PR
THE U... SITY ...GAN
JAN 18 1962
SCIENCE LIBRARY

The American Mineralogist

Journal of the Mineralogical Society of America

VOL. 46 NOVEMBER–DECEMBER, 1961 Nos. 11 and 12

Contents

Quantitative determination of kaolinite by x-ray diffraction ..... G. W. Brindley and S. S. Kurtossy 1205
Step height of spirals on hematite crystals ..... Ichiro Sunagawa 1216
Light scattering from heat treated synthetic quartz ..... J. A. Bastin and E. W. J. Mitchell 1227
Expandable chloritic clay minerals from carbonate rocks .. M. N. A. Peterson 1245
Polymorphism in bornite ..... N. Morimoto and G. Kullerud 1270
Crystallographic tables for the rhombohedral carbonates ..... Donald L. Graf 1283
Reaction of crystal structures and reaction fabric ..... W. R. Lauder 1317
Montmorillonite: High temperature reactions and classification ..... R. E. Grim and G. Kulbicki 1329
Ionic coordination in alumino-silicic gels in relation to clay mineral formation ..... C. De Kimpe, M. C. Gastuche and G. W. Brindley 1370
Relationship between unit-cell edges and composition of synthetic wurtzites ..... B. J. Skinner and P. M. Bethke 1382
Unit-cell edges of natural and synthetic sphalerites ..... B. J. Skinner 1399
New data for hisingerite and neotocite ..... J. A. Whelan and S. S. Goldich 1412
Carbonatic niobium-rare earth deposits, Ravalli Co., Montana ..... E. Wm. Heinrich and A. A. Levinson 1424
Arsenopyrite crystal-chemical relations .... Nobuo Morimoto and L. A. Clark 1448
Recognition of plagioclase twins in sections normal to the composition plane ..... Alexander C. Tobi 1470
Notes and News: Explanation of strain and orientation effects in perthites ..... J. V. Smith 1489

(Continued on Cover 2)

MINERALOGICAL SOCIETY OF AMERICA
CRYSTALLOGRAPHY PETROGRAPHY MINERALOGY
MCMXIX

EDITOR: LEWIS S. RAMSDELL
CO-EDITOR: E. WM. HEINRICH

BOARD OF ASSOCIATE EDITORS:

GEORGE W. BRINDLEY — ADOLF PABST (1959–61)
RICHARD H. JAHNS — EDWIN W. ROEDDER (1960–62)
CARL W. CORRENS — HERBERT INSLEY (1961–63)

Published bi-monthly by the Society

(*Contents continued*)

Indexed powder diffraction data for scapolite ..... G. V. Gibbs and F. D. Bloss 1493
A method of mineral separation using hydrofluoric acid ..... George J. Neuerburg 1498
N, N-dimethylformamide, a new diluent for bromoform used as a heavy liquid ..... N. Hickling, F. Cuttitta and R. Meyrowitz 1502
The chalcokyanite series ..... P. J. Rentzeperis 1503
The Weissenberg camera as a powder camera ..... Arrigo Addamiano 1504
Euclase in greisen pipes and associated deposits, Park Co., Colorado ..... William N. Sharp 1505
Ilvaite: a late magmatic occurrence in gabbro of Missouri ..... G. A. Desborough and D. H. Amos 1509
Book Reviews 1512
New Mineral Names 1513
Index to Volume 46; Title page; Table of contents 1521

Mineralogical Society of America

ASSOCIATED WITH THE GEOLOGICAL SOCIETY OF AMERICA

President: E. F. Osborn, Pennsylvania State University, University Park, Pennsylvania.
Past-President: Joseph Murdoch, University of California at Los Angeles, Los Angeles 24, California
Vice-President: Ian Campbell, State Division of Mines, San Francisco 11, Calif.
Secretary: George Switzer, U. S. National Museum, Washington 25, D. C.
Treasurer: Marjorie Hooker, U. S. Geological Survey, Washington 25, D. C.
Editor: Lewis S. Ramsdell, University of Michigan, Ann Arbor, Michigan.
Co-Editor: E. Wm. Heinrich, University of Michigan, Ann Arbor, Michigan.
Councilors:
(1959–61) Wilfrid R. Foster, Ohio State University, Columbus 10, Ohio.
(1959–61) Edward W. Nuffield, University of Toronto, Toronto 5, Ontario, Canada.
(1960–62) Julian R. Goldsmith, University of Chicago, Chicago 37, Illinois.
(1960–62) Horace Winchell, Yale University, New Haven, Connecticut.
(1961–63) Robert M. Garrels, Harvard University, Cambridge 38, Massachusetts.
(1961–63) O. F. Tuttle, Pennsylvania State University, University Park, Pennsylvania.
Advertising Manager: Martin L. Ehrmann, 369 South Robertson Blvd., Beverly Hills California.

The enlarged issues of this journal for 1961 are made possible by a grant from the Penrose Fund of the Geological Society of America.

The American Mineralogist—Journal of the Mineralogical Society of America

The journal, containing articles on mineralogy, crystallography, and allied sciences, is issued every two months. Contributions are invited.

The general conduct of the journal is in the hands of the editor, Lewis S. Ramsdell, Department of Mineralogy, University of Michigan, to whom all manuscripts should be submitted.

Second class postage paid at Menasha, Wis., under Act of March 3, 1879. Acceptance for mailing at the special rate of postage provided for in section 1103, Act of Oct 3, 1917, paragraph 4 section 429 P. L. & R. authorized March 13, 1922.

Notice of change of address, orders, and remittances should be sent to Marjorie Hooker, c/o U. S. Geological Survey, Washington 25, D. C.

Printed by George Banta Company, Inc., Menasha, Wisconsin
Printed in the United States of America

THE AMERICAN MINERALOGIST

JOURNAL OF THE MINERALOGICAL SOCIETY OF AMERICA

Vol. 46 NOVEMBER–DECEMBER, 1961 Nos. 11 and 12

QUANTITATIVE DETERMINATION OF KAOLINITE BY *X*-RAY DIFFRACTION*

G. W. BRINDLEY AND SARI S. KURTOSSY, *Department of Ceramic Technology, The Pennsylvania State University, University Park, Pennsylvania.*

ABSTRACT

An orientation index, $I(00l)/I(060)$, $l=1,2,$ is used to show that the degree of orientation of kaolinites ranging from well crystallized to poorly crystallized samples is high for samples giving sharp $00l$ reflections, and diminishes for samples with broader $00l$ reflections. A technique is employed involving the use of a thermoplastic cement which largely removes the preferential orientation in samples packed for *x*-ray diffractometer study. Van der Marel's experiments on the reflected basal intensities from kaolinite measured with respect to reflections from boehmite as an internal standard, are repeated, and the large variations found by him are confirmed when preferential orientation is not controlled. When the orientation is controlled, only small variations remain. Under this condition, the quantitative determination of kaolinite by *x*-ray diffraction is possible. However, the basal reflection intensities tend to diminish slightly as the reflection breadth increases, and therefore in analytical work a standard kaolinite will be preferred which gives basal reflections of the same angular width as those from the kaolinite to be determined.

INTRODUCTION

Quantitative *x*-ray diffraction provides a direct method for determining minerals in mixtures provided appropriate standards are available. Compared with other clay minerals, kaolinite presents relatively few problems because of the absence of significant amounts of isomorphous substitution. The basic assumption in determining kaolinites quantitatively by *x*-ray diffraction is that standard kaolinites can be obtained which diffract *x*-rays with the same intrinsic intensity as do the minerals to be measured. However, in a recent publication, van der Marel (1960) has brought forward data which seem to show that the reflected intensities from different kaolinites vary considerably. He gives values for the integrated intensities of the 001 reflections of a number of kaolinites ranging from about 1.9 down to 0.85 on a relative scale, a variation of about

* Contribution No. 60-60 from the College of Mineral Industries, The Pennsylvania State University, University Park, Pa.

100%. If this is indeed true, then the quantitative assessment of kaolinite in unknown mixtures by *x*-ray diffraction becomes quite unreliable unless standards can be chosen which correspond in *x*-ray reflection characteristics with the kaolinites to be measured.

Van der Marel gives diagrams showing both peak and integrated 001 reflection intensities plotted against the surface areas of the kaolinites measured by the B.E.T. method, from which it appears that the reflected intensity diminishes with increasing surface area. This decrease of intensity is attributed to the development of an amorphous surface layer of the order of 15–25 Å thickness and/or to an increasing internal disorder in the crystal lattice. He concludes that "*it is not possible to determine quantitatively the amount of kaolinite in samples of different origin,*" and that quantitative analysis is possible "*only when dealing with analyses of samples of one and the same particle size, order of crystallinity and composition.*"

One factor of considerable importance in relation to *x*-ray intensity measurements from kaolinite, particularly when the measurements are made by surface reflection, as in diffractometer techniques, is the marked tendency of the platy crystals to orient themselves parallel to the basal plane. Orientation is of extreme importance when measurements of the *basal* reflections are involved, as in the experiments of van der Marel. From the published account it appears that he gave little attention to this aspect of the work; he writes: "The samples were first dried at 105° C. for some hours (to prevent preferential orientation) and afterwards run with a Philips Geiger counter diffraction spectrometer. . . ." In the writers' view, this procedure is quite inadequate either to eliminate or even to control the preferential orientation of the platy clay particles.

Experiments have been undertaken, therefore, along similar lines to those of van der Marel, but with considerable attention to the question of preferential orientation. As a measure of orientation, the following intensity ratios have been measured: I(001)/I(060) and I(002)/I(060). Since orientation enhances I(001) and I(002), but diminishes I(060), these ratios provide convenient indications of the degree of orientation, and will be called "orientation indexes." It should be remarked that the prism reflection 020, although it occurs in the same angular range as the 001 and 002 reflections, is not suitable for measuring orientation because kaolinites with layer stacking disorder give diffuse scattering for the 020 and related reflections. On the other hand, the 060 and its associated reflections, $3\bar{3}1$ and $33\bar{1}$, are always clearly defined and can be measured fairly accurately.

An absolute value for the orientation index for randomly oriented crystals can be calculated from the crystal structure of the mineral.

The intensity diffracted by a randomly oriented powder in a surface-reflection diffractometer is proportional to

$$F^2 (1+\cos^2 2\theta)/(\sin^2 \theta \cos\theta) = F^2\phi(\theta),$$

where F is the structure factor and θ is the Bragg angle. This quantity was tabulated by Brindley and Robinson (1946) in their determination of the triclinic structure of kaolinite. They gave the values listed in the first and second columns of Table 1; the third column gives the calculated orientation indexes. The extent to which these results will agree with experimental values depends, of course, on the accuracy of the structure analysis as well as on the degree of preferential orientation in a powder sample. Since no attempt was made by Brindley and Robinson to refine the structure analysis beyond determining the general structural scheme, the importance of the calculated ratios must not be over-exaggerated.

TABLE 1. CALCULATED ORIENTATION INDEXES FOR KAOLINITE

hkl	$F^2\phi(\theta)\cdot 10^{-3}$		$I(00l)/I(060, 3\bar{3}\bar{1}, 33\bar{1})$
001	488		3.90
002	265		2.12
060	41.5		
$3\bar{3}\bar{1}$	42.5	125.4	—
$33\bar{1}$	41.4		

A purely experimental procedure is to measure the orientation indexes for many different kaolinites and to take the minimum values as representing the nearest approach to random orientation.

In the present experiments a technique has been applied for eliminating preferential orientation which appears to be largely successful, and the results now obtained go a long way towards proving that the intrinsic reflection intensities of the 001 and 002 reflections of kaolinite for different mineral samples exhibit relatively little variation, and that a large part of the variation observed by van der Marel is probably attributable to preferential orientation. His experiments and the present work both show the large variations which can arise when orientation is not adequately controlled, and the bearing of this result on the quantitative analyses of kaolinite in mixtures is very apparent.

THE PRESENT EXPERIMENTS

Materials

The experiments have been carried out using mainly a series of essentially pure kaolinites covering a range of particle sizes and degrees of

crystal structure perfection which were made available through the courtesy of Mr. S. C. Lyons and the Georgia Kaolin Company. These materials have already been described by Murray and Lyons (1956); they range from very well crystallized kaolinites showing sharp x-ray powder diffraction lines and well defined hexagonal forms in electron micrographs, to poorly crystallized kaolinites giving diffuse x-ray diffractions indicative of internal stacking disorder. These kaolinites were labelled A, B, C, . . . , L by Murray and Lyons, and the same designations are used here to facilitate comparison with their studies. Data are also given for several other kaolinites, which are labelled M, N, and P, and one sample of metahalloysite from Eureka, Utah.

Internal Standard

To facilitate comparison with the results of van der Marel, the same internal standard has been employed, namely boehmite, AlO(OH), and the same kaolinite/boehmite ratio, 3:1, has been used. Weighed quantities of kaolinite and boehmite were ground together under acetone for 7 minutes and then were dried at 105° C.

The following reflections have been compared:

kaolinite	(001)	$d=7.15$ Å
boehmite	(020)	$d=6.11$ Å
kaolinite	(002)	$d=3.57$ Å
boehmite	(021)	$d=3.16$ Å

Van der Marel made use of the first pair of reflections only, but as the second pair are equally convenient they also have been used.

Elimination of Orientation

As pointed out in the Introduction, orientation of the kaolinite flakes is potentially of great importance for the question under consideration. A technique for the elimination of preferred orientation, described to the writers by Mr. David Hinckley, has been applied in a modified form. The method consists of mixing a thermoplastic organic cement* with the clay, and then crushing after the mixture has hardened. Initially the cement was softened at about 80° C., but mixing with the clay was not easy and the cement was partly lost by vaporization. The following technique was then evolved: Powdered cement* was added to the clay in the ratio 1:5 and the mixture was ground for 7 minutes. Dioxane was then added to dissolve the cement; this was done on a hot-water bath.

* The cement used was "Lakeside, No. 70C," supplied by Hugh Courtright and Co., Chicago 20, Ill.

The cement dissolved readily and the mixing was continued with a spatula during the dissolution and eventual drying of the clay-cement mass. This had a granular texture and when fully dry was lightly ground for about 15 minutes to produce a fine powder. The material no longer had a "clayey feel."

Preliminary tests with various additions of the cement on the orientation of kaolinite as measured by the orientation index previously defined, showed that a cement:clay ratio of 1:5 was sufficient to reduce the orientation index to a minimum value.

The intensity ratios I (kaolinite)/I(boehmite), using the reflections previously listed, were measured with and without the cement addition. The measurements *without* cement were made with the object of comparing the results with those of van der Marel.

X-Ray Procedures

Measurements were made using filtered CuKα radiation and a Philips high-angle diffractometer with a scanning speed of $(\frac{1}{4})^\circ$ 2θ/minute and chart recording. *X*-ray intensities were kept within the range for which the recording system has an essentially linear characteristic. The sample was mounted in a 1″ diameter rotating holder constructed so that it could be packed from the back. To obtain uniform compaction of the powders, the same sample weight (0.5 gram) was used for each measurement. Integrated intensities were obtained by graphical integration, and each recorded value is the average of 3 runs on separately packed samples.

The angular widths of the 001 and 002 reflections were measured at half-maximum intensity. If, as van der Marel suggests, the reflected intensities are diminished by lattice disorder, then the widths of these reflections will be a useful parameter against which to plot the measured intensities. If the angular widths are related to the number of coherently reflecting planes, *i.e.*, effective crystal size, then again the widths will be a useful parameter to consider.

Results

The results are presented graphically in Figs. 1, 2, 3 and 4, where closed and open circles show respectively data for samples prepared with and without the thermoplastic cement.

Results for the Orientation Index

Figures 1 and 2 show the orientation indexes for kaolinite, I(001)/I(060) and I(002)/I(060), plotted against angular breadths B(001) and B(002). The open circles (samples without cement) are widely dis-

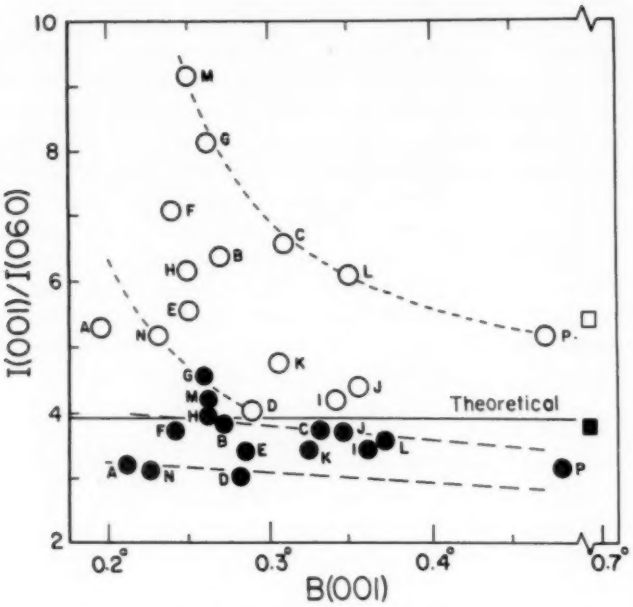

FIG. 1. Orientation index, I(001)/I(060), for fifteen kaolinite samples and one halloysite sample plotted against breadth B of the 001 reflections. Open circles for kaolinites without cement treatment. Solid circles for kaolinites with cement treatment. Squares show corresponding data for halloysite. Horizontal line shows theoretically calculated orientation index.

tributed, but have a general tendency to decrease in value as B increases. The closed circles (samples with cement) are confined to relatively narrow zones and the orientation indexes are nearly constant over the whole range of values of B.

The theoretically calculated orientation indexes also are shown in Figs. 1 and 2 by horizontal lines. Their agreement with the experimental values is particularly good for I(001)/I(060), but is less satisfactory for I(002)/I(060). The calculated value is *high* with respect to the experimental data in Fig. 1 but *low* in Fig. 2. The disagreements can be attributed, therefore, more to the approximate structure determinations than to the experimental data.

The experimental data for metahalloysite are shown by squares in Figs. 1 and 2. In order to include these values, it was necessary to break the horizontal axes, since the B values for the 001 and 002 reflections of halloysite lie far beyond the range of those for the kaolinite reflections. It is interesting to find that the halloysite reflections line up very well with

those for kaolinite despite the very different morphologies of the two minerals and the fact that the structural layers of halloysite are probably curved.

It can be concluded from the data in Figs. 1 and 2 that the cement technique has been largely successful in removing preferential orientation of the clay particles and that, in the absence of such a technique, orientation has a very large influence on the reflected intensities. Furthermore, the character of the results shows that orientation increases as the angular breadth B decreases. In so far as the angular breadth is related to morphology, it may be stated tentatively that kaolinites giving sharp reflections arise from well-crystallized forms which tend to be highly oriented.

Reflected Intensities

Figures 3 and 4 show values of the intensity ratios I(001)K/I(020)B and I(002)K/I(021)B, where K and B signify kaolinite and boehmite

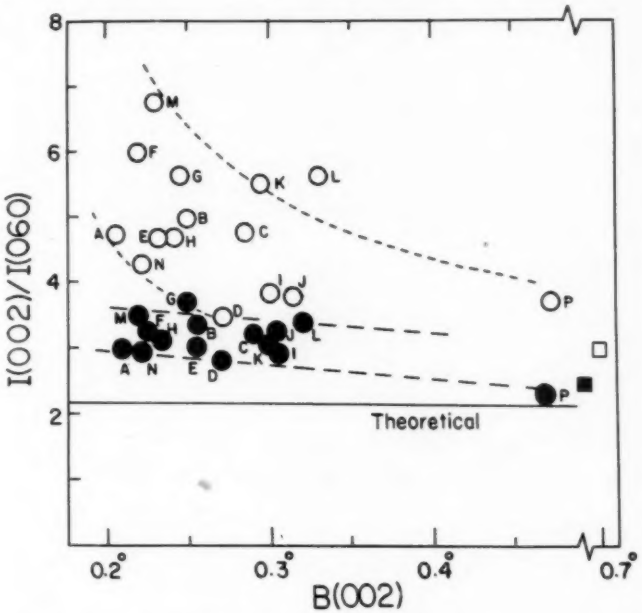

FIG. 2. Orientation index, I(002)/I(060), for fifteen kaolinite samples and one halloysite plotted against breadth B of the 002 reflections. Open circles for kaolinites without cement treatment; solid circles for kaolinites with cement treatment. Squares show corresponding data for halloysite. Horizontal line shows theoretically calculated orientation index.

respectively; the open and closed circles have the same significance as before.

Again it is seen that the open circles have wide ranges of values, with a marked tendency to decrease in magnitude as the breadth B increases. The data in Fig. 3 are comparable with those given by van der Marel in his Fig. 4. His values for I(001)K/I(020)B extend from about 1.9 down to 0.85, and the present values extend from about 2.2 down to 1.4. Both sets of values diminish as the breadth B, or as the surface area in van der Marel's Fig. 4, increases.

The closed circles in Figs. 3 and 4 are much more nearly constant and show relatively little variation as B increases. However, there remains a tendency for the intensities to diminish as the breadth B increases.

It is strikingly obvious that the intensity variations shown in Figs. 3 and 4 by the open circles run parallel with the orientation indexes given in Figs. 1 and 2. Conversely, when orientation is removed (or at least maintained constant) as shown by the solid circles in Figs. 1 and 2, the intensities in Figs. 3 and 4 also remain nearly constant.

Results for halloysite also are shown in Figs. 3 and 4. When account

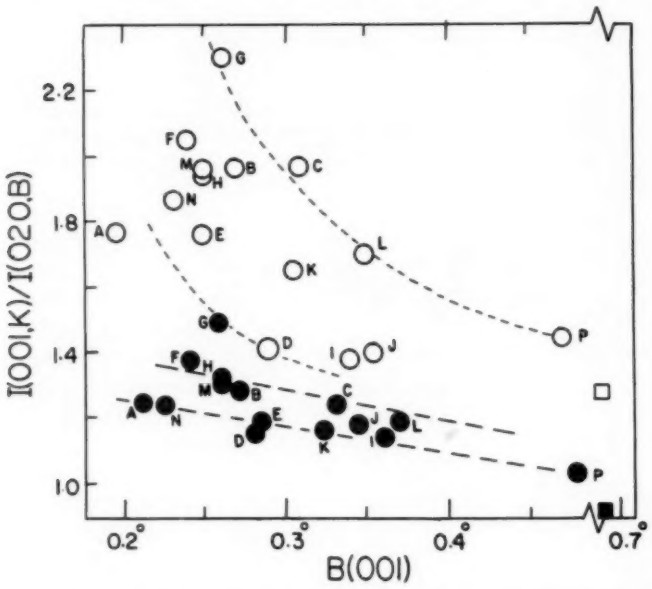

FIG. 3. Intensities of 001 reflections from fifteen kaolinite samples and one halloysite sample measured with respect to the 020 reflection from boehmite, plotted against breadth B of the 001 reflections. Open and solid circles and squares have the same significance as in Figs. 1 and 2.

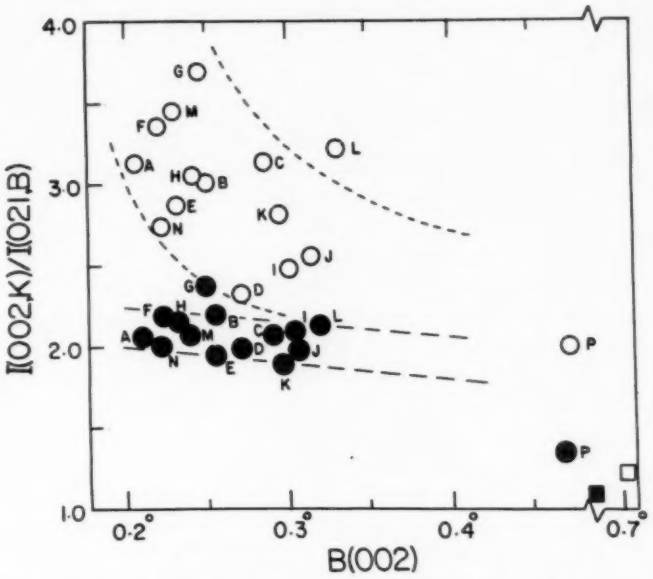

FIG. 4. Intensities of 002 reflections from fifteen kaolinite samples and one halloysite sample measured with respect to the 021 reflection from boehmite, plotted against breadth B of the 002 reflections. Open and closed circles and squares have the same significance as in Figs. 1 and 2.

is taken of the breaks in the B axis in these figures, the halloysite values are seen to lie roughly in line with those for the kaolinites, provided one accepts the conclusion that the intensities are diminishing slowly with increase of B. Indeed, the halloysite values provide additional support for this view. It is clear that for the kaolinites themselves, the decrease of intensity with increase of B is relatively small when preferential orientation is eliminated. It is not wholly negligible, however, and in the quantitative determination of kaolinites in mixtures it will be advantageous to choose standards having B values similar to those of the minerals being determined.

Discussion and Conclusions

The present experiments have confirmed those of van der Marel in showing large variations in the integrated intensities of the 001 and 002 reflections of kaolinites when no special precautions are taken to eliminate preferential orientation. An orientation index, $I(00l)/I(060)$ with $l=1$ and 2, is used to show that preferential orientation varies considerably from one kaolinite to another, the highest orientation and the highest $00l$

intensities corresponding to small values of B, the angular breadth of a basal reflection.

By using a thermoplastic cement, preferential orientation is largely eliminated (or at least controlled) and the reflected intensities are then nearly constant. Van der Marel's conclusion that "it is not possible to determine quantitatively the amount of kaolinite in samples of different origin" by *x*-ray diffraction analysis because of the large variation in reflected *x*-ray intensity is thus shown to be invalid. However, it appears that with increasing breadth of the kaolinite reflections, there is a small and not negligible tendency for the reflected intensity to diminish. Therefore it is advisable when selecting a standard kaolinite to choose one with approximately the same angular reflection breadth as the kaolinite to be measured. From the data shown in Figs. 3 and 4 it appears that it should be possible to select a kaolinite standard which reflects to within about 5% the same intensity as a kaolinite under investigation.

Van der Marel's results and those obtained in the present paper without using orientation control (*i.e.*, the open circles in Figs. 3 and 4) show the large errors which can arise in determining kaolinite by *x*-ray diffraction, if special precautions are not taken to diminish the orientation so readily assumed by clay mineral particles. An alternative solution to this problem, namely not to use basal reflections but to use more general-type reflections less subject to orientation errors, is generally impracticable. In many clay mineral mixtures in which kaolinite is present, the 001 reflection from the 7.15 Å layer spacing may be the only kaolinite reflection which is suitable for measurement and even this may be overlapped by a 002 chlorite reflection. Therefore, of necessity, the 001 and 002 kaolinite reflections, despite their sensitive dependence on preferential orientation, will be the only possible reflections which can be used in quantitative work. The present experiments emphasize the importance of eliminating (or controlling) the preferential orientation. The use of the organic cement is easy and simple and introduces very little additional labor in analytical determinations.

Acknowledgements

The participation of one of us (S.S.K.) in this work during the summer of 1960 was made possible by a grant from the National Science Foundation for Undergraduate Participation in Research. The kaolinite samples, A, B, C, . . . , L, were made available by Mr. S. C. Lyons and the Georgia Kaolin Company. The method for removing preferential orientation by the thermoplastic cement treatment was suggested by Mr. David Hinckley, though the method finally used was a modification of his suggestion.

References

Brindley, G. W. and Robinson, K. (1946), The structure of kaolinite. *Mineral. Mag.*, **27,** 242–253.

Murray, H. H. and Lyons, S. C. (1956), Correlation of paper-coating quality with degree of crystal perfection of kaolinite. *Proc. Fourth Nat. Conf. Clays and Clay Minerals, Nat. Acad. Sci.-N.R.C., Pub.* **456,** 31–40.

Van der Marel, H. W. (1960), Quantitative analysis of kaolinite. *Silicates Industriels*, **25,** 23–31, and 76–86.

Manuscript received December 22, 1960.

THE AMERICAN MINERALOGIST, VOL. 46, NOVEMBER-DECEMBER, 1961

STEP HEIGHT OF SPIRALS ON NATURAL HEMATITE CRYSTALS

ICHIRO SUNAGAWA,* *Physics Department, Royal Holloway College (University of London), Englefield Green, Surrey.*

ABSTRACT

The basal faces of hematite crystals from many localities have been observed with a phase contrast microscope. Different kinds of spirals are observed on the surface. The step heights are precisely measured by means of multiple-beam interferometry, and it is found that they are integral multiples of 2.3 Å, which is the height of a single layer in the structure, and not that of a unit cell height, which is 13.73 Å. Spirals having step heights close to 2.3 Å, 4.6 Å, 7 Å, 10 Å, 20 Å are observed.

Structural and theoretical consideration shows that the Burgers vector of screw dislocation or the unit of growth should be the height of the minimum component of the structure and not that of the unit cell. Therefore, both from theoretical consideration and the measurements, the widely accepted belief on the unit height of spirals is here contradicted.

INTRODUCTION

Ever since the importance of screw dislocations in crystal growth phenomena was predicted by Frank (1949), a wide variety of spiral patterns has been observed on many different crystals. Step heights of some of these spirals have been measured precisely by means of either multiple-beam interferometry or by the shadow-casting methods of electron microscopy. It has been widely believed that the step heights of the spirals are either one unit cell or a rational multiple thereof. However, it is not necessary to assume that the unit of growth is controlled only by the geometrical nature of the crystals.

Because of inadequate methods in some earlier studies, it is possible that the thinnest growth layers were missed. But there are cases in which the step heights of spirals less than the unit cell were found. Amelinckx (1951) observed spirals on SiC, type 6*H*, with a height of one half unit cell. He also reported (1955) spiral patterns on *n*-alcohol crystals having a height of one molecule, whereas the unit cell consists of two molecules. Verma and Reynolds (1953) detected spirals having half integral multiples of the unit cell on stearic acid. In this case, however, they did not find spirals having step heights less than one unit cell. Verma (1951) has also reported spirals on SiC having a smaller step height than the unit cell.

The most common spiral patterns found on hematite are deformed spirals revealing high step heights. They appear to have originated from scratches, misfit boundaries, etc., which have formed on the surface during growth, due to mechanical deformation, and external or

* Present address: Geological Survey of Japan, Hisamoto-cho 135, Kawasaki-shi, Japan.

internal stresses. Such high step spirals will not be discussed here. The spirals discussed in this paper are those having a regular form and spacing between successive layers. They might be called "typical spirals," and usually occur on the surface of thick growth layers, an indication that they are formed at the latest stage of growth. They sometimes cover nearly the whole crystal surface. They may be triangular, truncated triangular or circular. Precise measurements of the step heights of these spirals have been made with multiple-beam interferometry, and it is found that the step heights may be less than a unit cell, or greater. Successful phase contrast photomicrographs were obtained of steps, which measurements showed were 2.3 Å, 4.6 Å, 7 Å, 10 Å, 20 Å, etc.† Since c_0 for hematite is 13.73 Å, and as the unit cell consists of six layers of oxygen atoms sandwiching iron atoms, the height of the minimum component of the cell is indeed 2.3 Å. Therefore, it is concluded that the Burgers vector of screw dislocation of hematite, or the unit of growth, is not one unit cell in height, but is of the height of the minimum component of the unit cell. It is conjectured that this might be true not only for hematite but also, for other minerals having a layer structure, or having a structure which can be interpreted in terms of a layer structure. In the following section, the results of measurements of these very thin growth spirals are described and shown.

Methods of Observation and Measurement

With the usual metallurgical reflection microscope, growth layers of a thickness of less than a few hundred Å can hardly be observed. The very thin layers have been studied here with an "Olympus PMF type" phase contrast reflection microscope. Very absorbing phase disks give an exceptionally sensitive phase contrast effect, and permit observation of ultra-thin growth layers.

Multiple-beam interferometry has been applied to the measurement of step height of spirals, using the standard methods developed by Tolansky (1956). Since this method is well established, only a very brief account of the practice will be given here.

The surface is silvered to a thickness of about 1000 Å. It has been adequately established by Tolansky and Bhide (1956) that silvering with this thickness does not modify the surface structures. This silvered surface is matched against a silvered flat, and in accordance with familiar experimental arrangements, sharp, high precision multiple-beam Fizeau fringes are produced, using the green mercury line. Under normally good conditions, it is not difficult to measure step heights down to 15

† Photographs showing 2.3 Å, 4.6 Å and 7 Å spirals accompanied this paper, but lack of contrast made it impossible to reproduce them satisfactorily.

Å. However, in the case of layers thinner than 15 Å, it is necessary to apply indirect methods. For instance, when the spacing of the successive layers of a very shallow spiral is regular and narrow, it is easy to calculate the average step height of a single layer by dividing the easily measured total height of the spiral by the number of layers. The definite existence of spirals of layer height of only 2.3 Å has been confirmed this way. Quite often we observe that the thinner layers merge to form a thick layer. In such a case, we can derive the step heights of the thinner layers by dividing the measured step height of the thick layer by the number of thin layers present. Step heights of 4.6 Å, 7 Å, 10 Å, etc. have been obtained in this way. The 20 Å spiral was measured directly from the fringe displacement, using standard procedure.

Observations and Measurements

2.3 Å Spirals

On the basal planes of hematite crystals from many different localities, triangular structures have been commonly observed. When multiple-beam interference fringes are run across such structures, they show a very small shift, which clearly shows that the height of the structure is very small. Measurements of the total heights of these shallow hillocks have been made on one crystal of hematite from Ayumikotan in Japan. The smallest step height is about 20 Å, the maximum 110 Å, but the commoner step heights range from 30 Å to 50 Å (Sunagawa, 1958).

Under low magnification, no fine structure can be seen on the side faces of these triangular hills. However, when phase contrast photomicrographs of very high magnification and very high contrast sensitivity are taken, it is revealed that these actually consist of narrow spaced triangular spirals. Clearly the step height of each layer can be obtained by dividing total height by the number of clearly resolved spiral layers. The results measured and calculated for seven different cases show remarkably good agreement, ranging from 2.1 Å to 3.2 Å, with an average of 2.6 Å. Clearly this low value must be identified with the single layer of Fe_2O_3, which is 2.3 Å. This is quite a surprising result. This represents the smallest growth layer yet evaluated by multiple-beam interferometry. It clearly shows that there exists a screw dislocation with Burgers vector which is only one sixth of a unit cell. Many of our hematite crystals from different localities reveal that this type of unit spiral is quite common, and in some cases the whole surface is completely covered with this type.

The form of these spirals is always regular, consisting of straight-sided equilateral triangles. The spacings between successive layers are regular, and very narrow compared to most other spirals.

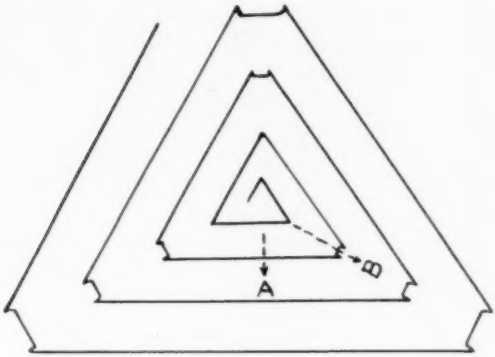

FIG. 1. Schematic drawing of horn-like projections at each corner of a 4.6 Å spiral.

4.6 Å Spiral

On one crystal from Saganoshima, Japan, nearly half the surface is covered with one triangular spiral originating form a single screw dislocation. At the center, the spiral has regular triangular form, but after several turns three of the corners truncate and a deformed hexagonal pattern appears. At each corner of this hexagon, a horn-like shape is observed as shown by the diagram in Fig. 1. This pattern is considered to be formed by the different rate of growth in the direction of A and B. A line crosses the whole crystal surface with a break at one portion. This line consists of two parallel twin boundaries (Sunagawa, 1959). Spiral fronts starting at a dislocation point on one side of the line spread out and cross this line at the break portion and cover nearly half the surface on the other side. This is schematically shown in Fig. 2. It is clear that the point A on the one side of the discontinuity line is higher

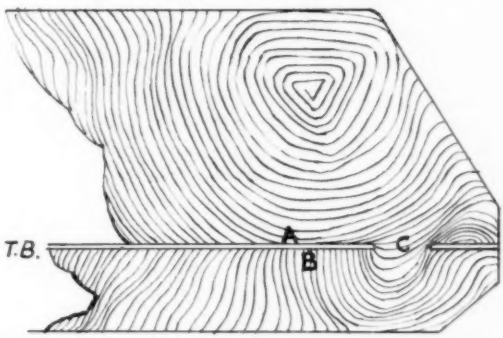

FIG. 2. Schematic drawing of crystal face covered with a 4.6 Å spiral.

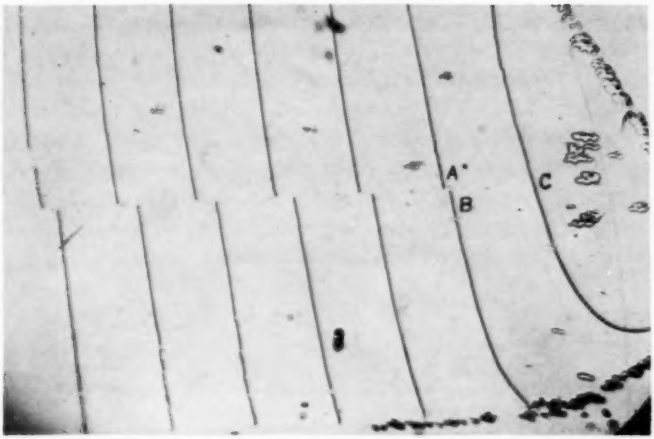

FIG. 3. Example of Fizeau fringes of a 4.6 Å spiral on a crystal from Saganoshima, Japan. ×27.

than point B on the other side, and that the level difference between A and B is equal to the multiple of the height of a single layer times the number of layers between two points. A multiple-beam interferogram for this area is shown in Fig. 3, which clearly shows the level difference between two sides of the discontinuity line. Measurements of the difference at several points have been made, and the number of layers counted on a phase contrast photomicrograph. The level differences, number of layers and the step heights of a single layer, calculated by dividing the level difference by the number of layers, are given in Table 1. The results at different points show remarkably good agreement, and the average step height is 4.5 Å, which effectively coincides with the predicted height of two layers in the structure.

TABLE 1. AVERAGE HEIGHT OF A SINGLE LAYER OF A 4.6 Å SPIRAL

Total level differences in Å	Number of layers	Height of a single layer in Å
116	29	4.0
186	37	5.0
266	60	4.4
422	95	4.4
450	97	4.6
601	132	4.6
655	139	4.7
		Average 4.5 Å

Another example of 4.6 Å spiral has been found on one crystal from the Ascension Islands. In this case, the spiral layers bunch together and form fairly thick layers, from which the total step heights can be measured, and so the individual spiral step is derived.

7 Å Spiral

On one crystal from Saganoshima, Japan, spirals with step height of about 7 Å have been observed. Two spirals start from either one screw dislocation point or alternatively two spirals of opposite sign are situated close together. On the spiral pattern, there are several tongue-like terraces at which the spiral growth fronts are intercepted. By dividing

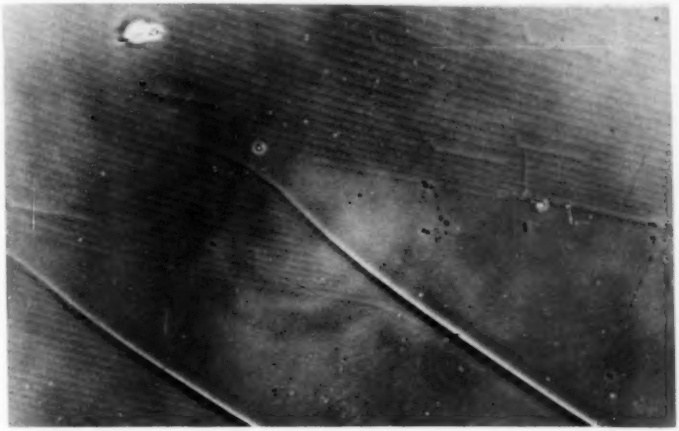

FIG. 4. Positive phase contrast photomicrograph showing bunching of 10 Å spiral layers. Ascension Island. ×160.

the total height of the tongue-like terrace by the number of intercepted spiral layers, the average step height is found to be 7 Å, which is clearly that of three layers in the structure, *i.e.*, $\frac{1}{2}$ unit cell height (Sunagawa, 1960). Similar spirals have been found on crystals from the Azores Islands, Portugal (Sunagawa, 1959).

10 Å Spiral

This spiral appears on a crystal from the Ascension Islands. At the marginal part of the spiral, growth layers bunch to form thick layers as shown in Fig. 4. No fringe shift is discernible at the edge of the spiral layer, but fortunately, very clear shifts can be obtained at the edges of the thick bunches. The number of spiral layers was easily counted with the phase contrast photomicrograph. Table 2 shows the results of meas-

urements, number of layers and the average step height of a single layer. The step heights thus calculated range from 9.0 Å to 12.1 Å, and average is 10.3 Å. This range of 9 to 11 Å effectively coincides with about four or five layers.

TABLE 2. AVERAGE STEP HEIGHT OF A SINGLE LAYER OF A 10 Å SPIRAL

Step heights of bunched thick layers in Å	Number of layers	Step height of a single layer in Å
43	4	10.8
124	11	11.3
157	13	12.1
159	17	9.3
169	17	9.9
174	16	10.8
249	23	10.8
283	29	9.7
316	30	10.5
365	37	9.9
368	37	10.0
406	38	10.7
427	47	9.0
434	47	9.2
		Average 10.3 Å

20 Å Spiral

This spiral was found on one crystal from Saganoshima, Japan. Nearly half of the surface of the crystal is covered with a spiral pattern originating from one dislocation point. At the center, the spiral has a triangular form. The spacing between successive layers is very narrow. But after several turns, the spacing suddenly increases and the triangular form changes into a deformed circle. In one direction of the spreading of this spiral, all the layers of the spiral split up into two thinner layers and form a characteristic interlacing pattern, part of which is shown in Fig. 5. Multiple-beam interferograms of very different dispersion have been obtained. In the case of high dispersion fringes, a very small fringe shift is detectable at each edge of the spiral layers, from which a direct measurement of the step height has been made. As the shifts are very small, the value so obtained is not very precise. Measurements range from 18 Å to 25 Å, and average value is 20 Å. It is certainly not 14 Å, which is the height of one unit cell, but exceeds this. The fact that the spiral layers split into two in one direction of spreading fits in with this

higher figure. (The interlacing pattern observed on this crystal is evidence which suggests the possibility of the existence of polytypism in hematite.) This spiral possibly originated from a screw dislocation with Burgers vector of value one and a half unit cell.

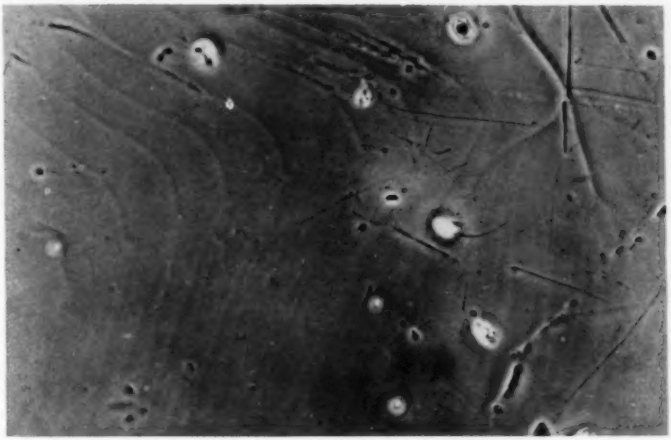

FIG. 5. Positive phase contrast photomicrograph showing interlacing pattern observed on portion of the 20 Å spiral. Saganoshima, Japan. ×180.

Spirals with Big Step Heights

On crystals from many localities, irregular formed spirals have been observed. These may owe their origin to scratches, distorted portions, misorientated portions, misfit boundaries, etc., formed by mechanical deformation and external or internal stresses taking place during growth. Judging from the visibility, width and the nature of white fringes appearing at the edges of layers on phase contrast photomicrographs, it is quite safe to say that the step heights of these spirals are large and variable.

SUMMARY AND DISCUSSION

As a result of detailed observations on the surface structures of hematite crystals from many localities, wide varieties of spiral patterns have been observed. Most spirals have relatively high step heights and are of irregular form. But some spirals appear having very small step height and are of regular triangular or circular form, often appearing on the surfaces of thick growth layers. At times they cover nearly the whole surface of a crystal. These shallow spirals originate from typical

screw dislocations. The step heights of these typical spirals have been measured precisely by means of multiple-beam interferometry. Spirals having step heights of 2.3 Å, 4.6 Å, 7 Å, 10 Å, 20 Å have been found. It is also found that spirals with one unit cell in height are not at all common, while those having 2.3 Å, 4.6 Å are quite common features.

The characteristics of these spirals are as follows:

1) 2.3 Å spirals always occur as close-spaced triangular spirals. The form is always regular triangular, and no special pattern formed by the difference of growth rate in different orientations are observed at the corner of the triangles.
2) In the case of 4.6 Å spirals, the spiral pattern is a regular triangle at the center, but after a few turns three corners truncate, forming a slight displacement at each corner. This is due to the different velocity of spreading in different orientations.
3) In the case of 7 Å spirals, two spirals start at a single dislocation point, or two opposite-handed spirals start from two closely situated dislocation points.
4) In the 20 Å spiral, the pattern is triangular at the center, but after several turns it becomes first hexagonal and then circular. Furthermore, in one direction of spreading, the layers split in two, forming an interlacing pattern.

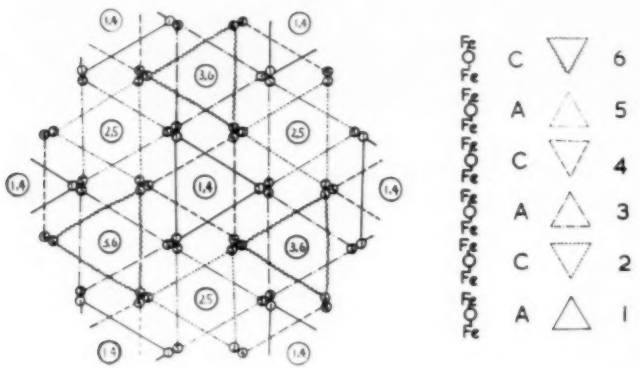

FIG. 6. Schematic drawing of the structure of hematite.

The unit cell of hematite consists of six layers of oxygen atoms parallel to 0001, alternating with Fe atoms. As shown in Fig. 6, triangles of three oxygen atoms are oppositely oriented in successive layers. Hence it is possible to subdivide the unit cell into six layers. It is quite reasonable to expect spirals of a step height of 2.3 Å, which is the height of one of these single layers, or step heights with rational multiples of 2.3 Å, but not multiples of a unit cell height. This conjecture is also supported from theoretical considerations on bond chains in the hematite structure, from the standpoint of the theory of Hartman.

If we consider the orientation of triangles consisting of three oxygen atoms, the characteristics of each spiral pattern can be explained clearly as follows. The 2.3 Å spiral should take on a simple and regular triangular pattern, as it consists of only one layer, on which triangles are arranged in the same direction. Since the 4.6 Å spiral consists of two layers, having triangles oppositely orientated, it will take on a hexagonal pattern, though in the center it will be of regular triangular form. In the case of the 7 Å spiral, it is considered that the screw dislocation of one unit cell height is split in two, thus forming a spiral having a half unit cell height. This is perhaps the reason why two 7 Å spirals usually are situated close together or start from a single dislocation point. In the case of the 10 Å spiral, no specific pattern has been observed. In the case of spirals having step height higher than the unit cell, the layer can split into two, or more than two. This is in fact observed in the case of 20 Å spiral.

Both from a theoretical and structural consideration and from precise measurements, it has been definitely clarified that the unit of screw dislocation or unit of growth is the minimum component of the unit cell and not one complete unit cell height. The step height of the spiral layer can be any rational multiple of the height of this minimum component. Since most measurements previously made on the step heights of spirals show that the heights of spiral layers are of unit cell height or rational multiples of this, it has been generally believed that the unit of screw dislocation is the *x*-ray repeat distance, but, as clearly seen here, this general idea is contradicted. It is conjectured that this may also be true in other crystal species, at least in the case of those crystals having a layer structure.

Acknowledgements

The writer expresses his heartfelt thanks to Professor S. Tolansky, in whose department the work was done, for his encouragement, helpful discussion and revising the first draft of this paper.

He also wishes to thank Professor F. C. Frank, S. Amelinckx and Drs. A. F. Seager, and P. Hartman for their constructive suggestions.

The specimens have been most generously supplied by the following people and organizations to whom the writer would like to express his gratitude.

Prof. Z. Harada, Dr. K. Sakurai, Messrs. N. Inai, K. Sawamura, H. Sato, K. Matsui.

British Museum (Natural History), Cambridge University (Department of Mineralogy and Petrology), Geological Survey of Portugal.

This work was undertaken while the writer was on leave from the Geological Survey of Japan, with the help of a Japanese Government grant.

References

AMELINCKX, S., Growth mechanism of carborundum crystals: *Nature*, **168,** 431 (1951).

———, Growth features on crystal of long-chain compounds, I, II, III: *Acta Cryst.*, **8,** 530 (1955); **9,** 16, 217 (1956).

FRANK, F. C., The influence of dislocations on crystal growth: *Disc. Farad. Soc.*, No. **5,** 48 (1949).

HARTMAN, P., Private communication.

SUNAGAWA, I., Crystal growth of hematite from Ayumikotan, Japan: *Jour. Miner. Soc. Japan*, **3,** 543 (1958).

———, Surface structures of twin boundary of hematite crystals: Symposium on twinning at IMA general meeting, Zurich (in press) (1959).

———, Growth and etch features of hematite crystals from the Azores Island, Portugal: *Serviços Geológicos de Portugal*, Memória No. 6 (Nova Série) (1960).

———, Growth history of hematite: Am. Mineral., **45,** 566–575 (1960).

TOLANSKY, S., Multiple-beam interferometry: Clarendon Press, Oxford (1948).

TOLANSKY, S. AND BHIDE, V. G., Sur la reproduction des reliefs par les couches minces utilisées en interférométrie a ondes multiples: *Jour. de Chim. Phys.*, 563 (1956).

VERMA, A. R., Growth spirals on carborundum crystals: *Nature*, **168,** 430 (1951).

VERMA, A. R. AND REYNOLDS, P. M., Interferometric studies of the growth of stearic acid crystals and their optical properties: *Proc. Phys. Soc.*, **B66,** 414 (1953).

Manuscript received January 16, 1960.

THE AMERICAN MINERALOGIST, VOL. 46, NOVEMBER-DECEMBER, 1961

LIGHT SCATTERING FROM HEAT TREATED SYNTHETIC QUARTZ

J. A. BASTIN* AND E. W. J. MITCHELL, *J. J. Thomson Physical Laboratory, The University, Reading.*

ABSTRACT

Many crystal plates of synthetic quartz appear milky after heating above about 650° C. In some specimens individual scattering particles can be resolved and are found to lie on planes, some of which (*e.g.* (00.1)) are crystallographically simple. In most specimens the scattering particles are grouped in more or less well-defined macroscopic regions. In a particular group of specimens these regions are well defined hexagonal prisms parallel to the *c*-axis. Before heat treatment it was shown that these prismatic regions were colored by ionizing radiation showing the well known broad band at about 4500 Å believed to be associated with Al impurity. Direct spectrographic analysis also showed that those specimens which contained most Al would have the highest light scattering coefficient after heat treatment.

The kinetics of the formation of the scattering particles was studied and the formation of the particles is limited by an activated process of energy 1.1 ± 0.1 eV.

A model is put forward to account for the results. It is suggested that the scattering particles result from the precipitation of Al which diffuses interstitially through the crystal to precipitation centers. These centers are frequently localized on planes; such centers might result from the intersection of edge dislocations with laminar faults.

INTRODUCTION

During experiments on the annealing of radiation damage in quartz it was noticed that synthetic specimens were invariably "milky" after heating above about 650° C. This effect was not found with natural (Brazilian) quartz. Subsequently an investigation was carried out of the conditions of formation of the scattering centers and of their spatial distribution. The results are described in this paper.

EXPERIMENTAL

The quartz crystals were grown by the hydrothermal method by the G.E.C., Wembley, England, and by Sawyer Products Inc., Cleveland, U.S.A. The G.E.C. crystals (see, for example, Brown and Thomas 1956) were grown on seeds in the form of plates cut perpendicular to the *c*-axis. The American crystals (see, for example, Bechmann & Hale 1955) were grown on long narrow bars of rectangular cross section. The long axis of each bar was parallel to the *y*-axis while the long narrow faces were perpendicular to either the *a*- or the *c*-axis. The G.E.C. supplied three types of crystals, differing in the amounts of Al impurity which had been incorporated. We refer to these as G I, G II and G III, and according to spectrographic analysis carried out by the G.E.C., the approximate concentrations of Al are as given in Table I.

* Now at Physics Department, Queen Mary College, London.

The specimens were heated in air in a temperature controlled silica tube furnace. It was found necessary, for plates of thickness greater than about 1.5 mm., to heat and cool slowly (1° per min.) in order to avoid cracking the specimens. For this reason the controller was fitted with an automatic drive and a given heat treatment was programmed with a specially cut cam. From time to time a chromel-alumel thermocouple was used to measure the temperature adjacent to the specimen. This temperature was found to be within 5° of that shown on the controller.

After heat treatment the crystals were examined with three kinds of microscopes:

(1) Low power (up to ×60).

(2) Leitz "ultramicroscope," which is a device for viewing light scattered at right angles to the incident beam. The scattered light was viewed through a low power microscope (up to ×60).

TABLE I

Type	Estimated weight % of Al	Mean Σ cm.$^{-1}$ defined	No. of specimens investigated for determination of Σ
G I	10^{-3}	7.2 ± 3	6
G II	$5-10\times10^{-3}$	38 ± 15	5
G III	2×10^{-2}	64	1

(3) Vickers projection microscope using a 4 mm. dark-field illumination objective to give magnifications on the screen of 1000. The fine adjustment head allowed the height of the specimen to be varied and set to 10^{-5} cm. The stage could be moved, by micrometers, in two perpendicular horizontal directions.

The spectral transmission of the specimens before and after heat treatment was measured with a Hilger Uvispek spectrophotometer. Measurements were also made using an integrating sphere in conjunction with the spetrophotometer as described by Bastin *et al.* (1959). In the former case light is removed from the straight-through beam by scattering and absorption, while in the integrating sphere the only losses recorded arise from absorption. Combining the two sets of data it is possible to separate scattering and absorption effects.

THE DISTRIBUTION OF SCATTERING CENTERS

All regions of the G.E.C. specimens and some regions of the Sawyer specimens were found to be permanently milky after heating above 650° C. The distribution of milkiness in the various specimens was as follows:

G.E.C. Type G I

Plates of thickness 0.05 cm. cut perpendicular to the *c*-axis showed an irregularly mottled appearance. Some unheated specimens were irradiated in the Harwell pile BEPO (1.7×10^{18} $n°$ cm^{-2}) and the induced smoky color was distributed in a similarly irregular way. However, in one case when the heat treatment was carried out on an irradiated specimen there was no obvious spatial correlation between the irradiation coloring and scattering patterns. Plates cut at right angles to a Y direction showed macroscopic striations in the basal plane. Similarly orientated striations were found in pile irradiated crystals of this type although the regions of preferentially dense radiation coloring tended to become regions of lower scattering power.

G.E.C. Type G II

Specimens cut parallel to the basal plane and viewed in the direction of the *c*-axis showed well-defined regions containing a preferentially high density of scattering centers. Fig. 1*a* shows a photograph taken with the Leitz ultra-microscope in which the regions appear in the form of equilateral triangles with the corners cut off by intersection with larger equilateral triangles. When the focal plane was moved through the

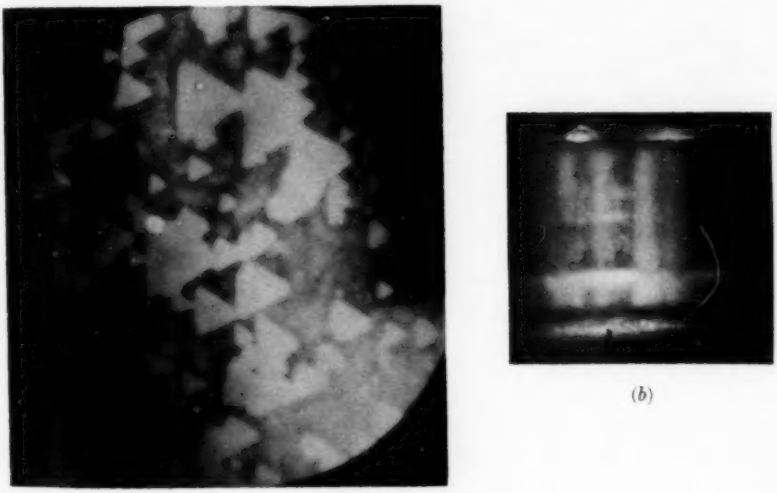

(*a*) (*b*)

FIG. 1. Photographs of specimen G II_2 taken by scattered light with a Leitz ultra-microscope viewed (*a*) in the *c*-axis direction (55×), and (*b*) at right angles to the *c*-axis, which is vertical (40×).

specimen in the direction of the *c*-axis the "triangles" remained in focus through most of the thickness of the specimen. This suggested that a high density of scattering centers existed within "triangular" *prisms* whose axes were parallel to the *c*-axis. Confirmation of this can be seen in Fig. 1*b* which shows a photograph taken by scattered light of the same specimen viewed in a direction at right angles to the *c*-axis. The prisms are now seen as striations. If the focal plane was lowered or raised the striations were found to remain in focus for a distance of about 0.01–0.02 cm. As the striations disappeared other randomly positioned

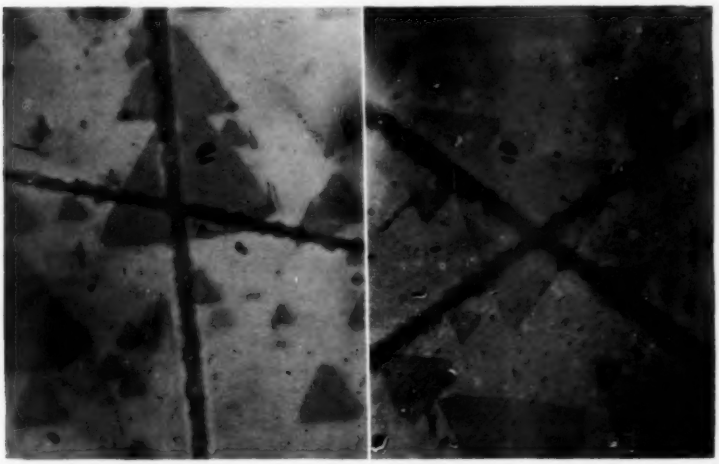

(*a*) (*b*)

FIG. 2. Photographs of specimen G II_2 taken by transmitted light (*a*) after neutron irradiation (1.7×10^{18} $n°$ cm.$^{-2}$). 85×; (*b*) after subsequent heating at 700° C. for 24 hours. 77×.

but parallel striations came into focus. This is consistent with the presence of prisms of cross-section dimensions of about 0.01–0.02 cm. (as indicated by Fig. 1*a*), randomly distributed in a basal plane but all parallel to the *c*-axis. Back reflection Laue photographs showed that, contrary to what might be expected, the directions of the "triangular" edges of the cross-section of the prisms do not coincide with *a*-axes. In the specimen examined these edges were at an angle of 13°.

The following experiment was carried out to see whether there was any correlation between the radiation darkening pattern and the scattering pattern. Two fine lines were cut on one of the surfaces of specimen G II_3. Before any treatment the plate was clear. After pile irradiation

(1.7×10^{18} $n°$ cm.$^{-2}$) the crystal appeared in transmitted light as in the photograph of Fig. 2*a*. Fig. 2*b* shows the appearance after heating at 700° C. for 24 hours. The radiation color is bleached by this treatment and the prismatic scattering regions are apparently induced as in an unirradiated crystal. A comparison of the two photographs shows that the regions of radiation coloring correspond with those which scatter light preferentially. The experiment also shows that previous neutron irradiation does not prevent the subsequent formation of light scattering centers.

A similar specimen was etched in 10% hydrofluoric acid for 12 hours

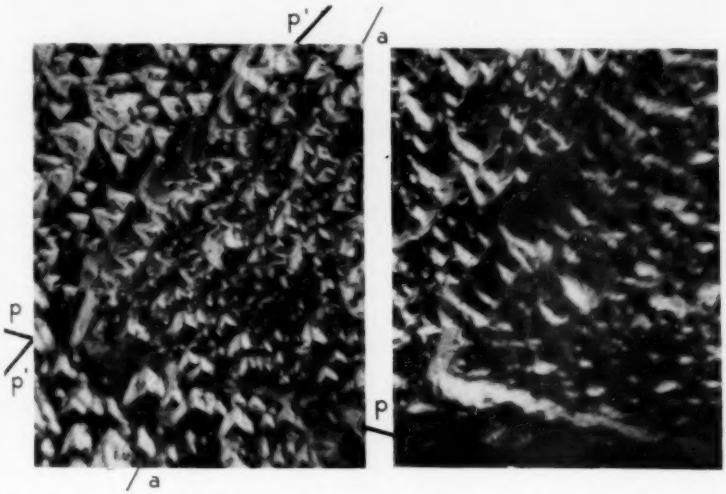

FIG. 3. Photographs of the 0001 surface of specimen G II_4 after etching in 10% HF. (Left) Focused on the surface within the prism boundary p-p and p′-p′ (a-a is *a*-axis direction. (Right) Focused on the surface outside the prism. 885×.

after having been heated at 700° C. Figure 3 shows a photograph of the etching pattern using a magnification (×400) such that only one prism surface appears in the field of view. It was also found, by focussing on to the surface of the crystal first within and then outside the prism, that more material had been removed from within the prism. The photographs show that there is a greater density of etch pits within the prism than outside it.

G.E.C. Type G III

Pile irradiation produces a non-uniform darkening in which triangular prismatic regions are evident but they are smaller and less geometrically exact than those produced in G II specimens. Figure 4 is a photograph

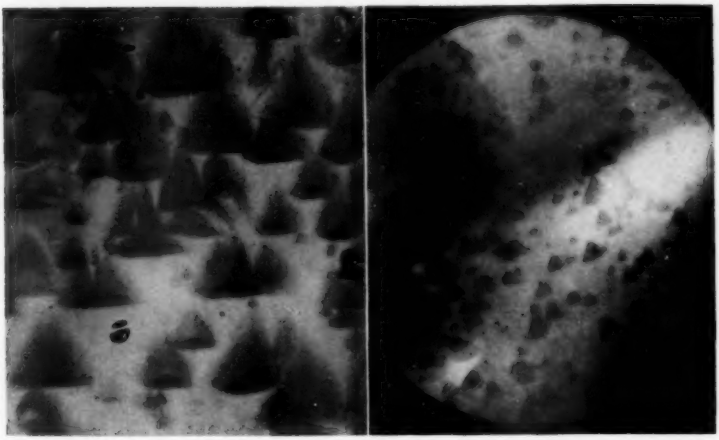

FIG. 4. (Left) Specimen G III_2 after neutron irradiation (1.7×10^{18} $n°$ cm.$^{-2}$) viewed in the c-axis direction. 148×.

FIG. 5. (Right) Specimen G III_3 after heating at 700° C. for 24 hours, viewed in the c-axis direction. 40×.

of specimens G III, after a neutron dose of 1.7×10^{18} $n°$ cm.$^{-2}$. It will be seen that there are light streaks running from the apices to the centers of the triangular regions.

In the case of G III_4, the only specimen of this type which has been heat treated, light is scattered from most of the crystal but there are prisms of approximately triangular cross-section within which there is a preferentially *lower* density of scattering centers (Fig. 5).

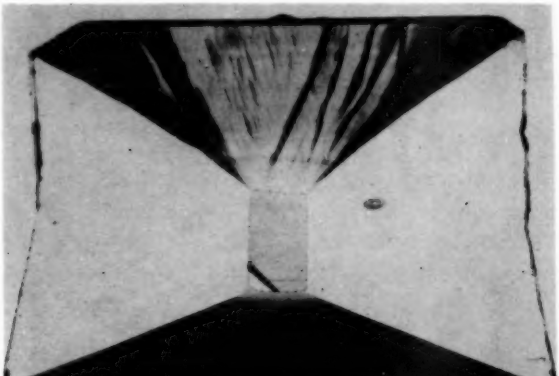

FIG. 6. Sawyer Products crystal viewed in the Y direction after neutron irradiation (1.7×10^{18} $n°$ cm.$^{-2}$). 3×.

Y-Bar Crystals (Sawyer Products)

The specimens were cut from the same crystal at right angles to the Y direction. In each case, the only region in which noticeable scattering was produced by heat treatment was in the slow growing X direction. The scattering density appeared fairly uniform throughout this region although there was a tendency for the density to be greater in laminated regions perpendicular to the growth direction and separated by about 0.05 cm. The effect of pile irradiation on unheated specimens is as shown in Fig. 6. Although the darkening in some parts of the crystal is extremely non-uniform, there are only slight variations in the part of the

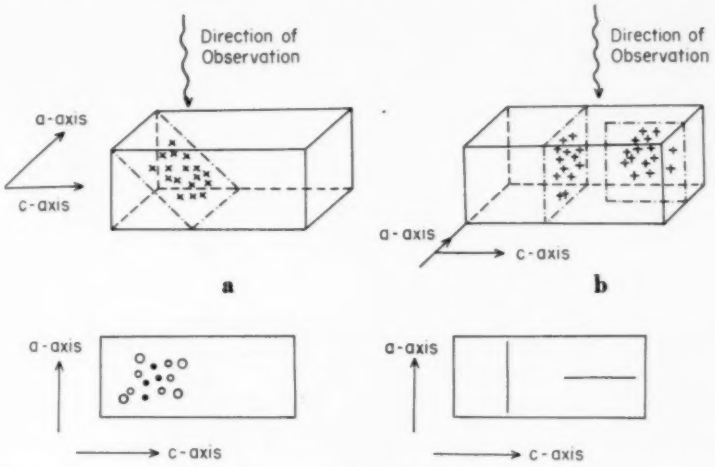

FIG. 7. Precipitation planes viewed (a) as planes, and (b) as lines in synthetic quartz.

crystal in which scattering centers are produced. Both Hale (1957) and Cohen (1957) have found similar patterns in the original Y bar crystals grown at the Clevite Research Center.

OBSERVATIONS OF INDIVIDUAL SCATTERING CENTERS IN G.E.C. TYPE G I SPECIMENS

Individual scattering centers were most clearly detected in Type G I specimens, from which, as described above, there was a relatively low intensity of scattered light. It is convenient to divide into two the distribution of centers revealed by the examination with the 4 mm. dark field objective (this was found to give optimum viewing conditions).

(a) Scattering centers grouped in apparently open clusters on planes not containing the direction of viewing (Fig. 7). It was found impossible to bring all the centers in a

given cluster into focus at once. This indicated that the centers were located at different depths within the crystal. If the specimen was moved slowly in the direction of observation the imaginary line, along which the centers were in focus, moved across the cluster. This type of grouping occurred principally in specimens heated for only a short time at comparatively low temperatures (700° C).

(b) Scattering centers grouped into planes containing the direction of viewing (Fig. 7). These centers are in planes which are viewed edge on so that they appear as lines which remains in focus when the specimen is moved in the direction of view. For a given specimen position the centers in focus were seen against a blurred background arising from the out of focus centers above and below the focal plane. Groups of this kind occurred most frequently in the higher temperature heat treatments.

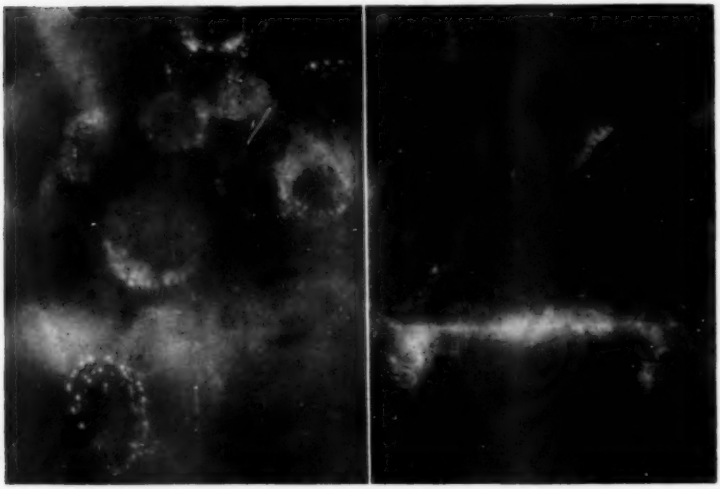

FIG. 8. Photographs of precipitation planes and particles in specimen G I_{16} viewed in an *a*-axis direction with the *c*-axis parallel to the base of each plate. 700×.

A particular region of specimen G I_{17} was examined both after a light and a subsequent heavy heat treatment. After the first heating (1 hour at 700° C.) a large number of open groups (*a*), and a few weak lines (*b*) were noticeable. After the second heat treatment (72 hours at 900° C.) the original lines were re-identified but were found to have extended much further into the crystal. It was not possible to re-identify the clusters which were much less apparent than after the heating at 700° C. These observations indicate that the two groups of centers are not only distinguished by their orientation but also by their condition of formation.

Photographs of both types of grouping are shown in Fig. 8.

Orientation of Planes

The orientation of type (*b*) clusters could be readily found by measuring the angle of the line relative to the *c*-axis. These angles (see Fig. 7) 0°; 36° 50′; and 90°. This data is summarized on the stereographic projection of Fig. 9.

The orientation of the planes containing the open clusters was found by determining the Cartesian co-ordinates of the in focus centers in a cluster. We suppose that for the first observation the focal plane of the microscope is in the crystal at $z_1=0$. The (x,y) co-ordinates were measured directly using the two micrometers on the stage, or by photographing and measuring the in focus spots on the plate. The microscope was then racked a distance d and a second set of (x,y) measurements taken (either directly or photographically) on the in focus spots at a depth in the crystal $z_2=nd$ (where n is the refractive index). The procedure was

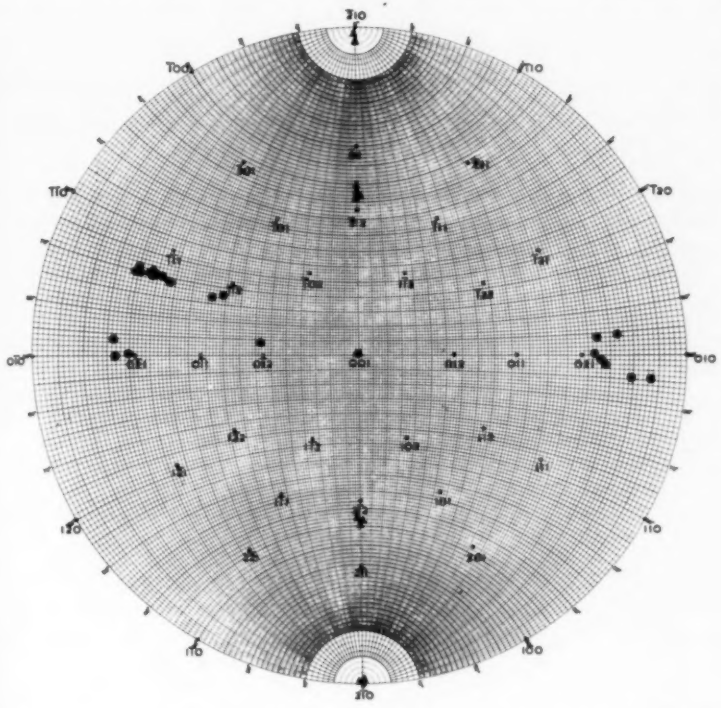

FIG. 9. Stereographic projection showing the directions of planes of scattering particles. ● planes seen as planes; ▲ planes seen as lines; • reference points of the projection.

repeated for various depths in the crystal $z_j = n(j-1)d$, for $j = 3,4$ etc. Using the 4 mm. objective the value of d used was 3×10^{-4} cm., giving for example $z_{11} = 46.2\times10^{-4}$ cm., with an uncertainty of $\pm 2\times10^{-4}$ cm. The errors in the determination of the (x,y) co-ordinates were about $\pm 1\times10^{-4}$ cm.

The measured co-ordinates for the scattering centers in a cluster were taken in groups of three and the values A, B, C of the equation of the plane: $Ax+By+Cz=1$ were determined. From the mean values of A:B:C determined for a given cluster the $(hk\cdot l)$ hexagonal indices for the plane of the cluster were found using the relation:

$$(hk\cdot l) \equiv \mathrm{A}; \qquad \frac{\mathrm{B}\sqrt{3}-\mathrm{A}}{2} : 1 \cdot 100\,\mathrm{C}$$

This data about orientation of planes containing scattering centers is also summarized in the stereographic plot of Fig. 9.

Rate of Production of Scattering Centers

From the transmission (T) measured with the spectrophotometer we have calculated the total light removal coefficient (Σ) from the equation:

$$T = (1-R)^2 e^{-\Sigma x}$$

where R is the fractional reflection loss from a specimen before heat treatment and x is the specimen thickness. This relation is the approximation to equation (7) of Bastin *et al.* (1959) when $R^2 e^{-2\Sigma x} \ll 1$.

It will be seen from Fig. 10 that Σ increases with length of heat treatment and finally reaches a saturation value. The rate of increase of Σ is temperature dependent; the rate increasing with increasing temperature.

The saturation value of Σ does not vary appreciably with the heating

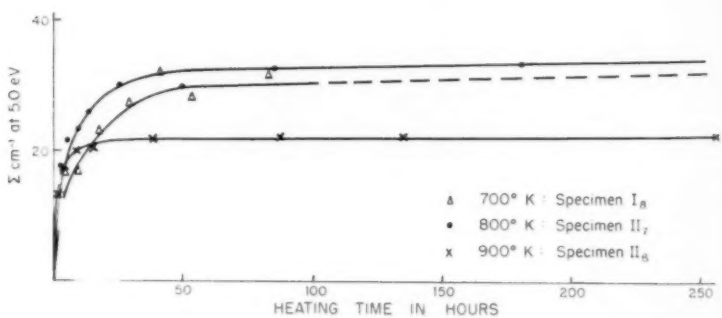

Fig. 10. Saturation of light scattering with heat treatment for specimens of type G II.

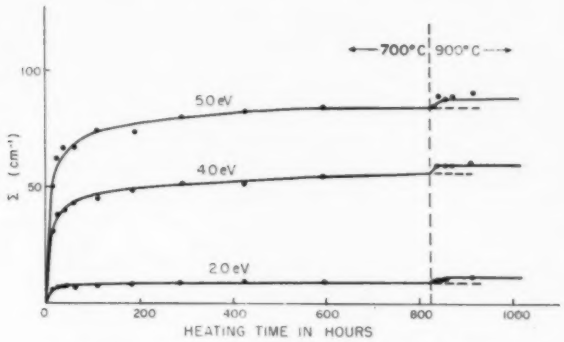

FIG. 11. Variation of Σ for specimen G II_2 heated first at 700° C. and then at 900° C.

temperature. In Fig. 11 results of heating specimen G II_2 for 830 hours at 700° C. are shown and a value of $\Sigma = 57$ cm.$^{-1}$ was reached at a wavelength of 3090 Å. Subsequent heating at 900° C. caused only a small increase in Σ to 61 cm.$^{-1}$ at the same wavelength.

The results of integrating sphere and transmission measurements are shown in Fig. 12. With the exception of the absorption band at 4200 Å which only occurred in a few specimens, the two sets of measurements indicate that most of the loss of light in the transmission experiments is due to scattering and not absorption. Determination of the coefficient Σ from spectrophotometer measurements thus gives a convenient measure of the light scattering within a specimen.

In order to determine whether the size of scattering particles is dependent on the heat treatment we have plotted Σ as a function of wavelength λ on logarithmic scales, for a crystal after a short and also a long high temperature heat treatment. The results are shown in Fig. 13. It will be seen that the wavelength dependence of log Σ has not changed markedly, indicating that although the amount of scattered light has increased, the mean size of the scattering particles has not changed significantly.

The saturation value of Σ was found to be highest in the G III and lowest in the G I specimens. We have already referred to the different concentrations of Al impurity in these crystals (Table I). The saturation values of Σ are also given in that table from which it is clear that Σ increases with increasing Al concentration.

DISCUSSION OF RESULTS

The results which have been described above may be summarized as follows:

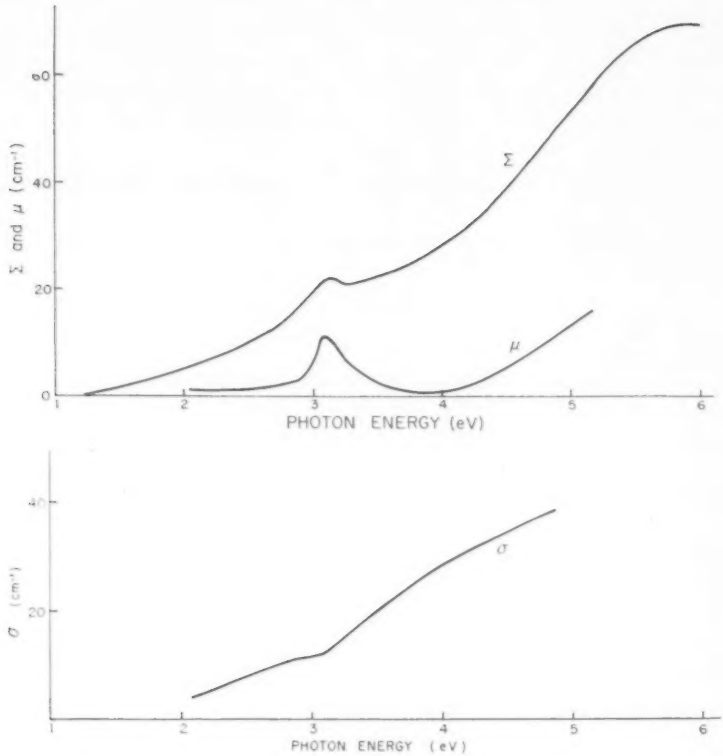

FIG. 12. Integrating sphere and transmission measurements for Specimen G III$_4$ after heating at 700° C. for 20 hours, (above) Σ from spectrophotometer measurements, and coefficients of absorption μ from integrating sphere measurements. (below) Coefficients of scattering σ calculated as the difference $\Sigma - \mu$.

(*a*) with the exception of growth in the *c*-axis directions in Y-bar crystals, heat treatment of synthetic quartz produces particles which scatter light.
(*b*) the spatial distribution of these particles varies in crystals grown under different conditions.
(*c*) the amount of scattering reaches a saturation value which takes longer to reach at lower temperatures.
(*d*) the saturation value is higher in specimens with high Al concentration.

We first consider two possible mechanisms for the formation of scattering particles. In subsequent sections we discuss the kinetics in relation to the second mechanism and the spatial orientation of the centers.

Bubble Mechanism

All the crystals were grown from aqueous solutions. It is possible,

as has been shown to be the case with some alkali halides, that the crystals contain cavities which are filled or partially filled, with aqueous growth solution. We may suppose that at high enough temperatures, the bubbles develop sufficient pressure to fracture the surrounding crystal which then causes light to be scattered.

Brown and Thomas (1956) observed light scattering which they attributed to this mechanism during their examination of some of the earlier and poorer quality synthetic quartz. In their case, however, the cavities were visible before heat treatment and the specimens also had

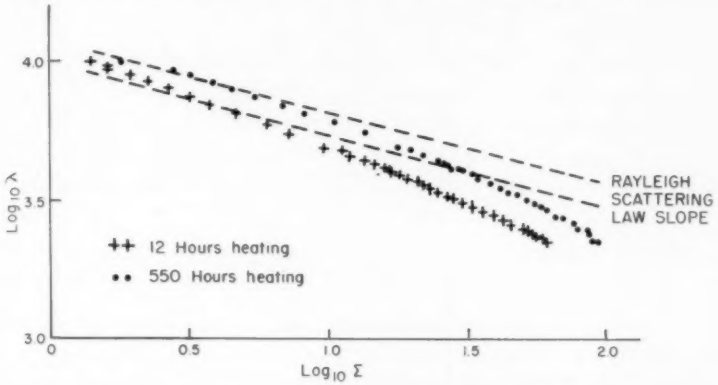

FIG. 13. Logarithmic plots of Σ as a function of wavelength for specimen G I_{18} after heating at 700° C.

a strong absorption band at 3μ corresponding to the O-H vibration in water. Neither of these features was observed in our specimens, although there was evidence of a weak (≈ 1 cm.$^{-1}$) absorption band at 2.8μ corresponding to isolated O-H vibrations.

Apart from the absence of spectroscopic evidence for the presence of water in the crystals examined, there is a further difficulty about the bubble mechanism. There will be a temperature at which most of the bubbles develop sufficient pressure to cause the surrounding crystal to fracture. We should expect that after heating at this temperature the amount of scattered light would have greatly increased, although the effect would presumably occur over a range of heating temperatures, corresponding to the range of filling of the cavities in the original crystal. Thus the "saturation" value reached at any temperature would be very temperature dependent, which is contrary to what was observed (see Fig. 11).

Precipitation Mechanism

In this mechanism we assume that there are precipitation sites in the

crystals at which impurity atoms are precipitated, and that the rate of precipitation is mainly governed by the thermally activated migration of the impurity atoms to these sites. The occurrence of regions of high scattering power in regions of strong radiation darkening indicates that Al may be the impurity involved, since there is considerable evidence that radiation darkening is associated with the presence of Al. Item (*d*) in the summary of results could also be accounted for if the impurity being precipitated were Al. The assignment may not be unique, however, for there may be other impurities which increase when the Al concentration increases.

Evaluation of the Activation Energy for the Precipitation Mechanism

Let N be the number of atoms per unit volume which at the start of the process are capable of being precipitated. The rate of precipitation at any time will be related to some function of N and also of n_t the number of atoms per unit volume which by time t have been precipitated. Thus:

$$\frac{dn_t}{dt} = Af(N, n_t)e^{-\epsilon/kT} \tag{1}$$

where $f(N, n_t)$ is a function of N and n_t, and A is a constant which may be specimen dependent.

As a measure of the light scattering we use the value of the coefficient Σ at a photon energy of 5 eV (2470 Å). Σ will be a function of the number of precipitation centers and of the size of the individual particles. We assume that the concentration of precipitation centers is a constant for a given crystal and that:

$$\Sigma_t = \alpha n_t^x \tag{2}$$

where α and x are constants. Thus:

$$\frac{dn_t}{dt} = \left(\frac{1}{\alpha}\right)^{1/x} \cdot \frac{1}{x}\, \Sigma^{1/x-1} \frac{d\Sigma_t}{dt}. \tag{3}$$

From (1) using results obtained at two temperatures on the same specimen and following Overhauser (1953) we can write, independently of the form of $f(N, n_t)$, that:

$$\epsilon = \frac{k}{\left(\frac{1}{T_2} - \frac{1}{T_1}\right)} \ln\left[\left(\frac{\partial n_t}{\partial t}\right)_{T_1} \Big/ \left(\frac{\partial n_t}{\partial t}\right)_{T_2}\right] \tag{4}$$

where the slopes $(\partial n_t/\partial t)_T$ have to be evaluated for the same value of t. If we measure the slopes at this value of t, using (3) we may write equation (4) as:

$$\epsilon = \frac{k}{\left(\frac{1}{T_2} - \frac{1}{T_1}\right)} \ln \left[\left(\frac{\partial \Sigma_t}{\partial t}\right) T_1 \Big/ \left(\frac{\partial \Sigma_t}{\partial t}\right) T_2 \right] \tag{5}$$

The results which may be used to evaluate ϵ from equation (5) must all refer to one specimen. Experimentally it is difficult to determine both slopes accurately. Two series of values of ϵ determined in this way on two specimens gave a mean of 0.9 eV, but the values ranged from 0.6 to 1.3 eV.

In order to improve the accuracy it is necessary to use results obtained on pairs of specimens, each member of a pair being heated at a different temperature. However, to deduce ϵ from the results we have to make more specific assumptions about the form of $f(N, n_t)$. We assume first that the rate of precipitation is proportional to the number of unprecipitated atoms. Thus:

$$\frac{dn_t}{dt} = (N - n_t) A e^{-\epsilon/kT} \tag{6}$$

where A is a constant which is related to the concentration of precipitation sites. Since $n_t = 0$ at $t = 0$ this equation may be integrated to give:

$$\ln \left(1 - \frac{n_t}{N}\right)^{-1} = tAe^{-\epsilon/kT}$$

or

$$\ln \left(1 - \frac{\Sigma_t^{1/x}}{\Sigma_\infty^{1/n}}\right)^{-1} = tAe^{-\epsilon/kT} \tag{7}$$

where Σ_∞ corresponds to saturation conditions in which all N atoms are precipitated. If we now determine the time t_1 needed at temperature T_1 for one specimen to reach a particular value of Σ_t/Σ_∞ and then the time t_2 for another specimen to reach the same value of this ratio at temperature T_2, we can calculate ϵ provided that A does not differ significantly between the two specimens. We do not have to specify x, and (from equation (7)) ϵ is given by:

$$\epsilon = \frac{k}{\left(\frac{1}{T_1} - \frac{1}{T_2}\right)} \ln \left(\frac{t_1}{t_2}\right) \tag{8}$$

We have used a value of $\Sigma_t/\Sigma_\infty = 0.8$ and following the above procedure measurements on 11 crystals (covering a temperature range 700°–900° C. and a corresponding time range 1–500 hours) give a value of $\epsilon = 1.15 \pm 0.3$ eV.

We now consider a modification of the above assumptions. If the scattering particles grow continuously throughout the process the number

of sites available for precipitation will increase with time, and will be proportional to the surface area of the particles. This surface area will be proportional to $n_t^{2/3}$ if the particles keep the same shape, so that equation (6) becomes:

$$\frac{dn_t}{dt} = (N - n_t)n_t^{2/3}A'e^{-\epsilon/kT} \tag{9}$$

where A' is a constant which is again related to the concentration of precipitation sites, and may thus be specimen dependent. Equation (9) gives on integration:

$$tA'e^{-\epsilon/kT} = \frac{1}{N^{2/3}}\left\{\ln\left[\frac{(n_t^{2/3}+N^{1/3}n_t^{1/3}+N^{2/3})^{1/2}}{(N^{1/3}-n_t^{1/3})}\right] + \sqrt{3}\tan^{-1}\left[\frac{2n_t^{1/3}+N^{1/3}}{\sqrt{3}N^{1/3}}\right] - \frac{\pi}{2\sqrt{3}}\right\}$$

which may be written as:

$$\begin{aligned} tA'e^{-\epsilon/kT} &= \frac{1}{N^{2/3}}f\left(\frac{n_t}{N}\right) \\ &= \left(\frac{\alpha}{\Sigma_\infty}\right)^{2/3x}f\left(\frac{\Sigma_t}{\Sigma_\infty}\right) \end{aligned} \tag{10}$$

Thus choosing a value of Σ_t/Σ_∞ which is obtained by conditions (T_1 t_1) in one specimen and (T_2 t_2) in another, we have by analogy to equation (8):

$$\epsilon = \frac{k}{\left(\frac{1}{T_1}-\frac{1}{T_2}\right)}\left[\ln\left(\frac{t_1}{t_-}\right) + \frac{2}{3x}\ln\left(\frac{\Sigma_{\infty_2}}{\Sigma_{\infty_1}}\right)\right] \tag{11}$$

In order to evaluate ϵ we have to make a specific assumption about x. If the dimensions of the scattering particle are small compared with the wavelength of the light, and if the attenuation of the wave within the particle is small, the scattering per particle is proportional to the 6th power of the radius r (i.e. $\Sigma_t \propto n_t^2$ or $x=2$, since $r^6 \propto V^2$ and $V \propto n_t$) for a fixed number of precipitation centers.

Using this procedure we find a value of $\epsilon = 1.08 \pm 0.10$ eV. This value does not differ appreciably from the previous value. It is interesting that this more detailed treatment gives a significant reduction in the spread of the values obtained for ϵ.

Values of ϵ for some impurities in quartz have been found from the study of the ionic conductivity arising from added ions. Such measurements have been made by Vogel and Gibson (1950), Verhoogen (1952), and Kirton (1960). The values found are all about 1 eV, but the accuracy is not sufficient to identify our value of 1.08 eV with that for any particular impurity.

Spatial Distribution

(*a*) Distribution of individual particles.

Figure 8 together with measurements of the co-ordinates of individual particles show that there are planes of area 10^{-6}–10^{-5} cm.^{2} on which the particles are located. Of these the 001, $\bar{2}10$ and $2\bar{1}0$ planes have been identified as simple crystallographic planes with low Miller indices. The reason for the arrangement of particles in this way is not clear, but it is possible that each plane is some kind of two dimensional defect. The intersection of dislocations with these defects could provide the precipitation sites for scattering particles.

(*b*) Large scale distribution of precipitate.

In general it is not clear why some regions give relatively dense precipitation on heating while other regions (*e.g.* *c*-axis growth direction of Sawyer crystals) show no measurable precipitation. Further it is not clear why precipitation should occur in synthetic and not in natural quartz.

In specimens of type G I, G II (see Fig. 2*b*) and in the slow X growth direction of Sawyer crystals (see Fig. 6), macroscopic laminae are found parallel to the growth surface. This laminated distribution would be expected if growth conditions were variable, or perhaps if the deposition of impurity were a co-operative phenomenon.

In G II type specimens the prismatic regions are of interest. No reasons can be given for the exact form of the prisms although trigonal symmetry in the basal plane would be expected and the regular axial propagation of the prism in the growth direction is also reasonable. Within the prisms both preferentially high precipitation and radiation darkening is observed. The results suggest Al as a possible constituent of the precipitate. This suggestion agrees with the correlation with radiation darkening since the latter has been attributed to Al by a number of workers (see for example E. W. J. Mitchell and E. G. S. Paige 1955). The presence of a high etch pit density on the exposed basal planes of the prisms (see Fig. 3) indicates a high density of defects within the prisms, a condition which might be expected to facilitate precipitation.

Acknowledgments

We should like to thank Professor R. W. Ditchburn for his interest in this work, and we are grateful to Mr. L. A. Thomas and Mr. C. S. Brown of the G.E.C. Research Laboratory, Wembley, Middlesex for the provision of specimens and for helpful discussions. It is also a pleasure to acknowledge the comments of Dr. A. J. Cohen of the Mellon Insti-

tute, Pittsburgh with whom some of the results were discussed, and Sawyer Products, Cleveland for the loan of a Y-bar crystal.

References

Bastin, J. A., Mitchell, E. W. J., and Whitehouse, J., *Brit. Journ. App. Phys.*, **10**, 412, 1959.

Brown, C. S., and Thomas, L. A., *Proc. Inst. Elect. Eng.*, **104**, 174, 1956.

Cohen, A. J., Private communication. 1957.

Bechmann, R., and Hale, D. R., *Journal of Brush Electronics Co.*, **4**, No. 1, 1, 1955, and Hale, 1957. Private communication. 1960.

Kirton, J., Ph.D. thesis, Reading University, 1960.

Mitchell, E. W. J., and Paige, E. G. S., *Phil. Mag.*, **46**, 1353, 1955.

Overhauser, A. W., *Phys. Rev.*, **90**, 393, 1953.

Verhoogen, J., *Amer. Min.*, **37**, 637, 1952.

Vogel, R. C., and Gibson, G., *J. Chem. Phys.*, **18**, 490 and 1094, 1950.

Manuscript received November 15, 1960.

THE AMERICAN MINERALOGIST, VOL. 46, NOVEMBER–DECEMBER, 1961

EXPANDABLE CHLORITIC CLAY MINERALS FROM UPPER MISSISSIPPIAN CARBONATE ROCKS OF THE CUMBERLAND PLATEAU IN TENNESSEE

M. N. A. PETERSON, *Department of Earth Sciences, University of California, San Diego, at La Jolla, California.*

ABSTRACT

The mineral assemblages of upper Mississippian carbonate rocks of the Cumberland Plateau in Tennessee may be considered in a six component system: MgO—CaO—Al_2O_3—SiO_2—CO_2—H_2O, and within this choice of components, the assemblages may be plotted on a ternary diagram MgO—CaO—Al_2O_3. CO_2 and H_2O are considered "perfectly mobile" and SiO_2 is present in excess. Compositional variation of the expandable chloritic minerals, determined by *x*-ray criteria, lies between the compositions of vermiculite and corrensite, and is consistent with the topologic requirements of the ternary diagram. Mixed-layer ordering, like that found in corrensite, occurs only in chlorite-vermiculite having a composition near a 1:1 ratio of chloritic to vermiculitic layers.

INTRODUCTION

Expandable chloritic clay minerals have been described from a number of localities in the United States and Europe. Many of these clays may be characterized as mixed-layer chlorite-vermiculites (Weaver, 1956). Some are randomly interstratified, and others have a basal spacing (001) near 29 Å, indicating that at least some of the material has a regular alternation of vermiculitic and chloritic layers. Lippman (1954) has proposed the name corrensite for the ordered material.

Table 1 summarizes described occurrences, in sedimentary rocks, of corrensite, or of materials which, on the basis of information given, seem to be corrensite. Two other occurrences of similar material, or hydrothermal origin, have been reported by Sudo *et al.* (1954) and Bailey and Tyler (1960).

Both random mixed-layer chlorite-vermiculite and corrensite have been found in Upper Mississippian rocks of the Cumberland Plateau in Tennessee. They were encountered during a study of the complete mineralogy of this group of rocks. The broad intentions of the study were to determine mineral assemblages, and to relate these assemblages to textures and general stratigraphy (Peterson, 1960).

During the investigation it became apparent that the expandable chloritic minerals displayed significant variations in composition and structure. These minerals will be discussed within the context of the lithologies and mineral assemblages in which they occur.

LITHOLOGY

Carbonate rocks of upper Mississippian strata of the Cumberland Plateau in Tennessee have exceptionally well preserved original sedi-

TABLE 1. PREVIOUSLY DESCRIBED OCCURRENCES OF CORRENSITE FROM SEDIMENTARY ROCKS

Described by:	Spacings in Å: Untreated (001)	Untreated (002)	Glycolated (001)	Glycolated (002)	Lithologic and Mineralogic Associations
Lippman (1954)	28.3	14.2	32–33	16.2	Middle Keuper of southern Germany. Marls show evidence of desiccation.
Earley *et al.* (1956)	29.		32		Yates formation, Permian of West Texas. Argillaceous siltstone. Quartz, feldspar, mica and dolomite.
Bradley and Weaver (1956)	29.	14.6	31.	15.5	Brazer formation, upper Mississippian of Colorado.
Lippman (1956)	29.	14.5	31.	15.5	Rot member of the Triassic, near Gottingen, Germany. Red and green shales. Siltstone and sandstone. Dolomite, halite and gypsum.
Braitsch, O. (1960)	30.	14.15	31.7	15.6	Stasfurtsalz, Permian, Reyershausen, Germany, Evaporite section.
Grim, R. E. *et al.* (1960)	30.0	14.48			Salado formation, Permian of Carlsbad, N. M., Evaporite section.
Echle, (1961)	29.4	14.6	31.1	15.44	Keuper near Gottingen, Germany. Dolomitic red bed sequence.

mentary structures; relatively little recrystallization has taken place. Fragments of some shells still have crystallites that appear to be oriented as they originally were in the organism. Also, many oolites have radial structure. Most of these carbonate rocks are very pure. Insoluble residues are usually less than five per cent and commonly only a few tenths of a per cent of the rock.

Strata from which specimens were collected are almost undeformed and dips are of the order of one degree. Younger Mississippian sandstones, shales and carbonates (Pennington group) have a maximum thickness of 500 feet (Vail, 1959); overlying Pennsylvanian formations have a composite thickness of 4,000 feet (Wilson *et al.*, 1956). Disregarding the possibility that rocks younger than Pennsylvanian in age were at one time present, 4,500 feet is a reasonable value for maximum burial. Such a depth of burial would correspond to about 400 bars of load

pressure if the pressure is assumed to have been hydrostatic. Specimens were collected, for the most part, from quarries and new road cuts, particular attention being given to sampling fresh and unweathered material.

These carbonate rocks exhibit a large range of textures including oolitic, fossiliferous fragmental, fine grained or microcrystalline and very fine grained or cryptocrystalline. Dolomitic rocks have proportions of dolomite varying from a barely detectable trace to 100%. Rocks containing an appreciable amount of dolomite are all fine grained, and may or may not contain scattered fragments of fossils or oolites. Many original features, such as thin bedding laminations, micro-cross-bedding, prelithification intrusions of soft sediment from overlying or underlying strata, and small pebbles of different lithologies, are present in beds of this type. Commonly these features are visible because of differences in dolomite content. Other rocks containing dolomite in only small amounts are composed, for the most part, of very small oolites.

Methods

Clays were extracted from carbonates by leaching the finely ground specimen, at room temperature, in a solution of acetic acid buffered at pH 4.5 with lithium acetate. Solution of dolomite is quite slow at this pH; it was usually necessary to allow reaction to proceed for about a day if much of it was present, even if the specimen was finely ground. Specimens that were mainly calcite leached much faster.

The highest possible pH consistent with a reasonable amount of time for leaching was chosen in order to do the least amount of damage to acid soluble clay minerals, especially those of chloritic type. Li^+ was chosen because it would be one of the ions least likely to replace other ions already in the clay structure (Grim, 1953, p. 147, Gedroiz, 1922). During the leaching process Ca^{++} and Mg^{++} ions are also produced. To keep the concentration of these ions low, a large excess of leaching solution was used. The solution was well buffered and change in acidity was less than 0.5 pH unit during the digestion of a specimen. About one gram of rock usually gave enough clay to prepare an oriented aggregate for *x*-ray diffraction purposes. Diffraction charts of clays left in the leaching solution for a week show no appreciable change from charts of clay minerals from the same specimen allowed to leach for only one hour.

The extracted clays and other insoluble materials were washed in distilled water several times to remove salts, so that the clays dispersed easily in aqueous suspension. Rapid contrifuging was used to expedite the process. Oriented aggregates of the clays were prepared for *x*-ray

diffraction study by allowing an aqueous suspension of the smaller than two micron fraction to dry on a microscope slide at slightly above room temperature, and then to remain at room temperature and humidity for several hours before study. Separation of the size fractions larger and smaller than 2 microns was done by centrifuging in aqueous suspension. Measurements of clay particles on electron photomicrographs verified that the amount of centrifuging used removed most of the particles larger than two microns; virtually all of the quartz grains were larger than two microns.

Minerals on the slides were identified using a Norelco recording Geiger counter diffractometer. Copper radiation and a nickel filter, scanning speed of 1° 2θ per minute, chart speed of $\frac{1}{2}''$ per minute, tube voltage of 45 kv. and current of 2θ amperes, and a time constant of 4 seconds were used. The divergent, scatter and receiving slits were 1°, 1°, and .003″ respectively. Heights of peaks were recorded as proportional to counts per second, rather than on a logarithmic basis. Heat treatment for the selective destruction of clay minerals was accomplished by loosely wrapping the slides in aluminum foil and heating for one hour at 215° C. and then again, after a diffractometer chart had been prepared, for one hour at 550° C.

Dolomite and calcite were identified by the presence of their principal peaks on *x*-ray diffractometer charts of the samples. The lower detection level, in untreated samples, was 0.2%. The presence of traces less than this was determined from *x*-ray diffractometer charts of insoluble residues which were prepared by digesting the ground rock, until all calcite was removed, in a solution of acetic acid buffered at pH 5 with ammonium acetate. For specimens containing more than 0.2% dolomite, the pH of the leach was adjusted to 4.5 in order to dissolve the dolomite also. Other trace minerals, such as albite, were identified from these charts. A thin section was prepared for each specimen.

Samples were chosen to be representative of all major lithologies in the stratigraphic sequence. Some of these lithologies contain nodular localizations of certain minerals, such as chalcedony (chert), dolomite and calcite. This introduces a sampling problem if one is trying to describe the typical mineralogy of a rock type. Fortunately such localizations usually form a very small proportion of the total rock, and samples were chosen purposely to avoid them. A total of 77 samples was studied.

Criteria of Clay Mineral Identification

10 Å clay

A 10 Å basal spacing and its associated integral series of higher order (001) reflections, which did not expand upon solvation with ethylene

glycol, was taken to be indicative of a clay with muscovite structure. The basal peak was usually seen to be asymmetric, as is common for "illite." Several determinations of the (060) spacing near 1.51 Å showed these specimens to be dioctahedral. This mineral will hereafter be referred to as muscovite. A small amount of glauconite, the only mineral likely to interfere with this determination, was evident in thin sections of two samples. When found, it was always in specific textural elements, such as inside of foraminifera, and was quantitatively unimportant.

Montmorillonite Containing Some Mixed 10 Å Layers

A broad basal peak, occurring anywhere between 10 Å and 13 or 14 Å, that readily expanded by solvation with ethylene glycol, and collapsed to about 10 Å upon heating to 215° C. was taken to indicate the presence of montmorillonite or montmorillonite containing some mixed 10 Å layers. (It was not necessary that a mineral expand all the way to 17 to 18 Å, as is common for true montmorillonite, for it to be placed in this category.) In some instances, only a small proportion of the clay sample was of this type of mineral, so no attempt was made to distinguish between true montmorillonite and montmorillonite containing non-expanding 10 Å layers.

Non-Expandable Chlorite

An integral series of peaks associated with a basal spacing of about 14.2 Å, that does not expand by solvating with ethylene glycol, identifies normal chlorites. Odd order reflections were weaker than even orders, but they were always clearly present. This is quite different from some of the weathered chlorites of modern sediments, for which the 14 Å peak may be almost completely missing. Commonly the non-expandable chlorite can be detected only after interfering lines of expandable chloritic minerals have been shifted by solvating with ethylene glycol (Fig. 1*a*, 75-9). The 14 Å and 7 Å peaks of the non-expanding chlorite remain unchanged upon heating to 215° C.

Chlorite-Vermiculite

A basal spacing of from 14.2 to 15.2 Å, that expands to a larger spacing upon solvating with ethylene glycol, and an associated series of peaks that is very nearly integral, indicates the presence of chlorite-vermiculite. Expansion is not the same for all samples, but is related to the spacing of the untreated material, such that the specimens showing the largest original spacing also expand the most (Fig. 1*a*, 78-6 and 75-9). Shifts in peak position are sufficient to reveal non-expandable chlorite, commonly present only in very small amounts. Heating the specimen to 550° C.

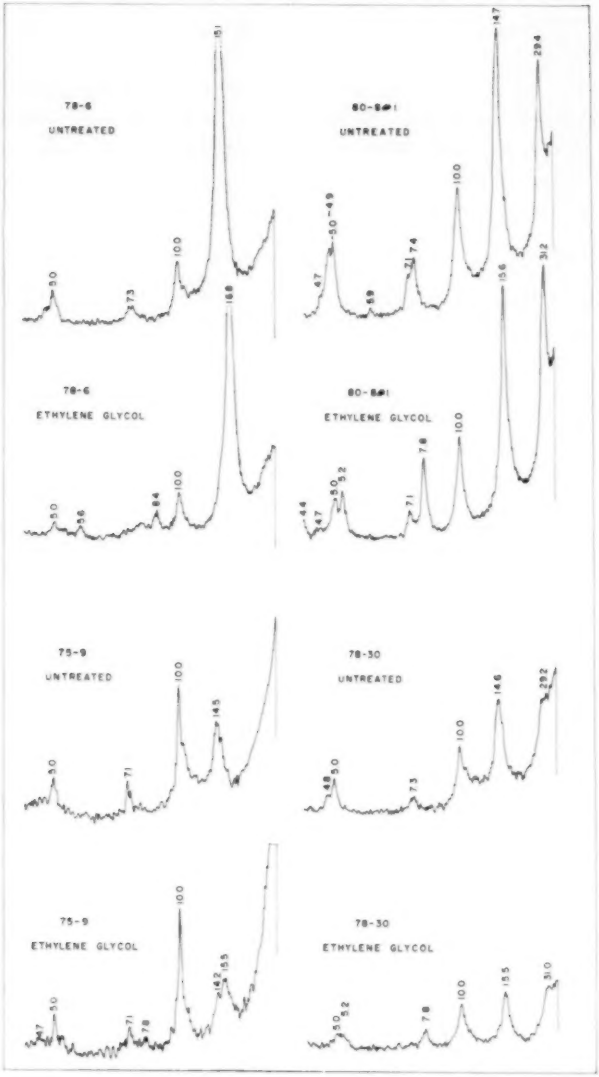

FIG. 1*a* *X*-ray diffractometer charts of samples of corrensite (80-8 No. 1 and 78-30) and chlorite-vermiculite (78-6 and 75-9) showing the differences in basal spacings of the air dried and glycolated samples. The specimens having the largest initial basal spacings expand the most upon solvation with ethylene glycol.

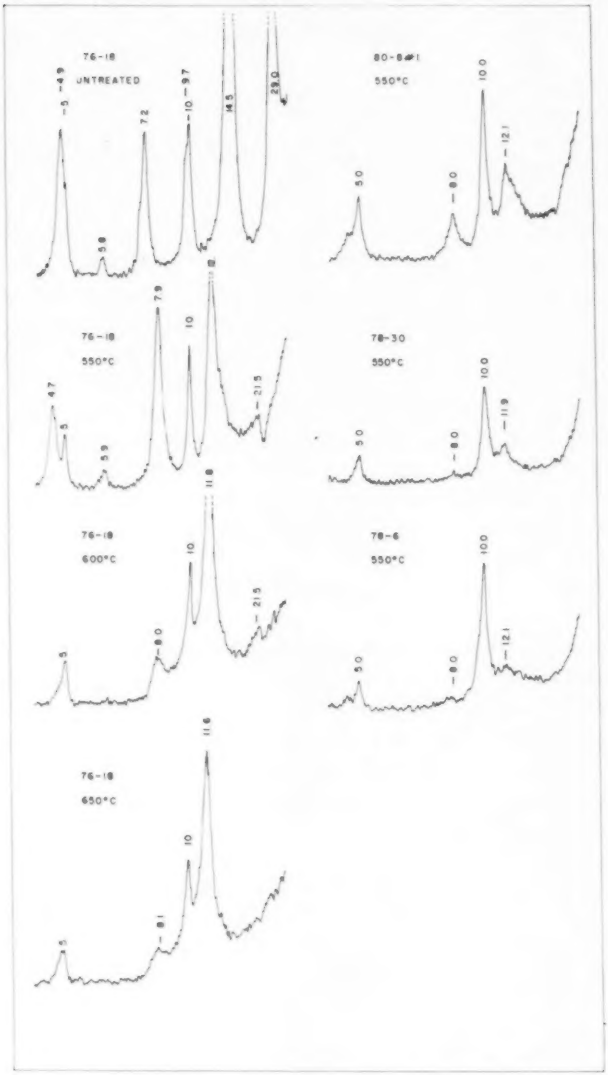

FIG. 1*b* *X*-ray diffractometer charts of samples of corrensite (76-18, 80-8 No. 1, and 78-20) and chlorite-vermiculite (78-6), showing the effect of heating. The non-integral character of the basal series is apparent from the manner in which the "7 Å" peak migrates toward lower angles upon heating.

verifies the identification, because the basal series behaves in a non-integral manner as the mineral collapses (Fig. 1*b*).

Corrensite

A basal spacing of from 28.5 to 29.5 Å is the essential criterion for corrensite (Fig. 1*a*, 80-8 No. 1, 78-30). The validity of using this spacing as the only feature of the mineral distinguishing it from chlorite-vermiculite will be discussed.

The (060) spacing is represented by an obvious line, in powder pattern, corresponding to 1.55 Å, and indicates that the mineral is trioctahedral. Other sedimentary clays of this type have also been described as trioctahedral by Bradley and Weaver (1956) and Lippman (1956). The chlorite-montmorillonite reported by Earley, *et al.* (1956) also appears to be trioctahedral on the basis of the fairly intense line at 1.54 Å. On the other hand, similar minerals of hydrothermal origin seem to be dioctahedral. Sudo, *et al.* (1954), report such a mineral from a fireclay mine, and Bailey and Tyler (1960) report another from an altered dike in an iron mine, the (060) spacings of which are 1.492 Å and 1.507 Å respectively.

The name corrensite is restricted, in this paper, to the trioctahedral mineral.

Kaolinite

No kaolinite was found in these samples. The important problem in identifying kaolinite is to distinguish its 7 Å basal spacing from the second order peak of non-expanding chlorite and chlorite-vermiculite, and from the fourth order peak of corrensite. Expansion with ethylene glycol will reveal the 7 Å peak masked in the untreated specimen by higher order peaks of corrensite and chlorite-vermiculite. This peak could belong either to non-expanding chlorite or to kaolinite. Well crystallized metamorphic or hydrothermal chlorite breaks down, upon heating, at temperatures above those at which kaolinite loses its crystallinity, whereas more or less degraded sedimentary chlorites break down at lower temperatures than does kaolinite. Some *a priori* judgment of the variety of chlorite is needed before thermal destruction can be used to discriminate between chlorite and kaolinite. Another convenient method for selective destruction of chlorite is leaching in strong, warm acid. Overnight treatment with a warm solution of one part water to one part concentrated HCl is sufficient to completely destroy chlorite. Thus, if the 7 Å peak is reduced in intensity or destroyed, upon acid treatment, the presence of chlorite is more clearly demonstrated. Reduction in intensity of the 7 Å peak, because of disorientation of mineral flakes during treatment, would be difficult to distinguish from destruc-

tion of one of the minerals contributing to it. This difficulty was not encountered, because destruction of the peak was always complete, indicating that no kaolinite was present. The presence of a significant 14 Å peak that does not expand also indicates that some, if not all, of the 7 Å peak is from chlorite.

General Mineralogy

Dolomite and calcite are the only two carbonates found. All but three specimens contain some calcite, and about one half of the specimens contain some dolomite. The dolomite, in all but one instance, has between 3% and 6% excess Ca, determined by *d* (211) (Goldsmith and Graf, 1958). *X*-ray spectrographic analyses indicate that the iron content of the dolomite is not sufficiently high to invalidate this determination. The calcite has an average *d* (211) corresponding to a Mg content of 0.5 to 1%. The method employed would have detected either ferroan-dolomite or siderite if they were present in significant quantities but neither was found.

Quartz is present in every specimen studied, either in the form of detrital grains, doubly terminated euhedra, or small authigenic overgrowths on detrital grains, or as cherty replacement of carbonate.

Potash feldspar and albite are present in some specimens. Albite, visible in thin section, is in euhedra that are clearly authigenic. Potash feldspar, not seen in thin section, is detected only in diffractometer charts of insoluble residues, and may be either detrital, authigenic or both; no distinction was made between its different structural states.

Of the clay minerals, a 10 Å phase, probably muscovite, is the only one present in every sample. Glauconite was identified in thin section in two specimens. Non-expanding chlorite, usually present only in very small quantities, was clearly identified in about two thirds of the samples; montmorillonite was distinguished in about one eighth of them. No kaolinite was found. Corrensite or chlorite-vermiculite is present in almost every sample.

Mineral Assemblages

In summary, the major minerals present are calcite, dolomite, corrensite, chlorite-vermiculite, montmorillonite, quartz and muscovite. Of these quartz and muscovite are in all samples. The remaining minerals fall into the following assemblages:

1. dolomite, corrensite
2. dolomite, calcite, corrensite
3. calcite, corrensite
4. calcite, chlorite-vermiculite
5. calcite, chlorite-vermiculite, montmorillonite

The simplicity of these mineral assemblages, and the uniformity with which they occur suggest that methods applicable to the portrayal of certain metamorphic mineral assemblages may also be applicable to these assemblages. These phases may be considered in a six component system, expressed as oxides. These are: CaO, MgO, Al_2O_3, SiO_2, CO_2 and H_2O. It is possible and convenient to regard the activities of some of these components as fixed, either because a phase having the composition of the pure component is in the system in excess, or because the component is "perfectly mobile" and its activity is determined by factors not controlled by the bulk composition of the system (Korzhinsky, 1950; Thompson, 1955; Zen, 1959).

The mineral assemblages do not suggest that there were any significant gradients in the activities of either H_2O or CO_2, at the time the assemblages formed, and thus the system has behaved as if both H_2O and CO_2 were "perfectly mobile." Quartz is present in every sample and therefore SiO_2 is present in excess and need not be considered as a component.

Having eliminated the need to consider three of the six components, it is now possible to plot the remaining three components on a ternary diagram (Fig. 2). The five mineral assemblages are also shown.

The composition of corrensite has been plotted on the basis of two analyses, one of which was reported by Bradley and Weaver (1956). The second analysis, prepared in connection with this study, was of a well crystallized specimen that contained only a small amount of muscovite and from which all quartz and carbonates were removed (Fig. 1*b*, No. 76-18; and appendix at the end of this article). It was assumed that the composition of the mica would be about that of "Fithian illite" (Grim and Rowland, 1942) and all K_2O was assigned to the mica. Recomputing to 100% gives a rough composition for corrensite that corresponds quite closely to that reported by Bradley and Weaver (1956), especially in regard to the Al_2O_3/MgO proportion. The average $MgO/(Al_2O_3+MgO)$ ratio, by weight, for the two analyses of corrensite is 65% (82 mole %). Iron has been ignored in this treatment because of the probability that an amorphous hydrate of Fe_2O_3 would have been concentrated from the large amount of dolomite during the leaching process. The specimen reported by Bradley and Weaver (1956) contained significantly less iron than the specimen analyzed for this study.

This ratio has a value of 67 weight % (84 mole %) for "Pauling formula" chlorite: $Mg_5Al(AlSi_3O_{10})(OH)_8$. Two low iron chlorites from Phillipsburg, Montana and West Chester, Pennsylvania (McMurchy, 1934) give values of 68 and 71 weight % respectively (85 and 87 mole %). Three analyzed low iron vermiculites from Bare Hills, Maryland, Webster, North Carolina (Gruner, 1934), and Kenya (Walter and Milne,

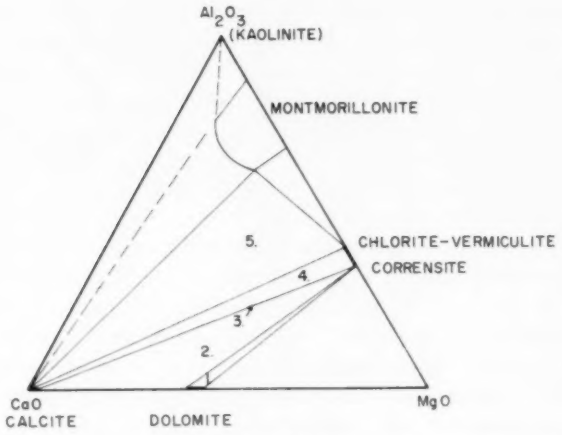

FIG. 2. Mineral assemblages, in the system Al_2O_3, CaO, MgO, SiO_2, CO_2 and H_2O, from relatively pure carbonate rocks from the upper Mississippian in the Cumberland Plateau in Tennessee. Quartz and muscovite are also present in every assemblage. The diagram may be considered as a projection from the composition of muscovite. The five mineral assemblages are shown by numbers. The field of montmorillonite has been drawn to include the compositions of several low iron montmorillonites, and has not been extended all the way to the calcite-kaolinite join so as to allow for the possibility of a *calcite, montmorillonite, kaolinite* assemblage, shown in dotted lines. About 0.5% to 1% Mg is in solid solution in the calcite. Temperature and pressure are considered to have been generally low, but variable.

1950), give an average value of about 60 weight % (79 mole %) for this ratio. The inadequacy of these data emphasizes the need for chemical analyses of the sedimentary analogues of these minerals.

The field of montmorillonite in Fig. 2 was drawn to include compositions of three low iron montmorillonites from Tatatilla, Mexico, Otay, California, and Montmorillon, France (Ross and Henricks, 1945). It is indicated as not extending to the kaolinite, calcite join so as to admit the possibility of a *calcite, montmorillonite, kaolinite* assemblage.

RELATIONSHIPS OF THE COMPLEX CHLORITIC MINERALS

The purpose in presenting the mineral assemblages has been to provide a basis for grouping the complex chloritic minerals.

In this study, observed variation in the (001) and (002) spacings of untreated chlorite-vermiculite and corrensite respectively, was from 14.2 to 15.2 Å. In an effort to determine if this variation was at all systematic, the 14.2 to 15.2 Å spacings were plotted in relation to the assemblages in which the mineral occurred (Fig. 3). Those from assemblages 1, 2 and 3 are essentially similar. Those from assemblage 4, however, have a larger

spread of values, and a larger average spacing than those from assemblages 1, 2 and 3; those from assemblage 5 have the largest spacings of all.

The basal spacing of vermiculite is somewhat larger than that of chlorite. Mathieson (1958) attributes the difference between the *d* (001) of Mg vermiculite (14.36 Å) and Mg chlorite (14.2 Å) to the difference between the H_2O—Mg—H_2O intersheet distance in vermiculite and the OH—MG—OH intersheet distance in chlorite.

The line in Fig. 3 at 14.28 Å indicates the spacing that would be expected for a mineral that was 1:1 mixed-layer chlorite and vermiculite. This value coincides closely with the lower limit of the observed spacings. Bradley and Weaver (1956) demonstrated by a Fourier analysis that a regularly interstratified specimen of this type of mineral was an alternation of vermiculitic and chloritic layers. Earley *et al.* (1956) arrived at essentially the same conclusion; however, they called their mineral a regularly interstratified montmorillonite-chlorite.

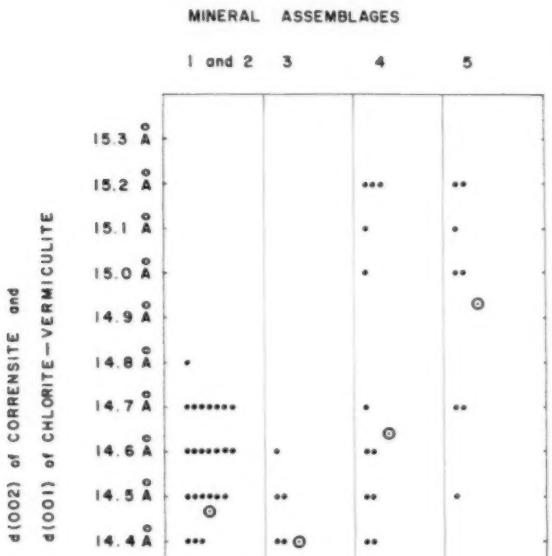

FIG. 3. The relation of mineral assemblages to content of vermiculite in chlorite-vermiculite and corrensite. The measures of content of vermiculite are *d* (001) of chlorite-vermiculite and *d* (002) of corrensite.

Increase in relative humidity tends to increase the basal spacing of vermiculite layers of these clays. At low relative humidity, however, the basal spacing of vermiculite stabilizes near a value of 14.4 Å and Weiss and Rowland (1956) have demonstrated in a heating camera that it remains so to a temperature near 80° C. They have also shown that the vermiculitic portion of chlorite-vermiculite behaves in a similar manner.

Variations in relative humidity cause much of the spread of values for spacings. Inasmuch as the data for each group were obtained under the same range of humidity conditions, the average value and relative spread would still be meaningful. Larger spacings would be associated with minerals having more vermiculite than a 1:1 ratio of vermiculite to chlorite, both because of the larger stable spacing of vermiculite at 14.36 Å and because of its ability to expand above this value.

It is therefore evident that the composition of chlorite-vermiculite in assemblage 4 is more nearly that of vermiculite than those of assemblages 1, 2 and 3. Their compositional range is also greater than in the other assemblages. The composition of chlorite-vermiculite from assemblage 5 is most nearly that of vermiculite.

Another measure of the proportion of vermiculitic layers to chloritic layers is the ratio of intensities of the (001) to (002) peaks of chlorite-vermiculite or the (002) to (004) peaks of corrensite (Weaver, 1956). This measure is more sensitive than changes in basal spacing, because the range of values is larger, but it is also more affected by variation in the iron content of the mineral. It is also a more difficult value to determine with accuracy because interfering peaks from non-expandable chlorite are commonly present, and because the 7 Å reflection from specimens near the composition of vermiculite is very weak. For these reasons it was impossible to evaluate this ratio for some specimens.

The (001)/(002) and (002)/(004) peak intensity ratios were plotted in relation to the mineral assemblages (Fig. 4) and demonstrate the same relationships as the basal spacings: that the more vermiculitic minerals are in assemblages 4 and 5, and that the largest spread of values is in assemblage 4.

The regression of one criterion for vermiculite content on the other is illustrated in Fig. 5.

The examples in Fig. 1*a* were chosen to demonstrate the variation found in expandable chloritic clays, and are more or less representative of the mineral assemblages from which they were taken. Samples 80-8 No. 1 and 78-30, both corrensite, are from assemblages 2 and 3 respectively, and have about the same vermiculite content. Samples 75-9 and 78-6 are chlorite-vermiculite from assemblages 4 and 5 respectively: 78-6 has a much larger vermiculite content than the other three specimens.

This compositional variation, in relation to the mineral assemblages, is

consistent with the only topologic possibility in constructing the ternary diagram (Fig. 2). Corrensite that is part of the two phase assemblage *dolomite, corrensite* has also been included in this group, but inasmuch as there are only three specimens from it, their contribution to the spread of values in negligible. Corrensite from the *calcite, corrensite* assemblage also seems to have a narrow range of composition, however, the peak intensity ratio (002)/(004), the most sensitive indicator of vermiculite content, shows it to be of slightly more vermiculitic composition (Fig. 4). In the two phase assemblage *calcite, chlorite-vermiculite*, however, composition of chlorite-vermiculite can vary all the way from that of corrensite to that of chlorite-vermiculite in the *calcite, chlorite-vermiculite, montmorillonite* assemblage. A paucity of values exists in the 14.7 to 14.8 Å range that may indicate either a compositional gap or inadequate sampling (Fig. 3). This gap may not be present in the distribution of (001)/(002)

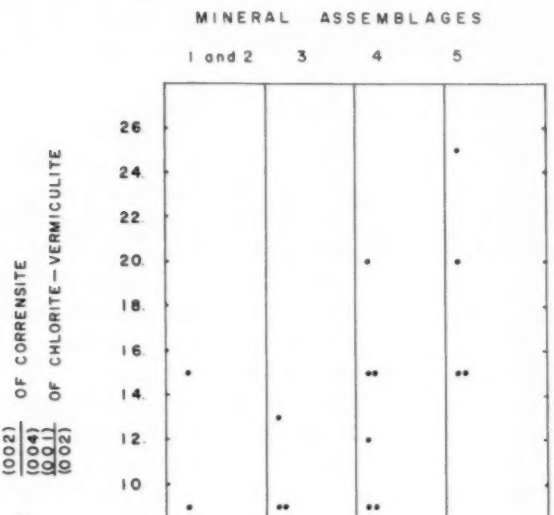

FIG. 4. The relation of mineral assemblages to content of vermiculite in chlorite-vermiculite and corrensite. The ratios of peak intensities (002)/(004) for corrensite and (001)/(002) for chlorite-vermiculite are used as measures of content of vermiculite.

ratios of peak intensities (Fig. 4) in assemblages 4 and 5; moreover, there are no compelling crystallographic reasons to believe such a compositional gap should exist. Chlorite-vermiculite from assemblage 5 should be the most vermiculitic, which it is. Being part of a three phase assemblage, this chlorite-vermiculite should also be invariant in composition. The data do not seem to bear this out, except that there is a suggestion of a decrease in its spread of values (Figs. 3 and 4) compared with that of assemblage 4. It is difficult to evaluate the influence of small amounts of iron and variations in humidity in contributing to this apparent compositional variation. Even the corrensite from assemblages 1 and 2 shows an appreciable spread of values.

Relationships of Corrensite

For the purpose of establishing mineral assemblages, corrensite was distinguished from chlorite-vermiculite by the presence of a basal spacing in the range of 28.4 to 30 Å. It is now of interest to examine variations within the group of minerals showing such a spacing.

Intensities of peaks corresponding to these large spacings vary greatly relative to other peaks in the basal series (Fig. 1*a*, 80-8 No. 1, 78-30) and may be used as a measure of dissimilarity of alternating vermiculitic and chloritic layers, and of the regularity of the alternation.

An independent criterion of dissimilarity of alternating layers is the degree to which the basal series behaves like a non-integral series. If the chlorite-vermiculite is not really a mixed-layer clay, but is composed of layers that are identical, then an integral series will characterized the mineral, even during heat treatment. On the other hand, if some layers are vermiculitic and other layers are chloritic the resultant series will only appear to be integral because the basal spacings of chlorite and vermiculite are so nearly the same. However, heat treatment will selectively crease the thickness of vermiculitic layers and the series will then be conspicuously non-integral.

In every instance heat treatment revealed a clearly non-integral series for both corrensite and chlorite-vermiculite, thus establishing that all the expanding chloritic minerals in these carbonate rocks are truly mixed-layer clays that are composed of dissimilar layers.

Figure 1*b* shows the effect of heat treatment on several specimens. Sample 76-18 is a well crystallized corrensite containing only a minor proportion of 10 Å clay. Heating to successively higher temperatures causes a rather symmetrical migration of the peaks on either side of the 10 Å peak, and illustrates the non-integral behavior of the basal series. Samples 80-1 No. 1, 78-30, and 78-6 are from assemblages 2, 3 and 5, respectively, and show similar behavior. This criterion indicates only that

certain of the layers have a higher thermal stability than others, but does not say how different they are.

If it is assumed that the layers are completely differentiated into ideal chlorite and ideal vermiculite, then the ratio of intensities of (001) to (002) peaks of corrensite is a measure of the proportion of the mineral composed of regularly alternating layers of chlorite and vermiculite. If this assumption is wrong, and the layers of chlorite are somewhat like vermiculite, and the layers of vermiculite are somewhat like chlorite, then a mineral of perfectly alternating layers would have a relatively reduced 28.4 to 30 Å peak and the (002)/(001) ratio would be larger. Inasmuch as magnesium is the only element available in important quantities for interlayer positions, at least in the corrensites that have been analyzed, preferential positioning of a more reflective ion, such as divalent iron, in alternating layers does not seem to be an important possibility.

The (002)/(001) ratio of intensities has been chosen therefore as a meas-

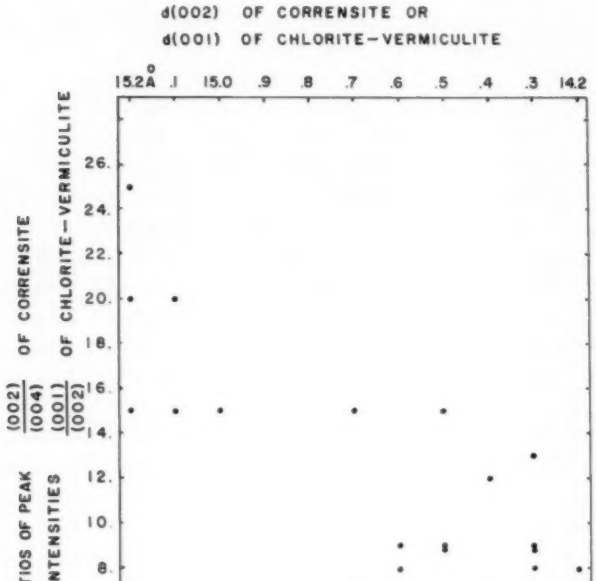

FIG. 5. The mutual relation of the two measures of vermiculite content in chlorite-vermiculite and corrensite.

ure of ordering of corrensite. Disorder would be present either as deviation of the individual layers from pure chlorite or vermiculite, or as a lack of perfect regularity of alternation of the layers. A well ordered mineral would have maximum differentiation of its layers and perfect alternation.

Height of peaks was used as the measure of intensity, and is somewhat difficult to determine with precision because the 28.4 to 30 Å peak is superimposed on a background that is rapidly descending from the direct *x*-ray beam. Intensity was measured above the interpolated background at the point of maximum height. The Lorentz-polarization factor and the area of irradiation were assumed, for this approximation of the degree of ordering, to be the same for all samples. Values of the ratio were determined only to the nearest 0.5.

Corrensite from assemblages 1, 2 and 3 has a much more limited range of compositional variation than that of the chlorite-vermiculite from assemblages 4 and 5, as can be seen from the small spread of values of both *d* (002) (Fig. 3) and (002)/(004) peak intensity ratios (Fig. 4). This limited variation may also be predicted from the fact that the portion of the mineral contributing to the 28.4 to 30 Å peak must have a 1:1 proportion of chloritic to vermiculitic layers. Variation does exist, however, and a plot of *d* (002) as a measure of vermiculite content, against (002)/(001) peak intensity ratio, as a measure of ordering, shows several interesting relationships (Fig. 6).

An abrupt upper limit to the degree of ordering exists, and probably represents a maximum ordering that can be achieved by the mineral with respect to chlorite and vermiculite alternation and differentiation.

Most of the specimens approach rather closely this maximum ordering; however, there are five specimens that do not. These fall in the more vermiculitic range, as indicated by their generally larger *d* (002). Poor ordering would also result if a mineral were more chloritic than the 1:1 ratio, but inasmuch as none of the poorly ordered specimens has a *d* (002) less than 14.4 Å, it would seem that compositional variation of expandable chloritic minerals in these carbonate rocks is between the compositions of corrensite and vermiculite. This generalization also includes the chlorite-vermiculites from assemblages 4 and 5.

Most of the specimens of corrensite occur in rocks containing dolomite, although some are from rocks that have only calcite as the carbonate. A plot of *d* (002) of corrensite against the proportion of dolomite in the rock in which it is found (Fig. 7) demonstrates that the composition of corrensite is not dependent on the bulk composition of the rock within the limits of the assemblages *dolomite, corrensite;* and *calcite, dolomite, corrensite.* A plot of (002)/(004) peak intensity ratios would demonstrate the

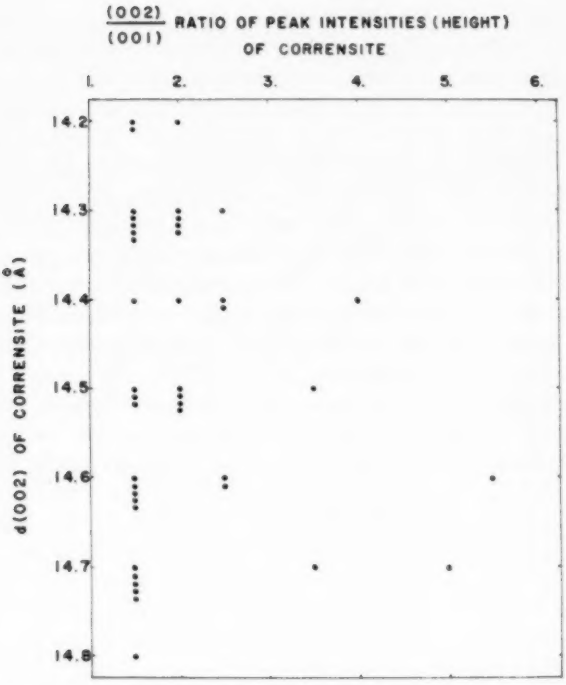

FIG. 6. A plot of d (002) of corrensite, a measure of the vermiculite content, against the (002)/(001) ratio of peak intensities, a measure of ordering.

same relationship. Minor exception to this generalization is found in the five examples of corrensite that show poor ordering with respect to chloritic and vermiculitic layers. A plot of the ordering criterion, (002)/(001) peak intensity ratios, against dolomite proportion of the host rock (Fig. 8) demonstrates that the better ordered corrensites show no relation to bulk composition of the rock. On the other hand, four of the five poorly ordered specimens fall on or near the join separating assemblages containing corrensite from those not containing it.

Important considerations concerning the relation of corrensite to the other expandable chloritic minerals are: (1) can chlorite-vermiculite of the same composition as a perfect 1:1 corrensite exist in these rocks without ordering, and (2) can ordering similar to that in corrensite exist in a mineral that is not very close to the ideal 1:1 composition? Using d (002) as the criterion for vermiculite content (Fig. 3) it can be seen that compositions of chlorite-vermiculite approach very closely that of corrensite, but are, in general, more vermiculitic. Ratios of peak intensities (002)/

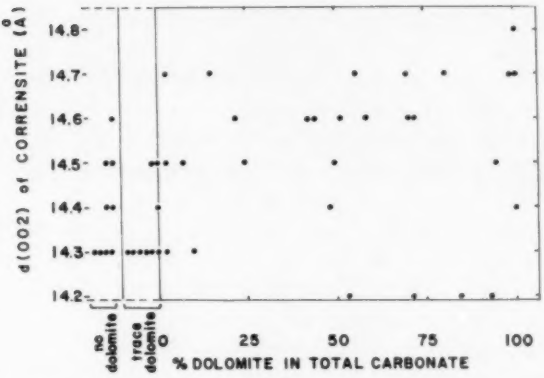

FIG. 7. A plot of d (002) of corrensite against the proportion of dolomite for each specimen, showing that there is no systematic variation in the proportion of vermiculite to corrensite in relation to the amount of dolomite also in the rock.

(004) for corrensite or (001)/(002) for chlorite-vermiculites of assemblages 4 and 5 really are more vermiculitic (Fig. 4). Unfortunately it was not possible to determine these ratios for all specimens. Evidence at hand seems to indicate that when the mineral has a composition very near that of corrensite, it tends to be ordered. The poorly ordered corrensites have (002) spacings within the range, although on the more vermiculitic side, of the well ordered corrensites. Humidity variations obscure some of the relations here, but it is safe to say that none of their compositions is far from that of well ordered corrensite.

It is also necessary to entertain the possibility that these poorly ordered

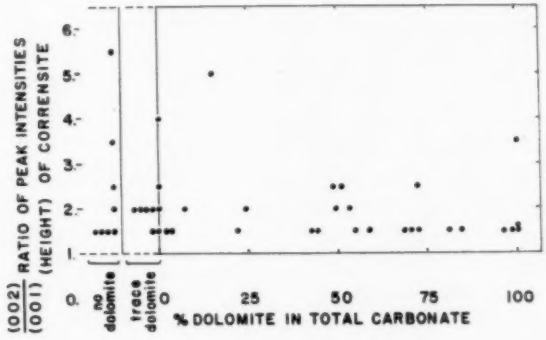

FIG. 8. A plot of (002)/(001) ratios of peak intensities against the proportion of dolomite for each specimen. The specimens containing poorly ordered corrensite, as shown by large (002)/(001) peak intensity ratios, also contain little or no dolomite.

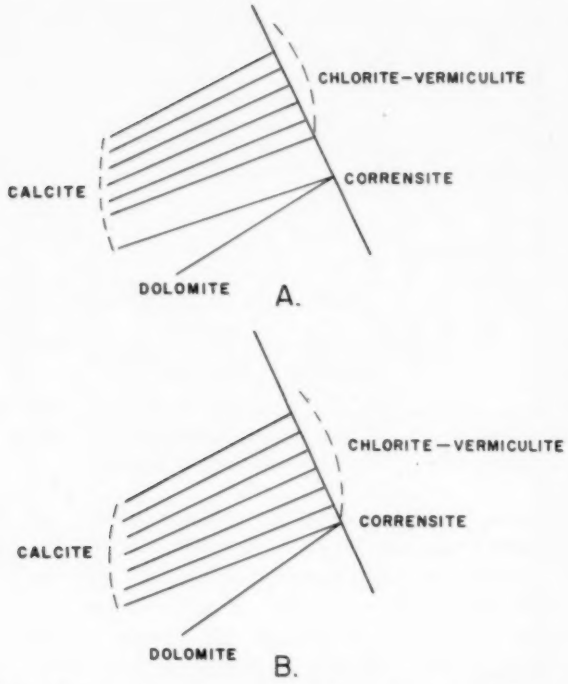

FIG. 9. Two alternative ways of constructing the portion of the ternary diagram Al_2O_3, MgO, CaO near corrensite in the system Al_2O_3, MgO, CaO, SiO_2, CO_2 and H_2O. There is no evidence for a compositional gap in the chlorite-vermiculites near the composition of corrensite. This fact would favor the interpretation shown in B.

corrensites are really mixtures of the well ordered mineral and chlorite-vermiculite of more vermiculitic composition. This possibility can be illustrated in the ternary diagram as shown in Fig. 9A. Alternatively this assemblage might be illustrated (Fig. 9B) as part of a two phase field *calcite, chlorite-vermiculite,* corrensite being somewhat variable in composition, grading into chlorite-vermiculite. Sufficient information is not available to revolve this point, except that there is no evidence of a compositional gap, however small, between chlorite-vermiculite of very nearly 1:1 composition and corrensite. Therefore, what evidence there is would favor the interpretation of a two phase field, *calcite, chlorite-vermiculite.* Corrensite would be an ordered member within the phase region of chlorite-vermiculite. Within the context of this study, corrensite assumes the role of an end member. The more magnesium rich part of the system is currently being investigated by the author. If it is assumed that

these assemblages are equilibrium products, and if the components have been sorted out properly, it is interesting to note that the mixed-layer minerals chlorite-vermiculite and corrensite have behaved as single thermodynamic phases, so far as satisfaction of the phase rule is concerned, because both are found as members of assemblages containing the maximum permissible number of phases, the variance having been arbitrarily set at two.

The purpose of this paper has been to present the information as it bears on compositional and structural variations in the complex chloritic minerals; however, the meaning would be quite incomplete without considering the question of what relation the mineral assemblages may bear to the true equilibrium products. The simplicity of the mineral assemblages, the uniformity with which they occur, and the fact that they can be used to construct an internally consistent phase diagram, which may be thought of as a graphic statement of the phase rule, all imply that the assemblages are the result of a mineral paragenesis, but not necessarily a complete equilibration, that took place during and after deposition. The fact that the compositional variations of the complex chloritic minerals are consistent with the topologic requirements of the phase diagram also carries the implication that these variations are indeed meaningful, and are related to the mineral paragenesis. The demonstration that minerals have formed or altered during or after deposition, or that they have been in some form of reactive equilibrium, does not prove that the rock in which they are found constitutes an equilibrium assemblage. Such a demonstration, however, does illustrate the importance of chemical processes in producing the properties of these carbonate rocks, and of the minerals forming them, even those minerals traditionally regarded as detrital. The question of whether these assemblages are true equilibrium products or are metastable assemblages will be discussed in more detail in a paper devoted to the geological implications of this study (Peterson, in press).

The processes contributing to this mineral paragenesis took place at temperatures and pressures far below those traditionally associated with metamorphism. Processes and conditions usually regarded as diagenetic grade with complete continuity into those regarded as metamorphic, and no clear distinction is possible. It is clear that diagenetic readjustment of sedimentary mineral constituents does take place, and can be thought of as the very beginning of metamorphism.

Acknowledgments

This work was done as part of a doctoral dissertation at Harvard University. I thank Professors R. Siever, J. B. Thompson, Jr., and C. Frondel

TABLE 2. CHEMICAL ANALYSIS OF CORRENSITE
Analyst: J. Ito

	Weight % Determined	Weight % Re-calculated		Weight % Determined	Weight % Re-calculated
SiO_2	37.2	34.	Na_2O[b]	0.2	—
Al_2O_3	15.5	13.	TiO_2[b]	0.4	—
Fe_2O_3 / FeO [a]	6.7	7.	MnO[b]	0.01	—
			V[b]	0.0001	—
MgO	18.9	24.	Zr[b]	0.0001	—
K_2O	1.4	—	Cu[b]	0.001	—
CaO	1.0	—	H_2O	18.4	22.
			Total	99.7	100.

[a] Total iron as F_2O_3.
[b] Determined spectrographically.

for their helpful guidance and friendly criticism, with regard to this part of the research. I would also like to thank Professors E. C. Dapples and L. L. Sloss of Northwestern University under those instruction I first became interested in this group of rocks.

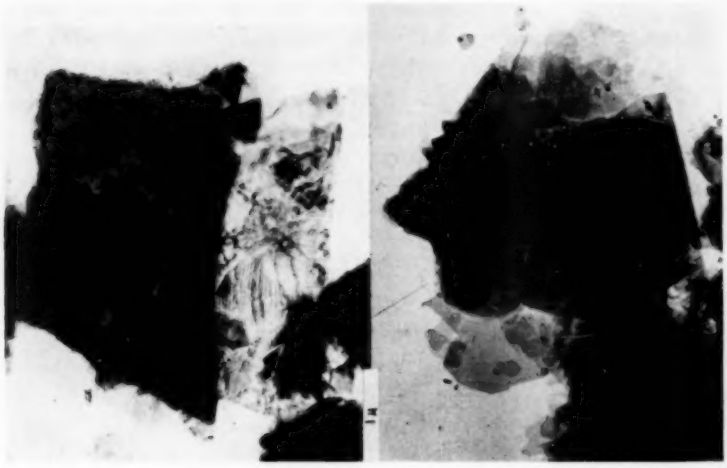

FIG. 10. Electron photomicrographs of corrensite from Sparta, Tennessee. Moiré patterns are clearly visible. (Courtesy of Dr. C. B. Chapman, Department of Biology, Harvard University).

TABLE 3. *X*-RAY DIFFRACTION DATA OF CORRENSITE
(County Rock Quarry, Sparta, Tennessee)

	Air Dried *d* Å (observed)	Solvated with ethylene glycol *d* Å (observed)
(001)	29.5 (29.0 computed)	32. (31.0 computed)
(002)	14.5	15.5
(003)	9.7	10.3
(004)	7.25	7.76
(005)	5.83	6.24
(006)	4.85	5.16
(007)	4.15	4.43
(008)	3.63	3.87
(009)	3.25	3.44
(00.10)	2.89	?
060	1.54	

APPENDIX

ANALYZED SPECIMEN OF CORRENSITE

The sample was collected from the county rock quarry four miles west of Sparta, Tennessee, on State Highway 42, about seventy-four feet above the floor of the quarry. It is from unit 18 of measured section number 76, descriptions of which are on file at the Division of Geology, G-5 State Office Bldg., Nashville, Tennessee. The carbonate fraction of the rock is composed of 96% dolomite and 4% calcite.

The clay was chosen for analysis because it was a relatively pure, well-ordered clay, as seen by *x*-ray diffractometer traces and was well crystallized, as seen from electron photo-

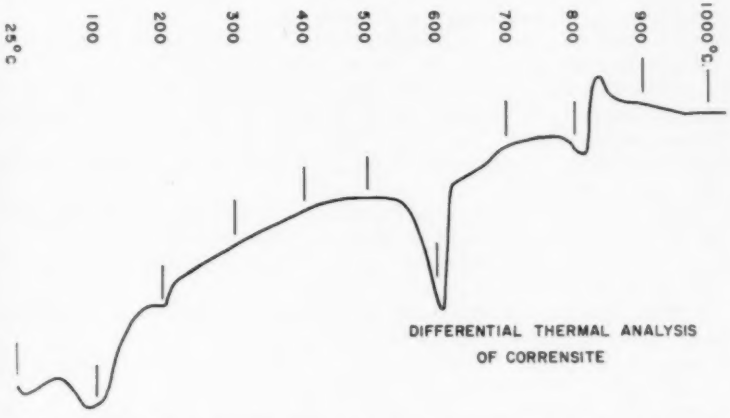

FIG. 11. Differential thermal analysis trace of corrensite from Sparta, Tennessee. The rate of heating was 5° C. per minute.

micrographs (Fig. 10), and was present in sufficient quantities in the rock. It was extracted by leaching the carbonate from the rock in a solution of acetic acid buffered at pH 4.5 with lithium acetate. Quartz was removed by size fractionation, leaving a small amount of muscovite, or "illite," as the only impurity detected by *x*-ray diffraction methods. Iron would be the least reliable part of the analysis because of the probability that it would be concentrated as an amorphous hydrate of Fe_2O_3 during the leaching of the dolomite. A faint brownish tinge to the dominant grey-green of the mineral may have been caused by uncombined Fe_2O_3. All K_2O was assumed to be in the mica, of the composition of "Fithian illite." Recomputing to 100% gives a rough composition for corrensite, as shown in Table 2.

Differential thermal analysis produces a curve essentially similar to that of the Brazer limestone corrensite (Bradley and Weaver, 1956) and is reproduced here for comparison (Fig. 11). The heating rate was 5° C. per minute.

X-ray diffraction data for this specimen are given in Table 3. A value of 1.54 Å for *d* (060) is within the range associated with trioctahedral phylosilicates.

References

Bailey, S. W. and Tyler, S. A. (1960); Clay minerals associated with the Lake Superior Iron Ores: *Econ. Geology*, **55,** 150–175.

Bradley, W. P. and Weaver, C. E. (1956); A regularly interstratified chlorite-vermiculite clay mineral: *Am. Mineral.*, **41,** 497–504.

Braitsch, O. (1960); Mineralparagenesis und Petrologie der Stassfurtsalz in Reyershausen: *Kali und Steinsalz* 1/1960, 1–14.

Earley, J. W., Brindley, G. W., McVeagh, W. J., Vanden Heuval, R. C. (1956); A regularly interstratified montmorillonite-chlorite: *Am. Mineral.*, **41,** 258–267.

Echle, W. (1961); Mineralogische Untersuchungen an Sedimenten des Steinmergelkeupers und der Roten Wand aus der Umgebrung von Göttingen: Beiträge zur Mineralogie und Petrographie **8,** 25–59.

Gedroiz, K. (1922); On the absorptive power of soils (translated by S. Waksman): Distributed by U. S. Department of Conservation.

Goldsmith, J. R. and Graf, D. L. (1958); Relation between lattice constants and composition of the Ca-Mg carbonates: *Am. Mineral.*, **43,** 84–101.

Grim, R. E. and Rowland, R. A. (1942); Differential thermal analysis of clay minerals and other hydrous materials, Part I: *Am. Mineral.*, **27,** 746–761.

———, (1953); Clay mineralogy: New York, McGraw-Hill Book Company, 500 p.

Grim, R. E., Droste, J. B. and Bradley, W. F. (1960); A mixed-layer clay mineral associated with an evaporite: *Clays and Clay Minerals*, **8,** 228–236.

Gruner, J. W. (1934); The structures of vermiculites and their collapse by dehydration: *Am. Mineral.*, **19,** 557–575.

Korzhinsky, D. S. (1950); Phase rule and geochemical mobility of elements: *18th. Internat. Geol. Cong. Proc., Section A, Problems of Geochemistry*, 50–57.

Lippman, F. (1954); Über einen Keuperton von Zaiserweiher bei Maulbronn: *Heidel. Beit. z. Min. u Petrol.*, **4,** 130–134.

———, (1956); Clay minerals from the rot member of the Triassic near Gottingen, Germany: *Jour. Sed. Petrology*, **26,** 125–139.

Mathieson, A. M. (1958); Mg-vermiculite: a refinement and re-examination of the crystal structure of the 14.36 Å phase: *Am. Mineral.*, **43,** 216–227.

McMurchy, R. C. (1934); The crystal structure of the chlorite minerals: *Zeists. Krist.*, **88,** 420–432.

Peterson, M. N. A. (1960); The mineralogy and petrology of upper Mississippian car-

bonate rocks of the Cumberland Plateau in Tennessee: Harvard University, Ph.D. Thesis, unpublished.

———, (in press); The mineralogy and petrology of upper Mississippian carbonate rocks of the Cumberland Plateau in Tennessee: *Jour. of Geol.*

Ross, C. S. and Hendricks, S. D. (1945); Minerals of the montmorillonite group: *U. S. Geol. Survey Prof. Paper* **205B.**

Sudo, T., Takahashi, H., Matsui, H. (1954); On *x*-ray properties of the fireclay from the Kurata mine, Yamaguchi Prefecture: *Japanese Jour. Geology and Geography*, **24,** 71–86.

Thompson, J. B., Jr. (1955); The thermodynamic basis for the mineral facies concept: *Am. Jour. Sci.*, **253,** 65–103.

Vail, P. R. (1959); Stratigraphy and lithofacies of upper Mississippian rocks in the Cumerland Plateau: Northwestern University Ph.D. Thesis, unpublished.

Walker, G. F. and Milne, A. (1950); Contribution: *Trans. 4th intern. Congr. Soil Sci.*, **2,** 62–67.

Weaver, C. E. (1956); The distribution and identification of mixed-layer clays in sedimentary rocks: *Am. Mineral.*, **41,** 202–221.

Weiss, E. J. and Rowland, R. A. (1956); Effect of heat on vermiculite and mixed layered vermiculite-chlorite: *Am. Mineral.*, **41,** 899–914.

Wilson, C. W., Jr., Jewell, J. W., and Luther, E. T. (1956); Pennsylvanian geology of the Cumberland Plateau: Nashville, State of Tennessee, Division of Geology, 21 p.

Zen, E-an (1959); Clay mineral-carbonate relations in sedimentary rocks: *Am. Jour. Sci.*, **257,** 29–43.

Manuscript received December 2, 1960.

THE AMERICAN MINERALOGIST, VOL. 46, NOVEMBER-DECEMBER, 1961

POLYMORPHISM IN BORNITE

N. MORIMOTO* AND G. KULLERUD, *Geophysical Laboratory, Carnegie Institution of Washington, Washington, D. C.*

ABSTRACT

Synthetic Cu_5FeS_4 and natural bornite were observed in three crystalline modifications: (1) a high-temperature form, face-centered cubic, with $a=5.50\pm0.01$ Å, Z=1, and probably anti-fluorite structure; (2) a metastable form, cubic, $Fd3m$ or $F\bar{4}3m$, with $a=10.94\pm0.02$ Å, Z=8; (3) a low-temperature form, primitive tetragonal, space group $P\bar{4}2_1c$, pseudo-$I\bar{4}2d$, with $a=10.94\pm0.02$, $c=21.88\pm0.04$ Å, Z=16. The high-temperature form is nonquenchable and is stable only above $228°\pm5°$ C. (for synthetic materials). The metastable form appears on rapid cooling from temperatures above that of the polymorphic inversion; it changes to the low-temperature form slowly at room temperature. The low-temperature and the metastable forms are closely related in crystal structure as shown by their similar intensity distributions in *x*-ray patterns. Twinning of the tetragonal form about a three-fold twin axis [221] accounts for other previously reported "modifications."

INTRODUCTION

Bornite is a common and widespread mineral occurring in numerous important copper deposits in considerable amounts. It forms under a variety of geological conditions and has been found in basic intrusives and disseminated in basic rocks, in contact metamorphic deposits in certain pegmatites and quartz veins, and even in monzonitic dikes and porphyries. It is usually found in aggregates of anhedral grains and only rarely in euhedral crystals. Previous studies of euhedral crystals indicated the existence of several polymorphs of bornite. The relationships between the various forms, however, remained almost entirely unknown. The purpose of this investigation is to study the polymorphism in both natural and synthetic bornites.

PREVIOUS STUDIES

Composition

Bornite has been recognized as a mineral since 1725. Its chemical composition was established by Harrington (1903) and confirmed by Allen (1916) and later by Zies and Merwin (1955). The analyses by these workers are the only ones, to our knowledge, that have been performed on pure materials. The mineral composition obtained from these analyses is Cu_5FeS_4 within the limits of error of the analytical methods.

At elevated temperatures, however, bornite forms extensive solid solution with numerous sulfide-type minerals, and its composition therefore

* Present address: Mineralogical Institute, Science Department, Tokyo University, Hongo, Tokyo, Japan.

often is significantly different from Cu_5FeS_4 at the time of mineral formation. On cooling, exsolution takes place, as is shown by the fine textures (such as chalcocite, chalcopyrite, and digenite lamellae) that occur in many bornites (Laney, 1911; Schwartz, 1931, 1939; Latsky, 1942; Kullerud, Donnay, and Donnay, 1960). Thus the structure of bornite, which at elevated temperatures tolerates variations in the Cu:Fe and metals:S ratios, shows a strong tendency, on slow cooling, to expel foreign atoms by exsolution and thus to bring the composition back to Cu_5FeS_4.

Crystallography

The first attempt to determine the crystal structure of bornite by *x*-ray diffraction methods was made by de Jong (1928). He reported a unit cell of cubic symmetry, with $a = 10.910 \pm 0.005$ kX, on natural bornite from Cornwall, England. The structure suggested by de Jong, however, did not account for the observed intensities. Lundqvist and Westgren (1936) studied synthetic bornite by means of powder photographs. They proposed a cubic structure, with $a = 10.93$ kX and space group $Fd3m$, in which the sulfur atoms are arranged in cubic close packing with the metal atoms situated in the interstices. Several schemes for distributing the metal atoms were suggested, but none could be confirmed by *x*-ray intensity data. Tunell and Adams (1949) examined crystals of "bornite" from the Carn Brea Mine, Illogan, Cornwall, and reported a unit cell of cubic symmetry with $a = 32.8 \pm 0.1$ Å. They proposed an approximate structure, giving reasonable intensities to all strong and medium reflections, based on a cubic sub-cell with $a = 5.47$ Å. A considerable number of weak reflections, however, were not accounted for. The very same specimens studied by Tunell and Adams (1949) were recently re-examined in polished sections and by *x*-ray precession photographs by Morimoto, Greig, and Tunell (1960) and found to consist of three phases.

Frueh (1950) investigated bornite crystals from Bristol, Connecticut, and from Butte, Montana, and produced *x*-ray, thermal, and electrical evidence indicating that bornite can exist in both a low- and a high-temperature form. Frueh considers the structural difference between the forms to be one of order-disorder. The disorder becomes measurable at 170° C. and reaches completion at 220° C. For the low-temperature form, Frueh (1950) reports orthorhombic symmetry with $a = b = 21.94$ Å and $c = 10.97$ Å. He later informed us, however (priv. comm., July 28, 1958), that he had been dealing with a "multiple crystal." Quoting him: "The reason it was called orthorhombic was that the intensity of reflections did not show four-fold symmetry. From the smaller fragment it appears to be truly tetragonal with $a = 10.97$ and $c = 21.94$ Å." Frueh (1950) reports that, after being heated at about 220° C. and then chilled rapidly in ice

cold water, the bornite crystals possess cubic symmetry with $a = 10.97$ Å.* He concludes that the high or disordered form is retained by rapid chilling, in other words that it is quenchable.

Kullerud and Roseboom (1958) confirm the existence of two forms of bornite and give the inversion temperature as about 190° C. for bornite coexisting with digenite along the Cu_9S_5-Cu_5FeS_4 join.

Kullerud, Donnay, and Donnay (1960) report two forms of bornite in a hand specimen from Coppercorp Mine in Ontario, Canada. One form is cubic with $a = 21.94 \pm 0.06$ Å and diffraction aspect P***. The other has a primitive orthorhombic lattice, with pseudotetragonal cell dimensions: $a = b = 21.90 \pm 0.06$ Å, $c = 10.95 \pm 0.03$ Å, in agreement with the low-temperature bornite described by Frueh (1950).

Synthetic Bornite

Bornite was synthesized by holding mixtures of copper, iron, and sulfur (of required composition) at fixed temperatures for various periods of time. The technique employed involves the use of rigid silica tubes. The products were chilled rapidly in cold water and identified at room temperature by optical and x-ray methods. Some of the bornite single crystals grown in this way were later investigated at elevated temperatures by Buerger's x-ray precession method.

Starting Materials

Bornite of Cu_5FeS_4 composition was grown from mixtures of the elements without catalytic agents or additional components. Experiments were carried out using copper, iron, and sulfur in the ratios 5:1:4. Since the vapor pressure of bornite of Cu_5FeS_4 composition even at 1000° C. is very low (Merwin and Lombard, 1937), the loss of sulfur and of metals to the vapor was negligible for the volume of free space allowed.

The copper was obtained from the American Smelting and Refining Company, ASARCO grade A-58. The analysis of this material shows it to consist of 99.999+ per cent Cu. No impurities are detectable by spectrographic analysis. The sum of selenium and sulfur is less than 1 ppm (<0.0001 per cent) by chemical analysis. This material was received as cast copper rods $\frac{3}{8}$ inch in diameter. Copper for each experiment was obtained by meticulous filing to avoid contamination. The grain size of these filings was about 0.5 to 1 mm. Reaction rates were high so further reduction in size was unnecessary.

The iron was obtained from the National Bureau of Standards, Standard sample 55, open-hearth iron. A chemical analysis of this material,

* This form is produced metastably during the cooling period, as will be shown later in this paper.

which contains 99.84 per cent Fe, is given by Kullerud and Yoder (1959).

The sulfur was of the same material as that used by Kullerud and Yoder (1959); it contains only 0.007 per cent impurity, all of which is carbonaceous material.

Equipment

All experiments were carried out in evacuated silica-glass tubes in the manner described by Kullerud (1953). The free space within the tube was reduced as described by Kullerud and Yoder (1959). The tubes were heated in regulated furnaces at temperatures accurate to $\pm 2°$ C. The outside wall of the tube was at 1 atm; no external supporting pressure medium was employed. The vapor pressure inside the tube containing a mixture of copper, iron, and sulfur in the 5:1:4 ratios reaches its maximum shortly after the tube has been placed in the hot furnace, because the temperature in the tube then rises rapidly (toward that of the furnace) and the vapor pressure over each element* increases with temperature. Some reaction will take place between the elements in the tube but, even when the temperature of the furnace has been reached, liquid sulfur is still present. At this point the pressure inside the tube can be estimated from the pure sulfur vapor pressure curve (Kullerud and Yoder, 1959). Thus, if the furnace temperature is 750° C. the pressure in the tube is about 25 atm. Free sulfur is consumed by the reaction with the metals and soon the liquid sulfur is gone. From then on the vapor is not saturated, and the vapor pressure decreases gradually until equilibrium is obtained in the tube. The vapor pressure over bornite of Cu_5FeS_4 composition, according to Merwin and Lombard, is about 400 mm Hg at 750° C. This initially high pressure may be sufficient to cause an explosion if the tube is heated much above 750° C. before the free sulfur has been consumed. For this reason each tube was first heated at 700° C. until all free sulfur had combined with the metals, which normally took less than 12 hours. Then the tube was extracted from the furnace and opened under acetone to avoid oxidation before and during the process of grinding. The fine homogeneous powder, while still covered by acetone, was placed in a new silica tube, which then was evacuated and sealed.

Quench Procedure

The silica tubes were removed from the furnace with tongs and plunged into water as quickly as possible at the termination of each experiment. Thus room temperature was reached in a few seconds. It was found that the form of bornite that is stable at elevated temperatures cannot be retained even by the most rapid chilling, thus quenching of this form is not

* The vapor pressures of copper and iron are negligible compared with that of sulfur.

possible. However, the rate of chilling, although never fast enough to produce a truly quenched phase, does influence the nature of the product. The effects of chilling are given later.

Description of the Cu_5FeS_4 Phase

The products obtained in silica tube experiments are identified by their physical, optical, and x-ray properties. Since bornite was synthesized in a two-step operation, the products of the first step, which lasted less than 24 hours, were identified by these methods in a number of experiments. The phases that are produced in addition to bornite are found as a non-equilibrium mixture of chalcopyrite, pyrrhotite, pyrite, and iron-rich chalcocite. These phases form a metastable assemblage and disappear on continued heating, even without grinding. However, grinding to a fine powder under a nonoxidizing medium shortens the time required for the establishment of equilibrium on further heating and greatly stimulates the growth of single crystals. Heating the finely ground material in evacuated silica tubes at 900° C. for 96 hours and then chilling it rapidly results in homogeneous Cu_5FeS_4 crystals. Examination under the binocular microscope shows that the cube is the predominant form. The cube edge ranges in length from 0.05 to about 0.5 mm. The "staircase" indentations replacing cube edges in natural bornite (Kullerud, Donnay, and Donnay, 1960) are common features also in these synthetic crystals. When inspected through the transparent wall of the unopened silica tubes, the crystals are seen to possess a brassy yellow or tombac color. However, on opening the tube in air, the color changes immediately owing to a reaction between the bornite and the atmosphere. Thus, after only a few seconds, the material appears pinkish, then changes through brownish purple and purple to an iridescent blue, identical with that seen on natural bornite (Kullerud, Donnay, and Donnay, 1960). Crushing the synthetic material under acetone, after it has been allowed to turn blue on exposure to air, demonstrates that the decoloration is a surface phenomenon. The fresh surfaces, developed by the crushing and while the material is submerged, show the original brassy yellow color observed inside the unopened tubes.

In polished sections bornite of Cu_5FeS_4 composition shows a pinkish or slightly orange color immediately after completion of the polishing process. However, owing to oxidation the color changes rapidly to purple and later to bluish violet. Bornite appears isotropic in polished sections after having been chilled from elevated temperatures. However, the same bornite appears slightly anisotropic when it is re-examined, after the necessary repolishing, a few weeks later.

In x-ray powder diffraction the freshly chilled material gives the cubic

bornite pattern, whereas the material re-examined several weeks later gives the pattern of tetragonal bornite. These patterns will be given by Yund and Kullerud (in preparation).

Natural Bornite

We examined bornite crystals from four localities: (1) Coppercorp Mine, Ontario, Canada (collected by G. Kullerud); (2) Mt. Con Mine, Butte, Montana (obtained from G. Tunell); (3) Centerville, Virginia* (obtained from the U. S. National Museum, Washington, D. C., specimen No. 106724); (4) Carn Brea Mine, Illogan, Cornwall (obtained from the U. S. National Museum, Washington, D. C., specimen No. C-525).

X-Ray Studies

The Buerger precession method was used extensively and the Weissenberg and oscillation methods were used on a number of occasions, during the investigations of synthetic and natural bornites. The *x*-ray targets were Fe, Cu, and Mo, with Kα wavelengths: Fe = 1.9373, Cu = 1.5418, and Mo = 0.7107 Å.

Because of the reported high-low inversion in bornite (Frueh, 1950; Kullerud and Roseboom, 1958), it was desirable to study the crystals not only below but also above the inversion temperature. The Buerger precession camera was modified to permit heating of the crystal during exposure. Thus it became routine to obtain precession photographs of bornite crystals at 300° to 400° C. The camera modification, which is described in detail by Morimoto and England (1960), may be summarized as follows. A small circular radiant-type platinum strip furnace is attached to the camera collimator. The crystal is mounted with epoxy cement on the junction of a (28 gauge) chromel-alumel thermocouple. The thermocouple wires are fastened to a fibre pin for mounting in the goniometer head. The temperature of the crystal during exposure fluctuates, partly because of limited furnace control, partly because of the movement of the crystal inside the furnace. The total variation in this specific furnace depends on the temperature control, on the angle μ, and on the furnace temperature. Thus at 200° C. with $\mu = 20°$ the temperature variation does not exceed $\pm 3°$ C. over a 30-minute period. Good photographs are obtained in 5 to 10 minutes with molybdenum radiation (50 KV, 20 mA).

In this technique the mounted crystals are heated in air; therefore, ex-

* Some of the bornite crystals from Centerville, Virginia, are partly covered by calcite. The crystal surface in contact with calcite has a yellow, brassy color very similar to that of the quenched synthetic materials; the surface exposed to the air shows the well-known blue iridescent bornite color.

treme caution is required. The first x-ray photograph of each crystal was made at room temperature. After rapid heating the next photograph was made in 5 to 10 minutes at the desired temperature. Then the crystal was cooled rapidly and a third exposure was made, again at room temperature. A final exposure was made after storing the crystals in air at room temperature for 2 days. The first and last photographs of each crystal were identical, indicating that oxidation, although it produced surface decoloration, did not affect the crystal structure sufficiently to be detected by x-rays.

Polymorphism

Synthetic Cu_5FeS_4 single crystals from a number of experiments were reheated in the unopened tubes at various temperatures and for various lengths of time as indicated in Table 1. After each reheating the tubes were chilled in cold water. As noted in Table 1, bornite crystals chilled from 230° C. or higher temperatures are of the "2a" type when studied at room temperature. Bornite crystals chilled from 226° and 220° C. are of the "modified 2a" type when studied at room temperature. The "2a"

TABLE 1. TYPES OF CRYSTALS OF SYNTHETIC BORNITE, OF Cu_5FeS_4 COMPOSITION, GROWN AT 900° C., COOLED, REHEATED TO AND CHILLED FROM VARIOUS TEMPERATURES, THEN STUDIED AT ROOM TEMPERATURE

Temperature of reheating, in ° C.	Time, in hours of reheating	Types of chilled crystals	Remarks
900	21	2a	Crystals have rounded edges and show no striation.
800	73	2a	Crystals have rounded edges and show no striation.
725	116	2a	Crystals have rounded edges and show no striation.
700	55	2a	No rounded edges. Some striation on {110}. Stepwise growth on {111}.
600	70	2a	No rounded edges. Some striation on {110}. Stepwise growth on {111}.
500	168	2a	No rounded edges. Some striation on {110}. Stepwise growth on {111}.
400	454	2a	No rounded edges. Some striation on {110}. Stepwise growth on {111}.
300	187	2a	No rounded edges. Some striation on {110}. Stepwise growth on {111}.
230	310	2a	Sharp edges, striation.
226	75	Modified 2a	Sharp edges, striation.
220	200	Modified 2a	Sharp edges, striation.

type crystals have a face-centered cubic cell with $a = 10.94 \pm 0.02$ Å and space group $Fd3m$ or $F\bar{4}3m$. The "modified $2a$" type crystals have a primitive cubic cell with $a = 21.88 \pm 0.1$ Å. Synthetic bornite thus appears to show two polymorphic modifications: a "high-temperature" form ($2a$) and a "low-temperature" form (modified $2a$). The transition temperature, as can be seen from Table 1, lies between $226° \pm 3°$ and $230° \pm 3°$ C., *i.e.* at $228° \pm 5°$ C. On re-examination, at various times after the chilling process, it was found that at room temperature the "high form" changes to the "low form" in a few days, whether the crystals are stored under atmospheric conditions or in vacuum. Both forms have also been reported from natural material: the "high form" is identical with the high-temperature polymorph that Frueh (1950) obtained by heating crystals from Bristol, Connecticut; the "low form" was observed in some of the bornite crystals from Coppercorp Mine, Ontario (Kullerud, Donnay, and Donnay, 1960). Since non-quenchable modifications are common in sulfides of the Cu—S and Cu—Fe—S systems, the possibility of phase changes in quench-type experiments even during the most rapid chilling could not be discounted without careful investigations. Both synthetic and natural crystals were studied at elevated temperatures by the method described above.

Synthetic crystals.—Cu_5FeS_4 crystals, synthesized at 900° C., later heated at 400° C. for 454 hours and then chilled, were studied by the precession method (Fig. 1). Photographs of $(100)_1$* were taken without the screen attachment. The photograph given in Fig. 1*a* was taken at room temperature of material that, after rapid cooling from 400° C., was kept in vacuum for 1 week before exposure. Figure 1*b* shows the same material at $240 \pm 3°$ C., and Fig. 1*c* shows the material within minutes after

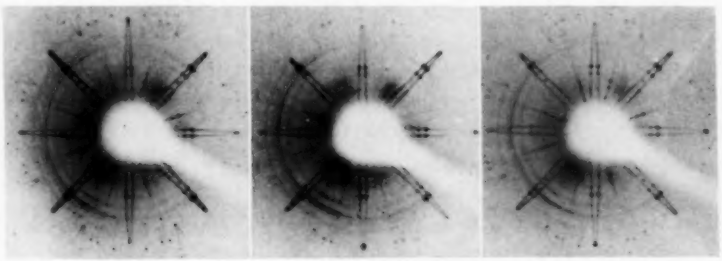

(*a*) (*b*) (*c*)

FIG. 1. High-temperature experiments on synthetic bornite. Precession photographs of $(100)_1$* taken without screen attachment: (*a*) at room temperature 1 week after rapid cooling from 400° C., (*b*) at $240° \pm 5°$ C., and (*c*) at room temperature within a few minutes after (*b*). The changes in the patterns are schematically shown in Fig. 2.

being cooled to room temperature again. Figure 2 gives schematical diagrams, with indexed reflections, of the photographs of Fig. 1. It is noted from Figs. 1*a* and 2*a* that the unheated material possesses the low-temperature bornite form with an apparently primitive cubic cell of the "modified 2*a*" type with $a=21.88$ Å. However, this cell, as will be discussed later, is the result of twinning of a tetragonal cell having $a=10.94$ Å and $c=21.88$ Å. It is noted from Figs. 1*b* and 2*b* that at $240°\pm3°$ C. bornite has a face-centered cubic cell with $a=5.50$ Å. Figures 1*c* and 2*c*

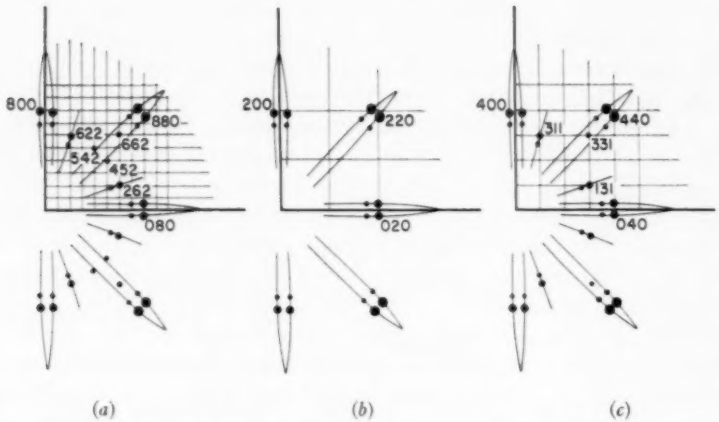

FIG. 2. Precession diagrams of Fig. 1, with reciprocal nets and index reflections.

show that at room temperature rapidly cooled bornite, at least shortly after being chilled, has the face-centered cubic cell, with $a=10.94$ Å, of the 2*a* type. Re-examination of this material, after it had been stored in vacuum for 2 days, shows transformation to the low-temperature cubic form with $a=21.88$ Å. It follows that the 2*a* cubic form must form during the chilling process and is metastable.

Natural crystals.—A bornite crystal from the Carn Brea Mine was likewise investigated by the modified precession method. Before heating, this crystal gives the pattern of the low-temperature form. At $205°\pm5°$ C. the pattern is that of the high-temperature form,* cubic with $a=5.47$ Å. When quickly cooled to room temperature this material, when investigated within a few hours after cooling, shows the metastable form, cubic with $a=10.94$ Å. Re-examination of this crystal after 4 days again

* This bornite is associated with chalcopyrite and is not of exact Cu_5FeS_4 composition. For this reason inversion to the high form takes place below $228°\pm5°$ C., the inversion temperature of stoichiometric Cu_5FeS_4.

showed inversion to the low-temperature cubic form with $a = 21.88$ Å.

Thus the high and low polymorphic forms as well as the metastable form occur both in synthetic bornite, of Cu_5FeS_4 composition, and in natural bornite.

In order to obtain real single crystals of the low-temperature form, natural crystals from the Coppercorp Mine were heated for 8 months at 150° C. in evacuated silica tubes. These crystals were then found to have tetragonal symmetry with $a = 10.94 \pm 0.02$ Å and $c = 21.88 \pm 0.04$ Å. The space group was determined without ambiguity as $P\bar{4}2_1c$ from the systematic extinctions or reflections. If weak reflections are neglected, the approximate space group is $I\bar{4}2d$.

X-ray patterns of "single" crystals of bornite from the four localities listed above show considerable variations, from one crystal to another, in the relative intensities of the reflections. None of the crystals studied gave the tetragonal patterns observed in the heated specimen from Coppercorp Mine. The intensity variations imply different symmetries and even different cell dimensions. Such changes in symmetry and in cell dimensions can be explained only as being due to twinning of individuals with varying volumes.

All the experimental data obtained on "single" crystals of natural bornite are accounted for by twinning about a three-fold twin axis [221], where the indices refer to the tetragonal cell. Figure 3 shows the inferred twin in stereographic projection. Five distinct cases of simulated symmetry and cell dimensions can be recognized, in terms of the volume fractions of the individual crystals in the twin. They are listed in Table 2.

The various symmetries and cell dimensions of natural bornites re-

TABLE 2. FIVE CASES OF SYMMETRY AND CELL DIMENSIONS THAT CAN BE SIMULATED BY THE INFERRED BORNITE TWIN

Case	Volumes of individuals			Apparent symmetry	Apparent cell dimensions, Å			Observer
	Crystal I	Crystal II	Crystal III		*a*	*b*	*c*	
Twin								
1	*u*	*u*	*u*	cubic	21.88	—	—	Donnay, Donnay, and Kullerud (1958)
2	*u*	*v*	*v*	tetragonal	21.88	—	21.88	
3	*u*	*v*	*w*	orthorhombic	21.88	21.88	21.88	
4	—	*u*	*u*	tetragonal	21.88	—	10.94	
5	*u*	*v*	—	orthorhombic	21.88	21.88	10.94	Donnay, Donnay, and Kullerud (1958); Frueh (1950)
Single crystal	*u*	—	—	tetragonal	10.94	10.94	21.88	Morimoto and Kullerud (1960); Frueh (priv. comm., 1958)

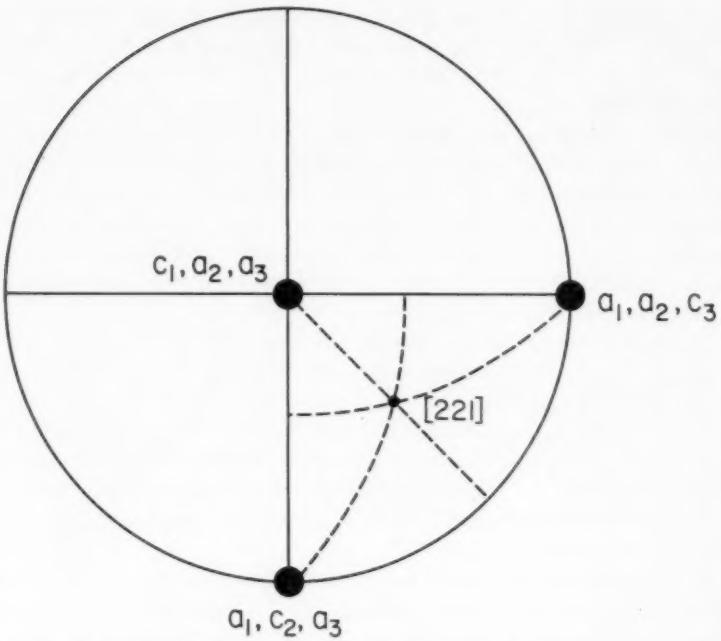

FIG. 3. Inferred bornite twin in stereographic projection. Three tetragonal crystals, I (a_1, c_1), II (a_2, c_2), and III (a_3, c_3), are related by a three-fold twin axis [221].

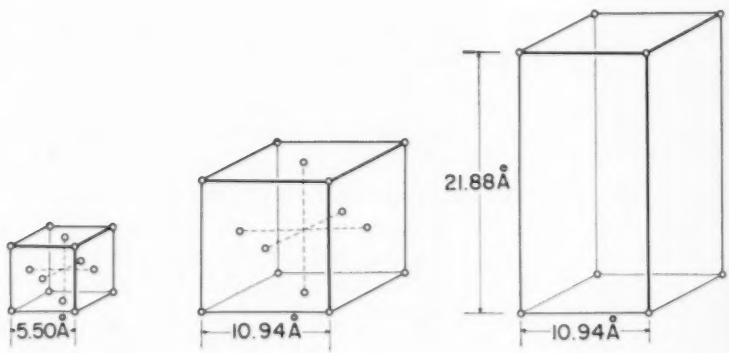

FIG. 4. Direct-lattice cells of the three forms of bornite: (a) high-temperature form, cubic; (b) metastable form, cubic; and (c) low-temperature form, tetragonal.

ported in the literature can now be easily understood as resulting from the inferred twinning. The low-temperature form of synthetic bornite with a primitive cubic cell of $a = 21.88$ Å, referred to above as the "modified $2a$" form, is also explained as a twin of three individuals with equal volumes. It is of particular interest to note here that twinning of tetragonal crystals may raise the symmetry to cubic, keep it tetragonal, or lower it to orthorhombic. These observations once more refute the notion that twinning always increases the symmetry of crystals, a "vague and mystical idea" the fallacy of which was already demonstrated by Friedel (1926).

The direct-lattice cells of the three polymorphic forms of bornite are shown on Fig. 4. The high-temperature form seems to have the antifluorite structure where metal atoms are statistically distributed. The low-temperature and the metastable forms must be closely related in crystal structure because of their similar intensity distributions. Their structural relationships will be discussed in a separate paper.

Acknowledgments

We are indebted to Mr. J. L. England, for his help in modifying the Buerger precession camera for use at elevated temperatures, and to Professor G. Tunell, Dr. G. Switzer, and Dr. P. E. Desautels, for specimens of natural bornite. We also want to express our gratitude to Professor J. D. H. Donnay, Dr. G. Donnay, and Dr. R. A. Yund, for discussions and critical reading of the manuscript.

References

Allen, E. T. (1916), The composition of natural bornite. *Am. J. Sci.*, **41,** 409–413.

Donnay, G., Donnay, J. D. H., and Kullerud, G. (1958), Bornite. *Carnegie Inst. Wash. Year Book*, **57,** 248–249.

Friedel, G. (1926), *Leçons de Cristallographie*, Paris, Berger-Levrault, p. 466.

Frueh, A. J., Jr. (1950), Disorder in the mineral bornite, Cu_5FeS_4. *Am. Mineral.*, **35,** 185–192.

Harrington, B. J. (1903), On the formula of bornite. *Am. J. Sci.*, **16,** 151–154.

de Jong, W. (1928), *Over de kristalstructuren van arsenopyriet, borniet en tetraëdriet*. Doctoral thesis, Delft, 25 pp.

Kullerud, G. (1953), The FeS-ZnS system: a geological thermometer. *Norsk geol. tidsskrift*, **32,** 61–147.

Kullerud, G., Donnay, G., and Donnay, J. D. H. (1960), A second find of euhedral bornite crystals on barite. *Am. Mineral.*, **45,** 1062–1068.

Kullerud, G., and Roseboom, E. H., Jr. (1958), Cu_9S_5-Cu_5FeS_4 system. *Bull. Geol. Soc. Am.*, **69,** 1602.

Kullerud, G., and Yoder, H. S. (1959), Pyrite stability relations in the Fe-S system, *Econ. Geol.*, **54,** 533–572.

Laney, F. B. (1911), The relations of bornite and chalcocite in the copper ores of Virgilina District of North Carolina and Virginia. *Econ. Geol.*, **6,** 399–411.

LATSKY, R. (1942), The magmatic copper ores of Namaqualand. *Trans. Geol. Soc. S. Africa*, **45,** 137.

LUNDQVIST, D., AND WESTGREN, A. (1936), On the crystal structure of bornite. *Arkiv for Kemi, Mineralogi och Geologi*, **12B,** No. 23, 1–6.

MERWIN, H. E., AND LOMBARD, R. H. (1937), The system Cu—Fe—S. *Econ. Geol.*, Suppl. to **32,** 203–284.

MORIMOTO, N., AND ENGLAND, J. L. (1960), High-temperature Buerger precession camera. *Carnegie Inst. Wash. Year Book*, **59,** 175.

MORIMOTO, N., GREIG, J. W., AND TUNELL, G. (1960), Re-examination of a bornite from the Carn Brea Mine, Cornwall. *Carnegie Inst. Wash. Year Book*, **59,** 122–126.

MORIMOTO, N., AND KULLERUD, G. (1960), Crystallography of the Cu_9S_8-Cu_5FeS_4 series. *Carnegie Inst. Wash. Year Book*, **59,** 116–122.

SCHWARTZ, G. M. (1931), Intergrowth of bornite and chalcopyrite. *Econ. Geol.*, **26,** 186–201.

SCHWARTZ, G. M. (1939), Significance of bornite-chalcopyrite microtextures. *Econ. Geol.*, **34,** 399–418.

TUNELL, G., AND ADAMS, C. E. (1949), On the symmetry and crystal structure of bornite. *Am. Mineral.*, **34,** 824–829.

ZIES, E. G., AND MERWIN, H. E. (1955), Analysis of Hamley bornite from South Australia. *Am. Mineral.*, **40,** 1001–1003.

Manuscript received January 12, 1961.

THE AMERICAN MINERALOGIST, VOL. 46, NOVEMBER-DECEMBER, 1961

CRYSTALLOGRAPHIC TABLES FOR THE RHOMBOHEDRAL CARBONATES

DONALD L. GRAF, *Illinois State Geological Survey, Urbana, Illinois.*

ABSTRACT

Cell constants are given for $CaCO_3$, $MgCO_3$, $CaMg(CO_3)_2$, $MnCO_3$, $FeCO_3$, $ZnCO_3$, $CoCO_3$, $NiCO_3$, and $CdCO_3$, together with listings of all possible *d*-values for powder diagrams taken with $CuK\alpha_1$ radiation. Less complete information is presented for $CuCO_3$, $Mg_3Ca(CO_3)_4$, $CaMn(CO_3)_2$, $CdMg(CO_3)_2$, and the hypothetical end member, $CaFe(CO_3)_2$. Samples of some of these materials prepared at or near room temperature have unit cells distinctly larger than those of equivalent samples prepared at higher temperature.

Amplitude contributions to the structure factors of calcite and dolomite powder reflections are given, based upon recently refined parameters cited in the literature. Front reflection intensities, based upon a simplified model essentially involving spherical neutral atoms at rest, are computed for a number of carbonates.

INTRODUCTION

The rhombohedral carbonate solid solutions, because of their widespread occurrence in a variety of geochemical environments, are important in evaluating the conditions under which various rocks formed. They are also of theoretical interest in a variety of solid-state studies. *X*-ray diffraction probably is the single most valuable technique for characterizing these materials. The change of unit-cell size among rhombohedral CaMg and CaMn carbonate solid solutions has been shown to be sufficient to allow the positions of suitably located individual back reflections on films taken with standard 114.59 mm. diameter powder cameras to be used as accurate measures of composition (Goldsmith, Graf and Joensuu, 1955; Goldsmith and Graf, 1957; Goldsmith and Graf, 1958b; Goldsmith, Graf, and Heard, 1961). The Debye-Scherrer method is particularly suitable for samples too small to utilize the maximum potential accuracy of the diffractometer.

Such back reflection measurements will yield useful information regardless of the indices of the particular reflection. Major advantages, however, are derived from considering the indices of the various back reflections:

1) More accurate values of the cell constants, a_0 and c_0, may be obtained by making extrapolations using reflections having, respectively, very large *a*-axis and *c*-axis components. Because reflections of this nature are limited in number, the procedure is most effective when various characteristic *X*-radiations may be utilized in order to bring the desired reflections as close as possible to $2\theta = 180°$;

2) The change in $c:a$ ratio between some pairs of carbonates is great enough to cause appreciable differential shifts in the positions of nearby reflections. The change of separation of such reflections becomes in itself an accurate measure of the extent of solid solution; film shrinkage can be

ignored over such a small portion of the film and errors varying with θ can be assumed to affect the two reflections equally and thus to cancel. The differential shift will be a maximum if one of the reflections has a strong *c*-axis component and the other, a strong *a*-axis component;

3) The spacings of reflections with strong *c*-axis components from carbonates with mixed-layer progressions along the *c*-axis (Graf, Blyth, and Stemmler, 1957; Goldsmith and Graf, 1958*b*; Graf, Blyth, and Stemmler, 1958) are altered because of this arrangement, and compositional measurements of such materials are best carried out using reflections with little or no *c*-axis component.

The back reflections of the rhombohedral carbonates are numerous enough so that interference or superposition of two or more reflections is not uncommon. Reliable unit-cell and *d*-spacing values for pure, well crystallized end members and ordered 1:1 compounds are, therefore, a prerequisite if diffraction diagrams of intermediate solid solutions and poorly crystallized materials are to yield maximum information. Tables 1 and 2 are a somewhat expanded version of a compilation of these quantities which has proved its usefulness. The accurate values given in Table 3 of the angles between [c] and the various plane normals of $CaMg(CO_3)_2$ may be used to estimate the orientation of planes in the other carbonates.

Intensities are important in evaluating cation and anion disorder and in estimating compositions of solid solutions between carbonates whose cations are very similar in size, such as $ZnCO_3$ and $CoCO_3$, and the ferroan dolomites, $Ca(Mg, Fe)(CO_3)_2$. The amplitude contributions of the several kinds of atoms to the structure factor are presented in Table 3 for the various reflections of $CaCO_3$ and $CaMg(CO_3)_2$, the only two rhombohedral carbonates for which variable parameters have been determined. These values were used in calculating the relative intensities of calcite and dolomite reflections out to $\{00\cdot12\}$ which are given in Table 4. The parameter approximations made in calculating analogous intensities for the other carbonates of Table 4 are discussed in a later section of the paper.

Measurements of reflection profiles and of the amounts of carbonates present in mixtures typically utilize low-angle reflections. Table 5 gives the 2θ values for such reflections from the more common rhombohedral carbonates for $CuK\alpha_1$ radiation.

Unit-Cell Dimensions

Table 6 summarizes the methods used in preparing the various materials for which unit-cell dimensions were determined. It also gives spectro-

TABLE 1. PREFERRED CELL CONSTANTS FOR THE RHOMBOHEDRAL CARBONATES*

Material	a_0	c_0	c_0/a_0	a_{rh}	α
$CaCO_3$					
20° C.	4.9900	17.061_5	3.4191	6.3753	46° 4.6′
26° C.	4.9899	17.064	3.4197	6.3760	46° 4.3′
$CaMg(CO_3)_2$					
(ordered)	4.8079	16.010	3.3299	6.0154	47° 6.6′
$Ca_{50}Mg_{50}$†	4.8114_5	16.039_5	3.3336	6.0251	47 4.0′
$MgCO_3$	4.6330	15.016	3.2411	5.6752	48° 10.9′
$MnCO_3$	4.7771	15.664	3.2790	5.9050	47° 43.1_5′
$CaMn(CO_3)_2$					
(disordered)	4.8797	16.367	3.3541		
$Ca_{50}Mn_{50}$†	4.8835	16.364	3.3509	6.1402_5	46° 51.8_5′
$FeCO_3$	4.6887	15.373	3.2787	5.7954	47° 43.3′
$Ca_{50}Fe_{50}$†	4.8393	16.218_5	3.3514	6.0855	46° 51.5′
$ZnCO_3$	4.6528	15.025	3.2292	5.6833	48° 19.6′
$CdCO_3$	4.9204	16.298	3.3123	6.1306	47° 19.1_5′
$CoCO_3$	4.6581	14.958	3.2112	5.6650_5	48° 33.1′
$Cd_{50}Mg_{50}$†	4.7767	15.657	3.2778	5.9028_5	47° 44.0′
$CdMg(CO_3)_2$					
(ordered)	4.7770 ±0.0009‡	15.641 ±0.003‡	3.2742		
$CdMg(CO_3)_2$					
(disordered)	4.7746 ±0.0009‡	15.678 ±0.03‡	3.2836		
$NiCO_3$	4.5975	14.723	3.2024	5.5795	48° 39.7′

* Pistorius (1960) has synthesized what appear to be mixtures of malachite and the anhydrous rhombohedral cupric carbonate, $CuCO_3$. Seven powder diffraction lines of the latter material give, from least square analysis, $a_0 = 4.796 \pm 0.005$ Å, $c_0 = 15.48 \pm 0.01$ Å, $c_0/a_0 = 3.227$, $\alpha = 48°11'$, $a_{rh} = 5.856$ Å.

† Hypothetical solid solutions with a_0 and c_0 midway between those of the two end members.

‡ The ranges given for a_0 and c_0 of ordered and disordered $CdMg(CO_3)_2$ indicate only the uncertainty that would result from a misreading of line position on the films (taken with a Guinier-type focusing camera) by the smallest unit measured, 0.05 mm. The procedure used in obtaining these $CdMg(CO_3)_2$ values is summarized in Table 7.

graphic analyses of those cations considered most likely to enter into solid solution in the carbonates. The analyses are computed with all cations as carbonates in solid solution, the most severe assumption possible inasmuch as some of the impurities may be present as traces of other compounds. Of the impurities detected, the 0.38 mol percent $CaCO_3$ in the $MgCO_3$ is the most significant, both because of the absolute amount and because the large size difference between Ca^{++} and Mg^{++} results in maximum spacing change. Assuming a linear relation between cell size

TABLE 2. POSSIBLE *X*-RAY REFLECTIONS FOR THE RHOMBOHEDRAL CARBONATES IN DEBYE-SCHERRER DIAGRAMS TAKEN WITH CuK_{α_1} RADIATION

hkl	$h_r k_r l_r$	$MgCO_3$	$CaMg(CO_3)_2$	$Ca_{50}Mg_{50}$*	$CaCO_3$ (26° C.)	$Ca_{50}Fe_{50}$*	$FeCO_3$	$Ca_{50}Mn_{50}$*	$MnCO_3$	$ZnCO_3$	$CdCO_3$	$CoCO_3$	$NiCO_3$
00·3	111		5.3366	5.3645		5.4062		5.4547					
10·1	100		4.0297	4.0330		4.0577		4.0947					
01·2	110	3.5387	3.6939	3.6975	3.8551	3.7233	3.5903	3.7570	3.6581	3.5509	3.7761	3.5505	3.5021
10·4	211	2.7412	2.8855	2.8893	3.0359	2.9141	2.7912	2.9404	2.8440	2.7476	2.9449	2.7424	2.7028
00·6	222	2.5027	2.6683	2.6733	2.8440	2.7031	2.5622	2.7273	2.6107	2.5042	2.7163	2.4930	2.4538
01·5	221		2.5382	2.5419		2.5651		2.5883					
11·0	101	2.3165	2.4039	2.4057	2.4949	2.4197	2.3443	2.4417	2.3886	2.3264	2.4602	2.3291	2.2988
11·3	210	2.1023	2.1918	2.1939	2.2848	2.2085	2.1318	2.2286	2.1721	2.1099	2.2411	2.1102	2.0817
02·1	11$\bar{1}$		2.0645	2.0661		2.0782		2.0972					
20·2	200	1.9832	2.0149	2.0165	2.0946	2.0288	1.9629	2.0473	2.0000	1.9460	2.0613	1.9474	1.9217
10·7	322		2.0046	2.0078		2.0277		2.0460					
02·4	220	1.7693	1.8470	1.8488	1.9275	1.8616	1.7952	1.8785	1.8290	1.7754	1.8880	1.7752	1.7511
01·8	332	1.7002	1.8037	1.8067	1.9127	1.8250	1.7369	1.8414	1.7698	1.7023	1.8380	1.6964	1.6705
11·6	321	1.7000	1.7860	1.7882	1.8755	1.8029	1.7296	1.8192	1.7623	1.7044	1.8235	1.7019	1.6776
00·9	333		1.7789	1.7822		1.8021		1.8182					
20·5	311		1.7454	1.7473		1.7601		1.7761					
21·1	20$\bar{1}$	1.5088	1.5662	1.5674	1.6259	1.5765	1.5271	1.5909	1.5559	1.5152	1.6028	1.5169	1.4971
12·2	21$\bar{1}$	1.4865	1.5442	1.5454	1.6042	1.5547	1.5050	1.5688	1.5334	1.4926	1.5800	1.4940	1.4744
02·7	331		1.5396	1.5415		1.5541		1.5682					
10·10	433	1.4063	1.4943	1.4969	1.5872	1.5125	1.4377	1.5261	1.4649	1.4078	1.5223	1.4025	1.3809
21·4	310	1.4061	1.4646	1.4659	1.5253	1.4754	1.4253	1.4889	1.4522	1.4114	1.4978	1.4119	1.3930
20·8	422	1.3706	1.4428	1.4447	1.5180	1.4570	1.3956	1.4702	1.4220	1.3728	1.4724	1.3712	1.3514
11·9	432	1.3538	1.4300	1.4320	1.5096	1.4453	1.3805	1.4583	1.4066	1.3563	1.4584	1.3529	1.3328
12·5	320	1.3537	1.4124	1.4137	1.4733	1.4234	1.3732	1.4363	1.3991	1.3585	1.4439	1.3585	1.3400
03·0	112	1.3374	1.3879	1.3889	1.4404	1.3970	1.3535	1.4097	1.3790	1.3432	1.4204	1.3447	1.3272

* Hypothetical solid solutions with a_0 and c_0 midway between those of the two end members.

hk·l	$h_1k_1l_1$	$MgCO_3$	$CaMg(CO_3)_2$	$Ca_{50}Mg_{50}$*	$CaCO_3$ (26° C.)	$Ca_{50}Fe_{50}$*	$FeCO_3$	$Ca_{50}Mn_{50}$*	$MnCO_3$	$ZnCO_3$	$CdCO_3$	$CoCO_3$	$NiCO_3$
01·11	443		1.3739	1.3763		1.3908		1.4034					
{30·3	300		1.3432	1.3443		1.3526		1.3649					
03·3}	22$\bar{1}$}												
00·12	444	1.2513	1.3342	1.3366	1.4220	1.3515	1.2811	1.3637	1.3053	1.2521	1.3582	1.2465	1.2269
21·7	421	1.2383	1.2965	1.2979	1.3569	1.3076	1.2580	1.3195	1.2817	1.2421	1.3246	1.2412	1.2239
02·10	442	1.2021	1.2691	1.2709	1.3391	1.2826	1.2256	1.2942	1.2488	1.2044	1.2945	1.2015	1.1837
12·8	431	1.1796	1.2371	1.2385	1.2968	1.2482	1.1992	1.2595	1.2219	1.1829	1.2634	1.1816	1.1650
{30·6	411}	1.1796	1.2313	1.2325	1.2850	1.2410	1.1968	1.2523	1.2194	1.1836	1.2587	1.1835	1.1674
03·6}	330												
22·0	20$\bar{2}$	1.1583	1.2020	1.2029	1.2475	1.2098	1.1722	1.2209	1.1943	1.1632	1.2301	1.1645	1.1494
20·11	533		1.1929	1.1946		1.2058		1.2167					
10·13	544		1.1810	1.1830		1.1957		1.2065					
22·3	31$\bar{1}$	1.1284	1.1726	1.1735	1.2185	1.1806	1.1427	1.1914	1.1642	1.1330	1.1997	1.1340	1.1191
11·12	543	1.1010	1.1665	1.1684	1.2354	1.1799	1.1242	1.1906	1.1454	1.1025	1.1890	1.0990	1.0824
13·1	21$\bar{2}$	1.1098	1.1518	1.1527	1.1956	1.1594	1.1232	1.1700	1.1444	1.1145	1.1787	1.1157	1.1012
31·2	30$\bar{1}$	1.1008	1.1430	1.1439	1.1869	1.1506	1.1143	1.1611	1.1353	1.1054	1.1696	1.1065	1.0921
21·10	532	1.0670	1.1223	1.1238	1.1799	1.1332	1.0861	1.1435	1.1066	1.0696	1.1456	1.0678	1.0524
13·4	32$\bar{1}$	1.0669	1.1096	1.1105	1.1539	1.1174	1.0807	1.1275	1.1011	1.0712	1.1351	1.0719	1.0577
01·14	554	1.0362	1.1027	1.1047	1.1731	1.1166	1.0600	1.1266	1.0801	1.0371	1.1230	1.0328	1.0168
22·6	420	1.0511	1.0959	1.0969	1.1424	1.1043	1.0659	1.1143	1.0860	1.0549	1.1206	1.0551	1.0409
{03·9	441}		1.0943	1.0955		1.1041		1.1141					
30·9}	522												
31·5	410	1.0435	1.0863	1.0873	1.1308	1.0942	1.0575	1.1042	1.0774	1.0475	1.1111	1.0480	1.0340
12·11	542	1.0146	1.0685	1.0700	1.1248	1.0792	1.0333	1.0890	1.0528	1.0169	1.0904	1.0148	1.0001
00·15	555		1.0673	1.0693		1.0812		1.0909					
02·13	553		1.0600	1.0616		1.0720		1.0816					

12·5	320	1.3537	1.4124	1.4137	1.4733	1.4234	1.3732	1.4363	1.3991	1.3585	1.4439	1.3585	1.3400
03·0	112	1.3374	1.3879	1.3889	1.4404	1.3970	1.3535	1.4097	1.3790	1.3432	1.4204	1.3447	1.3272

* Hypothetical solid solutions with a_0 and c_0 midway between those of the two end members.

TABLE 2—(*continued*)

$hk \cdot l$	$h_r k_r d_r$	$MgCO_3$	$CaMg(CO_3)_2$	$Ca_{50}Mg_{50}$*	$CaCO_3$ (26° C.)	$Ca_{50}Fe_{50}$*	$FeCO_3$	$Ca_{50}Mn_{50}$*	$MnCO_3$	$ZnCO_3$	$CdCO_3$	$CoCO_3$	$NiCO_3$
40·1	113		1.0387	1.0395		1.0456		1.0551					
04·2	222	.99424	1.0322	1.0330	1.0718	1.0391	1.0064	1.0486	1.0254	.99842	1.0563	.99947	.98641
13·7	430	.98781	1.0309	1.0319	1.0756	1.0390	1.0021	1.0484	1.0210	.99125	1.0538	.99119	.97772
40·4	400	.96908	1.0074	1.0082	1.0473	1.0144	.98147	1.0237	.99998	.97298	1.0307	.97372	.96087
20·14	644	.94587	1.0023	1.0039	1.0616	1.0138	.96585	1.0230	.98412	.94720	1.0216	.94414	.92987
31·8	521	.95723	1.0002	1.0012	1.0449	1.0084	.97162	1.0175	.98996	.96040	1.0223	.96008	.94690
22·9	531	.95146	.99593	.99701	1.0421	1.0045	.96649	1.0136	.98473	.95438	1.0175	.95371	.94045
04·5	331		.98994	.99078		.99702		1.0061					
11·15	654	.91893	.97550	.97713	1.0351	.98716	.93905	.99604	.95682	.92001	.99392	.91670	.90269
10·16	655	.91383	.97292	.97466	1.0354	.98525	.93499	.99410	.95269	.91455	.99071	.91073	.89656
21·13	643	.91889	.96987	.97125	1.0232	.98010	.93672	.98895	.95443	.92067	.98930	.91844	.90491
{30·12	633}	.91375	.96184	.96310	1.0120	.97135	.93041	.98014	.94799	.91586	.98163	.91415	.90093
{03·12	552}												
32·1	302	.91876	.95353	.95424	.98972	.95979	.92984	.96855	.94738	.92267	.97583	.92371	.91168
23·2	312	.91365	.94850	.94922	.98476	.95479	.92478	.96350	.94222	.91750	.97062	.91847	.90648
40·7	511		.94743	.94831		.95467		.96336					
13·10	541	.89406	.93659	.93764	.98078	.94478	.90849	.95335	.92564	.89671	.95677	.89594	.88341
32·4	41$\bar{1}$	.89400	.92914	.92988	.96565	.93553	.90533	.94406	.92241	.89763	.95061	.89837	.88654
12·14	653	.87568	.92512	.92647	.97685	.93508	.89303	.94352	.90991	.87728	.94348	.87498	.86202
04·8	440	.88467	.92348	.92438	.96377	.93079	.89758	.93925	.91452	.88772	.94402	.88762	.87553
01·17	665		.91856	.92021		.93023		.93858					
23·5	42$\bar{1}$	.88008	.91537	.91612	.95203	.92183	.89152	.93023	.90834	.88355	.93638	.88413	.87242
14·0	213	.87556	.90861	.90928	.94300	.91454	.88608	.92289	.90279	.87929	.92987	.88030	.86885
31·11	632	.86253	.90465	.90570	.94843	.91281	.87690	.92109	.89346	.86494	.92392	.86398	.85180
02·16	664	.85008	.90186	.90334	.95635	.91250	.86847	.92071	.88490	.85114	.91900	.84819	.83527
{14·3	322}	.86246	.89572	.89640	.93030	.90173	.87312	.90996	.88959	.86605	.91654	.86689	.85554
{41·3	401}												

31·11	632	.86253	.90469	.90576	.95976	.91618	.87215	.92440	.88859	.85483	.92268	.85188	.83527
02·16	664	.85008	.90186	.90334	.95635	.91250	.86847	.92071	.88490	.85114	.91900	.84819	.83527
14·3 / 41·3	322 / 401	.86246	.89572	.89640	.93030	.90173	.87312	.90996	.88959	.86605	.91654	.86689	.85554

hk·l	$h_1k_1l_1$	$MgCO_3$	$CaMg(CO_3)_2$	$Ca_{50}Mg_{50}$*	$CaCO_3$ (26° C.)	$Ca_{50}Fe_{50}$*	$FeCO_3$	$Ca_{50}Mn_{50}$*	$MnCO_3$	$ZnCO_3$	$CdCO_3$	$CoCO_3$	$NiCO_3$
22·12	642	.85001	.89301	.89411	.93777	.90143	.86479	.90960	.88113	.85219	.91173	.85095	.83881
00·18	666	.83422	.88944	.89109	.94801	.90103	.85405	.90911	.87022	.83472	.90545	.83099	.81794
32·7	520	.84590	.88144	.88224	.91835	.88805	.85759	.89613	.87377	.84902	.90136	.84924	.83783
40·10	622	.83409	.87269	.87363	.91278	.88007	.84711	.88806	.86310	.83671	.89171	.83620	.82461
23·8	530	.82646	.86206	.86288	.89903	.86873	.83824	.87663	.85406	.82939	.88136	.82943	.81820
41·6 / 14·6	510 / 431	.82644	.86011	.86084	.89508	.86630	.83741	.87420	.85321	.82964	.87975	.83007	.81902
20·17	755		.85805	.85948		.86827		.87609					
04·11	551		.84668	.84762		.85406		.86181					
03·15 / 30·15	663 / 744		.84608	.84729		.85505		.86277					
21·16	754	.79804	.84439	.84568	.89299	.85380	.81438	.86150	.82978	.79932	.86089	.79698	.78506
13·13	652	.80140	.84239	.84345	.88508	.85045	.81553	.85815	.83093	.80340	.85997	.80213	.79065
11·18	765	.78488	.83417	.83560	.88619	.84438	.80246	.85198	.81764	.78567	.84972	.78267	.77061
05·1	223		.83163	.83224		.83708		.84472					
50·2	114	.79792	.82828	.82890	.85987	.83375	.80761	.84136	.82284	.80129	.84761	.80216	.79169
10·19	766		.82589	.82738		.83643		.84394					
32·10	631	.78477	.82031	.82116	.85722	.82706	.79699	.83458	.81173	.78733	.83834	.78701	.77618
05·4	332	.78473	.81529	.81593	.84706	.82084	.79456	.82833	.80954	.78796	.83419	.78866	.77830
31·14	743	.77226	.81257	.81363	.85459	.82053	.78620	.82795	.80106	.77408	.82936	.77270	
14·9 / 41·9	540 / 621	.77529	.80916	.80995	.84433	.81553	.78655	.82295	.80139	.77798	.82719	.77792	
12·17	764		.80812	.80937	.85519	.81725	.77910	.82462	.79384		.82380		
50·5	500		.80594	.80659		.81154		.81893					
33·0	303	.77217	.80131	.80191	.83164	.80655	.78145	.81392	.79618	.77546	.82007	.77635	

TABLE 2—(*continued*)

hk·l	$h_rk_rl_r$	$MgCO_3$	$CaMg(CO_3)_2$	$Ca_{50}Mg_{50}$*	$CaCO_3$ (26° C.)	$Ca_{50}Fe_{50}$*	$FeCO_3$	$Ca_{50}Mn_{50}$*	$MnCO_3$	$ZnCO_3$	$CdCO_3$	$CoCO_3$	$NiCO_3$
23·11	641		.79859	.77945	.83537	.80537	.77513	.81268	.78977		.81598		
22·15	753		.79809	.79918	.84057	.80619	.77154	.81348	.78613		.81435		
40·13	733		.79500	.79595		.80233		.80960					
33·3	412		.79243	.79303	.82290	.79772	.77252	.80500	.78709		.81088		
01·20	776		.78610	.78752	.83705	.79616		.80331			.80040		
24·1	313		.78593	.78651	.81572	.79108		.79830	.78086		.80431		
42·2	402		.78310	.78369	.81294	.78827		.79546	.77797		.80139		
05·7	441		.78250	.78317		.78820		.79538					
02·19	775		.78108	.78240		.79053		.79764					
24·4	422		.77210	.77270	.80209	.77733		.78442			.79001		
04·14	662			.77074	.80847	.77707		.78411			.78590		
50·8	611				.80101	.77460		.78165			.78622		
33·6	521				.79822	.77288		.77993			.78507		
00·21	777					.77231		.77924					
42·5	511				.79424			.77643			.78178		
13·16	763				.79674			.77087			.77158		
20·20	866				.79358								
{30·18	855}				.79189								
{03·18	774}												
32·13	742				.79110						.77092		
21·19	865				.78698								
{41·12	732}				.78590								
{14·12	651}												
51·1	214				.77534								
24·7	531				.77436								
15·2	323				.77295								
11·21	876				.77263								
05·10	550				.77102								

TABLE 3. AMPLITUDE CONTRIBUTIONS TO STRUCTURE FACTORS, AND ANGLES BETWEEN [c] AND PLANE NORMALS, FOR CALCITE AND DOLOMITE

$hk \cdot l$	$h_r k_r l_r$	Amplitude contributions* to structure factors, F, for calcite			Amplitude contributions* to structure factors, F, for dolomite				Angle between plane normal and [c], for dolomite, in degrees
		f_{Ca}	f_C	f_O	f_{Ca}	f_{Mg}	f_C	f_O	
00·3	111				+1	−1	−0.2444	−0.6771	0
10·1	100				+1	−1	+0.0817	−0.3761	75.422
01·2	110	+2	−2	−1.8040	+1	+1	−1.9933	−1.7952	62.519
10·4	211	+2	+2	+1.8040	+1	+1	+1.9734	+1.8801	43.869
00·6	222	+2	−2	−6.0000	+1	+1	−1.9402	−5.8472	0
01·5	221				+1	−1	+0.4056	+0.7814	37.562
11·0	10$\bar{1}$	+2	+2	−2.1864	+1	+1	+2.0000	−2.1095	90
11·3	210			+4.1910	+1	−1	−0.2444	+4.1187 −3.6426	65.751
02·1	11$\bar{1}$				+1	−1	+0.0817	+1.6286	82.591
20·2	200	+2	−2	+1.9808	+1	+1	−1.9933	+1.9509	75.422
10·7	322				+1	−1	−0.5640	−0.0482	28.782
02·4	220	+2	+2	−1.9808	+1	+1	+1.9734	−2.3185	62.518
01·8	332	+2	+2	+1.8040	+1	+1	+1.8942	+1.6189	25.672
11·6	321	+2	−2	+2.1864	+1	+1	−1.9402	+1.1798 +2.9316	47.985
00·9	333				+1	−1	+0.7187	+1.9969	0
20·5	311				+1	−1	+0.4056	−2.0689	56.969
21·1	20$\bar{1}$			+3.7802	+1	+1	+0.0817	−4.4674 +2.7560	84.386
12·2	21$\bar{1}$	+2	−2	+1.7954	+1	+1	−1.9933	+0.6004 +2.8753	78.878
02·7	331				+1	−1	−0.5640	−1.1053	47.689
10·10	433	+2	−2	−1.8040	+1	+1	−1.8355	−1.8692	21.036
21·4	310	+2	+2	−1.7954	+1	+1	+1.9734	−1.8669 −1.2224	68.535
20·8	422	+2	+2	−1.9808	+1	+1	+1.8942	−1.4839	43.867
11·9	432			+4.1910	+1	−1	+0.7187	−4.3850 +3.0204	36.499
12·5	320			+3.7802	+1	−1	+0.4056	−2.8915 +3.8184	63.826
03·0	11$\bar{2}$	+2	+2	+2.5860	+1	+1	+2.0000	+1.9259	90
01·11	443				+1	−1	−0.8686	−1.1467	19.271
30·3 03·3	300 22$\bar{1}$				+1	−1	−0.2444	+0.8776 −1.3123	75.422
00·12	444	+2	+2	+6.0000	+1	+1	+1.7646	+5.3964	0
21·7	421			+3.7802	+1	−1	−0.5640	+4.8888 −2.4801	55.468

* The amplitude contributions have been divided by 6 in order to obtain expressions corresponding to the contents of the rhombohedral unit cell.

TABLE 3—(*continued*)

$hk \cdot l$	$h_r k_r l_r$	Amplitude contributions* to structure factors, F, for calcite			Amplitude contributions* to structure factors, F, for dolomite				Angle between normal and normal and [c], for dolomite, in degrees
		f_{Ca}	f_C	f_O	f_{Ca}	f_{Mg}	f_C	f_O	
02·10	442	+2	−2	+1.9808	+1	+1	−1.8355	+2.5679	37.562
12·8	431	+2	+2	−1.7954	+1	+1	+1.8942	+0.0523 −3.7372	51.818
30·6 03.6	411 330	+2	−2	−2.5860	+1	+1	−1.9402	−2.1240 −1.6297	62.519
22·0	202	+2	+2	−2.0192	+1	+1	+2.0000	−1.1830	90
20·11	533				+1	−1	−0.8686	+2.4039	34.955
10·13	544				+1	−1	+1.0127	+0.4701	16.470
22·3	31$\bar{1}$			−0.7811	+1	−1	−0.2444	−0.2913 +0.5583	77.307
11·12	543	+2	+2	−2.1864	+1	+1	+1.7646	−0.1901 −3.6045	29.035
13·1	21$\bar{2}$			−0.3704	+1	−1	+0.0817	+0.0978 −1.0696	85.875
31·2	30$\bar{1}$	+2	−2	−2.1566	+1	+1	−1.9933	+0.4957 −4.4963	81.791
21·10	532	+2	−2	+1.7954	+1	+1	−1.8355	+0.7635 +1.7822	45.493
13·4	32$\bar{1}$	+2	+2	+2.1566	+1	+1	+1.9734	+4.4742 −0.2543	73.905
01·14	554	+2	−2	−1.8040	+1	+1	−1.6819	−1.3600	15.365
22·6	420	+2	−2	+2.0192	+1	+1	−1.9402	+1.2488 +1.0570	65.751
03·9 30·9	441 522				+1	−1	+0.7187	+1.6801 −0.3982	52.036
31·5	410			−0.3704	+1	−1	+0.4056	+0.9577 +0.9170	70.169
12·11	542			+3.7802	+1	−1	−0.8686	+2.8797 −2.9749	42.766
00·15	555				+1	−1	−1.1500	−3.2150	0
02·13	553				+1	−1	+1.0127	+0.5257	30.603
04·$\bar{1}$	11$\bar{3}$				+1	−1	+0.0817	+0.3301	86.280
04·2	222	+2	−2	−5.9232	+1	+1	−1.9933	−4.8835	82.591
13·7	430			−0.3704	+1	−1	−0.5640	−1.1077 +1.1270	63.209
40·4	400	+2	+2	+5.9232	+1	+1	+1.9734	+4.8089	75.422
20·14	644	+2	−2	+1.9808	+1	+1	−1.6819	+0.9413	28.782
31·8	521	+2	+2	+2.1566	+1	+1	+1.8942	−0.7119 +4.2893	60.014
22·8	531			−0.7811	+1	−1	+0.7187	+0.0095 −0.7969	60.155
04.5	33$\bar{1}$				+1	−1	+0.4056	+0.7721	71.991

TABLE 3—(*continued*)

$hk \cdot l$	$h_r k_r l_r$	Amplitude contributions* to structure factors, F, for calcite			Amplitude contributions* to structure factors, F, for dolomite				Angle between plane normal and [c], for dolomite, in degrees
		f_{Ca}	f_C	f_O	f_{Ca}	f_{Mg}	f_C	f_O	
11·15	654			+4.1910	+1	−1	−1.1500	+4.4279 −2.1673	23.942
10·16	655	+2	+2	+1.8040	+1	+1	+1.5880	+1.7631	13.514
21·13	643			+3.7802	+1	−1	+1.0127	−5.0611 +2.0778	38.045
30·12	633	+2	+2	+2.5860	+1	+1	+1.7646	+2.2139 +1.2505	43.868
03·12	552								
32·1	302			−4.1145	+1	−1	+0.0817	+4.9874 −1.8593	86.586
23·2	312	+2	−2	+2.1826	+1	+1	−1.9933	+0.0903 +2.5584	83.195
40·7	511				+1	−1	−0.5640	−1.4156	65.528
13·10	541	+2	−2	−2.1566	+1	+1	−1.8355	−4.2242 −0.0001	54.197
32·4	411	+2	+2	−2.1826	+1	+1	+1.9734	−3.6841 +0.3294	76.577
12·14	653	+2	−2	+1.7954	+1	+1	−1.6819	−0.7023 +4.4086	36.005
04·8	440	+2	+2	+5.9232	+1	+1	+1.8942	+4.7092	62.519
01·17	665				+1	−1	+1.2797	+1.4537	12.745
23·5	421			−4.1145	+1	−1	+0.4056	+1.8389 −5.5649	73.389
14·0	213	+2	+2	+1.3784	+1	+1	+2.0000	+3.4131 −0.8908	90
31·11	632			−0.3704	+1	−1	−0.8686	−0.7970 −1.8852	51.570
02·16	664	+2	+2	−1.9808	+1	+1	+1.5880	−2.6866	25.671
14·3	322			+0.4469	+1	−1	−0.2444	+0.2011 +1.8240 −1.6229 −0.9715	80.338
41·3	401								
22·12	642	+2	+2	−2.0192	+1	+1	+1.7646	−1.2509 −0.8771	47.984
00·18	666	+2	−2	−6.0000	+1	+1	−1.4835	−4.6708	0
32·7	520			−4.1145	+1	−1	−0.5640	−4.1559 +1.7849	67.332
40·10	622	+2	−2	−5.9232	+1	+1	−1.8355	−4.4894	56.969
23·8	530	+2	+2	−2.1826	+1	+1	+1.8942	−0.5054 −1.3023	64.484
41·6	510	+2	−2	−1.3784	+1	+1	−1.9402	+1.2571 −3.1938 −3.4585 +0.4791	71.196
14·6	431								

TABLE 3—(*continued*)

$hk \cdot l$	$h_r k_r l_r$	Amplitude contributions* to structure factors, F, for calcite			Amplitude contributions* to structure factors, F, for dolomite				Angle between plane normal and [c], for dolomite, in degrees
		f_{Ca}	f_C	f_O	f_{Ca}	f_{Mg}	f_C	f_O	
20·17	755				+1	−1	+1.2797	−2.6163	24.341
04·11	551				+1	−1	−0.8686	−1.8350	54.428
03·15	663				+1	−1	−1.1500	−1.9624	37.561
30·15	744							−0.1016	
21·16	754	+2	+2	−1.7954	+1	+1	+1.5880	+0.3789	32.450
								−2.2512	
13·13	652			−0.3704	+1	−1	+1.0127	+2.0612	46.842
								−1.1270	
11·18	765	+2	−2	+2.1864	+1	+1	−1.4835	−0.8094	20.306
								+4.0937	
05·1	22$\bar{3}$				+1	−1	+0.0817	+2.0959	87.023
05·2	11$\bar{4}$	+2	−2	−1.0296	+1	+1	−1.9933	−0.5718	84.061
10·19	766				+1	−1	−1.4008	−0.8681	11.441
32·10	631	+2	−2	+2.1826	+1	+1	−1.8355	+4.6221	59.178
								−0.7322	
05·4	33$\bar{2}$	+2	+2	+1.0296	+1	+1	+1.9734	+0.0988	78.247
31·14	743	+2	−2	−2.1566	+1	+1	−1.6819	+0.8918	44.720
								−3.8638	
14·9	540			+0.4469	+1	−1	+0.7187	+0.5795	62.944
41·9	621							−1.9321	
								+1.3391	
12·17	764			+3.7802	+1	−1	+1.2797	+1.6923	30.897
								−2.7212	
								+1.9798	
50·5	500				+1	−1	+0.4056	−1.9669	75.422
33·0	30$\bar{3}$	+2	+2	−1.3282	+1	+1	+2.0000	−1.7691	90
23·11	641			−4.1145	+1	−1	−0.8686	−1.7248	56.723
								+5.8588	
22·15	753			−0.7811	+1	−1	−1.1500	+0.2729	41.605
								+0.9949	
40·13	733				+1	−1	+1.0127	+2.4289	49.794
33·3	41$\bar{2}$			−3.3772	+1	−1	−0.2444	−1.6477	81.460
								+2.0470	
01·20	776	+2	+2	+1.8040	+1	+1	+1.3691	+1.0319	10.883
24·1	31$\bar{3}$			+0.7735	+1	−1	+0.0817	−3.3813	87.186
								−2.4627	
42·2	40$\bar{2}$	+2	−2	+1.9430	+1	+1	−1.9933	+1.3808	84.386
								+2.1764	
05·7	44$\bar{1}$				+1	−1	−0.5640	+1.7233	69.993
02·19	775				+1	−1	−1.4008	+0.0808	22.036

TABLE 3—(*continued*)

$hk \cdot l$	$h_r k_r l_r$	Amplitude contributions* to structure factors, F, for calcite			Amplitude contributions* to structure factors, F, for dolomite				Angle between plane normal and [c], for dolomite, in degrees
		f_{Ca}	f_C	f_O	f_{Ca}	f_{Mg}	f_C	f_O	
24·4	42$\bar{2}$	+2	+2	−1.9430	+1	+1	+1.9734	−1.4132 −0.8250	78.878
04·14	66$\bar{2}$	+2	−2	−5.9232					48.448†
50·8	61$\bar{1}$	+2	+2	+1.0296					67.943†
33·6	52$\bar{1}$	+2	−2	+1.3282					73.700†
42·5	51$\bar{1}$			+0.7735					76.543†
13·16	76$\bar{3}$	+2	+2	+2.1566					41.664†
20·20	86$\bar{6}$	+2	+2	−1.9808					21.546†
30·18	85$\bar{5}$	+2	−2	−2.5860					33.350†
03·18	77$\bar{4}$								
32·13	74$\bar{2}$			−4.1145					52.937†
21·19	86$\bar{5}$			+3.7802					28.805†
41·12	73$\bar{2}$	+2	−2	−1.3784					56.449†
14·12	65$\bar{1}$								
15·$\bar{1}$	21$\bar{4}$			+4.5175					87.396†
24·7	53$\bar{1}$			+0.7735					71.479†
15·2	32$\bar{3}$	+2	−2	+2.4974					84.802†
11·21	87$\bar{6}$			+4.1910					18.040†
05·10	55$\bar{0}$	+2	−2	−1.0296					63.138†

† These angles are for calcite (26° C.).

and composition, 0.38 mol percent substituted $CaCO_3$ in $MgCO_3$ would produce a change of 0.0005 Å in a 1 Å basal reflection and 0.0003 Å in a 1 Å reflection with no *c*-axis component. These differences would be readily measurable in the back reflection region of films taken with a 114.59 mm. diameter powder camera such as that used in this work.*

The other impurities in Table 6, where they are greater than the limit of detection, would probably not produce detectable spacing changes. The Li_2CO_3 used to facilitate recrystallization of some of these samples in runs made with a squeezer-type apparatus (Griggs and Kennedy, 1956) has never been observed to lead to changed spacings in cases where carbonates were initially well crystallized and careful comparisons of back-reflection spacings before and after the run could be made.

* The slight equilibrium substitution of $CaCO_3$ in $MgCO_3$ at higher temperatures (Harker and Tuttle, 1955) suggests that the 0.38 mol percent $CaCO_3$ here computed is probably not all present in solid solution.

TABLE 4. COMPUTED RELATIVE INTENSITIES OF FRONT REFLECTIONS IN POWDER DIAGRAMS OF THE RHOMBOHEDRAL CARBONATES AND THE HYPOTHETICAL END MEMBER, $CaFe(CO_3)_2$, FOR COPPER RADIATION

$h_r k_r l_r$	$MgCO_3$	$Mg_3Ca(CO_3)_4$		$CaMg(CO_3)_2$	$CaCO_3$	$CaMn(CO_3)_2$	$CaFe(CO_3)_2$	$MnCO_3$	$FeCO_3$	$CoCO_3$	$NiCO_3$	$CuCO_3$	$ZnCO_3$	$CdMg(CO_3)_2$	$CdCO_3$
111				.021		(14.2)†	(16.4)†							67.6	
100				2.46		(9.17)	(12.7)							141	
110	.689	4.05	$11\bar{1}$*	3.38	17.3	42.1	48.1	75.4	90.1	105	122	136	154	125	565
211	78.9	196	200	146	213	231	231	246	243	246	249	323	296	342	779
222	9.73	17.9	111	6.65	4.96	1.59	1.15	.145	.0020	.0864	.346	.712	1.27	.817	28.0
221				7.20		(.039)	(.0052)							68.0	
$10\bar{1}$	5.17	22.7	$20\bar{2}$	17.0	30.2	40.2	41.3	50.7	52.7	58.1	61.8	82.3	80.3	87.6	267
210	39.4			34.9	44.6	43.4	42.5	41.6	40.4	39.4	38.6	41.2	39.5	97.7	47.2
$11\bar{1}$				6.07		(.465)	(.229)							45.2	
200	10.3	18.3	$3\bar{1}\bar{1}$	20.2	33.2	40.8	41.6	48.0	48.9	52.5	54.3	71.8	69.2	73.2	201
322				.260		(1.64)	(2.02)							20.5	
220	4.29	6.88	$22\bar{2}$	6.48	14.6	1.97	20.9	25.1	26.9	29.5	32.0	40.0	41.2	37.3	126
332	14.7	36.3	220	26.8	45.9	48.2	48.0	49.3	48.5	48.3	48.7	66.7	62.7	70.3	181
321	18.9	35.8	$31\bar{1}$	28.6	48.4	59.6	61.5	69.5	72.8	76.7	80.5	101	102	101	275
333				1.86		(.360)	(.247)							10.4	
311				.273		(3.64)	(4.09)							7.73	
$20\bar{1}$	4.09			6.95	8.98	7.78	6.72	5.88	5.06	4.38	3.71	6.11	4.33	23.7	7.94
$21\bar{1}$	6.24	6.94	$31\bar{3}$	14.9	21.4	28.6	28.9	33.0	33.2	35.9	37.3	52.6	49.9	57.9	163
331				.0416		(1.65)	(1.92)							6.21	
433	.324	.846	311	.782	2.15	3.93	4.40	5.69	6.64	7.29	8.29	10.7	11.7	11.7	46.7
310	5.17	7.34	$40\bar{2}$	8.46	13.6	18.7	19.8	21.9	25.9	28.6	31.1	38.6	40.3	41.4	121
422	1.76	3.62	400	4.00	6.20	8.14	8.50	9.89	10.6	11.4	12.4	16.1	16.6	19.1	56.1
432	5.85			5.05	7.92	6.74	7.05	6.42	6.17	5.73	5.52	6.18	5.81	19.1	7.00
320	2.50			4.78	5.74	4.61	4.23	3.63	2.91	2.65	2.24	3.70	2.63	22.3	4.90
$11\bar{2}$	11.2	7.81	$42\bar{2}$	10.4	17.7	21.5	22.2	25.1	26.4	28.4	30.0	34.6	35.7	30.6	81.6
443				.0534		(1.26)	(1.42)							4.02	
300				.455		(.970)	(1.14)							12.3	
$22\bar{1}$															
444	4.18	10.7	222	5.77	10.1	9.95	9.93	9.62	9.53	9.17	9.22	12.0	11.5	12.4	30.1

* The calcite rhombohedral cell, on the basis of which the intensities in this table are computed, contains only ½ $Mg_3Ca(CO_3)_4$ and is thus a pseudo-cell for huntite. The huntite reflections listed here may be indexed on this pseudo-cell; the corresponding index in the true huntite rhombohedral cell is given immediately after each huntite relative intensity value (see Graf and Bradley, in press).

† The intensities in parentheses were computed for a dolomite-type structure, the other $CaMn(CO_3)_2$ and $CaFe(CO_3)_2$ intensities, for a calcite-type structure (see text).

TABLE 5. VALUES OF 2θ FOR LOW-ANGLE *X*-RAY REFLECTIONS OF THE COMMON RHOMBOHEDRAL CARBONATES, COMPUTED FOR CuKα_1 RADIATION

$hk\cdot l$	$h_r k_r l_r$	$MgCO_3$	$CaMg(CO_3)_2$	$CaCO_3$ (26° C.)	$FeCO_3$	$MnCO_3$	$ZnCO_3$
00·3	111		16.597				
10·1	100		22.039				
01·2	110	25.143	24.071	23.051	24.777	24.310	25.056
10·4	211	32.637	30.964	29.394	32.038	31.428	32.561
00.6	222	35.850	33.557	31.427	34.989	34.319	35.827
01·5	221		35.331				
11·0	$10\bar{1}$	38.841	37.376	35.965	38.363	37.625	38.670
11·3	210	42.985	41.148	39.402	42.362	41.539	42.822
02·1	$11\bar{1}$		43.812				
20·2	200	46.832	44.950	43.152	46.208	45.302	46.633
10·7	322		45.193				
02·4	220	51.614	49.295	47.107	50.815	49.812	51.424
01·8	332	53.877	50.560	47.494	52.650	51.597	53.806
11·6	321	53.884	51.096	48.496	52.889	51.835	53.733
00·9	333		51.315				
20·5	311		52.374				
21·1	$20\bar{1}$	61.395	58.918	56.555	60.581	59.346	61.108
12·2	$21\bar{1}$	62.417	59.841	57.391	61.567	60.309	62.135
02·7	331		60.039				
10·10	433	66.420	62.056	58.063	64.789	63.448	66.340
21·4	310	66.431	63.459	60.660	65.423	64.065	66.149
20·8	422	68.386	64.533	60.983	66.996	65.595	68.204
11·9	432	69.354	65.182	61.359	67.828	66.405	69.210
12·5	320	69.360	66.097	63.042	68.239	66.806	69.081
03·0	$11\bar{2}$	70.329	67.419	64.654	69.372	67.911	69.981
01·11	443		68.199				
30·3	300		69.981				
03·3	$22\bar{1}$						
00·12	444	75.986	70.523	65.595	73.917	72.327	75.928

Table 6 also gives the a_0 and c_0 values obtained from $\cos^2\theta$ and

$$\left(\frac{\cos^2\theta}{\sin\theta}+\frac{\cos^2\theta}{\theta}\right)$$

extrapolations for various samples of $MgCO_3$, $FeCO_3$, $MnCO_3$, $CoCO_3$, $CdCO_3$, $NiCO_3$, $ZnCO_3$, and $CaMn(CO_3)_2$, together with measurements of $CdMg(CO_3)_2$ samples made on films taken with a Guinier-type focusing camera. The comparable information for $CaCO_3$ and $CaMg(CO_3)_2$ has been given in Goldsmith and Graf (1958*b*), together with a discussion of the extrapolation procedure, which involves successive approximations.

In making spacing measurements, film shrinkage and camera radius

TABLE 6. METHOD OF PREPARATION, PURITY, AND CELL CONSTANTS OF VARIOUS RHOMBOHEDRAL CARBONATE SAMPLES

$MgCO_3$, No. G-1219; basic Mg carbonate+CO_2+H_2O, 15 hours in Morey bomb at 300° C.; $0.38\pm0.06\%$ $CaCO_3$, $0.01\pm0.003\%$ $FeCO_3$, $<0.003\%$ $MnCO_3$, $<0.04\%$ $CdCO_3$, $<0.007\%$ $CoCO_3$, $<0.25\%$ $ZnCO_3$.

$a_0 = 4.6330$ Å, Cu radiation
$c_0 = 15.016$ Å (Goldsmith and Graf, 1958*b*)
$c_0/a_0 = 3.2411$

$MnCO_3$, reagent grade chemical; $0.1_1\pm0.03\%$ $CaCO_3$, $0.02\pm0.01_5\%$ $CdCO_3$, $<0.02\%$ $CoCO_3$, $<0.01\%$ $FeCO_3$, $0.1\pm0.05\%$ $MgCO_3$, $<0.2\%$ $ZnCO_3$. H_2O ($-110°$ C.), 0.85%*; H_2O ($+110°$ C.), 3.32%*.

$a_0 = 4.792$ Å, $\left(\frac{\cos^2\theta}{\sin\theta}+\frac{\cos^2\theta}{\theta}\right)$ extrapolation, Fe radiation

$c_0 = 15.71$ Å, $\left(\frac{\cos^2\theta}{\sin\theta}+\frac{\cos^2\theta}{\theta}\right)$ extrapolation, Fe radiation

$c_0/a_0 = 3.278$

$MnCO_3$, No. G-738; reagent grade $MnCO_3$+CO_2, 3 hours at 722° C. in cold-seal bomb; $0.09\pm0.02\%$ $CaCO_3$, $0.1\pm0.05\%$ $MgCO_3$, $0.01\pm0.008\%$ $FeCO_3$, $<0.02\%$ $CdCO_6$, $<0.02\%$ $CoCO_3$, $<0.2\%$ $ZnCO_3$.

$a_0 = 4.7771$ Å, Fe radiation
$a_0 = 4.7772$ Å, Cu radiation
$c_0 = 15.664$ Å, Fe radiation
$c_0/a_0 = 3.2790$

$FeCO_3$, No. G-613; $FeSO_4$+Na_2CO_3+CO_2+H_2O, 20 hours at 143° C. in Morey bomb;

$a_0 = 4.690_2$ Å, Co radiation
$c_0 = 15.369$ Å, Co radiation
$c_0/a_0 = 3.276_3$

$FeCO_3$, No. G-1219; $FeSO_4$+Na_2CO_3+CO_2+H_2O, 15 hours at 300° C. in Morey bomb; $0.038\pm0.020\%$ $CaCO_3$, $0.072\pm0.014\%$ $MgCO_3$, $0.13\pm0.013\%$ $MnCO_3$, $<0.08\%$ $CdCO_3$, $0.008\pm0.002\%$ $CoCO_3$, $0.18\pm0.04\%$ $ZnCO_3$.

$a_0 = 4.6887$ Å, Co radiation
$a_0 = 4.6888$ Å, Fe radiation
$c_0 = 15.373$ Å, Co radiation
$c_0/a_0 = 3.2787$

$FeCO_3$, material from No. G-1219+$NaHCO_3$, 3 hours in squeezer-type apparatus (Griggs and Kennedy, 1956), 14 kb, 659° C.

$a_0 = 4.6889$ Å, Fe radiation
$c_0 = 15.373$ Å, Fe radiation
$c_0/a_0 = 3.2786$

$CdCO_3$, reagent grade chemical; $<0.09\%$ $CaCO_3$, $<0.06\%$ $CoCO_3$, $0.01_2\pm0.009\%$ $FeCO_3$,

Unless otherwise noted, impurities reported in spectrographic analyses by Juanita Witters as weight per cent metal have been recalculated to mol per cent carbonate. Cell constants were obtained by $\cos^2\theta$ extrapolations unless otherwise noted. The ranges given for a_0 and c_0 of ordered and disordered $CdMg(CO_3)_2$ indicate only the uncertainty that would result from a misreading of line position on the films by the smallest unit measured, 0.05 mm.

* Analyst, L. D. McVicker.

TABLE 6—(*continued*)

$0.03_8 \pm 0.02_5\%$ $MgCO_3$, $0.06 \pm 0.03\%$ $MnCO_3$, $<0.08\%$ $ZnCO_3$. H_2O ($-110°$ C.), 0.23%*; H_2O ($+110°$ C.), 2.87%*.

$a_0 = 4.936$ Å, $\left(\frac{\cos^2\theta}{\sin\theta} + \frac{\cos^2\theta}{\theta}\right)$ extrapolation, Fe radiation

$c_0 = 16.29$ Å,
$c_0/a_0 = 3.300$ $\left(\frac{\cos^2\theta}{\sin\theta} + \frac{\cos^2\theta}{\theta}\right)$ extrapolation, Fe radiation

$CdCO_3$, No. G-1321; $CdSO_4 + Na_2CO_3 + CO_2 + H_2O$, 15 hours at 255° C. in Morey bomb; $0.09 \pm 0.07\%$ $CaCO_3$, $<0.01_5\%$ $MgCO_3$, $0.009 \pm 0.007\%$ $FeCO_3$, $0.003 \pm 0.002_5\%$ $MnCO_3$, $<0.06\%$ $CoCO_3$, $<0.08\%$ $ZnCO_3$.

$a_0 = 4.9207$ Å, Co radiation
$c_0 = 16.295$ Å, Co radiation
$c_0/a_0 = 3.3115$

$CdCO_3$, material from No. G-1321 plus Li_2CO_3 in squeezer-type apparatus for 3 hours at 10 kb, 500° C.

$a_0 = 4.9204$ Å, Co radiation
$c_0 = 16.298$ Å, Co radiation
$c_0/a_0 = 3.3123$

$ZnCO_3$, No. G-1316; reagent grade chemical $+H_2O+CO_2$, 15 hours at 250° C. in Morey bomb; $0.19 \pm 0.04\%$ $CaCO_3$, $0.01 \pm 0.008\%$ $MgCO_3$, $0.040 \pm 0.020\%$ $FeCO_3$, $0.002 \pm 0.001_5\%$ $MnCO_3$, $<0.02\%$ $CdCO_3$, $<0.02\%$ $CoCO_3$; H_2O ($-110°$ C.), 0.54%†; H_2O ($+110°$ C.), 3.73%†.

$a_0 = 4.6528$ Å, Cu radiation
$a_0 = 4.6525$ Å, Co radiation
$c_0 = 15.025$ Å, Cu radiation
$c_0 = 15.024$ Å, Co radiation
$c_0/a_0 = 3.2292$

$ZnCO_3$, transparent crystal from Broken Hill, Rhodesia; $0.03 \pm 0.01_5\%$ $CaCO_3$, $0.92 \pm 0.09\%$ $FeCO_3$, $0.30 \pm 0.03\%$ $MgCO_3$, $0.041 \pm 0.004\%$ $MnCO_3$, $<0.02\%$ $CdCO_3$, $<0.04\%$ $CoCO_3$, $<0.004\%$ $NiCO_3$.

$a_0 = 4.6534$ Å, Co radiation
$c_0 = 15.027$ Å, Co radiation
$c_0/a_0 = 3.2293$

$NiCO_3$ (prepared by Thelma Isaacs), $NiCl_2 \cdot 6H_2O + NaHCO_3 + H_2O + CO_2$, 2.5 months at 250° C. in Morey bomb; $0.06 \pm 0.03\%$ $CaCO_3$, $0.04 \pm 0.02\%$ $FeCO_3$, $0.01_5 \pm 0.008\%$ $MgCO_3$, $0.04 \pm 0.02\%$ $MnCO_3$, $0.09 \pm 0.05\%$ $ZnCO_3$, 0.02 wt % Cu, 0.2 wt % Na, 0.02 wt % Si. Infrared absorption curve shows no water in excess of that for the KBr blank.

$a_0 = 4.5975$ Å, Co radiation
$c_0 = 14.723$ Å, Co radiation
$c_0/a_0 = 3.2024$

$CoCO_3$, No. G-1319; "Specpure" $Co_3O_4 + KHSO_4 \xrightarrow{25°\text{ C.}}$ Co sulfate; Co sulfate + "Specpure" $Na_2CO_3 \xrightarrow{25°\text{ C.}}$ basic Co carbonate; basic Co carbonate $+H_2O+CO_2$ for 15 hours at 255° C. in Morey bomb; $<0.1_5\%$ $CaCO_3$, $0.04 \pm 0.03_5\%$ $MgCO_3$, 0.01

† Microanalyst, D. R. Dickerson.

TABLE 6—(*continued*)

±0.008% $FeCO_3$, <0.004% $MnCO_3$, <0.1% $CdCO_3$, <0.002% $NiCO_3$, <0.09% $ZnCO_3$. H_2O (−110° C.), none†; H_2O (+110° C.), 8.10%†.

a_0= 4.6620 Å, Co radiation
c_0=14.975 Å, Co radiation
c_0/a_0= 3.2121

$CoCO_3$, material from No. G-1319+Li_2CO_3, 2 hours in squeezer-type apparatus at 10 kb., 60° C.

a_0= 4.6581 Å, Co radiation
c_0=14.958 Å, Co radiation
c_0/a_0= 3.2112

$CdMg(CO_3)_2$, ordered; Li_2CO_3 added to equimolar mixture of $CdCO_3$ and $MgCO_3$, treated in cold-seal bomb for 23 hours under 27,000 psi CO_2 at 600° C.

$d_{\{444\}}$ and $d_{\{11\bar{2}\}}$ measured on film taken with Fe$K\alpha_1$ radiation, using a Guinier-type focusing camera, and calibrated against the closely similar $d_{\{444\}}$ and $d_{\{11\bar{2}\}}$ values of synthetic $MnCO_3$ run on the adjoining strip of the same film.

a_0= 4.7770±0.0009 Å
c_0=15.641±0.003 Å
c_0/a_0= 3.2742

$CdMg(CO_3)_2$, disordered; equimolar mixture of $CdCO_3$ and $MgCO_3$ treated at 10 kb. and 900° C. for 1.5 hours in sealed-tube gas system; spacing measurements made as for the ordered material.

a_0= 4.7746±0.0009 Å
c_0=15.678±0.003 Å
c_0/a_0= 3.2836

$CaMn(CO_3)_2$, disordered; equimolar mixture of $CaCO_3$ and $MnCO_3$ reacted in cold-seal bomb at 706–710° C. under 14,000 psi CO_2 pressure for 22 hours.

Line coincidence of {400} and {644} used to obtain accurate c_0/a_0 ratio, followed by a_0 and c_0 extrapolations of back reflections on film taken with Fe radiation. $I_{\{400\}}:I_{\{644\}}$ is computed to be about 3, and observed as such on films of CaMn carbonate solid solutions containing 40 and 60 mol per cent $MnCO_3$, for which the two reflections are resolved. Departure from coincidence in the $CaMn(CO_3)_2$ sample would thus readily be observable as line broadening relative to the line breadths of neighboring reflections.

a_0= 4.8797 Å
c_0=16.367 Å
c_0/a_0= 3.3541

errors were taken into account by using the Straumanis film mount and correction procedure. Reflections in the range θ=60°–90° were used for the $\cos^2\theta$ extrapolations, in accordance with the finding of Taylor and Sinclair (1945) that almost linear extrapolation curves which simultaneously eliminate eccentricity and absorption errors are obtained within this angular range.

COMPARISON OF CELL CONSTANTS WITH PUBLISHED VALUES

Cell constants cited in this paper are compared in Table 7 with values obtained from the literature. For most of the carbonates, the agreement

is excellent. The newly determined values for coarsely crystalline synthetic $NiCO_3$ are preferred over those of Pistorious (1959), and there is a small discrepancy for $CdCO_3$.

The range of a_0 values reported in Table 7 for several $CdCO_3$ samples, 4.9204 to 4.936 Å, includes the values published by Swanson *et al.* (1957) and Ramdohr and Strunz (1941), but the range of c_0 values, 16.298 to 16.29 Å, is clearly distinct from their 16.27 Å. Mr. Swanson (personal communication) finds $a_0 = 4.9279$ Å and $c_0 = 16.284$ Å on repeating the least squares calculation for his $CdCO_3$ sample.

The several sets of $CdCO_3$ values in Tables 6 and 7 suggest that a_0 increases and c_0 decreases with decreasing temperature of formation, although some of these differences are near the limit of error, and that Swanson's sample was made at fairly low temperature.

Enlarged Unit Cells of Lower Temperature Preparations

Effects analogous to the change in cell size of $CdCO_3$ prepared at lower temperatures are noted for other carbonates (Table 6). There is a considerable increase in both a_0 and c_0 of $CoCO_3$ prepared at 255° C., compared with that made at 600° C. Reagent-grade chemical $MnCO_3$ as received has a markedly enlarged cell compared with that of material crystallized at 722° C. Saint Léon Langlès (1952) reported values for two $NiCO_3$ preparations that indicate the higher temperature product has a smaller cell. Graf *et al.* (1961) have described a magnesite from the Lake Bonneville sediments of Quaternary age in the Great Salt Lake Desert, Utah, which has $a_0 = 4.669$ Å, $c_0 = 15.21$ Å, compared with $a_0 = 4.6330$ Å and $c_0 = 15.016$ Å given in Table 7 for material prepared at 250° C. The impurity content which could conceivably be in solid solution in the magnesite of the Utah sample, 0.7 wt% Fe, 0.01 wt% Mn, and about 0.2 wt% Ca (spectrographic analysis by Juanita Witters), fails by an order of magnitude to explain the change in cell size.

Calculations by Verwey (1946) for several alkali halides, which should be similar enough to the rhombohedral carbonates for order-of-magnitude comparison, indicated that near-surface shifts of position of positive and negative ions and their electron clouds should occur, but only for one or two atomic layers below the surface. The effect would thus be insignificant for particles of the order of 1 micron diameter such as those making up the lowest-temperature carbonate preparations. Rymer's recent (1957) review indicates extensive disagreement as to the size and magnitude of the effect of small particle-size *per se* on cell constants.

Lehovec (1953) computed that the space-charge zone in NaCl particles, which causes an electrostatic potential between the bulk and the surface of the crystal and affects the concentration of point defects, should extend inward from the surface about 0.013 micron at 627° C.,

TABLE 7. COMPARISON WITH PUBLISHED VALUES OF CELL CONSTANTS

Material	c_0 in Å	a_0 in Å	Reference	Remarks
$CaCO_3$	17.064	4.9900, 4.9896	Goldsmith and Graf (1958*b*)	Extrapolated values; spectrographic standard $CaCO_3$
	17.064 (26° C.)	4.9899 (26° C.)	See discussion in Graf and Lamar (1955)	Calculated from spectrometer measurements of α and $d_{\{211\}}$ of single crystals
	17.060±0.005 (18° C.)	4.9898±0.0003 (18° C.)	Andrews (1950)	Spectrographic standard $CaCO_3$
	17.063_8 (26° C.)	4.9896 (26° C.)		Andrews' values recalculated to 26° C. using thermal expansion data of Austin *et al.* (1940)
	17.062 (26° C.)	4.989 (26° C.)	Swanson and Fuyat (1953)	0.01–0.1% Sr is major residual impurity after purification
$MgCO_3$	15.016	4.6330	Goldsmith and Graf (1958*b*)	
	15.015	4.6332	Swanson *et al.* (1957)	Sample heated four days at 120,000 psi and 280° C.; 0.01–0.1% Ca
$MnCO_3$	15.664	4.7768	Goldsmith and Graf (1957)	
	15.67	4.777	Swanson *et al.* (1957)	Ppt. from solutions of $MnSO_4$ and $NaHCO_3$, heated in CO_2 atmosphere 3 days at 400° C.
	15.664	4.7771	This paper	Recrystallized at 722° C. (see Table 6)
$FeCO_3$	15.370±0.003	4.690±0.002	Sharp (1960)	$NaHCO_3$ and $FeSO_4 \cdot 7H_2O$ reacted at 200° C. under 500 bars (CO_2+H_2O) pressure, then held at 600° C. under 15 lb. pressure in squeezer apparatus of Griggs and Kennedy (1956); least squares treatment of diffractometer data
	15.373	4.6887	This paper	Prepared at 300° C. (see Table 6)

Material	c_0 in Å	a_0 in Å	Reference	Remarks
$ZnCO_3$	15.028 (25° C.)	4.6533 (25° C.)	Swanson *et al.* (1959)	U.S.N.M.#96155, Broken Hill, Rhodesia; 0.01–0.1% of Cd, Fe, Mg, and Pb; 0.001–0.01% of Ca, Mn, and Si; 0.0001–0.001% Cu.
	15.027	4.6534	This paper	Small transparent smithsonite crystals from Broken Hill, Rhodesia, supplied by C. S. Hurlbut, Jr. (see Hurlbut, 1954); spectographic analysis calculates to 0.92 mol per cent $FeCO_3$, 0.30 mol per cent $MgCO_3$ content
	15.024	4.6531	This paper	Previous entry corrected for $FeCO_3$ and $MgCO_3$, assuming straight-line relation between cell constants and composition in systems $ZnCO_3$-$FeCO_3$ and $ZnCO_3$-$MgCO_3$
	15.025	4.6528	This paper	Recrystallized at 250° C. (see Table 6)
$NiCO_3$	14.744±0.003 (25° C.)	4.602±0.001 (25° C.)	Pistorius (1959)	Ppt. from mixed $NiSO_4$ and $NaHCO_3$ solns. treated 15 min. at 500° C. and 2 kb. pressure in squeezer apparatus of Griggs and Kennedy (1956); 0.001% Fe, 0.01% Co, 0.005% Cu, <0.005% Pb
	14.723	4.5975	This paper	Prepared at 250° C. (see Table 6)
$CdCO_3$	16.27	4.92	Ramdohr and Strunz (1941)	Schering's (chemical) $CdCO_3$; kX values here converted to Å
	16.27	4.930	Swanson *et al.* (1957)	Fine-grained material; 0.001–0.01% of Cr, Ni, and Pb; 0.0001–0.001% of Ca, Cu, Fe, Mg, and Si
	16.298	4.9204	This paper	Recrystallized at 500° C. (see Table 6)
$CoCO_3$	14.957	4.659	Swanson *et al.* (1960)	$CoCl_2 \cdot 6H_2O$, $NaHCO_3$, and H_2CO_3 reacted in Morey bomb; 0.01–0.1% of Mo, Ni; 0.001–0.01% of Ba, Cu, Mg, Si, and Ag
	14.958	4.6581	This paper	Recrystallized at 600° C. (see Table 6)

0.22 micron at 327° C. However, the vacancy concentrations observed in the alkali halides even at high temperature hardly seem adequate to explain the larger of the cell-size anomalies described in this paper.

Some of the samples prepared at lower temperatures include several percent of H_2O or OH^- that is not released in 12 to 15 hours at 110° C. (Table 6). The remarkably high value reported for $CoCO_3$ is from a microanalysis that totals poorly and may be in error, but there is no reason to doubt the results given for $ZnCO_3$, $CdCO_3$, and $MnCO_3$. The structural location of this H_2O or OH^- (it may, of course, only be tightly adsorbed) and its possible effect upon cell constants will be discussed in a subsequent communication.

It is possible that some of the cell enlargement of dolomite in fine-grained precipitates formed at room temperature, hitherto attributed exclusively to excess calcium (Graf and Goldsmith, 1956; Goldsmith and Graf, 1958*a*), may actually result from structurally incorporated H_2O or OH^-. Such a hydration effect is, of course, ruled out for other dolomites with enlarged cells which were formed by high-temperature synthesis in an anhydrous system.

The Unit Cell of Huntite, $Mg_3Ca(CO_3)_4$

Graf and Bradley (In press) gave for the unit cell of huntite $a_0 = 9.505$ Å, $c_0 = 7.821$ Å, obtained from a powder diffraction film of huntite from Currant Creek, Nevada, by making a least squares analysis involving a drift error term of the form

$$\sin^2\theta\left(\frac{1}{\sin\theta} - \frac{1}{\theta}\right).$$

Their cell was of principal value in demonstrating the close agreement between observed and calculated d-spacings of front reflections. A more accurate a_0 value can be obtained by combining the c/a ratio obtained from the least squares analysis with measurements on a film taken with iron radiation of the positions of the $\{71\cdot3\}$ and $\{72\cdot2\}$ reflections, at $2\theta \cong 149°$ and 168°, respectively, to make a two-point $\cos^2\theta$ extrapolation. Then c_0 is calculated from $d_{\{00\cdot6\}}$, the latter first corrected by the amount that the measured spacing of the adjacent $\{25\cdot0\}$ reflection differs from the value calculated from a_0. Varying the c/a ratio by an amount corresponding to a_0 fixed at 9.4980 Å and c_0 changing from 7.81 to 7.82 Å changes the extrapolated a_0 value by only ± 0.0003 Å.

Measurements for three huntite samples, all very fine-grained naturally-occurring materials, are given in Table 8. The cell constants of the two samples from Currant Creek, Nevada, are identical within the general limits of error observed in such extrapolations for the other

rhombohedral carbonates. The sample from Tea Tree Gully has a significantly larger cell. Graf and Bradley estimated that the a_0 of the Currant Creek huntite was 0.61% greater than predicted from a straight-line interpolation between the values for magnesite and calcite; c_0, 0.75% larger. The corresponding values for the more accurately determined unit cells in Table 8 are a_0, 0.57–0.61%, c_0 0.66–0.70%.

Coarsely crystalline huntite will have to be found in nature or synthesized before it will be possible to attribute a particular cell size to

TABLE 8. UNIT CELL DIMENSIONS OF THE HEXAGONAL STRUCTURE CELL OF HUNTITE

Sample	a_0 by extrapolation	c_0		
		Using a_0 and the c/a ratio of the least squares analysis	From $d_{\{00\cdot6\}}$ corrected against $d_{\{25\cdot0\}}$	
			Diffractometer	Film
Currant Creek, Nevada (Collected by D. L. Graf)	9.4981	7.815_5	7.815_8	
Currant Creek, Nevada (Collected by G. T. Faust)	9.4979	7.815_5		7.815_0
Tea Tree Gully, South Australia	9.5020	7.818_7		7.818_8

material of strictly 3:1 molar $MgCO_3$:$CaCO_3$ composition, free of hydration effects.

EFFECT OF CATION ORDER ON CELL SIZE

Small but measurable changes in cell size take place with cation disordering of the 1:1 compounds. Comparison of a_0 and c_0 values for the ordered and disordered cells with those predicted by taking a_0 and c_0 values midway between those of the two end members is interesting. Thus far, the only composition for which all three sets of values are available is $CdMg(CO_3)_2$ (Goldsmith, 1958). The crystallinity of these preparations is not ideal, and back reflection measurements are therefore not of the highest quality. The most accurate data available are those obtained from films taken with a Guinier-type focusing camera. The change in a_0 on disordering is -0.0024 Å, that in c_0, $+0.037$ Å (Table 1). One might suspect that these slight differences resulted from a sampling or mixing error—it need involve only about 0.2 mol percent $CdCO_3$—were it not for the fact that the two axial lengths change in

opposite directions and that comparable effects, discussed below, are observed for dolomite. Actually, Goldsmith's mixing was achieved by prolonged hand mulling of small portions under alcohol, a method that leaves little reason to distrust the stated compositions.

The a_0 and c_0 cited for dolomite in Table 1 and used in computations elsewhere in this paper, 4.8079 and 16.010 Å, respectively, are those derived by Goldsmith and Graf (1958*b*) from study of several analyzed single-crystal dolomite samples. Goldsmith and Graf have discussed the relations between these values and those derived by averages of the a_0 values and of the c_0 values for calcite and magnesite. These averages also are included in Table 1.

The most probable Δa_0 and Δc_0 values for largely but not completely disordered materials having essentially the composition $CaMg(CO_3)_2$ are respectively, -0.003 Å and $+0.03_5$ Å (Goldsmith *et al.*, 1961). Most of the measurements were made on films taken with a Guinier-type focusing camera; the uncertainty in Δa_0 resulting from a possible Guinier measurement error on each pattern of the smallest unit recorded, 0.05 mm, is ± 0.0018 Å, and in c_0 is ± 0.006 Å.

The agreement among Δa_0 and Δc_0 values for the various $CaMg(CO_3)_2$ and $CdMg(CO_3)_2$ samples is good, in view of the difficulty in making accurate measurements on imperfectly crystallized materials and the fact that neither the compositions of the several dolomite samples nor the amounts of residual order remaining in them after quenching from temperatures near 1125° C. are precisely the same. Any variation that may exist in Δa_0 and Δc_0 with slight departures from equimolar composition is masked by the experimental uncertainty.

No 1:1 ordered calcium iron carbonate has yet been described, but a_0 and c_0 values predicted from those for $FeCO_3$ and $CaCO_3$ are presented in Table 1 because of their possible usefulness in studies of ferroan dolomite. The ordered compound $CaMn(CO_3)_2$, kutnahorite, is present in nature in well crystallized specimens, but none of the single-phase samples yet studied is sufficiently free of Mg and Fe in solid solution to permit precise comparison with predicted values. Order reflections for this composition can be detected with certainty only in single-crystal *x*-ray diagrams, so that it has not proved possible to determine whether ordered synthetic powders have been prepared. However, at a sufficiently high temperature, by analogy with single-crystal experiments (Goldsmith and Graf, unpublished data), one can be certain that such a powder is disordered, and values are given in Table 1 for a sample of this kind.

Reliability of Cell Constants

The extrapolated cell constants presented here and by Goldsmith and Graf (1958*b*) for materials recrystallized at high temperatures appear to

differ from comparable published data, and also among themselves where measurements of the same constant were made with several radiations, by from 0.0001 to 0.0003 Å in a_0 and by 0.001 or 0.001_5 Å in c_0, or from 2.5 to 10 parts per 100,000. The maximum uncertainty in the temperature for which cell constants are valid is $26 \pm 3°$ C., the range of temperature encountered in the laboratory where the films were taken, which is air-conditioned in summer. The correction for these materials for a temperature difference of 5° C., based upon available thermal expansion data, would be about 0.0001 Å in a_0 and about 0.002 Å in c_0, values comparable with the differences mentioned above.

The cell constants presented here should be satisfactory for most geochemical and mineralogical purposes, but they may not be adequate for some studies of defects in these solids. The extent to which they can be further refined appears to be limited by poor crystallinity for materials formed at moderate temperatures. Less than perfect cation ordering in 1:1 compounds such as dolomite appears, in principle, to be present in greater or lesser amount at all temperatures (Goldsmith and Graf, 1958*b*), and places a further limit on the accuracy with which cell constants can be obtained for these materials.

Interplanar Spacings

The a_0 and c_0 values selected for use in calculating d-values, typically those for well crystallized high-temperature materials giving the most accurate $\cos^2\theta$ extrapolations, are given in Table 1 together with a_{rh} and α values for the rhombohedral cells.

Table 2 includes all possible reflections of the carbonates listed there using Cu$K\alpha_1$ radiation. A list of such reflections was first prepared for a hypothetical dolomite-type structure having the a_0 and c_0 of $CaCO_3$. Deletions from this list were then made of reflections forbidden for calcite-type structures, and of reflections with $d < 0.77025$ for the carbonates with smaller cells. The spacings listed for $CaCO_3$ by Andrews (1950) and Swanson and Fuyat (1953), for $CaMg(CO_3)_2$ by Howie and Broadhurst (1958), for $MnCO_3$ by Goldsmith and Graf (1957) and Swanson *et al.* (1957), for $CdCO_3$ and $MgCO_3$ by Swanson *et al.* (1957), for $ZnCO_3$ by Swanson *et al.* (1959) and for $CoCO_3$ by Swanson *et al.* (1960) indicate which of the possible reflections for these compounds have sufficient intensity to be readily observed in routine diffraction analyses.

Structure Factors

Calcite belongs to space group $R\bar{3}c$, dolomite to $R\bar{3}$, and the huntite model proposed by Graf and Bradley (In press) to $R32$. The unit cells of these materials contain, respectively, $2CaCO_3$, $Ca > Mg(CO_3)_2$, and $Mg_3Ca(CO_3)_4$. All $\{h_r k_r l_r\}$ are possible reflections for dolomite and for

huntite, but for calcite reflections having $h_r+k_r+l_r$ odd are forbidden unless $h_r \neq k_r \neq l_r$.

Structure factor computations like those which follow are simplified considerably by using the rhombohedral cell. The amplitude contributions to the calcite structure factors, obtained by substituting in the appropriate expression (International Tables for *X*-ray Crystallography, volume 1, 1952, p. 473) for each atom in the rhombohedral unit cell and summing, fall into three types that may be represented by greatly simplified expressions. The types are defined using sign changes of amplitude contributions from atoms whose coordinates do not involve variable parameters, and the zero or non-zero character of amplitude contributions in general. Further definitions involving variable parameters which are very nearly equal to simple fractions could be made, but would break down for higher order reflections. The letter-designated subdivisions are not distinct types, but will be useful in a comparison of calcite, dolomite, and huntite reflection types which follow.

The calcite types are:

1. $(h_r+k_r+l_r)$ divisible by 4
   $2f_{Ca}+2sf_C+2f_O[\cos 2\pi x(h-k)+\cos 2\pi x(k-l)+\cos 2\pi x(l-h)]$
   (1a. Two or three indices alike)
   (1b. $h \neq k \neq l$)
2. $(h_r+k_r+l_r)$ even, but not divisible by 4
   $2f_{Ca}-2f_C-2f_O[\cos 2\pi x(h-k)+\cos 2\pi x(k-l)+\cos 2\pi x(l-h)]$
   (2a. Two or three indices alike)
   (2b. $h \neq k \neq l$)
3. $(h_r+k_r+l_r)$ odd, $h \neq k \neq l$
   $2f_O[\sin 2\pi x(h-k)+\sin 2\pi x(k-l)+\sin 2\pi x(l-h)]$.

These expressions are analogous to those presented by Tahvonen (1947) for the isostructural $NaNO_3$, but with calcium rather than the anion at the origin. Like the amplitude contributions which follow for dolomite and huntite, those for calcite have been divided by an appropriate constant so that they refer to the contents of one unit cell.

From the expression for the dolomite space group, given on page 463 of volume 1 of the International Tables for *X*-ray Crystallography, with calcium at the origin, three simplified expressions for the various types of dolomite reflections may be obtained:

1. $(h_r+k_r+l_r)$ even
   $f_{Ca}+f_{Mg}+2f_C[\cos 2\pi x(h+k+l)]\ 2f_O[\cos 2\pi(hx+ky+lz)+\cos 2\pi(kx+ly+hz)+\cos 2\pi(lx+hy+kz)]$
   (1a. $(h_r+k_r+l_r)$ divisible by 4; 2 or 3 indices alike)
   (1b. $(h_r+k_r+l_r)$ divisible by 4; $h \neq k \neq l$)
   (1c. $(h_r+k_r+l_r)$ even but not divisible by 4; 2 or 3 indices alike)
   (1d. $(h_r+k_r+l_r)$ even but not divisible by 4; $h \neq k \neq l$)

2. $(h_r+k_r+l_r)$ odd, two or three indices alike
   $f_{Ca}-f_{Mg}+2f_C[\cos 2\pi x(h+k+l)]+2f_O$[as in 1]
3. $(h_r+k_r+l_r)$ odd, $h\neq k\neq l$
   $f_{Ca}-f_{Mg}+2f_C[\cos 2\pi x(h+k+l)]+2f_O[\cos 2\pi(hx+ky+lz)+\cos 2\pi(kx+ly+hz)+\cos 2\pi(lx+hy+kz)]$;
   $f_{Ca}-f_{Mg}+2f_C[\cos 2\pi x(h+k+l)]+2f_O[\cos 2\pi(kx+hy+lz)+\cos 2\pi(hx+ly+kz)+\cos 2\pi(lx+ky+hz)]$

Dolomite reflections of type 2, a consequence of cation ordering, are forbidden in calcite. Those of dolomite type 3 are in calcite contributed to exclusively by oxygen.

From the expressions for the space group of the Graf-Bradley huntite model, given on page 466 of volume 1 of the International Tables for *X*-ray Crystallography, with calcium at the origin, the following four simplified expressions for the various types of reflections may be obtained. Lengthy trigonometric expressions which appear within the brackets have been omitted; those indicated by asterisks include both sines and cosines, the others, only cosines:

1. $(h+k+l)$ even, 2 or 3 indices the same
   $f_{Ca}+f_{C_I}+1/3[\ ]f_{C_{II}}+1/3[\ ]f_{Mg}+1/3[\ ]f_{O_I}+1/3[\ ]f_{O_{II}}+2/3[\ ]f_{O_{III}}$
   (a. h, k, l all even numbers)
   (b. Only one even index)
2. $(h+k+l)$ even, $h\neq k\neq l$
   $\sqrt{A^2+B^2}$, where
   $A=$ the expression given under 1
   $B=1/3[*]f_{C_{II}}+1/3[*]f_{Mg}+1/3[*]f_{O_I}+1/3[*]f_{O_{II}}+2/3[*]f_{O_{III}}$
   (2a. h, k, l all even numbers)
   (2b. Only one even index)
3. $(h+k+l)$ odd, 2 or 3 indices the same
   $f_{Ca}-f_{C_I}+\cdots$ remainder as in 1
   (3a. h, k, l all odd numbers)
   (3b. Only one odd index)
4. $(h+k+l)$ odd, $h\neq k\neq l$
   $\sqrt{A^2+B^2}$, where
   $A=f_{Ca}-f_{C_I}+\cdots$ remainder as in 1
   B as in 2
   (4a. h, k, l all odd numbers)
   (4b. Only one odd index)

Table 9 gives correlations among the several groups of reflections which have been described for calcite, dolomite, and huntite.

The number of cooperating planes for the various types of calcite and huntite powder reflections, expressed in hexagonal indices, is (See Internationale Tabellen, 1935, p. 502): $\{hkil\}$, 2·12; $\{hh2\bar{h}l\}$, 12; $\{0k\bar{k}l\}$, 2·6; $\{hki0\}$, 12; $\{hh2\bar{h}0\}$, 6; $\{0k\bar{k}0\}$, 6; $\{000l\}$, 2. For dolomite powder reflections the analogous values are: $\{hkil\}$, 4·6; $\{hh2\bar{h}l\}$, 2·6; $\{0k\bar{k}l\}$, 2·6; $\{hki0\}$, 2·6; $\{hh2\bar{h}0\}$, 6; $\{0k\bar{k}0\}$, 6; $\{000l\}$, 2. The 4·6 and 2·6

entries for dolomite indicate that atoms in general positions, namely, oxygens, will scatter with a different amplitude for some of the co-operating planes of a given $\{hkil\}$, $\{hh2\bar{h}l\}$, or $\{hki0\}$ reflection than for others.

Zero amplitudes result for particular sets of planes whose hexagonal indices do not transform to whole-number rhombohedral indices. Thus, there are for dolomite only two non-zero oxygen amplitudes for $\{21\cdot4\}$ and only one for $\{02\cdot7\}$. These relations are somewhat more simply stated in terms of rhombohedral indices: two non-zero oxygen amplitudes

TABLE 9. CORRELATION OF POWDER REFLECTION TYPES FOR THREE RHOMBOHEDRAL STRUCTURE CELLS (see text)

Calcite	Dolomite	Huntite
1*a*	1*a*	1*a*
1*b*	1*b*	2*a*
2*a*	1*c*	3*a*
2*b*	1*d*	4*a*
	2	
3	3	
		1*b*
		2*b*
		3*b*
		4*b*

result for all dolomite $\{h_rk_rl_r\}$ in which $h_r \neq k_r \neq l_r$, except for $\{h0\bar{h}\}$ reflections, which have a unique oxygen amplitude. The occurrence of zero amplitudes for calcite and huntite is such that there is only one non-zero oxygen amplitude for each $\{h_rk_rl_r\}$.

The amplitude contributions for calcite given in Table 3 have been calculated by using the value of $x=0.2578$ (corresponding to a C—O distance of 1.286 Å) given by Chessin and Post (1958). Sass *et al.* (1957) obtained closely similar values, $x=0.2593\pm0.0008$ and C—O $=1.294\pm0.004$ Å. The amplitude contributions for dolomite derive from Steinfink and Sans' (1959) oxygen parameters, $x=0.2374\pm0.0068$, $y=-0.0347\pm0.0068$, and $z=0.2440\pm0.00017$, and their value of $z=0.2435\pm0.00031$ for carbon, all in terms of the hexagonal unit cell. The corresponding values for the rhombohedral unit cell upon which the discussion in this paper is based are $x_0=0.4814$, $y_0=-0.0281$, $z_0=0.2787$, and $x_c=0.2435$. The C—O distance for dolomite corresponding to these parameters is 1.283 Å, in particularly good agreement with Chessin and Post's value. All three of the parameter determinations are based

upon single-crystal measurements. Those for calcite involve oxygen-only reflections, and those for dolomite are based on some 500 reflections of all types.

The variable parameters used for the other calcite structures (Table 10) were calculated by assuming that the C—O bond length remains constant at 1.286 Å; the parameter $x = \text{C—O}/a_0$. The dolomite x and y hexagonal unit-cell parameters were multiplied by the ratio of a_0 for $CaMg(CO_3)_2$ to that of a_0 for $CdMg(CO_3)_2$, so as to retain in $CdMg(CO_3)_2$ the same C—O value of 1.283 Å found for dolomite. In the absence of evidence for making other assumptions, the dolomite z parameters for

TABLE 10. ESTIMATED VARIABLE PARAMETERS USED IN INTENSITY CALCULATIONS

$MgCO_3$	$x=0.2776$			$CdCO_3$	$x=0.2614$
$MnCO_3$	$x=0.2692$			$CoCO_3$	$x=0.2761$
$FeCO_3$	$x=0.2743$			$NiCO_3$	$x=0.2797$
$ZnCO_3$	$x=0.2764$			$CuCO_3$	$x=0.2681$*
$CaMn(CO_3)_2$	$x=0.2635$			$CaFe(CO_3)_2$	$x=0.2657$
$CaMn(CO_3)_2$	$x_0=0.4779$,	$y_0=-0.0241$,	$z_0=0.2782$,	$x_C=0.2435$	
$CaFe(CO_3)_2$	$x_0=0.4799$,	$y_0=-0.0264$,	$z_0=0.2785$,	$x_C=0.2435$	
$CdMg(CO_3)_2$	$x_0=0.4829$,	$y_0=-0.0298$,	$z_0=0.2789$,	$x_C=0.2435$	

* Using the a_0 value given by Pistorius (1960).

oxygen and carbon were retained for $CdMg(CO_3)_2$, as was the slight rotation of the carbonate group relative to the hexagonal a axes, and the parameters for the hexagonal cell were then converted to values for the rhombohedral cell. Coplanarity of carbon with the oxygens of its carbonate group is not required by symmetry for the dolomite structure as is the case for calcite. The reality of the 0.0005 difference between the Steinfink and Sans z parameters for oxygen and carbon is indeterminate, because the uncertainty ranges attached to these values are just great enough to allow for coplanarity at $z=0.2438$. The intensity difference for this shift of carbon by about 0.01 Å is, in any event, insignificant compared with other sources of error.

Parameter assumptions of the same type as those for $CdMg(CO_3)_2$ were used in calculating the values given in Table 10 for dolomite structures having the compositions $CaMn(CO_3)_2$ and $CaFe(CO_3)_2$. These parameters involve a further approximation because, as discussed earlier, the a_0 values available for the calculations were not measured on ordered compounds. The a_0 available for $CaMn(CO_3)_2$ is that for disordered material, that for $CaFe(CO_3)_2$, merely the mean of the values for calcite and siderite. However, these parameters are the best that can

be derived at present for making intensity estimates for order reflections. Parameter estimates for calcite-type structures having the compositions $CaMn(CO_3)_2$ and $CaFe(CO_3)_2$ are also shown in Table 10.

The variable parameters given by Graf and Bradley (In press) for a huntite structure model derived from powder x-ray diffraction data are, for the rhombohedral unit cell, $x_{Mg}=0.541$, $x_{C_{II}}=-0.039$, $x_{O_I}=0.365$, $x_{O_{II}}=0.096$, $x_{O_{III}}=-0.033$, $y_{O_{III}}=0.180$, $z_{O_{III}}=0.371$.

Intensities

Intensities of front reflections in powder diagrams of the rhombohedral carbonates, computed for copper radiation, are given in Table 4. The change of intensities in the solid solution series between $CaMg(CO_3)_2$ and the hypothetical end member, $CaFe(CO_3)_2$, is shown graphically in Fig. 1. Estimated changes in cell size with composition have been considered in the ferroan dolomite computations, but these computations do not allow for departure of $CaCO_3$ content from 50 mol percent.

These intensities are simply the products of F^2 times multiplicity times the combined Lorentz and polarization correction for Debye-Scherrer lines on a cylindrical film,

$$\frac{1+\cos^2 2\theta}{\sin^2\theta\cos\theta}.$$

Absorption and temperature factors have not been considered, but could be added as corrective multipliers suitable for a given experimental situation. The scattering factors given by Berghius *et al.* (1955) were used for C, O, Ca, and Mg^{++}, all self-consistent field data with exchange, with the curve for Mg^{++} at $(\sin\theta/\lambda)<0.25$ diverted toward the value for the neutral Mg atom at $\sin\theta/\lambda=0$. Watson and Freeman (1961) give self-consistent field data with exchange for Mn, Fe, Co, Ni, and Cu^{+}; the latter curve at $(\sin\theta/\lambda)<0.25$ has been diverted toward the value for the neutral Cu atom at $\sin\theta/\lambda=0$.

The curve of Berghius *et al.* for Zn, based on self-consistent field data *without* exchange, gives expectably low values relative to the curves computed with exchange; it is essentially coincident with the Cu curve over part of the $\sin\theta/\lambda$ range. The values for Zn used in this paper were taken from a curve drawn, at each $\sin\theta/\lambda$ value, the same distance above the Cu curve as the separation between the Cu and Ni curves at that point. The scattering factor curve used for Cd, the only recent one available, was computed by Thomas and Umeda (1957) from the Thomas-Fermi-Dirac model.

These scattering factor curves fall off in generally concordant fashion and make it possible to observe the effect of progressively heavier cations upon the relative intensities of the various carbonate reflections. These

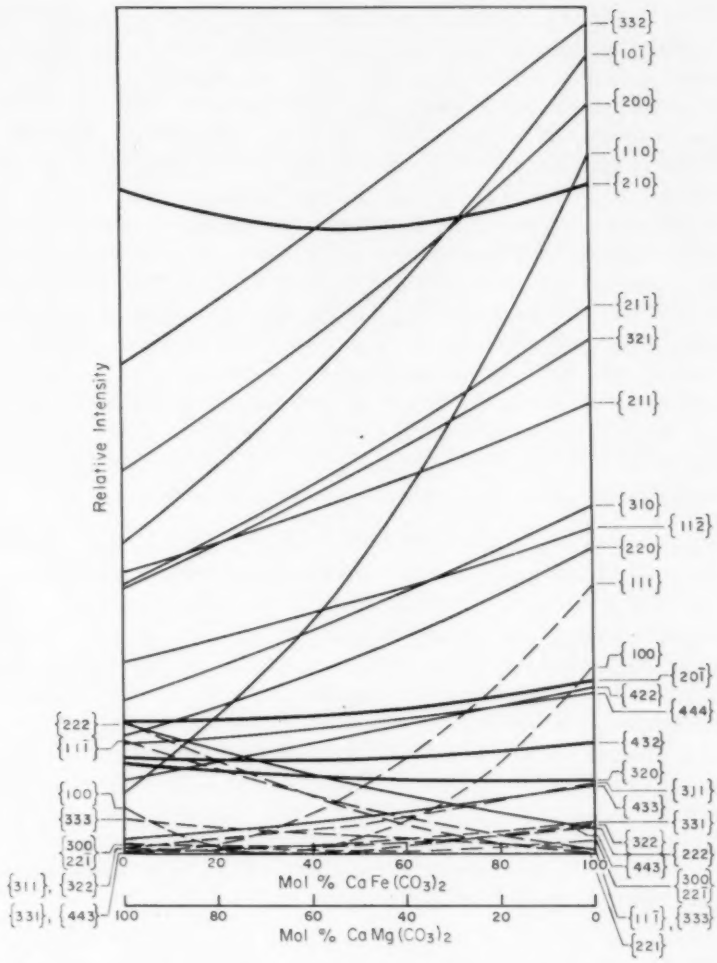

FIG. 1. Computed relative intensities for powder reflections in the front reflection region, using copper radiation, for the solid solution series between $CaMg(CO_3)_2$ and the hypothetical end-member, $CaFe(CO_3)_2$. Order reflections are shown by dashed lines, strong oxygen reflections by heavy lines. The intensity of the very strong {211} reflection is plotted reduced by a factor of ten relative to those of the other reflections; that of {321}, reduced by a factor of two.

relations are modified somewhat by differences in atomic arrangement in the related calcite, dolomite, and huntite structures. The increase in intensity of the $CdMg(CO_3)_2$ order reflections relative to those of the other ordered 1:1 carbonates is noteworthy.

The computed intensities of Table 4 and Fig. 1 are based upon a simplified model essentially involving spherical neutral atoms at rest, in accord with the empirical observation that observed intensities are better explained using neutral-atom scattering factor curves than those for ions. The radically different solubility rates of, for example, $CaCO_3$ and $NiCO_3$ in HCl solution indicate that an error is introduced for reflections at $(\sin \theta/\lambda) < 0.25$ by this uniform bonding approximation. The determination of scattering factor curves appropriate for specific carbonate structures is, however, beyond the scope of this paper. The third figure given in the computed intensities is obviously not generally significant, but may have meaning, for example, in computing an intensity ratio for two reflections of the same compound which lie at about the same 2θ angle and have similar structure factors.

It should be noted, in comparing observed intensities of two or more carbonates with the equivalent computed values in Table 4, that the observed values must be suitably corrected so that they all represent intensity diffracted from the same number of unit cells.

Acknowledgments

I am particularly indebted to J. R. Goldsmith for treating some of the samples in a squeezer-type apparatus and for taking many of the films upon which the measurements were made; to W. F. Bradley for many helpful suggestions made during the course of the calculations; to Daniel Appleman for using a computer program to prepare a list of all possible calcite reflections, as a check on the list arrived at by hand calculation; and to Juanita Witters, L. D. McVicker, and D. R. Dickerson for spectrographic and chemical analyses. C. S. Hurlbut, Jr., supplied the sample of single-crystal smithsonite from Broken Hill, Rhodesia; Brian Skinner, huntite from Tea Tree Gully, South Australia; George T. Faust, huntite from Currant Creek, Nevada. Permission from Dr. Goldsmith and Miss Isaacs to quote their results is gratefully acknowledged.

References

Andrews, K. W. (1950), An *x*-ray examination of a sample of pure calcite and of solid-solution effects in some natural calcites: *Mineral. Mag.*, **29**, 85–89.

Austin, J. B., Saini, H., Weigle, J., and Pierce, R. H. H. (1940), Direct comparison on a crystal of calcite of the *x*-ray and optical interferometer methods of determining linear thermal expansion: *Phys. Rev.*, **57**, 931–933.

Berghius, J., Jbertha, I., Haanappel, M., Potters, M., Loopstra, B. O., McGillavry, C. H., and Veenendall, A. L. (1955), New calculation of atomic scattering factors: *Acta Cryst.*, **8**, 478–483.

Chessin, Henry, and Post, Ben (1958), Positional parameter and thermal motions of oxygen atoms in calcite (Abst.): Annual Meeting of the American Crystallographic Association, Milwaukee, Wisconsin, June 23–27, 1958.

FREEMAN, A. J. (1959), Atomic scattering factors for spherical and aspherical charge distributions: *Acta Cryst.*, **12,** 261–271.

FREEMAN, A. J., AND WOOD, J. H. (1959), An atomic scattering factor for iron: *Acta Cryst.*, **12,** 271–273.

GOLDSMITH, J. R. (1958), Cadmium-dolomite and the system $CdCO_3$—$MgCO_3$: *Geol. Soc. Amer. Bull.*, **69,** 1570–1571.

GOLDSMITH, J. R., AND GRAF, D. L. (1957), The system CaO—MnO—CO_2: solid solution and decomposition relations: *Geochim. et Cosmochim. Acta*, **11,** 310–334.

GOLDSMITH, J. R., AND GRAF, D. L. (1958a), Structural and compositional variations in some natural dolomites: *Jour. Geology*, **66,** 678–693.

GOLDSMITH, J. R., AND GRAF, D. L. (1958b), Relation between lattice constants and composition of the Ca-Mg carbonates: *Am. Mineral.*, **43,** 84–101.

GOLDSMITH, J. R., GRAF, D. L., AND HEARD, H. C. (1961), Cell constants of the calcium magnesium carbonates: *Am. Mineral.*, **46,** 453–457.

GOLDSMITH, J. R., GRAF, D. L., AND JOENSUU, O. I. (1955), The occurrence of magnesian calcites in nature: *Geoch. et Cosmoch. Acta*, **7,** 212–230.

GRAF, D. L., BLYTH, C. R., AND STEMMLER, R. S. (1957), Mixed-layer effects in the rhombohedral carbonates: *Geol. Soc. Amer. Bull.*, **68,** 1737–1738.

GRAF, D. L., BLYTH, C. R., AND STEMMLER, R. S. (1958), Mixed-layer computations using ILLIAC: The three-layer case: *Geol. Soc. Amer. Bull.*, **69,** 1572.

GRAF, D. L., AND BRADLEY, W. F., The crystal structure of huntite, $Mg_3Ca(CO_3)_4$: In Press, *Acta Cryst.*

GRAF, D. L., EARDLEY, A. J., AND SHIMP, N. F. (1961), A preliminary report on magnesium carbonate formation in glacial Lake Bonneville: *Jour. Geology*, **69,** 219–223.

GRAF, D. L., AND GOLDSMITH, J. R. (1956), Some hydrothermal syntheses of dolomite and protodolomite: *Jour. Geology*, **64,** 173–186.

GRAF, D. L., AND LAMAR, J. E. (1955), Properties of calcium and magnesium carbonates and their bearing on some use of carbonate rocks: *Econ. Geol.*, **Fiftieth Anniversary Volume**, 639–713.

GRIGGS, D. T., AND KENNEDY, G. C. (1956), A simple apparatus for high pressures and temperatures: *Amer. Jour. Sci.*, **254,** 722–735.

HARKER, R. I., AND TUTTLE, O. F. (1955), Studies in the system CaO—MgO—CO_2: Part 2. Limits of solid solution along the binary join, $CaCO_3$—$MgCO_3$: *Amer. Jour. Sci.*, **253,** 274–282.

HOWIE, R. A., AND BROADHURST, F. M. (1958), *X*-ray data for dolomite and ankerite: *Am. Mineral.*, **43,** 1210–1214.

HURLBUT, C. S. (1954), Smithsonite from Broken Hill Mine, Rhodesia: *Am. Mineral.*, **39,** 47–50.

INTERNATIONAL TABLES FOR *X*-RAY CRYSTALLOGRAPHY (1952), The Kynoch Press, Birmingham, England, vol. I.

INTERNATIONALE TABELLEN ZUR BESTIMMUNG VON KRISTALLSTRUKTUREN (1935), Gebrüder Borntraeger, Berlin, vol. II.

LEHOVEC, KURT (1953), Space-charge layer and distribution of lattice defects at the surface of ionic crystals: *Jour. Chem. Physics*, **21,** 1123–1128.

PISTORIUS, C. W. F. T. (1959), High pressure preparation and structure of crystalline nickelous carbonate: *Experientia*, **15,** 328–329.

PISTORIUS, C. W. F. T. (1960), Synthesis at high pressure and lattice constants of normal cupric carbonate: *Experientia*, **16,** 447–448.

RAMDOHR, P., AND STRUNZ, H. (1941), Isomorphie von Otavite mit Kalkspat: *Zentralbl. Min.*, **A,** 97–98.

RYMER, T. B. (1957), The lattice constants of small crystals: *Nuovo Cimento*, **VI** (Suppl.), 294–305.

SAINT LÉON LANGLÈS, RENÉ DE (1952), Préparation et structure du carbonate neutre de nickel anhydre cristallisé: *Ann. chim.* (*Paris*), *ser. 12*, **7**, 568–583.

SASS, R. L., VIDALE, R., AND DONOHUE, J. (1957), Interatomic distances and thermal anisotropy in sodium nitrate and calcite: *Acta Cryst.*, **10**, 567–570.

SHARP, W. E. (1960), The cell constants of artificial siderite: *Am. Mineral.*, **45**, 241–243.

STEINFINK, H., AND SANS, F. J. (1959), Refinement of the crystal structure of dolomite: *Am. Mineral.*, **44**, 679–682.

SWANSON, H. E., COOK, M. I., EVANS, E. H., AND DE GROOT, J. H. (1960), Standard *x*-ray diffraction powder patterns: *U. S. National Bureau of Standards, Circ. 539*, **10**.

SWANSON, H. E., AND FUYAT, R. K. (1953), Standard *x*-ray diffraction powder patterns: *U. S. National Bureau of Standards, Circ.* 539, **2**.

SWANSON, H. E., GILFRICH, N. T., AND COOK, M. I. (1957), Standard *x*-ray diffraction powder patterns: *U. S. National Bureau of Standards, Circ. 539*, **7**.

SWANSON, H. E., GILFRICH, N. T., COOK, M. I., STINCHFIELD, ROGER, AND PARKS, P. C. (1959), Standard *x*-ray diffraction powder patterns: *U. S. National Bureau of Standards, Circ. 539*, **8**.

TAHVONEN, P. E. (1947), (The crystal structure of sodium nitrate and the atom form-factors of the atoms in the nitrate group): *Annales Acad. Scientiarum Fennicae*, 1 (Mathematica-Physica), 3–25.

TAYLOR, A., AND SINCLAIR, H. (1945), On the determination of lattice parameters by the Debye-Scherrer method: *Proc. Phys. Soc. London*, **57**, 126–135.

THOMAS, L. H., AND UMEDA, K. (1957), Atomic scattering factors calculated from the TFD atomic model: *Jour. Chem. Physics*, **26**, 293–303.

VERWEY, E. J. W. (1946), Lattice structure of the free surface of alkali halide crystals: *Rec. trav. chim.*, **65**, 521–528.

WATSON, R. E., AND FREEMAN, A. J. (1961), Hartree-Frock atomic scattering factors for the iron transition series: *Acta Cryst.*, **14**, 27–37.

Manuscript received Jan. 17, 1961.

THE AMERICAN MINERALOGIST, VOL. 46, NOVEMBER–DECEMBER, 1961

REACTION OF CRYSTAL STRUCTURES AND REACTION FABRIC

W. R. LAUDER, *Victoria University of Wellington, Wellington, New Zealand.*

ABSTRACT

Reaction fabric is the fabric resulting from the control of the orientation of one mineral by another. It may be produced by exsolution, simultaneous crystallization, parallel growth, and replacement. Such fabrics can be shown on a contoured reaction fabric diagram, which indicates the orientation of one mineral with respect to another that has known orientation. The reaction fabric diagrams of quartz with respect to microcline in micrographic intergrowth, and of albite with respect to labradorite which it replaces, indicate that there is some control of the orientation of quartz by microcline and albite by labradorite.

INTRODUCTION

When one mineral replaces another some ions from the host mineral often form part of the guest mineral. It is possible, therefore, that the orientation of the crystal structure of the guest will be influenced by the orientation of the structure of the host mineral. Control of the orientation of one mineral by another results in what is termed, in this paper, reaction fabric.

Reaction fabric is most readily recognized in crystals which contain chains, sheets, or bands of SiO_4 tetrahedra. These structural elements often determine the position of cleavages and the crystallographic form of a mineral, and the relative orientation of the guest and host can be obtained by reference to these properties, *e.g.* in the uralitization of pyroxene bands in the amphibole structure are sometimes parallel to the chains in the pyroxene structure (Fig. 1).

When considering minerals such as quartz and felspar, however, recourse must be made to the detailed optics of pairs of minerals for the determination of their relative orientation. Although the principal axes of the optical indicatrix do not, in general, coincide with chains, bands, and sheets of ions in such minerals, the relations between structural elements and optical properties are well known, and when using the stereographic net, deviation is easily allowed for. The purpose of this paper is to show how by using the optic properties of minerals the reaction fabric can be determined.

CONSTRUCTION OF THE REACTION FABRIC DIAGRAM

Hornblende granophyres from Pepin Island, Nelson, New Zealand, contain about thirty per cent of a micrographic intergrowth of quartz and microcline. Using the universal stage, the following procedure has

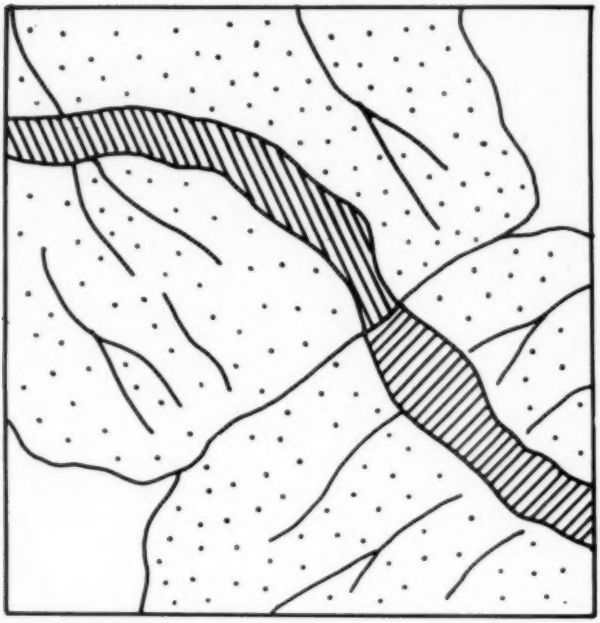

FIG. 1. A uralite vein (lined) crossing two pyroxene crystals (stippled). The fibres of uralite are parallel to the cleavage in the pyroxene.

been used to obtain the equal area plot of the reaction fabric of the *c* axis of quartz (E_q) with respect to the *X* indicatrix axis for microcline ($\doteqdot a$), here described X_m, in the intergrowths.

(*a*) Determine the positions of two of the indicatrix axes for microcline (X_m, Y_m, and Z_m) in an intergrowth and plot of a Schmidt net (Fig. 2A).

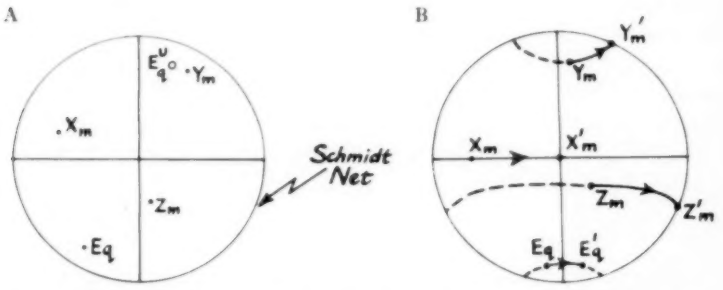

FIG. 2. Plotting of poles on the reaction fabric diagram. X_m, Y_m, and Z_m are *X*, *Y*, and *Z* of microcline. *E* is *e* of quartz. E_q^u is upper hemisphere. Other points are lower hemisphere.

The position of the third vibration direction is obtained by intersection.

(*b*) Determine the position of the *c* axis of quartz (E_q) in the same intergrowth and plot both upper and lower hemisphere poles on the same sheet as the microcline (Fig. 2A).

(*c*) Rotate the plot to bring X_m vertical (Fig. 2B; cf. Phillips 1953, p. 28). X_m', Y_m', and Z_m' are the new positions of X_m, Y_m, and Z_m, and E_q' is the new position of E_q. (Note:—$X_m \wedge X_m' = Y_m \wedge Y_m' = Z_m \wedge Z_m' =$

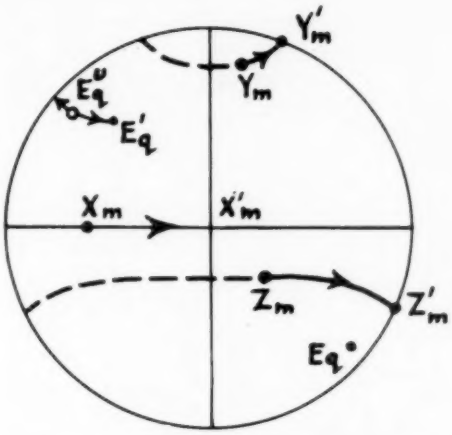

FIG. 3. Plotting of poles on the reaction fabric diagram. X_m, Y_m, and Z_m are X, Y, and Z of microcline. E_q^u is upper hemisphere plot of *e* for quartz. Other points are lower hemisphere.

$E_q \wedge E_q'$). If during rotation the lower hemisphere pole of quartz (E_q) moves on to the upper hemisphere, rotate the upper hemisphere pole E_q^u (Fig. 3).

(*d*) Orient the plot so that the Y vibration direction of microcline coincides with the N-S diameter of the net (Fig. 4A).

E_q'' is not a unique position for the *c* axis of quartz. There are four positions for a point so derived as shown in Fig. 5. In this diagram the ends of the vibration directions are differentiated to allow the rotations to be reconstructed. This is not so in practice and the four poles are identical. In plotting the reaction fabric diagram all poles have been transferred to the lower left hand quadrant *e.g.* E_q''' (Fig. 4B).

(*e*) The point E_q''' is now transferred to a new plot (Fig. 4B).

By using the above procedure one hundred *c* axes of quartz have been plotted and the contour diagram drawn (Fig. 6). This gives a reaction fabric diagram of quartz with respect to microcline in micrographic intergrowth.

THE STRUCTURE OF QUARTZ AND MICROCLINE

(*a*) Quartz (Bragg 1937, p. 83).

Quartz has a three dimensional framework with ε (the slow-ray vibration direction) parallel to the c crystal axis. There are spiral chains of SiO_4 tetrahedra with their spiral axes parallel to the c axis and these chains turn in opposite directions for right- and left-handed quartz.

(*b*) Microcline (cf. Orthoclase, Bragg 1937, p. 232).

Microcline has a three dimensional framework with the X vibration direction 5°–10° from the a crystal axis. Two cleavages (010 and 001)

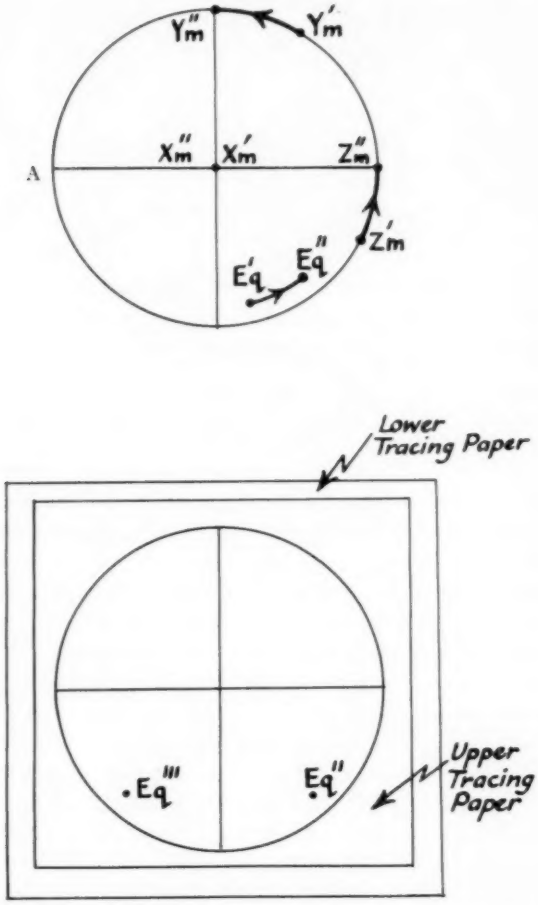

FIG. 4. Plotting of poles on the reaction fabric diagram. X_m, Y_m, and Z_m are X, Y, and Z of microcline. E_q is ε of quartz. Lower hemisphere plot.

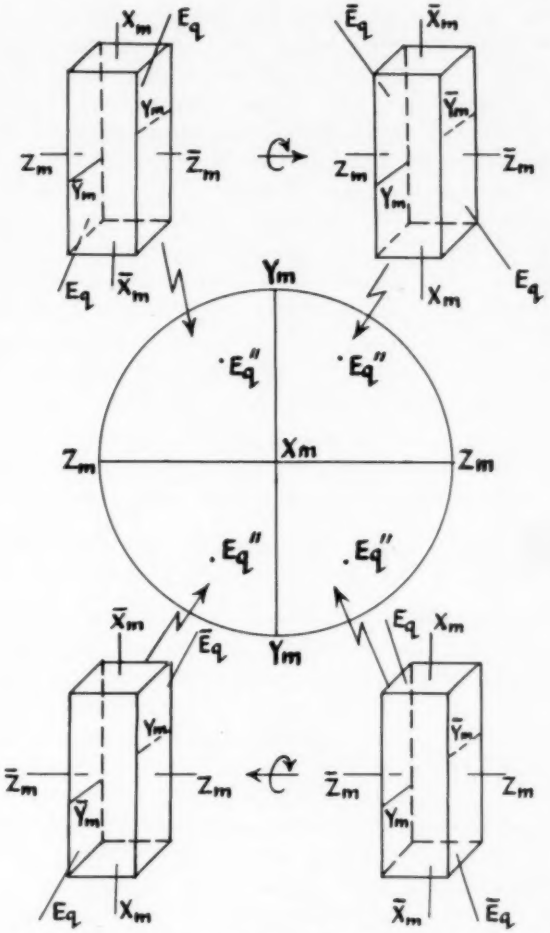

FIG. 5. Four equivalent positions for E_q'', cf. Fig. 4B. Lower hemisphere plot. X_m, Y_m and Z_m are X, Y, and Z of microcline. E_q is $e(=c)$ of quartz.

are parallel to a and these cleavage planes have a high concentration of K^+ ions. Zig-zag chains of SiO_4 tetrahedra run parallel to the a axis, $Y \doteqdot c$ and $Z \doteqdot b$.

INTERPRETATION OF THE REACTION FABRIC DIAGRAM OF QUARTZ WITH RESPECT TO MICROCLINE IN MICROGRAPHIC INTERGROWTH

Figure 6 is a reaction fabric diagram of the c axes of quartz with respect to microcline in micrographic intergrowth. The poles are dis-

tributed over the whole quadrant. This indicates that there is no single direction in microcline along which the *c* axes of quartz are oriented. However, there is a significant concentration of poles on the primitive. In this concentration the *c* axes of quartz are oriented more or less perpendicular to the *a* axis of microcline (a_m) and at about 45° to the *b* and *c* axes of microcline (b_m and c_m). Thus the spiral chains in the quartz structure are more or less perpendicular to the zig-zag chains in microcline and they intersect the cleavages in microcline at about 45°. By reference to the crystal structure model of microcline, it appears that the *c* axes of quartz in this concentration lie in the 001 plane of the felspar.

Micrographic intergrowth probably can be formed either by replacement or by simultaneous crystallization, and in either case a reaction fabric could be produced. In the replacement of microcline ($KAlSi_3O_8$) by quartz it is necessary to eliminate the K^+ ion and substitute silicon

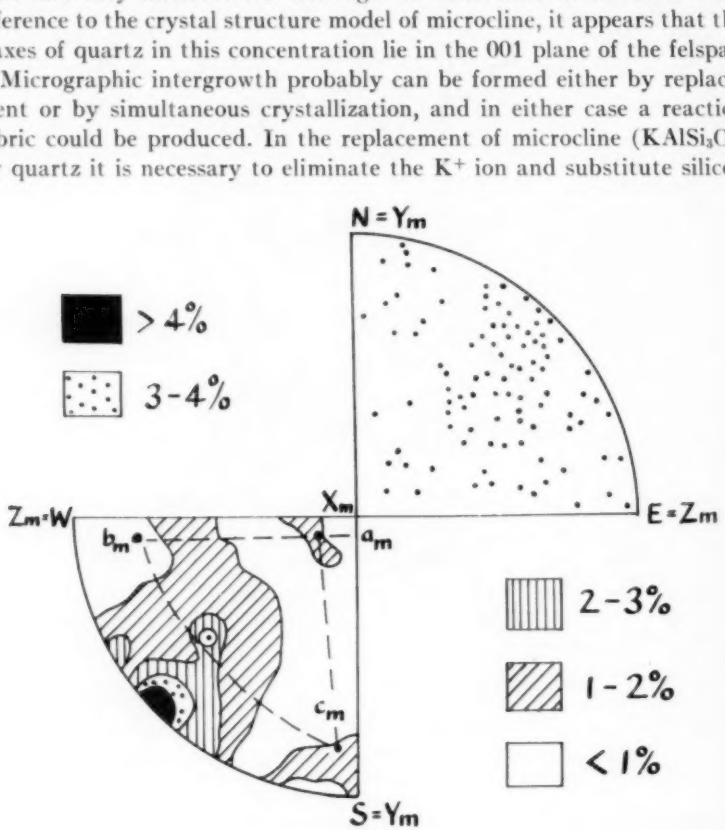

FIG. 6. The reaction fabric diagram of the *c* axis of quartz in micrographic intergrowth with microcline when the *X* vibration direction of microcline is vertical. X_m, Y_m, and Z_m are *X*, *Y* and *Z* for microcline. a_m, b_m, and c_m are *a*, *b* and *c* of microcline. Poles plotted and contour diagram. The four per cent contour encloses four per cent of 400 poles, *i.e.*, 16 poles.

for aluminium in the tetrahedra of the framework. The concentration of the *c* axes of quartz in the 001 plane of microcline suggests that the concentration of Si-O and Al-O tetrahedra in this plane has allowed the substitution to take place without complete disruption of the silicate framework. It might perhaps be expected that if this were the case the *c* axis would grow in this plane and parallel to the 010 cleavage. That this is not so suggests that the bonds in the framework which cross the 010 cleavage plane, although few in number, are Si-O rather than Al-O bonds. This allows the bridging of the cleavage planes without disruption of the silicate framework.

If simultaneous crystallization produced the intergrowths, then it is possible that the quartz nuclei encrusted the 001 plane of the microcline with a concentration of *c* axes parallel to 001 and at 45° to 010. However, in vugs and veins quartz crystals tend to grow so that the *c* axes are more or less perpendicular to the surface on which they start crystallization. It is unlikely, therefore, that the reaction fabric was produced by growth of quartz crystals on either the 001, or the 010, plane of the microcline.

The Reaction Fabric Diagram of the *a* Axis of Albite with Respect to Labradorite Which It Replaces

In basalts of Markle Type from Arthur's Seat, Edinburgh (Clark 1956), many of the labradorite phenocrysts are partially replaced by albite. The mineral fabric diagram of the *a* axes of albite with respect to the labradorite has been derived in the following way:—

For any one crystal the position of the *X*, *Y* and *Z* indicatrix directions of albite and labradorite were measured and plotted on a Schmidt net. The position of the *a* axis of ablite was located in relation to the vibration directions of that mineral. The plot was then rotated so that the *X* axis of labradorite (X_l) was vertical, the *Z* axis (Z_l) along the E-W diameter of the net, and the *Y* axis (Y_l) along the N-S diameter. The position of the *a* axis of albite was then transferred, if necessary, to the lower left hand quadrant and plotted on a separate oriented sheet.

The Structure of Albite and Laboradorite

The structures of these minerals are similar to that of orthoclase—a three dimensional framework of Si-O and Al-O tetrahedra with zig-zag chains parallel to the *a* crystal axes. The *c* axis of the unit cell of labradorite is twice as long as that in the unit cell of albite.

The Interpretation of the Reaction Fabric Diagram of Albite Replacements of Labradorite

Figure 7 shows a concentration of the poles of the *a* axis of albite in the a–c plane (010) of labradorite with a relatively strong concentration

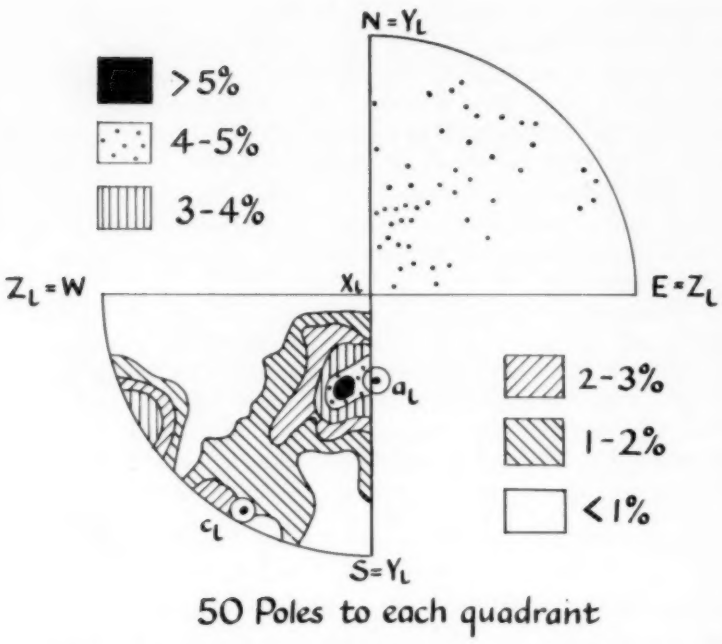

FIG. 7. The reaction fabric diagram of the *a* axis of albite replacing labradorite when the *X* vibration direction of labradorite is vertical. *X*, *Y*, and *Z* are *X*, *Y*, and *Z* of labradorite, and a_l and c_l are *a* and *c* of labradorite. Poles plotted and contour diagram. The five per cent contour encloses five per cent of 200 poles, *i.e.*, 10 poles.

of poles near the *a* axis of labradorite (a_l). This latter concentration suggests that when labradorite is replaced by albite the zig-zag chains in the former retain their identity, and that aluminium is replaced by silicon with only a small modification of the silicate framework. The general concentration of poles in the 010 plane probably indicates that the albite has a tendency to grow along the 010 cleavage.

The Optics of the Plagioclases

In determining the position of the *a* crystal axis of albite and labradorite with respect to the vibration directions of light through the minerals, an interesting relationship between the indicatrix and the *a* crystal axis was noted. Figure 8 shows a lower hemisphere stereographic plot of the *a* axes of plagioclase when the *X*, *Y* and *Z* vibration directions are in the positions shown. The *a* axes lie very close to the plane of *X* and *Y*. Figure 9 shows a lower hemisphere plot of the *XY* planes of the plagioclases when the *a* crystal axis is vertical (cf. Winchell 1951, Fig. 172, p. 274).

The rotation of the XY plane about the a axis in passing from anorthite to albite is worthy of note. Figure 10 is a series of three dimensional diagrams showing how in passing from anorthite to albite there is a clockwise rotation of the XY plane of the indicatrix about the a crystal axis with, at the same time, a rotation of X and Y in a clockwise direction within the plane.

This is a relatively simple way of visualising the position of the indicatrix in the plagioclase and perhaps indicates that the zig-zag chains in the plagioclase structure, which are parallel to the a crystal axes, are exerting some controlling influence over the orientation of the indicatrix.

The Preferred Orientation of Crystal Structures

Preferred orientation of one mineral with respect to another may possibly be brought about by exsolution, simultaneous crystallization, parallel growth, or replacement.

Exsolution

Minerals which form solid solutions contain ions of about equal radius and valency, and have similar crystal structures. When exsolution takes

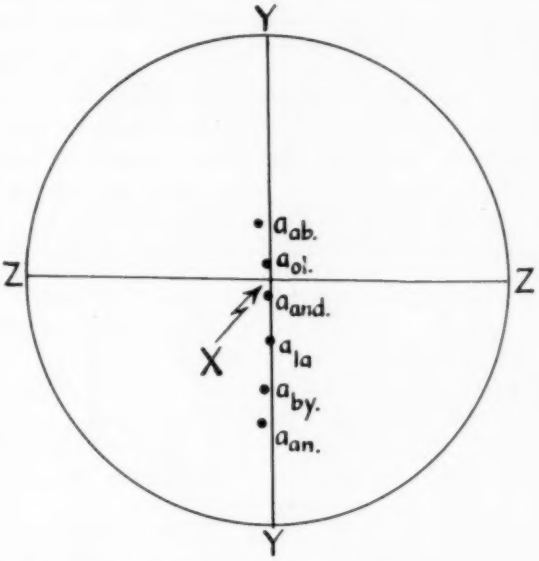

FIG. 8. Optic orientation of the plagioclases. Lower hemisphere, stereographic plot showing the movement of the a axes of the plagioclases in the XY plane. X, Y, and Z are the principal axes of the plagioclase indicatrix. $a_{ab}-a_{an}$ are the a axes of the plagioclases.

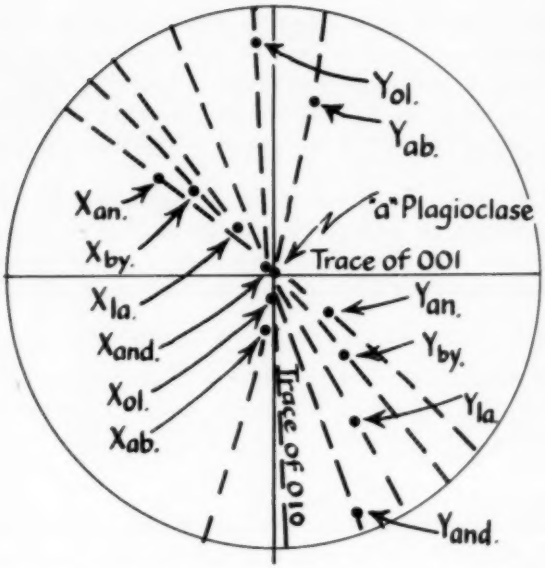

FIG. 9. Optic orientation of the plagioclases. Lower hemisphere stereographic plot showing the rotation of the XY plane of the plagioclases about the a crystal axis. X_{ab-an} and Y_{ab-an} are the X and Y indicatrix axes of the plagioclase.

place the solute and solvent minerals take up relative orientations determined by the structure, *e.g.*, when ilmenite unmixes from magnetite the (0001) planes in the former are parallel to the (111) planes in the latter. Both these planes contain some sheets of oxygen ions which have similar spacing within the sheets (Edwards 1954, p. 76). Again in the perthites the silicate framework is continuous throughout the whole

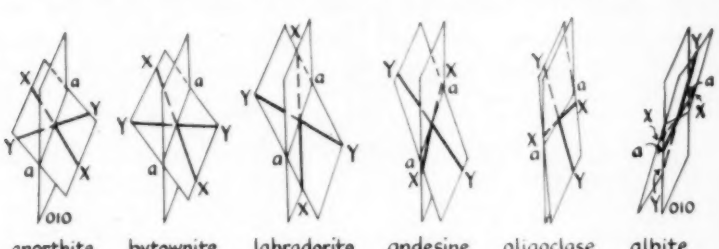

FIG. 10. Optic orientation of the plagioclases. Three dimensional diagram showing the rotation of the XY plane about the a axis in the plagioclases. X and Y are two principal axes of the plagioclase indicatrix.

crystal, the exsolution involving a redistribution of the Na^+ and K^+ ions (Bragg 1937, p. 40).

In both the above cases a reaction fabric diagram of one mineral with respect to the other should give a different but high concentration for each kind of pole.

Simultaneous Crystallization

Simultaneous crystallization usually involves two or more minerals of dissimilar structure. However, it is possible that, in certain cases, crystals may interfere with one another during growth so that one orients the other. Niggli (1954, p. 469) states: "At the outset, because of the Brownian movement, crystal nuclei may impinge on one another and grow by forming aggregates (aggregate growth or initial formation of secondary particles with micellar structure). The mutual orientation of the individual nuclei will be more or less perfect and often only have the character of a twinned intergrowth."

Parallel Growth

In some cases of parallel growth where the minerals have similar crystal structure, relative orientation is obvious from inspection, *e.g.* parallel growth in micas. It is possible also that a reaction fabric may be produced by overgrowth (Niggli 1954, p. 254), and it is apparent from Niggli's figure 150 that the orientation of the hornblende is controlled by the orientation of the augite upon which it has grown (the *c* axes are parallel).

Replacement

Whereas the above three processes are restricted, in general, to igneous rocks and pegmatites, usually as local phenomena, replacement is one of the most common geological processes. Almost all igneous masses show some replacement, whether of metasomatic or autometasomatic origin, and in contract rocks it is almost ubiquitous.

Replacement is generally conceded to be volume for volume, *i.e.*, the amount of a guest required to replace a given host depends on the relative specific gravities. This need not mean a complete destruction of the crystal structure of the mineral being replaced, and in many replacements involving silica and silicates it is probable that associated groups of SiO_4 tetrahedra from the host are incorporated in the guest mineral. Chemical reactions take the line of least resistance. If a mineral is stable under certain conditions of temperature, pressure, and concentration, then it is formed by that process in which least energy is expended. In the replacement of microcline by quartz for example, it is economical of

energy if SiO_4 tetrahedra are retained and built into the quartz with a minimum of reorientation, thus producing a reaction fabric.

References

Bragg, W. L., 1937. Atomic structure of minerals. Cornell University Press, New York.

Clark, R. H., 1956. Petrological study of the Arthur's Seat volcano. Trans. Roy. Soc. Edinburgh, Vol. 63, pp. 37–70.

Edwards, A. B., 1954. Textures of the ore minerals. Australasian Institute of Mining and Metallurgy, Melbourne.

Niggli, P., 1954. Rocks and mineral deposits. W. H. Freeman, San Francisco.

Phillips, F. C., 1954. The use of stereographic projection in structural geology. Edward Arnold, London.

Winchell, A. N., 1951. Elements of optical mineralogy. Part 2. Wiley, New York.

Manuscript received November 18, 1960.

THE AMERICAN MINERALOGIST, VOL. 46, NOVEMBER-DECEMBER, 1961

MONTMORILLONITE: HIGH TEMPERATURE REACTIONS AND CLASSIFICATION

R. E. GRIM AND GEORGES KULBICKI,* *University of Illinois, Urbana, Illinois.*

ABSTRACT

About forty samples of the montmorillonite group of clay minerals were heated to an elevated temperature (1400° C.) and the phase transformations studied by continuous *x*-ray diffraction. Chemical, cation exchange, differential thermal, infra-red, and optical data were obtained also on the samples.

All of the analytical data indicate that the dioctahedral montmorillonites do not form a single continuous isomorphic series. Two different aluminous types have been found, Cheto- and Wyoming-types, which differ primarily in the population of their octahedral layers. Also, it is suggested that some (probably a small number) of the silica-tetrahedra are inverted in the Cheto-type montmorillonite. Cation exchange capacity and other properties are also not the same for the two types.

Some bentonites are mixtures of discrete particles of the two types which can be separated by particle size fractionation.

The high-temperature phase transformations of montmorillonite show large variations depending on the composition and structure of the original material. The transformations are discussed in detail.

INTRODUCTION

The object of the investigation reported herein was to study the successive structural changes taking place when members of the montmorillonite group of clay minerals are heated to their fusion temperature. It was thought that the results of such a study would provide a better understanding of the structure of montmorillonites and the possible variations in their compositions. It was thought also that new light might be obtained on the general matter of solid state reactions in the layer silicates.

The major technique used was continuous high temperature *x*-ray diffraction using a spectrometer. This involved mounting a furnace in the position of the specimen holder in the *x*-ray unit with some manner of controlling and recording the temperature of the furnace. This method has advantages in comparison with a technique that involves heating, then cooling, followed by *x*-ray analysis in that it eliminates uncertainties concerning possible phase changes on cooling. Further it permits the study of the rate of development of new phases, and it is relatively rapid. In some cases *x*-ray diffraction recordings with a camera also were made on quenched samples to check the spectrometer data. The *x*-ray diffraction data were supplemented by differential thermal

* Currently Director of Geological Research, Société Nationale de Pétroles d'Aquitaine, Pau, France.

analyses carried to about 1400° C., infra-red absorption data, and optical determinations. Complete silicate analyses and cation exchange capacities were obtained for the samples.

The montmorillonite clay minerals are very common, being found in many soils, sediments, and hydrothermal alteration products. They are generally the dominant constituents of bentonites. The minerals of this group have a unique, so-called expandable lattice, which has a variable *c*-axis dimension depending on the thickness of layers of water molecules between silicate layers. The structure suggested by Hofmann, Endell, and Wilm (1933), Fig. 1, is made up of silicate layers consisting of two silica tetrahedral sheets tied together through a central sheet containing aluminum and/or magnesium, iron, and occasionally other elements in octahedral coordination. The silicate layers are continuous in the *a* and *b* directions and stacked one above another in the *c* direction with variable water layers between them. As first emphasized by Marshall (1935) and Hendricks (1942), a wide variety of substitutions in octahedral and tetrahedral positions are possible within the structure, and they always leave it with a net negative charge which is satisfied externally by cations which are exchangeable.

The foregoing structure is not accepted by all investigators. Thus, Deuel *et al.* (1950) believe that they have evidence that some of the tetrahedra of the silica sheets are inverted—an idea suggested earlier by Edelman and Favajee (1940). Other ideas concerning the montmorillonite structure have been published (McConnell, 1950), but the concept originating with Hofmann *et al.* (1933) is generally accepted as depicting the most probable framework of the mineral.

The substitution of various cations for aluminum in octahedral coordination can be essentially complete, in which case specific names are applied for example, nontronite (iron), saponite (magnesium). Ross and Hendricks (1945) have shown that there is considerable variation in composition within the aluminous montmorillonites.

Recently it has been suggested that some aluminous montmorillonites that appear to be single species are in fact complex mixtures. Thus, Byrne (1954) stated that the montmorillonites he studied were mixed-layer sequences in which adjacent layers differed from one another in composition and structure. Jonas (1955) concluded that montmorillonites showing dual dehydroxylation reactions are mixtures of two forms of the mineral, and McAtee (1958) concluded that the Wyoming bentonites he studied contained a sodium montmorillonite fraction and a calcium-magnesium montmorillonite fraction, and that these fractions were a consequence of differences in isomorphic substitution within the montmorillonite crystal lattice. One of the objectives of the present

study was to investigate the possible mixing of aluminous montmorillonites in bentonites.

The montmorillonite minerals have interesting plastic, colloidal, and other properties which frequently are quite different from one sample of the mineral to another. These differences cannot in many cases now be explained either by differences in the composition of the exchangeable cations or of the silicate layer, or by present concepts of the structure. Thus, some montmorillonites have catalytic properties towards certain organic substances, whereas others do not. It follows that there is much

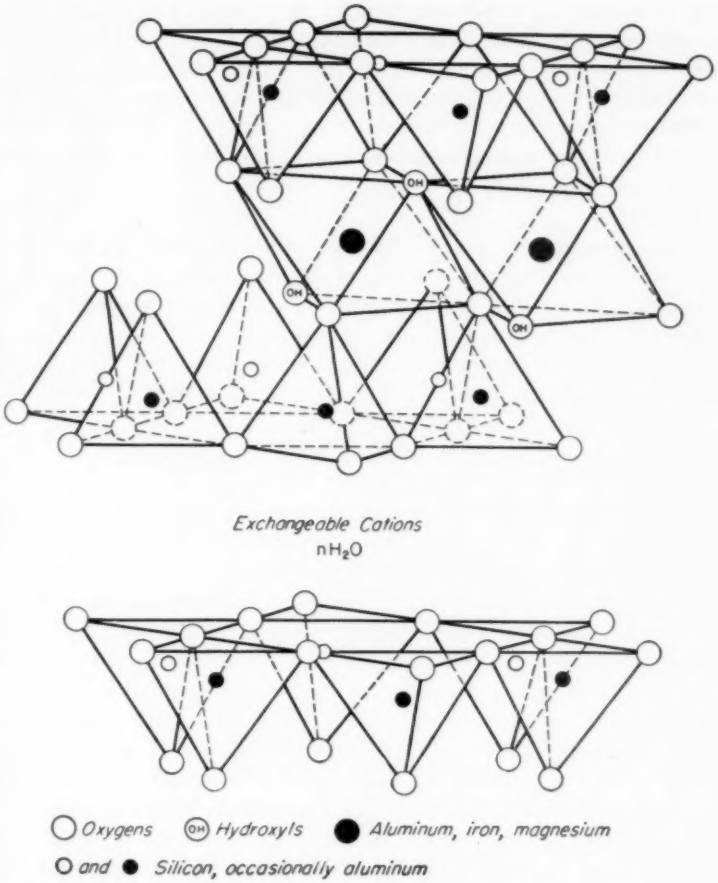

FIG. 1. Diagramatic sketch of the structure of montmorillonite according to Hofmann, Endell and Wilm (1933), Marshall (1935), and Hendricks (1942).

to be learned concerning the structure and compositional variations in this important group of minerals.

Procedure

Over a period of many years, *x*-ray diffraction diagrams of powders and oriented aggregates and differential thermal analyses have been obtained for several hundred samples of bentonites and other clays containing montmorillonite from all over the world that are in the University of Illinois collections. Preliminary studies of the high temperature reactions by continuous *x*-ray diffraction techniques were made also on many of these samples. Based on these data, about forty samples were selected for the present study which appeared to be substantially pure montmorillonite or montmorillonite plus small amounts of quartz or cristoballite. These samples were selected also to represent the variations in characteristics shown in the preliminary analyses. No claim is made that all types of montmorillonite are represented, but it is believed that there is good coverage of the aluminous variety.

Kulbicki and Grim (1957) have shown that the high temperature phases developed on heating montmorillonite are influenced greatly by the nature of the exchange cation composition. To study the relation of the montmorillonite itself to high temperature reactions it was necessary to prepare all samples with the same exchangeable cation composition. It was also deemed necessary to use material of about the same particle size, and in some cases to purify the samples. Accordingly, the following preparation procedure was followed for all samples:

The clays were dispersed in deionized water without the use of a chemical additive. If dispersion was difficult, the initial water was extracted through a porcelain filter candle, and new water added until dispersion was attained. The portion of the suspension containing the less than two micron fraction was separated by repeated decantations. Hydrochloric acid in concentrations kept less than 0.1 normal was added to the suspension containing the less than two micron particles. Within ten to twenty minutes after the addition of the acid, filtration of the clay on Buchner funnels was started. The clay was washed with acid of the same concentration until the total amount of acid to which the clay was subjected equalled about five times that necessary for complete cation exchange. This was followed by washing with deionized water until the concentration of salts in the wash water was about 1 part in 100,000.

A concentrated slurry of the material as prepared above was used to prepare oriented aggregates (Grim, 1934) for *x*-ray and optical study. The remainder of the sample was dried at room temperature for the other analyses. In cases where the influence of added cations were to be studied,

the prepared clay was not dried. Also, the cation exchange capacities were made on samples which had not been acid treated.

For high temperature *x*-ray diffraction study, oriented aggregate samples were prepared on platinum plates. The furnace used was of the design described by Kulbicki and Grim (1957). Runs were made with continuous heating at various rates, and also by soaking the samples at various temperatures. In many cases supplementary data were obtained by heating the samples in an electric furnace to various temperatures, air quenching, and then obtaining powder camera diffraction data.

Differential thermal analyses were made in a furnace with platinum wire as the heating element of the general design of Grim and Rowland (1942) with a platinum block as the sample holder. The analyses were made up to about 1400° C.

The other analyses were made by standard and well known procedures.

Location of Samples Studied

The location of each sample studied in detail is given in Table 1. No mention is made of the stratigraphic position or geologic setting of the samples although pertinent information for most of the samples has been obtained either by field studies of one of us (R.E.G.) or from the literature. Possible correlations of the character of the montmorillonite with its occurrence and mode of formation will be considered separately in a later report. All samples of the aluminous montmorillonites except possibly 6, 23, and 31 are bentonites in that their origin is by the alteration of volcanic ash in situ. The origin of the exceptions and the other montmorillonite samples is not established.

High Temperature Phase Development

Figures 2 to 7 show the high temperature phases developed when each of the samples is heated to a temperature causing the beginning of fusion. In these figures the intensity of a characteristic diffraction line is plotted against the temperature of the sample.

The data reported in Figs. 2 to 7 were obtained on samples whose temperature was continuously increased at a rate of 5° C. per minute. Other heating rates were used also on various samples, but the rate of 5° C. per minute was most satisfactory to permit the detection of the first appearance of a new phase and to record its development.

Differential thermal analyses to 1000° C. were made on all samples and for many of them the analyses were carried to 1400° C. The results of these analyses are given in Figs. 8 to 13.

The high temperature data show that all of the montmorillonites do

not develop the same crystalline phases on heating. A study of the data indicate that the highly aluminous samples investigated can be grouped into several types based on the characteristic high temperature phases developed, or as mixtures of these types. The types will be discussed separately.

TABLE 1. LOCATION OF SAMPLES

The aluminous montmorillonites are listed according to types as determined by the present study.

Cheto-type montmorillonites
1. Cheto, Arizona
2. Otay, California
3. Burrera, Jachal, San Juan, Argentina
4. El Retamito, Retamito, San Juan, Argentina
5. Mario Don Fernando, Retamito, San Juan, Argentina
6. Tatatilla, Vera Cruz, Mexico
7. Itoigawa, Niigata Prefecture, Japan

Wyoming-type montmorillonites
8. Hojun Mine, Gumma Prefecture, Japan
9. Tala, Heras, Mendoza, Argentina
10. Crook County, Wyoming
11. Rokkaku, Yamagata Prefecture, Japan
12. Amory, Mississippi
13. Santa Elena, Potrerillos, Mendoza, Argentina
14. San Gabriel, Potrerillos, Mendoza, Argentina
15. Emilia, Calingasta, San Juan, Argentina
16. Sin Procedencia, Argentina

Wyoming-type montmorillonites containing free silica
17. Usui Mine, Gumma Prefecture, Japan
18. Yakote, Akita Prefecture, Japan
19. Rokkaku, Yamagata Prefecture, Japan
20. Wayne, Alberta, Canada
21. Dorothy, Alberta, Canada
22. Cole Mine, Gonzales County, Texas
23. Cala Aqua Mine, Island of Ponza, Italy

Mixtures of Cheto- and Wyoming-type montmorillonites
24. Pembina, Manitoba, Canada
25. Polkville, Mississippi
26. Grand Junction, Colorado
27. Fadli, Mostaganem, Algeria
28. Taourirt, Morocco
29. Marnia, Algeria
30. Marnia, Algeria
31. Montmorillon, France
32. Yokote, Akita Prefecture, Japan

Miscellaneous aluminous montmorillonites
33. Colony, Wyoming
34. Amory, Mississippi
35. Weston County, Wyoming
36. Humber River, New South Wales, Australia

Iron-rich montmorillonite
37. Aberdeen, Mississippi
38. Santa Rosalina, Baja California

Nontronite
39. Manito, Washington

Hectorite
40. Hector, California

Saponite
41. Ksabi, Morocco

Talc
42. Gouverneur, New York

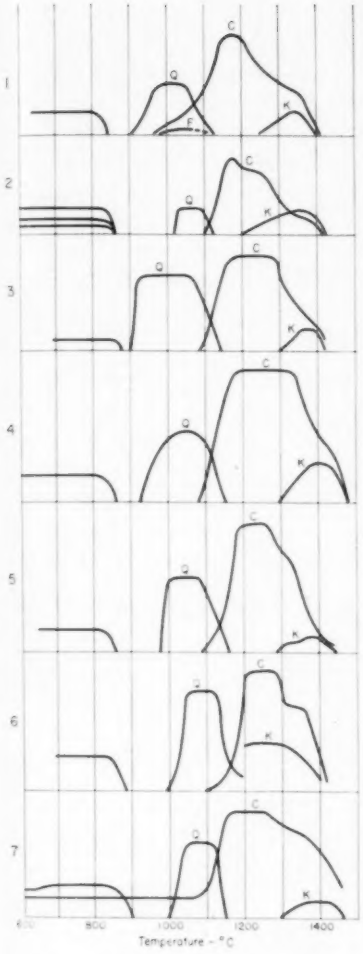

FIG. 2. High temperature phases developed on heating Cheto-type montmorillonites; Samples 1–7; Q, Beta Quartz; C, Beta Cristobalite; K, Cordierite; F, Feldspar.

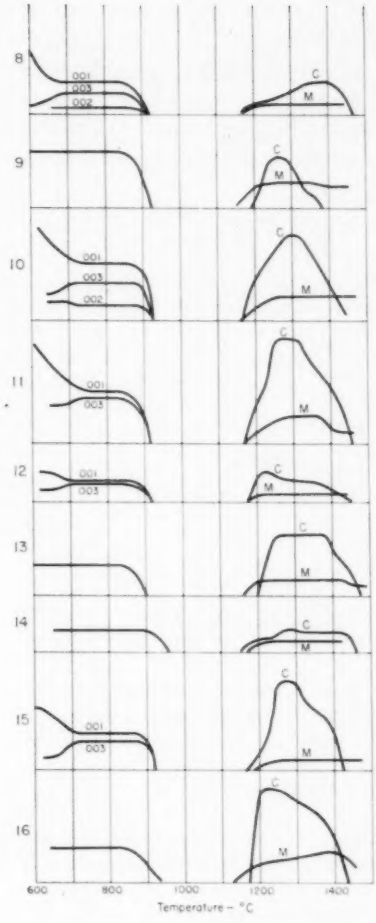

FIG. 3. High temperature phases developed on heating Wyoming-type montmorillonites; Samples 8–16; C, Beta Cristobalite; M, Mullite.

Cheto-Type

This type is so named because samples from the Cheto bentonite producing area in Arizona show very well its characteristics. Figure 2 illustrates the high temperature *x*-ray diffraction data for samples 1–7

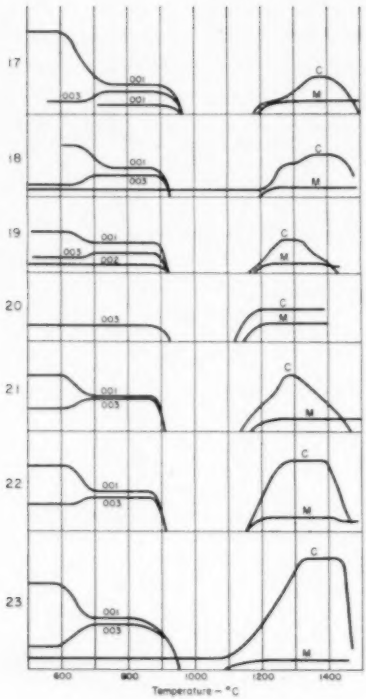

FIG. 4. High temperature phases developed on heating samples containing Wyoming-type montmorillonite plus free silica; Samples 17–23; C, Beta Cristobalite; M, Mullite.

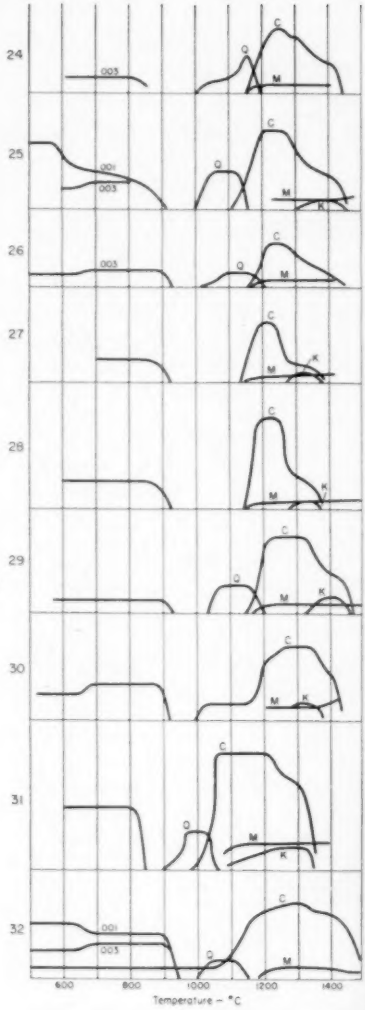

FIG. 5. High temperature phases developed on heating samples containing a mixture of Cheto-type and Wyoming-type montmorillonites; Samples 24–32; Q, Beta Quartz; C, Beta Cristobalite; M, Mullite; K, Cordierite.

showing the development of beta quartz, beta cristobalite, and cordierite, which are the characteristic high temperature crystalline phases for Cheto-type montmorillonite. Figure 8 shows the differential thermal analytical curves for the same samples.

The montmorillonite structure is preserved to 850°–900° C. where it is lost abruptly in a temperature interval of about 50° C. There does not seem to be any change in the intensity of the basal orders of the montmorillonite prior to the loss of structure.

The first high temperature phase to appear is beta quartz between about 900° C. and 1000° C. It develops at a temperature 50° to 125° higher than that for the loss of the montmorillonite structure. During the intervening interval the samples show no x-ray diffraction effects. The beta quartz develops rapidly as shown by the rapid increase in its diffraction intensity. The diffraction data indicate cell dimensions slightly larger (0.1 Å) than the values in the literature, suggesting the possibility of some stuffing of the lattice.

Beta cristobalite appears abruptly usually at 1100° C. and develops rapidly. The beta quartz phase disappears as the cristobalite develops, indicating a phase inversion. Sample 1 is exceptional in showing the development of cristobalite beginning before 1000° C. and before the

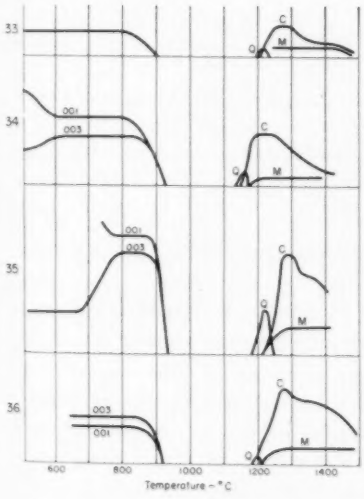

FIG. 6. High temperature phases developed on heating miscellaneous aluminous montmorillonites; Samples 33–36; Q, Beta Quartz; C, Beta Cristobalite; M, Mullite.

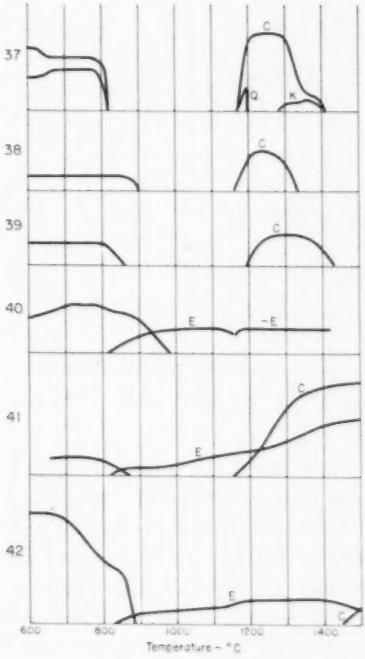

FIG. 7. High temperature phases developed on heating iron-rich montmorillonites (37 and 38), nontronite (39), hectorite (40), saponite (41), and talc (42); Q, Beta Quartz; C, Beta Cristobalite; K, Cordierite; E, Enstatite; C–E, Clinoenstatite.

FIG. 8. Differential thermal curves of Cheto-type montmorillonites; Samples 1–7.

FIG. 9. Differential thermal curves of Wyoming-type montmorillonites; Samples 8–16.

quartz starts to disappear. This same sample also yields a feldspar between about 1000° and 1100° C.

Cordierite appears at 1200°–1300° C. at about the temperature that cristobalite begins to disappear. Its diffraction effects increase in intensity as those of cristobalite decrease.

The samples start to fuse between 1400° and 1500° C. during which interval all of the diffraction effects disappear.

The differential thermal analytical (DTA) curves in Fig. 8 show considerable variation in intensity of the initial endothermic peak due to loss of adsorbed water, but no attempt has been made to study possible causes of this variation. Some samples exhibit a single endothermic reaction between 600° and 700° C. corresponding to the loss of hydroxyl water. Other samples exhibit a double endothermic reaction in the range 450°

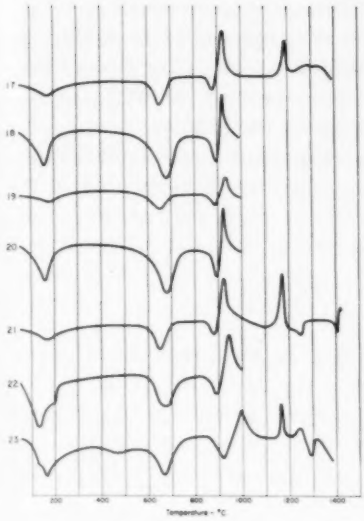

FIG. 10. Differential thermal curves of samples containing Wyoming-type montmorillonite plus free silica; Samples 17–23.

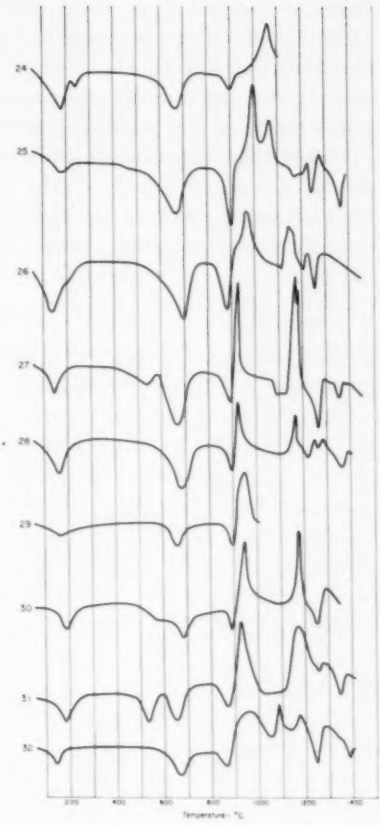

FIG. 11. Differential thermal curves of samples containing a mixture of Chetotype and Wyoming-type montmorillonites; Samples 24–32.

to 700° C. In all cases the endothermic reactions due to loss of hydroxyl water are of slight intensity. A comparison of Figs. 2 and 8 show that the structure of the montmorillonite is not lost with the loss of hydroxyls. It is significant that there is no important change in the *x*-ray diffraction data for the (002) reflections accompanying the loss of hydroxyls.

The DTA curves show a rather intense endothermic reaction between 850 and 900° C., which is the interval in which the structure of the montmorillonite is lost. This endothermic peak is followed after an interval of 50° to 150° C. by a sharp exothermic reaction which can be correlated with the appearance of beta quartz.

A second exothermic reaction appears at about 1100° C. which probably is a consequence of the formation of cristobalite. The DTA curves above about 1200° C. are too complex to be interpreted with certainty.

However, there is a suggestion of an exothermic peak between 1200° and 1300° C. which may correspond to the development of cordierite, an endothermic peak at about 1250° C. probably due to the break up of cristobalite, and another endothermic peak just short of 1400° C. at the temperature of the beginning of the fusion of the samples.

One of the samples (#7) contained cristobalite that could not be separated by fractionation from the montmorillonite. An inspection of the high temperature phase development and the DTA data shows no significant difference from samples of the same type without the excess silica.

Wyoming-Type

Many samples of bentonite from Wyoming are composed of montmorillonite with the characteristics of this type, hence the name.

Figure 3 shows the high temperature phases of samples 8–16 composed of Wyoming-type montmorillonite. The characteristic high temperature phases are cristobalite and mullite. Figure 9 illustrates the DTA data characteristic of this type of montmorillonite.

The montmorillonite on heating in the range of 600° to 700° C. shows generally a decrease in the intensity of the (001) reflection, an increase in the intensity of the (003) reflection and no significant change in the intensity of the (002) reflection.

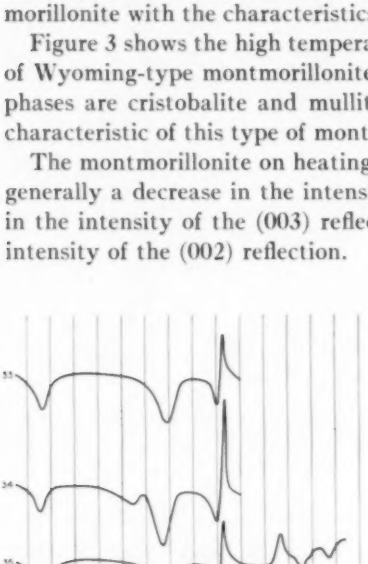

FIG. 12. Differential thermal curves of miscellaneous aluminous montmorillonites; Samples 33-36.

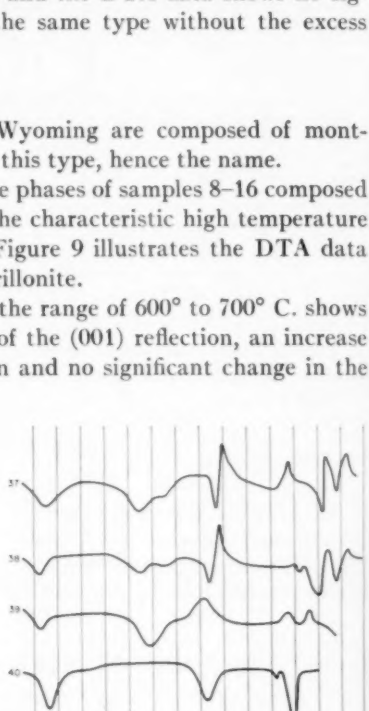

FIG. 13. Differential thermal curves of iron-rich montmorillonite (37 and 38), nontronite (39), hectorite (40), saponite (41) and talc (42).

The montmorillonite structure is lost at 900° to 950° C. and no x-ray diffraction effects are noted again for a temperature interval of 200° to 250° C., *i.e.*, until heating is carried to 1100° to 1150° C. at which temperature cristobalite and mullite appear at about the same time. Both of these phases persist until 1400° to 1500° C. when the material fuses. Frequently the cristobalite begins to disappear at about 1300° C. whereas the mullite generally persists unchanged until near the fusion temperature. However, the intensity of the mullite reflections is never very great indicating that this phase is never very abundant and/or very well crystallized. The lattice dimensions of the mullite vary slightly from published values for the pure mineral suggesting some replacements or defects.

The characteristics of the initial endothermic peaks on the DTA curves will not be considered herein. The curves all show a fairly intense endothermic reaction between 600° and 700° C. due to the loss of hydroxyl water. Some of the samples show another endothermic peak between 500° and 600° C. making a dual peak for the dehydroxylations. In general these dehydroxylation endothermic peaks are more intense for the Wyoming-type than for the Cheto-type montmorillonites. The x-ray data show that the structure of the montmorillonite persists through the loss of hydroxyls but that some structural changes take place which are adequate to cause changes in the relative intensities of the basal spacings. The DTA curves show an endothermic reaction of variable intensity at about 900° C., which is the temperature at which the diffraction effects from montmorillonite disappear. This endothermic peak is followed immediately by an exothermic reaction and it is of special interest that there is no crystalline phase shown at this temperature by the x-ray diffraction data, *i.e.*, this thermal reaction occurs at a temperature interval in which there are no x-ray reflections.

The DTA curve shows an exothermic reaction (sometimes more than one) at 1100° to 1200°C. which is the temperature at which mullite and cristobalite appear. The DTA curves beyond this temperature are quite irregular and variable, and cannot be interpreted.

Wyoming-Type With Excess Silica

Many of the samples containing the Wyoming-type montmorillonite also had quartz and/or cristobalite in small amounts (less than 15%) in particles so small that they could not be separated by fractionation from the montmorillonite. It is interesting that only one sample (#7) of Cheto-type montmorillonite was found with such free silica. The results of the high temperature diffraction studies of the Wyoming type samples with excess silica (numbers 17–23) are given in Fig. 4. DTA curves for the

same samples are given in Fig. 10. The diffraction effects of the quartz are not shown in Figure 4 since they did not influence the high temperature phase development.

A comparison of Figs. 3 and 4 show that the excess silica had no detectable effect on the development of high temperature phases. A comparison of the DTA curves in Figs. 9 and 10 show no large differences. The thermal reactions, especially the exothermic ones, are usually relatively less intense in the samples with excess silica. Also it is interesting, although the possible significance is not presently known, that none of the samples with excess silica show a double peak for the loss of hydroxyl water.

Mixtures of Cheto- and Wyoming-Types

Figure 5 shows high temperature phase data for samples (numbers 24–32) which exhibit characteristics of both of the Cheto- and Wyoming-types. Samples 27, 28 and 30 show cristobalite and mullite which are characteristic of the Wyoming-type plus cordierite which is characteristic of the Cheto-type. The DTA curves, Figure 11, of these same samples are like those of the Wyoming type and it seems likely that the dominant component of these samples is Wyoming-type montmorillonite.

Samples 24, 25, 26 and 29 show beta quartz and cristobalite high temperature phases like those of the Cheto-type plus mullite. In samples 24 and 26 cordierite has not developed. These samples except #29 show DTA curves characteristic of the Cheto-type montmorillonite and it seems likely that this type is dominant in these samples. The DTA curve of sample 29 resembles more those of the Wyoming-type than the Cheto-type, however, the first exothermic peak is unusually broad and could well be interpreted as a composite of the peaks in the Wyoming- and Cheto-types. The suggested interpretation is that sample 29 contains roughly equal amounts of Cheto- and Wyoming-type montmorillonites.

It is of interest that the sample investigated from the type locality at Montmorillon, France (#31) is a mixture of the Cheto- and Wyoming-types.

Sample 32 is composed of a mixture of the montmorillonite types plus cristobalite which could not be separated by fractionation. The high temperature phase development shows nothing unique. The exothermic reaction at about 900° C. seems unusually broad and may again be interpreted as due to the mixing of about equal parts of the two types of montmorillonite.

It is recognized that another possible interpretation is that these data do not indicate mixtures of two types of montmorillonite, but rather variations in the composition within a single type. It will be shown pres-

ently that there is strong additional evidence for mixing of types, although there is undoubtedly some variation in composition within each type.

Miscellaneous Samples

It is not meant to imply that all aluminous montmorillonites belong to the two classes indicated above. Figures 6 and 12 present high temperature phase and DTA data for samples that do not fit exactly in either of these two categories. Thus samples 33, 34, 35 and 36 have DTA curves like those of the Wyoming-type, and the high temperature phase characteristics are also like those of the Wyoming-type except for the small amount of quartz forming just prior to the development of cristobalite. It is expected therefore, that these samples would not differ in any very substantial way from those of the Wyoming type. A possible explanation for the presence of the beta quartz phase will be presented later in the Discussion.

Figures 7 and 13 present high temperature phase DTA data for a few montmorillonites with a high iron content (37, 38), a sample of nontronite (39), samples with a high magnesium content (40, 41), and a sample of talc (42). Samples with increasing replacements of aluminum by iron (samples 37, 38 and 39), show the absence of mullite at high temperatures. In samples with abundant iron (38, 39), cristobalite is the only high temperature phase. The destruction of the montmorillonite lattice tends to be at lower temperatures (800° to 900° C.) in the iron-rich samples as compared to the aluminous types. Also the cristobalite disappears finally at a slightly lower temperature in the iron-rich montmorillonites. The DTA curves for these high iron samples show a lower temperature for the endothermic dehydroxylation peaks than is the case for the aluminous types. Also the endothermic peak for the loss of structure is at a relatively lower temperature in the iron-rich types. In the nontronite sample (39) there is no peak accompanying the loss of structure, perhaps because of a gradual destruction of the structure which is in accordance with the *x*-ray data shown in Fig. 7. The DTA curves for the iron-rich samples show an exothermic reaction between 800° and 900° C. which is not accompanied by any crystalline phase detectable by *x*-ray diffraction. No definite explanation can be offered, but it is the authors' opinion that it represents the nucleation of a phase with a silica type crystallization. The slight second exothermic reaction just short of 1200° C. is at the temperature at which cristobalite appears in high temperature diffraction data. The DTA curves above 1200° C. are to complex to be interpreted.

In the case of hectorite (40) the structure is lost gradually from about 800° C. to 1000° C. Enstatite appears as soon as the structure of hector-

ite begins to disappear and the maximum diffraction of enstatite is attained while the hectorite is still producing considerable diffraction intensity. At about 1125° C. enstatite changes to clinoenstatite. No other high temperature phases were evident. The endothermic reactions at about 800° C. and 1200° C. are in the range of the loss of montmorillonite structure and the formation of enstatite, and the inversion of the enstatite to clinoenstatite, respectively. The saponite sample (41) loses its structure from about 800° C. to 875° C. without a corresponding DTA peak in accordance with its trioctahedal structure. Enstatite begins to form at a slightly lower temperature than that of the final loss of the saponite structure with no corresponding DTA peak. The intensity of the enstatite diffraction continues to increase to the highest temperature attained, 1500° C. Cristobalite begins to form at about 1150° C. and the intensity of its diffraction effects also continue to increase to the highest temperature attained. The DTA curve for saponite shows only one moderately intense thermal reaction, the exothermic reaction at about 975° C., and no definite correlation is possible between the DTA curve and the high temperature phase data.

The talc sample (42) loses its structure between about 700° C. and 880° C. Enstatite appears at a slightly lower temperature than that of the final loss of the talc structure and continues to diffract with moderate intensity up to the highest temperature attained, 1500° C. Cristobalite appears first at 1450° C. with very minor diffracting intensity which is, however, increasing at 1500° C. The DTA curve for talc shows a single thermal reaction, an endothermic one just short of 1000° C., which cannot be correlated with any of the high temperature phase reactions.

Chemical Analyses

Chemical analyses of all samples together with structural formulae computations according to the method of Ross and Hendricks (1944) are given in Tables 2 to 6.

The computed compositions of octahedral cations for all the montmorillonite samples are plotted in Fig. 14.

The chemical compositions of the aluminous samples fall into two groups corresponding to those derived from the high temperature diffraction and DTA data. The samples classed as Cheto-type, Table 2, have less than 5% of tetrahedral silicon replaced by aluminum; 25 to 35% of octahedral aluminum replaced by magnesium; and 5% or less of the octahedral positions populated by iron.

In general the Wyoming-type montmorillonites, Table 3, show about the same amount of the tetrahedral silicon replaced by aluminum, although in some samples the amount of tetrahedral aluminum is greater

Table 2. Chemical Analyses of Cheto-Type Montmorillonites

TABLE 2. CHEMICAL ANALYSES OF CHETO-TYPE MONTMORILLONITES

Sample Number	SiO_2	Al_2O_3	TiO_2	Fe_2O_3	FeO	MgO	CaO	Na_2O	K_2O	H_2O+	H_2O+ 105–500	H_2O+ 500–900	H_2O-	Si	Al. Tet.	Al. Oct.	Fe″	Fe‴	Mg	Total Oct.
1	61.77	19.85	.24	1.95*		5.56	1.89	.07	.09	7.72			9.49	3.91	.09	1.38		.09	.54	2.01
2	62.23	21.03		1.75	.48	5.70	0	.65	0		4.45	2.93	8.41	3.86	.14	1.39	.02	.08	.55	2.04
3	63.07	18.46	.28	1.99*		7.38	.24	.16	.16	7.17			13.03	3.93	.07	1.28		.09	.71	2.08
4	61.55	20.44		2.02	.38	6.06	0	.30	0		5.84	2.45	7.67	3.84	.16	1.34	.02	.09	.58	2.03
5	60.90	20.71		2.06	.36	6.84	.30	.23	0		5.99	2.03	7.08	3.81	.19	1.33	.02	.09	.65	2.09
6†	60.80	22.15		.07		4.44	3.74			8.71			14.75	3.98	.02	1.67			.38	2.05
7	65.97	19.10		1.09	.76	4.56	0	.13	0		4.80	2.40	5.49	‡		1.46	.03	.05	.46	

Analyses based on dry (105° C.) weight of samples.
* Total Fe as Fe_2O_3.
† Crude clay.
‡ Contains free silica.

TABLE 3. CHEMICAL ANALYSES OF WYOMING-TYPE MONTMORILLONITES

Sample Number	SiO_2	Al_2O_3	TiO_2	Fe_2O_3	FeO	MgO	CaO	Na_2O	K_2O	H_2O+	H_2O+ 105–500	H_2O+ 500–900	H_2O-	Si	Al. Tet.	Al. Oct.	Fe″	Fe‴	Mg	Total Oct.
8	64.80	24.54		1.27	.56	1.60	0	.40	0		2.84	3.87	6.22	3.96	.04	1.72	.03	.06	.15	1.96
9	62.00	23.42		3.74	.32	.93	.68	.72	2.63		3.86	1.35	6.44	3.92	.08	1.66	.02	.18	.09	1.95
10	62.30	23.50		3.35	.37	1.95	.31	.40	.03		2.01	4.44	7.81	3.90	.10	1.64	.02	.15	.19	2.00
11	62.70	22.20		4.62	.48	2.00	.58	.01	.12		2.44	4.62	7.13	3.92	.08	1.55	.03	.22	.19	1.99
12	59.73	24.30		5.54	.37	2.10	0	.80	.22		3.88	2.71	13.70	3.76	.24	1.56	.02	.26	.20	2.04
13	60.22	23.67	.34	6.28*		1.46	.13	.09	.19	6.86			6.81	3.80	.20	1.56		.30	.14	2.00
14	60.76	23.08	.38	6.10*		1.44	.17	.13	.21	6.07			7.65	3.84	.16	1.56		.29	.14	1.99
15	59.91	21.97	.33	6.72*		2.15	.34	.09	.11	6.66			8.81	3.83	.17	1.48		.32	.21	2.01
16	58.67	27.34		3.64	.38	2.00	0	.62	.18		3.22	3.82	10.88	3.66	.34	1.67	.01	.17	.19	2.05

Analyses based on dry (105° C.) weight of samples.
* Total Fe as Fe_2O_3.

than is the Cheto-type samples. In the Wyoming-type montmorillonite 5 to 10% of the octahedral aluminum is replaced by magnesium (less than for the Cheto-type); and 5 to more than 15% of the octahedral positions are populated by iron which is more than for the Cheto-type. The total octahedral population is generally 2 or slightly less in the Wyoming-type samples, whereas for the Cheto-type this value is generally slightly greater than 2.

The analyses of the Wyoming-type sample containing free silica show, Table 4, the expected relatively large amount of SiO_2.

Samples composed of mixtures of Cheto-and Wyoming-type montmorillonites have chemical compositions, Table 5, that are intermediate between the pure Wyoming- and Cheto-types.

Samples 33, 34, 35 and 36, which differ from the Wyoming-type samples because a small amount of beta quartz formed as an initial high temperature phase, and which are listed among the Miscellaneous samples in Table 6, have chemical compositions similar to those of the Wyoming-type samples, Fig. 14.

Samples 37 and 38, Table 6, show some characteristics of both the Cheto- and Wyoming types in the larger replacement of octahedral

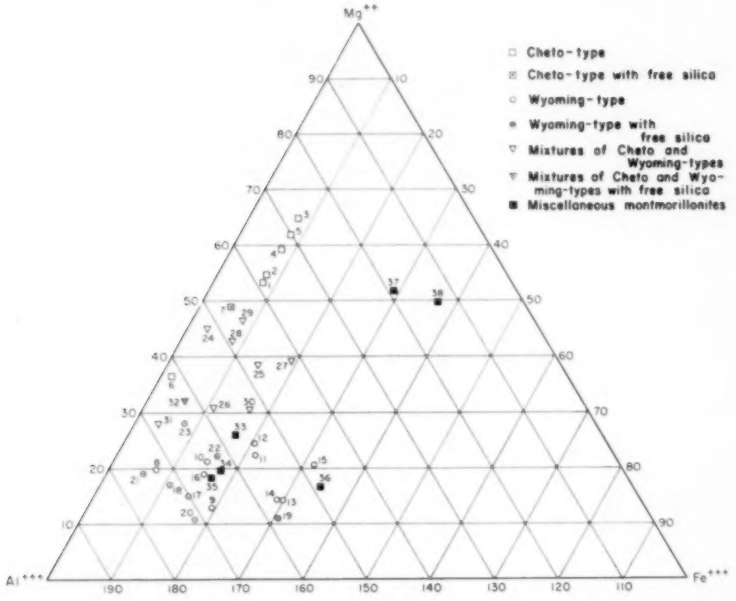

FIG. 14. Computed octahedral cation compositions of the montmorillonites.

TABLE 4. CHEMICAL ANALYSES OF WYOMING-TYPE MONTMORILLONITE CONTAINING ALSO QUARTZ AND/OR CRISTOBALITE

Sample Number	SiO_2	Al_2O_3	Fe_2O_3	FeO	MgO	CaO	Na_2O	K_2O	H_2O+ 105–500	H_2O+ 500–900	H_2O-
17	68.60	19.00	2.66	.45	1.07	2.52	.49	0	2.10	4.33	5.08
18	67.50	22.60	2.32	.35	1.41	.34	.09	.07	2.47	4.31	5.04
19	63.00	19.90	6.02	.57	.75	1.55	.40	.24	3.19	3.66	7.28
20	66.74	20.54	3.39	.38	.79	.42	.78	0	2.94	3.41	7.13
21	66.90	22.98	1.29	.28	1.76	0	.52	.01	3.61	2.51	5.34
22	66.26	20.49	3.25	.48	1.88	.45	.26	.03	3.78	2.55	10.26
23	72.45	17.52	1.45	.49	2.16	0	.10	0	2.58	2.97	7.57

Analyses based on dry (105° C.) weight of samples.

TABLE 5. CHEMICAL ANALYSES OF MIXTURES OF CHETO- AND WYOMING-TYPE MONTMORILLONITES

Sample Number	SiO_2	Al_2O_3	TiO_2	Fe_2O_3	FeO	MgO	CaO	Na_2O	K_2O	H_2O+	H_2O+ 105–500	H_2O+ 500–900	H_2O-	Si	Al. Tet.	Al. Oct.	Fe''	Fe'''	Mg	Total Oct.
24	61.63	24.92		.70	.78	4.51	0	.37	0		3.38	3.65	12.68	3.77	.23	1.56	.04	.03	.42	2.05
25	65.00	22.80		3.07	.40	3.90	.05	.17	.13		2.36	4.22	12.10	3.87	.13	1.47	.02	.14	.36	1.99
26	61.40	25.03		2.52	.23	3.26	.33	.62	0		3.06	3.76	11.03	3.78	.22	1.59	.01	.12	.31	2.03
27	60.70	20.28	.39	4.07*		3.98	.75	.62	.17	7.66			8.27	3.90	.10	1.43		.20	.39	2.02
28	61.56	22.99	.04	2.23*		4.48	.30	.12	.17	7.05			7.13	3.85	.15	1.51		.10	.43	2.04
29	60.62	22.18	.40	2.06*		4.80	.38	.06	.03	8.31			9.07	3.83	.17	1.48		.10	.49	2.07
30	63.37	23.37		3.82	.47	3.22	0	.63	0		3.35	2.67	7.80	3.91	.09	1.53	.02	.18	.30	2.03
31†	60.16	23.24		.98		3.79	1.91	.04	.13	9.39			14.81	3.97	.03	1.73		.05	.36	2.14
32	69.58	19.41		1.34	.75	2.57	0	.29	0		2.92	2.99	8.47	‡		1.62	.04	.06	.28	

Analyses based on dry (105° C.) weight of samples.
* Total Fe as Fe_2O_3.
† Crude clay.
‡ Contains free silica.

TABLE 6. CHEMICAL ANALYSES OF MISCELLANEOUS SAMPLES

Sample Number	SiO_2	Al_2O_3	TiO_2	Fe_2O_3	FeO	MgO	CaO	Na_2O	K_2O	H_2O+	H_2O+ 105–500	H_2O+ 500–900	H_2O-	Si	Al. Tet.	Al. Oct.	Fe''	Fe'''	Mg	Total Oct.
33	62.75	22.12	.15	3.94*		2.64	.29	.20	.06	6.70			8.96	3.94	.06	1.57		.17	.26	2.00
34	59.01	27.17		3.78	.27	2.20	0	.28	.22		3.96	3.13	8.44	3.70	.30	1.66	.01	.18	.21	2.06
35	60.20	26.20		3.76	.34	1.92	.04	.34	.02		2.31	4.58	7.05	3.75	.25	1.67	.02	.17	.18	2.04
36	60.00	19.70		6.70	.56	1.33	2.60	.53	.06		4.28	2.94	8.24	3.95	.05	1.48	.03	.33	.13	1.97
37	59.98	18.69	.20	6.47*		5.44	.22	.03	.30	7.99			7.77	3.81	.19	1.21		.31	.53	2.05
38	56.28	19.51		9.20	.23	4.95	0	.94	.92		5.32	2.22	11.80	3.65	.35	1.14	.01	.45	.49	2.09
39	50.10	3.75		34.87	.75	.63	.26	.14	.05		6.34	1.85	14.20							
40†	59.76	.15		.03		28.68	.18	3.37	.26	6.21	$Li_2O=1.35$		9.29	3.98	.02		Li=.35		2.81	3.61
41†	55.00	1.20		1.40		28.00	.01	—	.52		10.33			3.96	.04	.06		.07	2.92	3.05

Analyses based on dry (105° C.) weight of samples.
* Total Fe as Fe_2O_3.
† Crude clay.

aluminum by magnesium of the former and the relatively large replacement of tetrahedral silicon by aluminum of the latter. In addition these samples have a larger amount of iron than the Cheto- and Wyoming-type samples.

The sample of nontronite (39) has only a small amount of replacement of magnesium for iron in octahedral positions. The nontronite sample as well as the samples with considerable replacement of the aluminum by iron in octahedral positions (37 and 38) are dioctahedral forms, but the total population of octahedral positions is appreciably in excess of 2.

The samples of hectorite (40) and saponite (41) both are trioctahedral forms in which magnesium is the dominant component of the octahedral layer. It is interesting in both of these samples the tetrahedral layers have very little replacement of silicon by aluminum and in each case the total population of octahedral positions is slightly in excess of 3.

Cation Exchange Capacity

The cation exchange capacities of the samples determined and computed are listed in Table 7. The determined capacities of the Cheto-type montmorillonite ranges between 114 and 133 milliequivalents per 100

Table 7. Cation Exchange Capacity in Milliequivalents per 100 Grams

Sample No.	Determined	Computed	Sample No.	Determined	Computed
	Cheto-type			Mixture of Cheto- and Wyoming-types	
1	133	168			
2	114	160	25	113	151
3	118	151	26	114	126
4	125	182	27	114	126
5	125	161	28	118	129
6	122		29	110	126
			30	109	90
			30	103	
	Wyoming-type		32	57	(contains free silica)
8	109	95		Miscellaneous Samples	
9	91	95			
10	89	87	33	106	90
11	98	92	34	90	95
12	96	106	35	117	92
13	111	95	36	106	89
14	110	92	38	93	160
15	109	98	39	88	160
16	102	123	40	82	

Analyses based on dry (105° C.) weight of samples.
* Total Fe as Fe_2O_3.
† Crude clay.

gram, whereas the capacities of the Wyoming-type samples ranges from 89 to 111 milliequivalents per 100 gram. It is interesting that there is no overlap in the capacities between these types of montmorillonites.

The relatively higher exchange capacity of the Cheto-type is in agreement with a greater total replacement and higher net negative charge on the lattice of this type of montmorillonite as compared to the Wyoming-type. In the Wyoming-type most of the charge is derived from replacements in tetrahedral positions, but the total charge on the lattice is less than for the Cheto-type montmorillonite.

The samples which are mixtures of the two types have cation exchange capacities, which are intermediate as would be expected.

The miscellaneous samples with the exception of #35 have capacities similar to those of the Wyoming-type montmorillonite. The aluminous samples in this miscellaneous group (nos. 33, 34, 35 and 36) also have chemical compositions which are quite similar to those of the Wyoming-type. Miscellaneous samples 38, 39 and 40 are high iron or magnesium montmorillonite samples and data are not at hand to indicate whether or not these values have any general significance.

For the Wyoming-type montmorillonite, there is reasonable agreement between the determined and the computed cation exchange capacities. However, for the Cheto-type, the computed values are uniformly higher than the determined values by the order of about 35 milliequivalents per 100 grams. The only explanation that can be offered for this lack of agreement in the Cheto-type is that it is a consequence of the preparation of the samples. The samples for chemical analyses were prepared using acid, whereas for the exchange capacity determinations the samples were untreated. Perhaps the acid treatment removed some cations from within the lattice thereby increasing the computed value. If this is the explanation, it follows that the Cheto-type is more susceptible to leaching than the Wyoming-type montmorillonite.

In the case of mixtures, the computed values are in general higher than the determined values in accord with the presence of some Cheto-type material.

The foregoing explanation is supported by the much higher computed values for the iron rich samples (38, 39) as compared to the determined values. It would be expected that the lattice iron would be relatively more affected by the acid treatment.

X-Ray Diffraction of Unfired Samples

Powder Diagrams

The diagrams for the Cheto-type montmorillonites as compared to the Wyoming-type show somewhat better defined prism reflections, the (001)

reflections are frequently sharper, and there is a more definite indication of higher basal orders.

In the case of mixtures of the two types of montmorillonite, the prism reflections are like those of the Wyoming type. The (001) reflections are variable with similarities to both types represented in different samples.

The sample listed as containing free silica shows diffraction lines for cristobalite and/or quartz in addition to those from montmorillonite. Except for the expected reduction in intensity of the montmorillonite reflections, there is no significant difference in the patterns of these samples as compared to those with little or no free silica.

TABLE 8. COMPUTED AND MEASURED VALUES FOR b

Sample No.	Computed	Measured	Sample No.	Computed	Measured
Cheto type			Wyoming type (*cont.*)		
1	8.966	9.00	13	8.972	8.97
2	8.973	9.01	14	8.966	8.97
3	8.981	8.98	15	8.975	8.97
4	8.979	8.97	16	8.98	8.97
5	8.987	9.00	Miscella-		
6	8.938	8.95	neous types		
Wyoming type			33	8.951	8.95
8	8.933	8.965	34	8.978	8.965
9	8.944	8.94	35	8.97	8.98
10	8.95	8.97	36	8.958	8.97
11	8.956		37	8.998	9.00
12	8.979	8.97	38	9.03	9.04

Miscellaneous samples (33, 34, 35, 36) give diffraction data like those of the Wyoming-type. Sample 38 with a higher iron content is also like that of the Wyoming type. The sample of nontronite gives poorer data than the Wyoming-type in that the prism reflections are merely broad bands.

The values of b_0 determined from the (060) reflections observed on the powder diagrams and calculated according to the formula of MacEwan (1951) for the Wyoming, Cheto, and miscellaneous types are given in Table 8. All specimens appear to be dioctahedral montmorillonites. The agreement between the observed and computed values is reasonably good. The Wyoming-type samples observed values range from 8.94 to 8.97. The miscellaneous samples (33, 34, 35, 36) range from 8.95 to 8.98. The values for the Cheto type range from 8.97 to 9.01—higher than the

Wyoming type as would be expected because of the higher content of magnesium. An exception in the case of the Cheto-type is the Tatatilla sample (6) for which the value is unusually low probably because of the extremely small iron content. The values for the samples with a high iron content (37, 38) are 9.00 to 9.04 which is in the expected range. The

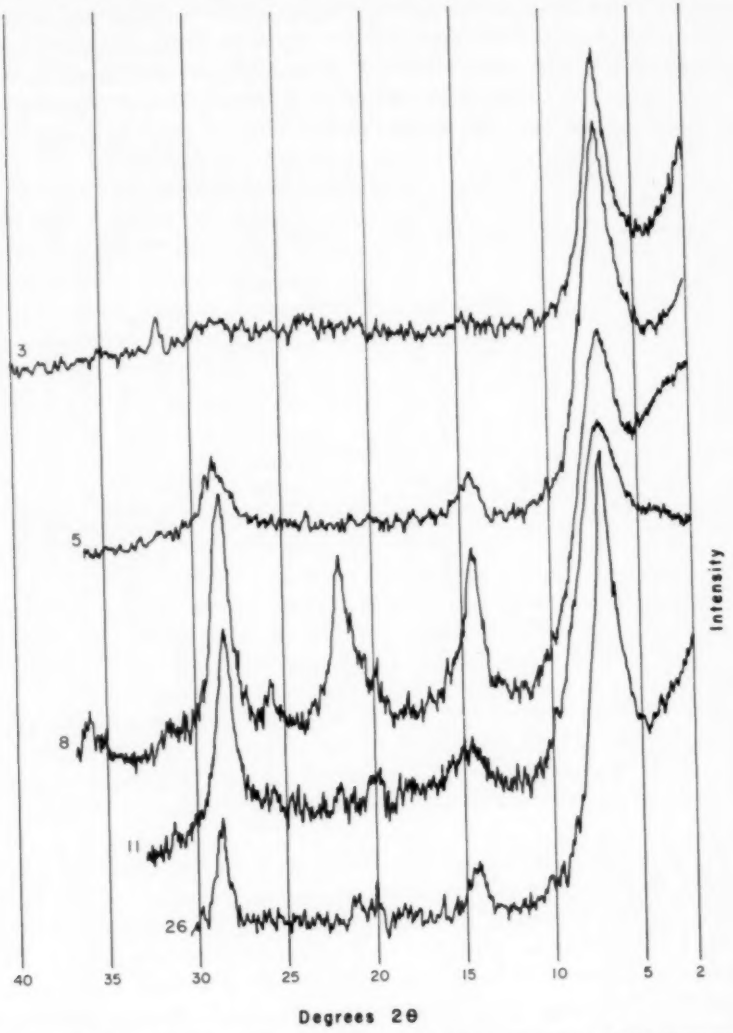

Fig. 15. *X*-ray diffraction spectrograms of oriented aggregates of Cheto-type montmorillonite (3 and 5), Wyoming-type montmorillonite (8 and 11), and a mixture of these types (26).

(060) reflection for most of the samples is fairly sharp but for others it is fairly broad, sometimes suggesting that it is a complex of several reflections. The samples composed of a single type of montmorillonite are in general sharper than those composed of mixtures. This is true for all of the Cheto-type samples but not for all of the Wyoming-type samples. Further, a few of the samples composed of mixtures yield quite sharp (060) reflections. It may be concluded from the foregoing statements that powder diffraction data may suggest that a given sample is composed of a particular type of montmorillonite or a mixture, but it is no more than a suggestion. The data seem to indicate that the population of cation positions in a mass of montmorillonite is more uniform in the Cheto-type than in the Wyoming-type mineral.

Oriented Aggregate Diagrams

The Cheto-type samples show intense sharp (001) reflections but higher orders are always of about uniform low intensity both with and without glycol treatment, Figs. 15 and 16. On the other hand, the Wyoming-type samples usually show sharp (001) reflections and also sharp intense higher orders up to about (006). The sharp higher orders were obtained from one sample without glycol treatment, but for the other samples glycol treatment was necessary to develop them.

The samples containing excess silica were substantially like those of the purer montmorillonites. The Wyoming-type with excess silica show the same sharp higher orders up to about (006) as those without the silica, indicating that the quartz or cristobalite is present in discrete particles even though it has been impossible to separate it from the montmorillonite.

The samples composed of mixtures, following glycol treatment, show the sharp higher orders like the Wyoming-type except that they are somewhat less intense. The (004) and (006) reflections are relatively weaker than the (002), (003), and (005) reflections and this characteristic is more pronounced in the mixtures than in the pure Wyoming-type mineral.

The miscellaneous samples of the aluminous montmorillonites show the development of higher orders comparable to the Wyoming type. The nontronite sample also shows the development of higher orders, but as would be expected the relative intensities are different from those of the aluminous samples.

It is planned to consider further the diffraction characteristics of these types of montmorillonite in a later paper. It appears, however, that the data warrant the conclusion that the Wyoming-type is composed of unit silicate layers less well bonded together than the Cheto-type, so that the montmorillonite can be more completely dispersed leading to more uni-

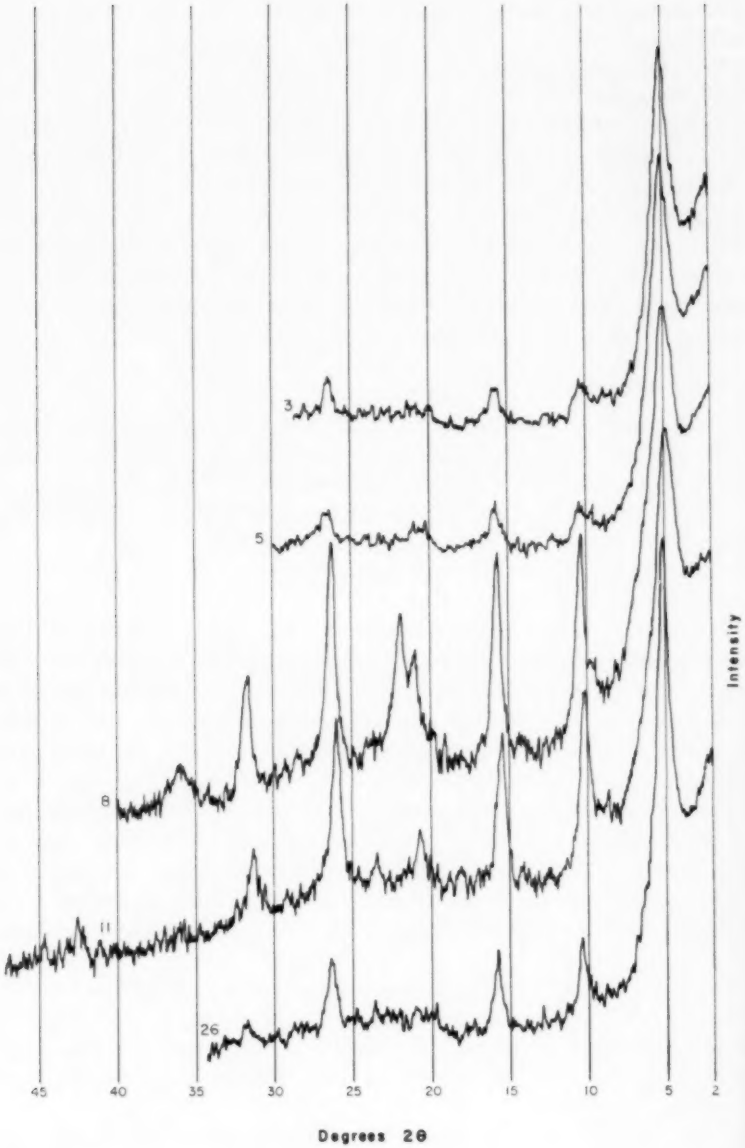

FIG. 16. *X*-ray diffraction spectrograms of oriented aggregates, glycol treated, of Cheto-type montmorillonite (3 and 5), Wyoming-type montmorillonite (8 and 11), and a mixture of these types (26).

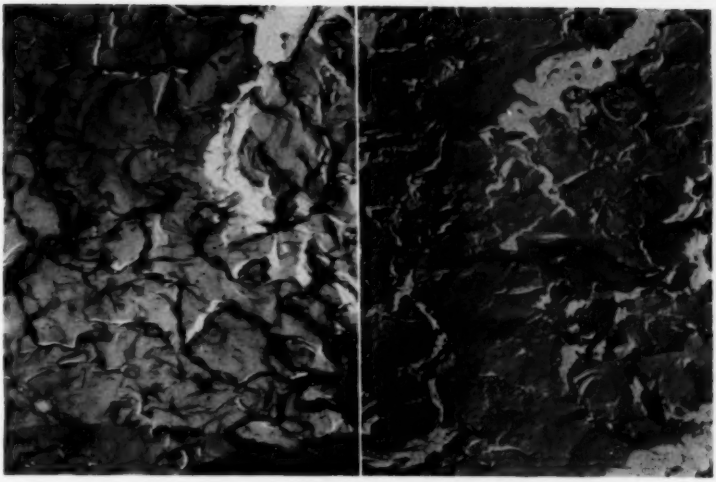

FIG. 17. Electron micrographs (carbon replicas) of Wyoming-type montmorillonite (10), 6500×.

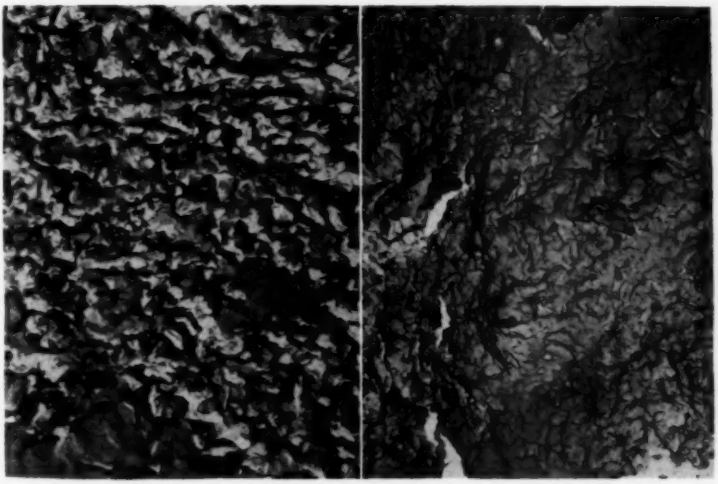

FIG. 18. Electron micrographs (carbon replicas) of Cheto-type montmorillonite (6), 6500×.

formly oriented aggregate flakes which are more thoroughly and completely penetratable by the glycol. This is in accord with the relatively low cation exchange capacity and hence lower charge on the lattice of the Wyoming type which in turn is the consequence of a relatively smaller amount of substitution within the lattice of the Wyoming-type montmorillonite.

Electron Diffraction and Microscopy

The electron diffraction and microscopic characteristics of the samples were not investigated exhaustibly but only to determine if there were obvious differences corresponding to the Wyoming- and Cheto-types of montmorillonite. No such differences could be found in the diffraction data.

Electron micrographs using the carbon replica technique indicate that the Wyoming type, Fig. 17, is composed of such extremely small particles that there is no suggestion of individual particles in the micrographs. On the other hand, micrographs of the Cheto-type, Fig. 18 and the sample from Montmorillon, Fig. 19, which is a mixture of types, have a granular appearance suggesting somewhat coarser particles. It is not felt that the electron micrographs present unequivocal evidence for separating the two types. However, the characteristics of the electron micrographs are gen-

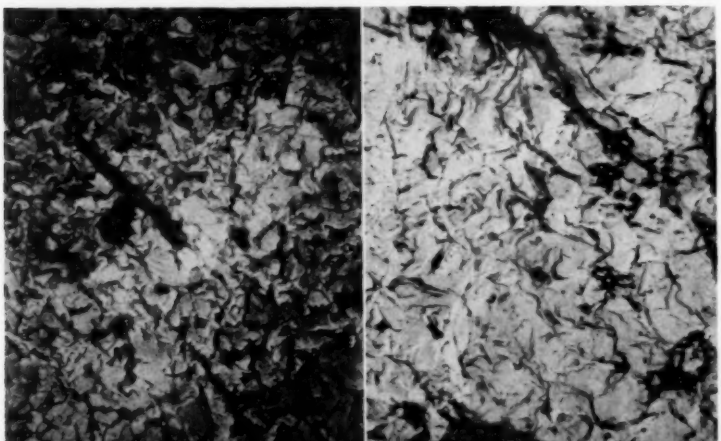

Fig. 19. Electron micrographs (carbon replicas) of samples composed of mixture of Wyoming- and Cheto-type montmorillonite, (31), 6500×.

erally in accord with the characteristics of the two types of aluminous montmorillonite derived from the other data.

Electron micrographs of the same samples after heating to a temperature just adequate to destroy the montmorillonite structure (900° C.±) showed no significant differences as compared to the unfired samples.

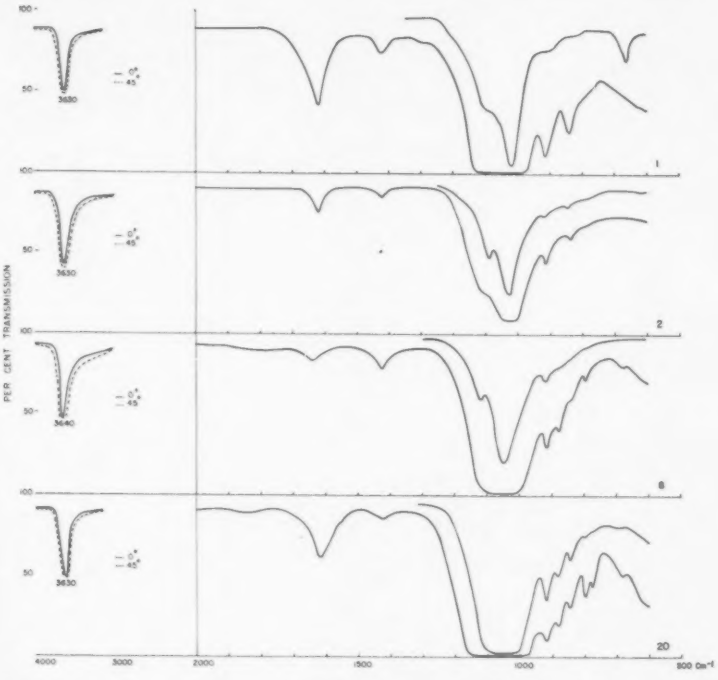

FIG. 20. Infra-red absorption curves of montmorillonites: Cheto-type (1 and 2), Wyoming-type (8), Wyoming-type plus quartz (20). All data from films except separate curves 600–1300 cm^{-1} from KBr pellets.

INFRA-RED ANALYSES

Infra-red absorption curves were obtained for a series of samples showing differences in chemical composition, *x*-ray diffraction, and DTA characteristics by Dr. J. M. Serratosa of the Illinois State Geological Survey. The authors are indebted to Dr. Serratosa for the interpretation of the infra-red data which are presented in Figs. 20 to 23.

Films composed of particles with parallel orientation of the basal cleavage planes were prepared by evaporating a suspension on plastic slides; when dried the films are easily separated with ethyl alcohol. These

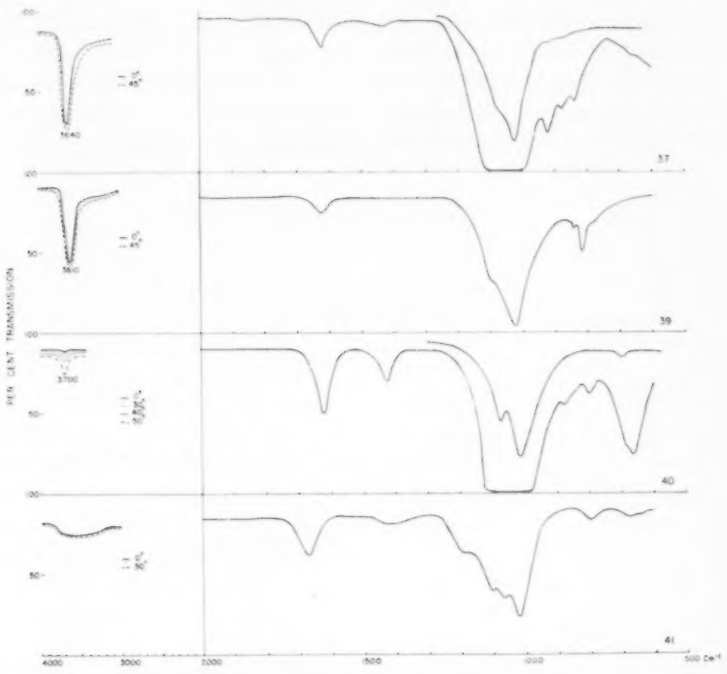

FIG. 21. Infra-red absorption curves of iron-rich montmorillonite (37), nontronite (39), hectorite (40), and saponite (41). All data from films except separate curves 600–1300 cm^{-1} from KBr pellets.

films were heated to 300° C. and protected with fluorolube oil in order to avoid rehydration. Infra-red spectra were obtained for different incident angles. Serratosa and Bradley (1958) have shown that among micas and related crystallizations trioctahedral compositions exhibit an OH bond axis normal to the cleavage flake with an infra-red absorption frequency near 3700 $cm.^{-1}$, but that the dioctahedral compositions exhibit OH bond axes near the plane of the cleavage flake and of lesser absorption frequency. Determination of the direction of the OH bond axis by obtained spectra of oriented aggregates for different incident angles therefore provides a means of identifying the dioctahedral or trioctahedral nature of such crystallization.

In the 3700 $cm.^{-1}$ region all of the samples of montmorillonite and nontronite examined showed a strong absorption for normal incidence with little sensitivity to the orientation of the flake, thereby indicating that the crystallization in these samples is dioctahedral. It must be noted that it is uncertain whether a mixture of dioctahedral and trioctahedral forms

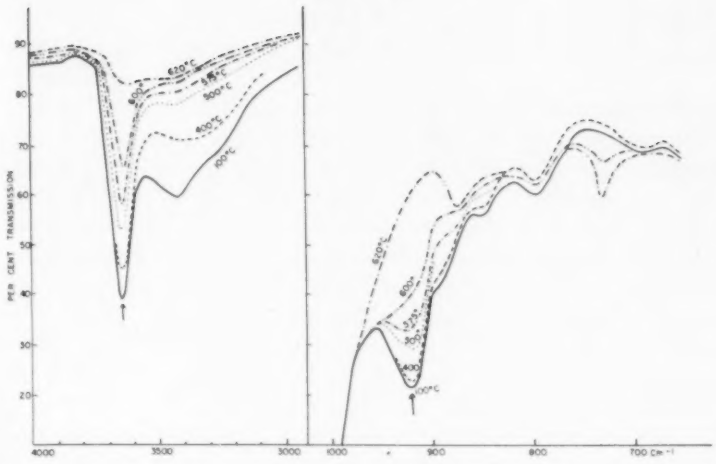

FIG. 22. Infra-red absorption curves of sample 27 composed of a mixture of Cheto- and Wyoming-type montmorillonite, and after heating to temperatures indicated.

could be detected with the equipment used (NaCl prism), if one of the components was present in small amounts. There is therefore, the possibility that a small amount of trioctahedral material may be present in these samples. It is of interest that the maximum absorption of the montmorillonites corresponds to that of muscovite (3640 cm.$^{-1}$), whereas that of the nontronites, is lower (3600–3610 cm.$^{-1}$).

The samples of saponite and hectorite, Fig. 21, show an absorption at higher frequencies (3700–3710 cm.$^{-1}$) which increases markedly with the incidence angle thereby indicating the trioctahedral nature of these minerals. The effect is more pronounced in the saponite than in the hectorite, probably because of the substitution of some OH by F in the hectorite.

In the 2000-600 cm.$^{-1}$ region the samples were examined as films without any protection, and as disseminated KBr pellets in concentrations of 0.3 to 0.8 per cent. All the samples show a band at 1625 cm.$^{-1}$ characteristic of the adsorbed water (deformation frequency of the H-O-H vibration). There is strong absorption at 1000–1050 cm.$^{-1}$ associated with the Si-O bonds, and a medium band between 1075 and 1125 cm.$^{-1}$ which cannot be explained. Also in the montmorillonites and nontronites there is a relatively weak band at 840–850 cm.$^{-1}$. The absorption at 775 and 800 cm.$^{-1}$ is due to quartz impurity.

In montmorillonites with aluminum as a principal cation in octahedral positions there is a relatively strong band at 920 cm.$^{-1}$. In the nontronites this band is not present, but instead there is an absorption at 820 cm.$^{-1}$, the shift in frequency being produced by the substitution of iron for

FIG. 23. Infrared absorption curves of nontronite (39) and after heating to temperatures indicated.

aluminum. To investigate this matter further spectra were obtained of montmorillonite and nontronite after heating to various temperatures up to 620° C. As shown in Figs. 22 and 23, the intensity to these two bands decreases regularly as the hydroxyls are lost. They must therefore, be related to the octrahedral layer, but at present it is not certain if these absorption bands correspond to a deformation vibration of the OH groups, or are associated with the vibration of the octahedra as a whole (O-Al-OH or O-Fe-OH vibrations).

In saponite and hectorite neither the 920 or 820 cm.$^{-1}$ band is present. Probably the strong absorption at about 650 cm.$^{-1}$ is the corresponding one in these minerals.

For the present study the salient conclusion from the infra-red data is that all the montmorillonites and the nontronite are dioctahedral. Any mixing of trioctrahedral crystallizations is believed to be very minor. The spectra do show slight variations in the 1200-600 cm.$^{-1}$ region which it is hoped future studies will relate to differences in the population of the tetrahedral and octahedral positions in the structure. In other words, it is not possible at the present time to relate these variations to differences in the type of montmorillonite, but there is considerable possibility that future investigations will permit such a correlation.

MICROSCOPIC STUDY AND OPTICAL PROPERTIES

Oriented aggregates produced by drying a suspension on a glass slide were examined with a petrographic microscope to determine the char-

acter of the aggregates and also, if possible, the optical properties of the montmorillonites.

In general the Wyoming-type montmorillonite shows much better aggregate orientation than the Cheto-type. The individual particles in the Wyoming-type aggregates are often too small to be seen individually and the aggregate has the appearance of the fragment of a single crystal. On the other hand, individual particles of the Cheto-type are easily visible in the aggregate which has a granular appearance. The uniformity of orientation of the individuals is much less in the Cheto-type than in the Wyoming-type. The particles of the Wyoming-type are not only smaller, but have aggregated together so perfectly that something akin to crystal growth has taken place.

As would be expected, the aggregates of the samples which are mixtures of the Wyoming- and Cheto-types are variable. Some are about like those of the Wyoming-type whereas other are distinctly granular. The aggregates of the miscellaneous type of montmorillonites are more like those of the Wyoming-type than the Cheto-type. Many of these samples provide aggregates which are composed of extremely small particles with a very high degree of uniformity of orientation. The sample of hectorite gives particularly excellent aggregates.

The optical properties were studied to determine if there was any consistent difference between values for the Cheto- and Wyoming-types. No such differences were found unequivocally and perhaps none are to be expected since, as Ross and Hendricks (1945) have shown, the indices vary with the iron content and as Mehmel (1937) has shown, the indices also vary with the content of magnesium. As both the iron and magnesium vary within the types, the influence of this variable might well conceal any variation between types. However, the data suggest that where the composition is similar the Wyoming type has slightly higher indices. Thus, sample 8, which is a Wyoming-type with a low iron content has a higher indice ($\beta = 1.530$) than sample 4 of the Cheto-type with a slightly higher iron content ($\beta = 1.520$). No satisfactory explanation can at the moment be offered for a possible consistent difference in optical properties from one type to the other.

Potassium and Magnesium Treatment

Samples of the various types of montmorillonite were treated with KCl (1N) and then washed until free of chloride. Diffraction diagrams were obtained on oriented slides after air drying with and without glycol treatment, and after oven drying and glycol treatment.

Wyoming-type samples, Fig. 24, collapsed to a c axis spacing of about 11.7 Å on air drying. Both the air dried and oven dried (at 100° C. for 2 hours) expanded to about 17.4 Å following glycol treatment. Therefore

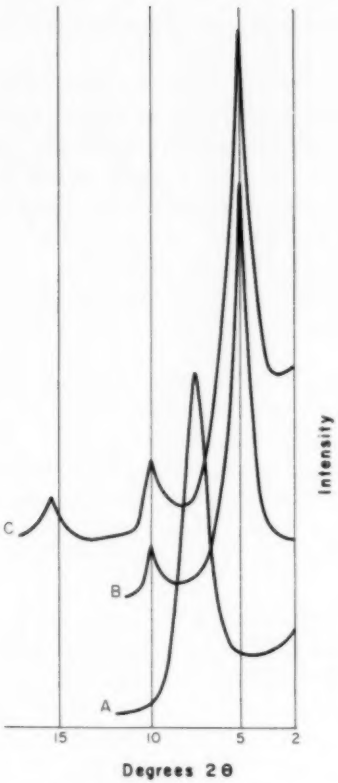

FIG. 24. *X*-ray diffraction data for Wyoming-type montmorillonite (10) treated with KCl. A—air dried, B—air dried and glycol treated, C—dried at 100° C. for 2 hours and glycol treated.

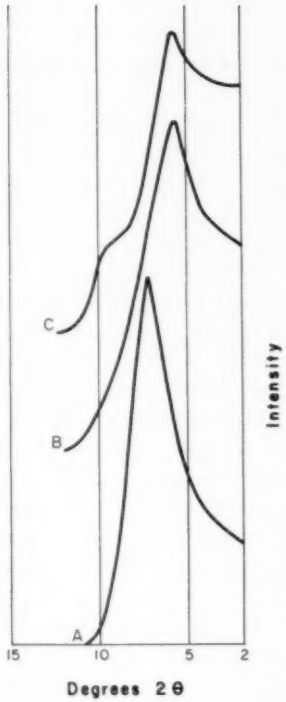

FIG. 25. *X*-ray diffraction data for Cheto-type montmorillonite (1) treated with KCl. A—air dried, B—air dried and glycol treated, C—dried at 100° C. for 2 hours and glycol treated.

it may be concluded that no permanent collapse of the structure or retardation of expansion was caused by potassium treatment of this type of montmorillonite.

The two samples of Cheto-type, Figs. 25 and 26, so treated collapsed on air drying to 12.1 and 11.9 Å. respectively. Following glycol treatment the air dried samples expanded to 15.5 and 14.7 Å, respectively. Glycol treatment of the oven dried samples produce material which expanded to about 15.5 and 14 Å, respectively. Results following the treatment of potassium chloride are therefore different for the two types of montmorillonite. This matter is being investigated further. Present data show

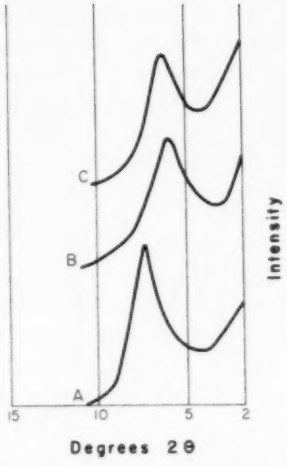

FIG. 26. *X*-ray diffraction data for Cheto-type montmorillonite (3) treated with KCl. A—air dried, B—air dried and glycol treated, C—dried at 100° C. for 2 hours and glycol treated.

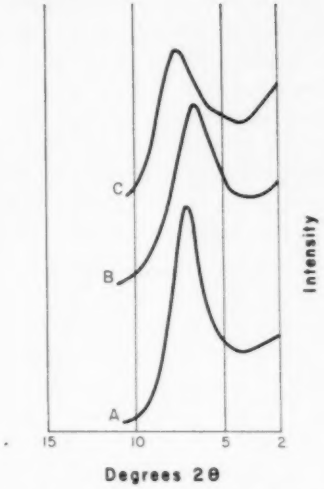

FIG. 27. *X*-ray diffraction data for iron-rich montmorillonite (37) treated with KCl. A—air dried, B—air dried and glycol treated, C—dried at 100° C. for 2 hours and glycol treated.

that the results are not the same for all montmorillonites derived from bentonites, and that the process must be used with caution in distinguishing expandable clay minerals derived from different parent materials (*e.g.* degraded micas versus montmorillonites from bentonites). It seems worthwhile to emphasize that the type of montmorillonite which shows no effect of potassium treatment, *i.e.* Wyoming type, is the one with a lower charge on the lattice and a lower cation exchange capacity. The type with a greater charge on the lattice shows retardation and reduction in amount of expansion, *i.e.* apparently in this type of montmorillonite enough potassium is held between the silicate layers to prevent complete expansion.

Miscellaneous sample 37 following potassium treatment shows, Figs. 26–27, a *c*-axis spacing of 12.5 Å without glycol treatment and 13.6 Å after glycol treatment. After oven drying the sample shows an expansion with glycol to only 11.6 Å. This sample has a larger amount of replacement within the octahedral positions than the Cheto-type samples, and as expected potassium treatment causes a greater reduction in expansion than for the Cheto-type samples.

The same samples were treated with magnesium chloride (1N) and then washed free of chloride. The results were the same for all the sam-

ples. Diffraction patterns obtained after air drying show a c-axis spacing of 13.8 Å. Following glycol treatment, the air dried samples and samples oven dried at 100° C. for 2 hours expanded to 17.2 Å. Thus the magnesium treatment has no effect in reducing the amount of expansion of the montmorillonites studied. The difference in the effect of potassium and magnesium is expected, since regardless of the charge, at least within the limits of the samples investigated, the size and coordination char-

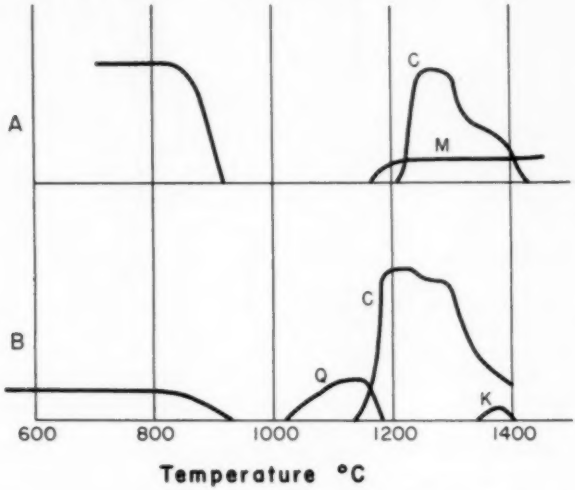

FIG. 28. High temperature phases developed by particle size fractions of a sample (29) composed of a mixture of Cheto- and Wyoming-type montmorillonites. A, Fraction < 1 micron; B, Fraction 2–1 micron; Q, Beta Quartz; C, Beta Cristobalite; M, Mullite; K, Cordierite.

acteristics of the magnesium ion would not cause it to aid in restricting the expansion of dried montmorillonites. Further magnesium treatment is a safer way to distinguish expandable material derived from chlorite as compared to montmorillonite derived from volcanic ash than is potassium treatment in distinguishing expandable material derived from mica as compared to montmorillonites from bentonites.

FRACTIONATION OF THE SAMPLE COMPOSED OF MIXTURE OF TYPES

Sample 29, indicated as a mixture of the Wyoming- and Cheto-type montmorillonite was fractionated by centrifuging a dilute suspension of the minus 2 micron component into the fractions containing particles of 2 − 1 microns and minus 1 micron. It can be seen from Fig. 28 that the finer fraction gave high temperature phase characteristics of the Wyoming-

type, whereas the coarser fraction exhibited such characteristics of the Cheto-type. It may be concluded that in this sample at least the mixture is one of discrete particles. Also, as expected, the Wyoming-type dispersed into smaller particles than did the Cheto-type montmorillonite.

Discussion

The present investigation indicates that dioctahedral montmorillonites do not form a single continuous isomorphic series. Two different aluminous types have been found, Cheto- and Wyoming-types, which differ primarily in the population of the octahedral layer; notably in the relatively higher amount of magnesium in the Cheto samples.

It is noteworthy that the addition of magnesium to the Wyoming-type montmorillonite does not cause the development of high temperature phases characteristic of the Cheto-type (unpublished data). Also repeated leaching of the samples with HCl in order to remove most of the octahedral cations did not change the high temperature reactions of either type. It seems, therefore, that there are structural as well as compositional differences between the two types. The analytical data suggest that these differences are as follows:

The Cheto-type has relatively more substitution of aluminum by magnesium in the octahedral layer causing a greater charge on the lattice. Further, the replacements are relatively more regular, *i.e.* the position of the magnesiums is in a fairly definite pattern in the Cheto-type. If the magnesiums were randomly distributed, the particles would have some Mg-rich areas as well as some Mg-poor areas. Therefore, they would have high-temperature phases of both types; indeed, this never happens with properly sized and purified fractions. Also it is thought that some (probably a small number) of the silica tetrahedra are inverted in the Cheto-type. There does not seem to be a difference in the population of the tetrahedral positions in the two types.

Figure 29 shows an ideal arrangement of octahedral cations with one fourth of the aluminums replaced by magnesium. This is close to the average Cheto-type composition and it seems reasonable to think that this type of montmorillonite has the magnesiums arranged in such a pattern. Considering this pattern the typical properties of the Cheto-type montmorillonite can be explained. Thus, the exchange sites being on a hexagonal net, the same kind of symmetry can be expected in the stacking of the elementary silica layers. Some of the exchangeable cations can also act as bonds between the layers. The net result of these factors would be the larger particles characteristic of the Cheto-type, the more difficult complete dispersion, and the development of a mica-like structure following potassium treatment. On the contrary, in the Wyoming-type mont-

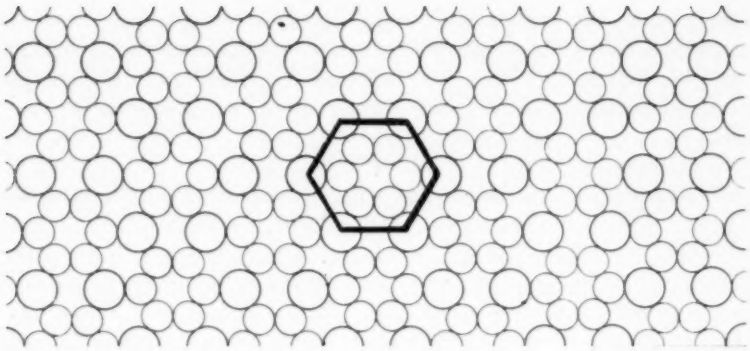

FIG. 29. Probable arrangement of octahedral cations in Cheto-type montmorillonite, showing suggested hexagonal arrangement of exchange sites. Large circles—Mg, small circles—Al.

morillonite, the exchange sites are randomly distributed, and no regular stacking and bonding of the silicate layers is to be expected. As a consequence, hydration and dispersion of the individual layers is relatively very easy.

The Cheto-type shows a greater loss of water in the 100–500° C. temperature interval which can be accounted for by some inversion of the silica tetrahedra. The hydroxyls of the exposed tips of the tetrahedra would probably be lost within this temperature interval.

No specific explanation can be offered for the variation in the dehydroxylation characteristics, i.e. dual versus single endothermic peak accompanying the reaction and the variation in intensity of the reaction. Samples with higher iron and magnesium contents have reactions of lesser intensity, so that variations in composition are a factor but structural attributes also are probably important. It seems likely that a dual peak means some sort of mixing of layers.

The intensities of the (001) reflections do not change on dehydroxylation of the Cheto-type samples whereas the relative intensities of these reflections do change for the Wyoming-type. It would seem likely that there would be less structural adjustment in the better crystallized Cheto-type with its regularity of substitution in the octahedral positions and hence less change in the intensity of the basal reflections accompanying the loss of hydroxyls.

The endothermic peak at about 900° C. varies in intensity and over a considerable temperature interval and is probably a matter of the abruptness of the loss of the montmorillonite structure causing it. For the Cheto-type the reaction is generally relatively intense in accordance

with the better crystallinity and hence the probable more abrupt loss of structure. The reaction for the Wyoming-type may be large or small, probably due to small variations in crystallinity and probably also to variations in composition. The intensity of the reaction decreases as the iron content increases, and in very iron-rich samples it is about absent. The presence of iron thus favors a gradual loss of the montmorillonite structure.

Electron micrographs show that the loss of the diffraction characteristics at about 900° C. is not accompanied by the complete loss of the external morphology, *i.e.* the flake shape of the units is still preserved. Data are not unequivocal, but the external form seems to be better preserved in the Cheto type than in the Wyoming-type montmorillonite. The reaction cannot be a complete structural breakdown but rather one in which the layer character is retained probably with lack of stacking order and some distortion in the *a* and *b* direction.

The formation of beta quartz from the Cheto-type probably involves whole reorganization of adjacent tetrahedral layers. It is thought that the presence of some inverted tetrahedra would favor the formation of this quartz phase which is not in the temperature domain of the formation of beta quartz as indicated in silica equilibrium diagrams. The postulated absence of inverted silica in Wyoming-type would explain the absence of a quartz phase from these montmorillonites (it has been pointed out that there is no difference in the composition of the tetrahedral positions in the two types). The differences in the temperature interval for various Cheto-type samples between the loss of montmorillonite diffraction and the formation of beta quartz and the variation in the intensity of the reaction accompanying the formation of quartz may be explained by variations in the amount of inverted tetrahedra and the consequent variation in the ease of formation of beta quartz.

The Wyoming-type montmorillonite shows a long temperature interval between the loss of montmorillonite diffraction and the formation of any high temperature phase. The absence of any inverted tetrahedra makes difficult the development of new phases. Cristobalite appears at a lower temperature in the Cheto- as compared to the Wyoming-type samples. That is, it appears at a lower temperature when formed by the inversion of beta quartz than when it develops directly from the silica of the montmorillonite structure.

At about 1200° C. mullite forms from the Wyoming-type samples. This phase does not form from the Cheto-type mineral as apparently magnesium in amounts in excess of about 1–2% MgO prevent the formation of mullite. Also, in the iron-rich samples, mullite does not appear so that small amounts of iron also block the formation of mullite. The

mullite that does form from the Wyoming-type montmorillonite probably is not pure aluminum silicate as the lattice parameters are slightly different from published values of pure material—in many instances it probably has about all the impurities that the structure will tolerate.

The intense exothermic peak shown on the differential thermal curves of the Wyoming-type samples at about 1000° C. is not accompanied by any crystalline phase detectable by *x*-ray diffraction. This reaction is interpreted as a consequence of a shift in bonding within the structure probably from face sharing octahedral units of dehydrated montmorillonite to the more stable edge sharing units which prevail in the high temperature structures that may form. This bonding shift is but one step in the development of new high temperature phases. A second step is the migration of cations into proper positions on a scale leading to crystal growth of a size detectable by *x*-rays. Higher temperature (about 1200° C.) is required to provide sufficient mobility of the cations so that this growth can take place. This second step may never take place if the composition is not proper for the specific network to form or if cations are present which block the growth or break up the network at relatively low temperatures. The potassium ion for example substantially inhibits the formation of any high temperature phase from the montmorillonite minerals (Kulbicki and Grim, 1957).

The phases that form at temperatures below about 1200° C., *i.e.* the beta quartz and cristobalite from it, form at this relatively low temperature because of their structural relation to the silica part of the montmorillonite structure. The first or nucleation stage of phases that appear prominently above about 1200° C. is closely dependent on the structure of the original mineral. Thus the arrangement of the magnesiums in the octahedral layer of the Cheto-type is such that the nucleation of cordierite is favored. The development of the high temperature phases beyond the nucleation stage is determined largely by the bulk composition of the material.

The presence of cristobalite in the unfired clay has no effect on the formation of high temperature cristobalite. This indicates that the new cristobalite is formed directly from montmorillonite rather than by a complete breakdown of a montmorillonite structure and then a regrouping around the primary cristobalite. That is, the formation of the new cristobalite is a solid state reaction from the montmorillonite.

The miscellaneous types of aluminous montmorillonites differ from the Wyoming-type only in the formation of a small amount of beta quartz. This can be explained by a varying small amount of inversion of the silica tetrahedra in these samples.

Nontronite and the very iron-rich montmorillonites only yield a silica

phase (cristoballite) at elevated temperatures. Iron apparently in substantial amounts blocks the development of any other crystalline phase.

For the trioctahedral magnesium-rich montmorillonites and talc, enstatite develops before the montmorillonite structure is completely lost and without any accompanying thermal reaction. This suggests a gradual breakdown of the structure of the original mineral with gradual growth from the debris of the enstatite—unlike the solid state reactions for the dioctahedral forms. In some cases, cristoballite develops at very high temperatures from the left over silica. The reason for the development of little or no cristoballite in some cases (hectorite) and much for other minerals (saponite) is not clear. The elongate structure of the hectorite as compared to the flake-shape of the saponite may be significant.

References

Byrne, P. J. S. (1954), Some observations on montmorillonite-organic complexes: *Proc. Second Nat. Clay Conference Pub.* **327,** *U. S. Nat. Acad. of Sci.*, 241–253.

Deuel, H., Huber, G., and Iberg, R. (1950), Organische Derivate von Tonmineralien: *Helv. Chim. Acta*, **38,** 1229–1232.

Edelman, C. H., and Favejee, J. Ch. L. (1940), On the crystal structure of montmorillonite: *Zeit. Krist.*, **102,** 417–431.

Grim, R. E. (1934), The petrographic study of clay minerals—A laboratory note: *Journ. Sed. Petrol.*, **4,** 45–46.

——— and Rowland, R. A. (1942), Differential thermal analyses of clay minerals and other hydrous materials: *Am. Mineral.*, **27,** 746–761, 801–818.

Hendricks, S. B. (1942), Lattice structure of clay minerals and some properties of clays: *Jour. Geol.*, **50,** 276–290.

Hofmann, U., Endell, K., and Wilm, D. (1933), Kristallstruktur und Quellung von Montmorillonit: *Zeit. Krist.*, **86,** 340–348.

Jonas, E. C. (1955), The reversible dehydroxylization of clay minerals: *Proc. Third Nat. Clay Conf., Publ.* **395,** *U. S. Nat. Acad. of Sci.*, 66–72.

Kulbicki, G., and Grim, R. E. (1957), Etude des Reactions de Hautes Temperatures dans les Mineraux Argileux au Moyen des Rayons X: *Bull. Soc. France Ceramique*, **36,** 21–28.

MacEwan, D. M. C. (1951), The Montmorillonite minerals, "*X*-ray Identification and Structure of the Clay Minerals." Monograph Min. Soc. Great Britain, 86–137.

Marshall, C. E. (1935), Layer lattices and base-exchange clays: *Zeit. Krist.*, **91,** 433–449.

McAtee, J. L. (1958), Heterogeneity of montmorillonites: *Proc. Fifth Nat. Clay Conf., Publ.* **566,** *U. S. Nat. Acad. of Sci.*, 270–288.

McConnell, D. (1950), The crystal chemistry of montmorillonite: *Am. Mineral.*, **35,** 166–172.

Mehmel, M. (1937), Beitrage zur Frage des Wasserhaltes der Minerale Kaolinit, Halloysit und Montmorillonit: *Chem. Erde*, **11,** 1–16.

Ross, C. S., and Hendricks, S. B. (1945), Minerals of the montmorillonite group: *Prof. Paper* **205-B,** *U. S. Geol. Survey*, 23–79.

Serratosa, J. M., and Bradley, W. F. (1958), Infra-red adsorption of OH bonds in micas. *Nature*, **181,** 111.

Manuscript received January 18, 1961.

THE AMERICAN MINERALOGIST, VOL. 46, NOVEMBER-DECEMBER, 1961

IONIC COORDINATION IN ALUMINO-SILICIC GELS IN RELATION TO CLAY MINERAL FORMATION

C. De Kimpe, M. C. Gastuche* and G. W. Brindley†

Abstract

Syntheses of aluminum and magnesium silicates have been carried out at low temperatures and normal pressures, with the production of various proportions of gels and crystalline phases. With aluminum, the gel phase is the more abundant and identification of the crystals is possible only by electron diffraction; with magnesium, the yield in crystals is much higher and *x*-ray identification is possible. It is shown that the properties of the gels influence the kind of crystals synthesized. The main factors are pH, salt concentration and the ratio of aluminum or magnesium content to the silica content. For aluminum, the change from six-fold to four-fold coordination increases with pH. Kaolinite has been identified at low pH and mica-like structures at higher pH. Serpentine minerals have been obtained in an intermediate pH range. The better yield of magnesium-bearing minerals may be attributed to the six-fold coordination of this cation.

Introduction

According to Hénin, Caillère and their collaborators (1953), the formation of clay minerals under ordinary conditions of temperature and pressure appears to be determined by the existence of a brucite-type hydroxide layer which, even in solution, induces the SiO_4 tetrahedra to develop a layer lattice. Various clay minerals are formed depending on the type of cation involved and on the pH of the solution, with high pH's (8–9) favoring formation of 2:1 lattices and lower pH's (6–7) favoring 1:1 lattices. In the pH range 6–7, precipitation of aluminum hydroxide occurs but, according to these authors, its rapid recrystallization to boehmite prevents the formation of kaolinite under these conditions.

The present experiments were undertaken with a view to studying the influence of simultaneous additions of Al and Si in the pH range of aluminum hydroxide precipitation with the hope that the recrystallization of the hydroxide might be retarded and the formation of a layer silicate structure facilitated. Experiments were also carried out with magnesium with a view to obtaining additional information on clay mineral formation.

Part of the present study carried out in the University of Louvain has been described by Gastuche and De Kimpe (1959) but subsequent work

* Laboratoire des Colloïdes des Sols Tropicaux, I.N.E.A.C., Institut Agronomique, Héverlé-Louvain, Belgium.

† Department of Ceramic Technology, The Pennsylvania State University, University Park, Pa. (U.S.A.).

Contribution No. 60-50 from the College of Mineral Industries, The Pennsylvania State University, University Park, Pa., U.S.A.

at the Pennsylvania State University, utilizing additional techniques, now enables an integrated account to be given of these investigations.

Procedure

The influence of the following factors on clay mineral formation was studied (see also Table 1):

a) *pH control:* Daily additions were made of normal solutions of either NaOH or HCl to maintain constancy of pH in a desired range between pH 4 and 9.

b) *Salt concentration:* Two series of experiments (experiments III*a* and III*b*) were run with and without a solution saturated with NaCl. High salt concentration favors gel flocculation but no evidence of preferential orientation is found.

c) *Aluminum in solution:* Initially (experiments I and II*a*) aluminum was brought into solution by slow dissolution of a metallic plate, but subsequently (II*a*, III) by daily additions of an ionic form, $AlCl_3.6H_2O$.

The experiments were made in a constant volume of 2 l which was maintained constant by evaporation of excess water; concentration increased, therefore, as the the experiments progressed.

d) *Silica sources:* Either the sol, 'Ludox SM,' (exp. I) or ethyl silicate (expts. II & III) was added daily in small amounts. In one experiment (exp. I) no silica was added apart from that extracted from the Pyrex flask.

e) *The ratio* $Al_2O_3/(Al_2O_3+SiO_2)$: In the first experiment, where the amount of aluminum dissolved from the plate depends on the pH, the relative content of this element is always low. Subsequently in order to keep this ratio as nearly as possible 50%, Al ions were used.

Each experiment lasted for at least two months. Afterwards, the samples were removed, washed and oven-dried at 105° C.

Study of the Gels

Alumina-silica gels

The slow addition of both Si and Al ions in the pH range studied was thought to be favorable to the fixation of SiO_4 tetrahedra at the time of formation of the aluminum hydroxide framework. *X*-ray studies of such gels give no indication of crystallized aluminum hydroxide, while in a similar experiment carried out at pH 4.2 with the Pyrex glass as the only source of silica, boehmite was found as the final result, as proved by both electron and *x*-ray diffraction techniques.

To explain the lack of *x*-ray reflections in most experiments, it can be supposed that silica controls the development of the sample, imposing mainly its three-dimensional framework.

A closer study provides further information. It has been concluded by Tamele (1950) and by Milliken, *et al.* (1950), that in fresh alumina-silica gels, obtained by coprecipitation, the aluminum is involved in the four-fold coordinated silica framework, provided the (Al_2O_3/Al_2O_3

TABLE 1. SURVEY OF EXPERIMENTS AND OF RESULTS

Exp.	Silica source	Aluminum source	pH	Solution	$\frac{Al_2O_3}{SiO_2+Al_2O_3}$ %	Gel H_2O %	B.E.C. meq./g.	So m²./g.	X-ray data	Electron microscope and diffraction data
0	Pure Ludox, ppt. by propyl alcohol	—	—	—	—	5	—	400	Gel	Gel
I_a	Ludox	Al "Merck" plate	4.2	H_2O	15.7	14.1	0.5	—	Gel	Gel+kaolinite (fire-clay)
			5.5		2.6	8.15	0.26	—	Gel	Gel+kaolinite
			7.5		1.3	7.33	0.15	—	Gel	Gel+kaolinite or mica
			9.0		12.3	5.5	0.29	—	Gel	Gel+mica
I_b	Pyrex flask	Al "Merck" plate	4.5	Sat. NaCl	88.1	26.5	0.18	—	Gel+boehmite	Boehmite+kaolinite
II_a	Ethyl silicate	Al "Merck" plate	4.5	Sat. NaCl	14.7	15.2	1.61	99.3	Gel	Gel+kaolinite
		Al "Merck" plate	4.5	H_2O	20	—	—	—	Gel	Gel alone
		Al^{+3}	4.5	H_2O	31.1	31.1	0.72	31.8	Gel	Gel+kaolinite
II_b	Ethyl silicate	Metallic magnesium	6.7	Sat. NaCl		21.0	0.20	156.3	Platy serpentine	Gel+platy serpentine
		Metallic magnesium	6.7	H_2O		20.2	0.18	193.1	Brucite	Gel+platy serpertine +chrysotile
		Mg^{+2}	4.5	H_2O		8.6	0.21	—	Gel	Ge'+antigo ite
III_a	Ethyl silicate	Al^{+3}	5.0	Sat. NaCl	32.4	16.2	1.07	128	Gel	
			6.5		28.1	15.9	1.63	37	Gel	Gel+kaolinite or mica
			8.0		27.1	17.6	2.32	40.9	Gel	
III_b	Ethyl silicate	Al^{+3}	5.0	H_2O	29.6	15.4	1.11	110.8	Gel	Gel+kaolinite or mica
			6.5		29.6	12.9	1.41	114.5	Gel	
			8.0		29.7	13.6	1.87	63.0	Gel	

$+SiO_2$) ratio remains less than 30–40%. As the ratio increases, the excess aluminum may take six-fold coordination. According to Iler (1955), the the following equilibria can be considered:

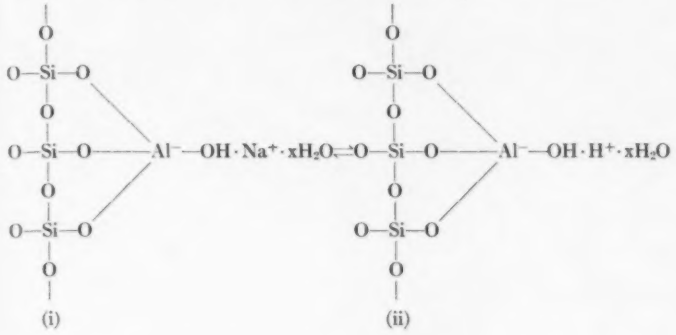

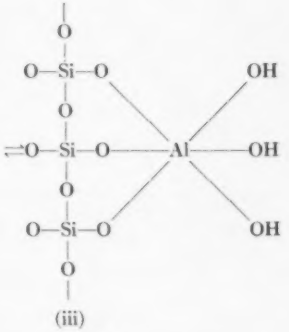

For each four-fold coordinated aluminum ion in formula (i), one negative charge arises, which is balanced by a cation. Gels of this form are stabilized under conditions of high pH and high salt concentration. With decreasing pH, at about pH 4.5, the unstable acid form of the gel, formula (ii), transforms quickly into an arrangement having uncharged six-fold coordinated aluminum, formula (iii).

a) The change in the base exchange capacity (B.E.C.) with respect to the relative content in Al_2O_3 (Fig. 1), shows a maximum as already proved by several authors, Tamele (1950), Milliken, *et al.* (1950), Bosmans and Fripiat (1958). It can be interpreted as follows: As long as the (Al_2O_3/$Al_2O_3+SiO_2$) ratio is small enough to allow the formation of tetrahedral aluminum, the charge will increase with aluminum content; when the ratio reaches the upper limit above which there are no further steric possibilities of Al-tetrahedra sharing corners with Si-tetrahedra, the charge decreases, and the excess aluminum adopts octahedral coordination.

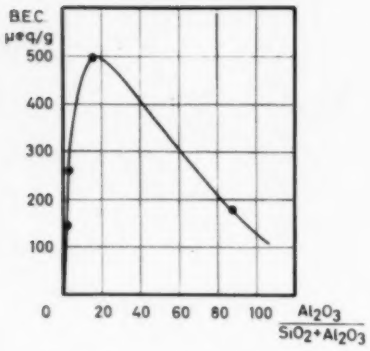

FIG. 1. Change in B.E.C. following relative aluminum content for experiment I_a.

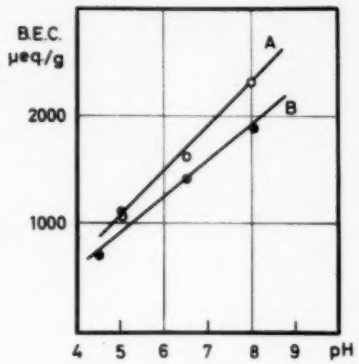

FIG. 2. Variation of B.E.C. according to pH of gel formation for the same relative aluminum content. A. Experiment III_a (in solution saturated in NaCl. B. Experiments II_a and III_b (in dilute solution).

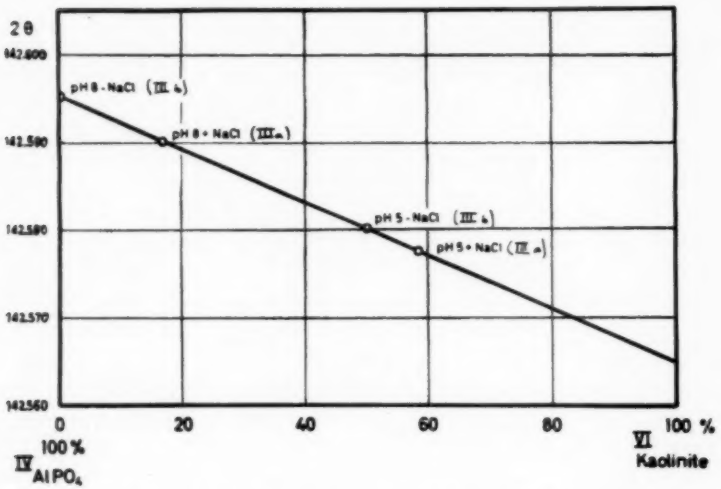

FIG. 3. Change in the diffraction angle 2θ with aluminum coordination.

b) In experiments II and III, where the aluminum content was kept constant, one observes the influence of pH and salt concentration on the transformation of aluminum coordination. In Fig. 2, it is seen that the B.E.C. of the gels increases with the pH of gel formation. For gels prepared in dilute solutions, the B.E.C. values are always smaller (*cf.* Fig. 2, line B) than those for gels prepared in more concentrated media (line A). This can be explained in terms of the equilibria discussed above.

To obtain more direct evidence for the interpretations (*a*) and (*b*), the aluminum coordination number was determined by *x*-ray fluorescence, following the method described by White, *et al.* (1958). In effect, one measures the emission wavelength of AlKα, using a reflection from an EDT crystal in the region of $2\theta = 142.5°$. A General Electric XRD-5 *x*-ray unit with a flow-proportional counter and helium path was employed. Small but significant shifts in the angular position of the AlKα line are obtained for different corrdination states. The results are calibrated by reference to $Al^{IV}PO_4$ and $Al_2{}^{VI}Si_2O_5(OH)_4$ (kaolinite). A calibration line is drawn between the 2θ-values obtained with $AlPO_4$ and

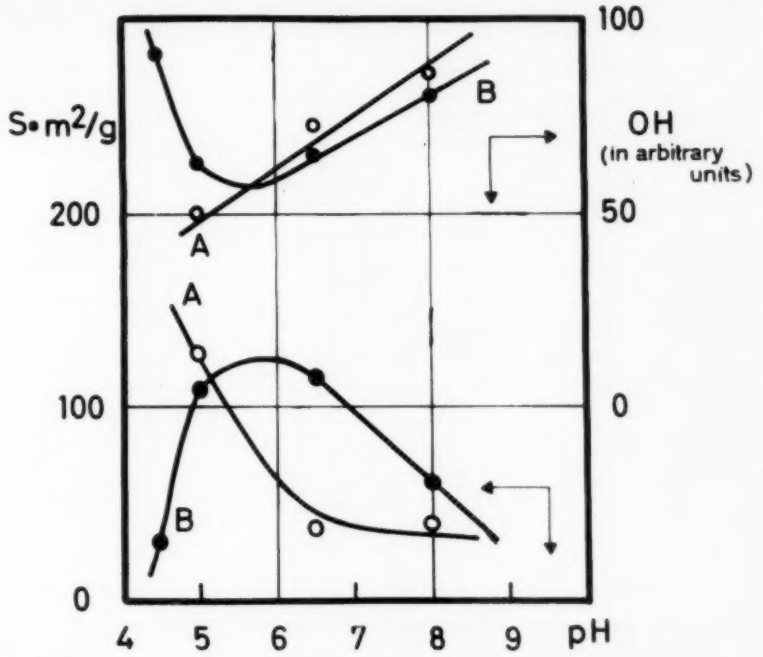

FIG. 4. Evolution of surface area and OH content following the pH of gel formation. A. Gels prepared in concentrated NaCl solution. B. Gels prepared in dilute solution.

with kaolinite, as in Fig. 3, from which an estimate is obtained of the proportions of Al ions in the two coordination states in a mixture. Although high accuracy cannnot be claimed for these estimates of Al^{IV} and Al^{VI}, nevertheless when the results for the gels are inserted in the diagram a clear trend is seen towards six-fold coordination as the pH conditions become more acidic.

c) Valuable data also are provided by surface area (S_0) measurements, which are compared with the OH content of the gels (Fig. 4). The former determinations were made following the Brunauer, Emmett and Teller (B.E.T.) method, by adsorption of nitrogen at low temperature. The OH contents of the gels were obtained by infra-red spectrophotometry; the intensity of the OH stretching vibration band at 2.85μ was compared with the intensity of the H_2O deformation band at 6μ, and this ratio, when multiplied by the total water content of the gel determined by chemical analysis, gives a value related to the total OH content of the sample.

The curve for the specific surfaces of gels obtained under conditions of great dilution (see lower part of Fig. 4), shows a maximum around pH 5.5 which, according to Iler (1955), is the pH of maximum instability for a silica gel. It is noticeable that this disorganization appears also in the formation of mixed gels.

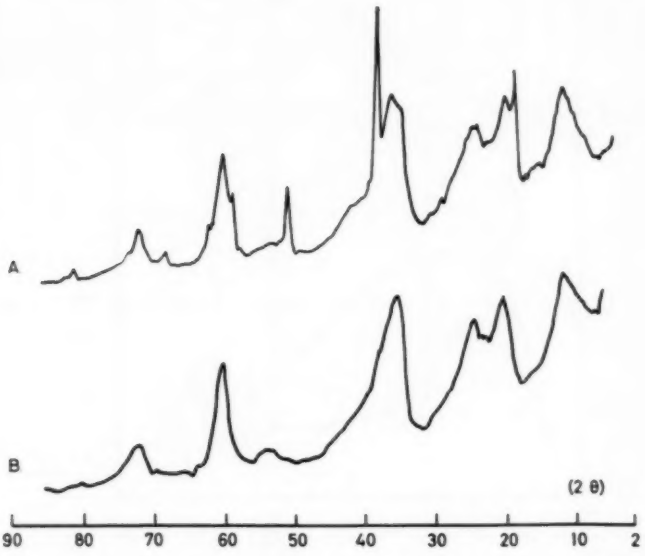

FIG. 5. *X*-ray patterns of the magnesium products. A. Serpentine mineral, plus brucite. B. Serpentine mineral; in the presence of NaCl, the reaction is complete and brucite is wholly transformed.

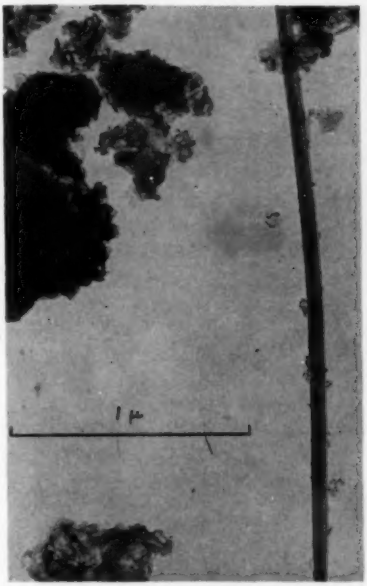

FIG. 6. Example of a fiber formed in the experiment with magnesium and ethyl silicate, in dilute solution.

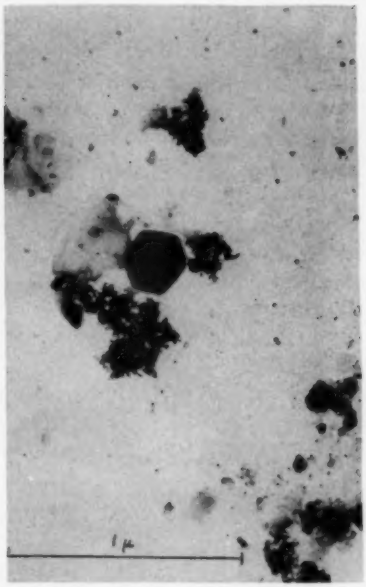

FIG. 7. Formation of kaolinite crystals. Notice the variable thickness of the platy crystals. Experiment II_a; ionic aluminum and ethyl silicate at pH 4, 5.

The decrease in surface area observed at high pH can be explained by a strain due to the water held by the cations. Iler (1955) admits this possibility for alumina-silica gels. Bosmans and Fripiat (1958) observe also, for such freshly coprecipitated gels, that the maximum in B.E.C. at about 30 to 40% of relative aluminum content is connnected with the minimum in surface area, measured by the B.E.T. method.

The slow increase in OH groups along with increasing B.E.C. for these samples (compare data in upper part of Fig. 4 with data in Fig. 2), comes from the stabilization of the tetrahedral aluminum form. The low surface area measured for the gel prepared at pH 4.5 comes along with a sharp increase in OH groups and a very low B.E.C.; in this case, the six-fold coordinated aluminum is stabilized.

Magnesia-silica gels

Experiment II_b was performed in order to investigate the formation of gels starting from a cation which takes only the six-fold coordination.

Two kinds of magnesium sources have been used. The ionic form, $MgCl_2 \cdot 6H_2O$, was added slowly along with ethyl silicate at pH 5.5. Two

other experiments were performed with metallic magnesium; one in a solution saturated in NaCl, the other in dilute solution. The metal quickly transformed into hydroxide; the reaction was more rapid in presence of NaCl.

Though the pH had to be kept constant in the acid pH range, the rapid dissolution of magnesium into hydroxide increased the pH up to 7.5.

The products obtained in these experiments are characterized by very high specific surface, high water content and very low B.E.C.

The Crystalline Phase

Magnesium products

For the reasons given above, the yield in crystalline phase is important and good *x*-ray patterns of a 1:1 serpentine mineral were obtained.

The presence of NaCl promoted considerably the result; in the case of dilute solutions, the brucite pattern is still present (Fig. 5).

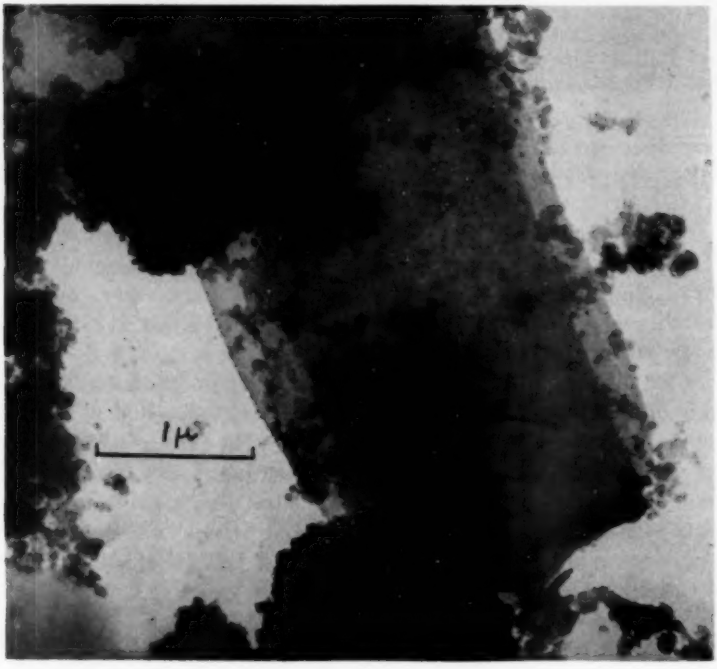

Fig. 8. Formation of mica-like plates. Crystal coming from experiment I_a, with Ludox and metallic aluminum at pH 9.

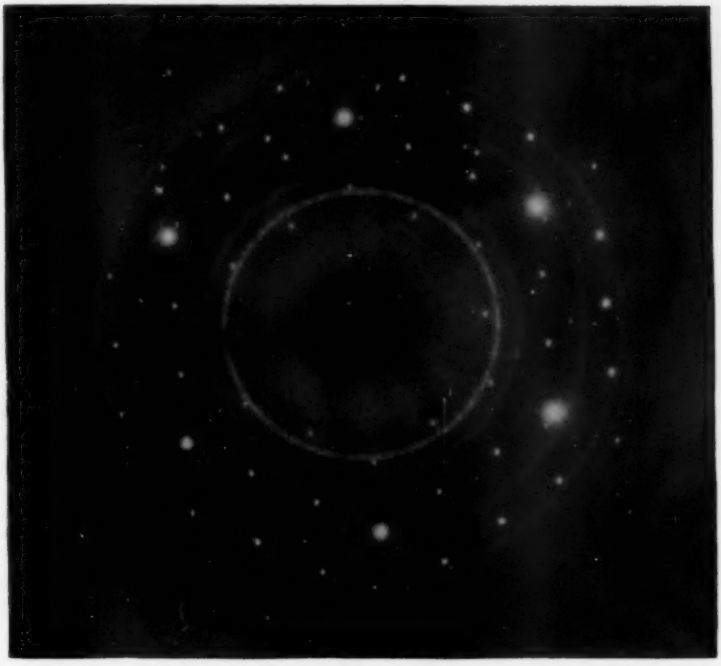

FIG. 9. Example of diffraction by pseudo-hexagonal crystal found at low pH, kaolinite. Ring pattern formed by aluminum metal used as internal standard.

Under the electron microscope, two different crystalline forms were observed. A platy form was obtained which yielded an electron diffraction pattern showing a hexagonal distribution of spots with *no* evidence for the long *a*-parameter of antigorite found by Zussman, *et al.* (1957). This form is therefore a platy serpentine, possibly lizardite, but complete identification is not possible. At least it can be said that the platy form is *not* antigorite in the strict sense of this term. Fibrous forms are also observed in the electron microscope and these appear to be chrysotile (Fig. 6).

Aluminum products

As said previously, the yield in crystalline phase was never sufficient to give a useful *x*-ray pattern. Therefore, all the determinations on these crystals were made using electron microscope and electron diffraction techniques.

In most cases, the first step in the crystalline process appears to be the formation of plates with a widely variable thickness. Their development in the 001 plane depends on the pH. In the low pH range, several pseudo-hexagonal crystals were found (Fig. 7) some showing 120° angles, very similar to those of a well crystallized kaolinite. In the high pH range, the crystals are better developed in the 001 plane, but their morphology is less well defined. They do not show any obvious geometrical form except that occasionally they are platy in appearance (Fig. 8).

The diffraction unit of the R.C.A. microscope E.M.U. 2D was used, equipped with an aperture specially designed by Charteron and Oberlin (1956) which permitted selected area diffraction. Single-crystal patterns were obtained showing *hk*0 reflections. Identification on the basis of these reflections is difficult and has been discussed fully by Brindley and De Kimpe (1961). They find that a clear distinction between the *hk*0 diagrams of different layer lattices is possible only by accurate measurement of the lattice parameters, using metallic aluminum shadowing as an internal standard. By this method it is possible to measure the *b*-parameter with an accuracy better than $\pm 0.2\%$, which is sufficient to distinguish between the principal clay lattices (see Fig. 9).

Using this method, *b*-parameters were measured for crystals among the gel phase: At pH 4.5, the *b*-parameter is 8.93 ± 0.03 Å. It can be correlated with kaolinite. At higher pH, a value of *b* equal to 9.02 ± 0.02 Å corresponds to a mica or mica-like mineral. The sodic mica, paragonite, is a possible explanation.

Conclusions

Though the yield of crystalline phase is very poor in the experiments carried out in the presence of aluminum, a detailed study of the gel phase shows its tendency to organization, confirmed by the crystalline phase study. Kaolinite appears at low pH, where the six-fold coordinated structure of aluminum is stabilized. At higher pH, a mica-like clay mineral appears, while the four-fold coordinated aluminum increases in the gel structure.

The low yield in crystalline phase can be attributed to:

(i) The insolubility of silica at the pH studied induced the polymerization of an alumina-silica gel.

(ii) The aluminum ion easily gives an isomorphous substitution with silicon, the hexacoordinated form being stable only at low pH.

The latter difficulty does not arise with magnesium ions and in consequence magnesian clays are developed more easily.

Acknowledgments

Thanks are due to Professor J. J. Fripiat for his interest and encouragement during this work.

Some of the experimental measurements were performed at the Department of Ceramic Technology, The Pennsylvania State University, and form part of the program of Project 55, sponsored by the American Petroleum Institute to whom our thanks are due.

References

Bosmans, H., and Fripiat, J. (1958), Ionenuitwisselingsvermogen en oppervlakte ladingsdichtheid van SiO_2-Al_2O_3 gelen. *Pédologie*, **8**, 184–198.

Brindley, G. W., and De Kimpe, C. (196–), Identification of clay minerals by single crystal electron diffraction. *Am. Mineral.* **46**, 1005–1016.

Caillere, S., and Henin, S. (1948), Essais de synthèse des minéraux argileux. *Verres et Silicates Ind.*, **12**, 63–64.

Caillere, S., Henin, S., and Esquevin, J. (1953), Recherches sur la synthèse des mineraux argileux. *Bull. Soc. Fr. Min.*, **76**, 300–314.

Charteron, R., and Oberlin, A. (1956), Description d'un selecteur pour microdiffraction électronique. *Bull. Soc. Fr. Min. Crist.*, **79**, 479–490.

Gastuche, M. C., and De Kimpe, C. (1959), Tentative de synthèse des argiles du groupe du kaolin dans des conditions normales de température et de pression. *Acad. Royale de Belgique, Bull. Cl. Sc., 5th series*, **45**, 1087–1104.

Henin, S., and Robichet, O. (1954), Resultats obtenus du cours de nouveaux essais de synthèse des minéraux argileux. *C. R. des Réunions du Groupe Fr. des Argiles*, **VI**, Nouvelle serie no. 1 (1954) 19–22.

Iler, R. K. (1955), The colloid chemistry of silica and silicates. Cornell Univ. Press, Ithaca, N. Y.

Milliken, J. H., Mills, G. A., and Oblad, A. G. (1950), The chemical characteristics and structure of cracking catalysts. *Disc. Farad Soc.*, **8**, 279.

Tamele, M. W. (1950), Chemistry of the surface and the activity of alumino-silica cracking catalysts. *Disc. Farad. Soc.*, **8**, 270–279.

White, E., McKinstry, H., and Bates, T. F. (1958), Crystal chemical studies by *X*-ray fluorescence. Seventh Ann. Conf. Ind. App. *X*-Ray Analysis, Univ. of Denver, 239–245.

Zussman, J., Brindley, G. W., and Comer, J. J. (1957), Electron diffraction studies of serpentine minerals. *Am. Mineral.*, **42**, 133–153.

Manuscript received January 18, 1961.

THE AMERICAN MINERALOGIST, VOL. 46, NOVEMBER-DECEMBER, 1961

THE RELATIONSHIP BETWEEN UNIT-CELL EDGES AND COMPOSITION OF SYNTHETIC WURTZITES[1]

BRIAN J. SKINNER AND PHILIP M. BETHKE, *U. S. Geological Survey, Washington 25, D. C.*

ABSTRACT

Synthetic 2H wurtzites have been prepared in the composition planes ZnS-FeS-MnS and ZnS-FeS-CdS. In both planes, the unit-cell edges are linear functions of the composition expressed in mol per cent.

The cell edges of Fe- plus Mn-bearing wurtzites are described by the linear functions

$$a = 3.8230 + 0.000490\ X + 0.001628\ Z$$
$$c = 6.2565 + 0.000886\ X + 0.002089\ Z$$

where a and c are in Ångstrom units and X and Z are the FeS and MnS contents respectively.

The cell edges of Fe- plus Cd-bearing wurtzites are defined by the linear functions

$$a = 3.8230 + 0.000490\ X + 0.003124\ Y$$
$$c = 6.2565 + 0.000886\ X + 0.004555\ Y$$

where a and c are in Ångstrom units and X and Y are the FeS and CdS contents respectively, in mol per cent.

INTRODUCTION

Wurtzite (ZnS) is hexagonal, space group $P6_3mc$, $Z = 2$. Like sphalerite, it does not appear to deviate measurably from the stoichiometric formula. It can, however, tolerate very extensive solid solutions, whereby iron, manganese, cadmium and other cations can replace zinc in the structure, and anions such as selenium and oxygen can replace the sulfur. Numerous previous studies have demonstrated that measurable changes in the unit-cell edges of wurtzite accompany the compositional changes of the solid solutions.

Wurtzite is the high temperature polymorph of ZnS, sphalerite being the phase stable at room temperature. Allen and Crenshaw (1912) determined the temperature of the sphalerite-wurtzite transition for pure ZnS as 1020° C. and demonstrated that the transition temperature was lowered by the presence of iron in solid solution. Kullerud (1953) studied the effect of iron, manganese and cadmium on the sphalerite-wurtzite transition, showing that all three caused a significant decrease in the transition temperature.

Frondel and Palache (1950), Strock and Brophy (1955) and others have demonstrated that regular one-dimensional stacking faults may occur in wurtzites, giving rise to higher periodicities along the c-axis than the 2-layer repeat of common, or 2-layer hexagonal (2H) wurtzite. All

[1] Publication authorized by the Director, U. S. Geological Survey.

wurtzites prepared in the present study have the basic 2H structure. This statement is based on the *x*-ray work of D. Appleman, who kindly studied a number of single crystals by the Buerger precession method and found them all to be 2H. In addition, *x*-ray diffractometer tracings and *x*-ray powder diffraction films were made of all compounds prepared, and no lines were observed that could be attributed to a stacking sequence other than 2H.

Sample Preparation and Measurement

All wurtzite samples were prepared by heating mixtures of the requisite amounts of ZnS, FeS, MnS and CdS in sealed, evacuated, silica-glass tubes. The starting compounds were prepared from the same zinc, iron and sulfur described by Skinner *et al.* (1959) and the same manganese and CdS described by Skinner (1961).

Unit-cell edge measurements were all made with the *x*-ray diffractometer using copper radiation. The (110), (200), (210) and (300) spacings were used to determine a and the (103), (004), (203) and (114) to determine c. NaCl was used as an internal standard of measurement; the unit-cell edge of NaCl was taken from Frondel (1955) and converted from kX to Å by the conversion factor 1.00202 (Bragg, 1947).

Individual diffraction lines were measured by successive oscillations, each oscillation including both the reference line of the internal standard and the wurtzite line under observation. A minimum of six oscillations were made over each line. The samples prepared by Bethke (samples labeled B, Table 5) were measured against NaCl, using the step-scanner attachment on the *x*-ray diffractometer. Two individual measurements were made for each composition, the sample being rotated 180° about an axis perpendicular to the surface, after each measurement.

A value for a, independent of c, was calculated directly from each measurement of the $h00$ and $hk0$ spacings selected. The calculated a's were combined by taking the average, and the average a used to calculate a value for c from the measured spacings of the (103), (203) and (114) reflections. A value for c, independent of a, can be calculated directly from the (004) spacing. All the calculated c's were averaged to get the value of c quoted for a given composition.

The values quoted in Tables 4–9 for the cell edges of individual compounds are the numerical averages of all measurements of the compound. The precisions stated have no statistical significance and are simply the maximum observed deviation from the numerical average. Previous studies have shown that the methods employed allowed the same reproducibility to be attained by different workers, using different equipment (Skinner *et al.*, 1959).

Unit-Cell Edges of Pure Wurtzite

The cell edges of pure wurtzite have been measured by a number of workers, and these values have been gathered for comparison in Table 1.

It is apparent that there is reasonable agreement between various workers for the value of a. Agreement on the value of c, however, is less satisfactory. Swanson and Fuyat (1953) and the present authors are in essential agreement, but the values of other workers are widely scattered. The reason for these discrepancies cannot readily be found in compositional differences, except perhaps in the case of Ulrich and Zachariasen (1925) who recorded both a and c significantly greater than anyone else. The discrepancies may possibly be found in differences of measurement procedure, but unfortunately most workers did not describe their methods in sufficient detail to allow adequate review. However, Smith *et al.* (1957) specifically state that they used the (110) reflection to determine a and the (006) to determine c. Although (006) is a permissible reflection in the space group $P6_3mc$, it was not observed in powder patterns taken in the present study, nor in the extremely careful and detailed study of Swanson and Fuyat (1953). It is probable that Smith and his co-workers mistook the strong (302) reflection for that of the (006). Recalculating their data on this assumption, a value for c of 6.257 Å is obtained, in good agreement with our results and those of Swanson and Fuyat (1953).

Lacking further details on which to evaluate the other measurements we have used the cell edges of pure wurtzite determined in the present study to construct the curves of cell edge versus composition.

Table 1. Unit-Cell Edges of Wurtzite (ZnS)

Investigator	Unit-cell edges	
	a, Å	c, Å
Ulrich and Zachariasen (1925)	3.844[1]	6.290
Fuller (1929)	3.819[1]	6.247
Kroger (1938)	3.819[1]	6.247
Swanson and Fuyat (1953)	3.820[2]	6.260
Kullerud (1953)	3.8217 ± 0.0003[1]	6.2702 ± 0.0003
Smith *et al.* (1957)	3.8226	6.244
Skinner and Barton (1960)	3.8232	Not reported
Skinner and Barton (1960)	3.8237	Not reported
Present study	3.8230 ± 0.0005[3]	6.2565 ± 0.0006

[1] Converted from kX to Å by the kX/Å conversion factor, 1.00202.
[2] At 26° C.
[3] At 25° C.

TABLE 2. UNIT-CELL EDGES OF GREENOCKITE (CdS)

Investigator	Unit-cell edges	
	a, Å	c, Å
Ulrich and Zachariasen (1925)	4.150[1]	6.738
Kroger (1939)	4.139[1]	6.705
Swanson, *et al.* (1955)	4.136[2]	6.713
Smith (1955)	4.1348±0.0015	6.7490±0.0010
Hurlbut (1957)	4.143	6.729
Present study	4.1354±0.0008[2]	6.7120±0.0007

[1] Converted from kX to Å.
[2] At 25° C.

UNIT-CELL EDGES OF GREENOCKITE (CsS)

Greenockite (CdS) has the same structure as wurtzite, but a considerably larger unit cell. The values of $a=4.1354\pm0.0008$ Å and $c=6.7120\pm0.0007$ Å at 25° C. for the cell edges of pure greenockite, recorded in the present study, are in good agreement with the careful study of Swanson *et al.* (1955) (Table 2). The a value is also in excellent agreement with the 4.1348 ± 0.0015 Å reported by Smith (1955). Smith's c value of 6.7490 ± 0.0010 Å is in poor agreement with the present study, however. As in the case of wurtzite, Smith used the (006) reflection to determine c, but since neither Swanson *et al.* (1955) nor the present author recorded the (006) on powder films or diffractometer tracings, it is believed Smith mistook the (302) for the (006). Recalculating his data on this assumption gives a value of 6.724 ± 0.001 Å for c, in better agreement with the present study.

TABLE 3. UNIT-CELL EDGES OF FeS-BEARING WURTZITES DETERMINED BY KULLERUD (1953). CONVERTED FROM kX TO Å UNITS AND CORRECTED FOR ERRORS IN MOL PER CENT CALCULATIONS

FeS content		Unit-cell edges (corrected)	
Weight per cent	Mol per cent (corrected)	a, Å	c, Å
0	0	3.8217±0.0003	6.2702±0.0003
4.75	5.24	3.8233±0.0004	6.2733±0.0004
9.30	10.21	3.8243±0.0004	6.2765±0.0004
22.00	23.82	3.8296±0.0004	6.2880±0.0004
30.00	32.20	3.8324±0.0004	6.2943±0.0004

Binary Wurtzites

Fe-bearing wurtzites

Kullerud (1953) demonstrated that a discontinuous solid-solution series with the wurtzite structure extends from ZnS to approximately 42 mol per cent FeS. He also presented a series of measurements for the cell edges of Fe-bearing wurtzites. His measurements are incorrectly stated as being in Å, whereas they are actually in kX units. Kullerud used NaCl as an internal standard of measurement, taking the unit-cell edge of pure NaCl from Wyckoff (1948). The confusion over units arose from an error by Wyckoff who misquoted the cell edge of NaCl in Å when it should have been in kX. There is also a minor numerical error in Kullerud's conversions of weight per cent to mol per cent. Corrected values of Kullerud's data are presented in Table 3 and Fig. 1. Cell edges of Fe-bearing wurtzites determined in the present study are presented in Table 4 and graphically in Fig. 1. The disagreement between Kullerud's data and the present study is disturbingly large. The curves for *a* versus composition diverge slightly, in the same manner that the *a* versus composition curve for Fe-bearing sphalerites was found to diverge from Kullerud's curve (Skinner *et al.*, 1959). The explanation possibly lies, as suggested for the sphalerite case (Skinner *et al.*, 1959), in the use of

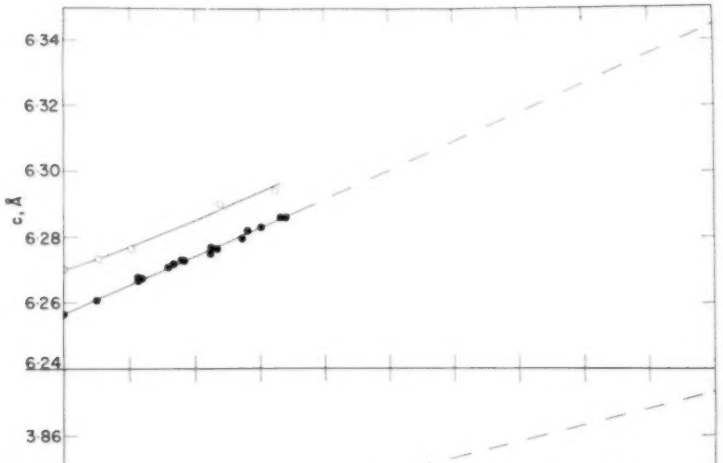

Fig. 1. Unit-cell edges, in Å, of Fe-bearing wurtzites.

TABLE 4. UNIT-CELL EDGES OF Fe-BEARING WURTZITES

FeS content		Temp. ° C.	Time (hours)	Unit-cell edges	
Weight per cent	Mol per cent			a, Å ±0.0006	c, Å ±0.001
4.57	5.04	1150	88	3.8250	6.2607
10.30	11.29	1150	48	3.8276	6.2678
10.31	11.30	1110	127	3.8286	6.2667
10.88	11.92	1150	88	3.8285	6.2674
14.56	15.89	1110	127	3.8310	6.2707
15.35	16.73	1150	88	3.8307	6.2719
16.46	17.92	1150	48	3.8316	6.2730
16.85	18.34	1110	127	3.8317	6.2727
20.64	22.38	1150	88	3.8340	6.2750
20.70	22.44	1150	48	3.8346	6.2769
21.57	23.36	1110	27	3.8345	6.2764
25.23	27.22	1150	88	3.8365	6.2795
26.05	28.08	1150	48	3.8369	6.2820
28.00	30.12	1110	27	3.8380	6.2829
30.89	33.13	1150	48	3.8394	6.2861
31.66	33.93	1150	88	3.8405	6.2860

slightly oxidized FeS as a starting material by Kullerud. The c versus composition curves, however, have a further serious and unexplained discrepancy, since Kullerud's curve lies significantly above that of the present study. The reason for the lack of agreement is unknown, but may, as suggested for the pure wurtzite measurements, be due to differences in measurement procedures.

Both the a and c values of Fe-bearing wurtzites change linearly with composition. Functions suitably describing these relations are:

$$a = 3.8230 + 0.000490X$$
$$c = 6.2565 + 0.000886X$$

where a and c are in Ångstrom units and X is the FeS content in mol per cent. These equations are derived from least squares analysis for the best fitting straight line that passes through the values for pure wurtzite. The standard deviation of measured values of a from the best fitting line is ±0.0004 Å; and of c, ±0.0007 Å. The cell edges of the hypothetical FeS compound with a wurtzite structure are, by extrapolation: $a = 3.8720$ Å and $c = 6.3451$ Å.

Mn-bearing wurtzites

An extensive, but discontinuous solid-solution series extends from wurtzite towards MnS. Kroger (1938) observed that the series was stable to at least 55 mol per cent MnS.

TABLE 5. UNIT-CELL EDGES OF Mn-BEARING WURTZITES

MnS content		Temp. ° C.	Time (hours)	Unit-cell edges		Sample prepared by[1]
Weight per cent	Mol per cent			a, Å ±0.0005	c, Å ±0.0008	
1.67	1.86	1200	120	3.8270	6.2603	B
2.33	2.60	1120	160	3.8274	6.2611	S
3.63	4.05	1200	120	3.8292	6.2671	B
4.30	4.79	1120	160	3.8310	6.2687	S
5.46	6.08	1200	120	3.8322	6.2709	B
6.46	7.18	1120	160	3.8350	6.2713	S
7.32	8.13	1120	160	3.8360	6.2737	S
7.35	8.16	1200	120	3.8357	6.2740	B
9.00	9.97	1200	120	3.8380	6.2777	B
9.48	10.50	1120	160	3.8400	6.2770	S
12.65	13.96	1120	160	3.8457	6.2858	S
13.70	15.10	1200	120	3.8475	6.2880	B
17.76	19.48	1120	160	3.8550	6.2966	S
18.37	20.13	1200	120	3.8561	6.3000	B
19.91	21.78	1120	160	3.8584	6.3000	S
27.63	29.95	1200	120	3.8718	6.3212	B
29.20	31.60	1120	160	3.8742	6.3205	S
37.27	39.96	1200	120	3.8888	6.3371	B
37.46	40.15	1120	160	3.8882	6.3411	S
43.91	46.72	1120	160	3.8990	6.3515	S
47.01	49.84	1200	120	3.9050	6.3618	B

[1] S refers to samples prepared by Skinner, B to those by Bethke.

The cell edges of Mn-bearing wurtzites determined in the present study are presented in Table 5 and graphically in Fig. 2. Similar measurements by Juza *et al.* (1956) and Smith *et al.* (1957) are also plotted. It is apparent that there is good agreement between the values obtained in the present study and those of Juza *et al.* (1956), but that serious disagreements arise with the data of Smith *et al.* (1957). Kroger (1938) stated that he observed a linear change of cell edges versus composition for Mn-bearing wurtzites, and that the projected linear plot passed through the measured cell edges of metastable hexagonal MnS.*

Our data also confirm the linearity of the relationships between both

* Three modifications of MnS are known. A cubic form, metastable at room temperature, having a sphalerite-type structure; a hexagonal form, with a wurtzite-type structure, also believed metastable at room temperature, but recently reported in nature from thin manganiferous layers in marine, organic muds by Baron and Debyser (1957); and a second cubic form with a sodium chloride-type structure, occurring in nature as the mineral alabandite.

a and c and composition, but our projected c value for pure MnS is 0.02 Å higher than that measured by Schnaase (1933). Smith *et al.* (1957) on the other hand reported a discrepancy of 0.065 Å between their projected plot of a versus composition, assuming linearity, and the measured value of a for hexagonal MnS.

Kroger (1938), Juza *et al.* (1956) and the present study are in excellent agreement on the cell edges of Mn-bearing wurtzites, in spite of a diversity of preparation and measurement methods. It is suggested, therefore, that Smith *et al.* (1957) must be mistaken in the compositions they assign their synthetic wurtzites.

Least squares analysis of our data yield best fitting straight lines passing though the values for pure wurtzite that are described by the following equations:

$$a = 3.8230 + 0.001628Z$$

$$c = 6.2565 + 0.002089Z$$

where a and c are in Ångstrom units and Z is the MnS content in mol per cent. The standard deviation of measured values of a from the best fitting straight line is ± 0.0005 Å, and of c, ± 0.0011 Å. The extrapolated cell edges of pure MnS with a wurtzite structure are $a = 3.9858$ Å and

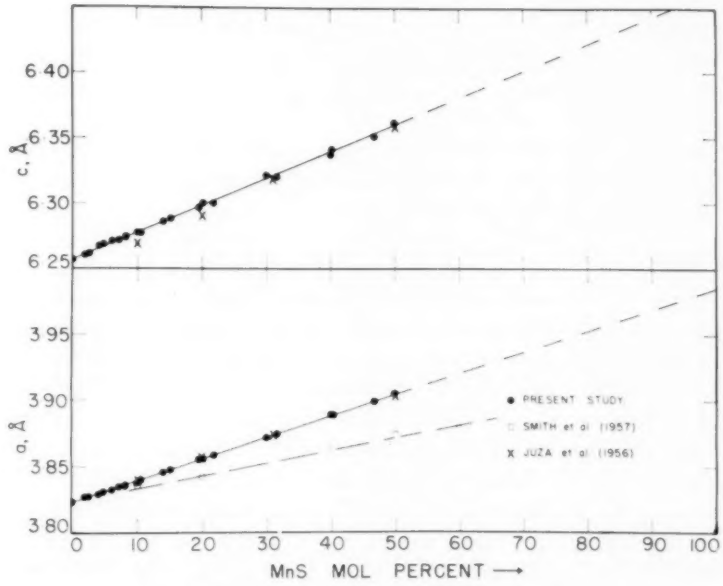

FIG. 2. Unit-cell edges, in Å, of Mn-bearing wurtzites.

TABLE 6. UNIT-CELL EDGES OF COMPOUNDS IN THE WURTZITE-GREENOCKITE SOLID-SOLUTION SERIES

CdS content		Temp. ° C.	Time (hours)	Unit-cell edges	
Weight per cent	Mol per cent			a, Å ±0.0006	c, Å ±0.001
5.12	3.51	965	162	3.8328	6.2736
9.59	6.68	965	162	3.8440	6.2888
10.03	6.99	1145	40	3.8430	6.2938
19.81	14.28	858	531	3.8674	6.3226
20.41	14.75	1145	40	3.8682	6.3238
34.46	26.18	1145	40	3.9020	6.3728
40.21	31.21	858	531	3.9194	6.4006
42.70	33.45	1145	40	3.9260	6.4068
50.23	40.50	1145	40	3.9507	6.4430
61.08	51.42	1145	40	3.9832	6.4938
69.32	60.38	1000	95	4.0112	6.5318
69.99	61.14	858	531	4.0136	6.5388
78.42	71.02	1145	40	4.0434	6.5804
79.60	72.47	1000	95	4.0482	6.5934
89.05	84.58	1000	95	4.0900	6.6398

$c = 6.4654$ Å. Schnaase (1933) measured the cell edges of pure MnS with a wurtzite-type structure and reported $a = 3.984$ Å,* in excellent agreement with our results; and $c = 6.445$ Å,* in poor agreement. The material measured by Schnaase was precipitated from an aqueous solution at low temperatures and was therefore subject to possible serious complications from polytypism. Since polytyping affects the measured c values much more strongly than it does the a values, little weight can be placed on Schnaase's determination of c.

Cd-bearing wurtzites

Kroger (1939), Hurlbut (1957) and others have demonstrated that a complete solid solution exists between wurtzite and greenockite (CdS). A number of compounds in the series were prepared in the present study and their cells edges measured. These data are presented in Table 6 and Fig. 3. Hurlbut (1957) presented a series of cell-edge measurements for the same solid-solution series. His data are in error, however (Hurlbut, written communication, 1959), as he incorrectly labeled the compositions of his synthetic compounds as mol per cent when actually they are in weight per cent. His measurements, converted to mol per cent, are plotted on Fig. 3. The plot of a versus composition is in excellent agree-

* Converted from kX to Å.

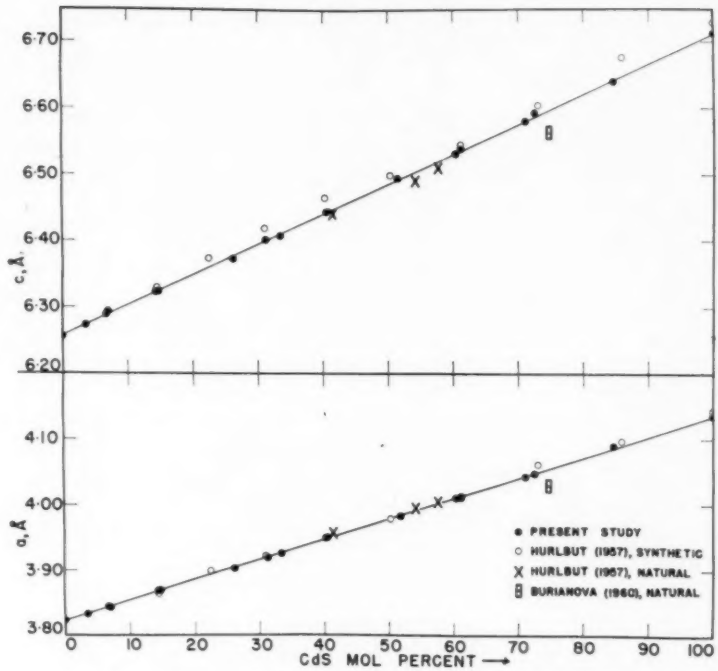

FIG. 3. Unit-cell edges, in Å, of compounds in the wurtzite-greenockite solid-solution series.

ment with that of the present study and also with the natural compounds described by Hurlbut (1957). The plot of c versus composition, however, is not in good agreement. A linear relation was found in the present study but all of Hurlbut's measurements fall above the observed line. The natural compounds reported by Hurlbut, however, are in good agreement with the synthetic compounds prepared in the present study. The curves are sensibly linear, the curvature observed by Hurlbut (1957) appearing only when compositions are expressed as weight per cent.

Burianova (1960) reports a zincian greenockite with the composition $(Cd_{0.746}Zn_{0.254})S$ from a sedimentary deposit at Tuva. The reported unit-cell edges are $a=4.030\pm0.004$ Å and $c=6.563\pm0.004$ Å.* Burianova's data fall somewhat below the unit-cell edge versus composition curves (Fig. 3) but, within the limits of measurement and analysis, must be considered in reasonable agreement with the synthetic compounds.

On plots of a and c versus CdS content, lines drawn through the values

* Converted from kX to Å.

TABLE 7. UNIT-CELL EDGES OF Fe-BEARING GREENOCKITES

FeS content		Temp.	Time	Unit-cell edges	
Weight per cent	Mol per cent	° C.	(hours)	a, Å ±0.0008	c, Å ±0.001
5.55	8.81	900	238	4.1158	6.6826
10.58	16.28	800	431	4.0954	6.6543
15.38	22.59	900	238	4.0752	6.6243
19.79	28.85	800	431	4.0644	6.6037
25.50	36.00	900	238	4.0400	6.5780
30.59	42.00	950	238	4.0280	6.5490
35.18	47.14	950	238	4.0078	6.5400

for pure wurtzite and pure greenockite also fit the observed values of the various intermediate compositions rather well. Because of the good fit and the minimum compositional uncertainty of the pure end members, these relationships have been chosen to describe our data. The corresponding functions defining the variation in cell dimensions with composition are:

$$a = 3.8230 + 0.003124\mathrm{Y}$$
$$c = 6.2565 + 0.004555\mathrm{Y}$$

where a and c are in Ångstrom units, and Y is the CdS content in mol per cent. The equations fit our data to ±0.001 Å for a and ±0.003 Å for c.

Fe-bearing greenockites

An extensive but incomplete solid-solution series, having a wurtzite structure, extends from greenockite towards FeS. Fe-rich greenockites containing up to 47 mol per cent FeS were prepared at high temperatures and quenched to room temperature. The iron replaces cadmium in the greenockite structure, with a resultant marked decrease in the cell edges of the greenockite. Measurements demonstrating this effect are presented in Table 7, and graphically in Fig. 4. It is apparent that within the limits of measurement error the decrease in cell edges with increasing FeS content must be considered linear.

On plots of a and c versus FeS content, lines drawn through the values for pure CdS and for FeS with a wurtzite structure (obtained by extrapolation of the Fe-bearing wurtzite data presented above) fit our data well. The functions are:

$$a = 4.1354 - 0.002634\mathrm{W}$$
$$c = 6.7120 - 0.003669\mathrm{W}$$

where a and c are in Ångstrom units and W is the FeS content in mol per cent. The functions define both a and c to ± 0.003 Å.

Kroger (1939) demonstrated that greenockite can accommodate extensive replacement of Cd by Mn in the structure. He further states that the observed reductions in cell edges consequent on this replacement are identical with those computed on the assumption of additivity of the unit-cell edges of hexagonal CdS and hexagonal MnS. Apparently then, both FeS and MnS cause linear decreases in the cell edges of greenockite.

Ternary Wurtzites

Fe- plus Mn-bearing wurtzites

During the course of systematic phase-equilibria studies a number of wurtzites whose compositions fall in the ternary composition plane ZnS-FeS-MnS were prepared. The cell edges of these compounds have been measured and are presented in Table 8. Also given in Table 8 are the cell edges calculated on the assumption of additivity using the functions developed for the binary solid solutions above. It can be seen that the agreement between the calculated and experimental values of a is

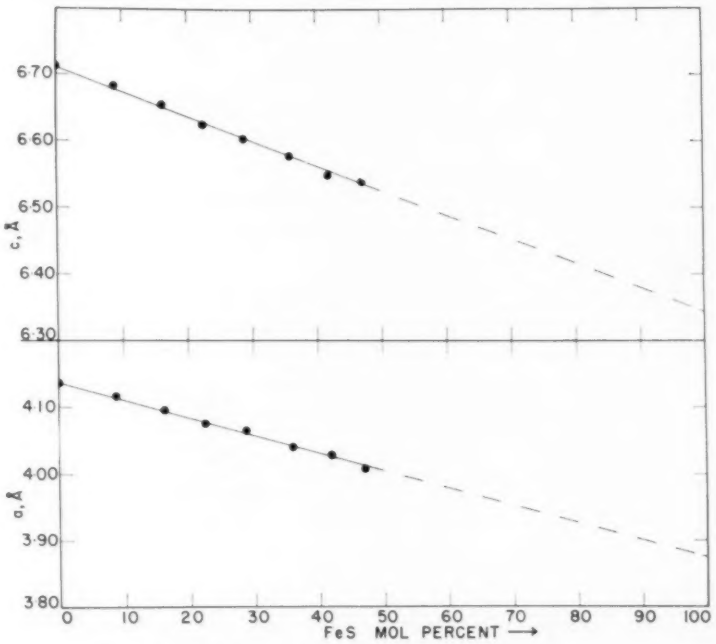

Fig. 4. Unit-cell edges of Fe-bearing greenockites.

TABLE 8.—UNIT-CELL EDGES OF Fe- PLUS Mn-BEARING WURTZITES

Composition						Temp. ° C.	Time (hours)	Unit-cell edges					
Weight per cent			Mol per cent					*a*, Å			*c*, Å		
ZnS	FeS	MnS	ZnS	FeS	MnS			Measured ±0.001	Calculated	Difference ×10⁴	Measured ±0.002	Calculated	Difference ×10⁴
88.18	6.16	5.66	87.01	6.74	6.25	1150	48	3.8368	3.8365	+ 3	6.2759	6.2755	+ 4
87.47	6.87	5.66	86.24	7.51	6.25	1100	127	3.8370	3.8369	+ 1	6.2766	6.2761	+ 5
84.56	7.18	8.24	83.11	7.82	9.07	800	450	3.8410	3.8416	− 6	6.2785	6.2823	−38
84.26	4.97	10.77	82.75	5.40	11.85	800	450	3.8453	3.8449	+ 4	6.2806	6.2861	−55
82.13	13.01	4.86	80.52	14.14	5.34	1100	127	3.8390	3.8386	+ 4	6.2788	6.2802	−14
82.09	12.87	5.04	80.48	13.99	5.53	1150	48	3.8391	3.8388	+ 3	6.2786	6.2805	−19
80.86	7.97	11.17	79.12	8.64	12.24	1100	127	3.8466	3.8471	− 5	6.2846	6.2897	−51
80.59	7.33	12.08	78.82	7.95	13.23	1100	127	3.8488	3.8484	+ 4	6.2866	6.2911	−45
79.87	12.95	7.18	78.10	14.04	7.86	800	240	3.8440	3.8427	+13	6.2815	6.2853	−38
79.40	10.40	10.20	77.58	11.26	11.16	1150	48	3.8480	3.8467	+13	6.2849	6.2898	−49
78.79	10.00	11.21	76.93	10.82	12.25	800	240	3.8487	3.8482	+ 5	6.2923	6.2917	+ 6
77.74	8.12	14.14	75.78	8.78	15.44	800	240	3.8525	3.8524	+ 1	6.2941	6.2965	−24
77.68	13.16	9.16	75.76	14.23	10.01	800	456	3.8470	3.8463	+ 7	6.2887	6.2900	−13
77.54	15.31	7.15	75.64	16.55	7.81	800	765	3.8450	3.8438	+12	6.2856	6.2875	−19
77.52	14.06	8.41	75.61	15.20	9.19	800	456	3.8455	3.8454	+ 1	6.2896	6.2892	+ 4
75.63	11.97	12.40	73.58	12.91	13.51	1100	127	3.8512	3.8513	− 1	6.2932	6.2961	−29
74.48	9.93	15.59	72.35	10.69	16.96	1150	48	3.8555	3.8558	− 3	6.2959	6.3014	−55
74.32	20.74	4.94	72.27	22.35	5.38	1100	48	3.8423	3.8428	− 5	6.2857	6.2875	−18
73.51	20.39	6.10	71.41	21.95	6.64	1100	127	3.8450	3.8446	+ 4	6.2872	6.2898	−26
72.65	2.75	24.60	70.36	2.96	26.68	1100	127	3.8668	3.8678	−10	6.3100	6.3148	−48
72.18	21.59	6.23	70.02	23.21	6.77	800	765	3.8460	3.8454	+ 6	6.2890	6.2912	−22
70.12	21.96	7.92	67.86	23.56	8.58	800	765	3.8482	3.8485	− 3	6.2955	6.2953	+ 2
69.66	9.97	20.37	67.29	10.67	22.04	1150	48	3.8588	3.8641	+53	6.3098	6.3119	−21
69.66	7.97	22.37	67.27	8.53	24.20	1100	127	3.8652	3.8666	−14	6.3110	6.3147	−37
68.92	21.48	9.60	66.60	23.01	10.39	1150	48	3.8503	3.8512	− 9	6.2974	6.2986	−12
65.33	19.36	15.31	62.86	20.64	16.50	1150	48	3.8606	3.8600	+ 6	6.3085	6.3093	− 8
64.62	20.24	15.14	62.13	21.57	16.30	1150	48	3.8610	3.8601	+ 9	6.3052	6.3096	−44
63.77	11.26	24.97	61.19	11.98	26.83	1150	48	3.8714	3.8726	−12	6.3197	6.3231	−34
60.14	22.82	17.04	57.54	24.21	18.25	800	456	3.8655	3.8646	+ 9	6.3176	6.3160	+16
60.09	19.73	20.18	57.47	20.91	21.62	1150	48	3.8667	3.8684	−17	6.3194	6.3202	− 8
59.78	21.04	19.18	57.17	22.29	20.54	800	456	3.8685	3.8673	+12	6.3186	6.3191	− 5
59.63	9.61	30.76	56.94	10.17	32.89	1150	48	3.8797	3.8815	+18	6.3318	6.3342	−24
58.73	27.99	13.28	56.13	29.65	14.22	1100	127	3.8584	3.8607	+23	6.3090	6.3125	−35
55.08	9.88	35.04	52.32	10.40	37.28	1150	48	3.8876	3.8888	−12	6.3411	6.3436	−25

close, the standard deviation being less than ± 0.001 Å. The experimental c values, although in relatively good agreement, in general fall below the calculated values. However, there is no obvious systematic relationship between composition and deviation of the experimental values of c from those calculated from the binary relationships. Certainly, to a reasonable approximation, the additivity assumption adequately describes the relationship between composition and unit-cell edges.

The functions used to calculate the cell dimensions of the ternary wurtzites are:

$$a = 3.8230 + 0.000490\mathrm{X} + 0.001628\mathrm{Z}$$
$$c = 6.2565 + 0.000886\mathrm{X} + 0.002089\mathrm{Z}$$

where X and Z are the FeS and MnS contents in mol per cent respectively.

Kroger (1939) observed additivity for a versus composition in the system ZnS-CdS-MnS. He states, however, "the c-axis experimental values were slightly greater than the calculated ones; in the center of the system the difference was about 0.03 Å, decreasing continuously in the direction of the pure substances."

It is apparent, then, that in both ternary systems, ZnS-FeS-MnS and ZnS-CdS-MnS, Vegard's Law (the assumption of additivity) does hold for a but at best can only be considered an approximation in the case of c.

Fe- plus Cd-bearing wurtzites

Compounds having the wurtzite structure can be prepared across much of the composition plane ZnS-FeS-CdS. Four ternary compounds were prepared during the present study, sufficient only to check the assumption of additivity. The results are presented in Table 9. It is immediately apparent that compounds in the system do obey Vegard's Law and hence that functions defining a and c in the ternary compounds can be derived by simple addition from the binary functions, so that

$$a = 3.8230 + 0.000490\mathrm{X} + 0.003124Y$$
$$c = 6.2565 + 0.000886\mathrm{X} + 0.004555\mathrm{Y}$$

where a and c are in Ångstrom units and X and Y are the FeS and CdS contents respectively in mol per cent. Calculated values of a and c using these functions are presented in Table 9 for comparison with the measured values.

Conclusions

The unit-cell edges of all compounds having the wurtzite (2H) structure, with compositions lying in the ternary planes ZnS-FeS-MnS and

TABLE 9. UNIT-CELL EDGES OF Fe- PLUS Cd-BEARING WURTZITES

Composition						Temp. °C.	Time (hours)	Unit-cell edges					
Weight per cent			Mol per cent					a, Å			c, Å		
ZnS	FeS	CdS	ZnS	FeS	CdS			Measured ±0.001	Calculated	Difference $\times 10^4$	Measured ±0.002	Calculated	Difference $\times 10^4$
74.21	8.30	17.49	77.95	9.66	12.39	1100	70	3.8674	3.8664	+10	6.3227	6.3215	+12
50.19	30.21	19.60	51.80	34.56	13.64	1100	70	3.8830	3.8825	+ 5	6.3484	6.3492	− 8
29.99	19.78	50.23	34.96	25.55	39.49	1100	70	3.9586	3.9589	− 3	6.4592	6.4590	+ 2
10.11	20.39	69.50	12.70	28.40	58.90	1100	70	4.0220	4.0219	+ 1	6.5490	6.5500	−10

ZnS-FeS-CdS, are linear functions of their compositions expressed in mol per cent. Wurtzite structure-type compounds in the plane ZnS-CdS-MnS were found by Kroger (1939) to have a linear relation between a and composition, but to have small departures from linearity at high CdS plus MnS content in the case of c.

It is a reasonable conclusion therefore that a linear relation exists between a and compositions expressed in mol per cent for the wurtzite structure-type compounds whose compositions can be expressed in terms of the components ZnS, FeS, MnS, and CdS. The function defining this relation is:

$$a = 3.8230 + 0.000490X + 0.003124Y + 0.001628Z$$

where a is in Å and X, Y, and Z are the FeS, CdS, and MnS contents in mol per cent respectively. The function should define a to ± 0.001 Å.

Because of Kroger's observations on the small departures from linearity of c versus composition in the plane ZnS-CdS-MnS, the assumption of additivity for c, of wurtzite structure-type compounds in the quaternary system ZnS-FeS-MnS-CdS, can only be considered approximate. The maximum systematic deviation observed by Kroger was 0.03 Å, and if we make the assumption that this is the maximum deviation in the system, the function:

$$c = 6.2565 + 0.000886X + 0.004555Y + 0.002089Z$$

where c is in Å and X, Y, and Z are the FeS, CdS, and MnS contents in mol per cent respectively, should be true to ± 0.03 Å.

The uncertainty raised by Kroger's observations clearly suggests that the a versus composition function is a more suitable one to use in determining the compositions of wurtzites from their unit-cell edges.

References

Allen, E. T., and Crenshaw, J. L., 1912, The sulphides of Zn, Cd and Hg; their crystalline forms and genetic significance: *Am. Jour. Sci., Ser. 4*, **34**, 341–396.

Baron, G., and Debyser, J., 1957, Sur la présence dans des vases organiques de la mer Baltique, du sulfure manganese β hexagonal: *Acad. sci. Paris Comptes rendus*, **245**, 1148–1160.

Bragg, W. L., 1920, The crystalline structure of zinc oxide: *Phil. Mag.*, **39**, 647.

———, 1947, The conversion factor for kX units to Ångstrom units: *Am. Mineral*, **32**, 592.

Burianova, E. Z., 1960, On the mineralogy and geochemistry of cadmium in sedimentary rocks of Tuva: *Geokhimiya, no. 2*, 177–182.

Frondel, Clifford, 1955, A precision x-ray powder camera: *Am. Mineral.*, **40**, 876–884.

——— and Palache, Charles, 1950, Three new polymorphs of zinc sulfide: *Am. Mineral.*, **35**, 29–42.

Fuller, M. L., 1929, The crystal structure of wurtzite: *Phil. Mag.*, **8**, 658–663.

Hurlbut, C. S., Jr., 1957, The wurtzite-greenockite series: *Am. Mineral.*, **42**, 184–190.

International Tables for *X*-Ray Crystallography, 1952, Kynoch Press, Birmingham, England.

JUZA, R., RABENAU, A., AND PASCHER, G., 1956, Über feste Lösungen in den Systemen ZnS/MnS, ZnSe/MnSe, ZnTe/MnTe: *Zeit. Anorg. und allgem. Chemie*, **285,** 61–69.

KROGER, F. A., 1938, Formation of Solid Solutions in the System Zincsulfide-Manganesesulfide: *Zeit. Krist.*, **A100,** 543–545.

———, 1939, Solid solutions in the ternary system ZnS-CdS-MnS: *Zeit. Krist.*, **A102,** 132–135.

KULLERUD, GUNNAR, 1953, The FeS-ZnS system. A geologic thermometer: *Norsk geol. tidsskr.*, **32,** 61–147.

SCHNAASE, H., 1933, Kristallstruktur der Manganosulfid und ihrer Mischkristalle mit Zinksulfid und Cadmiumsulfid: *Zeit. phys. chemie*, **B20,** 89–117.

SKINNER, B. J., 1961, Unit-cell edges of natural and synthetic sphalerites: *Am. Mineral.* This issue.

SKINNER, B. J., AND BARTON, P. B., JR., 1960, The substitution of oxygen for sulfur in wurtzite and sphalerite: *Am. Mineral.*, **45,** 612–625.

SKINNER, B. J., BARTON, P. B., JR., AND KULLERUD, G., 1959, Effect of FeS on the unit cell edge of sphalerite. A revision: *Econ. Geology*, **54,** 1040–1046.

SMITH, F. G., 1955, Lattice constants of cadmium sulfide: *Am. Mineral.*, **40,** 696–697.

———, DASGUPTA, S. K., AND HILL, V. G., 1957, Manganoan ferroan wurtzite from Llallagua, Bolivia (1): *Canadian Mineral.*, **6,** 128–135.

STROCK, L. W., AND BROPHY, V. A., 1955, Synthetic zinc sulfide polytype crystals: *Am. Mineral.*, **40,** 94–106.

SWANSON, H. E., AND FUYAT, R. K., 1953, Standard *x*-ray diffraction powder patterns. Volume II: *Nat. Bur. Stds. Circ.* **539,** 65 pp.

———, ——— AND UGRINIC, G. M., 1955, Standard *x*-ray diffraction powder patterns. Volume IV: *Nat. Bur. Stds. Circ.* **539,** 75 pp.

ULRICH, F., AND ZACHARIASEN, W., 1925, Über die Kristallstruktur des α- und β-Cds, sowie des Wurtzits: *Zeit. Krist.*, **62,** 260–273.

WYCKOFF, R. W. G., 1948, Crystal structures: Interscience.

Manuscript received January 17, 1962.

THE AMERICAN MINERALOGIST, VOL. 46, NOVEMBER-DECEMBER, 1961

UNIT-CELL EDGES OF NATURAL AND SYNTHETIC SPHALERITES*

BRIAN J. SKINNER, *U. S. Geological Survey, Washington, D. C.*

ABSTRACT

The unit-cell edges of a number of synthetic Fe-, Mn-, and Cd-bearing sphalerites have been measured. The effects of the components in solid solution on the unit-cell edge of sphalerite are linear and additive. The unit-cell edge of a sphalerite can be expressed in terms of its composition by the function $a = 5.4093 + 0.000456X + 0.00424Y + 0.00202Z$, where X, Y, and Z are the contents of FeS, CdS, and MnS in mol per cent and a is in Ångstroms.

Measurements of nineteen analyzed natural sphalerites show good agreement with the synthetic materials.

INTRODUCTION

Sphalerite (ZnS) is cubic, space group $F\bar{4}3m$, Z = 4, with a unit-cell edge (a) at 25° C. of 5.4093 ± 0.0002 Å (Skinner and Barton, 1958 and 1960).

Sphalerite does not deviate measurably from the stoichiometric formula, although it can tolerate extensive solid solutions in which the zinc is replaced by other cations such as iron, manganese, cadmium, and copper (Kullerud, 1953). Anionic substitutions may also occur, whereby elements such as selenium and oxygen (Skinner and Barton, 1960) may replace the sulfur. In the present study care has been exercised to prevent any anionic substitutions.

The individual substitutions of iron, manganese, and cadmium for zinc in the sphalerite structure have been studied in the past, the most detailed and recent study being that of Kullerud (1953), and for the effect of iron alone, Skinner *et al.* (1959). In these studies it has been amply demonstrated that a precise determination of the cell edge of sphalerite provides a sensitive measure of composition.

As a portion of a larger study on phase relations in the system ZnS-FeS-MnS and ZnS-FeS-CdS, the cell edges of a number of synthetic and natural sphalerites have been determined.

SAMPLE PREPARATION

Charges of appropriate composition were prepared by weighing together the requisite amounts of ZnS, FeS, MnS, and CdS. The ZnS and FeS were prepared from the same zinc, iron, and sulfur, and in the same manner, as described by Skinner and Barton (1960). MnS was prepared from metallic manganese (Johnson, Matthey and Co. Ltd., Laboratory No. 3770, Catalogue No. J. M. 810, Table 1) and sulfur. Stoichiometric

* Publication authorized by the Director, U. S. Geological Survey.

TABLE 1. SEMIQUANTITATIVE SPECTROGRAPHIC ANALYSES OF MANGANESE (BY JOHNSON, MATTHEY AND CO. LTD.), AND CdS (ANALYSIS BY K. V. HAZEL, U. S. GEOLOGICAL SURVEY)

Element	Mn	CdS	Element	Mn	CdS
Si	0.0002%	0.015%	Cd	—	Major
Al	—	0.0015	Cr	—	0.0003
Fe	0.0003	0.07	Cu	0.0001	0.015
Mg	0.001	0.03	Ni	—	0.003
Ca	<0.0001	0.03	Pb	—	0.0015
Mn	Major	—	Sr	—	0.0003
Ag	—	0.000015	V	—	0.0015
Ba	—	0.0015	Zn	—	0.15
Bi	—	0.0015			

Specifically sought, but not detected: As, Au, B, Be, Co, Cs, Ga, Ge, Hf, Hg, In, Ir, K, Li, Mo, Na, Nb, Os, P, Pt, Rb, Re, Rh, Ru, Sb, Se, Sn, Ta, Te, Ti, Tl, W, Zr.

mixtures of manganese and sulfur were weighed into silica-glass tubes; then the evacuated and sealed tubes were heated at 800° C. for 48 hours. To ensure complete reaction the tubes were opened after 48 hours, the contents ground, a slight excess of sulfur added and the charge reheated at 800° C. for a further 48 hours. There is no indication that MnS_2 is formed by the excess sulfur. Excess sulfur in the final product was removed by washing with carbon disulfide.

CdS was obtained as a fine yellow powder from British Drug Houses Ltd. Analysis of this material (Table 1) showed it to be pure, but as a handling precaution it was always recrystallized in sealed silica-glass tubes at 900° C. for 24 hours. This produced a larger grain size and consequently led to easier handling during weighing procedures.

The preparation of Fe-bearing sphalerite has been discussed in detail by Kullerud (1953) and by Skinner *et al.* (1959). Exactly the same methods as those described by Skinner were used to produce the sphalerites for the present study.

UNIT-CELL EDGE MEASUREMENT

All *x*-ray measurements of the cell edges reported in this study were made in exactly the same manner, using the same equipment and internal standards, as reported by Skinner and Barton (1960) and Skinner *et al.* (1959). The precision stated for measurements is the maximum observed deviation from a numerical average of repetitive measurements and is therefore a non-statistical statement of the range. Previous studies have shown that the methods employed allowed the same reproducibility to

be attained by different workers, using different equipment (Skinner *et al.*, 1959).

All measurements were made at a room temperature of 25°±3° C. Thermal expansion data for sphalerite (Birch *et al.*, 1942) and calculations based on these data indicate the variation in cell edge of sphalerite per degree centigrade to be 0.00004 Å. The uncertainty introduced by making cell edge measurements at room temperature and not introducing a correction factor for thermal expansion is thus only ±0.0001 Å, a figure significantly less than the reproducibility of measurement.

Unit-Cell Edges of Synthetic Binary Sphalerites

The effect of FeS on the unit-cell edge of sphalerite was discussed, and previous studies summarized, by Skinner *et al.* (1959). They derived the linear function $a=5.4093+0.000456X$, where a is the cell edge, in Ångstrom units, of a sphalerite containing X mole per cent FeS.

The cell edges of a number of Mn- and Cd-bearing sphalerites have been measured in the present investigation and data for these are presented in Tables 2 and 3. The cell edges of both Mn- and Cd-bearing sphalerites change linearly with composition (Fig. 1).

CdS is known in two polymorphic modifications; a hexagonal type with a wurtzite structure (greenockite), and a cubic modification with a sphalerite structure, found in nature as the mineral hawleyite (Traill and Boyle, 1955). The cell edge of the cubic modification of CdS has been

Table 2. Unit-Cell Edges of Cd-Bearing Sphalerites

Composition, CdS		Temp. ° C.	Time (hours)	Unit-cell edge a, Å
Weight per cent	Mol per cent			
0.83	0.56	880	400	5.4116±0.0003
1.19	0.81	880	400	5.4124±0.0003
1.64[1]	1.11	650	7800	5.4143±0.0003
2.33	1.58	880	400	5.4160±0.0003
2.94	2.00	880	400	5.4172±0.0003
3.17[1]	2.16	650	7800	5.4186±0.0003
4.03	2.75	850	350	5.4205±0.0003
5.01[1]	3.47	650	7800	5.4229±0.0004
5.30	3.64	750	450	5.4244±0.0004
7.13	4.92	750	450	5.4300±0.0003
8.89[1]	6.18	650	7800	5.4354±0.0004

[1] Samples prepared by Paul B. Barton Jr., and cell edges measured by P. M. Bethke.

TABLE 3. UNIT-CELL EDGES OF Mn-BEARING SPHALERITES

Composition, MnS		Temp. ° C.	Time (hours)	Unit-cell edge a, Å
Weight per cent	Mol per cent			
1.06	1.19	850	350	5.4116±0.0003
1.24	1.39	880	400	5.4117±0.0003
1.98	2.21	850	350	5.4140±0.0005
2.06	2.30	880	400	5.4140±0.0006
2.93	3.27	880	400	5.4155±0.0005
3.82	4.26	850	350	5.4172±0.0003
5.06	5.63	880	400	5.4196±0.0003
5.18	5.77	750	450	5.4200±0.0003
6.01	6.68	750	450	5.4216±0.0003
7.20	7.99	750	450	5.4236±0.0003

measured by Goldschmidt (1927) who reported $a = 5.823 \pm 0.005$ kX, and by Ulrich and Zachariasen (1925) who reported $a = 5.820$ kX. Converted to Å by the kX/Å conversion factor, 1.00202, these values become 5.835 ± 0.005 Å and 5.832 Å respectively. Selecting 5.833 ± 0.005 Å as a reasonable average value for a of cubic CdS, the cell edges of the Cd-bearing sphalerites prepared in the present study fall on the straight line joining a for pure sphalerite (5.4093) and a for cubic CdS. The function relating the cell edge of Cd-bearing sphalerites with composition is $a = 5.4093 + 0.00424Y$ where Y is the CdS content in mol per cent, and a is in Ångstrom units. The standard deviation of measured values of a from the straight line is ± 0.0003 Å.

The sphalerite-structure type modification of MnS is not known to occur in nature but may be prepared as an unstable compound at room temperature. Schnaase (1932) demonstrated that homogeneous sphalerite-type solid solutions could be prepared in the system ZnS-MnS, with an interruption between 89 and 20 mol per cent MnS, by precipitation from aqueous solutions. He also reported a cell edge of 5.600 ± 0.002 kX for the sphalerite form of MnS (Schnaase, 1932). This converts to 5.611 ± 0.002 Å.

The cell edges of the Mn-bearing sphalerites measured in the present study fall on, or close to, the straight line joining 5.4093 (a for pure sphalerite) and 5.611, indicating that Mn-bearing sphalerites obey Vegard's law within the limits of measurement. The equation for this line, which defines the cell edge of Mn-bearing sphalerite is $a = 5.4093 + 0.00202Z$, where Z is the MnS content in mol per cent, a is the cell edge

in Å. The standard deviation of measured values of a from the straight line is ± 0.0003 Å.

Kullerud (1953) also related the change of cell edge of sphalerite with its cadmium and manganese contents. Kullerud's data contain numerical errors in the conversion of weight per cent to mol per cent and his cell edge measurements which are reported in Å are actually in kX units. The conversion from kX to Å can be made by applying the kX/Å conversion factor 1.00202 (Bragg, 1947). The corrected values for Kullerud's measurements are presented in Table 4. Agreement between the present measurements and those of Kullerud (1953), considering the precision of measurement in each case, is poor (Fig. 1). Initial Mn- and Cd-bearing sphalerites prepared for this study had cell edges in excellent agreement with those of Kullerud. However, my colleague, Philip M. Bethke, could not satisfactorily reproduce these results. This apparent inconsistency led to the suspicion that the synthetic preparations used may have been inhomogeneous and hence that the measured cell edges were spurious. Further work by Bethke and by the writer confirmed this suspicion. The inhomogeneity develops because the MnS and CdS grains loaded into the capsules saturate the ZnS grains nearest them. Further diffusion of the Mn and Cd, leading to a homogeneous charge, is apparently slow. This

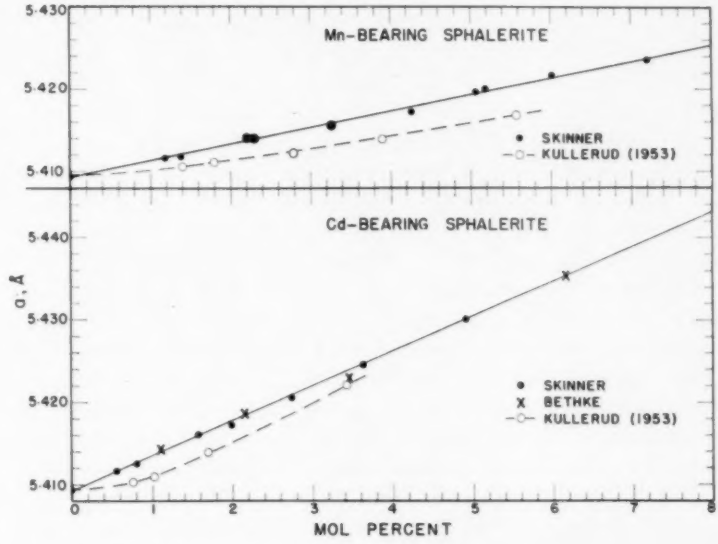

FIG. 1. Relation between unit-cell edge and composition of Mn- and Cd-bearing sphalerite.

TABLE 4. UNIT-CELL EDGES OF Mn- AND Cd-BEARING SPHALERITES DETERMINED BY KULLERUD (1953), CONVERTED FROM kX TO Å UNITS AND CORRECTED FOR ERRORS IN MOL PER CENT CALCULATIONS

Composition		Unit-cell edge a, Å	
MnS Weight per cent	MnS Mol per cent	Original	Corrected
0	0	5.3985±0.0001	5.4094±0.0001
1.25	1.40	5.3996±0.0003	5.4105±0.0003
1.80	2.01	5.4002±0.0003	5.4111±0.0003
2.50	2.79	5.4013±0.0003	5.4122±0.0003
3.50	3.90	5.4030±0.0003	5.4139±0.0003
5.00	5.57	5.4059±0.0003	5.4168±0.0003
CdS Weight per cent	CdS Mol per cent		
1.10	0.76	5.3994±0.0003	5.4103±0.0003
1.50	1.02	5.4000±0.0003	5.4109±0.0003
2.50	1.70	5.4030±0.0003	5.4139±0.0003
5.00	3.43	5.4112±0.0003	5.4221±0.0003

effect can be minimized in several ways. First, by using well-mixed, finely ground starting materials. Second, by working at the highest possible temperatures at which sphalerite of the desired composition is stable (that is, just below the temperature at which a wurtzite phase first appears). Third, if the capsule is opened after several days heating, the contents very finely ground (preferably under acetone to prevent loss of any particles) and the ground charge replaced and reheated under the same conditions, equilibration occurs much more rapidly. The inhomogeneity is most marked when the starting ZnS, CdS and MnS are in coarse grains and at low CdS and MnS concentrations. It seems probable that this effect gives rise to the "hooks" previously observed in the cell edge versus composition curves for Mn- and Cd-bearing sphalerites.

The measurements reported in this paper represent the relations for homogeneous compounds. Because the initial compounds prepared in this study were inhomogeneous and gave non-linear cell edge versus composition curves, it seems probable that the compounds measured by Kullerud (1953), who also obtained non-linear curves, were inhomogeneous.

Unit-Cell Edges of Synthetic Ternary Sphalerites

Fe- plus Mn-bearing sphalerites were prepared over a wide range of compositions, and the cell edges measured. These data are gathered in Table 5 and presented diagrammatically in Fig. 2. Contours of equal *a* are, within the limits of error of the data, straight lines. The contours are essentially parallel throughout the composition range studied.

Fe- plus Cd-bearing sphalerites also have an essentially linear relation between the cell edge and composition (Table 6, Fig. 3). The contours of equal *a* are straight lines, and are essentially parallel. Thus the cell edges of both Fe- plus Mn- and Fe- plus Cd-bearing sphalerites are linear functions of their compositions and obey Vegard's law.

It is a reasonable assumption that the cell edges of Fe- plus Mn- plus Cd-bearing sphalerites should also be linear functions of their composi-

Table 5. Unit-Cell Edges of Fe- Plus Mn-Bearing Sphalerites

Composition						Temp. °C.	Time (hours)	Unit-cell edge, *a*, Å		
Weight per cent			Mol per cent					Measured ±0.0004	Calculated	Difference
ZnS	FeS	MnS	ZnS	FeS	MnS					
95.74	2.61	1.65	95.28	2.88	1.84	750	912	5.4143	5.4143	0.0000
94.28	5.22	0.50	93.69	5.75	0.56	922	305	5.4126	5.4130	+0.0004
93.84	2.23	3.93	93.17	2.46	4.37	750	912	5.4192	5.4192	0.0000
93.27	4.53	2.20	92.57	4.98	2.45	750	912	5.4164	5.4165	+0.0001
92.87	3.61	3.52	92.12	3.97	3.91	750	912	5.4190	5.4190	0.0000
92.63	2.78	4.59	91.84	3.06	5.10	750	912	5.4210	5.4210	0.0000
91.54	7.56	0.90	90.70	8.30	1.00	830	403	5.4148	5.4151	+0.0003
90.33	4.53	5.14	89.34	4.97	5.69	830	603	5.4238	5.4231	−0.0007
90.02	6.39	3.59	89.02	7.00	3.98	750	912	5.4201	5.4205	+0.0004
87.97	11.58	0.45	86.83	12.67	0.50	922	305	5.4155	5.4161	+0.0006
86.34	11.57	2.09	85.06	12.64	2.30	750	912	5.4210	5.4197	−0.0013
85.80	9.00	5.20	84.44	9.82	5.74	750	800	5.4245	5.4254	+0.0009
83.24	12.03	4.73	81.73	13.08	5.19	830	603	5.4255	5.4258	+0.0003
83.12	12.88	4.00	81.59	14.01	4.40	750	800	5.4243	5.4246	+0.0003
82.04	16.21	1.75	80.46	17.62	1.92	750	800	5.4213	5.4212	−0.0001
81.16	17.16	1.68	79.52	18.64	1.84	750	800	5.4213	5.4215	+0.0002
80.93	18.24	0.83	79.28	19.81	0.91	830	603	5.4202	5.4201	−0.0001
80.04	16.82	3.14	78.32	18.24	3.44	750	800	5.4245	5.4245	0.0000
79.63	17.24	3.13	77.88	18.69	3.43	800	240	5.4244	5.4247	+0.0003
78.93	16.69	4.38	77.13	18.08	4.79	830	603	5.4273	5.4272	−0.0001
78.46	21.13	0.41	76.67	22.88	0.45	830	603	5.4204	5.4206	+0.0002
78.00	19.00	3.00	76.16	20.56	3.28	800	480	5.4253	5.4253	0.0000
77.47	18.39	4.14	75.58	19.89	4.53	800	765	5.4272	5.4276	+0.0004
77.39	21.84	0.77	75.53	23.63	0.84	830	603	5.4219	5.4218	−0.0001
76.52	17.41	6.07	74.57	18.80	6.63	700	800	5.4312	5.4313	+0.0001
73.70	23.91	2.39	71.63	25.76	2.60	800	450	5.4263	5.4263	0.0000
72.99	25.00	2.01	70.90	26.91	2.19	800	480	5.4260	5.4260	0.0000
72.75	26.14	1.12	70.65	28.13	1.22	800	765	5.4248	5.4246	−0.0002
71.30	28.31	0.39	69.15	30.43	0.42	830	603	5.4245	5.4240	−0.0005
66.62	19.07	4.31	74.69	20.60	4.71	830	603	5.4280	5.4282	+0.0002

tions, and that the following relation should hold

$a = 5.4093 + 0.000456X + 0.00424Y + 0.00202Z$, where X, Y, and Z are the FeS, CdS, and MnS contents in mol per cent. To test the validity of this function three Fe- plus Mn- plus Cd-bearing sphalerites were prepared and measured. Results of the measurements are presented in Table 7, and show excellent agreement with the calculated cell edges.

Kullerud (1953) first suggested and demonstrated that the effects of Fe, Mn, and Cd on the cell edge of sphalerite were additive. He did not, however, obtain linear relations between cell edge and composition. The present work has shown that the binary, ternary, and quaternary relations are additive as well as linear. Although some of the present measurements are in disagreement with those of Kullerud, it is apparent that they amply substantiate his suggestion concerning the additivity of cell edges.

Natural Sphalerites

Cell edges were carefully determined for nineteen analyzed sphalerites

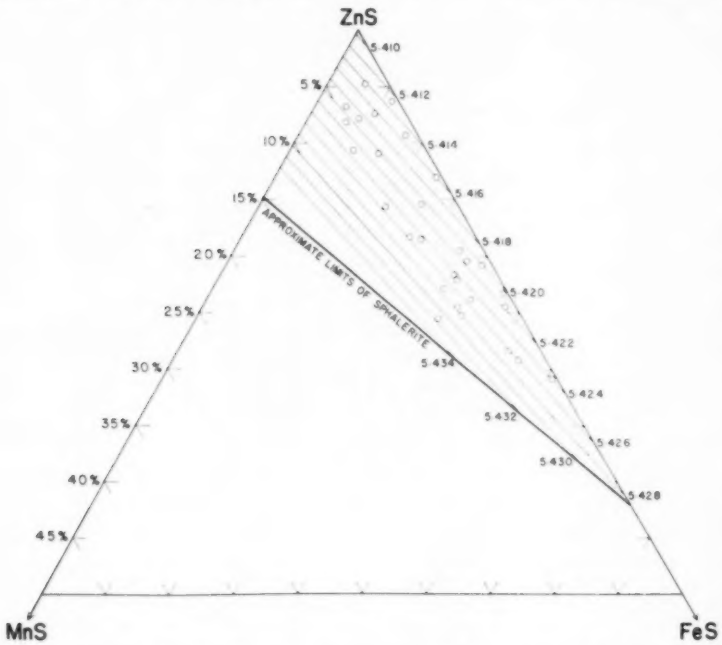

Fig. 2. Unit-cell edge (in Å) of synthetic sphalerite in the system ZnS-FeS-MnS. Compositions plotted in mol per cent. Approximate limits of sphalerite determined experimentally.

TABLE 6. UNIT-CELL EDGES OF Fe- PLUS Cd-BEARING SPHALERITES

Composition						Temp. ° C.	Time (hours)	Unit-cell edge, a, Å		
Weight per cent			Mol per cent					Measured ±0.0005	Calculated	Difference
ZnS	FeS	CdS	ZnS	FeS	CdS					
94.72	4.37	0.91	94.55	4.84	0.61	765	750	5.4140	5.4141	+0.0001
92.51	4.80	2.69	92.84	5.34	1.82	765	750	5.4190	5.4194	+0.0004
90.27	8.51	1.22	89.90	9.38	0.82	765	750	5.4175	5.4171	−0.0004
86.94	10.03	3.03	86.85	11.11	2.04	765	750	5.4222	5.4230	+0.0008
86.45	4.97	8.58	88.44	5.64	5.92	765	750	5.4370	5.4370	0.0000
86.34	8.82	4.84	86.88	9.84	3.28	765	750	5.4275	5.4277	+0.0002
85.80	13.18	1.02	84.87	14.45	0.68	765	750	5.4188	5.4188	0.0000
84.69	12.65	2.48	84.39	13.94	1.66	765	750	5.4211	5.4227	+0.0016
81.64	10.20	8.16	82.93	11.48	5.59	800	360	5.4387	5.4382	−0.0005
80.69	16.65	2.66	79.94	18.28	1.78	765	750	5.4243	5.4251	+0.0008
80.25	15.32	4.43	80.08	16.94	2.98	765	750	5.4296	5.4296	0.0000
80.02	19.00	0.98	78.65	20.69	0.66	800	360	5.4212	5.4215	+0.0003
80.00	16.00	4.00	79.66	17.66	2.68	800	360	5.4289	5.4288	−0.0001
79.99	14.01	6.00	80.34	15.60	4.06	800	360	5.4333	5.4336	+0.0003
79.95	18.00	2.05	78.93	19.70	1.37	800	360	5.4239	5.4241	+0.0002
79.93	17.08	2.99	79.23	18.77	2.00	800	360	5.4267	5.4264	−0.0003
79.86	15.15	4.99	79.85	16.79	3.36	800	360	5.4312	5.4312	0.0000
79.25	19.81	0.94	77.82	21.56	0.62	765	750	5.4217	5.4217	0.0000
73.99	25.00	1.01	72.27	27.07	0.66	800	532	5.4250	5.4244	−0.0006
72.86	26.13	1.01	71.08	28.25	0.66	800	532	5.4242	5.4250	+0.0008
72.00	26.99	1.01	70.18	29.16	0.66	800	532	5.4256	5.4254	−0.0002
72.00	25.00	3.00	70.77	27.24	1.99	800	532	5.4300	5.4300	0.0000
71.77	22.12	6.11	71.48	24.42	4.10	800	789	5.4381	5.4378	−0.0003
71.00	28.00	1.00	69.13	30.22	0.65	800	532	5.4253	5.4259	+0.0006
70.89	22.11	7.00	70.81	24.48	4.71	800	789	5.4397	5.4405	+0.0008
70.01	29.00	0.99	68.09	31.26	0.65	800	532	5.4268	5.4264	−0.0004

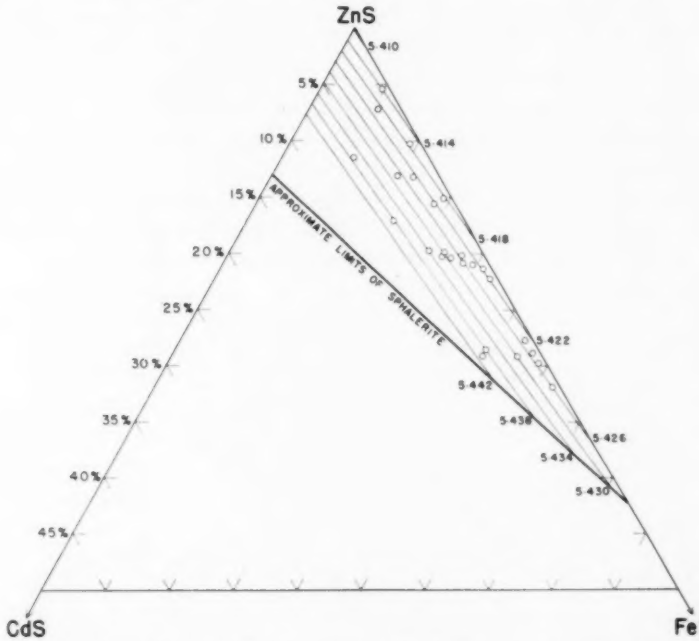

FIG. 3. Unit-cell edge (in Å) of synthetic sphalerite in the system ZnS-FeS-CdS. Compositions plotted in mol per cent. Approximate limits of sphalerite determined experimentally.

and the data compared with those for the synthetic compounds (Table 8). The sphalerites chosen cover a wide range of composition and were selected so that pure material could be hand-picked. Samples containing visible inclusions of other sulfide minerals were rejected. Polished section mounts were prepared of splits of all samples separated for analysis. Microscopic examination led to the rejection of various samples that showed exsolution bodies or intergrowths of other sulfide minerals. Any sample showing an obvious compositional zoning was also rejected, but it is realized that all of the samples undoubtedly contained some compositional inhomogeneities.

All samples were analyzed for their iron, manganese, cadmium, and copper contents. Zinc was not specifically determined in all samples, and

TABLE 7. COMPARISON OF MEASURED AND CALCULATED UNIT-CELL EDGES FOR Fe- PLUS Cd- PLUS Mn-BEARING SPHALERITES

Composition						Temp. ° C.	Time (hours)	Unit-cell edge, a, Å		
Weight per cent			Mol per cent					Measured ±0.0004	Calculated	Difference
FeS	CdS	MnS	FeS	CdS	MnS					
5.15	1.43	2.26	5.68	0.96	2.53	850	350	5.4213	5.4211	−0.0002
8.88	1.44	1.37	9.78	0.97	1.52	850	350	5.4212	5.4210	−0.0002
18.02	1.04	2.20	19.60	0.69	2.42	750	450	5.4258	5.4260	+0.0002

where not determined was assumed to account for the remainder of the cations in the mineral. Sulfur was not determined in any sample and was assumed to be the only anion present. Natural sphalerites would not be expected to contain oxygen replacing the sulfur, although significant amounts of oxygen can be put into synthetic sphalerites (Skinner and Barton, 1960). In calculating the composition of the individual sphalerites in terms of the sulfide "molecule," any element present in amounts less than 0.1 per cent was ignored, and the totals adjusted to 100 per cent. This procedure is justified since compositional differences of less than 0.1 per cent cause changes in the cell edge less than the limit of error in the measurement of the cell edge.

The agreement between the measured and calculated cell edges is excellent; only two of the nineteen samples show differences between the calculated and measured a greater than the limit of measurement error in a. There is, however, a statistical preference for the calculated a to be slightly larger than the measured a (see Table 8). It is believed the reason for this lies in the difficulty of obtaining absolutely clean samples for analysis. Any slight amount of admixed impurity will of course contribute to the final analysis and accordingly be treated in calculation as if it were

TABLE 8.—COMPARISON OF CALCULATED AND MEASURED UNIT-CELL EDGES OF NATURAL SPHALERITES

	Composition									Unit-cell edge, a, Å			Location
	Element, Weight per cent					Sulfide content, Mol per cent				Measured ±0.0005 Å	Calculated	Difference	
	Zn	Fe	Cd	Mn	Cu	ZnS	FeS	CdS	MnS				
1	N.D.	0.20	0.40	<0.01	<0.04	99.30	0.35	0.35	—	5.4106	5.4110	+0.0004	Joplin, Mo.
2	N.D.	0.30	0.41	<0.01	<0.05	99.12	0.52	0.36	—	5.4109	5.4110	+0.0001	Joplin, Mo.
3	N.D.	0.50	0.23	<0.01	<0.03	98.93	0.87	0.20	—	5.4099	5.4105	+0.0006	Belgium
4	N.D.	0.30	0.74	<0.01	<0.03	98.83	0.52	0.65	—	5.4121	5.4123	+0.0002	Hungary
5	N.D.	1.40	0.12	<0.01	<0.04	97.64	2.25	0.11	—	5.4110	5.4108	−0.0002	Wallaroo, So. Australia
6	N.D.	5.10	0.42	<0.05	<0.04	90.84	8.84	0.36	—	5.4144	5.4148	+0.0004	Broken Hill, N.S.W.
7	N.D.	3.12	1.70	0.02	Tr.	93.04	5.45	1.48	—	5.4176	5.4181	+0.0005	Keystone, S. Dak.
8						88.31	10.97	0.72	—	5.4169	5.4174	+0.0005	Sevnningdalen, Helgeland, Norway[1]
9						91.83	7.90	0.27	—	5.4131	5.4140	+0.0009	Breitenbrunn, Germany[1]
10	N.D.	7.20	0.22	1.40	0.05	84.97	12.39	0.19	2.45	5.4202	5.4206	+0.0004	Broken Hill, N.S.W.
11	56.2	7.60	0.22	1.37	<0.03	84.06	13.31	0.19	2.44	5.4215	5.4211	−0.0004	Broken Hill, N.S.W.
12	56.1	8.30	0.22	1.90	0.08	82.25	14.25	0.18	3.32	5.4230	5.4233	+0.0003	Broken Hill, N.S.W.
13	54.1	9.40	0.19	2.60	0.10	79.20	16.11	0.16	4.53	5.4260	5.4265	+0.0005	Broken Hill N.S.W.
14	54.2	8.70	0.19	1.79	<0.03	81.35	15.29	0.17	3.20	5.4234	5.4235	+0.0001	Broken Hill, N.S.W.
15	N.D.	12.50	0.30	2.70	<0.01	74.30	20.87	0.25	4.58	5.4289	5.4292	+0.0003	Broken Hill, N.S.W.
16	56.72	8.10	0.25	1.50	<0.02	83.26	13.92	0.21	2.61	5.4220	5.4218	−0.0002	Zagoran, Mont.
17	53.54	12.50	0.14	0.21	<0.01	78.16	21.36	0.12	0.36	5.4197	5.4202	+0.0005	Cumberland, England
18	55.1	9.0	0.19	2.3	<0.03	80.5	15.3	0.16	4.0	5.4250	5.4251	+0.0001	Nairne, So. Australia[2]
19	55.0	8.8	0.18	2.5	<0.03	80.4	15.1	0.15	4.4	5.4242	5.4257	+0.0015	Nairne, So. Australia[2]

Analyses 1–6, 10–19, by Defense Standards Laboratories, Adelaide, South Australia.
Analysis 7 by Isidore Adler, U. S. Geological Survey.
[1] Analyses from Kullerud (1953), unit-cell edge measurements by Kullerud (personal communication).
[2] Skinner (1958).

in solid solution in the sphalerite. This will lead to too high a figure for the calculated *a*.

It can be concluded then, that the function relating the cell edges of synthetic sphalerites with their compositions also satisfactorily defines the relation for natural Fe- plus Mn- plus Cd-bearing sphalerites.

Other Studies

Bizouard and Roering (1958) measured the cell edge of an analyzed natural sphalerite and noted a large discrepancy between the observed and computed cell edges. The discrepancy becomes small when the data from the present study are used to compute the cell edge from the composition, although it would be necessary to measure the cell edge with greater precision to actually prove or disprove their point. They refer their measurements to a unit-cell versus composition curve determined by Henriques (1957). Henriques' data, however, do not show an internal consistency of measurement and are not determined with sufficient precision to allow adequate comparison with the present study.

Cell edge measurements of numerous analyzed sphalerites have been reported in the literature. Most of these studies, however, have limitations preventing reasonable comparison with the present work. Chudoba and Mackowsky (1939) found variations in the cell edges of natural sphalerites, but unfortunately their samples were only partially analyzed. Lazarenko (1955) states that he did not observe any change in the cell edge with changing composition. His measurements were insufficiently precise to record cell differences in the samples he studied, however, and his observations should be modified accordingly.

The suggestion has been made by Henriques (1957) that the thermal history of a sphalerite may affect the cell edge. Henriques apparently had a quenchable order-disorder effect in mind, because he draws an analogy to the feldspars. This is an inexact choice for an example; the mechanism of the complex order-disorder effects in the feldspar structures is not yet fully understood, and there is no evidence to suggest that such effects should or could occur in either natural or synthetic sphalerites. Some sphalerites may contain a certain amount of hexagonal close-packing (Smith, 1955), but this would not lead to the effects suggested by Henriques.

Acknowledgments

This study was begun while the author was a member of the staff of the University of Adelaide, South Australia. The assistance of Robin Offler in making certain of the unit-cell edge measurements is gratefully acknowledged. Brian Daly of the South Australian Museum and J. J.

Norton, U. S. Geological Survey, kindly loaned specimens for study. Gunnar Kullerud, Geophysical Laboratory, Carnegie Institution of Washington, generously allowed quotation of his unpublished measurements of the unit-cell edges of two analyzed sphalerites.

My colleagues Philip M. Betkhe and Paul B. Barton, Jr. have at all times been generous in their efforts and assistances.

References

1. Birch, Francis, Schairer, J. F., and Spicer, H. C., 1942. Handbook of Physical Constants: *Geol. Soc. America Spec. Paper, No.* **36,** 325 p.
2. Bizouard, H. and Roering, C., 1958, An investigation of sphalerite: *Geol. Foren. Stockholm Forh,* **B 80,** 309–314.
3. Bragg, W. L., 1947, The conversion factor for kX units to Ångstrom units: *Am. Mineral.*, **32,** 592.
4. Chuboda, K. F. and Mackowsky, M. T., 1939, Über die Isomorphie von Eisen und Zink in der Zinkblende: *Zentr. Mineral. Geol., Abt.* **A,** No. 1, 12–21.
5. Goldschmidt, V. M., 1927, Geochemische Verteilungsgesetze der Elemente VIII. Untersuchungen über Bau und Eigenschaften von Krystallen: *Skrifter Norsk. Viden-Akad. Oslo. I Mat. Natur. Klasse.* 1926, No. 8.
6. Henriques, Å., 1957, Cell dimensions of sphalerite: *Arkiv. for Mineral. och Geol.*, **2,** p. 275.
7. Kullerud, Gunnar, 1953, The FeS-ZnS system. A geologic thermometer: *Norsk. geol. tidsskr.*, **32,** 61–147.
8. Lazarenko, E. K., 1955, Blendes from pyritic deposits of the Middle Urals: *Sci. Annals Lvov State Univ., Ser. Geol.*, **35,** no. 8, 72–119.
9. Schnasse, H., 1932, Kristallstruktur der Manganosulfide und ihrer Mischkristalle mit Zinksulfid und Cadmiumsulfid: *Zeit. Physik. Chem.* (**B**) **20,** 89–117.
10. Skinner, B. J., 1958, The geology and metamorphism of the Nairne Pyritic Formation, a sedimentary sulfide deposit in South Australia: *Econ. Geol.*, **53,** 546–562.
11. Skinner, B. J. and Barton, P. B., Jr., 1958, Recent work on sphalerite. Its bearing on the sphalerite geothermometer: (Abs.) *Geol. So. America Bull.*, **69,** 1768.
12. ———, 1960, The substitution of oxygen for sulfur in wurtzite and sphalerite: *Am. Mineral.*, **45,** 612–625.
13. Skinner, B. J., Barton, P. B., Jr., and Kullerud, Gunnar, 1959, Effect of FeS on the unit edge of sphalerite. A revision: *Econ. Geol.*, **54,** 1040–1046.
14. Smith, F. G., 1955, Structure of zinc sulfide minerals: *Am. Mineral.*, **40,** 658–675.
15. Traill, R. J. and Boyle, R. W., 1955, Hawleyite, isometric cadmium sulfide, a new mineral: *Am. Mineral.*, **40,** 555–559.
16. Ulrich, F. and Zachariasen, W., 1925, Über die Kristallstruktur des α- und β-CdS, sowie des Wurtzits: *Zeit. Krist.*, **62,** 260–273.

Manuscript received January 17, 1961.

THE AMERICAN MINERALOGIST, VOL. 46, NOVEMBER-DECEMBER, 1961

NEW DATA FOR HISINGERITE AND NEOTOCITE

J. A. WHELAN AND S. S. GOLDICH*

ABSTRACT

New chemical and *x*-ray data are given for three samples of hisingerite from northern Minnesota. The variable chemical composition of hisingerite, a hydrous iron silicate, is shown by the new analyses representing two samples from gabbros of the Beaver Bay complex and one from veins in the Biwabik iron-formation at Babbitt, Minnesota.

The *x*-ray diffraction patterns consist of a few diffuse lines that resemble the pattern for nontronite and also bear some similarity to the published data for iron-rich saponite. Structural formulas computed for the Beaver Bay hisingerites fit a saponite structure reasonably well; however, the hisingerite from Babbitt, as well as analyzed samples from Parry Sound, Ontario, and from Montauban, Quebec, show excess Fe_2O_3 for the saponite structure.

Hisingerite occurs in a variety of geologic environments, and commonly results from alteration of pyroxene and olivine. So-called hisingerites may represent mixtures of two or more minerals or stages in the alteration of ferromagnesian minerals.

A sample of hisingerite-like material from the Montreal Mine, Iron County, Wisconsin, closely resembling hisingerite in physical properties, was found to be a hydrous manganese silicate, neotocite. A chemical analysis and *x*-ray data are given for the neotocite.

INTRODUCTION

Hisingerite is a soft, black, hydrous iron silicate with a characteristic resinous luster and conchoidal fracture. It has been reported throughout the world in rocks of various ages and in many geologic settings. It occurs with ores of uranium, tin, copper, lead, zinc, iron, and manganese. Recent studies of hisingerite are by Bowie (1955), Nikolsky (1953), Sudo and Nakamura (1952). The present study is concerned with occurrences of hisingerite in gabbros in the vicinity of Beaver Bay and in iron formation at Babbitt in northeastern Minnesota. Some new data are presented for hisingerite from Parry Sound, Ontario, previously described by Schwartz (1924) and for hisingerite from the Montauban Mines, Quebec, described by Osborne and Archambault (1950).

DESCRIPTION OF SAMPLES

Beaver Bay complex. Hisingerite is a common alteration produced in the iron-rich gabbroic rocks of the Beaver Bay complex. The present study was started on material collected by R. B. Taylor who noted the widespread occurrence of hisingerite in the Beaver Bay area during the course of field work in 1953. Additional material was collected by H. M. Gehman, Jr., in 1955. The mineral described by Muir (1954) as bowlingite, an alteration product of olivine in iron-rich diabase from Beaver Bay,

* Present addresses: Department of Mineralogy, University of Utah, Salt Lake City, Utah, and U. S. Geological Survey, Washington, D. C.

is the hisingerite of the present paper. In describing the olivine in the Beaver Bay specimen, Muir notes that it "is invariably surrounded either by a reddish-brown highly-birefringent alteration product which is mostly bowlingite, or, more rarely, by deep-green isotropic chlorophaeite."

The Beaver Bay complex was named by Grout and Schwartz (1939, p. 13) and was related by them to the Middle Keweenawan intrusive action at the time of emplacement of the Duluth gabbro. The gabbroic intrusives, where concordant with the Keweenawan flows, are sills, but Grout and Schwartz (1939, p. 33) noted that transgressive and dike-like masses of diabase form some high bluffs. More recent studies by H. M. Gehman, Jr. (unpublished Ph.D. thesis, University of Minnesota, 1957) show that the Beaver Bay complex consists of a number of intrusions.

Sample No. 1 (Table 1, etc.) was collected by R. B. Taylor from laminated ferrogabbro in a quarry that supplied large blocks for the construction of the breakwaters of the Silver Bay harbor. The quarry is situated west of Highway 61 in SW$\frac{1}{4}$ Sec. 6, T. 55 N., R. 8 W., approximately one mile southwest of the Reserve Mining Company plant at Silver Bay.

Sample No. 2 was collected by H. M. Gehman, Jr. from ferrogabbro in a freshly blasted cut behind the thickening plant of the taconite concentrator of the Reserve Mining Company. The locality is east of Highway 61 in SE$\frac{1}{4}$ Sec. 31, T. 56 N., R. 7 W.

East Mesabi. Hisingerite has been reported in very small amounts in the Biwabik formation in the Morris Mine near Hibbing, Minnesota (Gruner, 1946, p. 22), but it is a common and locally abundant mineral in the Eastern Mesabi district where it occurs in veinlets in the iron formation. We are indebted to J. N. Gundersen who collected the material for this study from the Peter Mitchell Pit, Reserve Mining Company, Babbitt, Minnesota. According to Gundersen, the hisingerite veinlets average about 1 mm. in width, with a maximum of 5 mm. The veinlets are usually more common in phases of the iron formation which contain more fayalite and hypersthene than average for the locality.

The Babbitt hisingerite is black, resinous, and brittle, with a hardness of 3 and a specific gravity of approximately 2.67. Under the microscope it appears to be isotropic, greenish-brown in color, and in very thin fragments at high magnification (400×) is apple green. The refractive index is 1.66.

Wilcox Mine, Parry Sound, Ontario. Hisingerite from the Wilcox Mine was generously supplied by G. M. Schwartz, and the description that follows is taken from the earlier paper by Schwartz (1924). In the Wilcox Mine hisingerite is intimately associated with pyrite and chalcopyrite and forms a matrix for the sulfides. The ore occurs as masses and dis-

seminations in Precambrian garnet-biotite schists. In addition to the garnet and biotite, minerals of the schists include plagioclase, hypersthene, hornblende, apatite, quartz, and others. Schwartz (1924, p. 144) concluded that the hisingerite was formed for the most part by the alteration of the hypersthene.

The Parry Sound hisingerite is black, resinous, and brittle. The hardness is approximately 2.5. The specific gravity is given as 2.50 by Schwartz (1924, p. 142) who noted that the "streak is yellow and similar to that of limonite." Schwartz estimated that three-fourths of the material he studied is isotropic and one-fourth anisotropic. He found a range in refractive index, $n = 1.50$–1.56, which was confirmed, $n = 1.50$–1.57, in the present investigation.

Montauban Mines, Quebec. The hisingerite was first noted in the Tetreault mine by Osborne in 1938 and described in detail by Osborne and Archambault (1950), and the notes that follow are taken from their description. The sample was presented by Osborne to J. W. Gruner who made it available for the present study.

The zinc and lead ores at Montauban occur in crystalline limestone in a gangue that is largely diopside and tremolite. The hisingerite, according to Osborne and Archambault (1950, p. 289), is largely a replacement of diopside, and complete pseudomorphs after diopside were found. Some of the hisingerite apparently also formed as a replacement of calcic plagioclase and of siderite. The hisingerite is cut by veinlets of pyrite from one-tenth to one inch wide and by paper-thin veinlets of calcite. The calcite veinlets are attributed to fillings of contraction cracks by Osborne and Archambault.

The Montauban hisingerite is black, resinous, and brittle. Osborne and Archambault give the hardness as 2.5 and the specific gravity as 2.53–2.55. They found the material to be isotropic with variable refractive index which they determined as $n = 1.65$ in 1948 and as $n = 1.51$ in 1951. The sample in the Minnesota collection is variable in refractive index, but the results generally were close to $n = 1.66$.

Montreal Mine, Wisconsin. A sample labeled hisingerite in the Minnesota collection comes from the 94th crosscut on the 30th level of the Montreal Mine, Gogebic range, Iron County, Wisconsin. This sample was collected by J. W. Gruner. It is dark brown, resinous, brittle with good conchoidal fracture, and has a hardness of 3 and specific gravity of 2.43. The mineral is neotocite as shown by its chemical analysis (Table 1). The sample is essentially isotropic with small amounts anisotropic when viewed at high magnification. The index of refraction is variable but is close to 1.62.

Chemistry

Three new chemical analyses of hisingerite from Minnesota (Table 1) were made for the present investigation in the Rock Analysis Laboratory at the University of Minnesota. For comparison, the published analyses of hisingerite from the Wilcox Mine, Parry Sound, Ontario, and from the Tetreault Mine at Montauban, Quebec, are included. The variability in chemical composition of so-called hisingerite is apparent from these analyses. The molecular ratio of Fe_2O_3/FeO in these samples ranges from 3.67 for the Parry Sound sample to 0.35 for the sample from Babbitt. The chemical variability is further discussed in a later section concerned with the probable structural formula.

The chemical analysis (Table 1, No. 6) of neotocite was made of two small fragments which appeared to be homogeneous, and no impurities

Table 1. Chemical Analyses of Hisingerites and of Neotocite

	1	2	3	4	5	6
SiO_2	39.11	42.35	38.19	35.57	37.54	31.74
Al_2O_3	3.89	3.65	0.00	0.38	0.56	0.50
TiO_2	0.16	0.13	0.01	0.12	0.00	0.01
Fe_2O_3	22.22	23.28	19.91	39.20	37.02	1.88
FeO	5.90	5.54	24.64	4.80	4.66	0.00
MnO	0.92	0.38	0.66		0.75	12.29
MnO_2						27.05
MgO	5.21	8.22	2.36	1.60	2.81	9.55
CaO	2.52	2.06	0.61	0.85	1.52	0.28
Na_2O	0.27					0.02
K_2O	0.07					0.01
H_2O+	5.82	6.85	8.40	11.60	9.20	8.86
H_2O-	13.54	6.95	5.53	6.00	6.00	7.04
CuO						0.78
Organic Matter					0.05	
Total	99.63	99.41	100.31	100.12	100.11	100.01
S.G.			2.67—.02	2.50	2.53–2.55	2.43—.02

1. Hisingerite, gabbro, Beaver Bay complex. S. S. Goldich, analyst.
2. Hisingerite, gabbro, Beaver Bay complex. S. S. Goldich, analyst.
3. Hisingerite, Biwabik iron-formation, East Mesabi range. C. O. Ingamells, analyst.
4. Hisingerite, Parry Sound, Ontario. R. J. Leonard, analyst (Schwartz, 1924, p. 142).
5. Hisingerite, Montauban Mines, Quebec. H. Boileau, analyst (Osborne and Archambault, 1950, p. 286).
6. Neotocite, Montreal Mine, Wisconsin. Doris Thaemlitz and C. O. Ingamells, analysts.

were recognizable in the powder used for determination of the refractive index.

X-Ray Diffraction Data

Samples for powder photographs were obtained by hand picking under a binocular microscope. The hisingerite (No. 2) from gabbro of the Beaver Bay complex was further purified by magnetic separation with a Franz magnetic separator. Data from the powder photographs, together with the data of Sudo and Nakamura (1952) and of Bowie (1955), are given in Table 2. The lines on all patterns were broad and diffuse.

The *x*-ray diffraction pattern of neotocite is similar enough to those of the hisingerites that considering the broad and diffuse lines in the patterns of both of these minerals it is impossible to differentiate them by *x*-ray diffraction.

Infra-Red Absorption Spectra

The infra-red absorption spectra of the chemically analyzed samples of hisingerite and of neotocite are shown in Fig. 1. The silicate bands of the spectra at approximately 10 microns are poorly defined as is typical of the montmorillonite group. The maxima at about 6.2 microns represents O-H bending.

Differential Thermal Analyses

The DTA curves of the hisingerites and neotocite are shown in Fig. 2. The runs were made in air with a heating rate of 10° C. per minute. The endothermic reactions between 100° C. and 200° C. on these curves represent the loss of water. The only other characteristic reaction is exothermic and occurs at about 1000° C. This reaction probably represents the formation of ferrites. The exothermic reactions between 400°C. and 500° C. on the curves of the Montauban Mines and Parry Sound hisingerites represent the oxidation of a very small amount of pyrite contaminating these samples. The strong exothermic reaction between 700° C. and 800° C. on the DTA curve of neotocite represents the formation of braunite.

Structure

The fact that hisingerites give poor *x*-ray diffraction patterns makes a unique determination of structure impossible. Gruner (1935), Sudo and Nakamura (1952), and Bowie (1955) all have noted the general similarity between the *x*-ray diffraction patterns of hisingerites and those of nontronites. The strong 12–17 Å basal reflection of nontronites, however, is absent in *x*-ray diffraction patterns of hisingerite. The poor *x*-ray diffraction patterns of hisingerites, together with their variable ferric-ferrous

TABLE 2. *X*-RAY DIFFRACTION PATTERNS OF HISINGERITE AND NEOTOCITE

1		2		3		4		5		6		7		8		9		10		11		12	
d(Å)	I	d(Å)	I	d(Å)	I	d(Å)	I	d(Å)	I	d(Å)	I	d(Å)	I	d(Å)	I	d(Å)	I	d(Å)	I	d(Å)	I	d(Å)	I
				7.53	w																		
4.42	w	4.51	w	4.33	w	4.55	w			4.36	w	4.45	s	4.40	s	4.40	s	4.39	s	4.43	s	4.40	ss
				3.50	w					3.59	w	3.53	s	3.55	s	3.55	s	3.58	s				
2.48	w	2.54	w	2.55	w	2.59	w	2.51	2	2.59		2.56	s	2.56	s	2.58	s	2.57	s	2.56	s	2.60	ss
		1.70	w									1.71	w	1.70	w	1.70	w	1.71	w				
1.54	vw	1.53	w	1.55	w	1.54	w	1.54	w	1.54	w	1.54	s	1.53	s	1.53	s	1.54	s	1.53	s	1.50	ss
1.21	vw			1.21	w																		

1-6 unfiltered iron radiation, camera radius 57.3 mm., 24-hour exposures.
Intensities are as follows: s, strong; w, weak; vw, very weak.

1. Hisingerite No. 1, Beaver Bay complex.
2. Hisingerite No. 2, Beaver Bay complex.
3. Hisingerite, East Mesabi range.
4. Hisingerite, Parry Sound.
5. Hisingerite, Montauban Mines.
6. Neotocite, Montreal Mine.
7. Hisingerite, Riddarhyttan, Sweden (Bowie, 1955).
8. Hisingerite, Blaine County, Idaho (Bowie, 1955).
9. Hisingerite, Nicholson Mine, Saskatchewan (Bowie, 1955).
10. Hisingerite, Langanshyttan, Sweden (Bowie, 1955).
11. Hisingerite, Weal Jane, Cornwall (Bowie, 1955).
12. Hisingerite, Kawayma Mine, Japan (Sudo and Nakamura, 1952)

ratio, lead the writers to suggest that hisingerites may form as a metastable iron saponite which then undergoes oxidation in different degrees. On this basis the analyzed samples described in this paper were fitted to saponite structures by the method of Ross and Hendricks (1945). Trivalent iron was equated to divalent iron. The results of these calculations are given in Table 3. The analyses of the hisingerites from the Beaver Bay complex fit a saponite structure reasonably well. Hisingerite No. 2, for example, gives a structural formula of $(Fe''_{1.90}Mn_{0.03}Mg_{1.05}Al_{0.01})Al_{0.36}Si_{3.64}O_{10}(OH)_2 \cdot nH_2O$, $Ca/2=0.38$ (analysis), $X=0.37$ (calculated).

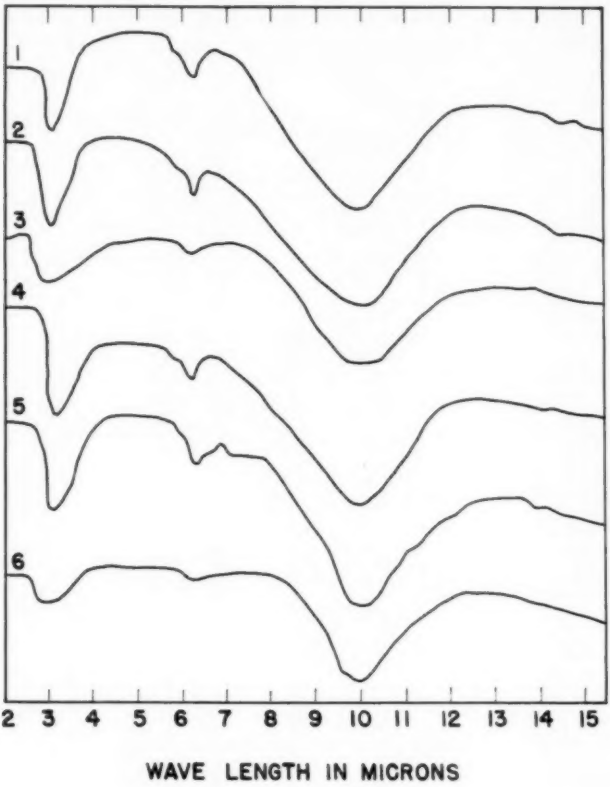

FIG. 1. Infra-red Spectra.

1. Hisingerite No. 1, Beaver Bay complex
2. Hisingerite No. 2, Beaver Bay complex
3. Hisingerite, East Mesabi range
4. Hisingerite, Parry Sound
5. Hisingerite, Montauban Mines
6. Neotocite, Montreal Mine

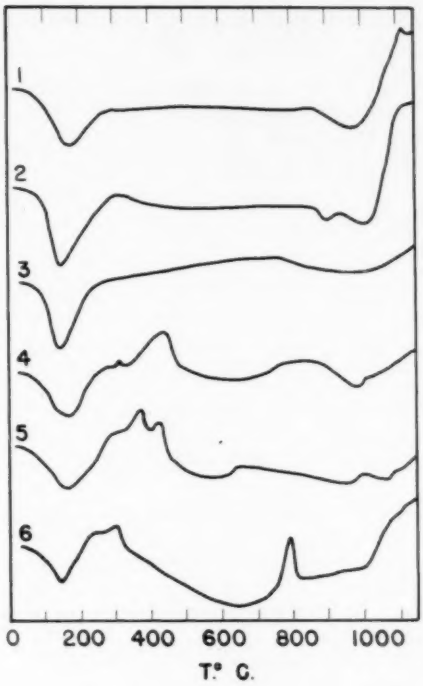

FIG. 2. DTA Curves.

1. Hisingerite No. 1, Beaver Bay complex
2. Hisingerite No. 2, Beaver Bay complex
3. Hisingerite, East Mesabi range
4. Hisingerite, Parry Sound
5. Hisingerite, Montauban Mines
6. Neotocite, Montreal Mine

The analyses of the other hisingerites, however, indicate more cations than can be fitted into a saponite structure. In these, Al+Si was assumed to occupy the four tetrahedral positions of the sheet structures, and Fe″, Mn″, Mg, and Fe‴ recalculated to Fe″ were used to fill three octahedral positions. This method of calculation left excess Fe_2O_3. No goethite or hematite appeared in the *x*-ray diffraction patterns of these hisingerites. The DTA curves likewise do not show an endothermic reaction at about 400° C. which would be characteristic of goethite. In the Parry Sound and Montauban Mines hisingerites, however, this reaction may have been masked by the exothermic reactions due to the oxidation of sulfides contaminating the samples.

The *x*-ray diffraction pattern of the East Mesabi hisingerite has a 7.5 Å

TABLE 3. STRUCTURAL FORMULAS OF HISINGERITES CALCULATED AS SAPONITE[a]

	1	2	3	4	5
Octahedral					
Fe''^{b}	2.01	1.90	2.57	2.73	2.49
Mn''	0.07	0.03	0.06		0.07
Mg''	0.72	1.05	0.37	0.27	0.44
Al'''	0.06	0.01			
Tetrahedral					
Al'''	0.36	0.36		0.05	0.07
Si''''	3.64	3.64	4.00	3.95	3.93
Exchangeable					
$Ca''/2$	0.50	0.38	0.14	0.20	0.34
Na'	0.05				
K'	0.01				
Calculated	0.58[c]	0.37	0.00	0.05	0.07
Excess Fe_2O_3 (%)			14.63	11.87	10.55

[a] Calculated by the method of Ross and Hendricks (1945) using analytical results of alkaline earths and alkalies as "X." When excess cations for octahedral positions were indicated in analyses, Si+Al was considered as 4.00 and excess cations considered to be Fe_2O_3. Oxygen considered as 10, hydroxyl as 2.

[b] Fe''' recalculated as Fe'' in structure.

[c] 0.22 octahedral and 0.36 tetrahedral.

1. Hisingerite No. 1, Beaver Bay complex.
2. Hisingerite No. 2, Beaver Bay complex.
3. Hisingerite, East Mesabi range.
4. Hisingerite, Parry Sound.
5. Hisingerite, Montauban Mines.

line which suggests a possible incipient chlorite structure. This sample has a high ferrous to ferric ratio. The other hisingerites whose analyses cannot be fitted to a saponite structure have low ferrous to ferric ratios, and their *x*-ray diffraction patterns did not show 7.5 Å lines. For these reasons, a chlorite structure is not considered probable.

Wilshire (1958), studying iddingsites which are similar chemically and physically to hisingerites, concluded they consist of mixed-layer chlorite-smectite minerals. Brown and Stephen (1959) found iddingsite from New South Wales, Australia, to consist of goethite and a layer silicate lattice. Sun (1957) found material considered iddingsite from basaltic rocks in New Mexico was cryptocrystalline goethite plus amorphous silica and other oxides. A possible explanation is that ferromagnesian

minerals first alter to an iron saponite, then to a mixture of goethite and a layer silicate lattice and finally to a mixture of goethite and amorphous oxides. Perhaps the hisingerites with iron in excess of that which can be fitted to a saponite structure represent an alteration intermediate between the first and second steps listed above. A. C. Waters (personal communication, November 23, 1955) suggests that hisingerite and chlorophaeite may be equivalent. Wilshire (1958) has published *x*-ray data on isotropic alteration products of olivines and orthopyroxenes which are in good agreement with the data for hisingerite, except that the chlorophaeite patterns have a 14 Å basal reflection. Since this basal reflection was not affected by treatment with ethylene glycol or heating, he postulated an incipient chlorite structure for chlorophaeite.

Canbyite (Hawkins and Shannon, 1920; Bowie, 1955) and an iron-rich saponite from Japan (Sudo, 1954) are also similar to hisingerite. Some typical chemical data for the various iron silicates, selected from the literature, are given in Table 4. *X*-ray data are given in Table 5.

TABLE 4. CHEMICAL ANALYSES OF CANBYITE, IRON-RICH SAPONITE, CHLOROPHAEITE, AND IDDINGSITE

	1	2	3	4
SiO_2	32.85	39.68	40.35	38.63
Al_2O_3	2.64	3.93	5.11*	1.78
TiO_2	0.26	0.37	0.20	
Fe_2O_3	40.70	19.82	24.99	32.49
FeO		1.12	3.55	
MnO	0.74	0.19	0.22	
MgO	2.05	11.21	5.48	6.64
CaO	1.50	2.37	1.32	2.79
Na_2O			0.18	
K_2O			1.44	
H_2O+	7.90	6.16	8.51	17.70
H_2O-	11.40	15.11	8.51	
Total	100.04	99.96	99.86	100.03

* With possible P_2O_5. CO_2, SO_3, S, NiO, BaO, SrO not found.

1. Canbyite, Brandywine Quarry, Wilmington, Delaware. E. V. Shannon, analyst (Hawkins and Shannon, 1924).
2. Iron-rich saponite, iron sand bed at Monuia, Oide-Mura, Natorigun, Miyagi Prefecture, Japan. J. Ossaka, analyst (Sudo, 1954).
3. Chlorophaeite, New Reservoir, Holyoke, Massachusetts. G. Steiger, analyst (Emerson, 1905).
4. Iddingsite, La Jara Creek, Conejos quadrangle, Colorado (Ross and Shannon, 1925).

TABLE 5. X-RAY DIFFRACTION PATTERNS OF IRON-RICH SAPONITE, CANBYITE, AND CHLOROPHAEITE

Indices	d(kX)	I	d(Å)	I	d(Å)	I
	1		2		3	
001	15.7	40–150			15.0–14.0	s
11·0·2	4.55	10	4.40	s	4.5	w
					4.48	vw
			3.54	s		
13·2·0	2.62	8			2.59	vw
			2.56	s		
	2.47	5				
31·15·24	1.70	5	1.70	w		
33·0·6	1.533	10	1.53	s	1.55	vvw
	1.323	5				

1. Iron-rich saponite, Japan (Sudo, 1954).
2. Canbyite, Wilmington, Delaware (Bowie, 1955).
3. Chlorophaeite, Walla Walla, Washington (Wilshire, 1958).

CONCLUDING REMARKS

Hisingerite is found in a number of differing geologic occurrences. The Beaver Bay material is attributed to deuteric and late-stage hydrothermal alteration of olivine, pyroxene, and possibly other minerals. The hisingerite that occurs in veinlets cutting the Biwabik iron-formation on the East Mesabi range is related to the later stages of metasomatism in connection with the metamorphism at the time of intrusion of rocks of the Duluth complex. The hisingerites at Parry Sound, Ontario, and at Montauban, Quebec, appear to be closely related to the sulfide ore deposition and probably represent late-stage hydrothermal activity.

The origin of hisingerite as an alteration product replacing a variety of minerals suggests that this material might easily be a mixture of two or more minerals. The fineness of grain makes optical and chemical studies difficult, and even the more strongly birefringent materials give poor *x*-ray diffraction patterns. Hisingerite, however, appears to be a rather common mineral that warrants further study.

ACKNOWLEDGMENTS

We are indebted to a number of persons indicated in the text who, in supplying samples and in other ways, contributed to the investigation. The greater part of the laboratory work was done in the Department of Geology of the University of Minnesota. Part of this study was done by Whelan in connection with a Ph.D. thesis under the supervision of Pro-

fessor J. W. Gruner, and financial assistance to Whelan in the form of a U. S. Steel Foundation Fellowship is gratefully acknowledged. A part of the cost of the chemical analyses made in the Rock Analysis Laboratory was defrayed by a grant to Goldich from the Graduate School of the University of Minnesota. The careful work of the analysts is deeply appreciated. Thanks are due to Hatten S. Yoder, Jr., for numerous helpful suggestions.

References

Bowie, S. H. U. (1955), Thucholite and hisingerite-pitchblende complexes from Nicholson Mine, Saskatchewan, Canada. *Bull. Geol. Surv. Gr. Britain*, **10,** 45–57.

Brown, G. and Stephen, I. (1959), Structural study of iddingsite from New South Wales, Australia. *Am. Mineral.*, **44,** 251–260.

Emerson, B. K. (1905), Plumose diabase and palagonite from the Holyoke Trap Sheet. *Bull. Geol. Soc. Am.*, **16,** 91–130.

Grout, F. F. and Schwartz, G. M. (1939), The geology of the anorthosites of the Minnesota coast of Lake Superior. *Minn. Geol. Surv. Bull.* **28,** 119 p.

Gruner, J. W. (1946), The mineralogy and geology of the taconites and iron ores of the Mesabi range, Minnesota. Office of the Commissioner of the Iron Range Resources and Rehabilitation, 127 p.

Gruner, J. W. (1935), The structural relationships of nontronite and montmorillonite. *Am. Mineral.*, **20,** 475–483.

Hawkins, A. C. and Shannon, E. V. (1924), Canbyite, a new mineral. *Am. Mineral.*, **9,** 1–5.

Muir, I. D. (1954), Crystallization of pyroxenes in an iron-rich diabase from Minnesota. *Mineral. Mag.*, **30,** 376–388.

Nikolsky, A. P. (1953), On hisingerite of the Schsagen (Saksogan) belt. *Min. Sbornik, Lvov Geol. Soc.*, 127–134. Abs. *Mineral. Mag.*, **31,** 61.

Osborne, F. F. and Archambault (1950), Hisingerite from Montauban-les-mines. *Le Naturaliste Canadien*, **77,** 283–290.

Ross, C. S. and Hendricks, S. B. (1945), The minerals of the montmorillonite group, their origin and relation to soils and clays. *U. S. Geol. Surv. Prof. Paper* **205 B,** 41–43.

Ross, C. S. and Shannon, E. V. (1925), The origin, occurrence, composition and physical properties of the mineral iddingsite. *Proc. U. S. Nat. Museum*, **67,** 1–19.

Schwartz, G. M. (1924), On the nature and origin of hisingerite from Parry Sound, Ontario. *Am. Mineral.*, **9,** 141–144.

Sudo, T. (1954), Iron-rich saponite found from Tertiary iron sand beds of Japan. *Jour. Geol. Soc. Japan*, **60,** 18–27.

Sudo, T. and Nakamura, T. (1952), Hisingerite from Japan. *Am. Mineral.*, **37,** 618–621.

Sun, Ming-shan (1957), The nature of iddingsite in some basaltic rocks of New Mexico. *Am. Mineral.*, **42,** 525–533.

Wilshire, H. G. (1958), Alteration of olivine and orthopyroxene in basic lavas and shallow intrusives. *Am. Mineral.*, **43,** 120–146.

Manuscript received February 17, 1961.

THE AMERICAN MINERALOGIST, VOL. 46, NOVEMBER-DECEMBER, 1961

CARBONATIC NIOBIUM-RARE EARTH DEPOSITS, RAVALLI COUNTY, MONTANA*

E. Wm. Heinrich and A. A. Levinson, *The University of Michigan, Ann Arbor, Michigan and The Dow Chemical Company, Freeport, Texas.*

Abstract

Carbonatic Nb-RE deposits of Ravalli County, Montana contain chiefly dolomite and Sr-Ba calcite and variable amounts of biotite, chlorite, actinolite, allanite, quartz, barite, apatite, monazite, pyrite, magnetite, and columbite. Rarer unusual constituents are ancylite, fersmite, niobian rutile, eschynite, andradite, glaucophane and wollastonite. The tabular deposits which are in pre-Beltian (?) hornblendic metamorphic rocks are an inch to 10 feet thick, as much as 450 feet long, and crosscutting as well as conformable. They range in texture and composition from metasomatized marble layers to banded, comb-structure veins, resulting from the action of hydrothermal solutions of alkalic derivation, which supplied mainly Sr, Ba, RE, Nb, and S.

Introduction

General Statement

Mineral deposits of unusual characteristics occur in the southwestern corner of Montana in Ravalli County, in the headwaters of the West Fork of the Bitterroot River along the eastern flank of the Bitterroot Range. The area is approximately 38 miles by road south of Darby. Deposits have been discovered in the general area of Woods, Beaver, and Sheep Creeks, all tributaries to the West Fork Bitterroot River (Fig. 1). The purpose of this investigation has been to study the mineralogy and paragenesis of these deposits and to formulate conclusions regarding their origin.

History

Rare-earth minerals from western Montana were first described by Penfield and Warren (1899), who analyzed parisite crystals which were reportedly found near the ghost settlement of Pyrites, east of Florence, in northern Ravalli County. The description of the matrix material containing the parisite, apparently an altered rhyolite or trachyte, indicates, however, that this occurrence of a rare-earth carbonate is not directly related to the deposits described in this report.

Sahinen (1957) states that columbite was discovered at Sheep Creek in 1953. Fersmite was first detected in the columbite ore in January 1954 (Hess and Trumpour, 1959) in a sample submitted by Mr. Louis Eriksen

* Contribution No. 238 from the Mineralogical Laboratory, Dept. of Geology and Mineralogy, The University of Michigan, Ann Arbor, Michigan.

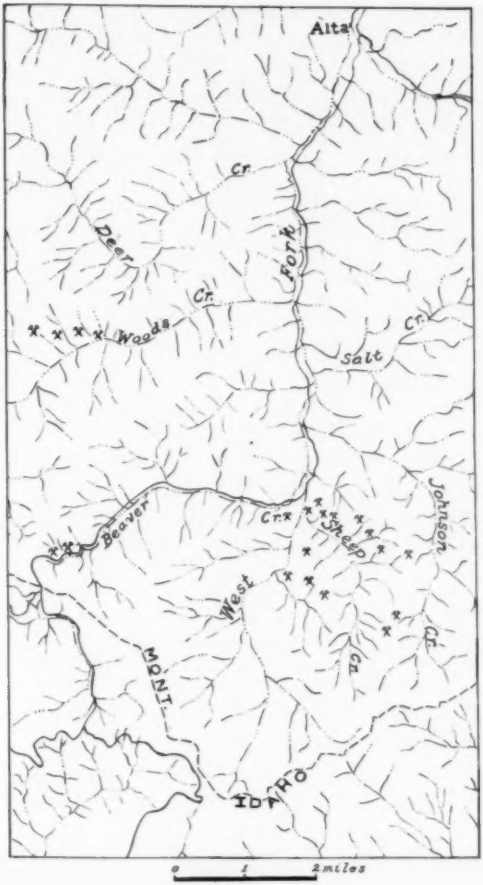

FIG. 1. Outline map of the niobium-rare earth district, Montana and Idaho.

of Corvallis to the U. S. Bureau of Mines Petrographic Laboratory at Albany, Oregon.

Only the Sheep Creek deposits have been actively developed; all of the other Montana occurrences have been merely prospected. The former are owned by the Sheep Creek Mining Company, a subsidiary of the Continental Columbium Corporation of California, which began activities in 1957, driving four adits. The Idaho counterparts, first described by Abbott in 1954, have since been studied in detail by Anderson (1958, 1960).

The senior author studied the deposits during the early summer of

1957 and again in August 1958, when he also examined a number of the Idaho occurrences. The Montana Bureau of Mines and Geology also has investigated the deposits (Crowley, 1958, 1960).

The field work and part of the laboratory work has been supported by Michigan Memorial-Phoenix Project, No. 150. The writers gratefully acknowledge assistance from the following individuals: for laboratory aid, R. A. Borup, J. A. Greear, R. W. Vian, R. W. Deane, and E. B. Gross; for information and specimens, Dr. Charles Milton and Dr. Mary Mrose, Professor Clifford Frondel and Frank A. Crowley. The writers are grateful to Dr. E. R. Wright and The Dow Chemical Company for their encouragement and permission to publish the results of this study.

Geology

Definition of the District

The district lies in the southwestern corner of Montana, continuing generally southward into Idaho (Fig. 1). Deposits are known in a north-northwest-trending belt that extends from near North Fork, Idaho, to Deer Creek, just north of Woods Creek in Montana (Fig. 1). The belt is approximately 18 miles along its northwesterly axis and 3 or 4 miles across the axis.

General

The mineralized area is underlain chiefly by metamorphic rocks, shown on the geological map of Montana (Ross *et al.*, 1955) as metasediments of the Ravalli group, Belt Series. Reconnaissance study suggested however, that the rocks might be pre-Beltian in age. This is supported by Sahinen (1957, p. 6). Crowley (1958, 1960) also regards these rocks as pre-Beltian. In many respects their lithology resembles that of the Cherry Creek group, a unit widespread elsewhere in southwest Montana (Heinrich, 1953). The other possibility is that these rocks represent higher-grade metamorphic facies, grading northward into more typical Belt rocks.

Main rock types noted near the deposits include: 1) Hornblende gneiss and amphibolite, weakly foliated to coarsely gneissic; some banded or streaked. This is the most common wall rock of the deposits. 2) Light colored quartz-feldspar gneiss streaked with biotite-rich lenticles. 3) Augen gneiss, a relatively dark hornblendic rock studded with ovoid feldspar metacrysts, an inch long. This may represent local, partly granitized amphibolite. 4) Biotite and muscovite schists, highly fissile, light gray to dark. 5) Biotitic and feldspathic quartzite. 6) Iron formation—banded quartz-magnetite rock. This rock is characteristic of the Cherry Creek group elsewhere in Montana. 7) Marbles. Crowley (1958, 1960) also reports diabase dikes cutting these metamorphic rocks.

Along Woods Creek the metamorphic foliation strikes generally N. 30–50° W., dipping rather uniformly northeast at 40–70°. Near the mouth of Sheep Creek it strikes N. 60–70° W. and dips steeply northeast. The West Fork Bitterroot River north of Sheep Creek apparently follows a major north-south fault that passes just west of the Sheep Creek deposits.

The metamorphic rocks are intruded by scattered, relatively small, undifferentiated, granitic pegmatites and are also cut by a few small quartz and quartz-chlorite veins. These pegmatites and veins are probably related to granodiorite of the Idaho batholith, which intrudes the metamorphic rocks at the very southern tip of the West Fork area. Locally fine-grained felsic dikes (Laramide or Tertiary?) transect the metamorphic complex.

Deposits

Most of the smaller deposits generally are parallel with the metamorphic foliation and most of them occur within hornblendic rocks. Some of the thicker ones transect the foliation at slight angles, or locally send off apophyses that cut across at considerable angles. The deposits range in thickness from about an inch to as much as 10 feet (Fig. 2). Some have been traced for only several feet, whereas others are known to be continuous along the strike for as much as 450 feet. The thinner deposits tend to occur in closely spaced subparallel clusters of three or more, separated by a few inches to several feet of wall rock.

Most deposits have sharply defined walls. Most are tabular; a few of the larger ones are lensoid to irregular, showing branching as well as pinch-and-swell structures. The deposits appear to have been formed

FIG. 2. Hanging-wall part of thick baritic carbonatic deposit, Rocky Point No. 5, Woods Creek, Montana.

chiefly along two types of structures: 1) the metamorphic foliation, and 2) contacts between hornblende gneiss and other metamorphic rocks. Some of the cross-cutting deposits may also have been emplaced along faults.

On the basis of texture, the deposits are divisible into three types: 1) Very fine grained, essentially aphanitic, showing a very weakly developed gneissoid texture. This is characteristic of some of the deposits along Woods and Beaver Creeks. This carbonate-rich rock resembles a fine-grained limestone, with a porcelanoid fracture and an average grain size of 1 mm. or less. Thin-sections show a well developed foliation, with the carbonate in highly elongate, equigranular, subparallel spindles that are conspicuously twinned. 2) A somewhat coarser-grained, megascopically granular and streaked texture occurs in Rocky Point No. 5 and some of the other Woods Creek deposits. The gneissoid texture results from the alignment of barite lenses within a dominantly carbonate matrix. The grain size ranges from 3 to 10 mm. Under the microscope the carbonates are seen to be heterogranular, poorly to non-foliated, with but minor twinning. 3) More variable and much coarser-grained structures characterize the Sheep Creek veins. Irregular comb structures may be developed marginally, and the interiors vary greatly in grain size, from coarse grained (4 cm.) to fine grained (1 mm. or less). Gneissoid structure is only locally and marginally present.

A few small vugs (several mm. to several cm. across) were found in the lower Beaver Creek deposits and in some parts of the Sheep Creek vein. They are generally partly filled with calcite rhombohedra. Some vugs in the lower Beaver Creek deposits have an outer lining of small quartz crystals, central crystals of clear calcite, corroded by very fine-grained hematitic carbonate which fills the remaining space.

Thus the deposits range in appearance from some resembling fine-grained limestones, through others that look like coarse-grained, weakly foliated marbles, to several that have the textural characteristics of ordinary veins.

Post-consolidation disturbance of the deposits is shown by 1) numerous late veinlets of clear calcite and/or of quartz, and 2) slickensided surfaces (in the Sheep Creek deposits) across all of the minerals including ancylite. The Sheep Creek veins have been offset and displaced by at least two sets of faults.

Exomorphic and Endomorphic Effects

Most of the deposits are characteristically surrounded by thin envelopes of altered wall rock, in which much of the hornblende has been transformed to biotite (Table 1, A and B). Metacrysts of biotite as large

TABLE 1. MODES OF WALL ROCKS

	A	B	C
Hornblende	49.6%	31.9%	70.0%
Biotite	2.4	23.2	—
Quartz	15.6	9.6	3.6
Plagioclase	30.8	32.8	6.2
Epidote	tr	—	13.8
Barite	—	—	4.4
Magnetite	0.5	—	1.4
Apatite	0.4	2.5	—
Rutile	tr	—	—
Sphene	0.7	—	—
Pyrite	—	—	0.6
	100.0	100.0	100.0

A. 6—RP2 Amphibolite, Rocky Point No. 2, several feet from deposit.
B. 4—RP2 Altered amphibolite, Rocky Point No. 2, directly adjacent to deposit.
C. 11—RP5 Altered amphibolite, Rocky Point No. 5, directly adjacent to deposit.

as 1 cm. in diameter appear in the selvages of carbonate layers that are only a few inches thick. Subsequently much of the biotite directly at the contacts was chloritized. These biotitized selvages also have been impregnated by considerable calcite, which appears both as fine-grained disseminated aggregates and as hair-like, crisscrossing veinlets.

Along the Rocky Point No. 5 the amphibolite has been coarsened, epidotized, and has had barite introduced (Table 1, C). The hornblende also shows unusual greenish blue pleochroism and abnormal interference tints, indicating a transition toward glaucophane.

Many carbonate bands contain small inclusions of altered wall rocks or aggregates of amphiboles formed by the alteration of incorporated wall-rock hornblende. Angular pieces of chloritized biotite amphibolite as much as several centimeters across have been noted.

MINERALOGY

General

The chief minerals are rhombohedral carbonates, which usually constitute 80–95% of the deposits. Present also in most of the occurrences, but in variable amounts, are biotite, chlorite, actinolite, allanite, quartz, barite, apatite, monazite, pyrite, magnetite and columbite. Of these, the Fe-Mg silicates, barite, monazite and apatite become major constituents (>10%) in some parts of deposits.

TABLE 2. CHARACTERISTICS OF THE RHOMBOHEDRAL CARBONATES
(ANALYSES BY EMISSION SPECTROGRAPH)

Deposit	Max. grain size of carbonate	Fabric	Appearance and paragenetic positions	*X*-ray diffraction identities	Composition (in weight per cent)
Calhoun	1 cm.	Heterogranular, non-foliated, no twinning	Main = Clear (Carb. I)	Dolomite	———
			Minor = dusty, interstitial (Carb. II)	?	
Rocky Pt. No. 1	6 mm.	Equigranular, strongly foliated, sheared (?), twinning strong	Main = Dusty (Carb. I)	Dolomite	———
			Vein = Carb. III	Calcite	———
Rocky Pt. No. 2	2 mm.	Foliation moderately well developed, twinning minor, heterogranular	Clear (Carb. I)	Dolomite	———
			Dusty (Carb. II) Ratio 1:1	Calcite	———
Rocky Pt. No. 3 (Cresthill)	3 mm.	Heterogranular, non-foliated	Main = Clear (Carb. I)	Dolomite	Calcite (Carb. II): Sr-1.1, Ba-0.51, Mn-0.55
			Minor = dusty and brown-weathering (Carb. II)	Calcite	
Rocky Pt. No. 3—West	3 mm.	Equigranular, well foliated	Clear (Carb. I)	Dolomite	———
			Dusty (Carb. I)	Calcite	———
Rocky Pt. No. 4	1 mm.	Heterogranular, poor foliation in clear grains	Clear (Carb. I)	Dolomite	
			Dusty (Carb. II)	Calcite	
Rocky Pt. No. 5	1 cm.	Heterogranular	Clear (Carb. I)	Calcite	Calcite (Carb. II) Sr-1.4, Ba-0.11, Mn-0.46
			Dusty (Carb. II)	Calcite	
			Clear, vein (Carb. III)	Calcite	
Upper Beaver Creek (Jackie)	1 mm. or less	Equigranular, well foliated twinning common	Clear (Carb. I)	Dolomite	
		Heterogranular, non-foliated	Dusty (Carb. II)	Calcite	
			Vein (Carb. III)	Calcite	
Lower Beaver Creek	1 cm.	Non-foliated, highly twinned, twin lamellae are bent	Dusty (Carb. II)	Calcite	
Sheep Creek (Columbine, Van Matre)	4 cm.	Comb, at vein margin	Clear (Carb. I)	Dolomite	
Sheep Creek (Columbine, Van Matre)	2 cm.	Remnants in ancylite	Dusty (Carb. II)	Calcite	Sr-0.35, Ba-0.59, Mn-0.42
Sheep Creek (Columbine, Van Matre)	3 cm.	Bladed	Dusty (Carb. II)	Calcite	Sr-1.3, Ba-0.42, Mn-0.42
Sheep Creek (Columbine, Van Matre)	3 cm.	Bladed	Dusty (Carb. II)	Calcite	Sr-1.2, Ba-0.32, Mn-0.19
	3 mm.	Equigranular	Veined by Carb. III	Calcite	
Sheep Creek (Columbine, Van Matre)	1 cm.	Equigranular vein	Clear (Carb. III)	Calcite	Sr-0.07, Ba-0.37, Mn-0.73

The complete list of minerals found is:

Sulfides: pyrite, pyrrhotite, chalcopyrite, molybdenite
Oxides: magnetite, hematite, rutile, niobian rutile, ilmenite, columbite, fersmite, eschynite
Halide: fluorite
Carbonates: dolomite, strontian-barian calcite, calcite, ancylite, malachite
Sulfate: barite
Phosphates: apatite, monazite
Silicates: quartz, albite, andradite, biotite, chlorite, muscovite, hornblende, actinolite, soda-actinolite, glaucophane, allanite, wollastonite

NOTES ON INDIVIDUAL MINERALS

Rhombohedral carbonates: The rhombohedral carbonates show a considerable variation in grain size, texture, and composition. On the basis of paragenetic position, three main types are recognizable:

Carbonate I—Earliest. Microscopically clear, megascopically gray to blue-gray if unweathered. With weathering, it first develops films of limonite along cleavage surfaces and finally turns entirely brown, resembling siderite megascopically. It is usually dolomite, rarely calcite (Table 2).

Carbonate II—Of intermediate position. Microscopically dusty to "dirty"; in hand specimen gray, pale buff or greenish. It is the only carbonate present in a few veins or locally in parts of some veins. If it occurs subordinate to Carbonate I, it is interstitial to I; if it exceeds I, it embays and replaces it (Fig. 3). It is invariably a strontian and/or barian calcite also containing Mn (Table 2).

Carbonate III—A megascopically snow-white carbonate forms veinlets across nearly all other species (post-ancylite and post-sulfide). In thin section it is clear. The veinlets may consist solely of this carbonate or of quartz-carbonate (Fig. 3), or, rarely, of quartz, carbonate and a second generation of barite (Fig. 4). They range

FIG. 3. Sr-Ba calcite (II) enclosing corroded remnant of iron stained dolomite (I), Rocky Point No. 5 deposit. 70×.

FIG. 4. Veinlet of chlorite (dark marginal fringe), quartz (clear), barite euhedra, and calcite (III) (central, gray), cutting Sr-Ba calcite (II), Sheep Creek vein. 42×.

in thickness from less than a millimeter to about 1.3 cm. This carbonate is invariably calcite, and the one analysis shows it to be Sr-low (Table 2).

This carbonate also forms coarse rhombohedra in vugs of the Lower Beaver Creek deposit, which also contain a fourth carbonate that fills the remainder of the vugs, corroding the white calcite (III). This youngest carbonate is uniformly very fine grained and deep brick-red in color owing to included hematite.

Textural relations and compositions of the carbonates indicate that the initial carbonate (I) was chiefly dolomite, which in some of the thinner deposits displays a strongly foliated fabric. In some deposits or parts of some deposits dolomite was 1) recrystallized, or 2) recrystallized and partly replaced by Sr-Ba calcite, or 3) nearly entirely replaced by Sr-Ba calcite (Fig. 3).

Ancylite: Ancylite has been found by the writers only in the Sheep Creek vein. The ancylite content varies considerably, with the color of the specimen serving as an index to the rare earth carbonate content: specimens low in ancylite are faintly pink; higher grade material is colored light cherry red; the highest grade rock, containing slightly less than 50% ancylite, is dark reddish-lilac in color. The Sheep Creek vein contains material relatively rich in ancylite in masses as much as several feet across, generally segregated in the central parts.

Most of the ancylite is very fine grained (0.007–.030 mm.) and is intimately intergrown with quartz of similar grain size and with Sr-Ba calcite and some barite, both of which are replaced by the ancylite-quartz aggregates (Fig. 5). Veinlets of quartz and of clear calcite (III) transect the ancylite aggregates (Fig. 6). Ancylite varies considerably in form: most is anhedral (Fig. 5); some is euhedral (Fig. 7) and in a few cases it forms radial aggregates (Fig. 8). *X*-ray data are given in Table 4.

Complete purification of an ancylite sample for analysis proved impossible. Analysis of a high-grade specimen containing ancylite, strontian calcite, quartz and a little barite gave the results of Table 3A. Since no other rare-earth mineral was present, all of the rare-

FIG. 5. Corroded remnants of Sr-Ba calcite (II) in fine-grained ancylite quartz aggregate. Late veinlet of calcite (III) cuts both. Sheep Creek vein. 70×.

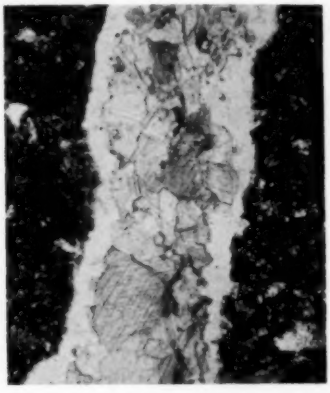

FIG. 6. Veinlet of marginal quartz and central calcite (III) cutting very fine-grained ancylite (dark)-quartz-carbonate aggregate. Sheep Creek vein. 42×.

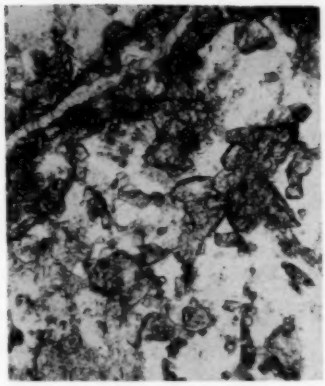

FIG. 7. Auhedral ancylite in quartz matrix, with irregular Sr-Ba calcite (II) remnants (gray) and a late calcite (III) veinlet. Sheep Creek vein. 70×.

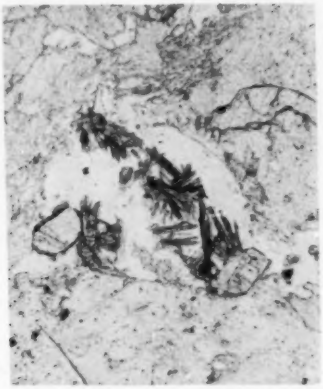

FIG. 8. Radial groups of ancylite in quartz. Also rounded monazite (gray, high relief) in Sr-Ba calcite (III). Sheep Creek vein. 70×.

earth elements are assignable to ancylite. By comparing the amount of rare-earth elements in the sample to that required by pure ancylite, the sample can be calculated to contain 44% ancylite. The ratio

$$\frac{\text{Wt\% Sr}}{\text{Wt\% RE}} = 0.25.$$

For pure strontium ancylite this ratio (Palache *et al.*, 1951, p. 292) is calculated to be 0.47. Since some of the Sr in the Ravalli sample is contained in the calcite (Table 2) and a little in the barite, there is considerable substitution of Ca for Sr in the ancylite, certainly sufficient to regard the Sheep Creek mineral as a calcian ancylite. Probably the small amount of Ba reported may be assigned entirely to barite.

Barite: Barite is especially abundant in the Rocky Point No. 5 deposit, in which it occurs in irregular to lensoid snow-white, coarsely crystalline aggregates, many grains of which are 3 mm. across. Nearly all barite is pre-calcite II, being veined and corroded by it (Fig. 9). Parts of the Sheep Creek deposit contain microscopic quartzose veinlets containing scattered barite euhedra (Barite II) (Fig. 4). The Rocky Point No. 5 barite (by *x*-ray fluorescence) contains 0.4% Sr.

Monazite: Monazite was identified in nearly all the deposits studied, in most cases microscopically. However, in the Rocky Point No. 1 and in the Sheep Creek vein it appears in coarse, rounded anhedra, in the former as much as 8 mm. across and in the latter as much as several centimeters in diameter. These tend to be concentrated in marginal parts of veins. The color is somewhat variable, ranging from a light honey-yellow to a deep orange-red. Microscopically monazite appears most commonly as irregular to ellipsoidal and rounded grains intergrown with carbonate. Some grains are skeletal; others are lobate, markedly embayed by carbonate II (Fig. 10). In the Sheep Creek vein some monazite, which forms overgrowths on subhedral apatite, is dactylicly intergrown with strontian calcite (Fig. 11).

TABLE 3. PARTIAL ANALYSES OF THE RE MINERALS, BY X-RAY FLUORESCENCE

A Ancylite ore[1]	B Monazite[2]	C Allanite[4]
Ce —9.0%	Ce_2O_3 —35.8%	Ce_2O_3 —12.9%
La —6.8	La_2O_3 —26.5	La_2O_3 —10.1
Nd —1.7	Nd_2O_3— 6.4	Nd_2O_3— 2.0
Pr —0.5	Pr_2O_3 — 2.7	Pr_2O_3 — 1.1
Sm —0.1	Sm_2O_3— tr.	Y_2O_3 — tr.
Y —0.01	Gd_2O_3— tr.	ThO_2 — tr.
Gd — tr.	Y_2O_3 — tr.	SrO — tr.
Th —0.05	ThO_2 — 0.7	TiO_2 — tr.
Ca —34		
Sr —4.6	Total—72.1	Total—26.1
Ba —1.3		
Fe —0.2		
Mn—0.1		
W[3] —0.3		

Analysts: A. A. Levinson and R. A. Borup.

[1] Sheep Creek vein. Estimated to be 44% ancylite, rest mainly Sr-Ba calcite and minor quartz.

[2] By emission spectrography.

[3] Rocky Point No. 1 deposit. Average of three analyses.

[4] Sheep Creek vein. Average of two analyses.

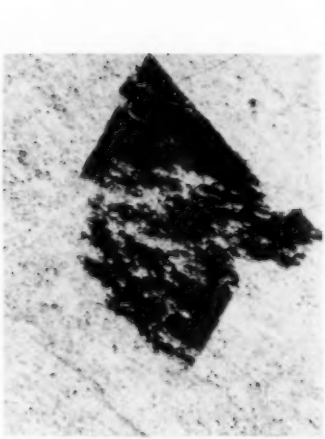

FIG. 9. Zoned, euhedral barite, partly replaced by Sr-Ba calcite (II). Sheep Creek vein. 70×. Crossed polars.

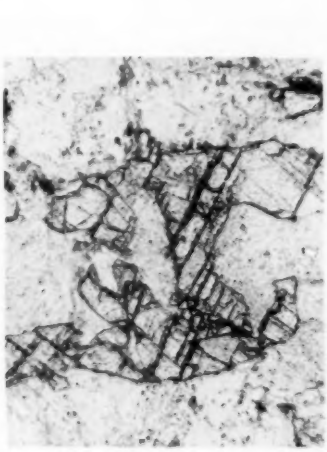

FIG. 10. Lobate monazite embayed by Sr-Ba calcite (II). Sheep Creek vein, 70×.

Monazite is intergrown with both allanite and columbite. Much of it is veined by clear calcite and less commonly by pyrite. For the composition of the monazite see Table 3B; it is but feebly radioactive.

Apatite: Apatite is widespread as microscopic anhedra to subhedra intergrown with dolomite and with Sr-Ba calcite, which may vein it. It is especially abundant in the Western Rocky Point No. 3 vein in which it forms thin phosphate-rich layers.

Fluorite: Small, very rare anhedra of fluorite, pale lilac in color, were noted in two specimens from the deposits in the upper part of Beaver Creek. Microscopic colorless fluorite occurs in the Lower Beaver Creek deposits associated with the altered andradite and wollastonite.

Sulfides: Pyrite is widespread as minute subhedra to euhedra but is locally abundant only in the Sheep Creek vein in which it forms coarse-grained masses as large as 7 cm. across. The other sulfides, chalcopyrite, pyrrhotite and molybdenite appear to be largely restricted to the Sheep Creek vein. Molybdenite is very rare, having been noted as small flakes in but two specimens. Pyrrhotite, only slightly more abundant, was identified only in polished sections. In the Sheep Creek vein the sulfide-rich material also contains much coarse magnetite. Quartz and calcite veinlets transect all of the sulfides.

Columbite: Columbite forms ellipsoidal to irregular aggregates as much as 5 cm. long, with all of the masses over 0.5 cm. in size coming from the Sheep Creek vein. Smaller particles are widespread but not common in many of the other veins, but it is not always possible to distinguish them from grains of niobian rutile by inspection.

The larger columbite aggregates are polycrystalline, composed of numerous unoriented subhedra having a maximum length of about 2 mm. The aggregates include considerable intergrown carbonate as well as some barite and a little monazite and fersmite. Columbite particles from acid insoluble residues therefore are highly porous and resemble minute "clinkers" (Fig. 12). In some instances columbite euhedra project into the included carbonate. These interlaced crystals are of stout prismatic habit, showing closely

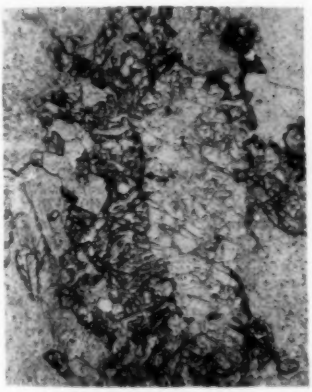

FIG. 11. Apatite grain with dactylic overgrowth of monazite in Sr-Ba calcite (II). Sheep Creek vein. 42×.

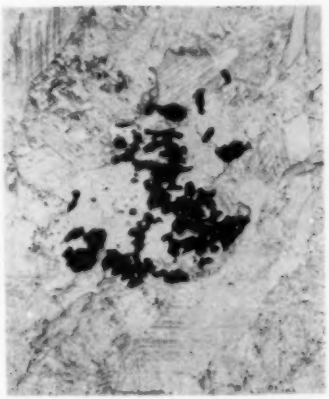

FIG. 12. Skeletal columbite in carbonate I, with scattered biotite flakes. Rocky Point No. 1 deposit. 70×.

spaced vertical striations and simple terminal development, with {001} dominant. By emission spectrograph the mineral was determined to be tantalum-free, agreeing with Sahinen (1957).

Fersmite: The second world occurrence of fersmite is represented by that in the Sheep Creek vein (Hess and Trumpour, 1959). Small amounts of fersmite also were found intergrown with columbite from the Rocky Point No. 1 deposit. Fersmite occurs as irregular to angular inclusions in columbite, commonly close to larger calcite particles. Some fersmite is distinctly vein-like in form.

Eschynite: Crowley (1958, 1960) found a dark brown, radioactive, submetallic mineral in aggregates of parallel fibers as much as 6 inches long and 4–5 inches across in a deposit in the upper part of Sheep Creek. A 200 mg. specimen of the mineral, which he suggested might be euxenite, was analyzed by wet methods by J. A. Greear and found to contain 2.8% barite, 0.7% SiO_2 and 0.4% H_2O as impurities. The original analysis (total 102.7%), excluding the impurities, recalculated to 100% yields:

CaO = 4.2%	ThO_2 = 3.3%	TiO_2 = 15.7%
RE_2O_3 = 25.4%	Nb_2O_5 = 49.4%	Fe_2O_3 = 2.0%

By *x*-ray fluorescence analysis it was found that (1) the rare-earths are chiefly of the cerium sub-group, (2) the mineral contains no Ta or U and (3) Greear's chemical separations were good. ThO_2 was precipitated with RE_2O_3 and determined by *x*-ray fluorescence.

Microscopically the mineral is partly metamict. The crystalline remnants are brown, feebly pleochroic, biaxial (−), 2V moderate. $\alpha > 2.00$; $\gamma - \alpha = 0.010$–0.015. G = 4.20. *X*-ray data are given in Table 4. These data, together with the analytical results, indicate the mineral is eschynite, low in Ti and Th. Eschynite has not been found up to now in carbonate-rich deposits.

TABLE 4. *X*-RAY DIFFRACTION DATA FOR ANCYLITE AND ESCHYNITE FROM SHEEP CREEK, RAVALLI CO., MONTANA. FILTERED Fe RADIATION

Ancylite				Eschynite	
d Å	I	*d* Å	I	*d* Å	I
4.3	1	1.83	3	1.66	ms
3.7	1	1.74	4	1.62	s
2.95	5	1.72	4	1.54	w
2.65	5	1.68	5	1.50	w
2.53	5	1.65	2	1.44	ms
2.44	4	1.62	3	1.37	m
2.35	10	1.59	5	1.34	w
2.18	1	1.55	2	1.28	m
2.14	3	1.53	6	1.24	m
2.09	10+	1.49	5		
2.05	3	1.46	2		
2.02	10	1.42	5		
1.95	8	1.38	4		
1.90	2	1.32	10		
1.85	6				

FIG. 13. Twinned allanite with inclusions of monazite, cut by calcite veinlets (III). Sheep Creek vein. 42× Crossed polars.

FIG. 14. Partial pseudomorph of chlorite (dark gray) and calcite (clear blades) after zoned and sector-twinned andradite (high relief). Sheep Creek vein. 70×.

Iron and titanium oxides: Magnetite occurs in all the deposits, appearing in the narrower carbonate bands of Woods and Beaver Creeks as minute disseminated octahedra. In the Sheep Creek vein it also forms irregular to ellipsoidal aggregates as large as 5×9 cm. Polished sections show that these are replaced by metallic hematite, particularly along fractures. Minor amounts of supergene red hematite coatings occur in several other veins. Minute morphologically complex hematite crystals also were found in insoluble residues from the upper Beaver Creek deposits.

Niobian rutile, the most abundant niobium mineral of the Idaho deposits, appears to be much less common in the Montana counterparts. It was identified with certainty only in the Rocky Point No. 4 by its *x*-ray powder pattern. However columbite is present in the same vein. The Idaho niobian rutile contains 13% Nb and <0.1% Ta (Heinrich, *et al.*, 1958). Small grains of golden rutile were noted in thin sections of the Rocky Point No. 1 deposit. Crowley (1958, 1960) also reports ilmenite in the Beaver Creek deposits.

Allanite: Nearly all the deposits contain some allanite; locally in several it forms conspicuous clusters of prismatic subhedra, several centimeters long, concentrated near the walls. It is commonly intergrown with some monazite. The allanite crystals are segmented by veinlets of clear calcite and marginally replaced and corroded by actinolite and chlorite. None of the allanite shows any metamictization whatsoever, and its thorium content is very low (Table 3C). It is strongly pleochroic in shades of deep red, brown and dark green. Some of the larger crystals show color zoning with darker shades in the central parts of crystals. Twinning is conspicuous (Fig. 13).

Amphiboles: Hornblende and actinolite, which are widespread, are concentrated in the thicker deposits near the walls but in thinner ones are disseminated, with the former showing sub-parallel orientation. Dark green hornblende forms single crystals; light green actinolite forms clusters of fibers, usually in radiating groups.

Glaucophane, black in hand specimen, is locally abundant in outer parts of the Sheep Creek vein, forming subparallel bundles as much as 4 cm. long. It also occurs in the

Rocky Point No. 4 deposit. Several amphiboles, which from their optical properties are member of soda-actinolite—glaucophane series, appear in minor amounts as disseminated prismatic subhedra in the Rocky Point No. 4 and 5 deposits.

Micaceous minerals: In the larger deposits much of the biotite forms single foils as much as several centimeters across in marginal parts of veins. It shows varying degrees of alteration to chlorite. In the narrower bands biotite usually is disseminated and may show parallel orientation. Most of it is pleochroic in shades of brown, rarely green. It is veined by strontian calcite along cleavage directions. Biotite is generally more abundant in deposits that contain strontian calcite rather than dolomite as the principal carbonate. Muscovite is an uncommon, late mineral in a few deposits.

There are three types of chlorite: 1) a variety pseudomorphous after biotite, 2) a type which, together with fine-grained carbonate, replaces zoned andradite (Fig. 14), and 3) a variety forming spherulitic aggregates interstitial to calcite (Lower Beaver Creek deposit).

Andradite: Garnet occurs as remnants of partly replaced euhedra in the Lower Beaver Creek and Sheep Creek deposits. It was observed only microscopically. Its properties are: very pale golden yellow in color; isotropic or very weakly birefringent with B as much as 0.004; $n = 1.85$–1.86. The former euhedra are zoned concentrically and show sector twinning. The x-ray powder diffraction pattern has the spacings of andradite, with a $a_o = 11.98$ Å. The crystals have been largely replaced in the Sheep Creek vein by a very fine-grained chlorite-carbonate-hematite mixture (Fig. 14) and in the Lower Beaver Creek deposit they are corroded by wollastonite.

Wollastonite: Wollastonite was discovered in the Lower Beaver Creek deposit in which it forms fibrous, pink lenses as much as 5 cm. long and 1 cm. thick. Under the microscope it appears as finely felted aggregates of radial or irregular aspect. It is minutely intergrown (and replaced) by fine-grained calcite, quartz, and fluorite. Wollastonite corrodes andradite, actinolite, and carbonate I. The wollastonite is also replaced by several very fine-grained unidentified hydrated calcium silicates.

Other silicates: Quartz is a minor constituent of many of the deposits, occurring in four ways: 1) As disseminated ellipsoidal grains. 2) As very fine-grained lacy aggregates with ancylite replacing Sr-Ba calcite (Sheep Creek only). 3) In late veinlets. 4) As euhedral crystals lining small vugs in the Lower Beaver Creek vein.

Rounded relicts of sodic plagioclase corroded by a strontian calcite appear in the Rocky Point No. 4 vein.

Paragenesis

Clearly defined textural relations indicative of age differences (cross-cutting veinlets, corroded relicts, pseudomorphs, crustification and overgrowths) abound in the veins, and their interpretation leads to a generally consistent paragenetic sequence which is divisible into the following stages (oldest to youngest; a question mark indicates a doubtful positional assignment):

Metamorphic

I. Dolomite, aparite, magnetite I, hornblende, quartz I, plagioclase, andradite, wollastonite, hematite

Metasomatic replacement

II. Silicate stage: biotite, actinolite, Na-actinolite, glaucophane
III. RE-Nb stage: allanite, monazite, barite, columbite, Nb-rutile, eschynite (?)
IV. Carbonate stage: Sr-Ba calcite
V. Sulfide stage: Pyrite, magnetite II, molybdenite, chalcopyrite, pyrrhotite
VI. Ancylite stage: chlorite, muscovite, ancylite, quartz II, fersmite (?) hematite, fluorite (?)

Veinlet stage

VII. Quartz III, calcite III, barite II, chlorite, hematitic calcite

Supergene

VIII. Hematite, limonite, malachite

For the metasomatic stages it is noteworthy that this sequence agrees well, although not exactly, with that first determined by Anderson (1958, p. 30), independently for the similar Idaho deposits: 1) silicates, 2) phosphates, 3) sulfates, 4) oxides, 5) carbonates, 6) sulfides. In his later publication (Anderson, 1960, p. 1196) he changes the order to 1) silicates, 2) phosphates, 3) carbonates, 4) sulfates, 5) oxides, and 6) sulfides. In our sequence the position of the sulfide phase is in considerable doubt. Pyrite is clearly post-monazite, but may be as late as post-ancylite.

Within individual stages, save that of the sulfides, age relationships among member species are less clearly defined than between stages. It appears that wall rock hornblende was altered in the sequences:

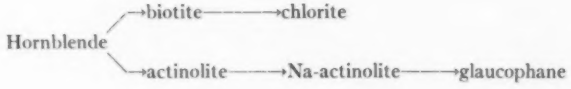

There is also the possibility that allanite represents the final mineral in the alteration of wall rock plagioclase which locally has been transformed to epidote along vein margins (Table 1C). The alteration, andesine→epidote, would release Na for the change, actinolite→glaucophane. Allanite appears to overlap the silicate and RE-Nb stages; some of it is included in monazite, whereas some of it contains monazite inclusions. Monazite is at least in part post-apatite (Fig. 11).

Strontian-barian calcite, which forms the bulk of many of the veins, is an excellent reference mineral. Most of the other species can readily be determined as older or younger than it.

The sequence within the sulfide stage is: 1) pyrite, 2) magnetite, 3)

chalcopyrite, and 4) pyrrhotite. The position of molybdenite is not known.

Nor are the columbite-fersmite relations well defined. Their intergrowths suggest that fersmite replaced columbite, resulting from reaction of Ca- and RE-bearing solutions upon the Mn-Fe niobate. For eschynite all that is known is that it is intergrown with barite.

Nearly all of the ancylite-quartz lenticles and elongated irregular "streaks" transect the fabric of vein material rich in Sr-Ba calcite (Fig. 5). In banded parts of veins the sequence from walls inward is 1) biotite selvage, 2) patches of actinolite, 3) dolomite, some in comb structure, 4) Sr-Ba calcite, 5) ancylite-rich material. It is noteworthy that the RE elements for the ancylite were not obtained by the destruction of earlier monazite or allanite. Although some monazite is embayed by Sr-Ba calcite and many sections of ancylite-rich ore show little or no monazite, ancylite and monazite do occur together.

In the veinlet stage, simple quartz veinlets cut clear calcite veinlets, but in complex veinlets calcite usually occupies interior parts and quartz is marginal. This is also the relative positions of the two in the rare vugs of the Beaver Creek deposits. In some of these the sequence inward is: 1) chlorite, 2) quartz, 3) barite euhedra (Fig. 7), and 4) carbonate. Thus for this stage the sequence appears to be: 1) complex veinlets, 2) calcite veinlets, 3) quartz veinlets.

TABLE 5. COMPOSITION OF THE DEPOSITS (IN WEIGHT PER CENT) (BY *X*-RAY FLUORESCENCE)

	Calhoun No. 1	Rocky Point No. 2	Rocky Point No. 4	Rocky Point No. 4	Rocky Point No. 5	Rocky Point No. 5 barite-rich phase	Beaver Creek	Beaver Creek	Sheep Creek
Sr	0.34		1.4	0.88	1.7	1.5	0.27	0.24	1.4
Ba	0.26		0.96	0.40	1.3	11.7	0.08		3.6
Ca	11.0		20.4	23.8	35.0	10.2	30.6	34.0	12.4
Nb	0.073		0.11	0.19	0.11	0.007	0.03	0.02	0.035
Ti	0.15			0.08			0.06	0.1	
Mn	0.29		0.27	0.29		0.09	0.2	0.1	0.09
Fe	5.0		2.4	3.1	3.5	0.54	2.4	2.7	0.67
K	<1				0.36	0.4			
Zn	tr							tr	
La		0.5	0.70	0.24	0.76				3.3
Ce		0.4	0.98	0.30	1.0				4.3
Pr		<0.1							0.3
Nd		<0.1	0.17	0.064	0.16				1.0
Sm		<0.1							<0.01
Gd		<0.1			0.08				<0.1
Y				0.02	nil	0.005	0.006		0.006
Cu					0.018				
Ta					nil		nil	nil	nil
Zr								0.08	

Geochemical Considerations

General

Analyses of vein samples (Table 5) show that the principal determined elements of the deposits are Ca, Ba, Sr, and Fe. Other known major constituents not sought in the analyses are CO_2, P, S, Si, Al, and H_2O. Of lesser quantitative significance are Nb, Ti, Mn, K, Na and several rare earths of the cerium group. Also present but in very minor amounts are yttrium-group rare earths, Zn, Cu, and Th.

The group of elements concentrated in these deposits resembles strongly the assemblage characteristic of carbonatites (Heinrich, 1958, pp. 225–226). Like carbonatites radioactivity is low and stems almost entirely from Th. Also like carbonatites the deposits are essentially Ta-free. However, these deposits appear to be somewhat lower in F and possibly Zr than most carbonatites. The columbite is Zr-free.

Rare Earths

Rare earths are represented almost entirely by the cerium group, with La and Ce predominating greatly, Pr and Nd subordinate, and Sm minor. The yttrium group is represented only by Y and Gd. Noteworthy also is the rare-earth distribution on atomic weight per cent basis for the three chief rare-earth minerals.

	Allanite	*Monazite*	*Ancylite*
La	39	37	38
Ce	49	50	50
Pr	4	4	3
Nd	8	9	9
	100	100	100

These species, within the experimental, measurable limits, show no rare-earth fractionation. The individual rare-earths of the Ravalli fersmite have not been determined. In the eschynite the principal RE elements also are Ce, Nd and La.

Niobium

The presence of columbite in these deposits represents an essentially unique occurrence of this mineral. Previously it has been recorded as 1) a widespread accessory mineral in granite pegmatites; 2) a rare accessory in a few aplites, e.g., the Meldon aplite of Devonshire (von Knorring, 1951); 3) an accessory in some alkalic granites, e.g., the famous biotite granite of the Jos-Bukuru younger granite complex of Nigeria and the alkali granites of the Erzin Massif of Eastern Tuva, U.S.S.R. (Pavlenko *et al.* 1958); and 4) pseudomorphs after pyrochlore in two Tanganyika

carbonatites (James and McKie, 1958). In the Ravalli deposits its occurrence represents a rare example of a Nb-Ca-CO_2 association in which most of the Nb does not occur as a Ca-Nb oxide or silicate (pyrochlore, betafite, niobian perovskite, niocalite). Likewise this occurrence of eschynite is unique.

Strontium

Gundlach (1959) has determined the Sr contents of many hydrothermal carbonate-rich veins from several German districts and reports their Sr content to range from 0.1–0.7%. These are chiefly sulfide-bearing veins with gangues of variable amounts of quartz, fluorite, barite, and calcite, dolomite, siderite, and ankerite. In this type of deposit 95–100% of the Sr occurs in barite. The Ravalli County veins contain 0.24–1.7% Sr (Table 5), with the rhombohedral carbonates containing 0.07–1.4% Sr (0.35–1.4% if the late clear vein calcite is excluded) (Table 2). The barite contains but 0.4% Sr. Thus the Montana veins not only contain from 2 to nearly 2.5 times as much Sr as typical sulfidic hydrothermal veins, but also have most of the Sr in carbonate rather than in sulfate species. The Sr content of these deposits also is in the order of 400–2800 times that of normal limestones (Turekian and Kulp, 1956). Such high Sr contents, are, however, characteristic of feldspathoidal rocks (Gerasimovskii and Lebedev, 1958).

The presence of such, apparently unusually, large amounts of Sr and Ba in calcite aroused the suspicions of the writers. The analyzed material was carefully checked for 1) strontianite and 2) aragonite. Neither was detected. That not all Ba- and Sr-rich calcium carbonates need have the orthorhombic (aragonite) structure has been demonstrated by Terada (1952), who synthesized rhombohedral Ba-Ca and Sr-Ca carbonates.

Origin

General

Ideas on the origin of the Montana-Idaho RE-Nb deposits are highly diverse. Abbott (1954) believed that originally clastic rare earth-bearing minerals, deposited in argillaceous and arenaceous Belt sediments, were destroyed during regional metamorphism and the liberated RE elements migrated to beds of phosphatic marble, where they reacted to form monazite. Kaiser (1956) likewise favored the idea that, during metamorphism, solutions carrying RE elements, derived either from an unknown source or from the rocks themselves, precipitated monazite selectively in carbonate rocks in certain favorable structural settings. Sahinen (1957) refers to the Sheep Creek deposit as a "dike" or "vein."

Hess and Trumpour (1959, p. 1) state simply "The fersmite . . . occurs . . . with a tantalum-free columbite associated with monazite, ancylite,

barite, quartz, and apatite in a fine-grained buff-colored marble." Crowley (1958) has summarized arguments for and against three hypotheses: 1) carbonatites, 2) hydrothermal replacement in marbles, and 3) lateral secretion (actually metamorphic segregation).

Anderson (1958) classed the Idaho deposits as replacement veins and lodes, and pointed out (p. 24) that, "Although others have regarded the carbonates as representing beds of crystalline limestone or marble replaced by the monazite and associated minerals, . . . much of the carbonate intimately associated with the mineralization is younger than the marble beds and indeed younger than the monazite and most of the other minerals." This conclusion is supported by the observations of the writers for the Montana deposits. Anderson (1958, 1960) believes that RE, Ba, Nb, Ti and other substances were introduced by fluids from a deep, probably magmatic, source and that these fluids entered the rocks not long after metamorphism to deposit their minerals along structurally favorable channelways.

Similar Deposits

The mineralogy and composition of these deposits are totally unlike those of most other types of metalliferous veins that have predominantly carbonate gangues. However, a few other occurrences have been described to which the Montana-Idaho deposits show similarities. Pecora (1942, 1948; Pecora and Kerr, 1953) has described deposits in the Bearpaw Mountains of Montana which are calcitic veins also containing essential sanidine, biotite, aegirine, pyrite and pyrrhotite in varying abundance, with lesser amounts of other sulfides (chalcopyrite, galena, tetrahedrite), ilmenite, barite, pyrochlore, and rare-earth carbonate minerals (ancylite, lanthanite, burbankite and calkinsite). The deposits are crudely zoned, 1–8 inches thick, cutting shonkinite, mafic monzonite, and syenite of the Bearpaw Mountains alkalic complex.

In the Salmon Bay area of Prince of Wales Island, southern Alaska, rare-earth carbonate veins cut graywacke (Houston *et al.*, 1958). The chief minerals are ankerite, ferroan dolomite and dolomite, with appreciable amounts of alkali feldspar, hematite, pyrite, and locally siderite and magnetite. Small amounts of the following also have been identified (in decreasing order of abundance): quartz, chlorite, calcite, parisite, bastnaesite, muscovite, fluorite, apatite, thorite, zircon, monazite, epidote, topaz, garnet, chalcopyrite, and marcasite. Niobium minerals are apparently absent. The veins appear to be related genetically to lamprophyre dikes which " . . . may be associated with alkalic rocks which have not yet been exposed by erosion." (Houston *et al.*, 1958, p. 21.)

Zoned phosphatic veins occur 35 miles northeast of Uranium City,

Saskatchewan, cutting chiefly quartz-feldspar gneisses (Hogarth, 1957). Marginal amphibole-rich zones (hornblende, diopside, sphene, biotite, and allanite) are succeeded by phosphatic zones (cerian and yttrian apatite with inclusions of monazite, uranothorite and allanite), with central units that are feldspathic (chiefly hyalophane) and carbonatic (chiefly calcite, quartz and barite). Lamprophyres occur on the flanks of the area; syenite and a barium-rich syenitic gneiss also are present.

Also similar in many respects to the Montana-Idaho veins are the carbonate-rich veins and mineralized zones adjacent to and genetically related to the Iron Hill, Gunnison County, Colorado, alkalic intrusive complex, in which carbonatite body occurs (Olson and Wallace, 1956). These Th-RE veins contain rhombohedral carbonates (calcite, dolomite, ankerite, siderite), minor sulfides (pyrite, sphalerite, chalcopyrite, galena), barite, phosphates (monazite, xenotime, apatite), fluorite, quartz, alkali feldspars, phlogopite, sodic amphiboles, thorite, bastnaesite, cerite (?) and synchisite (?).

Age

Age determinations have been made on three monazites from the Idaho deposits (Jaffe *et al.*, 1959, pp. 96–97). The lead-alpha ages are 99, 95, and 90 (mean 95) m.y. The mean age of rocks from the main mass of the Idaho batholith has been determined as 108 ± 12 m.y. by Larsen *et al.* (1958), who conclude that the batholith was emplaced within a short time, not over a few million years, in early Late Cretaceous. Anderson (1958, p. 32) suggests that the mineralizing fluids came " . . . from some deep, probably magmatic, source, possibly the root region of the Idaho batholith." The age difference between the monazite mineralization and the Idaho batholith rocks appears to be too great to support the idea that the solutions were derivatives of the batholith. Geochemical considerations further hamper linkage of the two: the batholith being of calc-alkalic character, whereas the deposits are alkalic in nature.

Conclusions

The Montana-Idaho RE-Nb deposits are primarily of metasomatic origin. They grade in structure, texture, mineralogy and chemical composition from nearly undisturbed phosphatic dolomitic marbles through recrystallized and reconstituted marbles to typical veins formed by combined replacement and fracture filling. Even the carbonate layers of the Upper Beaver Creek deposits, which most closely resemble marbles in structure, and mineralogy, contain abnormal Sr concentrations and small amounts of monazite. Crowley (1960, p. 42) also distinguishes two types of carbonate bodies: mineralized and unmineralized ("blue marble").

In addition to the textural evidence, other factors supporting the thesis that the deposits are epigenetic are: 1) Some are slightly discordant to the metamorphic foliation and some have apophyses that transect the foliation. 2) The deposits are usually enclosed in selvages of altered wall rocks, and in a general way the intensity of this alteration appears to be more pronounced around the thicker, more persistent veins. A few even contain what are apparently altered wall rock inclusions. 3) The deposits are characterized by assemblages and concentrations of elements that are anomalous to dolomites, limestones and their metamorphosed equivalents. 4) The monazite, at least, is much younger than the wall rocks of the carbonate deposits. Furthermore, in Idaho, the host rocks are probably of Beltian age, whereas those in Montana may be pre-Beltian.

The writers believe that the deposits were formed by hydrothermal solutions that may well have been derivatives of an alkalic subsilicic magma. Although rocks of this character are not known in the vicinity of the deposits, a small peridotite-syenite complex occurs to the north, east of Hamilton (Heinrich, 1948), and the region as a whole contains other deposits suggesting the imprint of alkalic mineralization (*e.g.*, barite veins in Missoula County to the north and thorite-rare earth veins at Lemhi Pass to the south).

The chief extrinsic elements supplied by the solutions were Sr, Ba, RE, Nb, and S, and minor K, Cu, Mo, Th. Largely available to the solutions from the marbles or the adjacent gneisses were Ca, Mg, Fe, Al, Si, PO_4, and CO_3.

Anderson (1958, p. 24) has aptly stated that "The deposits possess all the compositional characteristics of . . . carbonatites, differing from the type only in the apparent absence of usually associated alkaline rocks," and he further (p. 32) characterizes " . . . the deposits as hypothermal, occurring as hypothermal replacements in carbonate and other rocks. They should, perhaps, be classed as carbonatite veins and lodes."

The writers conclude that the deposits are alkalic-type hydrothermal lodes and veins generally developed in compositionally favorable layers of marble. The presence of such species as columbite, eschynite, rutile, allanite, and actinolite certainly suggests that at the beginning of their formation temperatures were high, probably, as Anderson believes, within the hypothermal range. Terminal stages, characterized by chlorite, fine-grained quartz, ancylite, and ordinary calcite, were marked by much lower temperatures.

References

Abbott, Agatin T. (1954), Monazite deposits in calcareous rocks, northern Lemhi County, Idaho. *Idaho Bur. Mines Geol. Pamph.* **99.**

Anderson, Alfred L. (1958), Uranium, thorium, columbium, and rare earth deposits in the Salmon region, Lemhi County, Idaho. *Idaho Bur. Mines Geol. Pamph.* **115.**

——— (1960) Genetic aspects of the monazite and columbium-bearing rutile deposits in northern Lemhi County, Idaho. *Econ. Geol.*, **55,** 1179–1201.

CROWLEY, FRANCIS A. (1958), Niobium-rare earth deposits in southern Ravalli County, Montana. *Mont. School Mines MS Thesis.*

——— (1960) Columbium-rare-earth deposits, southern Ravalli County, Montana. *Mont. Bur. Mines, Geol., Bull.* **18.**

GERASIMOVSKII, V. I., AND V. I. LEBEDEV (1958), Proportions of strontium and calcium in rocks of the Lovozero massif. *Geochemistry* 1958, 699–705.

GUNDLACH, HEINRICH (1959) Untersuchungen zur Geochemie des Strontiums auf hydrothermalen Lagerstätten. *Geol. Jahrb.* **76,** 637–712.

HEINRICH, E. WM. (1948), Pegmatite mineral deposits in Montana. *Mont. Bur. Mines Geol. Mem.* **28.**

——— (1953), Pre-Beltian geologic history of Montana (abs.). *Bull. Geol. Soc. Am.*, **64,** 1432.

——— (1958), Mineralogy and Geology of Radioactive Raw Materials. McGraw-Hill Book Company, Inc., New York.

———, A. A. LEVINSON, J. M. AXELROD, AND CHARLES MILTON (1958), Niobium-titanium-rare earth minerals of Ravalli County, Montana, and Lemhi County, Idaho (abs.). *Bull. Geol. Soc. Am.*, **69,** 1580–1581.

HESS, H. D., AND H. J. TRUMPOUR (1959), Second occurrence of fersmite. *Am. Mineral.*, **44,** 1–8.

HOGARTH, D. D. (1957), The apatite-bearing veins of Nisikkatch Lake, Saskatchewan. *Can. Mineral.*, **6,** 140–150.

HOUSTON, J. R., R. G. GATES, R. S. VELIKANJE, AND HELMUTH WEDOW, JR. (1958), Reconnaissance for radioactive deposits in southeastern Alaska, 1952. *U. S. Geol. Surv. Bull.* **1058-A.**

JAFFE, H. W., DAVID GOTTFRIED, C. L. WARING, AND H. W. WORTHING (1959), Lead-alpha age determinations of accessory minerals of igneous rocks (1953–1957). *U. S. Geol. Surv. Bull.* **1097-B.**

JAMES, T. C., AND DUNCAN MCKIE (1958), The alteration of pyrochlore to columbite in carbonatites in Tanganyika. *Mineral. Mag.*, **31,** 889–900.

KAISER, E. P. (1956), Preliminary report on the geology and deposits of monazite, thorite, and niobium-bearing rutile of the Mineral Hill district, Lemhi County, Idaho, *U. S. Geol. Surv. Open File Report.*

LARSEN, E. S., JR., DAVID GOTTFRIED, H. W. JAFFE, AND C. L. WARING (1958), Lead-alpha ages of the Mesozoic batholiths of western North America. *U. S. Geol. Surv. Bull.* **1070-B.**

OLSON, J. C., AND S. R. WALLACE (1956), Thorium and rare-earth minerals in Powderhorn district, Gunnison County, Colorado, *U. S. Geol. Surv. Bull.* **1027-0.**

PALACHE, CHARLES, HARRY BERMAN, AND CLIFFORD FRONDEL (1951), The System of Mineralogy, Vol. II. John Wiley and Sons, New York.

PAVLENKO, A. S., E. E. VAINSHTEIN, AND M. M. KAKHANA (1958), On Nb/Ta ratios in some minerals from igneous and metasomatic rocks. *Geochemistry*, 1958, 706–720.

PECORA, W. T. (1942) Nepheline syenite pegmatites. Rocky Boy stock, Bearpaw Mountains, Montana. *Am. Mineral.*, **27,** 397–424.

——— (1948), Telescoped, xenothermal mineral association in alkalic pegmatites and related veins, Vermiculite prospect, Bearpaw Mountains, Montana (abs.). *Am. Mineral.*, **33,** 205–206.

——— AND JOE H. KERR (1953), Burbankite and calkinsite, two new carbonate minerals from Montana. *Am. Mineral.*, **38,** 1169–1183.

PENFIELD, S. L., AND C. H. WARREN (1899), On the chemical composition of parisite and a new occurrence of it in Ravalli County, Montana. *Am. Jour. Sci.*, **VIII,** 21–24.

ROSS, CLYDE P., DAVID A. ANDREWS, AND IRVING J. WITKIND (1955), Geologic Map of Montana, U. S. Geol. Surv.

SAHINEN, UUNO M. (1957), Mines and mineral deposits of Missoula and Ravalli counties, Montana. *Mont. Bur. Mines Geol., Bull.* **8.**

TERADA, JITSUO (1952), Rhombohedral crystals of Ba-Ca and Sr-Ca double carbonates. *Jour. Phys. Soc. Japan*, **7,** 432–434.

TUREKIAN, KARL K., AND J. L. KULP (1956), The geochemistry of strontium. *Geochim. Cosmochim. Acta*, **10,** 245–296.

VON KNORRING, OLEG (1951) A note on the occurrence of columbite in the Meldon aplite, Devonshire. *Mineral. Mag.*, **29,** 799–801.

Manuscript received February 1, 1961.

THE AMERICAN MINERALOGIST, VOL. 46, NOVEMBER-DECEMBER, 1961

ARSENOPYRITE CRYSTAL-CHEMICAL RELATIONS

NOBUO MORIMOTO* AND LLOYD A. CLARK,† *Geophysical Laboratory, Carnegie Institution of Washington, Washington, D. C.*

ABSTRACT

The composition of naturally occurring arsenopyrite varies from about $FeAs_{0.9}S_{1.1}$ to $FeAs_{1.1}S_{0.9}$, as indicated by the more credible published chemical analyses and one new analysis. Analytical errors probably account for any apparent deviations of the Fe:(As+S) ratio from 1:2.

Five arsenopyrites of different compositions were studied by single-crystal *x*-ray methods. The changes caused by increasing arsenic content are (1) the triclinic symmetry approaches monoclinic, and (2) metrically the cell approaches the orthorhombic. These pseudosymmetries give rise to two types of twinning. Although refinements of the arsenopyrite crystal structure by means of (*h*0*l*) and (*hk*0) data were hampered by twinning, the atomic coordinates obtained in this investigation confirm those of Buerger (1936). The interatomic distances Fe-As, Fe-S, and As-S are 2.35, 2.25, and 2.33 Å, respectively.

Indexed *x*-ray powder data are given. The metrically monoclinic cell constants for six analyzed arsenopyrites relate linearly to arsenic content and inversely to sulfur content. Provided the combined minor element content is below 1%, the curve $d_{131}=1.6106+0.00098x$, where x is the arsenopyrite arsenic content in atomic per cent, enables rapid determination of arsenopyrite compositions to within 1 atomic per cent.

INTRODUCTION

Although arsenopyrite is relatively common in ore deposits, it has not received the careful attention often given to less common and economically less important minerals. A recent investigation of the phase relations in the Fe-As-S system (Clark, 1960) demonstrated that certain physical factors control the variation in composition of synthetic arsenopyrite. This warranted an examination of the compositional variations in naturally occurring arsenopyrite and a search for quantitative relations between composition and crystallographic properties.

Buerger's (1936, 1939) single-crystal *x*-ray investigations made a significant contribution to our knowledge of arsenopyrite symmetry and crystal structure. His work was hampered, however, by the use of twinned crystals, and the structure was finally derived by analogy with related structures. The importance of the mineral warranted a search for untwinned crystals, re-examination of the symmetry, and refinement of the structure.

Previously published *x*-ray powder diffraction data are entirely inadequate to explain the complexities in the powder pattern of arsenopyrite,

* Present address: Mineralogical Institute, Tokyo University, Tokyo, Japan.

† Present address: Department of Geological Sciences, McGill University, Montreal, Canada.

and the available cell is of the wrong geometry for satisfactory indices to be calculated.

The present work on arsenopyrite symmetry, twinning, and crystal structure is the principal responsibility of Morimoto. For the most part Clark developed the discussions on arsenopyrite composition, indexing of *x*-ray powder data, and the composition-cell constant relation.

Previous Work

Arsenopyrite cell and symmetry

The arsenopyrite cell was first determined by de Jong (1926) using the powder and rotation methods on arsenopyrite from Sulitjelma, Norway, which contained almost 7% cobalt. The orthorhombic crystallographic data were $a=6.45$, $b=9.54$, $c=5.53$ Å (from kX) and $Z=8$; the specific gravity was 6.28. The space group, determined from the indices of 1/ powder reflections, was *Pmmm* or *Pmmn*.

Buerger (1936) studied arsenopyrite from Franklin, N. J., by the rotation and oscillation methods. The symmetry was orthorhombic with cell dimensions: $a=6.43$, $b=9.57$, and $c=5.72$ Å (from kX). In addition Buerger investigated arsenopyrite from the St. Peter Mine, Spindelmühle, Bohemia, by the Weissenberg method. Again the symmetry was orthorhombic, with cell dimensions of $a=6.43$, $b=9.53$, and $c=5.66$ Å (from kX). In both cases the possible space groups were *Cmmm*, *Cmm*2, and *C*222. Attempts to determine the arsenopyrite crystal structure on the basis of orthorhombic symmetry failed, and Buerger concluded that the symmetry was ideally monoclinic and commonly triclinic. By merely interchanging the axes mentioned above (we call it the first setting) by the transformation 001/100/010, Buerger adopted a conventional orientation of a monoclinic crystal (we call it the second setting). Thus, the respective space groups were $B2_1/d$ and $B\bar{1}$. Using the data obtained from twinned crystals, he determined the structure, by the trial and error method, as a derivative structure of marcasite, on the basis of space group $B2_1/d$. He attributed the deviation from monoclinic symmetry in "common" arsenopyrite to variations from the ideal chemical formula (FeAsS).

Huggins (1937) criticized the structures of marcasite and arsenopyrite, as determined by Buerger (1931, 1936), on the grounds that the structure led to interatomic distances not in harmony with those calculated from electron-pair bond radius sums. Buerger (1937) refined the structure of marcasite and confirmed its abnormal interatomic distances. For arsenopyrite, refinements were hampered by the difficulty of obtaining untwinned crystals; nevertheless, Buerger (1939) was able to suggest qualitative corrections to his published arsenopyrite parameters on the basis

of the crystal structure of gudmundite (FeSbS) and confirmed that the interatomic distances in the arsenopyrite group are quite different from those derived from pyrite group minerals.

Incomplete powder patterns for natural arsenopyrite were published by de Jong (1926), Harcourt (1942), and Van Tassel (1954). Only de Jong's pattern was indexed, and that was on the basis of an orthorhombic cell.

Compositional variation of synthetic arsenopyrite

The report of an earlier investigation (Clark, 1960) includes a résumé of previous experimental works pertinent to arsenopyrite, most of which were thermal decomposition studies. Clark found that the composition of arsenopyrite synthesized in sealed, evacuated tubes in the presence of equilibrium vapors varied as a function of temperature and that no one composition was stable throughout the temperature range of arsenopyrite stability. Arsenopyrites synthesized in the 630° to 660° C. range had the approximate composition $FeAs_{1.1}S_{0.9}$, whereas arsenopyrites richer in arsenic became stable at temperatures up to 702° ± 3° C., the invariant temperature for the incongruent breakdown of arsenopyrite. Arsenopyrites richer in sulfur than is indicated by the theoretical composition FeAsS became stable only at temperatures below 450° to 500° C. The majority of natural arsenopyrites, as represented by published chemical analyses, lie in this sulfur-rich lower temperature range. Preliminary tests indicated that the composition and temperature limits of the sulfur-rich arsenopyrites were considerably extended by confining pressures of 2000 bars.

With various experiments Clark demonstrated that arsenopyrite, either natural or synthetic, would not equilibrate to new physical and chemical conditions even after months of heating at near-melting temperatures. Differences in the free energies of formation of arsenopyrites of different composition are very small.

Since arsenopyrites are frequently, perhaps universally, twinned, Clark explored for high-temperature crystallographic transitions, using differential thermal analysis with the samples in sealed, evacuated glass tubes. Neither natural nor synthetic arsenopyrite showed evidence of any transition from room temperature to 630° C.

Indexing of Powder Patterns

The powder diffraction patterns of some natural arsenopyrites show doubling of some of the major reflections, and the patterns are more complex in general than the published data would indicate (see, for example, pattern *a* in Fig. 1). The reflections cannot be indexed on the basis of an orthorhombic cell.

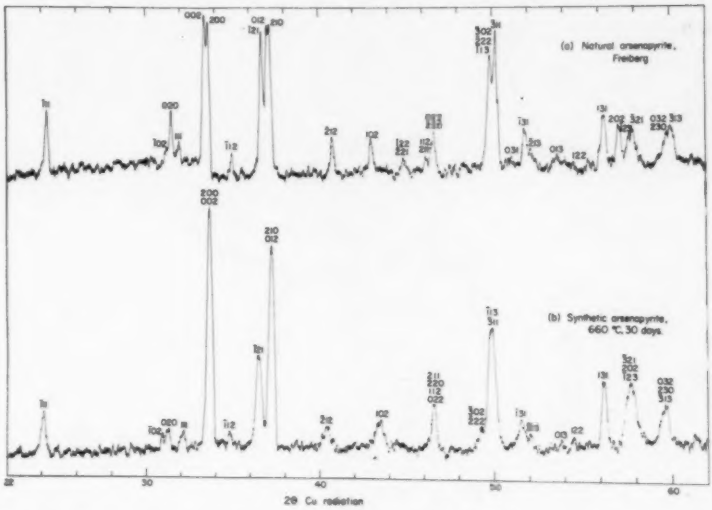

FIG. 1. Powder diffraction patterns of natural and synthetic arsenopyrites. They were obtained from smear-type mounts on a Norelco diffractometer with goniometer speed of one-half degree/minute. The intensity scale is linear.

A primitive monoclinic cell (we call it the third setting), derived from Buerger's (1936) double monoclinic, but metrically orthorhombic cell (the second setting) by transformation $\frac{1}{2}0\frac{1}{2}/0\bar{1}0/\frac{1}{2}0\frac{1}{2}$, was employed as a first approximation in indexing the powder pattern.* The cell values were $a=c=5.76$, $b=5.66$ Å (from kX), $\beta=111°\ 47'$, with space group $P2_1/c$. Using arsenopyrite from Freiberg, Germany (Smithsonian Institution No. 103651), new primitive monoclinic cell dimensions were calculated from eight sets of measurements on the reflections $\bar{1}11$, 020, and the doublet 002,200. The improved cell values then facilitated revision of the initial indexing for the reflections that occur between 40° and 60° 2θ (Cu radiation).

The powder diffraction patterns of all synthetic arsenopyrites are very similar. A typical one for arsenopyrite with a composition near $FeAs_{1.1}S_{0.9}$ is shown in Fig. 1*b*. The principal differences from the natural arsenopyrite pattern (Fig. 1*a*) are that the major peaks show no tendency to split and that the 202 reflection, which is isolated in natural arsenopyrite patterns, joins with the $\bar{3}21$ and $\bar{1}23$ reflections to form a single broad peak in synthetic arsenopyrite patterns. There are more subtle changes in the interplanar spacings of most of the other reflections. The pattern for

* All crystallographic data and indices in the present paper are based on a primitive monoclinic cell (the third setting) unless otherwise indicated.

synthetic material could probably be indexed on a pseudo-orthorhombic cell, but the indexing based upon a primitive monoclinic cell is retained for ease of comparison. The variations in the powder patterns of natural and synthetic arsenopyrites are due to variations in the cell constants, which reflect compositional differences.

The arsenopyrite *x*-ray powder data are given in Table 1. The data for the Freiberg arsenopyrite are rather typical of natural arsenopyrites found in coexistence with pyrite or other sulfides from a sulfur-rich deposition environment. The synthetic arsenopyrite data more closely represent natural arsenopyrites grown in association with arsenide minerals such as loellingite ($FeAs_2$). There are all variations between, and slightly beyond, the limits of these sets of data. The observed spacings and intensities are averaged from two diffractometer patterns standardized with CaF_2. The values shown to five significant figures were determined more carefully for use in the least-squares calculation of the cell constants, which is discussed later. The cell constants for the Freiberg arsenopyrite are: $a=5.744\pm0.002$, $b=5.675\pm0.001$, $c=5.785\pm0.002$ Å, and $\beta=112.17°\pm0.02°$. Those for synthetic arsenopyrite are: $a=5.828\pm0.002$, $b=5.720\pm0.001$, $c=5.792\pm0.002$ Å, and $\beta=113.20°\pm0.02°$. The calculated spacings are based on these cells. Even excluding the absent reflections in space group $P2_1/c$, there are twice as many calculated reflections as are shown in Table 1. Using Weissenberg photographs of Freiberg arsenopyrite crystals, we were able to eliminate approximately 50% of the calculated reflections as being too weak to appear in a powder diffractometer pattern. For example, some of the higher angle peaks (Fig. 1) are assigned to three reflections. It was possible to omit as many as three other reflections because they made no significant contribution to the observed peak. Powder-camera films show, at *d* values below 1.5, five weak and several very weak reflections, which were not observed with the diffractometer, but show no additional reflections at higher *d* values.

Composition of Natural Arsenopyrite

Sixteen published analyses, only two of which antedate 1928, are compiled in Table 2 to demonstrate the compositional variations of natural arsenopyrites. Analyses containing a few per cent cobalt, along with those which obviously have been performed on impure material, are not included. The sample location, the reference, the analyst, and, when available, pertinent information such as associated minerals and methods of purification and analysis, are listed.

It was hoped to supplement analysis No. 1, which represents carefully purified material from a sulfur-rich environment of deposition, with an

TABLE 1. *X*-RAY POWDER DATA FOR NATURAL ARSENOPYRITE FROM FREIBERG, GERMANY, AND SYNTHETIC ARSENOPYRITE GROWN IN COEXISTENCE WITH ARSENIC AND A SULFUR-ARSENIC LIQUID AT 660° C.

CuKα radiation, $\lambda = 1.5418$ Å, Ni filter, Norelco diffractometer. Intensities taken proportional to the peak heights.

Freiberg arsenopyrite				Synthetic arsenopyrite			
hkl	*d* (obs.)	*d* (calc.)	I	*hkl*	*d* (obs.)	*d* (calc.)	I
$\bar{1}11$	3.6581*	3.6576	40	$\bar{1}11$	3.6970*	3.6994	20
$\bar{1}02$	2.866	2.866	5	$\bar{1}02$	2.890	2.878	5
020	2.8382	2.8377	30	020	2.8632	2.8601	10
111	2.7963	2.7979	10	111	2.800	2.792	5
002	2.677	2.678	100	200	2.665	2.678	100
200	2.662	2.660	100	002		2.662	
$\bar{1}12$	2.557	2.558	10	$\bar{1}12$	2.561	2.571	5
$\bar{1}21$	2.4402	2.4405	90	$\bar{1}21$	2.4645	2.4637	40
012	2.418	2.422	95	210	2.415	2.426	90
210	2.412	2.408	95	012		2.413	
$\bar{2}12$	2.2041	2.2040	25	$\bar{2}12$	2.2330	2.2328	10
102	2.0955	2.0955	20	102	2.0797	2.0797	10
$\bar{1}22$	2.017	2.016	5	221	2.022	2.034	5
221		2.010		$\bar{1}22$		2.029	
112	1.961	1.966	5	211		1.959	
211		1.960		220	1.947	1.955	20
022	1.943	1.948	25	112		1.954	
220		1.941		022		1.949	
$\bar{3}02$	1.824	1.830	70	$\bar{3}02$	1.846	1.860	10
$\bar{2}22$		1.829		$\bar{2}22$		1.850	
$\bar{1}13$		1.824		$\bar{3}11$	1.824	1.836	50
$\bar{3}11$	1.814	1.812	90	$\bar{1}13$		1.826	
031	1.787	1.784	5	031		1.795	
$\bar{1}31$	1.7591	1.7592	20	$\bar{1}31$	1.7741	1.7745	10
$\bar{2}13$	1.750	1.748	5	$\bar{2}13$	1.758	1.763	5
013	1.703	1.703	5	013		1.695	
131	1.6307	1.6306	30	131	1.6378	1.6378	25
202	1.6080	1.6080	25	$\bar{3}21$	1.597	1.605	25
$\bar{1}23$	1.594	1.594	15	202		1.599	
$\bar{3}21$	1.589	1.586	20	$\bar{1}23$		1.598	
032	1.543	1.545	20	$\bar{3}13$	1.555	1.556	15
230		1.542		230		1.553	
$\bar{3}13$	1.537	1.535	20	032		1.550	
$\bar{3}23$	1.390	1.390	5	$\bar{3}23$		1.407	
$\bar{1}14$		1.389		$\bar{2}14$		1.396	
$\bar{2}14$		1.389		$\bar{1}14$		1.388	
123		1.345		$\bar{3}21$	1.339	1.343	15
$\bar{3}21$	1.343	1.340	15	123		1.339	
004		1.339		004		1.331	

* Observed *d* values used in the least-squares calculation of cell constants are shown to four decimal places.

TABLE 2. RECENT ANALYSES OF ARSENOPYRITE IN WEIGHT PER CENT

	FeAsS	1	2	3	4	5	6	7	8	9	10	11	12	13	14	15	16
Fe	34.30	34.34	34.40	33.84	34.13	34.09	34.30	33.72	34.41	34.18	35.23	33.01	35.63	33.91	33.13	34.53	32.48
Co		0.00	<0.1	~0.3	~0.4	—	—	—	0.07	0.43	—	—	—	trace	—	0.09	1.16
Ni		0.00	~0.03	~0.1	~0.03	—	—	—	nil	0.05	—	—	—	—	—	—	—
Mn		—	≪0.03	<0.03	≪0.03	0.004	—	—	—	—	trace	—	—	trace	—	—	—
As	46.01	44.33	43.82	44.45	44.00	43.82	43.64	46.52	42.28	42.37	41.77	49.91	43.03	45.10	45.83	44.34	48.72
Bi		0.00	—	—	—	—	—	—	0.03	—	—	—	—	—	—	0.79	—
Sb		—	—	—	—	—	—	1.44	0.18	trace	0.32	—	—	—	—	—	—
S	19.69	20.89	19.86	19.91	20.20	20.95	21.25	18.09	21.43	21.93	22.59	16.27	21.30	20.77	20.43	20.22	18.80
Cu		0.15	—	—	—	—	—	—	0.04	0.78	0.15	trace	—	—	—	—	—
Pb		—	—	—	—	—	—	—	0.22	0.24	trace	—	trace	—	—	—	—
Zn		—	—	—	—	—	—	—	—	—	0.32	—	trace	—	—	—	—
Insoluble		0.00	—	—	—	0.87	—	—	1.06	0.55	0.08	0.23	0.42	—	0.50	—	?
Total	100.00	99.71	98.16	98.62	98.76	99.73	99.19	99.77	99.79*	100.53	100.46	99.42	100.38	99.78	99.89	99.97	101.16
S.G.	6.18	6.08				6.088			5.903				5.67	6.01			6.199

ANALYSES RECALCULATED TO 100% SUBTRACTING: INSOLUBLE, Cu AS $CuFeS_2$, Pb AS PbS, AND Zn AS (Zn, Fe)S CONTAINING 7.5% Fe

	FeAsS	1	2	3	4	5	6	7	8	9	10	11	12	13	14	15	16
Fe	34.30	34.46	35.04	34.32	34.56	34.48	34.58	33.80	35.02†	34.38	35.27	33.28	35.64	33.98	33.33	34.54	32.11
Co		0.00	<0.1	~0.3	~0.4	—	—	—	0.07	0.44	—	—	—	trace	—	0.09	1.15
Ni		0.00	~0.03	~0.1	~0.03	—	—	—	nil	0.05	—	—	—	—	—	—	—
Mn		—	≪0.03	<0.03	≪0.03	0.004	—	—	—	—	trace	—	—	trace	—	—	—
As	46.01	44.65	44.64	45.07	44.55	44.32	44.00	46.63	43.02	43.48	42.02	50.32	43.05	45.20	46.11	44.35	48.16
Bi		0.00	—	—	—	—	—	—	0.03	—	—	—	—	—	—	0.79	—
Sb		—	—	—	—	—	—	1.44	0.06	trace	0.32	—	—	—	—	—	—
S	19.69	20.89	20.23	20.19	20.46	21.19	21.42	18.13	21.73	21.65	22.39	16.40	21.31	20.82	20.56	20.23	18.58
									Se=0.07								

* Includes 0.07% Se.

† In analysis 8 the Pb and Cu were subtracted as a mixture of sulfosalts with an estimated average composition of Pb=47, Sb=26, Cu=9, and S=18%.

Localities of Analyzed Arsenopyrites

1. Freiberg, Germany. (Smithsonian Institution, Washington, D. C., specimen No. 103651.) Clark, 1960. Asp* associated with py, cp, sp, and gn. Analysis performed by H. B. Wiik and P. Väänänen on >1.5 g of hand-picked material. S.G. is the mean of three measurements (6.13, 6.04, and 6.08) with a Berman balance.

2, 3, and 4. Brabant, Belgium. Van Tassel, 1954. Small asp crystals embedded in qtz veins in Cambrian phyllites. Some insoluble material was observed but was not recorded in per cent. It is supposed that inclusion of these insoluble fractions would bring the analysis totals nearer to 100%.

5. Nodatamagawa Mine, Iwate Prefecture, Japan. Kitahara, 1952. Prismatic crystals of arsenopyrite, together with qtz, filling fissure veins in country rock. Deposition presumably preceded the Mn, Fe, Pb, and Zn mineralizations. S.G. of 6.088 was calculated from the measured value of 6.008 by subtracting qtz.

6. Iname Mine, Aichi Prefecture, Japan. Yoshino, 1951. The mineral associations were not recorded. This analysis was performed by conventional means (As separated from Fe with H_2S and determined by Volhard's method, Fe with $KMnO_4$, and S as $BaSO_4$) to check a new method of As determination using ion-exchange resin. The new technique gave similar results: Fe=34.13, As=43.89, S=21.11.

7. Varuträsk pegmatite, Sweden. Ödman, 1942. Analysis by Th. Berggren. Asp found in rock which may have been xenolith of amphibolite. Asp was microscopically homogeneous and no Sb mineral was observed.

8. Boliden Mine, Sweden. Ödman, 1941. Analysis by Th. Berggren. Asp in stubby, euhedral crystals up to 1 cm. These are cut by late veinlets, mostly of microscopic width containing a variety of Pb-Sb sulfosalts which probably account for most of the Pb and Sb in the analysis. There are many late minerals but py and cobaltite are the principal early associates of asp.

9. Felsöszalánk, com. Szepes, Hungary. Tokody, 1936. Analysis by G. Vavrinecz. Asp associated with tetrahedrite, cp, and qtz.

10. Kap-san, Kankyônandô, Korea. Tsurumi, 1934. Asp in 2–3 cm prismatic crystals cut by veinlets of cp. Asp crushed to ~1 mm grains and hand picked. Tsurumi attributed the Cu in the analysis to cp. He stated that the method of As determination was not very good; this analysis was performed on the condensed vapor from asp heated at 700° C.

11. Ashio Mine, Totigi Prefecture, Japan. Okada, 1933. Asp associated with py, ms, cp, sp, and qtz. Okada indicated that the asp was difficult to purify—he hand picked asp with the aid of a microscope. He used Stokes' method for S and determined As as As_2S_2 which he believed gave a high value. Spectrographic analysis showed little other than Fe, As, and S.

12. Nogarè, Trentino, Italy. Andreatta, 1928*b*. Stubby asp crystals in veins with py, gn, sp, and qtz. The low S.G. is due to some siliceous impurities.

13. Calceranica, Trentino, Italy. Andreatta, 1928*a*. Asp in prismatic crystals from microscopic size up to 3 cm., which occur in talc mica schist adjoining mined pyrite vein.

14. Ronchi near Caldonazzo, Trentino, Italy. Andreatta, 1928*a*. Asp in crystalline masses with qtz in sericite and chlorite schists. Limonite prevalent and occasional pockets of py and sulfosalts.

15. O'Brien Mine, Cobalt, Ontario. Ellsworth, 1916. Asp as basal plates up to 2.5 mm in calcite and attached to arsenide masses. Both As and S were determined by fusion followed by titration of Ag_3AsO_4 or precipitation as $BaSO_4$.

16. Franklin Iron Company quarry, Franklin, New Jersey. Palache, 1910, 1935. Analysis by E. C. Sullivan. Asp crystals up to 1 inch long in limestone associated with py, po, spinel, humite, tourmaline, and phlogopite. The analysis was performed on 0.25 g. of material, and Sullivan noted that the As determination was probably too high and that silica and organic matter were also present.

* Abbreviations of mineral names are in accordance with Chace (1956).

* Includes 0.07% Se.
† In analysis 8 the Pb and Cu were subtracted as a mixture of sulfosalts with an estimated average comp

analysis of material from an arsenic-rich environment. Unfortunately, loellingite ($FeAs_2$) cannot be completely separated from arsenopyrite because they have very similar physical properties. The efficiency of a separation is difficult to estimate because the two minerals are almost indistinguishable optically, especially when the loellingite contains more than 1% sulfur in solid solution. Arsenopyrite coexisting with native arsenic is rare, and such material was unavailable. The only practical alternative was to use arsenopyrite that was not associated with either arsenide or sulfide minerals.

A specimen from Llallagua, Bolivia, obtained through the Smithsonian Institution (No. R-8069), contained stubby arsenopyrite crystals up to $\frac{1}{4}$ inch long occurring with minor amounts of quartz in what may have been a vug filling. One of the larger arsenopyrite crystals was fragmented and, upon microscopic examination of polished surfaces, was found to be completely homogeneous and free from other phases. After 90 seconds of etching with saturated $FeCl_3$ solution, no loellingite was detected. This material was chemically analyzed for Fe, Co, Ni, As, Bi, S, and Cu by Drs. H. B. Wiik and P. Väänänen, Helsinki, Finland. The results are given in Table 3.

To gain a visual comparison of the compositional variations recorded in Tables 2 and 3 the data have been plotted, in Fig. 2, on the expanded central portion of the Fe-As-S system. In plotting Fig. 2, Co, Ni, and Mn were included with Fe; Bi and Sb with As; and Se with S.

TABLE 3. ANALYSIS OF ARSENOPYRITE FROM LLALLAGUA, BOLIVIA, IN WEIGHT PER CENT

Element	Content	Recalculated to 100% after subtracting SiO_2
Fe	33.01	33.05
Co	0.58	0.58
Ni	0.21	0.21
As	45.56	45.61
Bi	0.88	0.88
S	19.65	19.67
Cu	<0.01	
Insoluble	0.04	
	99.93	
Specific gravity*	6.11	

* This is the mean of three determinations (6.16, 6.14, and 6.03) made with a Berman density balance.

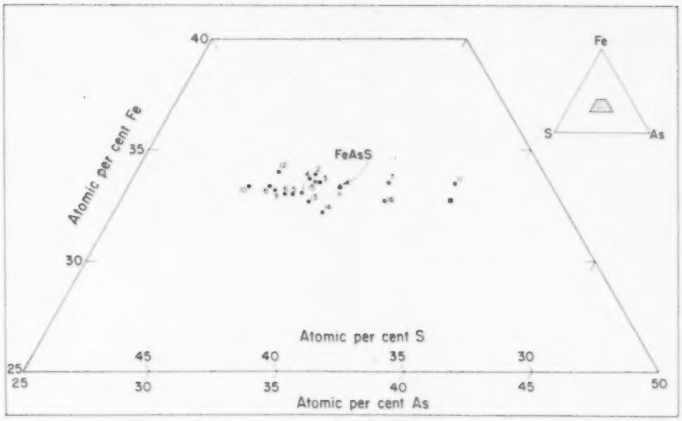

FIG. 2. Compositional variation of arsenopyrite shown on the central portion of the Fe-As-S diagram. The numbers correspond to specimen localities which are listed in the text. The cross represents the composition of arsenopyrite from Llallagua, Bolivia (Table 3); the solid square is an analyzed, synthetic arsenopyrite grown at 660° C.

The Bolivian analysis (shown by cross in Fig. 2) has equal proportions of arsenic and sulfur, as might have been expected from its environment. An arsenopyrite synthesized at 660° C. in the arsenopyrite-arsenic-liquid-vapor region (shown by solid square in Fig. 2) has a relatively high As:S ratio, with 4.64 atomic % more As than has the ideal FeAsS (Clark, 1960, Table 16). Only three of the natural materials have As:S ratios greater than unity, and for at least two of these (Nos. 11 and 16) the analyses are questionable. Arsenopyrite No. 11 occurred in a sulfur-rich environment! The analyst indicated that the sample was difficult to purify, and he believed the analyzed value for As was high. Analysis No. 16 was performed on only 0.25 g of material; this analyst also suspected that the As determination was high.

One analysis on material from Broken Hill, Australia, reported by Ramdohr (1950, p. 313) to be arsenic-rich arsenopyrite, has not been included in this compilation. On Fig. 2 it would fall beyond the limits of the diagram on the upper right-hand side, and on a phase diagram would plot in or near the pyrrhotite-loellingite two-phase region. Clearly, this analysis does not represent an arsenopyrite composition.

The majority of analyses in Fig. 2 are grouped on the high-sulfur side of the ideal FeAsS composition. Again some are more credible than others. With No. 10 the analyst suspected a poor As determination, and one of the older analyses, No. 15, was performed on arsenopyrite from an arsenic-rich environment. It should be noted that the composition of the

Freiberg arsenopyrite (No. 1), in which we have confidence, is 1.61 atomic % richer in sulfur than ideal FeAsS.

It is uncertain whether the variations of iron content, all within about ±0.6 atomic % of the mean value, truly represent different cation:anion ratios or reflect sampling and analytical errors. We believe that the differences represent errors, and that arsenopyrite does not vary measurably from the 1:2::cation:anion ratio* because three analyses by one analyst (Nos. 2, 3, and 4) are all iron rich, and three more by a different analyst (No. 1, cross, and solid square in Fig. 2) are all iron deficient by approximately the same amount. If these are errors they are consistent and may represent built-in biases in the two analytical procedures. (We do not know what procedures were used.) Three analyses (Nos. 12, 13, and 14) were performed by a third analyst and show the maximum and minimum iron contents of all the 18 analyses plotted in Fig. 2. Errors, if present in these last mentioned analyses, are random.

It is noteworthy that about 75% of the analyzed arsenopyrites have compositions richer in sulfur than ideal FeAsS. From experimental findings (Clark, 1960), it is clear that these arsenopyrites could only form at temperatures below 500° C.; however, this limit would be raised to about 650° C. under combined sulfur and arsenic activities equivalent to 2000 bars pressure. Arsenic-rich arsenopyrites could only form above about 300° to 400° C. The uneven distribution of analyses about ideal FeAsS relates principally to the frequence of suitable deposition environments, *i.e.* the predominance of sulfide-type over arsenide-type mineral deposits. Also, arsenopyrite when associated with arsenide minerals is much more difficult (if not impossible) to separate for chemical analysis than when it is associated with sulfides.

Variation of Cell Dimensions and d_{131} with Composition

The composition of arsenopyrite is variable, and since this causes measurable changes in the *x*-ray powder diffraction patterns, it seemed desirable to determine the nature of the change in each of the four cell dimensions with changing composition. Only six chemically analyzed arsenopyrites were available for this part of the investigation; their source, composition, etc., were discussed earlier. These arsenopyrites were from Freiberg, Boliden, Nogaré, Calceranica (Table 2, Nos. 1, 8, 12, and 13), and Llallagua (Table 3), in addition to synthetic arsenopyrite grown at 660° C. in an arsenic-rich environment (Clark; 1960, Table 16).

* Buerger (1936) postulated a small amount of proxy replacement of iron by arsenic in Franklin, N. J., arsenopyrite. This postulation was unwarranted because the cation deficiency is only 0.64 atomic %, and the analysis (No. 16, Table 2) is somewhat unreliable.

Theoretically, measurement of four appropriate reflections on the powder diffraction pattern would be sufficient to yield the four cell constants. However, the arsenopyrite pattern is not characterized by sharp reflections amenable to accurate measurement (see Fig. 1), and most of the strong peaks are due to two or more reflections. Therefore, it was decided to measure all the isolated reflections having reasonable definition and derive the best fitting cell by submitting the data to a least-squares calculation. The reflections measured were: $\bar{1}11$, 020, 111, $\bar{1}21$, $\bar{2}12$, 102, $\bar{1}31$, 131, and 202. (With the synthetic material, 111 and 202 were not measured.) The reflections were each measured in four diffractometer patterns obtained from two separate smear-type mounts with CaF_2 as internal standard ($a=5.4626$ Å, Swanson and Tatge, 1953). The least-squares calculations were performed on the IBM 704 computer at the U. S. National Bureau of Standards, Washington, D. C.

In Fig. 3 the various cell constants are plotted as functions of the sulfur and arsenic contents. The sulfur and arsenic contents are shown to vary inversely. A plot of cell constants versus iron content of arsenopyrite gave a scatter of points. This was not surprising since Fig. 2 indicated very little variation in the iron content of 18 chemically analyzed arsenopyrites. The compositions are grouped in such a way as to place undue reliance upon the points representing the synthetic arsenopyrite; however, this composition is relatively well known. It should be noted that h is equal to l for all the reflections except 102. Therefore, the 102 reflection was the only one that differentiated between a and c. Fortunately, relatively precise measurement of d_{102} was possible. Using the cell constants so obtained, the differences between computed and observed d values were almost always in the fourth decimal place as was shown in Table 1. In Fig. 3 the sizes of the data points are indicative of the precision. Larger errors are indicated for a and c than for b and β. With respect to composition the points were arbitrarily given a width of $\pm 0.1\%$, which was, perhaps, too optimistic. Part of the scatter in the plotted points is due to fractional percentages of elements (other than Fe, As, and S) in solid solution. Through measurement of cell dimensions the composition of an arsenopyrite can be estimated. However, the result may not be reliable if the combined minor-element content exceeds 1 %.

The d_{131} values for the various arsenopyrites are also shown in Fig. 3. In the previous investigation of the Fe-As-S system (Clark, 1960) the 131 interplanar spacing was used as a relative measure of arsenopyrite composition although the exact relationship was not established. This procedure was followed because the 131 spacing could be measured precisely and with relative ease, as compared with the time and labor required to derive the cell constants. Since the iron content never departs greatly

from 33.3 atomic %, the curves shown here relate the 131 spacing quantitatively to the arsenopyrite composition. The sulfur and arsenic contents vary inversely indicating the mutual solid solution of these elements in arsenopyrite. Measurement of d_{131} in a natural arsenopyrite will give the composition within 1%. The expression $d_{131}=1.6106+0.00098x$ relates

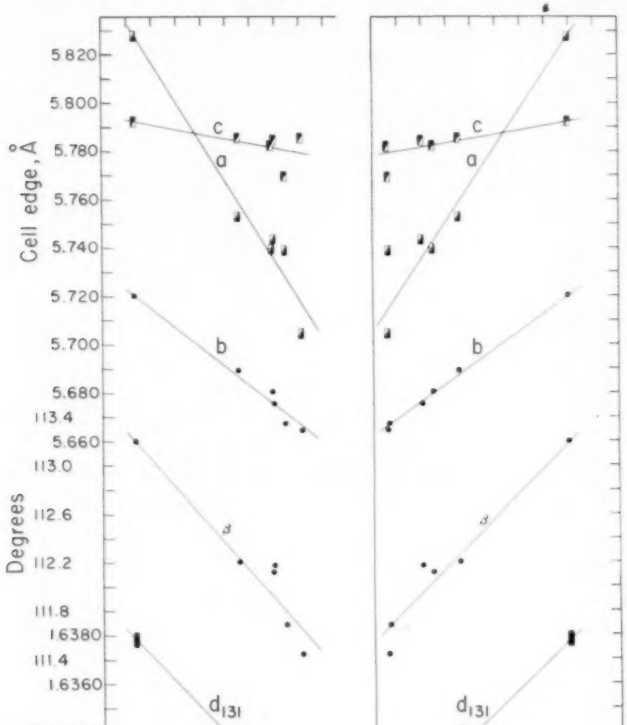

FIG. 3. Variations are shown in the arsenopyrite primitive monoclinic cell dimensions and d_{131} values as functions of sulfur and arsenic content. The sizes of the data points represent the precision in the crystallographic quantities, but with respect to composition the points are arbitrarily estimated at ±0.1%. The arsenopyrite specimens used are: synthetic, Llallagua, Calceranica, Freiberg, Nogaré, and Boliden, in order of increasing sulfur content (decreasing arsenic content).

the arsenopyrite arsenic content (x) in atomic % to the d_{131} value measured in angstroms.

Crystal Structure of Freiberg Arsenopyrite

The Weissenberg photographs of Freiberg arsenopyrite, taken by Mo radiation ($\lambda = 0.71069$ Å), were used for the intensity data. The intensities were estimated visually and were corrected for the polarization and Lorentz factors. No absorption corrections were applied. The intensity data were placed on an absolute scale by comparing them with the calculated values.

Comparison of calculated and observed structure factors confirmed that Buerger's (1936) arsenopyrite structure is fundamentally correct. To explain the appearance of $h0l$ reflections with l odd, in the Freiberg arsenopyrite, on the basis of Buerger's structure, we have to destroy the glide plane c in $P2_1/c$ leaving the possible space groups $P2_1$ and $P\bar{1}$. It will be shown that arsenopyrite has triclinic symmetry; therefore, $P\bar{1}$ remains the only possible space group. Starting from Buerger's (1936) structure and adopting space group $P\bar{1}$, we obtained a structure which gave a residual, $R = \sum \big| |F_o| - |F_c| \big| / \sum |F_o|$, of 0.29 for 172 $h0l$ reflections and 0.20 for 135 $hk0$ reflections after four cycles of least-squares refinement. Using the final coordinates, the signs of $h0l$ and $hk0$ were determined and used in the calculation of electron-density projections on (010) and (001). Figure 4 shows the electron-density map on (010).

Arsenopyrite Symmetry and Twinning

Freiberg arsenopyrite

Crystals of Freiberg arsenopyrite were studied by the oscillation, precession, and Weissenberg methods using Fe, Cu, and Mo radiations. Of the ten specimens examined, all showed splitting of some reflections on the single-crystal photographs. In some instances this was merely a matter of slight randomness of orientation; however, most of the splittings were due to intrinsic properties of the crystals. In order to explain all the splittings, at least two types of twinning are required. The first type, described in detail by Buerger (1936) and referred to here as type-I twinning, has twin plane $(10\bar{1})$ or (101) or has twin axis $[10\bar{1}]$ or [101], respectively. The second type of twinning requires the assumption that arsenopyrite is triclinic; the postulated twin law is twin axis [010], which is equivalent to twin plane (010)*. We designate it type-II twinning. The deviations of α^* and γ^* from 90° are less than 30′ and were not determined more closely.

Thus the Freiberg arsenopyrite has at least two types of twinning.

Type I results from the pseudo-orthorhombic symmetry of the lattice and type II from its pseudomonoclinic symmetry. Since the amount of type-I twinning, or volume ratio of the twin individuals, varies from specimen to specimen, it is supposed that this twinning takes place on a large scale, whereas type-II twinning occurs on a small scale, relative to the size of x-ray "single" crystals ($\sim$0.05 to 0.2 mm.). A photomicrograph, Fig. 5, shows the two types of twinning.

Triclinic symmetry of Freiberg arsenopyrite is most clearly revealed by the fact that the intensities of some ($hk0$) reflections are definitely different from those of the corresponding ($h\bar{k}0$) reflections. This justifies the existence of type-II twinning. Wilson's method (1949), applied on ($hk0$) reflections, confirmed the existence of a symmetry center. Thus, $P\bar{1}$ is the only possible space group.

Some crystals of Freiberg arsenopyrite were heated at 600° C. for 30 days in a sealed, evacuated, silica-glass tube and then rapidly cooled in cold water. Since the Weissenberg and precession photographs show no differences between the heated and unheated specimens, there is no evidence of a sluggish high-low polymorphic inversion.

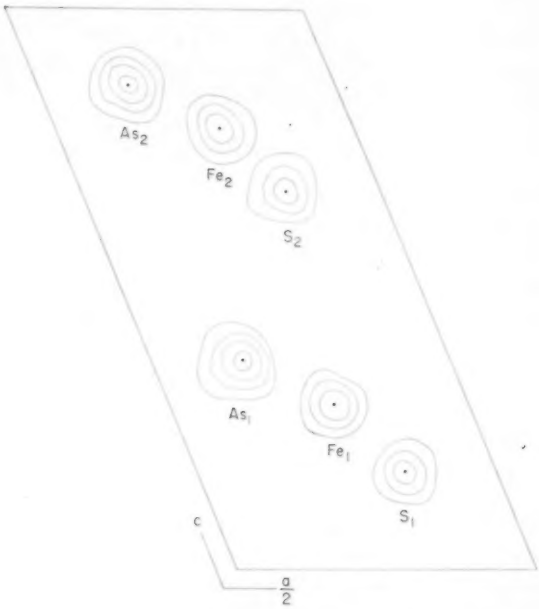

FIG. 4. Electron-density projection on (010). Contours are drawn at intervals of 11 $e/\text{Å}^2$ beginning at 10 $e/\text{Å}^2$.

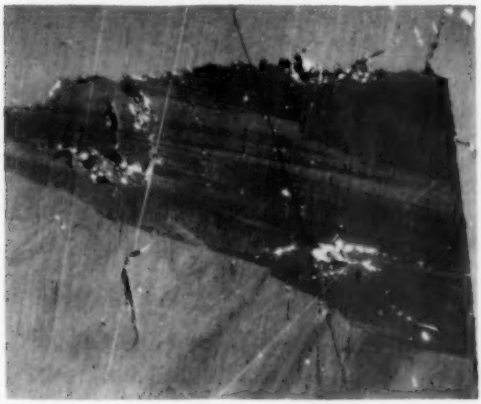

FIG. 5. In addition to the fine twinning of type II, the Freiberg arsenopyrite grain, which occupies about 90% of the photograph, also shows a type-I twin plane which divides it into two parts. White and black areas are pits. Taken with reflected light polarized in two directions.

Synthetic arsenopyrite

Owing to the failure of experiments planned to synthesize crystals of the required size for use with the *x*-ray precession and Weissenberg cameras, only one synthetic arsenopyrite "single" crystal was examined.* The precession and Weissenberg photographs give orthorhombic symmetry, and the cell dimensions obtained from the precession photographs: $a=9.669$, $b=5.720$, and $c=6.400$ Å (all ± 0.005). If the primitive monoclinic cell is employed for ease of comparison with the Freiberg arsenopyrite,† the above cell values transform to: $a=c=5.796$, $b=5.720\pm 0.005$ Å, and $\beta=113°\ 21'\pm 5'$. Using these values of b and β the composition of this synthetic arsenopyrite crystal is obtained from Fig. 3 as about 38 atomic per cent arsenic, or approximately $FeAs_{1.1}S_{0.9}$. The zero-level Weissenberg photograph of synthetic arsenopyrite about the b axis, Fig. 6*b*, is compared with that of a Freiberg crystal, Fig. 6*a*. As fully discussed by Buerger (1936) in his investigation of arsenopyrite from Franklin,

* Crystals of suitable size were grown under rather peculiar conditions of disequilibrium Arsenopyrite and arsenic were intergrown as an impervious mass at one end of a small, sealed tube at 600° C. This tube, open at the other end, was then heated for 3 days at 350° C. inside a larger sealed tube. A portion of the arsenopyrite decomposed to satisfy the vapor requirement of the large tube, and a 0.5 mm. layer of needle-shaped arsenopyrite crystals grew at the surface of the undecomposed arsenopyrite.

† The transformation from the pseudo-orthorhombic double cell (the second setting) to primitive monoclinic cell (the third setting) is given in the discussion of the powder pattern indices.

N. J., the apparent orthorhombic symmetry observed in the synthetic arsenopyrite is the result of type-I twinning of crystals of lower symmetry. Assuming space group $P2_1/c$, all the observed reflections but one can be explained by twinning. The one exception is $(10\bar{1})$, which proves that, although this synthetic arsenopyrite is nearly monoclinic, it really is triclinic, as fully discussed later.

Effect of chemical composition

Single-crystal investigations of the Freiberg and synthetic arsenopyrites show definite differences, not only in lattice constants, but also in

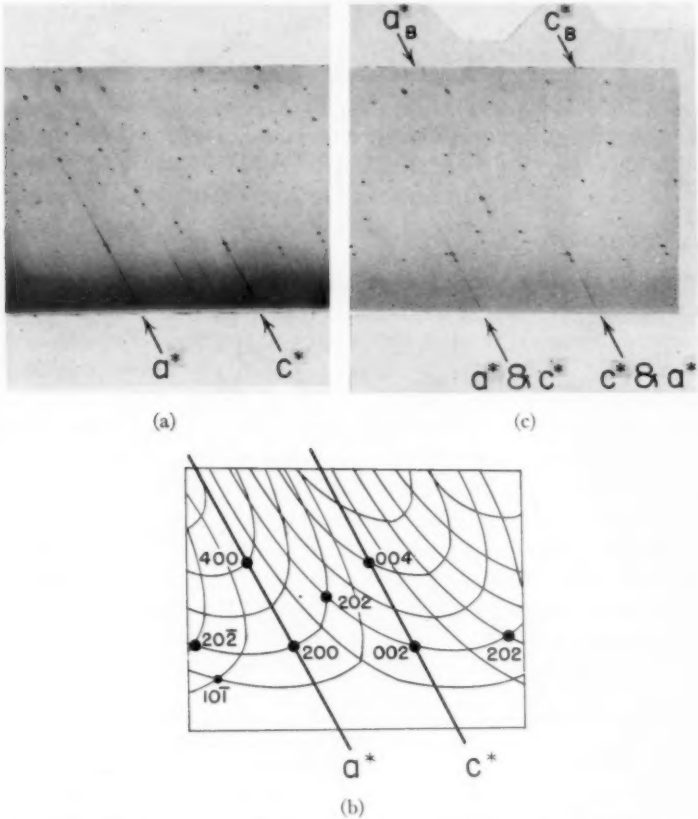

FIG. 6. (Upper left) Zero level *b*-axis Weissenberg photograph of Freiberg arsenopyrite. (Upper right) Synthetic arsenopyrite. Apparent orthorhombic symmetry is clear where a_B^* and c_B^* represent Buerger's pseudo-orthorhombic axes. The intensities of $h0l$ with l odd differ greatly. (Below) Diagram showing indexing of some reflections.

apparent symmetry. As previously discussed (see Fig. 2), these arsenopyrites differ in arsenic content by 6 atomic per cent. The composition of the Freiberg arsenopyrite lies on the sulfur-rich side of ideal FeAsS and appears to typify the majority of natural arsenopyrites, while that of the synthetic arsenopyrite is arsenic-rich relative to FeAsS and is near the limit of solid solution. It is reasonable to assume that these differences in the sulfur-to-arsenic ratio underlie the observed differences in reflection intensities and extinctions. To confirm this assumption, other specimens of natural arsenopyrite of known chemical compositions were studied using the Buerger precession method. The specimens are from (1) Llallagua, Bolivia; (2) New Consols Mine,* Cornwall; and (3) Boliden Mine, Sweden. The compositions and descriptions of these arsenopyrites are given in Tables 2 and 3. For the five specimens investigated the arsenic content decreases as follows: synthetic, New Consols, Llallagua, Freiberg, and Boliden.

The compositional variation in this series correlates with the following crystallographic observations:

(a) Crystals apparently free from type-I twinning† were found only in sulfur-rich arsenopyrite, i.e. in the Boliden and Freiberg specimens. These specimens show symmetry variations from pseudomonoclinic to pseudo-orthorhombic according to the relative volumes of the individuals in the twin. Type-I twinning was always observed for the Llallagua, New Consols, and synthetic specimens. The precession photographs for all the specimens from each of these three localities gave apparent orthorhombic symmetry without exception. Both types of twinning were observed in polished sections of some Freiberg specimens (see Fig. 5), but no twinning was observed microscopically in any of the other specimens. Our failure to observe this twinning microscopically is puzzling. Arsenopyrite anisotropic effects are small, and adjacent twin individuals may be so oriented as to show no visible difference. On precession and Weissenberg photographs of arsenic-rich "single" crystals, twinning is always visible. This implies that twinning occurs on a finer scale, so that it accounts for the more even volume distribution of the twin individuals in randomly selected specimens.

(b) The intensities of the $h0l$ reflections with l odd decrease with increasing arsenic content. These reflections, clearly observed on the x-ray

* Although a chemical analysis of the New Consols arsenopyrite is not available, its composition can be estimated from cell dimensions. Precession photographs give $b=5.718$ Å and $\beta=112.50°$. From x-ray powder data, $d_{131}=1.635$ Å. On Fig. 3 these values give mean compositions of 31 atomic % sulfur and 36% arsenic.

† The crystals may not be completely free from type-I twinning, but they give photographs like that shown in Fig. 6*a*.

photographs of Freiberg specimens, become weaker for specimens containing more arsenic, and are not observed in synthetic material except for the $(10\bar{1})$ reflection (see Fig. 6*c*). From the structural viewpoint the absence of these reflections indicates monoclinic symmetry. Therefore, the space group which is valid for sulfur-rich arsenopyrite specimens, namely $P\bar{1}$, approaches space group $P2_1/c$ with increasing arsenic content. Although none of the specimens examined had truly monoclinic symmetry, since the $(10\bar{1})$ was observed in all specimens, we presume that a crystal slightly more arsenic-rich than $FeAs_{1.1}S_{0.9}$ would have the space group $P2_1/c$. Thus, the replacement of sulfur by arsenic causes a gradual change in the arsenopyrite properties which raises the symmetry of the structure from triclinic to monoclinic.*

We can offer no reasonable theoretical explanation of these observations, which, it will be noted, do not fit the hypothesis of Buerger (1936), namely that arsenopyrite of the "ideal" composition FeAsS is monoclinic whereas compositional variations from the ideal render the symmetry triclinic. In view of the peculiar nature of the arsenopyrite stability field (Clark, 1960, Fig. 14), apparently the concept of any specific composition being "ideal" is invalid.

The electron-density maps give the following ratios of peak heights for the different atoms:

As:Fe:S::1.30:1.11:1.00

These peak heights require one of two assumptions: either the crystal used to collect the intensity data contains a small amount of type-I twinning, or there is 30% replacement of arsenic atoms by sulfur atoms and vice-versa. It has already been concluded that there is no appreciable substitution of iron for arsenic or sulfur. Comparisons were made between intensities of some strong $h0l$ reflections with h odd and of their counter reflections $l0h$ in the supposed twin. The average ratio was 33:1. This is a direct measure of the relative volumes of the twin individuals if $h0l$'s were absent when l is odd. However, some $h0l$'s with l odd do appear; the volume contributed by the counterpart individual is thus even smaller than 1/33 of the total volume of the specimen.

When the volume difference between the twin individuals is so large, it is difficult to decide the relative effects of twinning and of the assumed partial sulfur-arsenic disorder on the intensity data. Both causes may be responsible, though twinning is probably the more important. This ambiguity renders further refinements of the structure impossible.

* Rather than calling on further arsenic substitution, it is possible that the monoclinic structure may be attained by incorporation of minor amounts of elements such as cobalt or antimony in the arsenopyrite structure.

TABLE 4. ATOMIC COORDINATES IN ARSENOPYRITE

(in thousandths of cell edge)

	Buerger, 1936			Present study		
	x	*y*	*z*	*x*	*y*	*z*
As_1	147	372	353	154	371	363
As_2	(147	128	853)*	155	129	863
Fe_1	275	0	275	272	000	289
Fe_2	(275	500	775)	275	502	787
S_1	333	−368	167	346	−370	175
S_2	(333	−132	667)	343	−131	675

* The coordinates given in parentheses are crystallographically equivalent to those immediately above.

The atomic coordinates adopted are those obtained in the first stage of the analysis without considering the effects on the intensities of either twinning or partial disorder. The *R* values for the coordinates are 0.29 for *h*0*l* and 0.21 for *hk*0. The coordinates are compared, in Table 4, with those given by Buerger (1936). The differences are slight. The accuracy of the coordinates cannot be estimated. Interatomic distances are calculated and given in Table 5. Average interatomic distances Fe-As, Fe-S, and As-S are 2.35, 2.25, and 2.33 Å, respectively. These values are in good agreement with those obtained for marcasite (Buerger, 1931) and loellingite (Buerger, 1932). Atomic radii derived from these interatomic distances are: $r(Fe) = 1.14$, $r(As) = 1.21$, and $r(S) = 1.11$ Å. The structure is not accurate enough to warrant a discussion of the atomic distances, but it does support Buerger's (1936) arsenopyrite structure and atomic distances.

TABLE 5. INTERATOMIC DISTANCES IN ARSENOPYRITE

(in Ångströms)

As_1–Fe_1	2.30	S_1–Fe_1	2.29	As_1–S_1	2.34
–Fe_2	2.39	–Fe_2	2.22	As_2–S_2	2.33
	2.32		2.25		
As_2–Fe_1	2.38	S_2–Fe_1	2.24	As –S	2.33
	2.41		2.26		
–Fe_2	2.32	–Fe_2	2.26		
As –Fe	2.35	S –Fe	2.25		

Acknowledgments

All calculations for structure refinements were carried out by Dr. D. Appleman at the U. S. Geological Survey, Washington, D. C., to whom we are very grateful. We express appreciation to Drs. H. B. Wiik and P. Väänänen, Helsinki, for the chemical analysis of an arsenopyrite and to Mr. H. E. Swanson, U. S. National Bureau of Standards, Washington, D. C., for assistance in programming the electronic computation of the *x*-ray powder data.

For critical reading and constructive criticism of the manuscript we are indebted to Drs. M. J. Buerger, G. Donnay, J. D. H. Donnay, G. Kullerud, and R. A. Yund.

The arsenopyrite specimens used in this investigation were obtained from the following institutions and persons, to whom we wish to express our thanks: Mr. P. E. Desautels and the Smithsonian Institution, Washington, D. C.; Dr. P. G. Embrey and the British Museum (Natural History), London; Professor C. Andreatta, Istituto di Mineralogia e Petrografia, Universita di Bologna, Bologna; and Dr. E. Grip, Bolidens Gruvaktiebolag, Boliden, Sweden.

References

Andreatta, C. (1928*a*), Sulle arsenopiriti dei giacimenti minerari di Calceranica e Caldonazzo nel Trentino: *Riv. Studi Trentini Sci. Nat.*, **9** (1), 15 pp.

——— (1928*b*), Sull'arsenopirite di Nogarè (Trentino): *Riv. Studi Trentini Sci. Nat.*, **9** (2), 12 pp.

Buerger, M. J. (1931), The crystal structure of marcasite: *Am. Mineral.*, **16,** 361–395.

——— (1932), The crystal structure of löllingite, $FeAs_2$: *Z. Krist.*, **32,** 165–187.

——— (1936), The symmetry and crystal structure of the minerals of the arsenopyrite group: *Z. Krist.*, **95,** 83–113.

——— (1937), Interatomic distances in marcasite and notes on the bonding in crystals of löllingite, arsenopyrite, and marcasite types: *Z. Krist.*, **97,** 504–513.

——— (1939), The crystal structure of gudmundite (FeSbS) and its bearing on the existence field of the arsenopyrite structural type: *Z. Krist.*, **101,** 290–316.

Chace, F. M. (1956), Abbreviations in field and mine geological mapping: *Econ. Geol.*, **51,** 712–723.

Clark, L. A. (1960), The Fe—As—S system: phase relations and applications: *Econ. Geol.*, **55,** 1345–1381, 1631–1652.

Ellsworth, H. V. (1916), A study of certain minerals from Cobalt, Ontario: *Ontario Dept. of Mines Ann. Rept.*, **25,** pt. I, 200–243.

Harcourt, G. A. (1942), Tables for the identification of ore minerals by *x*-ray powder patterns: *Am. Mineral.*, **27,** 63–113.

Huggins, M. L. (1937), The crystal structures of marcasite, arsenopyrite, and löllingite: *Z. Krist.*, **96,** 384–385.

Jong, W. F. de (1926), Bepaling van de absolute aslengten van markasiet en daarmee isomorfe mineralen: *Physica, Nederl. Tijds. Natuurk.*, **6,** 325–332.

——— (1928), Over de kristalstructuren van arsenopyriet, borniet, en tetraëdriet: Gedrukt

bij de Technische Boekhandel en Drukkerij, Delft. (Abstr. in *Z. Krist.*, Strukturbericht, 1913–1928, p. 283.)

KITAHARA, J. (1952), On the arsenopyrite from the Nodatamagawa Mine, Iwate Prefecture: *J. Geol. Soc. Japan*, **58,** 545–549.

ÖDMAN, O. H. (1941), Geology and ores of the Boliden deposit, Sweden: *Sveriges Geologiska Undersökning*, **35,** 1–190.

——— (1942), Minerals of the Varuträsk pegmatite. XXXIII. Native elements and sulphides: *Geol. Fören. Förh.*, **64,** 277–282.

OKADA, I. (1933), On the existence of arsenic in the ore from the Ashio Mine, and on the iron sulphides from the same mine: *J. Geol. Soc. Tokyo*, **40,** 443–472.

PALACHE, C. (1910), Contributions to the mineralogy of Franklin Furnace, N. J.: *Am. J. Sci.*, **29,** 177–187.

——— (1935), The minerals of Franklin and Sterling Hill, Sussex County, N. J.: *U. S. Geol. Surv. Prof. Paper* 180, 135 pp.

RAMDOHR, P. (1950), Die Lagerstätte von Broken Hill in New South Wales: *Heidelberger Beitr. Mineral. u. Petrog.*, **2,** 291–333.

SWANSON, H. E., AND TATGE, E. (1953), Standard *x*-ray diffraction powder patterns: *U. S. Nat. Bur. Standards Circular* 539, v. I, 69–70.

TOKODY, L. (1936), Adatok a Szepes-Gömöri Érchezység ásványainak ismeretéhez: *Mat. Term.-tud. Értesítö, Budapest*, **54,** 650–671. [Abstr. in *Min. Abstr.*, **7,** 116.]

TSURUMI, S. (1934), Chemical composition of arsenopyrite from Kap-san, Chôsen: *J. Japanese Assoc. Min. Pet. Geol.*, **12,** 189–190.

VAN TASSEL, R. (1954), Le mispickel du Brabant: *Volume jubilaire Victor Van Straelen, Inst. roy. sci. nat. Belg.*, **1,** 95–113.

WILSON, A. J. C. (1949), The probability distribution of *x*-ray intensities: *Acta Cryst.*, **2,** 318–321.

YOSHINO, Y. (1951), Separation of arsenic from iron by ion-exchange resin: *Bull. Chem. Soc. Japan*, **24,** 39–41.

Manuscript received February 25, 1961.

THE AMERICAN MINERALOGIST, VOL. 46, NOVEMBER-DECEMBER, 1961

THE RECOGNITION OF PLAGIOCLASE TWINS IN SECTIONS NORMAL TO THE COMPOSITION PLANE

ALEXANDER C. TOBI, *Geological Institute, University of Amsterdam, Holland.*

ABSTRACT

In sections of plagioclase twins cut normal to the composition plane, the law of twinning can often be recognized without the aid of the universal stage by considering the birefringences and extinction angles of the twin individuals. Three diagrams, one for each of the important composition planes, facilitate this recognition. When the twinning is lamellar, the distinction between the albite and acline-pericline laws is always easily accomplished.

INTRODUCTION

In the beginning of this century the development of the universal stage gave the opportunity of studying in great detail the optical properties of the members of the plagioclase group. In the period from 1914 to 1924 their optical orientation and their various laws of twinning were studied exhaustively (Fedorov and Nikitin, Wülfing, Duparc and Reinhard, Berek and others). Yet, in most cases the types of twinning were not studied for their own sake: they served, in conjunction with the optical orientation, to determine the chemical composition (*i.e.* the percentage of anorthite) of the plagioclase.

Several other methods to determine the composition are practicable without the universal stage. They make use of characteristic extinction angles in specific sections or zones (Michel-Lévy, Schuster, Fouqué, Köhler and others). These methods are now used far more universally than those designed for the universal stage. Their application does not require much knowledge of the basic facts and concepts underlying them. Yet lack of insight may lead to wrong results. Even the directions for the use of these methods, as given in many textbooks, often contain inaccuracies.

In the last decade a growing interest can be noted in the mode of occurrence and the distribution of the various laws of plagioclase twinning in different rocks. Gorai (1951) distinguishes between two groups, "A-twins" (usually lamellar) and "C-twins" (non-lamellar or composite).* His study of the frequency of A- and C-twins in many rocks shows interesting differences between plagioclase of magmatic and of metamorphic origin. Attractive in his method is the possibility to distinguish between both groups without the aid of the universal stage. Yet a more detailed classification would have advantages. For instance, in

* The criteria given by Gorai to distinguish between simple A-twins and C-twins are only correct for twins with (010) as composition plane.

medium-grade metamorphic rocks the pericline or acline law is often more frequent than the albite law, while the reverse is true for most magmatic rocks (Turner 1951, Tobi 1959). Again, in albite porphyroblasts of certain low-grade metamorphic schists the Carlsbad and albite laws are both found, whereas twins with composition planes other than (010) are rigorously absent (Tobi 1959). As a final example it may be mentioned that rocks such as spilites and trondhjemites occasionally show a large number of Ala-A twins, combined with albite lamellae. Under favorable circumstances these patterns may serve to distinguish between otherwise similar rocks, or to indicate the origin of clastic grains in an arenite. Eventually, a more extensive research into the occurrence of the various twin laws in different rocks might shed some light upon the conditions favoring their development, which would be of great petrological importance. *The present article has been written with the double purpose of stressing some basic facts underlying current determination methods, and of facilitating the recognition of the various laws of twinning without the aid of the universal stage.*

The Properties to Be Studied

When studying a plagioclase twin without a universal stage our information consists chiefly of the *extinction angles* and the *birefringences* found in both individuals of the twin. Nieuwenkamp (1948) constructed charts for the determination of the An-content from these properties in random sections of albite twins. In the present paper our chief aim will be to determine not the An-content, but the law of twinning. *To this end we will use only sections of twins cut perpendicular to their composition plane.*

This following portion deals with the question of how such sections are found and how the necessary information is obtained from them. To make an intelligent use of this information, it should be realized that the optical properties of the individuals of a twin are chiefly conditioned by:

1) the optical orientation of the particular plagioclase.
2) the law of twinning.
3) the orientation of the section.

Selecting sections normal to the composition plane

A plagioclase twin is usually visible with crossed nicols only. This visibility may be caused by a difference in extinction angle, in birefringence, or in both. The plane of contact between the twin individuals is called the composition plane. In sections normal to this plane, to

which the present method is confined, the trace of this plane should be a sharp line. It should not move laterally when the focus of the objective with the highest magnification is lowered from the upper to the lower surface of the thin section.

When the composition plane is irregular or in other ways does not agree with the "ideal" composition plane, the method is not practicable.

Distinguishing between symmetrical and asymmetrical extinctions

When the extinctions are symmetrical with regard to the trace of the composition plane, the twin individuals show equal illumination in each 0° and 45° position of this trace. This means that the twin becomes almost invisible in those positions. When the extinctions are asymmetrical, one would expect the twin to be visible in both the 0° and 45° positions. In reality, the difference in intensity of the transmitted light is often visible in one of these positions only, *viz.* in that nearest to the extinction positions.

Determining the elongation with regard to the composition plane

It suffices to insert the gypsum plate while *the trace of the composition plane* is in the NE 45° position. With most microscopes the twin individuals will become yellow when the elongation is negative (length fast), blue when it is positive (length slow). In the following this is assumed to be the case. It should be noted that the term elongation is used here in a not too literal way, as the form of the crystals is of no importance. It should be borne in mind too that the extinction angles given in the literature always refer to X′ (the vibration direction of the ray with the smaller refractive index). Thus, when the elongation is positive the extinction angle must be over 45°. The sign of the elongation should not be confused with the sign of the extinction angle.

Determining the sign of the extinction angle

Some special attention should be given to the confusing matter of the extinction sign. According to common usage, *extinction angles measured from a cleavage or composition plane in a clockwise direction are considered positive, those measured in counter clockwise direction negative.* This extinction sign has only relative importance, because it is reversed by turning the section upside down. To avoid ambiguity in the reading of tables and diagrams, it became customary to give the extinction angle $X'\wedge(010)$ on (001) as seen from the *positive* side of the *c*- axis, the angle $X'\wedge(001)$ in sections on (010) as seen from the *positive* side of the *b*-axis, and the angles $X'\wedge(010)$ and $X'\wedge(001)$ in sections normal to *a* as seen from the *negative* side of the *a*-axis (cf. Duparc and Reinhard,

1924, p. 22). Unfortunately, it is seldom possible to ascertain the crystallographic orientation of plagioclase crystals in a thin section. An exception must be made for the section normal to *a*, to which will be devoted a separate paragraph (page 1480).

In this paper, the extinction sign will be chiefly used in a relative way to compare the extinction angles of the two individuals of a twin: if both angles are measured from the trace of the composition plane in the same direction the signs agree, if they are measured in opposite directions the signs are opposite.

The extinction positions are easily determined on rotating the stage. When the extinction angles are large, or when composite twins are studied, it may prove useful to insert the gypsum plate while the trace of the compsition plane is in the 0° position. Twin individuals with positive extinction will then become yellow, those with negative extinction blue. Thus, in this position twin individuals with symmetrical extinctions will always show different colors.

Estimating the birefringence

For the present purpose a rough estimation of the birefringences found in twins cut normal to the composition plane will usually be sufficient. In the diagrams four groups are distinguished, limited by the following values:

0.002: almost optically isotropic
0.004: birefringence like that of apatite
0.008: birefringence near that of quartz.

The Optical Orientation of Plagioclase

In the plagioclase group a distinction can be made between a *high-temperature* and a *low-temperature form*, the former being virtually restricted to volcanic rocks. The optical properties are slightly different, but for the problems under consideration these differences do not seem to be of great importance. The diagrams given here refer to low-temperature optics.

The *optical orientation of plagioclase* may be studied in a stereographic projection on a plane normal to the crystallographic *a*-axis (Wulff net, Fig. 1)*. In this projection the important cleavage- and composition

* The original diagram given by Duparc and Reinhard (1924) was oriented on the negative side of the *a*-axis, as the conventional extinction signs are based on this orientation. The present author has chosen the orientation on the positive side of the *a*-axis to facilitate comparison with crystal drawings, which are always drawn with the positive *a*-axis pointing to the observer and the positive *c*-axis pointing upward. Winchell and Winchell (1951) use the same orientation in their Fig. 172, but here the optical orientation is not correct.

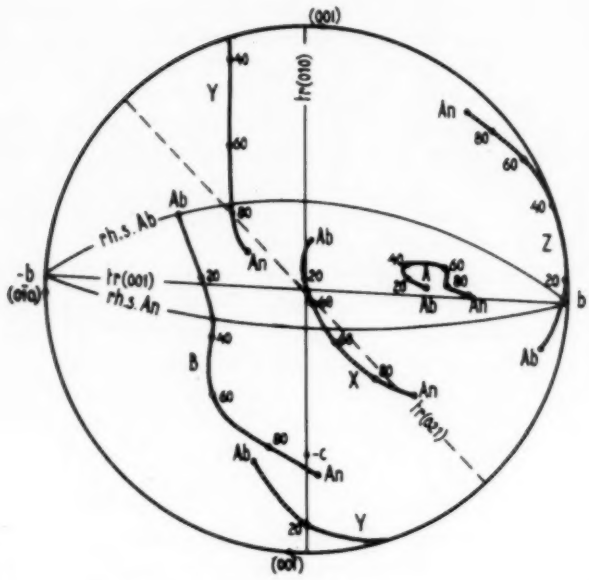

FIG. 1. Optical orientation of the low-temperature plagioclases, shown in stereographic projection on a plane normal to the *a* axis. The cleavage- or composition-planes (010), (001) and (021) appear as straight lines. The rhombic sections (rh.s.) of the end members albite (Ab) and anorthite (An) are indicated by great circles. The left Baveno composition plane (021) is not indicated. (Modified after Duparc and Reinhard)

planes (010) and (001), making an angle of 94° with each other, appear as diameters of the net. Therefore, the properties of sections cut normal to these planes are read conveniently from this diagram. The composition trace of one of the Baveno laws appears as a dashed line (tr. (021)). The composition plane of the pericline law is obtained by tilting from the (001) plane around the *b*-axis over an angle dependent on the An-content (Fig. 2). The position of this plane (the "rhombic section") for the end members of the plagioclase group (albite and anorthite) is indicated by great circles in Fig. 1.

The change of orientation of the indicatrix with increasing An-content can be roughly described as a rotation around the optic axis A. The change in the positions of the optic axes A and B is also controlled to some extent by differences in optic axial angle.

Let us now consider how the optical properties of sections normal to the various composition planes are controlled by this optical orientation, so that we may distinguish between those planes in favorable cases.

Sections normal to (010)

In plagioclase with less than 75% An, Z is the indicatrix axis nearest to the normal on (010) (Fig. 1). Hence, this plagioclase must show *negative elongation with regard to (010)*. The closer Z is to the normal on (010), the smaller is the extinction angle. Generally the optic axes A and B are distinctly oblique to (010). Only when the An-content surpasses 75% the axis B lies in or nearly in (010). This implies that sections normal to (010) always show appreciable birefringence when the An-content is below 75%.

The actual properties as shown in Fig. 3 confirm these statements. In this diagram the birefringences and extinction angles are drawn as "contours." The chemical composition is plotted along the abscissa, the orientation of the normal on the section in the zone normal to (010) along the ordinate. *Thus, the line marked c indicates the section cut perpendicular to the c-axis.* Each imaginary vertical line in the diagram indicates the extinction angles and birefringences found when a plagioclase of definite composition is turned in the zone normal to (010). The maximum extinction angle to occur in this plagioclase is indicated by the extinction curve tangent to this vertical line. The dominance of negative elongation (angles smaller than 45°) and appreciable birefringence in the

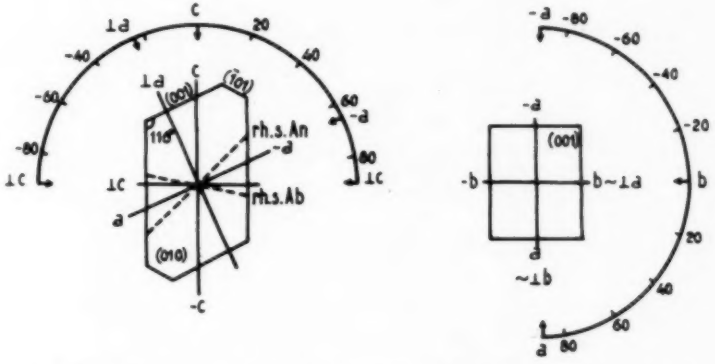

FIG. 2. (Left) Section parallel to (010), with indication of the crystal- and twin-axes lying in this plane, and of the traces of the rhombic section (rh.s.) for albite and anorthite. The arc shows that part of the zone perpendicular to (010) covered by Fig. 3, with indication of the angles used to fix the orientation.

FIG. 2. (Right) Section parallel to (001), with indication of the crystal- and twin-axes lying in this plane. The *a*- and *b*-axes are nearly at right angles, so that the normal of one of them in the plane (001) is optically indistinguishable from the other. The arc shows that part of the zone perpendicular to (001) covered by Fig. 4, with indication of the angles used to fix the orientation.

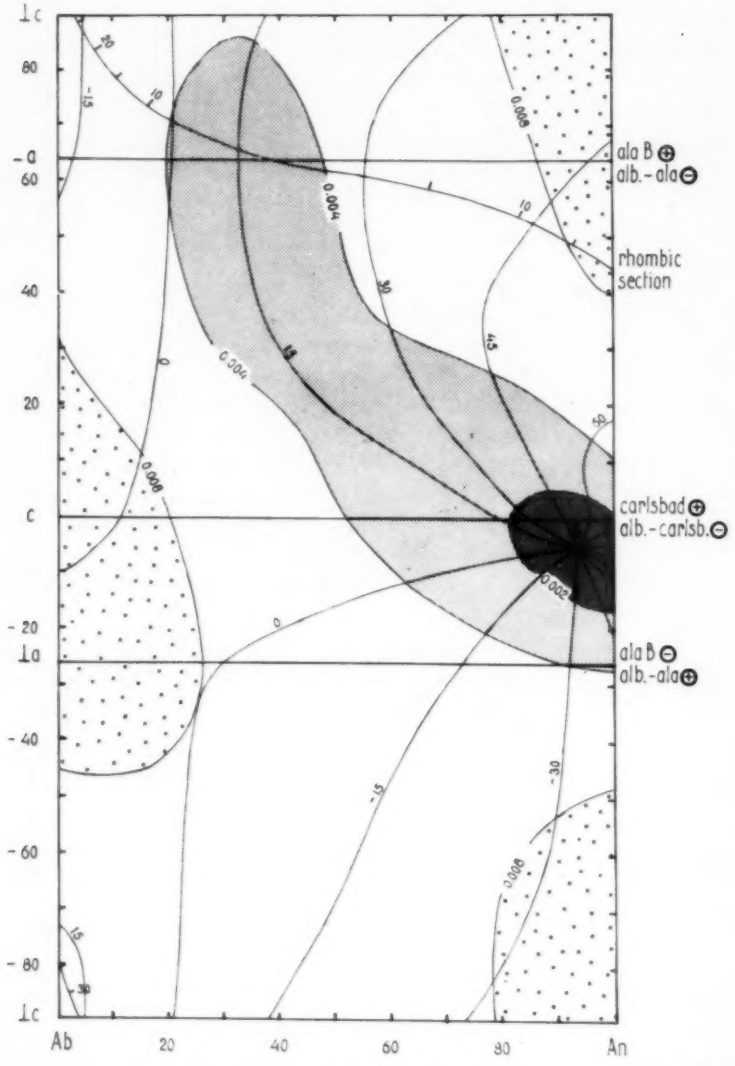

FIG. 3. Extinction angles $\chi' \wedge 010$ and birefringences in the zone normal to (010). *The optical properties refer to sections normal to the directions indicated along the ordinate.* The individuals of a *normal twin, i.e.* an albite twin, occupy one and the same point in the diagram, the extinction of the second individual being found by reversal of sign. The individuals of a *parallel or complex twin* are represented by two points situated symmetrically with regard to the horizontal line bearing the name of that twin law in the margin of the diagram. These points indicate the optical properties of the twin individuals, when the

zone normal to (010) stands out clearly in the diagram.

It should be borne in mind that the chart shows only half of the zone normal to (010). The other half is identical but for the extinction signs, which are opposite. This fact need not worry us, because the extinction signs will be used here in a relative way only. For cases where the conventional extinction signs of specific sections are needed, that part of the zone covered by the diagram is indicated by an arc in Fig. 2 (left).

Sections normal to (001)

In Na-rich and intermediate plagioclase, Y is nearest to the normal on (001). Hence, *the elongation of this plagioclase with regard to (001) may be positive or negative* depending on the orientation of the section. The optic axis A always makes a small angle with (001).When the An-content is between 10% and 35%, the same holds true for the axis B. This means that *in the zone normal to (001) all plagioclases may show sections remaining dark on turning the stage.* The neighborhood of the optic axes results also in widely varying extinction angles.

These tendencies appear clearly from Fig. 4, which gives the extinction angles and birefringences in the zone normal to (001). The fields representing sections with nearly isotropic character or very weak birefringence cover a large part of the diagram. Large extinction angles are frequently encountered. The orientation in this zone is given with regard to the *b*-axis. As the *a*-axis is very nearly normal to the *b*-axis (with small variations depending on the An-content), the section parallel to *b* may be considered identical with that normal to *a*. For cases where the conventional extinction signs of specific sections are needed, that part of the zone covered by the diagram is indicated by an arc on Fig. 2 (right).

Sections normal to the rhombic section

The position of the rhombic section differs appreciably from (001) for compositions near the end members of the plagioclase group. For compositions of ca 20–80% An the angle between both planes is less than 10°; at about 40% An both planes coincide (Figs. 1, 2, 3). The resulting differences in extinction angles and birefringences appear clearly

---

name of the twin law is provided with a ⊕ sign. The ⊖ sign denotes that the sign of one of the extinction angles as found in the diagram should be reversed to obtain the optical properties for that twin law.

Along the line representing the rhombic section, the angle with (001) is indicated in degrees. That part of the zone covered by the diagram is indicated by an arc in Fig. 2 (left). For further explanation see text.

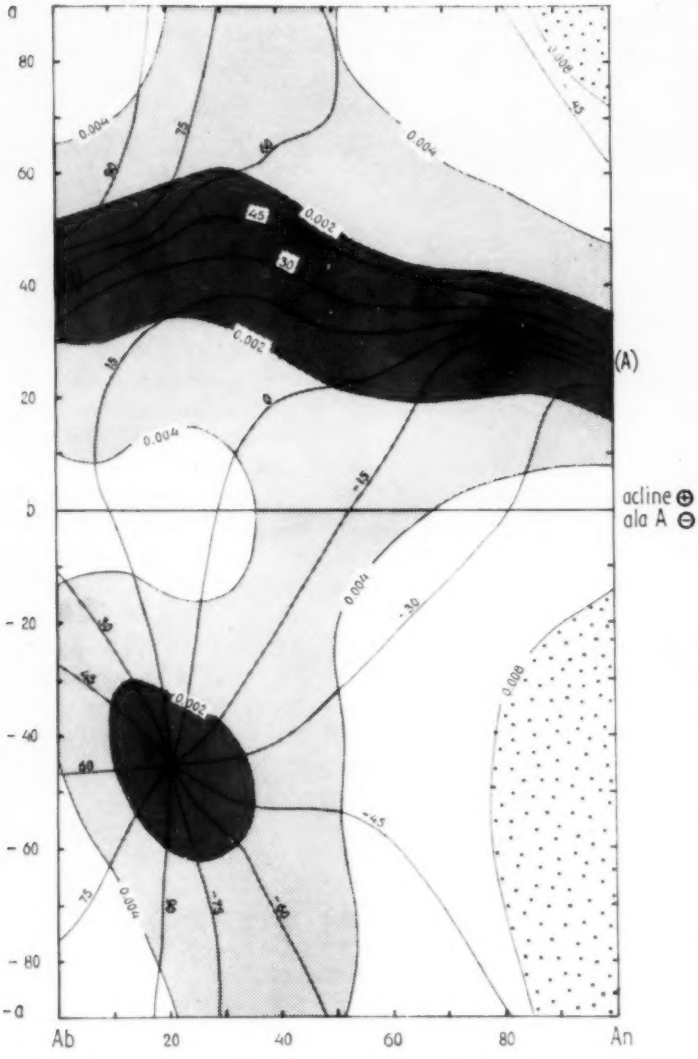

FIG. 4. Extinction angles $\chi' \wedge 001$ and birefringences in the zone normal to 001. That part of the zone covered by the diagram is indicated by an arc in Fig. 2 (right). For explanation see Fig. 3.

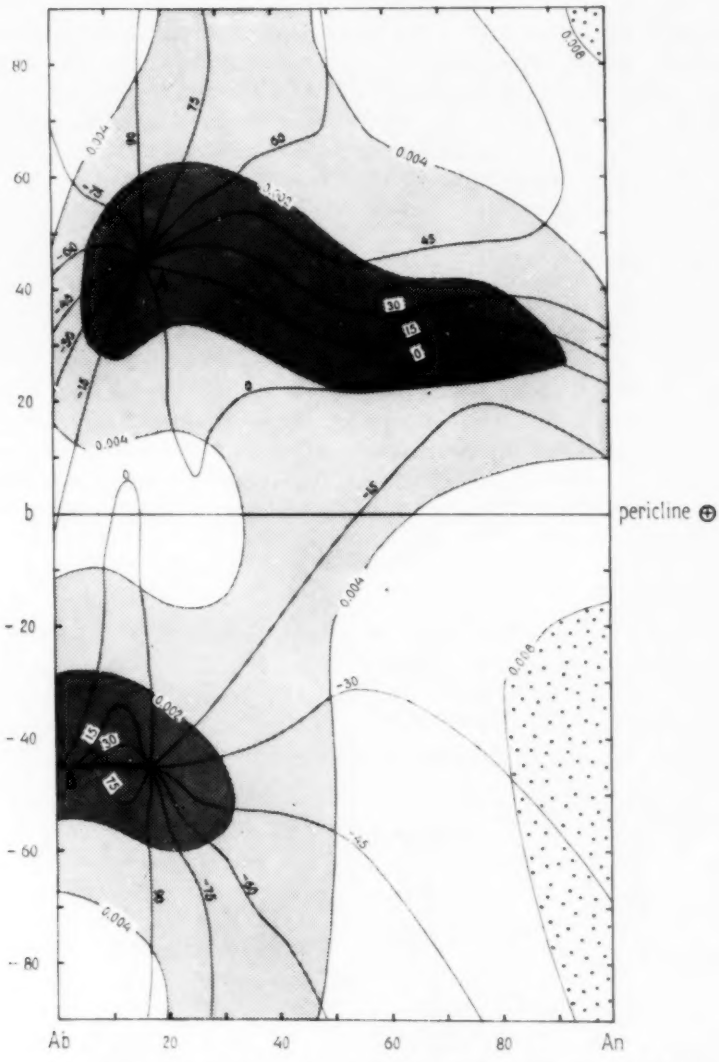

FIG. 5. Extinction angles $\chi' \wedge$rh.s. and birefringences in the zone normal to the rhombic section. For explanation see Fig. 3 and text.

by comparison of Figs. 4 and 5. These differences are best explained by considering the position of the optic axes A and B with regard to both planes. Thus, for pure albite the axis B lies just in the rhombic section, while the axis A makes a considerably larger angle with that plane than with (001). At a composition near 20% An the axis B lies again in the rhombic section, while in the interval between 0 and 20% the angle remains very small. In Fig. 5 this interval is represented by a heavy black line. Again, the larger angles with the axis A for the end members result in the 0.002 contour closing around A in the upper part of the diagram.

Sections normal to (021) or ($0\bar{2}1$)

These composition planes may be recognized by their making angles of roughly 45° with the cleavage directions (010) and (001). Even if no cleavage is visible, their nature is often betrayed by their oblique position with regard to the crystal outlines. No attempt is made here to distinguish between the zones normal to (021) and ($0\bar{2}1$). Therefore, no diagrams are given for these zones. Some general rules may be read from Fig. 1 in the same way as was done for the other composition planes. The trace of ($0\bar{2}1$) is not indicated; it should be approximately normal to the dashed trace of (021).

Section normal to a

In this section both cleavage- or composition planes (010) and (001) are visible as sharp traces enclosing an angle of 94°. The optical properties of this section for the various members of the plagioclase group may be read along the line marked -*a* in Fig. 3. When the An-content is between 0% and 75%, the elongation is always negative with regard to (010),

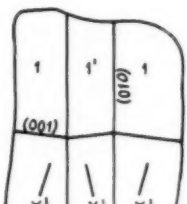

FIG. 6. Section normal to *a* of an albite twin of albitic composition. The conventional negative extinction sign for this section, as given in tables and charts, refers to the individual 1', which is seen from the negative side of the *a*-axis.

positive with regard to (001). Thus, the elongation is now alone sufficient to distinguish between both traces.*

To obtain the conventional extinction sign, this section should be regarded from the negative side of the *a*-axis. If the (010) trace is oriented in the N-S position, the (001) trace dips to the right when the section is observed from the positive, to the left when it is observed from the negative side of the *a*-axis. In the albite twin of albitic composition shown in Fig. 6, the conventional negative extinction sign refers to the individual 1′, in which the negative *a*-axis points to the observer. The extinction angle of this individual complies with two rules:

1) X′ points to the obtuse angle between (010) and (001);
2) X′ is measured anticlockwise from (010).

When we now consider the individual 1, the attachment of an extinction sign is a matter of free choice. If we need the conventional extinction angle to determine the An-content, we choose the first rule: both individuals now have the negative sign demanded for albite in current tables and charts. The rule is valid for this particular section only. In the present paper the second rule is chosen: for our method the individuals of an albite twin should always have opposite extinction signs, as their extinction angles are measured from the (010) trace in opposite directions.

If the trace with positive elongation is not a cleavage, but a composition plane of lamellar twinning, the section might be normal to the rhombic section instead of normal to (001). The ensuing differences in extinction angle and birefringence, which may be read from Fig. 3, are only important for Ca-rich plagioclase.

The Laws of Twinning

In Table I the various laws of twinning are arranged according to composition plane and type of twinning. In the preceding section we have studied the extinction angles and birefringences occurring in sections normal to these composition planes. The Carlsbad B twin is not here considered, since it is extremely rare. We will now see how the position of the twinning axis determines the particular combination of optical properties found in the twin individuals. Before starting our enquiry into the various types of twinning, we should remember that the plagioclase crystal has a center of symmetry. Therefore, each twin must have a symmetry plane, situated perpendicular to the twinning axis.

* Above 75% An, the large extinction angles make a distinction more difficult.

TABLE I. LAWS OF PLAGIOCLASE TWINNING

Composition plane	Normal twinning	Parallel twinning		Complex twinning	
		Axis	Law	Axis	Law
(010)	**albite** (often lamellar)	*c*	**Carlsbad A**	$\perp c$ in (010)	**albite-Carlsbad**
=cleavage		*a*	*Ala B*	$\perp a$ in (010)	albite-Ala
(001)	Manebach	*b*	**acline** (often lamellar)	$\perp b$ in (001)	=Ala A
=cleavage		*a*	Ala A	$\perp a$ in (001)	=**acline**
$\|\|b \sim (001)$ rhombic section		*b*	**pericline** (often lamellar)		
$\|\|c \sim (100)$		*c*	*Carlsbad B*		
(021), (02$\bar{1}$)	Baveno				

Laws in **bold face:** very common.
Laws in *italics:* rare.

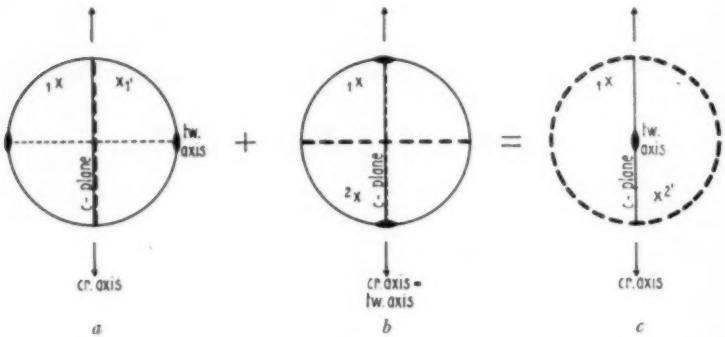

FIG. 7. Stereograms indicating the positions of the twin axis and symmetry plane (heavy dashes) with respect to the composition plane for the three types of plagioclase twinning. (*a*) Normal twinning, (*b*) parallel twinning and (*c*) complex twinning. c-plane=composition plane; tw. axis=twinning axis; cr. axis=crystal axis. One of the crystal axes is horizontal and lies in the composition plane. The effect of the symmetry operation is shown for one particular direction (1) in one of the individuals. It will be seen that complex twinning is equivalent to an addition of the symmetry operations of normal and parallel twinning.

Normal twinning

The twin axis of the normal twin is situated normal to the composition plane. Accordingly, the symmetry plane of the twin coincides with this composition plane (Fig. 7*a*). Therefore, in sections normal to this plane the individuals of such twins show the same birefringence, while the extinction angles are equal and of opposite sign, *i.e.*, the extinctions are symmetrical with regard to the trace of the composition plane.

In Figs. 3 and 4 the optical properties of both individuals of a normal twin are represented by one point only, the extinction angle of the second individual being found by reversal of sign. The composition plane of the normal twin should be a rational lattice plane: irrational planes such as the rhombic section are not found here.

Parallel and complex twinning. Basic concepts

The twin axis of a parallel twin is a crystallographic axis lying in the composition plane (Fig. 7*b*). The twin axis of a complex twin is also situated in this composition plane, but at right angles to a crystallographic axis (Fig. 7*c*). Perhaps the name complex twin is unfortunate: it should refer only to the position of the twinning axis, not to a possible complex appearance of the twin. A complex twin may well consist of two single individuals. The complex twin may also be thought of as having resulted from the successive operation of a normal law and a parallel law with the same composition plane (*cf.* the positions of 1, 1′ and 2′ in Fig. 7). When a twin shows several individuals with parallel composition planes, but with three or more different extinction positions or birefringences, more than one type of twinning must be present.

In the plane (010) the *a*- and *c*-axes enclose an angle of 116°. Thus, the complex twin axes $\perp a$ and $\perp c$, differing markedly in direction from the crystallographic axes, give rise to the complex albite-Carlsbad and albite-Ala twins (Fig. 2, left). On the other hand, in the plane (001) the *a*- and *b*-axes are very nearly perpendicular to each other (Fig. 2, right). Therefore, the complex twin belonging to one of these axes is optically indistinguishable from the parallel twin of the other.

Since an immediate distinction between parallel and complex twin laws is usually impossible, these laws will be treated together.

Parallel and complex twinning. Optical characteristics

In both twin types the twin axis lies in the composition plane, so that the symmetry plane must be at right angles to this plane. Thus, sections normal to the composition plane may make any angle with the symmetry plane of the twin. Theoretically, the twin individuals in these sections

should generally have asymmetrical extinctions and different birefringences. This may be illustrated by considering the change in position of the directions 1 and 2 on turning the section of Fig. 7*b* about the normal of the composition plane. Two sections in this zone need our special attention:

(1) The section parallel to the twin axis, being perpendicular to both the composition and symmetry planes, has symmetrical extinctions, and is optically indistinguishable from a normal twin with the same composition plane.

(2) The section normal to the twin axis coincides with the symmetry plane, hence the extinction angles are equal and at the same side of the composition plane, and the twin is invisible.

In Figs. 3, 4 and 5 the position of the symmetry plane of a twin is indicated by a horizontal line at a distance of 90° from the position of the twin axis. Thus, in Fig. 3 the symmetry plane of the Ala B twin is represented by the line marked $\perp a$. The intersections of the extinction curves with this line give the extinction angles of one of the twin individuals in the section normal to the symmetry plane. The extinction angle of the other individual is found by reversal of sign. If the section is not normal to the symmetry plane, the two points representing the twin individuals should be situated at equal distances on either side of the line representing the symmetry plane. Again, one of the extinction signs as found in the diagram should be reversed. The necessity of this reversal of sign is indicated by $\ominus$ after the name of the twin in the margin of the diagrams. Thus, Ala B $\ominus$ means that the positions of the individuals of an Ala twin should be symmetrical with regard to the line marked $\perp a$, while the sign of one of the two extinction angles thus found should be reversed.

In a similar way, the extinction angle of the section normal to the twin axis, in which the twin is invisible, is found along the line representing that axis. If the section is not normal to the twin axis, the positions of both twin individuals must be situated at equal distances on either side of the line representing this axis. The extinction angles thus found in the diagram are used without reversal of sign, which fact is indicated by $\oplus$ after the name of the twin in the margin of the diagrams.

Summarizing, we can state that the points of the diagrams indicating the optical properties of the individuals of a twin should be situated at equal distances on either side of:

1) the line representing the symmetry plane, with reversal of the extinction sign of one individual ($\ominus$);
2) the line representing the twinning axis, without any reversal of extinction sign ($\oplus$).

The Procedure of Twin Determination

With the aid of the three diagrams it is possible to determine the law of twinning in many cases. The procedure is essentially a trial-and-error method. Of course, simple twins, consisting of two individuals only, are the most likely to present difficulties. Generally speaking, the composition plane is easier to determine than the twin axis. It is well brought out in Fig. 3 that in most sections of not too Ca-rich plagioclase the Ala-B twin is nearly invisible. Could this be the reason that this twin is so rarely recorded? A discussion of the specific properties of each twinning law would be rather tedious: these properties follow from the more general considerations presented and from the diagrams. An exception will be made for lamellar twinning and for twins cut approximately normal to *a*.

The determination of lamellar twinning

In the case of lamellar twinning, we are generally dealing with the albite, acline or pericline law. Of these, albite twinning is readily distinguished from the other two, while acline and pericline twinning often show little difference.

In plagioclase with less than 75% An, albite twins cut normal to the composition plane must show each of the following properties:

1) symmetrical extinctions (normal twin)
2) appreciable birefringence } composition plane (010)
3) negative elongation }

These properties are *never* simultaneously present in acline or pericline twins, as may be judged from Figs. 4 and 5. Over a large part of these diagrams the extinction angles are over 45° (positive elongation). In the remaining parts, either the birefringence is too low, or the extinctions are obviously asymmetrical or even situated at the same side of the composition plane (in the central part of the diagrams). These distinctions are an essential preliminary to all determination methods based upon the properties of albite or Carlsbad twinning. Thus far they have seldom been clearly stated in textbooks.

It appears from a comparison of Figs. 4 and 5 that the extinction angles and birefringences generally do not serve to distinguish between acline and pericline twins. As a rule, this distinction is only possible in sections where the angle between the (001) cleavage and the rhombic section is visible. As the interesecting line of both planes is the *b*-axis, this angle will be best visible in sections approximately normal to this axis, which is the twin axis of both laws. These sections are represented by the central parts of both diagrams: they have negative elongation with extinc-

tions situated at the same side of the composition plane. The angle between the rhombic section and (001) for plagioclases of different composition may be read from Fig. 3. According to some authors smaller angles are also found, giving rise to twins intermediate between acline and "ideal" pericline twins. This discrepancy is due, at least partly, to a change in the chemical composition of the crystals after their formation.

Recognition of twins in the section normal to a

Sections normal to *a* are readily recognized. In plagioclase with less than 75% An the cleavage with negative elongation is (010), that with positive elongation (001). When the composition plane is (010) and the extinctions are symmetrical, the twin is an albite twin. Both twin individuals are normal to *a*, their (001) traces make an angle of 8°. When the composition plane is (010) and the extinction angles are different and situated on either side of this plane, the twin is a Carlsbad twin. When they are different and on the same side of the composition plane, it is an albite-Carlsbad twin. In both cases, only one individual can be normal to *a*: in the other individual no (001) cleavage should be visible.

When the composition plane is (001) and the extinctions are symmetrical, the twin is an acline or Manebach twin. The (010) cleavage traces in both individuals make an angle of 8° with each other. If the twin is lamellar, it is an acline twin. When, the other properties being equal, the trace of the composition plane is rather vague, while the (001) cleavage is distinctly normal to the section, the twin is a pericline twin.

In sections exactly normal to *a* the Ala twins are invisible, *a* being their twinning axis. In sections slightly differing from that position these twins become visible by small differences in extinction angle. The extinctions are always on the same side of the composition plane. Characteristically, the transverse cleavage-traces or composition planes of other twins are parallel in both individuals, because their direction is not altered by the twinning operation.

The Aid of the Universal Stage

The method has thus far been outlined for use without the universal stage. Yet it will be clear that this accessory is of great value if a systematical investigation of feldspar twinning is undertaken. With the aid of the universal stage it will be possible to bring the composition plane of most twins in the vertical NS position. On turning on A4 (or OEW) the behavior of the twin in the zone normal to the composition plane becomes evident at once. The elongation occurring in this zone may be judged from a rotation around A4 with the table in the 45° position.

Furthermore, sections may be made normal to *a*, to the twinning axis

or to the symmetry plane of the twin. In favorable cases, these procedures will lead immediately to the composition as well as to the law of twinning.

When the composition plane is irregular, or when the results prove to be ambiguous, recourse can still be made to the zone method of Rittmann (1929) or to the method of Emmons and Gates (1939), where the twin axis, found in a similar way with a 5-axis stage, is subsequently plotted on a Wulff net.

Sources and Acknowledgments

To my knowledge the kind of diagram proposed here was first used by Köhler (1923), as far as the extinction angles are concerned. By folding the diagram of Fig. 3 along the line marked *c*, this author obtained a valuable chart for the determination of the composition of plagioclase from the corresponding extinction angles of the Carlsbad twin.

Figs. 3 and 4 were newly constructed according to data compiled by van der Kaaden (1950, p. 46, 47). The extinction angles of Fig. 5 were found with the aid of the Fresnel construction on the Wulff net, starting from data compiled by Reinhard (1931, p. 114*). The curves were drawn by rather rough interpolation between the measured points: no great precision should be expected. The diagrams should be used in a qualitative rather than a quantitative way. The birefringences in all diagrams were taken from the charts of Nieuwenkamp (1948).

I am grateful to Prof. Nieuwenkamp (Utrecht), Prof. den Tex (Leiden) and Prof. de Roever (Amsterdam) for their advice and criticism, and to Prof. H. Winchell (New Haven) for his critical reading of the manuscript.

References

Duparc, L. and Reinhard, M. (1924), La détermination des plagioclases dans les coupes minces: *Mem. Soc. Phys. Hist. Nat. Genève*, **40,** 1–149.

Emmons, R. C. and R. M. Gates (1939), New method for the determination of feldspar twins: *Am. Mineral.*, **24,** 577–589.

Gorai, M. (1951), Petrological studies on plagioclase twins: *Am. Mineral.*, **36,** 884–901.

Kaaden, G. van der (1951), Optical studies on natural plagioclase feldspars with high- and low-temperature optics: *'s Gravenhage*, 105 p. (thesis Utrecht).

Köhler, A. (1923), Zur Bestimmung der Plagioklase in Doppelzwillingen nach dem Albit- und Karlsbader-Gesetz: *Tscherm. Min. Petr. Mitt., N.F.*, **36,** 42–64.

Köhler, A. (1942), Drehtischmessungen an Plagioklaszwillingen von Tief- und Hochtemperaturoptik: *Tscherm. Min. Petro. Mitt., N.F.*, **53,** 159–179.

* The plagioclases with 4, 29, 64 and 97% An are omitted as they belong to the high-temperature form. N.B. In the table of p. 114 the symbols (100) and (001) should be reversed.

KÖHLER, A. (1949), Recent results of investigations on the feldspars: *Jour. Geol.*, **57,** 592–599.

NIEUWENKAMP, W. (1948), Stereograms for the determination of plagioclase feldspars in random sections. Spectrum Publishers, Utrecht, 29p.

REINHARD, M. (1931), Universaldrehtischmethoden. Basel.

RITTMANN, A. (1929), Die Zonenmethode. *Schweiz. Min. Petr. Mitt.*, **9,** 1–46.

TOBI, A. C. (1959), Petrographical and geological investigations in the Merdaret-Lac Crop region. (Belledonne Massif, France): *Leidse geol. Meded.*, **24,** 181–282.

TURNER, F. J. (1951), Observations on twinning of plagioclase in metamorphic rocks: *Am. Mineral.*, **36,** 581–589.

Manuscript received February 4, 1961.

THE AMERICAN MINERALOGIST, VOL. 46, NOVEMBER–DECEMBER, 1961

NOTES AND NEWS

EXPLANATION OF STRAIN AND ORIENTATION EFFECTS IN PERTHITES

J. V. SMITH, *Department of Geology, University of Chicago.*

Laves (1952, p. 562), Coombs (1954) and others have noted that the compositions of the two phases of a perthite, determined from ($\bar{2}01$) spacings, are sometimes impossible: for example values have been obtained indicating minus ten per cent $NaAlSi_3O_8$ in the potassium-rich phase and more than one hundred per cent in the sodium-rich phase. Laves pointed out that there must be serious distortions of the Si, Al-O framework, but so far no detailed explanation has been put forward. It is the purpose of this note to show that the anomalous results can be explained semi-quantitatively if the volume of a perthite unit remains constant even when the lattice is distorted to enable it to maintain continuity with the other component. In addition an explanation of the position of the perthite composition plane is given.

The major contact plane of orthoclase micro-perthites can be seen in a microscope to lie near ($\bar{6}01$), making an angle of about 73° to the trace of the (001) cleavage in an (010) section. Because the schiller plane in crypto-perthites is also near ($\bar{6}01$) it is quite certain that the contact plane of the exsolved component and its host is the same for both crypto- and micro-perthites. The shape of the exsolved units varies from regular discs with the minor axis normal to the ($\bar{6}01$) plane to somewhat irregular units. Laves (1952, Fig. 16) has shown from *x*-ray photographs of an orthoclase crypto-perthite that the lattice rows coincide for two directions near [106] and [301], the former direction lying in the plane ($\bar{6}01$). The author has confirmed this for several cryptoperthites and has also shown that the repeat distances along [106], but not [301], agree in length. Examination of many *b*-axis oscillation photographs of cryptoperthites has shown that the *b*-axes of the monoclinic potassium-rich component and of the pericline-twinned sodium-rich unit are parallel and of equal length: in addition, the reciprocal lengths $1/b^*$ of the b^* axes of the albite-twinned sodium-rich phases are also equal to the monoclinic *b*-repeat. Consequently the ($\bar{6}01$) lattice planes of the two components in the cryptoperthites are identical if the deviation from monoclinic symmetry of the Na-rich phase is neglected. The small deviation that occurs is in opposite directions for the two components of either an albite or a pericline twin so that the average deviation is zero.

If the volume of a perthite unit is independent of distortion, the direction normal to the ($\bar{6}01$) plane must undergo readjustment to take account of the change in area at the ($\bar{6}01$) plane. Because all three axes expand from Na-feldspar to K-feldspar, the spacing of the ($\bar{6}01$) planes

must expand even more in a perthite when the ($\bar{6}01$) plane is common to both. From the cell dimension data listed in Table 1, it may be seen that the cell volumes vary comparatively little with the Si, Al ordering. Because orthoclase is thought to be partly ordered, the most suitable comparison is between its cell dimensions and those of an albite part-way between high and low-albite. The *a*-azis expands 5.1%, the *b*-axis 1.2%, the *c*-axis 0.9% and the volume 8.1% in going from the Na- to the K-feldspar. Consequently in a perthite with identical composition plane and no change of the volume of each unit, the spacing of the ($\bar{6}01$) planes should differ by 8.1%, a value considerably greater than the expansion for the isolated phases. The Bowen and Tuttle (1950) method for estimating composition utilizes change in the ($\bar{2}01$) spacing. As the ($\bar{2}01$) and ($\bar{6}01$) planes lie at an angle of 24°, the spacing expansion for the ($\bar{2}01$) planes should be approximately 8.1 cos 24° = 7.4%. For isolated units the spacing expansion for the ($\bar{2}01$) planes is 4.5% in going from the Na-feldspar to the K-feldspar. Consequently, the measured compositional gap should be about 7.4/4.5 = 1.64 times too large, if the assumption mentioned here holds true. Values observed by Laves and Coombs for the exsolved phases of certain cryptoperthites indicate compositional gaps of 120%. Correcting by 1.64 gives a value of 73% which turns out to be quite reasonable. By examination of many analyzed specimens to see if they were homogeneous or unmixed, MacKenzie and Smith (1955, 1956) found that the immiscibility gap for orthoclase perthites was about 85%, and for sanidine perthites about 40%. The specimens examined by Coombs and Laves would be expected to show an immiscibility gap similar to that for orthoclase perthites but perhaps somewhat less because of incomplete transformation from a sanidine perthite to an orthoclase perthite. The predicted value of 73%, therefore, is quite reasonable, showing that the volume is independent of distortion, at least to a first approximation.

In microcline perthites, where the perthite is coarsely developed, there is good reason to believe that the compositions of the two phases are near Or_{95} and Or_2. Nevertheless the $\bar{2}01$ spacings do not show the gross anom-

TABLE 1. CELL DIMENSIONS OF CERTAIN FELDSPARS

Name	Composition	*a* (Å)	*b* (Å)	*c* (Å)	α	β	γ	V
low albite	Or_0	8.138	12.789	7.156	94°20[1]	116°34[1]	87°39[1]	664.2
high albite	Or_0	8.149	12.880	7.106	95°22[1]	116°18[1]	90°17[1]	666.7
orthoclase	Or_{92}	8.562	12.996	7.193	—	116°01[1]	—	719.3
sanidine	Or_{92}	8.564	13.030	7.175	—	116°00[1]	—	719.7

[1] Data from Cole, Sorüm and Kennard (1949) and Ferguson, Traill and Taylor (1958).

alies found for the orthclase and sanidine perthites described previously. The cell dimensions of these microcline perthites are close to or identical with those for the isolated units (Goldsmith and Laves, in course of publication). In these coarse perthites, the units are many thousands of unit cells thick and the surface strain will have little effect on the center of the unit. It seems probable that as the perthitic units grow, the surfaces can no longer resist the forces tending to return the units to their normal geometry: the bonds at the surface will break and there will no longer be any continuity of the Si, Al-O framework across the boundary. Such a process would be encouraged by the movement of Si, Al atoms during ordering and by external shearing stress acting on the feldspar crystals. The result of this process would be a fine network of internal discontinuites, especially suitable for the migration of ions. Complete recrystallization of a feldspar, as suggested by Tuttle (1952), would be made easier by the existence of these discontinuities. The *x*-ray photographs of many microcline perthites show some disorientation—the largest, 2–3°, has been observed in charnockitic specimens kindly supplied by Howie (1955). Deviations from parallelism of the *b* and *b** axes of the K-rich and Na-rich components have been found to occur for some microperthites in conformity with the findings of Laves and Soldatos (1961). These disorientations may be the result of readjustment when the perthitic units break contact. A detailed study of the cell dimensions of perthitic components would be well worth while, for it should reveal intermediate effects between the gross distortion in cryptoperthites and the lesser effects in microcline micro-perthites.

Laves (1952) has postulated that the $(\bar{6}01)$ plane is chosen as the contact plane in perthites because this leads to the smallest angular deviation between corresponding lattice rows. Actually the situation is more complex. As shown earlier, the largest difference in the axial lengths is for *a*, which changes about five times as much as for *b* and *c*. Consequently to get the smallest dilatational strain, the contact plane should be nearly perpendicular to the *x*-axis. In Fig. 1 (curve a) are the actual calculated values for directions in the (010) plane. It may be seen that the smallest percentage deviation occurs near the direction [106], which indeed is the trace of the schiller plane. It is a remarkable concidence that the smallest angular deviation also occurs when the schiller plane is $(\bar{6}01)$. Curves (b) and (c) of Fig. 1. show the angular deviatien between corresponding lattice directions, calculated for unstrained sodium and potassium feldspars. To obtain curve (b) it was assumed that the *z*-axes were parallel. It may be seen that the angular deviations are not symmetical, with a maximum value of 58′ in one direction and 104′ in the other direction. By rotating one feldspar 23′ with respect to the other, the angular devia-

tions can be made symmetrical and thereby a minimum as shown in curve (c). Zero deviations occur for two directions, one about 2° from the trace of the schiller plane [106] and the other 90° away. Curve (d) shows the actual deviations measured by Laves for a cryptoperthite. The correspondence with curve (c) is very good, except that the deviations for all directions are about 50% greater than those for the isolated feldspars. This arises from the distortion described earlier.

One might ask whether the dilatational or the angular distortion governs the choice of $(\bar{6}01)$ as the schiller plane. Although it seems likely that angular factors contribute to the strain, the dilatational effect must be paramount: otherwise the other plane with zero angular distortion could be a possible contact surface. Although the author is skeptical

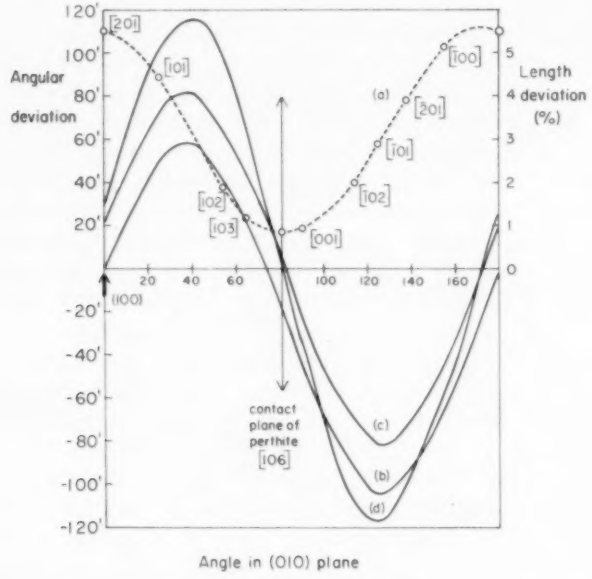

FIG. 1. Geometrical differences between K- and Na-feldspars. Curve (a) shows the deviation in repeat distance for several zone axes in the $(h0l)$ plane. Curve (b) shows the angular deviation between corresponding lattice directions if the c-axis of the two feldspars are in contact. Curve (c) shows the angular deviation if one feldspar is rotated so that the maximum positive deviation equals the maximum negative deviation. Curve (d) contains the data measured by Laves (1952) for a natural cryptoperthite. Curves (a), (b) and (c) were calculated by using the orthoclase in Table 1 as a representative K-feldspar and an intermediate albite as the Na-component. For simplicity, the deviations of α and γ from 90° were neglected: albite and pericline twinning cancel out the effects of the triclinic geometry, anyway.

about the validity of such simple considerations as those used here, he is nevertheless gratified to find how well they do explain phenomena that must really be based on very complex systems of chemical forces.

Thanks are expressed to Drs. J. R. Goldsmith, F. Laves and W. S. MacKenzie for critical examination of the manuscript and to the National Science Foundation for support from grant G14467.

References

Bowen, N. L. and Tuttle, O. F. (1950), The system $NaAlSi_2O_8$—K $AlSi_3O_8$-H_2O: *Jour. Geol.*, **58**, 489–511.

Cole, W. F., Sörüm, H. and Kennard, O. (1949), The crystal structures of orthoclase and sanidinized orthoclase: *Acta Cryst.*, **2**, 280–287.

Coombs, D. S. (1954), Ferriferous orthoclase from Madagascar: *Mineral. Mag.*, **30**, 409–427.

Ferguson, R. B., Traill, R. J., and Taylor, W. H. (1958), The crystal structures of low-temperature and high-temperature albite: *Acta Cryst.*, **11**, 331–348.

Howie, R. A. (1955), The geochemistry of the charnockite series of Madras, India: *Trans. Roy. Soc. Edinburgh*, **62**, 725–768.

Laves, F. (1952), Phase relations of the alkali feldspars: *Jour. Geol.*, **60**, 436–450, 549–574.

Laves, F. and Soldatos, K. (1961), Die Albit/Mikroklin-Orientierungs-Beziehungen und ihre genetische Deutung: *Zeit. Krist.*, in press.

MacKenzie, W. S. and Smith, J. V. (1955), The alkali feldspars I: *Am. Mineral.*, **40**, 707–732.

——— and ——— (1956), The alkali feldspars III: *Am. Mineral.*, **41**, 405–427.

THE AMERICAN MINERALOGIST, VOL. 46, NOVEMBER-DECEMBER, 1961

INDEXED POWDER DIFFRACTION DATA FOR SCAPOLITE

Gerald V. Gibbs, *Metallurgy Research Laboratory, Norris, Tenn.*

and

F. Donald Bloss, *Dept. of Geology, Southern Illinois University, Carbondale, Ill.*

During a study of the similarities between natural scapolites and fibrous potassium lead silicates synthesized by Shell (1957), no indexed powder diffraction data for scapolite for comparison could be found in the literature nor in the *x*-ray powder data file. Recently, Eugster and Prostka (1960, p. 1859) published data on seven indexed peaks for two synthetic scapolites. However, it is felt that additional indexed data, particularly for natural scapolites, might be a desirable addition to the literature since future comparisons might be desired. This note thus presents indexed data for some 40 peaks for scapolites from Arendal, Norway and from Grenville, Quebec.

TABLE 1. X-RAY POWDER DIFFRACTION DATA FOR SCAPOLITE

Arendal				Grenville			
hkl	d_{obs}	I/I_0	d_{calc}	*hkl*	d_{obs}	I/I_0	d_{calc}
110	8.556	5	8.553	110	8.600	5	8.605
101	6.439	5	6.419	200	6.087	20	6.085
200	6.040	20	6.048	211	4.422	<5	4.419
211	4.397	5	4.402	220	4.306	5	4.303
220	4.282	10	4.276	310	3.846	45	3.849
310	3.824	60	3.826	301	3.577	10	3.577
301	3.558	20	3.560	112	3.465	95	3.465
112	3.464	100	3.463	202	3.210	10	3.214
321	3.069	70	3.067	321	3.085	75	3.083
400	3.027	55	3.024	400	3.043	55	3.043
222	2.833	10	2.835	330	2.869	<5	2.869
411	2.734	15	2.736	222	2.843	<5	2.842
420	2.703	25	2.705	411	2.750	5	2.750
312	2.693	30	2.691	420	2.721	5	2.722
510	2.370	<5	2.372	312	2.700	100	2.699
431	2.306	15	2.304	510	2.387	<5	2.387
332	2.278	5	2.277	431	2.317	15	2.317
422	2.204	5	2.201	332	2.287	15	2.286
521	2.152	10	2.153	422	2.209	<5	2.209
303	2.141	20	2.140	521	1.164	15	2.165
530	2.074	5	2.073	303	2.142	20	2.143
611	1.932	15	1.923	530	2.086	5	2.087
620	1.912	30	1.912	512	2.091	10	2.019
004	1.892	10	1.893	611	1.933	15	1.935
541	1.832	5	1.833	620	1.923	30	1.925
532	1.820	5	1.819	413	1.918	15	1.918
631	1.753	10	1.754	004	1.893	15	1.893
710	1.712	15	1.711	541	1.843	10	1.844
640	1.677	5	1.677	532	1.827	<5	1.828
721	1.622	5	1.623	631	1.764	10	1.765
613	1.562	5	1.562	503 / 433	1.752	<5	1.752
712	1.558	5	1.559				
543	1.512	5	1.512	710	1.721	5	1.721
732	1.464	10	1.465	640	1.687	<5	1.688
325	1.381	<5	1.381	721	1.632	<5	1.633
624	1.346	15	1.345	404	1.607	<5	1.607
910	1.335	<5	1.336	613	1.567	15	1.568
653	1.319	<5	1.320	543	1.518	<5	1.518
921 / 761	1.293	<5	1.293	811 / 741	1.514	5	1.514
435 / 505	1.284	<5	1.284	732	1.472	10	1.472
				505	1.459	5	1.459
				325	1.381	<5	1.381
				822	1.376	15	1.375
				624	1.349	5	1.349
				910	1.344	<5	1.344
				653	1.325	<5	1.326
				921 / 761	1.301	<5	1.301
				505 / 435	1.286	5	1.286

The Arendal scapolite was white in color and non-fluorescent whereas the Grenville scapolite was yellow and fluoresced a brilliant canary yellow under long wave ultraviolet radiation. Each scapolite was mottled with

less transparent areas which, when examined as grains under the polarizing microscope, appeared to contain a finely dispersed alteration product. Thus it was necessary to coarse-crush each scapolite and isolate the clear grains, then crush these clear grains to −400 mesh for the *x*-ray and chemical analysis. Smear mounts of the −400 mesh crushed fragments of each scapolite were scanned at $\frac{1}{4}$ degree per minute with a Norelco high-angle diffractometer operated in conjunction with an automatic strip chart recorder. Instrumental settings were: divergence and scatter slits, 1 degree; receiving slits, 0.006 inches; strip chart scale, $\frac{1}{2}$ degree per inch; time constant, 4; multiplier, 1; scale factor, 8 and 16; filtered CuKα radiation.

The 2θ values for resolved Kα_1 peaks on the strip charts were read at the midpoints at $\frac{2}{3}$ the height of the peak (Donnay and Donnay, 1951); the 2θ values for unresolved or partly resolved peaks were read at the midpoints at $\frac{1}{2}$ the height of the peak (Smith and Sahama, 1954). These

TABLE 2. CHEMICAL ANALYSIS AND CALCULATION OF THE UNIT CELL CONTENT OF THE ARENDAL SCAPOLITE

(Analyst R. E. Hooper) U. S. Bureau of Mines, Norris, Tenn.

	Analysis wt. %	Mass units per unit cell (atomic-wt. units)	Gram-molecular wt. of oxide, or constituent of column 1	No. of oxides, etc. per unit cell	No. of metal ions per unit cell	No. of anions per unit cell
SiO_2	50.38	894.48	60.06	14.89	14.89	29.78
Al_2O_3	24.18	429.31	101.94	4.21	8.42	12.63
Fe_2O_3	0.29	5.15	159.70	0.03	0.06	0.09
TiO_2	0	—	—	—	—	—
CaO	13.06	231.88	56.08	4.13	4.13	4.13
MgO	0	—	—	—	—	—
Na_2O	7.09	125.88	61.97	2.03	4.06	2.03
K_2O	0.51	9.06	94.20	0.10	0.20	0.10
CO_2	0.94	16.69	44.01	0.38	0.38	0.76
Cl	4.32	76.70	35.46	2.16	—	2.16
F^-	0.31	5.50	19.00	0.29	—	0.29
SO_3	0	—	—	—	—	—
H_2O	n.d.					
	101.07					
Less O equivalent to F and Cl, resp.	.13					
	.95					
	99.99[1]					

[1] The total reported by the analyst, *i.e.* 100.25%, has been readjusted to 100.00%.

peak readings were then corrected to an internal standard—a synthetic spinel ($MgAl_2O_4$) with cell dimensions that had been carefully determined with respect to transistor grade silicon.

The data of Table 1 for the Arendal specimen were indexed on the basis of a tetragonal, body-centered cell: a 12.095, c 7.571A $\pm$0.05%; for the Grenville on a similar cell: a 12.163, c 7.569A $\pm$0.05%. In the case of the former precession photographs were taken to confirm the diffraction indices assigned to the peaks of the powder diffraction record. These photographs exhibited the symmetry $4/m$ and a systematic absence of reflections with $h+k+l$ odd. The space groups consistent with these diffraction data are $I4$, $I\bar{4}$ and $I4/m$. Piezoelectric tests were made on the Arendal scapolite as a possible means of discerning whether scapolite possesses space group symmetry $I4$, $I\bar{4}$ (noncentric), or $I4/m$

TABLE 3. CHEMICAL ANALYSIS AND CALCULATION OF THE UNIT CELL CONTENT OF THE GRENVILLE SCAPOLITE

(Analyst R. E. Hooper)

	Analysis wt. %	Mass units per unit cell (atomic wt. units)	Gram-molecular wt of oxide, or constituent of column 1	No. of oxides, etc. per unit cell	No. of metal ions per unit cell	No. of anions per unit cell
SiO_2	44.46	806.74	60.06	13.43	13.43	26.85
Al_2O_3	29.14	528.75	101.94	5.19	10.38	15.57
Fe_2O_3	0.23	4.17	159.70	0.03	0.06	0.09
TiO_2	0	—	—	—	—	—
CaO	16.36	296.87	56.08	5.29	5.29	5.29
MgO	0	—	—	—	—	—
Na_2O	2.43	44.09	61.97	0.71	1.42	0.71
K_2O	2.23	40.46	94.20	0.43	0.86	0.43
CO_2	0.95	17.24	44.01	0.39	0.39	0.78
Cl	0.35	6.35	35.46	0.18	—	0.18
F^-	0.15	2.72	19.00	0.14	—	0.14
SO_3	1.07	19.42	80.07	0.24	0.24	0.72
H_2O^-	0.11	—	—	—	—	—
H_2O^+	2.66	48.27	18.02	2.68	5.36	2.68
	100.14					
Less O equivalent to F and Cl	.06 .08					
	100.00[1]					

[1] The total reported by the analyst, *i.e.* 100.16%, has been readjusted to 100.00%.

(centric).* The test was made at 50° intervals between 20° C. and the boiling temperature of liquid nitrogen with the piezoelectric detector at the Pennsylvania State Crystallographic Laboratory, University Park, Pennsylvania. The results of the tests gave no indication of non-centrosymmetry, although it is realized that a negative result is not conclusive. However, Professor Pepinsky is of the opinion that the piezoelectric detector used for the test is very sensitive and that a negative result is a good indication of centrosymmetry. Thus, it appears probable that scapolite belongs to the centrosymmetric space group $I4/m$ which is in agreement with Pauling's (1930) postulated structure for scapolite. However, definite confirmation of this conclusion will have to await a detailed structural analysis of scapolite.

Other physical constants measured for these scapolites were, for the Arendal scapolite: ω_D1.566, ϵ_D1.544, ρ2.66 and for the Grenville scapolite: ω_D1.588, ϵ_D1.559, and ρ2.69.

The unit cell content of the two scapolites was found by calculating the atomic-weight units in the unit cell from the relation $\rho V/1.66$ and allocating these units to the various oxides, etc., on the basis of their respective weight percentages reported in the chemical analysis (Tables 2 and 3). The notation ρ and V refer to the measured density and unit cell volume, respectively, of the scapolites. No determination of H_2O was made in the chemical analysis of the Arendal scapolite because the 1.89 gm sample available for the analysis was expended in the analytical determination of the other chemical constituents.

References

Burley, B. J., Freeman, E. B. and Shaw, D. M. (1961), Studies on Scapolite: *Canadian Mineral.* **6,** 670–679.

Donnay, G. and Donnay, J. D. H. (1952), The Symmetry Change in the High-Temperature Alkali-Feldspar Series: *Am. J. Sci.*, **Bowen Vol.,** 118.

Eugster, H. P. and Prostka, H. J. (1960), Synthetic Scapolites: *Proc. G.S.A., Denver,* Abstract, p. 92.

Gibbs, G. V. and Lewis, R. M. (in press), Quadratic Functions for Copper Radiation $-0°$ to $180°2\theta$.

Pauling, L. (1930), The Structure of Some Sodium and Calcium Alumino-Silicates: *Proc. Nat. Acad. Sci.*, **16,** 453.

Shell, H. R. (1957), Synthetic Asbestos Investigations III. Synthesis and Properties of Fibrous Potassium-Lead Silicate: *Department of the Interior, Bureau of Mines Report of Investigations* **5293.**

Smith, J. V. and Sahama, Th. C. (1954), Determination of the Composition of Natural Nephelines by an *X*-Ray Method: *Min. Mag.*, **XXX,** No. 226, 440.

* While this article was in press, "Studies on Scapolite" by B. J. Burley, E. B. Freeman and D. M. Shaw appeared in *Canad. Mineral.* **6,** part 5, 670–679, with powder photograph data and a discussion of symmetry.

THE AMERICAN MINERALOGIST, VOL. 46, NOVEMBER–DECEMBER, 1961

A METHOD OF MINERAL SEPARATION USING HYDROFLUORIC ACID*

GEORGE J. NEUERBURG, *U. S. Geological Survey, Denver, Colo.*

The major minerals and many minor minerals of most rocks are readily decomposed by hydrofluoric acid. Some of the minor minerals, however, which generally must be isolated for positive identification and study, are decomposed extremely slowly or not at all by hydrofluoric acid. These include most sulfides and sulfosalts, many beryllium minerals, anatase, barite, bastnaesite, carbon, graphite, rutile, topaz, zircon, and doubtless others not yet investigated. This fortuitous contrast in solubility is the basis for a separation method that offers some useful advantages over physical methods of mineral separation.

Briefly, the method consists of decomposition of a rock fragment, weighing about 200 grams, by repeated application of hydrofluoric acid over a period of several weeks. Water-insoluble reaction products are removed by boiling in a solution of aluminum chloride. The method is slow and somewhat hazardous, but requires little attention. Only a few minutes work with a sample is required each day the process is in operation, and the operator is free for other less routine work.

For those minerals to which it is applicable, this method is advantageous in several respects. Separated mineral grains are exceptionally clean and pure, and crystal breakage is held to a minimum, which facilitates and enlarges possibilities for studies of crystal morphology. The true size distribution and abundance in a rock can be determined for those minerals that do not react at all with hydrofluoric acid. Easy separation can be made of at least three mineral groups that are normally very difficult to separate: (1) minerals of such fine grain as to be almost inseparable physically, as pigmenting carbon in slates; (2) minerals present in extremely minute proportions in a rock; and (3) minerals whose densities do not differ appreciably from the common rock minerals, beryl for example. The suitability for chemical studies of minerals separated by this method has not been investigated.

The following minerals, apparently unchanged in form, have been recovered by this method from a limited variety of ordinary crystalline rocks: anatase, arsenopyrite, barite, bastnaesite, bertrandite, beryl, bornite, carbon, chalcocite, chalcopyrite, chrysoberyl, covellite, euclase, graphite, molybdenite, pyrite, rutile, silver, sphalerite (Fe-poor), topaz, and zircon. *X*-ray patterns made of most of these minerals showed

* Publication authorized by the Director, U. S. Geological Survey.

no evidence of their having reacted with hydrofluoric acid or aluminum chloride. I am indebted for contributions to this list to Theodore Botinelly, Keith Ketner, and W. N. Sharp, who have found this method useful.

Finely ground samples of a few additional minerals were tested by digesting them in cold 48 per cent hydrofluoric acid for two days, decanting, washing, and drying before bringing to a 1-minute boil in aluminum chloride solution. Apatite, cinnabar, cuprite, monazite, uraninite, and xenotime were partly or completely decomposed in this test. The minerals that survived are boulangerite, cassiterite, digenite, enargite, gold, loellingite, melonite, pyrargyrite, stibnite, tetrahedrite, tourmaline, and zinckenite. Some in the latter group, however, might not last through the full decomposition of a rock, as this involves much more intense and prolonged treatment with hydrofluoric acid. Also, some rocks might react with hydrofluoric acid to produce compounds that would in turn decompose some of these minerals.

The effect of hydrofluoric acid on some sulfides was tested quantitatively by treating finely ground samples of pure minerals in parallel with a group of rocks being separated by the procedure given at the end of this note. The results are shown in Table 1. No changes were visible in the appearance of chalcopyrite, molybdenite, and pyrite; the losses for these minerals could be mainly from repeated handling of such small quantities of finely divided material. Galena was etched and coated with a thin iridescent film. Pyrrhotite was largely dissolved, the residue being partly coated with a brown film. The grain form and crystal structure of sphalerite persist, but the mineral is partly dissolved and is heavily filmed by a black substance.

The sulfide mineralogy of 37 samples of quartz monzonite and granodiorite from the Boulder batholith, Montana, was studied by means of polished sections, heavy media separation, and hydrofluoric acid separa-

TABLE 1. SOLUBILITY OF SULFIDES IN HF

	Sample weight	Recovered weight	Weight loss
Chalcopyrite	0.0497 g (0.0518 g)*	0.0473 g (0.0508 g)*	4.8% (1.9%)*
Galena	0.0986 g (0.0591 g)*	0.0705 g (0.0508 g)*	28.5% (14.0%)*
Molybdenite	0.0245 g	0.0244 g	0.4%
Pyrite	0.0431 g (0.0278 g)*	0.0410 g (0.0260 g)*	4.9% (6.5%)*
Pyrrhotite	0.0881 g	0.0056 g	93.6%
Sphalerite (Fe-rich)	0.0549 g	0.0450 g	20.0%

* Treated with technical instead of analytical grade HF.

tion. The results of the three methods of study are in substantial agreement, except that the relative abundance and variety of sulfides found with hydrofluoric acid are greater. The amount of total sufide separated with hydrofluoric acid indicates a sulfide abundance in the rock of 2 to 3 times that indicated by the results of heavy media separation.

Further study of the method, particularly of its quantitative effect in partly dissolving some minerals, is obviously needed. However, sufficient experience has been had with the method to demonstrate its usefulness in solving some difficult problems in mineral separation. I am particularly indebted to Professor Paul Ramdohr for his spoken suggestion (1960) that I try to isolate sulfides from the Boulder batholith rocks with hydrofluoric acid.

Procedure

The detailed procedure developed for use on the Boulder batholith rocks serves to illustrate the method. It should be considered only as a guide. Modifications may be necessary in treating rocks of different compositions and in separating minerals that react with difficulty but that do react finally with hydrofluoric acid or with aluminum chloride. For example, most of the magnetite of a rock can be preserved by removing it physically just before the final residue of rock is treated with hydrofluoric acid in step 3, below.

The initial, preferred sample is a single piece of rock, weighing about 200 grams. Crushed or ground samples pose the danger of violent reaction with hydrofluoric acid; addition of hydrofluoric acid to rock powders as coarse as 10 mesh can result in as much effervescence as that produced by the addition of concentrated hydrochloric acid to powdered chalk. Fragmentation of the sample unneccessarily breaks desired grains, especially of the brittle sufides, and introduces possibilities of inter-sample contamination and selective loss of some components. Apart from finely ground samples, the rate of decomposition of a rock by hydrofluoric acid appears to be slow and not materially affected by grain size; no more than one-third saving in time is had by fragmenting to a pea-sized product.

All work with hydrofluoric acid must be done in a well-ventilated hood, and the operator must take every caution to avoid contact with the acid or its fumes. An ordinary laboratory hood may be used and will apparently suffer no damage from long contact with hydrofluoric acid fumes. Analytical grade reagents are not required in the following procedure.

STEP 1. Add about 70 ml. of approximately 52% hydrofluoric acid to the sample in a polyethylene beaker, which is conveniently cut from emptied hydrofluoric acid bottles of

the size used for 1-lb quantities of the acid and of the type not requiring cardboard reinforcement. The reaction is allowed to proceed at room temperature for 24 hours, after which the liquid phase is evaporated overnight to moist dryness on a steam bath. The beaker now contains unreacted rock, water-soluble reaction products, and water-insoluble reaction products. These reaction products are removed in the next step before further addition of acid, lest they interfere with the efficiency of the further acid treatment of the unreacted rock.

STEP 2. The residue from step 1 is digested in 150 ml. of water for one hour on the steambath, with occasional stirring. The reaction products are washed into another polyethylene beaker; 70 ml. more of hydrofluoric acid is added to the remaining undecomposed rock and step 1 is repeated. The separated material is filtered and washed to remove most of the water-soluble reaction products. The undissolved material, consisting of HF-insoluble minerals, loose fragments of reaction products, and small rock particles, some of which are armor-plated with reaction products, is dried and set aside. Filtering rather than decanting is necessary because some of the sulfides float on the surface of the liquid. If loss of materials less than 200 mesh in size can be tolerated, appreciable time, bother, and reagent are saved by wet-sieving through 200-mesh silk bolting cloth instead of filtering through paper.

The first and second steps are repeated until no more rock is visible in the first beaker. This point is reached in 4 to 6 weeks, apparently varying with mineralogy and with texture; each 70 ml. of hydrofluoric acid decomposes from 10 to 30 grams of the sample.

STEP 3. The residues from step 2 are combined and gently pulverized by grinding with a rubber-tipped (soil) pestle. These residues still contain some water-soluble reaction products, which are removed by heating to boiling with 1 to 1½ liters of water and filtering or sieving. The residue remaining at this point is dried and then treated once more—or oftener if necessary—with hydrofluoric acid to dissolve any included rock particles. Some minerals such as magnetite and pyrrhotite may be quite resistant up to this step, then dissolve with considerable rapidity.

STEP 4. The material from step 3 is brought to a 1-minute boil in 200 ml. of a solution of aluminum chloride (227 grams of $AlCl_3 \cdot 6H_2O$ in 1 liter of water) in pyrexware, allowed to settle for 1 minute and filtered. Again it is preferable to wet-sieve through 200-mesh silk bolting cloth, here for the additional reason that the liquid phase may gelatinize on cooling. Gelatinization has been uncommon in practice and it can be avoided by diluting with hot water. The residue on the screen or filter is washed back into the beaker, 200 ml. of aluminum chloride solution is added to it, and the mixture is allowed to stand overnight before boiling and filtering once again.

STEP 5. The residue from step 4 is again treated with hydrofluoric acid, to remove HF-soluble minerals that were armor-plated with water-insoluble reaction products in earlier steps. The addition of hydrofluoric acid at this point *must* be made with extreme caution, because the first increment of acid usually reacts violently and may cause dangerous spattering.

Steps 4 and 5 can be repeated as often as necessary to clean the minerals concentrated by the first application of step 5. Attempts to shortcut the method by heavy media separations were unsatisfactory owing to very inefficient recoveries, presumably because of a tendency for adhesion of some insoluble reaction products to the HF-insoluble minerals.

Besides a mixture of minerals, the final product contains organic material, principally filter paper fibers. Lichens, or some modification thereof, are obtained from samples taken from the surfaces of natural outcrops. Paint or paper labels, if left on the sample, may also contaminate the product.

THE AMERICAN MINERALOGIST, VOL. 46, NOVEMBER-DECEMBER, 1961

N, N-DIMETHYLFORMAMIDE, A NEW DILUENT FOR BROMOFORM USED AS A HEAVY LIQUID

NELSON HICKLING, FRANK CUTTITTA AND ROBERT MEYROWITZ,
U. S. Geological Survey, Washington 25, D. C.

N, N-Dimethylformamide (DMF), $HCON(CH_3)_2$, which has already been used as a diluent for methylene iodide (diiodomethane) in heavy liquid separations (Meyrowitz, *et al.* 1960), is recommended as a diluent for bromoform also. This diluent can be used in place of dimethyl sulfoxide (DMSO), $(CH_3)_2SO$, for the preparation of heavy liquids of constant specific gravity for the same range of specific gravity for which the dimethyl sulfoxide-bromoform liquids were recommended (Meyrowitz, *et al.*, 1959). This new diluent for bromoform is suggested only as an alternate to dimethyl sulfoxide. At present (1961) the dimethyl sulfoxide-bromoform and dimethylformamide-bromoform liquids are to be considered as equivalent and can be used interchangeably. Because one set of liquids may be chemically reactive to a particular mineral, it is well to have both diluents on hand for substitution when necessary.

The physical properties of dimethylformamide are similar to those of dimethyl sulfoxide (Meyrowitz, *et al.*, 1960). Its vapor pressure is low; its boiling and flash points are high; and it is completely miscible with water and acetone.

The combining volumes of dimethylformamide-bromoform solutions are additive and a straight-line mixing curve (volume+volume) can be used to prepare a liquid of desired specific gravity. Acetone, dimethylformamide, and water are miscible in all proportions. The separated minerals can be washed free of a dimethylformamide-bromoform liquid using acetone. The bromoform can be recovered from the washings by mixing the washings with large volumes of water in the manner conventionally used when alcohol or acetone is the diluent. When a dimethylformamide-bromoform solution, prepared for a specific job, is no longer needed, the bromoform can be recovered in the same way.

To test the constancy of the dimethylformamide-bromoform solutions during use, a series of solutions were prepared. During a 3 month period from 30 to 40 mineral separations were made with each liquid. The specific gravities of these liquids before and after the 3 month period are given below. There is a slight darkening in the color of these solutions after use. This color is lighter than that developed in the dimethyl sulfoxide-bromoform liquids after use.

Specific gravity before use	*Specific gravity after use (3 months later)*	*Change in specific gravity*
2.5584 (27° C.)	2.5560 (28° C.)	−0.0024
2.6000 (27° C.)	2.5954 (28° C.)	−0.0046
2.6866 (26.5° C.)	2.6883 (28° C.)	+0.0017
2.5804 (27° C.)	2.5739 (28° C.)	−0.0065
2.6460 (28° C.)	2.6449 (28° C.)	−0.0011

Precautions to be taken when using dimethylformamide have been mentioned in a previous paper (Meyrowitz, *et al.*, 1960).

References

Meyrowitz, Robert, Cuttitta, Frank and Hickling, Nelson, 1959, A new diluent for bromoform in heavy liquid separation of minerals: *Am. Mineral.*, **44,** 884–885.

Meyrowitz, Robert, Cuttitta, Frank and Levin, Betsy, 1960, N, N-Dimethylformamide, a new diluent for methylene iodide heavy liquid: *Am. Mineral.*, **45,** 1278–1280.

THE AMERICAN MINERALOGIST, VOL. 46, NOVEMBER–DECEMBER, 1961

THE CHALCOKYANITE SERIES

P. J. Rentzeperis, *Department of Mineralogy, University of Thessaloniki, Thessaloniki, Greece*

In the table giving *x*-ray data for the chalcokyanite series (Strunz 1961), the data for $CoSO_4$ are those of the high temperature α-modification (Rentzeperis 1958), with space group *Pmnb*. Anhydrous $CoSO_4$ also has a low temperature β-modification isomorphous with $MgSO_4$ (Rentzeperis and Soldatos 1958), $MnSO_4$ (Rentzeperis 1958), $FeSO_4$ (Coing-Boyat 1959), and $NiSO_4$ (Dimaras 1957). The space group for this $NiSO_4$ series is *Cmcm*.

References

Coing-Boyat, J. (1959), *Acta Cryst.*, **12,** 939.

Dimaras, P. I. (1957), *Acta Cryst.*, **10,** 313.

Rentzeperis, P. J. (1958), *Neues Jb. Mineral., Monatshefte*, **210,** 226.

——— and Soldatos, C. T. (1958), *Acta Cryst.*, **11,** 686.

Strunz, H. (1961), *Am. Mineral.*, **46,** 758.

THE AMERICAN MINERALOGIST, VOL. 46, NOVEMBER–DECEMBER, 1961

THE WEISSENBERG CAMERA AS A POWDER CAMERA

ARRIGO ADDAMIANO, *General Electric Company, Lamp Research Laboratory, Cleveland, Ohio*

The suggestion has been made by Christ (1956) that powder patterns of substances of known cell-dimensions be taken at the edges of Weissenberg photographs to serve as standards for film calibration. In our laboratory we have often used the Weissenberg camera as a "powder" camera in order to get the diffraction patterns of related substances (e.g., a series of mixed crystals of different composition) side by side on the same film, thereupon facilitating the comparison between different patterns, reducing the time for processing the films and eliminating the need to do independent calibrations for film shrinkage and for the determination of the actual radius of the camera. The technique is very simple. The samples to be examined are centered one after another on the goniometer of the Weissenberg camera, the layer line screen is introduced and the powder patterns recorded in the desired order, taking care to read the position of the camera each time and to shift the camera a known amount (say, 5 mm) in the same direction after each picture.

When all the samples have been used the pattern of a substance of known cell dimensions is recorded at one edge of the film. In this way not only a calibration of the film is obtained but the order followed in taking the pictures becomes evident by inspection of the film after developing.

As mentioned above, this technique affords a considerable saving of the time involved in loading and unloading the camera and for processing the films. Also, independent film calibrations are eliminated. Furthermore, when not only the spacings of the lines but their intensities have to be compared, it is very convenient to have all the patterns collected on the same film and developed simultaneously.

In our experience the method is particularly attractive when the time involved for obtaining good sharp pictures is short, of the order of one hour, so that the collection of the whole set of diffraction data can be done in about one day.

REFERENCE

CHRIST, C. L. (1956), Precision determination of lattice constants of single crystals using the Weissenberg camera: *Am. Mineral.*, **41**, 569.

THE AMERICAN MINERALOGIST, VOL. 46, NOVEMBER-DECEMBER, 1961

EUCLASE IN GREISEN PIPES AND ASSOCIATED DEPOSITS, PARK COUNTY, COLORADO*

WILLIAM N. SHARP, *U. S. Geological Survey, Denver, Colo.*

INTRODUCTION

Euclase, $AlBe(SiO_4)(OH)$, apparently was first found in Brazil, and was brought to Europe as early as 1785. The mineral was classified and named by Hauy about 1792. Several other early European mineralogists studied the crystallography of euclase from Brazil, the Austrian Alps, and the Urals. Even though euclase was recognized very early, it has remained a rare species. So far as the writer can determine the mineral has not previously been reported from North America.

Euclase was first noted by the author in the greisen deposits of Park County, Colo., during field studies in the summer of 1960. Shortly thereafter the identification as euclase was confirmed by *x*-ray powder patterns. Euclase had been found only in vein deposits and placer material before its present discovery in greisen. The features of the vein occurrences denote a relatively high temperature of formation for euclase. In Brazil euclase is found in clay-rich quartz lenses in phyllite, associated with topaz and rutile; euclase also occurs in pegmatites with topaz and beryl (Leonardos, 1945). The Austrian euclase accompanies pericline and rutile in vuggy quartz vein deposits in mica-schist. Euclase in granite-pegmatite is recorded for Silesia (Kolbeck and Henglein, 1908), Bavaria (Durrfeld, 1910), and Tanganyika (McKie, 1955). Euclase is associated with bertrandite in an altered beryl crystal in pegmatite at Iveland, Norway (Strand, 1953). Euclase is found in placer material in Russia and British Guiana. At all these places the mineral is relatively rare.

Euclase may, however, be more common than it appears to be, especially in beryl-bearing pegmatites. The apparent rarity may be due to the inconspicuous nature of the mineral. Euclase is colorless, whitish, blue, or green; and though it customarily occurs in well-formed crystals, these commonly are small and can be easily overlooked if associated with such minerals as quartz, calcite, or topaz.

LOCATION AND FIELD RELATIONS

Euclase in Park County, Colo., is in small pipe-shaped bodies of greisen in the Redskin Gulch area within the Pikes Peak granite mass,

* Publication authorized by the Director, U. S. Geological Survey.

but near its western edge; and it also appears in more irregularly shaped greisen zones and closely related quartz-beryl deposits at the Boomer mine in a small outlying stock of the Pikes Peak granite (Sharp and Hawley, 1960).

In the greisen pipes of the Redskin Gulch area, euclase occurs as small well-formed crystals ½ to 2 mm across, which commonly are on clear to milky quartz crystals in vugs in granular quartz-muscovite greisen (Fig. 1). The euclase is closely associated with quartz, fluorite, muscovite (gilbertite), and bertrandite, all of which are found in well-formed crystals. Some of the minerals in the pipes carry evidence that they are a product of the alteration of material of an earlier stage of greisen development, a stage in which a beryl-bearing rock is present. Lens-shaped parts of some beryllium-bearing pipes consist of a reddish stained, finely to coarsely textured rock made up mostly of quartz, bertrandite and muscovite. At places in this rock fine-grained muscovite and pink cryptocrystalline bertrandite form bands and zones with conspicuous hexagonal shapes as much as 1 inch across. That these aggregates were beryl crystals at one stage seems reasonable. Euclase crystals accompanied by purple and white zoned fluorite are attached to quartz crystals in small vugs, and evidently formed at a late stage.

In the Boomer mine area euclase occurs as crystal clusters and coatings on fluorite in vugs in gray quartz-muscovite-fluorite greisen. Here, as in the pipes of the Redskin Gulch area, euclase was a late-forming

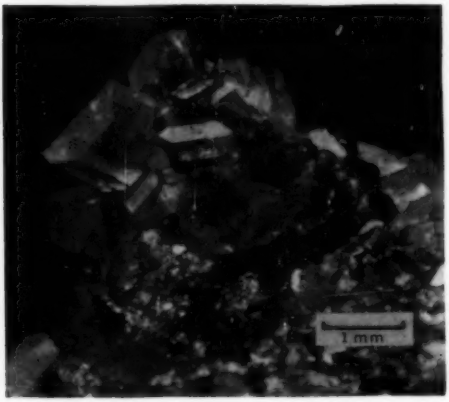

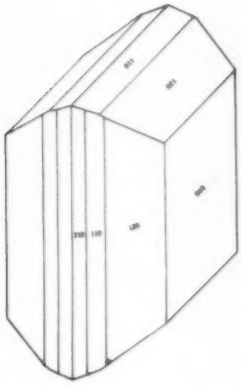

FIG. 1. (Left) Photograph of euclase crystals attached to quartz, Park County, Colorado.

FIG. 2. (Right) Crystal habit of euclase showing probable dominant forms, Park County, Colorado.

mineral. Green fluorite, which is common in the greisen, is overgrown with clear and purple-zoned fluorite crystals. Clusters and coatings of euclase crystals, together with some quartz crystals, cover both types of fluorite. Rosettes of muscovite are intergrown with the euclase. A bertrandite-bearing phase of the greisen (Sharp and Hawley, 1960), occurring in the same deposit, does not appear to contain euclase.

An altered beryl-bearing part of a quartz vein associated with greisen at the Boomer mine contains both well-formed euclase crystals as much as 2 mm across and bertrandiate crystals as much as several millimeters in size. These euclase crystals are mixed with quartz and muscovite crystals in small vugs and porous aggregates pseudomorphic after beryl. This occurrence is similar to that reported by Strand (1953) from a Norwegian pegmatite.

Mineralogy

Euclase in the greisen in Park County, Colo., appears to be consistently simpler in habit than that described from other localities. The Park County crystals are colorless thick plates on which the (010) face is dominant. Cleavage parallel to (010) is conspicuous. The habit is shown in the clinographic sketch on figure 2. Euclase is monoclinic and holohedral. Crystals previously described commonly are of elongate prismatic habit and have many faces (Meixner, 1957; Saldanha, 1939, 1941; Dana, 1914).

The crystal structure has been studied and described by Biscoe and Warren (1933) and more recently by Mrose and Appleman (oral communication, 1960). *X*-ray diffraction data for euclase from Park County, Colo., agree well with those of Mrose and von Knorring (1959) for euclase from Minas Gerais, Brazil. Powder films of the Park County euclase were compared visually with a film prepared from euclase from near Ouro Preto (Villa Rica), Brazil, that was supplied by the U. S. National Museum. The patterns of both minerals appear to be identical in *d*-spacings and intensities.

Optical measurements of the Park County euclase match closely those given by Dana (1914, p. 508–509) and Winchell (1951, p. 357–358).

Optic sign (+) Dispersion $r>v$
Indices

α	1.652±0.001 (Na)	
β	1.655±0.001 (Na)	$2V=48°$ meas. with
γ	1.670±0.001 (Na)	spindle stage
$\gamma-\alpha$	0.028	

Optic plane is (010)
G=2.987±0.005 (by liquid immersion method)

A semiquantitative spectrographic analysis by A. T. Myers of the Park County euclase, sample S60-Bd-1, gave the following results:

Si	Major	Cu	.003 per cent
Al	Major	Ge	.15 per cent
Fe	.003 per cent	Sc	.003 per cent
Ca	.005 per cent	Sn	.015 per cent
Be	7. per cent		

Acknowledgments

The writer is indebted to Dr. George Switzer, U. S. National Museum, for a crystal fragment of Brazilian euclase; and to Alfred T. Myers, a colleague in the U. S. Geological Survey, who made the spectrographic analysis. Other colleagues who contributed helpful suggestions include John W. Adams, Arthur J. Gude, Mary E. Mrose, Theodore Botinelly, and Fred A. Hildebrand.

References

Biscoe, J., and Warren, B. E., 1933, The structure of euclase, $HBeAlSiO_5$: *Zeit. Krist.*, **86,** 292–297.

Dana, J. D., 1914, System of mineralogy, 6th ed., New York, John Wiley & Sons, Inc., 508–509.

Durrfeld, V., 1910, Über die Aufstellung und optische Orienterung das euklas von San Isabel de Paraguassú und von Epprechtstein: *Zeit. Krist.*, **47,** 372–373.

Kolbeck, F., and Henglein, M., 1908, Über ein neues Vorkommen von euklas aus dem pegmatite von Dobschütz bei Görlitz in Schlesien: *Centralblatt Min.*, 335.

Leonardos, O. H., 1945, Occurrências de euclasio no Brazil: *Mineração e Metalurgia*, **8,** 383–384.

McKie, Duncan, 1955, Notes on some minerals from Tanganyika: Records, *Geol. Survey Tanganyika*,, **V,** 86–87.

Meixner, Heinz, 1957, Ein neues Euklasvorkommen in den Ostalpen: *Tschermaks Min. u. Petr. Mitt. Bd.* **6,** H. 3, 246–249.

Mrose, M. E., and von Knorring, O., 1959, The mineralogy of väyrynenite, (Mn,Fe) $Be(PO_4)(OH)$: *Zeit. Krist.*, **112,** 275–288.

Saldanha, Reynaldo, 1939, Sobre o euclasio de Dom Bosco: Sao Paulo, Univ. Fac. Filos., Ciencios, e Letros, B. 18, Min. N° 3, p. 29–37; 1941, Nota sobre o euclasio de Cachoeiro de Santa Leopoldina: B. 21, Min. N° 4, p. 25–31.

Sharp, W. N., and Hawley, C. C., 1960, Bertrandite-bearing greisen, a new beryllium ore, in the Lake George district, Colorado, *in* Short papers in the geological sciences: *U. S. Geol. Survey Prof. Paper* **400-B,** 73–74.

Strand, Trygve, 1953, Euclase from Ireland, occurring as an alteration product of beryl: *Norsk Geologisk Tidsskrift*, **31,** 1–5.

Winchell, A. N., 1951, Elements of optical mineralogy, 4th ed., New York, John Wiley & Sons, Inc., 357–358.

THE AMERICAN MINERALOGIST, VOL. 46, NOVEMBER-DECEMBER, 1961

ILVAITE: A LATE MAGMATIC OCCURRENCE IN GABBRO OF MISSOURI

GEORGE A. DESBOROUGH* AND DEWEY H. AMOS†

Ilvaite occurs in Precambrian intrusive gabbroic rocks which are exposed in Madison and Iron Counties of southeastern Missouri. The rocks are principally gabbro, olivine gabbro and olivine diabase; plagioclase and augite, with or without olivine are the major silicates. About 35 polished surfaces and 35 companion thin sections of the basic rock have been studied.

Ilvaite is present in 8 of 13 fresh gabbroic rocks collected from various localities 5 to 15 miles apart. Identification of ilvaite is based on: (1) *x*-ray powder patterns, (2) the observed (apparent) angle of rotation, which is more than 9° for a section showing maximum bireflectance (Cameron, 1959, p. 56), (3) polarization colors, and (4) dispersion properties. Vonsenite, a mineral recently described by Leonard and Vlisidis (1960), has several characteristics similar to ilvaite, but the latter has a larger angle of rotation in reflected light. *X*-ray powder patterns of ilvaite from the Hanover Mine, Hanover, New Mexico were prepared and found to be essentially identical to the patterns given by the ilvaite of the Missouri gabbroic rocks.

Point counts (1500 per 530 sq. mm. surface) of ore minerals revealed that where ilvaite is present, it ranges in amount from less than 0.1% to about 2% of the rock. Percentages of ilvaite are comparable to those of pyrrhotite and exceed those of chalcopyrite. Other ore minerals in the fresh rock include ilmenite, magnetite with ulvöspinel cloth texture and and traces of pentlandite in pyrrhotite.

Ramdohr (1960, p. 1001) cited two occurrences of ilvaite in olivine gabbros, one in Elfdalen, Sweden and another in the Skaergaard intrusion of East Greenland. He (1960, p. 1001) states that ilvaite is a reaction product of plagioclase and iron-rich olivine at these localities. Other than these, no other occurrences of ilvaite in gabbroic rocks were found in reviewing the literature.

The most frequent occurrence of ilvaite is with the skarn minerals of contact metamorphic deposits and particularly those rich in copper and iron sulfides and minor iron oxides. Gorbunov and Kornilov (1954) report the presence of disseminated ilvaite in pyrrhotite-pentlandite-chalcopyrite ore (locality not given); ilvaite replaces magnetite and is

* Geology Department, The University of Wisconsin, Madison.
† Geology Department, Southern Illinois University, Carbondale.

replaced by epidote and zoisite. Baker (1953) observed ilvaite in a micropegmatite diorite in New Guinea where it is associated with ilmenite near veins of prehnite and replaces some of the pyroxenes in the diorite. He considers that ilvaite (and prehnite) are the products of hydrothermal alteration, that ilvaite formed later than ilmenite, and that locally ilvaite hydrothermally replaces pyroxene. Ramdohr (1960, p. 1001) doubts the strictly hydrothermal origin of ilvaite which has been suggested for some localities. In view of the fact that prehnite may be an alteration product in intermediate and basic rocks, ilvaite in the diorite described by Baker (1953) may have been derived from the late volatiles expelled from the intrusion as he suggested (p. 842). However the relationships described by Baker (1953, p. 840) do not indicate that ilvaite and prehnite were necessarily contemporaneous and of the same origin.

In the gabbroic rocks of Missouri ilvaite is not a hydrothermal mineral. Quartz and calcite veins locally cut the gabbro and are probably of hydrothermal origin, but thin sections and polished surfaces of the gabbro cut by these veins contain no ilvaite.

Deuterically altered gabbroic rocks of the area are considered as those showing the following alterations: olivine to minerals commonly identified as iddingsite, bowlingite and serpentine; plagioclase to saussurite; augite to amphibole or a chlorite-like mineral; titaniferous magnetite to a turbid mass of sphene and leucoxene; pyrrhotite to pyrite. Ilmenite is unaffected. Carbonate and quartz are common and more mesostatsis is present than in the unaltered rocks. The altered rocks are apparently more abundant than those which are unaltered. Two gabbro specimens from the same exposure (one of which is deuterically altered and the other is not), less than one foot apart vertically, clearly show ilvaite in the unaltered specimen while it is lacking in the altered one. Eighteen specimens systematically collected from a gabbroic sill less than 300 feet thick show the same relationships as above. Unaltered gabbro contains ilvaite and altered gabbroic rocks do not.

Ilvaite is present in olivine diabase, olivine gabbro, and gabbro which have not been affected by deuteric or hydrothermal solutions. Ilvaite is not necessarily associated with plagioclase or olivine and iron-rich olivine is lacking in the rocks examined. It is most abundant in specimens without olivine. According to the paragenetic sequence ilvaite was the last magmatic mineral to crystallize; it is most closely associated with pyrrhotite, ilmenite and magnetite and occurs as minute grains in small aggregates. Ilvaite also incipiently replaces the pyroxene component of ilmenite-pyroxene micrographic (myrmekitic) intergrowths in which ilmenite shows optical continuity.

Baker (1953) observed ilvaite incipiently replacing pyroxene of ilmenite-pyroxene micrographic intergrowths and implied the ilvaite was of hydrothermal replacement origin. In the Missouri rocks the presence of ilvaite in unaltered gabbros and its absence in the deuterically altered and hydrothermally altered gabbros indicates it is of magmatic origin. If pyrrhotite and chalcopyrite may be considered as late magmatic minerals in the gabbroic rocks of Missouri, then ilvaite must also be placed in this category. The association of ilvaite with pyrrhotite, chalcopyrite, ilmenite and magnetite is consistent with mineralogical assemblages found in ore deposits like those of Hanover, New Mexico, those described by Gorbunov and Kornilov (1954) and some contact metamorphic deposits.

Acknowledgments

The writers extend their thanks to Robert Carpenter for preparation of *x*-ray powder patterns. The facilities of the Economic Geology Laboratory, The University of Wisconsin, were used for petrographic and mineragraphic investigation. Thin section preparation and field expenses were financed by the Mississippi Valley Investigations and Research Organization of Southern Illinois University. Thanks are due E. N. Cameron for helpful suggestions regarding the manuscript.

References

Baker, G. (1953), Ilvaite and prehnite in micropegmatite diorite, Southeast Papau: *Am. Mineral.*, **38,** 840–844.

Cameron, E. N. (1959), The study of opaque minerals in reflected light: *Am. Soc. For Testing Materials, Spec. Tech. Pub.* **257,** 39–74.

Gorbunov, G. I., and Kornilov, N. A. (1954), On a discovery of ilvaite in copper-nickel sulphide ores: *Doklady Acad. Sci. USSR.*, **94,** 323–325.

Leonard, B. F., and Vlisidis, A. C. (1960), Vonsenite from St. Lawrence County, Northwest Adirondacks, New York: *Am. Mineral.*, **45,** 439–442.

Ramdohr, P. (1960), Die Erzmineralien und ihre Verwachsungen: Akademie-Verlag, Berlin.

BOOK REVIEWS

SPECTROCHEMICAL ANALYSIS, 2nd Edition, L. H. AHRENS AND S. R. TAYLOR. Addison-Wesley Publishing Company, Reading, Mass., and London, England. 454 +xxiii pages. $15.00.

SPECTROCHEMICAL ANALYSIS by Ahrens and Taylor is well known to workers in the spectrochemical analysis of rocks, minerals, and related substances. The general coverage of the work is the same as that of the first edition with particular emphasis on newer techniques in quantitative determination of major constituents, the development of general sensitive methods for determining many elements in a single operation, and the use of enrichment techniques to extend greatly detection limits of many elements.

The entire treatment is based upon the D.C. arc source, an approach fully justified in the results obtained. A table of most sensitive lines of the elements with interfering lines is given. General principles and techniques as well as specific discussions of each of the detectable elements and a choice of internal standards are given. Important band spectra are covered in addition to the spectra of the usable elements. Forty-five pages of bibliography are included.

The book has already earned its place as an important reference and will certainly continue to maintain this position among students and research workers.

REYNOLDS M. DENNING
Department of Geology and Mineralogy
University of Michigan

THE INTERPRETATION OF *X*-RAY DIFFRACTION PHOTOGRAPHS, by N. M. F. HENRY, H. LIPSON, AND W. A. WOOSTER. Macmillan and Co., Inc., London. (St. Martin's Press, New York); 2nd Edition, 1960, X+282 pages, price $12.00.

A review of the first edition of this book was given in *Am. Mineral.*, **37,** 1952. In the second edition (1960), the authors have attempted to expand certain sections, particularly the one on the precession method, and change the use of kX to angstrom units to conform with international nomenclature.

The book consists of 17 chapters, followed by 9 appendices, and 13 tables. Titles of chapters include Crystal Lattices and Symmetry Classes, Nature of *x*-rays, Geometry of *x*-rays Reflections, and Single Crystal and Fibre Photographs. Following these chapters are interpretations of the various methods, namely, oscillation photographs (22 pages), Laue method (10 pages), moving film methods (20 pages) which include Weissenberg and rotation-retigraph methods, precession method (27 pages), and powder photograph method and interpretation (43 pages). The authors also discuss orientation in single crystals and twins, and preferred orientation in polycrystalline aggregates, with examples of calculations for two triclinic crystals and one trigonal crystal.

Space groups are only briefly mentioned, although adequate references are given for further investigation. More emphasis is given to the powder method than to the more difficult single crystal Weissenberg photographic interpretations so widely used at present.

In conclusion, the book is of great value to the student who carries out calculations in interpretation of *x*-ray diffraction photographs and to the researcher who needs a review of the methods.

EUGENE B. GROSS
Department of Geology and Mineralogy
The University of Michigan

NOTICE

New Mineral Names has been prepared by Michael Fleischer for many years with extraordinary coverage and critical evaluation, and remains one of the most important sections of *The American Mineralogist*. Dr. Fleischer continues to find the task enjoyable but increasingly burdensome. This is a call for volunteers to assist him in combing and reviewing the literature for descriptions of new minerals and new mineral data. Mineralogists interested, please contact Dr. M. Fleischer, U. S. Geological Survey, Washington 25, D. C., and specify the language(s) and journals you can and are willing to cover. Especially helpful would be the services of three good mineralogists to cover *Mineralogical Magazine*, *Bulletin Société Française Minéralogie*, and *Neues Jahrbuch für Mineralogie* etc., Monatshefte.

NEW MINERAL NAMES

Farringtonite

E. R. Dufresne and S. K. Roy. A new phosphate mineral from the Springwater pallasite: *Geochim. et Cosmochim. Acta*, **24**, 198–205 (1961).

The mineral was found in the Springwater pallasite, from near Springwater, Saskatchewan. It occurs as colorless to wax-white to yellow material peripheral to olivine nodules. The meteorite also contains metallic iron (kamacite) and troilite.

Spectrographic analyses were made on two 25 mg. samples; the first was cleaned magnetically, the second by gravity separation in a centrifuge as well. These gave: P_2O_5 37.6 ± 0.6, 49.7 ± 1.0; MgO 49.2 ± 0.2, 41.6 ± 1.3; SiO_2 11.1 ± 0.2, 2.9 ± 0.1; Fe 5.4 ± 0.1, 3.7 ± 0.2%. The final content of metallic iron in the samples was "quite negligible"; the Fe reported must be present as FeO or Fe_2O_3 or both. Microscopic and *x*-ray study of the second sample showed no olivine; it is probable that at least some SiO_2 was present in solid solution. The composition is therefore essentially $Mg_3(PO_4)_2$, but with Fe and Si present; it is known that synthetic $Mg_3(PO_4)_2$ can take MgO into solid solution up to a composition $MgO \cdot 3Mg_3(PO_4)_2$. The mineral is virtually insoluble in water, attacked slowly by dilute HNO_3.

Farringtonite is monoclinic, cleavage "fair to good (100) and (010)," distinguished by "parallel partings along 100." Optically biaxial, positive, *ns* α 1.540, β 1.544, γ 1.559, all ± 0.002, 2V 54–55°, birefringence "0.010–0.014," extinction inclined Z:c = 16–17° in β obtuse. G. approx. 2.80 (method of determination not stated).

X-ray powder data agree with those for synthetic $Mg_3(PO_4)_2$. The strongest of the 28 lines given are 3.83 (vs, d), 3.41 (vs), 2.39 (ms), 2.77 (m, d), 2.11 (m), 1.074 (m), 1.071 (m), 1.002 (m), 0.984 (m).

The name is for O. C. Farrington (1864–1933), for many years Curator of Geology, Field Museum, an authority of meteorites.

Michael Fleischer

Tin-tantalite (Olovotantalit)

V. V. Matias. Tin-tantalite (olovotantalit), a new variety of tantalite: *Geol. Mestorozhd. Redkikh Elementov No.* **9**, 30–41 (1961) (in Russian).

The mineral occurs in "one of the pegmatite deposits of the U.S.S.R." as brown, well-formed crystals 0.5–1 mm. in diameter. Analysis by K. A. Dorofeeva and T. A. Ukhina gave Ta_2O_5 62.53, Nb_2O_5 12.50, SnO_2 9.06, TiO_2 0.50, ZrO_2 none, Fe_2O_3+FeO 0.57, MgO none, MnO 13.06, UO_2 0.03, rare earths 0.17, CaO 0.18, SiO_2 0.20, H_2O^+ 0.04, H_2O^- 0.06, sum 98.90%, corresponding to $(Mn_{0.87}Fe_{0.04}TR_{0.01})_{0.92}$ $(Ta_{1.34}Nb_{0.44}Sn_{0.28}Ti_{0.03})_{2.09}$ O_6. Spectrographic analysis showed also Sb, Al, Zr, each about 0.1%, Mg, Ga, Bi, La, Y, Zn, each about 0.01%, Cu, Yb, Ag each about 0.001%. The mineral is completely dissolved when heated with H_2SO_4+$(NH_4)SO_4$, so that cassiterite cannot be present.

The mineral is dark brown to black, opaque to translucent. Luster greasy on fracture, vitreous on crystal faces. H. 5½–6 (660 kg. sq. mm.), G. 7.4. Not luminescent in cathode rays. Optically biaxial, positive, *ns* α 2.19±0.02, γ 2.28±0.02, 2V 30–40°. Pleochroism distinct X reddish-brown, Z yellowish, absorption X>Z. Reflecting power in polished section somewhat lower than for manganotantalite and much lower than that of stibiotantalite. Strongly anisotropic with yellow-brown internal reflections. Two cleavages were noted under the microscope, the less perfect one at 26–28° to X, the perfect cleavage parallel to X. Simple and polysynthetic twinning was observed. Dielectric constant 4.84. Infra-red spectra made by L. S. Ivanova are given for tin-tantalite, tantalite, thoreaulite, and cassiterite; that for tin-tantalite is similar to those for tantalite and thoreaulite but differs in showing absorption at 10–11 mμ.

The crystals appeared to be monoclinic, but Laue diagrams were not decisive. The *x*-ray powder diagram is given; the strongest lines are 1.468 (10), 1.780 (8), 2.95 (7), 2.51 (7), 1.743 (7), 1.723 (7), 1.917 (6–7). The pattern is similar to that of manganotantalite, but contains some additional lines.

The mineral occurs in small (0.5–1 mm. diameter) crystals of irregular form, also as pseudomorphs after simpsonite; in a strongly albitized pegmatite. It is associated with simpsonite, microlite, lepidolite, and spodumene; rarely stibiotantalite. The mineral is later than spodumene and simpsonite, earlier than stibiotantalite.

Discussion.—An unnecessary name for stannian mangano-tantalite.

M. F.

Alumobritholite

M. A. Kudrina, V. S. Kudrin, and G. A. Sidorenko. Britholite and alumobritholite from alkalic pegmatites of Siberia: *Geol. Mestorozhdenii Redkikh Elementov No.* **9**, 108–120 (1961) (in Russian).

Silicophosphates of the rare earths occur in abundance in "a large alkalic masif of Siberia"; britholite (an analysis is given of thorian britholite, ThO_2 9.77%) in nepheline syenite pegmatites, alumobritholite in pegmatites of aegirine-riebeckite granites. Analyses of alumobritholite by T. I. Ivanova and Z. V. Vasil'eva gave SiO_2 21.93, 19.02; P_2O_5 3.96, 1.87; B_2O_3 ——, 0.15; CaO 17.34, 22.55; rare earths 27.58, 32.32; ThO_2 4.76, 9.25; VO_2 0.63, 2.05; Al_2O_3 14.91, 9.45; Fe_2O_3 5.42, 0.42; FeO 0.32, ——; ZrO_2 0.98, ——; MgO ——, 0.34; K_2O ——, 0.06; Na_2O 0.30, 0.13; H_2O^+ 0.33, 1.15; H_2O^- 0.37, ——; F 1.66, 1.44; sum 100.49, 100.20, $-(O=F_2)$ 0.69, 0.60=99.80, 99.60%. Calculation of the analyses on the basis of the apatite group formula, $X_5(ZO_4)_3F$, gave unsatisfactory results with (Si+P)=3 or with (Si+P+Al)=3; the Al is therefore divided and the formula calculated is $(Ca_{1.89}Al_{1.36}Fe_{0.44}Ce_{1.09}Th\ etc_{0.21})_{5.0}$ $(Si_{2.2}P_{0.4}Al_{0.4})_{3.0}$ $(F_{0.53}OH_{0.22})$. *X*-ray spectrographic analysis by N. V. Turanskaya of the rare earths showed La 18.55, Ce 28.8, Pr 2.9, Nd 9.3, Sm 2.0,

Gd 1.8, Dy 2.5, Ho 0.7, Er 2.3, Tu 0.5, Yb 3.65, Lu 0.8, Y 26.2%; in containing both Y and Ce elements, the mineral is intermediate between britholite and abukumalite. DTA study showed an exothermic effect at 575° (transition to crystalline state?).

The mineral is yellowish-brown, slightly greenish; color nonuniform, deeper in the center of grains. Luster vitreous to greasy. Fracture conchoidal. Hardness 5.4, microhardness 471 kg./mm.^{2}. Isotropic (metamict), n 1.72. Slightly soluble in HCl.

Amorphous to x-rays; after being heated to 900° for 30 minutes gives a pattern corresponding to a 9.45 ± 0.01, c 6.91 ± 0.01 Å. The strongest lines (20 given) are 2.827 (10), 1.851 (7), 1.952 (6), 3.112 (5).

The mineral alters readily on weathering.

DISCUSSION.—The postulated replacement of Ca by Al is surprising. The name is an unnecessary one for aluminian britholite.

M. F.

Calzirtite

T. B. ZDORIK, G. A. SIDORENKO, AND A. V. BYKOVA. A new calcium titanozirconate-calzirtite: *Doklady Akad. S.S.S.R.*, **137,** No. 3, 681–684 (1961) (in Russian).

YU. A. PYATENKO AND Z. V. PUDOVKINA. The crystal structure of calzirtite—a new derivative of the structural type of CaF_2-CeO_2: *Kristallografiya*, **6,** No. 2, 196–199 (1961) (in Russian).

The mineral occurs in metasomatic calcite-forsterite-magnetite rocks of an alkalic ultrabasic massif, Eastern Siberia. It forms tabular concretions 3×4×1 mm. in size, composed of complex trillings. Single crystals are tetragonal, prismatic, bipyramidal.

Analysis by A.V.B. gave CaO 11.26, TiO_2 16.04, Nb_2O_5 0.10, ZrO_2 70.12, HfO_2 0.44, Fe_2O_3 1.64, SiO_2 0.41, loss ign. 0.17, sum 100.18%. Spectrographic analysis showed Mn, Rb, Ce, Y, and Sr 0.0X, Sn and Sb 0.00X%. This corresponds very closely to $CaZr_3TiO_9$. The unit cell (see below) contains $Ca(Ca_{0.81}, Zr_{1.16})_2\ Zr_4\ (Ti, Fe)_2O_{16}$. The mineral is infusible, but lightens in color before the blowpipe in O.F. Partly soluble when heated in concentrated H_2SO_4, H_3PO_4, or HCl.

The color is dark brown, nearly black. Luster semi-metallic to adamantine. Streak brown. Brittle, hardness varies with crystallographic direction from 626–1035 kg./mm.^{2}, = 6–7. G. 5.01. Dielectric constant 5.03. Does not luminesce in UV light, gives a wavy red luminescence in cathode rays, after heating, a fiery red. Non-pleochroic. Optically uniaxial, positive, $ns\ \omega$ between 2.19 and 2.27, ϵ between 2.30 and 2.36, ϵ-ω 0.07–0.08. In polished sections light gray. Reflecting power Re 16.4, Ro 15.0. Birefringence distinct in immersion, not observed in air. Internal reflections strong, reddish-brown.

Indexed x-ray powder data are given by Z., S., and B. (50 lines). The strongest lines are 2.945 (10), 1.801 (10), 1.537 (9), 1.170 (7), 2.552 (6), 0.981 (6), 0.871 (6). Most of the reflections correspond to a cubic cell with a 10.195 kX, but some lines did not; P. and P. find the mineral to be tetragonal, space group $I4_1/acd$, a 15.30 ± 0.06, c 10.20 ± 0.04 A.

Atomic co-ordinates are given.

The name is for the composition.

M. F.

Yoshimuraite

TAKEO WATANABE, YOSHIO TAKEUCHI, AND JUN ITO. The minerals of the Noda-Tamagawa Mine, Iwate Prefecture, Japan. III. Yoshimuraite, a new barium-titanium manganese silicate mineral: *Mineralogical Jour. (Japan)*, **3,** 3, 15%–167 (1961) (in English).

A preliminary note was abstracted in *Am. Mineral.*, **45,** 479 (1960).

The mineral occurs in coarse-grained pegmatite along the boundary between massive Mn ore (tephroite with rhodonite, braunite, and hausmannite) and massive hornfels containing manganophyllite, richterite, and urbanite. The pegmatite contains K-Ba feldspar, quartz, richterite, urbanite, and rhodonite.

Analysis (by J. I.) of yoshimuraite gave SiO_2 18.25, TiO_2 10.00, Fe_2O_3 1.32, FeO 1.47, MnO 17.64, MgO 0.56, ZnO 0.50, BaO 33.51, SrO 4.62, Na_2O 0.16, K_2O 0.03, P_2O_5 3.98, SO_3 5.40, Cl 0.41, $H_2O \pm 2.34$, sum 100.19 $-(O=Cl_2)$ 0.09 = 100.10%. This corresponds to $(Ba,Sr)_{1.84}(Ti,Fe''')_{0.96}$ (Mn, Fe'', Mg)$_{1.97}$ $(SiO_4)_2$ $[(P_{0.76}S_{0.92})O_4]$ $(OH,Cl)_{1.45}$ or $(Ba,Sr)_2$ (Ti,Fe''') Mn_2 $(SiO_4)_2$ [(P, S)O_4] (OH, Cl). The unit cell contains 2 formula weights.

The mineral occurs as blades or mica-like forms up to 5 cm. long. Hardness 4½ brittle, G. (pycnometer) 4.13, calcd. 4.21. Optically biaxial, positive, *ns* α 1.763, β 1.777, γ 1.785, 2V 85–90°, r > v. Pleochroic with X bright yellow, Y orange-brown, Z brown, absorption $X < Y \leqq Z$. The optical orientation could not be determined exactly; α' is nearly parallel to *a*, γ' nearly parallel to *c*. Polysynthetic twinning on (010) was observed.

Precession photographs showed yoshimuraite to be triclinic, space group PT, *a* 7.00 ±.01, *b* 14.71 ±.02, *c* 5.39 ±.01 Å., α 93.5°, β 90.2°, α 95.3° (all ±0.2°), axial ratio *a*:*b*:*c* = 0.476:1:0.366. Tests for piezoelectricity were negative. Cleavages {010} perfect, {10$\bar{1}$} and {101} distinct. Indexed *x*-ray powder data (32 lines) are given. The strongest lines are 3.40 (10)(1$\bar{3}$1), 2.94 (10)(041, $\bar{2}$01), 4.90 (6)(011), 3.24 (6) ($\bar{1}$30), 2.78 (6) ($\bar{3}$21, $\bar{1}$41).

A similar mineral has also been found at the Taguchi Mine, Aichi Prefecture, and will be described later.

The name is for Professor Toyofumi Yoshimura of Kyushu University, who first studied the Mn minerals of the mine.

M. F.

Ekanite

B. W. Anderson, G. F. Claringbull, R. J. Davis, and D. K. Hill. Ekanite, a new metamict mineral from Ceylon: *Nature*, **190,** No. 4780, 997 (1961).

Several specimens, the largest about 44 g., of a green transparent-translucent mineral have reached Europe. It occurs in the gem pits of Eheliyagoda, Raknapura district, Ceylon. Analysis by D. I. Bothwell gave SiO_2 55.6, ThO_2 27.6, UO_2 2.1, Fe_2O_3 0.5, CaO 13.7, PbO 0.8, Al_2O_3, MgO, MnO traces, sum 100.3%, corresponding to (Th, U)(Ca, Fe, Pb)$_2$ Si_8O_{20}. *n* 1.5969, G. 3.280; after the mineral is heated at 510° for 24 hours, *n* is 1.5933, G. 3.276; after it is heated at 1000° C. for 24 hours, G. is 3.313.

The mineral is metamict. At temperatures between 650° and 1000° C., it recrystallizes to a phase that can be indexed on a body-centered tetragonal cell with *a* 7.46, *c* 14.96 Å. "Heating at higher temperatures involving re-melting leads to the development of the thorium silicate huttonite. If the mineral is fully melted and then recrystallized at 1000° C., the product appears to be a thorium analogue of the britholite-cerite-lessingite group."

The mineral is named for Mr. F. L. D. Ekanayake, who first found it.

F. D.

Alpha-fergusonite, Beta-fergusonite

S. A. Gorshevskaya, G. A. Sidorenko, and I. E. Smorchkov. A new modification of fergusonite: β-fergusonite. *Geol. Mestorozhdenii Redkikh Elementov No.* **9,** 28–29(1961) (in Russian).

Nearly all fergusonites are metamict, but are transformed when heated at 575–765° to a tetragonal material, which in turn is transformed to monoclinic material at higher temperatures. Komkov, *Zapiski Vses. Mineral. Obshch.*, **87,** 432–444 (1957), described naturally crystalline tetragonal fergusonite with *a* 5.15, *c* 10.89 Å from Ural pegmatites.

This is now called alpha-fergusonite. When heated about 900°, the material becomes monoclinic, a 5.05, b 10.89, c 5.27 A., $\beta = 85°30'$.

The authors have now found natural monoclinic crystals in crystals 0.05–0.2 mm. in cross section from the apical parts of microcline granite stocks, Central Asia. It is light yellow, G. 5.65. *X*-ray spectrographic analysis showed much Y, Nb, U; Fe (about 2.5%), about 1% Ta and Th, about 0.5% Ca and Zr, about 0.2% Ti, and about 0.1% Pb. It is monoclinic, a 5.12, b 10.89, c 5.20 Å, beta 88°10′. When heated at 950° for 1 hour, the unit cell became a 5.06, b 10.92, c 5.30 Å, $\beta = 85°48'$. This natural monoclinic modification is called beta-fergusonite.

M. F.

Unnamed

J. Zemann. Über den Botryogen vom Rammelsberg: *Fortschr. Mineral.*, **39,** 84 (1961).

Reddish-brown, poorly formed crystals up to a few mm. in size occur on zincian melanterite. Analysis of a few tenths of a gram selected under the binoculars gave MgO 1.6, ZnO 7.7, MnO 3.6, FeO 1.2, Fe_2O_3 18.4, SO_3 36.1, $H_2O > 50°$ C. 30.9, sum 99.5%, a member of the botryogen group' $M^{+2}\,Fe^{+3}\,(SO_4)_2(OH)\cdot 7H_2O$, with Zn:Mn:Mg:Fe = 47:25:20:8. G. 2.19. Optical constants close to those of Bandy (Dana's System, 7th Edition, **2,** 617) for the Mg member of the group. *X*-ray study shows it to be monoclinic, C $P2_1/n$, a 10.51 ±0.02, b 17.85 ±0.03, c 7.14 ±0.02 Å, β 100°00′ ± 15′, Z = 4. The crystals are prismatic with forms {110} and {$\bar{1}$01} dominant, also {120} and {010}.

Discussion.—This is dominantly the zinc analogue of botryogen. Dr. Zemann (letter of Aug. 18, 1961) prefers that this not be given a name, the name botryogen being used as a group name.

M. F.

Benstonite

Friedrich Lippmann. Benstonit, $Ca_7Ba_6(Co_3)_{13}$, ein neues Mineral: *Naturwissenschaften,* **16,** 550–551 (1961).

The mineral occurs in white to ivory masses up to 1 cm. in size as fissure fillings, associated with quartz, barite, and calcite, in the barite mine near Magnet Cove, Hot Springs County, Arkansas. Analysis of material whose *x*-ray pattern showed the presence of some calcite gave CO_2 31.35, BaO 43.05, SrO 4.02, CaO 19.52, MgO 1.69, MnO 0.35, sum 99.98%, corresponding to $(Ca, Mg, Mn)_{7.419}\,(Ba, Sr)_6\,(CO_3)_{13.419}$, or, deducting calcite $(Ca, Mg, Mn)_7(Ba, Sr)_6(CO_3)_{13}$, with Ca:Mg:Mn = 0.87:0.11:0.01, and Ba:Sr = 0.88:0.12. G. 3.596 (measured), 3.648 (calcd.). Optically uniaxial, negative, *n*s (Na) ω 1.690$_5$ ±0.0005, ϵ 1.527 ±0.001. H. 3–4.

Weissenberg photographs show the space group to be probably R_3, or perhaps R $\bar{3}$, with a_0 18.28 ±0.01, c_0 8.67 ±0.02 Å.

The mineral is named for O. J. Benston, metallurgist, of Malvern, Arkansas, who first called attention to the mineral.

M. F.

Boleslavite

Cz. Haranczyk. The PbS gel—boleslavite. *Bull. Acad. Polonaise Sci., Ser. sci. geol. et geogr.* **9,** No. 2, 85–89 (1961).

Colloform ZnS and PbS occur in colloform varieties with marcasite as impregnations in the Gogolin limestones in the "Boleslaw" mine near Olkusz. The colloform PbS is silvery with a strong bluish tint; hardness (by Vickers sclerometer PMT-3) 40–80 kg./sq. mm. It shows "a diffraction pattern characteristic for crystalline galena." The *x*-ray

powder data (by J. Kubisz) are given. Chemical analysis gave Pb 86.33, S 13.24; spectrographic analysis showed As 0.1, Fe 0.08, Zn 0.03, Sb 0.015, Mn 0.003, Tl 0.003, Mo 0.0006, Cu 0.0004, Ag 0.0004%, Ca and Ba present. A D.T.A. curve is given.

The name is for the mine.

DISCUSSION.—A useless and unnecessary name.

M. F.

Geversite and Unnamed Pt Minerals and $(Fe, Ni)_2S$

E. F. STUMPFL. Some new platinoid-rich minerals, identified with the electron microanalyser. *Mineralog. Mag.*, **32,** 833–847 (1961).

Concentrates of Pt minerals were examined from the Driekop mine, eastern Transvaal. Geversite is light gray, reflectivity lower than that of Pt, but higher than that of sperrylite. Non-pleochroic, not anistropic, presumably cubic. Hardness similar to that of Pt, perhaps slightly higher. Analysis by microprobe gave Pt 45.0, Sb 51.5%, corresponding to Pt Sb_2, the antimony analogue of sperrylite. A variety with 7.2% Bi was also noted. Synthetic Pt Sb_2 is cubic with pyrite structure, a 6.428 A., H. 4½–5, m.p. 1230° C. The name is for T. W. Gevers, geologist, of South Africa.

Other new minerals, not given names are:

Pt(Sb, Bi). Color distinctly pinkish. Reflectivity lower than that of Pt, higher than that of geversite. Pleochroic from pink to light brown. Under crossed nicols, intense anisotropy effects. Hardness slightly less than that of Pt. The anisotropy suggests a hexagonal layer lattice. Microprobe analysis gave Pt 50.5, Sb 26.4, Bi 15.3%, corresponding to $Pt_7Bi_2Sb_6$ or approximately Pt(Sb, Bi).

PtSb. Color light brown with a touch of pink. Reflectivity lower than that of Pt(Sb, Bi), much higher than that of Pt. Analysis by microprobe gave Pt 50.5, Sb 34.7%. Synthetic PtSb is hexagonal (NiAs type), a 4.130, c 5.472 A.

(Pt, Ir)$_2$. Color grayish, reflectivity high, but lower than that of $PtSb_2$. Non-pleochroic, no anisotropy, evidently cubic. Hardness higher than those of Pt or $PtSb_2$, probably about 6. Microprobe analysis gave Pt 47.0, As 46.8, Ir 5.0%. Perhaps an iridian sperrylite.

Pt(Ir, Os)$_2$*As*$_4$ (?). Color distinctly brownish in reflected light. Reflectivity similar to that of sperrylite, lower than that of (Pt, Ir)As_2. Hardness higher than that of (Pt, Ir)As_2. No anisotropy, presumably cubic. Contains lamellae of iridosmine. Microprobe analysis gave As 32.5, Pt 22.0%, much Ir and Os; the Ir and Os contents vary greatly in opposite directions within a few microns. Occurs in grains and as lamellae in Pt.

Pt$_4$*Sn*$_3$*Cu*$_4$. Color pinkish, like PtSb. Reflectivity very high, lower than that of Pt, slightly lower than that of Pt$(Sb, Bi)_2$. Anisotropy visible in oil immersion. Hardness near that of Pt, lower than that of $PtSb_2$. Microprobe analysis gave Pt 51.7, Sn 22.0, Cu 16.8%. Very rare.

Pd$_2$*CuSb*. Strong violet color. Reflectivity much lower than any other associated mineral. Under crossed nicols, good anisotropy effects with orange colors. Hardness near that of Pt. Microprobe analysis gave Pd 53.5, Sb 31.3, Cu 16.0%, corresponding to Pd_2CuSb.

Pd$_8$*CuSb*$_3$. Intergrown or closely associated with the preceding mineral. Color pale yellow. Reflectivity slightly lower than that of $PtSb_2$. Anisotropic. Hardness near that of Pt. Microprobe analysis gave Pd 62.0, Pt 6.0, Sb 30.0, Cu 5.0%, corresponding to $(Pd, Pt)_8CuSb_3$.

Pd(Sb, Bi). Color light yellow. Reflectivity high. Non-pleochroic, anisotropy effects of medium intensity with gold-yellow colors under crossed nicols. Hardness distinctly less than that of sperrylite. Microprobe analysis gave Pd 43.6, Sb 25.2, Bi 32.2%, corresponding to $Pd_8Sb_4Bi_2$, or approximately Pd(Sb, Bi). Synthetic PdSb is reported to be hexagonal (NiAs type) with a 4.070, c 5.582 A., G. 9.4; synthetic PdBi is reported to be orthorhombic with a 7.203, b 8.707, c 10.662 A.

(Fe, Ni)$_2$S. In small grains resembling pyrrhotite in color, but with slightly higher reflectivity. Anisotropic under crossed nicols. Hardness comparatively low. Microprobe analysis gave Fe 51.0, Co 1.0, Ni 28.0, S 22.5%. An early mineral in this paragenesis.

Names are not given to these minerals pending further study.

M. F.

REDEFINITION OF SPECIES

Betafite

D. D. HOGARTH, A study of pyrochlore and betafite: *Canadian Mineral.*, **6,** 610–633 (1961).

A restudy of the group, with new analyses, *x*-ray study, and D.T.A., shows that betafite is a member of the pyrochlore group, with the general formula $A_{18-x}B_{16}(O, OH)_{16}(F, OH)_8$, with up to 67% of the A positions vacant (A = Na, K, Ca, Fe^{+2}, ΣCe, ΣY, Th, U, Pb, Ba, Sr, Bi; B = Nb, Ta, Ti, Zr, Sn, Fe^{+3}, W). It is suggested that the name betafite be reserved for members of the pyrochlore group containing U 15% or more (2.5 or more U atoms per unit cell). Hatchettolite and ellsworthite then become intermediate members of the pyrochlore-betafite series and these names can be dropped.

M. F.

NEW DATA

Scholzite

H. STRUNZ AND CH. TENNYSON. Kristallographie von Scholzit, $CaZn_2(PO_4)_2 \cdot 2H_2O$: *Zeitschr. Krist.*, **107,** 318–330 (1956).

Analysis of material from Hagendorf-South gave P_2O_5 35.99, ZnO 35.70, FeO 0.38, MnO 1.36, MgO 0.94, CaO 14.29, H_2O 10.36, insol. 0.88, sum 99.90%, corresponding to $CaZn_2(PO_4)_2 \cdot 2H_2O$, with some substitution by Mn, Mg, and Fe. Oscillation photographs showed it to be orthorhombic, space group Pbmm, with *a* 17.14, *b* 22.19, *c* 6.61 Å. Z = 12. Unindexed *x*-ray powder data are given (56 lines); the strongest lines are 8.588 (10), 2.788 (9), 4.230 (7), 3.376 (6), 2.652 (6), 2.240 (6), 1.892 (6). Cleavage (100) fair. The mineral is colorless to white, H. 3–3½, G. 3.11. Optically biaxial, positive, *n*s 1.581, *β* 1.586, *γ* 1.596, 2V70°, X = *a*, Y = *b*.

DISCUSSION.—My attention was recently called to the fact that I had not abstracted this paper, which changes, without explanation, the composition, symmetry, unit cell, and 2V given in the original description (see *Am. Mineral.*, **36,** 382 (1951)). I regret the oversight.

M. F.

DISCREDITED MINERALS

Dillnite (= Zunyite)

J. KONTA AND L. MRAZ. Dillnite and its relation to zunyite: *Am. Mineral.*, **46,** 629–636 (1961).

The name dillnite, first given in 1849 but long considered to apply to a mixture, was revived in 1955 (see *Am. Mineral.*, **41,** 673–674 (1956)). New study shows it to be zunyite,

higher in F content than any previously described. It is suggested that the name be kept for material of higher fluorine content and lower index of refraction.

DISCUSSION.—The limits of division are not specified. The analysis still show OH>F, so that the name is unnecessary.

M. F.

Henwoodite (=Turquoise)

E. FISCHER. Henwoodit, ein Glied der Türkis-chalkosiderit-Reihe: *Chem. der Erde*, **21**, 97–100 (1961).

Analysis (on 12.2 mg) of a sample labelled henwoodite from Redruth, Cornwall, obtained in 1878, gave CaO 0.57, CuO 8.81, Al_2O_3 28.01, Fe_2O_3 9.58, P_2O_5 34.90, H_2O 17.13, sum 99.00%, *i.e.* a ferrian turquoise. This was confirmed by the *x*-ray powder pattern.

DISCUSSION.—Hey, Chemical Index of Minerals, 2nd Ed., 1955, p. 449, lists henwoodite as a synonym of turquoise (F. A. Bannister, private communication).

M. F.

Gouréite (=Narsarsukite)

E. JÉRÉMINE AND M. CHRISTOPHE-MICHEL-LÉVY. Un nouveau gisement de narsarsukite (Identification d'un minéral dénommé provisoirement "gouréite" par A. Lacroix en 1934): *Bull. soc. franc. mineral. crist.*, **84**, 191–194 (1961).

The name gouréite was given by A. Lacroix (*Acad. Sci. Paris, Mem. No.* **61**, 318, 1934) to a mineral from an aegirine-riebeckite granite from Gouré, Sudan. Only optical data were obtained. *X*-ray study shows that the mineral is narsarsukite, with *ns* α 1.610, γ 1.632, positive (originally stated to be negative), values close to those for narsarsukite from Greenland. A qualitative test showed high Ti.

M. F.

Hjelmite (= Pyrochlore + Tapiolite (?))

V. V. MATIAS. Tin-tantalite, a new variety of tantalite: Geol. Mestorozhdenii Redkikh Elementov No. 9, p. 30–41 (1961) (in Russian).

Hjelmite (see Dana's System, 7th Ed., Vol. I, p. 779–780) was found by Nordenskiöld in 1860 and is supposed to be $(Fe^{+2}, Mn, U, Ca)(Nb, Ta, Sn)_2O_6$. Material from the type locality contained 6.56% SnO_2. There are no modern analyses and the mineral has long been considered dubious. Matias reports results obtained on a sample of hjelmite "from Norway," from the Mineralogical Museum, Academy of Sciences, U.S.S.R. Optical and *x*-ray studies showed it to be a mixture of tapiolite, pyrochlore, and an unidentified phase.

DISCUSSION.—The type material from the Kararfvet mine, Sweden, might well be such a mixture, but the mineral cannot be considered discredited since the work was done on a specimen, the locality and history of which are not given.

M. F.

INDEX TO VOLUME 46

Leading articles are in **bold face** type; notes, abstracts and reviews are in ordinary type. Only minerals for which definite data are given are indexed.

Abdel-Gawad, A. M., and Kerr, P. F. Urano-organic mineral association 402

ABO_3 type rare earth borates, polymorphism of (Levin, Roth, Martin) 1030

Addamiano, A. Weissenberg camera as a powder camera 1504

Adler, H. H. and Puig, J. A. Thermal behavior of brannerite 1086

Adler, I. (Book review) 460

Advances in *x*-ray research. Vols. 1, 2, 3. Edited by W. M. Mueller (Book review) 462

Advances in *x*-ray analysis. Vol. 4. Edited by W. M. Mueller (Book review) 764

Agrell, S. O. 1203

Ag_2Te and Ag_2S, polymorphism of (Frueh) 654

Ahrens, L. H. and Taylor, S. R. Spectroscopic analysis (Book review) 1512

Allanite and its radioactivity (Gindy) 985

Alling, Harold Lattimore, memorial of (Jensen) 471

Alumobritholite (Kurdrina, Kudrin, Sidorenko) 1514

Alumocobaltomelane (Ginzberg, Rukavishnikova) 766

Ames, L. L. Cation sieve properties of open zeolites 1120

Ammentorp, W. F., with Johnson, N. M. and Daniels, F. Thermoluminescence measurements with rapid heating ... 447

Amos, D. H. with Desborough, G. A. Ilvaite: a late magmatic occurrence in gabbro of Missouri 1509

Ampangabeite (discredited) 770

Amphiboles and pyroxenes, rapid determination of composition of (Parker) 892

Amphiboles, calciferous, oxyhornblende, kaersutite and barkevikite (Wilkinson) 340

Analytic classification and quadriplanar charting of analyses with nine or more components (Mertie) 613

Andalusite, kyanite and sillimannite, relative stability of. (Weill, Fyfe) 1191

Anderson, B. W. 1516

Andreatta, Ciro, memorial of (Gallitelli) 475

Ankinovich, E. A. 1200

Antlerite, *x*-ray data (Mrose) 146

Aramaki, S. Sillimanite and cordierite from volcanic xenoliths) 1154

Arsenopyrite crystal-chemical relations (Morimoto, Clark) . 1448

Arsenothorite (Bonshtedt-Kupletskaya) 1200

$AsBr_3$ immersion liquids, stability of (Meyrowitz and Westly) . 761

Austin, C. F. and Slawson, W. F. Isotopic analyses of single galena crystals 1132

Autunite, *x*-ray study of (Takano) 812

Balashov, Y. A. 769

Ballman, A. A. Growth and properties of colored quartz 439

Baotite (Simonov) 466

Baranova, E. N. 1202

Baric, L. J. 467

Barker, F. Phase relations in cordierite-garnet-bearing Kingsman quartz monzonite and enclosing schist, New Hampshire 1166

Barkevikite (Wilkinson) 340

Barth, Tom. F. W. Acceptance of the Roebling Medal of the Mineralogical Society of America 509

Bastin, J. A. and Mitchell, E. W. Light scattering from heat treated synthetic quartz 1227
Bates, R. L. Geology of industrial rocks and minerals (Book review) 235
Bauxite deposits near Weipa, Queensland, mineralogy of (Loughnan, Bayliss) 209
Bayliss, P. with Loughnan, F. C. Mineralogy of bauxite deposits near Weipa, Queensland 209
Behier, J. 767
Behierite (Behier) 767
Beljankin, D. S., Iwanow, B.W., Lapin, W. W. Technical petrography of products of refractories, whiteware-ceramics and hydraulic binders (Book review) 235
Bel'kov, I. V. and Volkova, M. I. 1004
Benford plate (Craig) 757
Benjamin, B. M. with Kohn, H. W. Radiation coloration of silica minerals 218
Benstonite (Lippmann) 1517
Beryllosodalite (beryllium sodalite) (Semonov, Bykova; Sørensen) 241
Betafite (Hogarth) 1519
Bethke, P. M. with Skinner, B. J. Relationship between unit-cell edges and composition of synthetic wurtzites 1382
Beus, A. A. 244
Blade, L. V. with Milton, C. and Ingram, B. L. Kimzeyite, a Zr garnet from Magnet Cove 533
Bloss, F. D. and Gibbs, G. V. Nomograms for determining 2θ from precession photographs 26
——— Indexed powder diffraction data for scapolite 1493
Boleslavite (Haranczyk) 1517
Bollin, E. M. and Kerr, P. F. Differential thermal pyrosynthesis 823
Boltwoodite, an alkali uranyl silicate, new data on (Honea) .. 12
Bonshtedt-Kupletskaya, E. M. .. 1200
Bornite from Cheshire (Howie) .. 458
Bornite, polymorphism in (Morimoyo, Kullerud) 1270
Borodin, L. S. 465
Borovskii, I. B. 464
Bovenkerk, H. P. Morphology and physical characteristics of synthetic diamond 952
Bradford, E. F. 768
Brannerite, thermal behavior of (Adler, Puig) 1096
Brindley, G. W. Reaction series, gibbsite-chialumina-kappa alumina-corundum. II 1187
——— **and Choe, J. O. Reaction series gibbsite-chi alumina-kappa alumina** 771
——— **and DeKimpe, C. Identification of clay minerals by single crystal electron diffraction** 1005
——— **with De Kimpe, C. and Gastuche, M. C. Ionic coordination in alumino-silicic gels in relation to clay mineral formation** 1270
——— with Hoffmann, R. W. Adsorption of ethylene glycol and glycerol by montmorillonite 450
——— **and Kurtossy, S. S. Quantitative determination of kaolinite by *x*-ray diffraction** ... 1205
Broch, O. A. Identification of potash feldspar, plagioclase and quartz for quantitative thin-section analysis 752
Buckley, Harold Eugene, memorial of (Deer) 481
Buerger, M. J. with Prewitt, C. T. Crystal structure of cahnite .. 1077
——— Crystal-structure analysis (Book review) 461
Bültemann, H. W. 465
Bulakh, A. G. 1202
Buryktalskite (Ginzberg, Rukavishnikova, Nikitin) 766
Bykova, A. V. 241, 465, 1515

Cahnite, crystal structure of (Prewitt, Buerger) 1077
Calciostrontianite (Mitchell, Pharr) 193
Calzirtite (Zdorik, Sidorenko, Bykova; Pyatenko, Pudovkina) 1515
Cameron, E. N. and Threadgold, I. N. Vulcanite, a new copper telluride from Colorado 258
Ca-Mg carbonates, lattice constants of (Goldsmith, Graf, Heard) 453
Carbocernaite (Bulakh, Konrat'eva, Baranova) 1202
Cation sieve properties of open zeolites (Ames) 1120
Celestite and calciostrontianite from Virginia (Mitchell, Pharr) 189
Chakravarty, P. S. Sheared ilmenite in a quartz vein 969
Chalcedony, origin and synthesis of (White, Corwin) 112
Chalcokyanite series (Rentzperis) 1503
Chalcokyanite series (Strunz) 758
Chao, E. C. T., Evans, H. T. Skinner, B. J., Milton, C. Neighborite, $NaMgF_3$, a new mineral from the Green River formation in Utah 379
——— with Mrose, M. E., Fahey, J. J. and Milton, C. Norsethite, $BaMg(CO_3)_2$, a new mineral from the Green River formation in Wyoming 420
Chemical composition of rocks, estimation of (Heier) 728
Chodos, A. A. with Doe, B. R., Rose, A. W. and Godijn, E. Determination of iron in sphalerite by *x*-ray fluorescence 1056
——— and Engel, C. G. Fluorescent *x*-ray spectrographic analysis of amphibolite rocks 120
Choe, J. O. with Brindley, G. W. Reaction series gibbsite-chi alumina-kappa alumina 771
Christ, C. L. (Book review) 460
Christophe-Michel-Levy, M. 1520
Chrysotile fiber, synthetic, growth of (Yang) 748
Claringbull, G. F. 1516
Clark, L. A. with Morimoto, N. Arsenopyrite crystal-chemical relations 1448
Clark, G. W. with Kopp, O. C. and Harris, L. A. Hydrothermal conversion of muscovite to kalsilite and an iron-rich mica 719
Clausthalite, D. T. A. of (Dunne, Kerr) 1
Clay mineral formation, ionic coordination in alumino-silicic gels in relation to (DeKimpe, Gastuche, Brindley) 1370
Clay minerals, density separation of, in thallous formate solutions (Kittrick) 744
Clay minerals, identification by single crystal electron diffraction (Brindley, DeKimpe) ... 1005
Cobaltomelane, cryptonickelmelane (Ginzberg, Rukavishnikova, Nikitin) 766
Coesite and kyanite, formation of, from pyrophyllite at very high pressures and high temperatures (Giardini, Kohn, Eckart, Tydings) 976
Colburn, Burnham Standish, memorial of (Schaller) 485
Cole, W. F. and Rowland, N. M. Abnormal effect in D.T.A. of clay minerals 304
Corrensite (Vivaldi, MacEwan) .. 769
Corwin, J. F. with White, J. F. Synthesis and origin of chalcedony 112
Cox, K. G. 766
Craig, D. B. The Benford plate .. 757
Crestmore, past and present (Murdoch) 245
Crook, K. A. W. Vein minerals from New South Wales 1017
Cryptonickelmelane (Ginzberg, Rukavishnikova) 766
Crystal-structure analysis (Buerger) (Book review) 461
Cuspidine, occurrence of, in phos-

phorous furnace slag (Wilson, Leary) 759
Cuttitta, F. with Hickling, N. and Meyrowitz, R. N,N-dimethylforamide, a new diluent for bromoform used as a heavy liquid 1502

Dachiardite (Gottardi) 769
Daniels, F. with Johnson, N. M. Ammentorp, W. F. Thermoluminescence measurements with rapid heating 447
Davidite, *x*-ray crystallography of (Pabst) 700
Davis, R. J. 1516
Deer, W. A. Memorial of Harold Eugene Buckley 481
Deev, A. N. 464
DeKimpe, C. with Brindley, G. W. Identification of clay minrals by single crystal electron diffraction 1005
———, Gastuche, M. C. and Brindley, G. W. Ionic coordination in alumino-silicic gels in relation to clay mineral formation 1370
Delatorreite (discredited) 467
Deltaite (discredited) 467
Denning, R. M. Lamellar structure in a type I diamond 740
——— (Book reviews) 240, 1512
DeNoyer, J. (Book review) 461
Desborough, G. A. and Amos, D. H. Ilvaite: a late magmatic occurrence in gabbro in Missouri 1509
Deweylite, new data on (Lapham) 168
Diamond, synthetic, morphology and physical characteristics of (Bovenkerk) 952
Dielectric behavior of rocks and minerals (Howell, Liscastro) 269
Differential thermal analysis of clay minerals, abnormal effect in (Cole, Rowland) ... 304
Differential thermal analysis of galena and clausthalite (Dunne, Kerr) 1
Differential thermal analysis of shattuckite (Sun) 67
Differential thermal pyrosynthesis (Bollin, Kerr) 823
Diffractometer mount for small samples (Gude, Hathaway) . 993
Diffractometer patterns of A.P.I. reference clay minerals (Molloy, Kerr) 583
Dillnite and its relation to zunyite (Konta, Mráz) 629, 1519
Discredited minerals (Fleischer) 467, 769, 1520
Doe, B. R., Chodos, A. A., Rose, A. W. and Godijn, E. Determination of iron in sphalerite by *x*-ray fluorescence 1056
Dolerophanite, *x*-ray data (Mrose) 148
Drovenik, M. 465
Dufresne, E. R. 1513
Dunne, J. A. and Kerr, P. F. D.T.A. of galena and clausthalite 1

Eckart, D. W. with Giardini, A. A. Kohn, J. A. and Tydings, J. E. Formation of coesite and kyanite from pyrophyllite at very high pressures and high temperatures 976
Edwards, Austin Burton, memorial of (Stillwell) 489
Eitel, W. (Book review) 235
Ekanite (Anderson, Claringbull, Davis, Hill) 1516
Elberty, W. T. 467
Elements of crystallography and mineralogy (Wade, Mattox) (Book review) 1001
Elizavetinskite (Mikheev, Ginzburg) 767
Ellweilerite (Bultemann) 465
Engel, C. G. with Chodos, A. A. Fluorescent *x*-ray spectrographic analyses of amphibolite rocks 120
Erd, R. C., McAllister, J. F. and Vlisidis, A. C. Nobleite, a new hydrated calcium borate 560
Errata 459, 763, 1000

Eskebornite (Tischendorf) 467
Eskolaite, Cr_2O_3, morphology of (Tennyson) 998
Euclase in greisen pipes and associated deposits, Park Co., Colorado (Sharp) 1505
Evans, H. T. Jr. with Chao, E. C. T., Skinner, B. J. and Milton, C. Neighborite, $NaMgF_3$, a new mineral from the Green River formation in Utah 379
Expandable chloritic clay minerals from Upper Mississipian carbonate rocks of the Cumberland Plateau in Tennessee (Peterson) 1245

Fahey, J. J. with Mrose, M. E., Chao, E. C. T. and Milton, C. Norsethite, $BaMg(CO_3)_2$, a new mineral from the Green River formation in Wyoming 420
Fanale, F. and Kulp, J. L. Helium in limestone and marble 155
Farquahar, R. M. with Russell, R. D. Lead isotopes in geology (Book review) 764
Farringtonite (Dufresne, Roy) ... 1513
Fayalite-bearing pegmatite, Burnet Co., Texas (King) 747
$(Fe,Ni)_2S$ (Stumpfl) 1518
Fergusonite, alpha and beta (Gorshevskaya, Sidorenko, Smorchkov) 1516
Fischer, E. 1520
Fischer, W. Gesteins- und Lagerstättenbildung im Wandel der Wissenschaftlichen Anschauung (Book review) 1003
Fleischer, M. Ten more years of new mineral names 463
Fluorescent *x*-ray spectrographic analysis of amphibolite rocks (Chodos, Engel) 120
Fournier, R. O. with Morey, G. W. Decomposition of microcline, albite and nepheline in hot water 688
Frenzel, G. 765
Freudenbergite (Frenzel) 765
Frondel, C. Systematic mineralogy of uranium and thorium (Book review) 238
——— 1204
Frueh, A. J., Jr. Use of zone theory in problems of sulfide mineralogy. III. Polymorphism of Ag_2Te and Ag_2S 654
Fyfe, W. S. and Weill, D. F. Relative stability of andalusite, kyanite and sillimanite 1191
Fynchenite (Bonshtedt-Kupletskaya) 1200

Gajite (discredited) 467
Galena and clausthalite, D. T. A. of (Dunne, Kerr) 1
Gallitelli, Paolo. Memorial of Ciro Andreatta 475
Garronite (Walker) 466
Gastuche, M. C. with DeKimpe, C. and Brindley, G, W. Ionic coordination in alumino-silicic gels in relation to clay mineral formation 1370
Gay, P. and LeMaitre. Some observations on "iddingsite" .. 92
——— 1203
Gedrite from Oxford Co., Maine (Milton, Ito) 734
Gelatin mounts for mineral grains (Jeffries) 458
Genkin, A. D. 464
Geologie und Bodenschätze Afrikas. (Krenkel) (Book review) 1001
Geology of industrial rocks amd minerals. (Bates) (Book review) 235
Gesteins- und Lagerstättenbildung im Wandel der Wissenschaftlichen Anschauung (Fischer) (Book review) 1003
Geversite (Stumpfl) 1518
Giardini, A. A., Kohn, J. A., Eckart, D. W. and Tydings, J. E. Formation of coesite and kyanite from pyrophyl-

lite at very high pressures and high temperatures..... 976
Gibbs, G. V. with Bloss, F. D. Nomograms for determining 2θ from precession photographs..... 26
——— and Bloss, F. D. Indexed powder diffraction data for scapolite..... 1493
Gibbsite-chi alumina-kappa alumina reaction series (Brindley, Choe)..... 771
Gibbsite vermiforms in the Pensauken formation of New Jersey (Lodding)..... 394
Gillberg, M..... 765
Gindy, A. R. Allanite and its radioactivity..... 985
Ginzburg, I. I.....766, 767
Gladovskii, A. K..... 243
Glauconite, factors concerning nature and origin of (Hower) 313
Gleason, S. Ultraviolet guide to minerals (Book review)..... 238
Godijn, E., with Doe, B. R. Chodos, A. A. and Rose, A. W. Determination of iron in sphalerite by x-ray fluoescence..... 1056
Goldich, S. S. with Whelan, J. A. New data for hisingerite and neotocite..... 1412
Goldsmith, J. R., Graf, D. L. and Heard, H. C. Lattice constants of Ca-Mg carbonates. 453
Goldsmith, J. R. Presentation of the 1960 Mineralogical Society of America Award to Donald L. Graf..... 511
Gorshevskaya, S. A..... 1516
Gottardi, G..... 769
Gouréite (=Narsarsukite) (Jérémine, Christophe-Michel-Levy)..... 1520
Graf, D. L. Acceptance of the 1960 Mineralogical Society of America Award..... 513
——— **Crystallographic tables for the rhombohedral carbonates**..... 1283
——— with Goldsmith, J. R. and Heard, H. C. Lattice constants of the Ca-Mg carbonates..... 453
Graf, R. B. with Wahl, F. M. and Grim, R. E. Phase transformations in silica as examined by continuous x-ray diffraction..... 196
——— **Phase transformations in SiO_2-Al_2O_3 mixtures by continuous x-ray diffraction**..... 1064
Greenberg, S. S..... 467
Grim, R. E. with Wahl, F. M. and Graf, R. B. Phase transformations in silica as examined by continuous x-ray diffraction..... 196
——— **Phase transformations in SiO_2-Al_2O_3 mixtures by continuous x-ray diffraction**..... 1064
——— **and Kulbicki, G. Montmorillonite: high temperature reactions and classification**..... 1329
Gross, E. B. (Book reviews)...764, 1512
Gude, A. J. and Hathaway, J. C. Diffractometer mount for small samples..... 993
Gutsevichite (Ankinovich)..... 1200
Gyrolite and reyerite (Meyer, Jaunarajs)..... 913

Hak, J. with Johan, Z. Novakite, a new mineral..... 885
Hale, W. E. Memorial of Graham Stewart MacKenzie..... 501
Halotrichite and melanterite, decomposition of pyritized carbonaceous shale to (Sclar)... 754
Haranczyk, C..... 1517
Harris, L. A. with Kopp, O. C. and Clark, G. W. Hydrothermal conversion of muscovite to kalsilite and an iron-rich mica..... 719
Hathaway, J. C. with Gude, A. J. Diffractometer mount for small samples..... 993
Hausen, D. M..... 464

Hawes, L. Direct determination of hexagonal lattice parameters 763
Heard, H. C. with Goldsmith, J. R. and Graf, D. L. Lattice constants of the Ca-Mg carbonates 453
Heier, K. S. Estimation of the chemical composition of rocks 728
Heinrich, E. Wm. Memorial of John Tipton Lonsdale 497
——— Book reviews 237, 238, 1001
——— **and Levinson, A. A. Carbonatic niobium-rare earth deposits, Ravalli, Co., Montana** 1424
Helium in limestone and marble (Fanale, Kulp) 155
Henry, N. M. F., Lipson, H. and Wooster, W. A. Interpretation of *x*-ray diffraction photographs (Book review) 1512
Henwoodite (=turquoise) (Fischer) 1520
Hexagonal lattice parameters, direct determination of (Hawes) 763
Hexastannite (Ramdohr) 1204
Hickling, N., Cuttitta, F. and Meyrowitz, R. N,N-dimethylforamide, a new diluent for bromoform used as a heavy liquid 1502
Hill, D. K. 1516
Hisingerite and neotocite, new data for (Whelan, Goldich) 1412
Hjelmite (Matias) 1520
Hoffmann, R. W. and Brindley, G. W. Adsorption of ethylene glycol and glycerol by montmorillonite 450
Hogarth, D. D. 1519
Honea, R. M. New data on boltwoodite, an alkali uranyl silicate 12
Howell, B. F., Jr. and Licastro, P. H. Dielectric behavior of rocks and minerals 269
Hower, J. Some factors concerning the nature and origin of glauconite 313
Howie, R. A. 458
Hsianghualite (Beus) 244
Hurlbut, C. S., Jr. Tephroite from Franklin, N. J. 549
Hydronium jarosite (Kubisz) 243
Hydrothermal conversion of muscovite to kalsilite and an iron-rich mica (Kopp, Harris, Clark) 719

"Iddingsite," some observations on (Gay, LeMaitre) 92
Ilmenite, sheared, in a quartz vein (Chakravarty) 969
Ilvaite: a late magmatic occurrence in gabbro of Missouri (Desborough, Amos) 1509
Imbibometry, a new method for investigation of clays (Konta) 289
Ingham, F. T. 768
Ingram, B. L. with Milton, C. and Blade, L. V. Kimzeyite, a Zr garnet from Magnet Cove 533
Innelite (Balashov, Turanskaya) 769
Interpretation of *x*-ray diffraction photographs (Henry, Lipson, Wooster) (Book review) 1512
Ionic coordination in aluminosilicic gels in relation to clay mineral formation (DeKimpe, Gastuche, Brindley) 1370
Iron in sphalerite, determination of, by *x*-ray fluorescence (Doe, Chodos, Rose, Godijn) 1056
Isomorphous substitution and infra-red spectra of layer lattice silicates (Stubičan, Roy) 32
Isotopic analyses of single galena crystals: A clue to history of deposition (Austin, Slawson) 1132
Ito, J. with Milton, D. J. Gedrite from Oxford Co., Maine 734
——— 1515
Iwanow, B. W., Beljankin, D. S., Lapin, W. W. Technical petrography of products of refractories, whiteware-ceramics and hydraulic binders (Book review) 235

Jaffe, H. W., Groeneveld, W. O. J. and Selchow, D. H. Manganoan cummingtonite from Nsuta, Ghana 642
Jaunarajs, K. L. with Meyer, J. W. Gyrolite and reyerite .. 913
Jensen, David E. Memorial of Harold Lattimore Alling 471
Jérémine, E. 1520
Johan, Z. and Hak, J. Novakite, a new mineral 885
——— 467
Johnson, M. M., Ammentorp, W. F. and Daniels, F. Thermoluminescence measurements with rapid heating 447

Kaersutite (Wilkinson) 340
Kaolinite, monoclinic, from Yugoslavia (Krstanović, Radošević) 1198
Kaolinite, quantitative determination of, by *x*-ray diffraction (Brindley, Kurtossy) 1205
Kaolin minerals, lattice expansion of, with potassium acetate (Wada) 78
Kapitonova, T. A. 465
Karooite (Von Knorring, Cox) ... 766
Katsura, T. and Kushiro, I. Titanomaghemite in igneous rocks 134
Kazakova, M. E. 1202
Kennedyite, karooite (Von Knorring, Cox) 766
Kerr, P. F. with Abdel-Gawad, A. M. Urano-organic mineral association 402
——— **with Bollin, E. M. Differential thermal pyrosynthesis** 823
——— **with Dunne, J. A. Differential thermal analysis of galena and clausthalite** 1
——— **with Molloy, M. W. Diffractometer patterns of A.P.I. reference clay minerals** 583
Kilchoanite (Agrell, Gay) 1203
Kimzeyite, a Zr garnet from Magnet Cove (Milton, Ingram, Blade) 533
King, E. A. Jr. Fayalite-bearing pegmatite, Burnet Co., Texas 747
Kittrick, J. A. Density separation of clay minerals in thallous formate solutions 744
Kneller, W. A. (Book review) 238
Kohn, H. W. and Benjamin, B. M. Radiation coloration of silica minerals 218
Kohn, J. A. with Giardini, A. A., Eckart, D. W. and Tydings, J. E. Formation of coesite and kyanite from pyrophyllite at very high pressures and high temperatures 976
Kondrat'eva, V. V. 1202
Konta, J. Imbibometry, a new method for the investigation of clays 289
——— **and Mraz, L. Dillnite and its relation to zunyite** 629, 1519
Kopp, O. C., Harris, L. A. and Clark, G. W. Hydrothermal conversion of muscovite to kalsilite and an iron-rich mica 719
Kordes, E. Optische Daten zur Bestimmung anorganischer Substanzen mit den Polarisations-Mikroskop (Book review) 237
Koutekite (Johan) 467
Krenkel, E. Geologie und Bodenschätze Afrikas (Book review) 1001
Krstanović, I. and Radošević, S. Monoclinic kaolinite from Yugoslavia 1198
Kudrin, V. S. 1514
Kudrina, M. A. 1514
Kubisz, J. 242, 243
Kulbicki, G with Grim, R. E. Montmorillonite: high temperature reactions and classification 1329
Kullerud, G. with Morimoto, M. Polymorphism in bornite 1270
Kulp, J. L. with Fanale, F. Helium

in limestone and marble.... 155
Kurtossy, S. S. with Brindley, G. W. Quantitative determination of kaolinite by *x*-ray diffraction..... 1205
Kuo, C..... 1200
Kushiro, I. with Katsura, T. Titanomaghemite in igneous rocks..... 134

Lamellar structure in a type I diamond (Denning)..... 740
Landes, K. K. (Book review).... 235
Lapham, D. M. New data on deweylite..... 168
Lapin, W. W., Beljankin, D. S., Iwanow, B. W. Technical petrography of products of refractories, whiteware-ceramics and hydraulic binders (Book review)..... 235
Lattice expansion of kaolin minerals by treatment with potassium acetate (Wada)..... 78
Lauder, W. R. Reaction of crystal structures and reaction fabric..... 1317
Lawsonite, synthetic, lattice constants of (Pistorius)..... 982
Layer lattice silicates, isomorphous substitution and infrared spectra of (Stubican, Roy)..... 32
Lazarevićite (Sclar, Drovenik)... 465
Lead-alpha age measurements, new results from (Stern, Rose)..... 606
Lead isotopes in geology (Russell, Farquahar) (Book review).. 764
Leary, J. K. with Wilson, A. Occurrence of cuspidine in phosphorous furnace slag..... 759
LeMaitre, R. W. and Gay, P. Some observations on "iddingsite"..... 92
Leonard, B. F. and Vlisidis, A. C. Vonsenite at the Jayville magnetite deposit, St. Lawrence Co. N. Y...... 786
Lepp, H. with Whelan, J. A. Occurrence of saponite near Silver Bay, Minnesota..... 430
Levin, E. M., Roth, R. S. and Martin, J. B. Polymorphism of ABO_3 type rare earth borates..... 1030
Levinson, A. A. Poorly crystallized, low barium, psilomelane-type mineral..... 355
——— **with Heinrich, E. W. Carbonatic niobium-rare earth deposits, Ravalli Co., Montana**..... 1424
Licastro, P. H. with Howell, B. F. Dielectric behavior of rocks and minerals..... 269
Liebhafsky, H. S., Pfeiffer, H. G., Winsloe, E. H. and Zemany, P. D. *X*-ray absorption and emission in analytical chemistry (Book review)..... 460
Lippmann, F..... 1517
Lipson, H. with Henry, N. M. F. and Wooster, W. A. Interpretation of *x*-ray diffraction photographs (Book review).. 1512
Lobanova, V. V..... 768
Lodding, W. Gibbsite vermiforms in the Pensauken formation of New Jersey..... 394
Lonsdale, John Tipton, memorial of (Heinrich)..... 497
Loughnan, F. C. and Bayliss, P. Mineralogy of bauxite deposits near Weipa, Queensland..... 209
Ludwigite, aluminian, from Crestmore, California, composition of (Schaller, Vlisidis)..... 335
Lueshite (Safriannikoff)..... 1004

MacChesney, J. B. and Muan, A. Phase equilibria in the system iron oxide-titanium oxide..... 572
MacEwan, D. M. C..... 769
MacKenzie, Graham Stewart, memorial of (Hale)..... 501
Magnesium (=magnesian) szomolnokite (Kubisz)..... 243

Magnetic susceptibility as a measure of total Fe plus Mn in ferromagnesian silicates (Vernon) ... 1141
Mandarino, J. A. ... 1201
Manganoan cummingtonite, first U.S. occurrence of (Segeler) ... 637
Manganoan cummingtonite from Nsuta, Ghana (Jaffe, Groenveld, Selchow) ... 642
Marchukova, I. D. ... 464
Martin, J. B. with Levin, E. M. and Roth, R. S. Polymorphism of ABO_3 type rare earth borates ... 1030
Martinez, E. Effect of particle size on thermal properties of serpentine ... 901
Mason, B. Trap rock minerals of New Jersey (Book review) ... 764
——— ... 769
Matias, V. V. ... 1514, 1520
Mattox, R. B. with Wade, F. A. Elements of crystallography and mineralogy (Book review) ... 1001
McAllister, J. F. with Erd, R. C. and Vlisidis, A. C. Nobleite, a new hydrated calcium borate ... 560
McDougall, I. Optical and chemical studies of pyroxenes in a differentiated Tasmanian dolerite ... 661
Meijer, W. O. J. G., with Jaffe, H. W., Selchow, D. H. Manganoan cummingtonite from Nsuta, Ghana ... 642
Mertie, J. B. Jr. Analytic classification and quadriplanar charting of analyses with nine or more components ... 613
Metaschoderite (Hausen) ... 464
Methods and techniques in geophysics. Vol. 1. Edited by S. K. Runcorn (Book review) 461
Methods in geochemistry. Edited by A. A. Smales and L. R. Wager (Book review) ... 460
Meyer, J. W. and Jaunarjs, K. L. Gyrolite and reyerite ... 913
Meyrowitz, R. with Hickling, N. and Cuttitta, F. N,N-dimethyl-dimethylforamide, a new diluent for bromoform used as a heavy liquid ... 1502
——— and Westly, H. Stability of $AsBr_3$ immersion liquids during storage ... 761
Microcline, albite and nepheline, decomposition of, in hot water (Morey, Fournier) ... 688
Microspectrochemical analysis of minerals (Waring, Worthing, Weeks) ... 1177
Mikheev, V. I. ... 767
Milton, C., Ingram, B. L. and Blade, L. V. Kimzeyite, a Zr garnet from Magnet Cove ... 533
——— **with Chao, E. C. T., Evans, H. T. and Skinner, B. J. Neighborite, $NaMgF_3$, a new mineral from the Green River formation in Utah** ... 379
——— **with Mrose, M. E., Chao, E. C. T. and Fahey, J. J. Norsethite, $BaMg(CO_3)_2$, a new mineral from the Green River formation in Wyoming** 420
——— (Book review) ... 1003
Milton, D. J. and Ito, J. Gedrite from Oxford Co., Maine ... 734
Mineral separation method, using hydrofluoric acid (Neuerburg) 1498
Mineralogical Society of America Award, acceptance of (Graf) ... 513
Mineralogical Society of America Award, presentation to Donald L. Graf (Goldsmith) ... 511
Mineralogy and petrology of the system Al_2O_3-SiO_2-H_2O in pyrophyllite deposits of North Carolina (Zen) ... 52
Mitchell, E. W. with Bastin, J. A. Light scattering from heat treated synthetic quartz ... 1227
Mitchell, R. S. and Pharr, R. F. Celestite and calciostrontianite from Virginia ... 189
——— (Book review) ... 1001

Moleva, V. A. 241
Molloy, M. W. and Kerr, P. F. Diffractometer patterns of A.P.I. reference clay minerals 583
Montmorillonite, adsorption of ethylene glycol and glycerol by (Hoffman, Brindley) 450
Montmorillonite: high temperature reactions and classification (Grim, Kulbicki) 1329
Morey, G. W. and Fournier, R. O. Decomposition of microcline, albite and nepheline in hot water 688
Morimoto, N. and Clark, L. A. Arsenopyrite crystal-chemical reactions 1448
——— and Kullerud, G. Polymorphism in bornite 1270
Mraz, L. with Konta, J. Dillnite and its relation to zunyite 629, 1519
Mrose, M. E., Chao, E. C. T., Fahey, J. J. and Milton, C. Norsethite, $BaMg(CO_3)_2$, a new mineral from the Green River formation in Wyoming 420
——— Vernadskite discredited: pseudomorphs of antlerite after dolerophanite 146
Muan, A. with MacChesney, J. B. Phase equilibria in the system iron oxide-titanium oxide 572
——— and Sōmiya, S. Phase equilibria at liquidus temperatures in the system iron oxide-manganese oxide-silica 364
Murdoch, J. Crestmore, past and present 245

Nakhla, F. M. Polianite pseudomorphs 964
Namaqualite (discredited) 769
Natrolite from Somerset Co., N. Jersey (Sinkankas) 1195
Neighborite, $NaMgF_3$, a new mineral from the Green River formation in Utah (Chao, Evans, Skinner and Milton) 379
Neotocite and hisingerite, new data for (Whelan, Goldich) .. 1412
Nepheline-albite system (Saha) . 859
Neuerburg, G. J. A method of mineral separation using hydrofluoric acid 1498
New minerals, five unnamed (Mandarino, Williams) 1201
New Mineral names (Fleischer) 241, 464, 765, 1004, 1200, 1513
New mineral data (Fleischer) 244, 466, 769, 1519
Nickelemelane, nickel-cobaltomelane (Ginzberg, Rukavishnikova) 766
Nikitin, K. K. 767
Niobium-rare earth deposits, carbonatic, Ravalli Co., Montana (Heinrich, Levinson) .. 1424
Niobozirconolite (Borodin, Bykova, Kapitonova, Pyatenko) 465
N,N-dimethylforamide, a new diluent for bromoform used as a heavy liquid (Hickling, Cuttitta, Meyrowitz) 1502
Nobleite, a new hydrated calcium borate (Erd, McAllister, Vlisidis) 560
Nomograms for determining 2θ from precession photographs (Bloss, Gibbs) 26
Norsethite, $BaMg(CO_3)_2$, a new mineral from the Green River formation, Wyoming (Mrose, Chao, Fahey, Milton) 420
Novakite, a new mineral (Johan, Hak) 885

Olsen, E. J. Six-layer orthohexagonal serpentine from the Labrador trough 434
Optical crystallography (Wahlstrom) (Book review) 240
Optische Daten zur Bestimmung anorganischer Substanzer mit den Polarisations-Mikroskop. (Kordes) (Book review) 237
Organova, N. I. 241

Orientite from Oriente Province, Cuba, optical orientation of, and *x*-ray data (Sclar) 226
Orthopinakiolite (Randmets) 768
Oxyhornblende (Wilkinson) 340

Pabst, A. X-ray crystallography of davidite 700
Parker, R. B. Rapid determination of composition of amphiboles and pyroxenes 892
Paulite (Bültemann) 465
Peacock Memorial Prize 458
Perite (Gillberg) 765
Perthites, explanation of strain and orientation effects in (Smith) 1489
Peterson, M. N. A. Expandable chloritic clay minerals from Upper Mississippian carbonate rocks of the Cumberland Plateau in Tennessee 1245
Pfeiffer, H. S. with Liebhafsky, H. S., Winsloe, E. H. and Zemany, P. D. *X*-ray absorption and emission in analytical chemistry (Book review) 460
Pharr, R. F. with Mitchell, R. S. Celestite and calciostrontianite from Virginia 189
Phase equilibria in the system iron oxide-manganese oxide-silica in air at liquidus temperatures (Muan, Sōmiya) 364
Phase equilibira in the system iron oxide-titanium oxide (MacChesney, Muan) 572
Phase relations in cordierite-garnet-bearing Kingsman quartz monzonite and enclosing schist (Barker) 1166
Phase transformations in silica as examined by continuous *x*-ray diffraction (Wahl, Grim, Graf) 196
Phase transformation in SiO_2-Al_2O_3 mixtures by continuous *x*-ray diffraction (Wahl, Grim, Graf) 1064
Photoelastic effects in quartz and feldspars (Ramberg) 934
Pistorius, C. W. F. T. Lattice constants of synthetic lawsonite 982
Plagioclase, polysynthetic twinning in (Vance) 1097
Plagioclase twins in sections normal to the composition plane, recognition of (Tobi) 1470
Polianite pseudomorphs (Nakhla) 964
Prewitt, C. T. and Buerger, M. J. Crystal structure of cahnite 1077
Proceedings of the 41st annual meeting of the Mineralogical Society of America 516
Psilomelane-type mineral, poorly crystallized, low barium (Levinson) 355
Pt and Pd minerals, unnamed (Borovskii, Deev, Marchukova) (Stumpfl) 464, 1518
Pudovkina, Z. V. 1515
Puig, J. A. with Adler, H. H. Thermal behavior of brannerite 1086
Pyatenko, Y. A. 465, 1515
Pyroxenes in a differentiated Tasmanian dolerite, optical and chemical studies of (McDougall) 661

Quantitative thin section analysis, identification of potash feldspar, plagioclase and quartz for (Broch) 752
Quartz, colored, growth and properties of (Ballman) 439

Radiation coloration of silica minerals (Kohn, Benjamin) 218
Radošević, S. with Krstanović, I. Monoclinic kaolinite from Yugoslavia 1198
Ramberg, H. Photoelastic effects in quartz and feldspars 934
Ramsdell, L. S. (Book review) ... 461
Ramdohr, P. 1204
Randmets, R. 768
Rare earth borates, ABO_3 type, polymorphism of (Levin, Roth, Martin) 1030

Rare-earth calcium phosphate-silicate, unnamed (Bel'kov, Volkova) 1004
Reaction of crystal structures and reaction fabric (Lauder) 1317
Reaction series gibbsite-chi alumina-kappa alumina (Brindley, Choe) 771
Reaction series, gibbsite-chi alumina-kappa alumina-corundum. II (Brindley) 1187
Redledgeite (Strunz) 1201
Rentzperies, P. J. The chalcokyanite series 1502
Reyerite and gyrolite (Meyer, Jaunarajs) 913
Rezhikite (Soboleva, Sobelev) 244
Rhombohedral carbonates, crystallographic tables for (Graf) 1283
Roebling Medal of the Mineralogical Society of America Acceptance of (Barth) 509
Roebling Medal, presentation to Tom. F. W. Barth (Tunell) 505
Rose, A. W. with Doe, B. R., Chodos, A. A. and Godijn, E. Determination of iron in sphalerite by *x*-ray fluorescence 1056
Rose, H. J. Jr. with Stern, T. W. New results from lead-alpha age measurements 606
Roth, R. S. with Levin, E. M. and Martin, J. B. Polymorphism of ABO_3 type rare earth borates 1030
Rowland, N. M. with Cole, W. F. Abnormal effect in D.T.A. of clay minerals 304
Roy, R. Comments on "Growth and properties of colored quartz" 446
——— **with Stubičan, V. Isomorphous substitution and infrared spectra of layer lattice silicates** 32
Roy, S. K. 1513
Rozenite (Kubisz) 242
Rukavishnikova, I. A. 766, 767
Russell, R. D. and Farquahar, R. M. Lead isotopes in geology (Book review) 764
Safiannikoff, A. 1004
Saha, P. System nepheline-albite 859
Saponite, occurrence of, near Silver Bay, Minnesota (Whelan, Lepp) 430
Scapolite, indexed powder diffraction data for (Gibbs, Bloss) 1493
Schaller, W. T. Memorial of Burnham Standish Colburn 485
——— **and Vlisidis, A. C. Composition of aluminian ludwigite from Crestmore, California** 335
Schoderite (Hausen) 464
Scholzite (Strunz, Tennyson) 1519
Sclar, C. B. Decomposition of pyritized carbonaceous shale to halotrichite and melanterite 754
——— **Optical orientation of orientite from Oriente Province, Cuba** 226
——— 465
Seaman's mineral tables (Book review) 239
Segeler, C. G. First U. S. occurrence of manganoan cummingtonite, tirodite 637
Selchow, D. H. with Jaffe, H. W. and Groenveld, W. O. J. Manganoan cummingtonite from Nsuta, Ghana 642
Semenov, E. I. 241
Serpentine, effect of particle size on thermal properties of (Martinez) 901
Serpentine, six-layer orthohexagonal, from the Labrador trough (Olsen) 434
Shappiro, J. (Book review) 240
Sharova, A. K. 243
Sharp, W. N. Euclase in greisen pipes and associated deposits, Park Co., Colorado 1505
Shattuckite, differential thermal analysis of (Sun) 67
Sidorenko, G. A. 1514, 1515, 1516
Silica, phase transformations in,

as examined by continuous x-ray diffraction (Wahl, Grim, Graf) 196
Sillimanite and cordierite from volcanic xenoliths (Aramaki) 1154
Simonov, V. I. 466
Sinkankas, J. Natrolite from Somerset Co., N. Jersey 1195
Skinner, B. J. Unit-cell edges of natural and synthetic sphalerites 1399
——— and Bethke, P. M. Relationship between unit-cell edges and composition of synthetic wurtzites 1382
———with Chao, E. C. T., Evans, H. T., and Milton, C. Neighborite, $NaMgF_3$, a new mineral from the Green River formation in Utah 379
Slawson, W. F. with Austin, C. F. Isotopic analyses of single galena crystals 1132
Smith, J. V. Explanation of strain and orientation effects in perthites 1489
Smol'yaninova, N. N. 241
Smorchkov, I. E. 1516
Sobolev, N. D. 244
Soboleva, M. V. 244
Sokolovite (Sharova, Gladovskii) 243
Sōmiya, S. with Muan, A. Phase equilibria at liquidus temperatures in the system iron oxide-manganese oxide-silica 364
Sørensen, H. 241
Spectrochemical analysis (Ahrens, Taylor) (Book review) 1512
Spencite (Frondel) 1204
Sphalerites, natural and synthetic, unit-cell edges of (Skinner) .. 1399
Spirals on natural hematite crystals, step height of (Sunagawa) 1216
Spiroff, K. (Book review) 239
Stern, T. W. and Rose, H. J. New results from lead-alpha age measurements 606
Stillwell, F. L. Memorial of Austin Burton Edwards 489
Strontioborite (Lobanova) 768
Strunz, H. The chalcokyanite series 758
——— 1201, 1519
Stubičan V. and Roy, R. Isomorphous substitution and infrared spectra of layer lattice silicates 32
Stumpfl, E. F. 1518
Sunagawa, I. Step height of spirals on natural hematite crystals 1216
Sun, Ming-Shan. Differential thermal analysis of shattuckite 67
Synthetic quartz, light scattering from (Bastin, Mitchell) 1227
Systematic mineralogy of uranium and thorium (Frondel) (Book review) 238

Takano, Y. X-ray study of autunite 812
Takeuchi, Y. 1515
Taylor, S. R. with Ahrens, L. H. Spectroscopic analysis (Book review) 1512
Technical petrography of products of refractories, white-ware-ceramics and hydraulic binders. (Beljankin, Iwanow, Lapin). German edition (Winkler) (Book review) 235
Teineite (Zemann, Zemann) 466
Ten more years of new mineral names (Fleisher) 463
Tennyson, C. Morphology of eskolaite, Cr_2O_3 998
——— 1519
Tephroite from Franklin, New Jersey (Hurlbut) 549
Thermoluminescence measurements with rapid heating (Johnson, Ammentorp, Daniels) 447
Threadgold, I. M. with Cameron, E. N. Vulcanite, a new copper telluride from Colorado 258
Tikhonenkova, R. P. 1202
Tin-tantalite (Olovotantalit) (Matias) 1514

Tirodite, manganoan cummingtonite, first U. S. occurrence of (Segeler) 637
Tischendorf, G. 467
Titanomaghemite in igneous rocks (Katsura, Kushiro) 134
Tobi, A. C. Recognition of plagioclase twins in sections normal to the composition plane 1470
Trap rock minerals of New Jersey (Mason) (Book review) 764
Tunell, G. Presentation of the Roebling Medal to Tom. F. W. Barth 505
Turanskaya, N. V. 769
Tydings, J. E. with Giardini, A. A., Kohn, J. A. and Eckart, D. W. Formation of coesite and kyanite from pyrophyllite at very high pressures and high temperatures 976

Ultraviolet guide to minerals (Gleason) (Book review) 238
Urano-organic mineral association (Abdel-Gawad, Kerr) 402

Vance, J. A. Polysynthetic twinning in plagioclase 1097
Van Wambeke, L. 770
Vdovykin, G. P. 244
Vein minerals from New South Wales (Crook) 1017
Vernadskite discredited (pseudomorphs of antlerite after dolerophanite (Mrose) 146
Vernon, R. H. Magnetic susceptibility as a measure of total Fe plus Mn in ferromagnesian silicates 1141
Vivaldi, J. L. M. 769
Vlasovite (Tikhonenkova, Kazakova) 1202
Vlisidis, A. C. with Leonard, B. F. Vonsenite at the Jayville magnetite deposit 786
——— **with Erd, R. C. and McAllister, J. F. Nobleite, a new hydrated calcium borate** 560
——— **with Schaller, W. T. Composition of aluminian ludwigite from Crestmore, California** 335
Volkova, M. I. 1004
Von Knorring, O. V. 766
Vonsenite at the Jayville magnetite deposit, St. Lawrence Co., N. Y. (Leonard, Vlisidis) 786
Vulcanite, a new copper telluride from Colorado (Cameron, Threadgold) 258

Wada, K. Lattice expansion of kaolin minerals by treatment with potassium acetate 78
Wade, F. A. and Mattox, R. B. Elements of crystallography and mineralogy (Book review) 1001
Wahl, F. M., Grim, R. E. and Graf, R. B. Phase transformations in silica as examined by continuous *x*-ray diffraction 196
——— **Phase transformations in SiO_2-Al_2O_3 mixtures by continous *x*-ray diffraction** 1064
Wahlstrom, E. E. Optical crystallography (Book review) 240
Walker, G. P. L. 466
Waring, C. L., and Worthing, H. W. Microspectrochemical analysis of minerals 1177
Watanabe, T. 1515
Weeks, A. D. Note on microspectrochemical analysis of minerals 1185
Weill, D. F. and Fyfe, W. S. Relative stability of andalusite, kyanite and sillimanite 1191
Weissenberg camera as a powder camera (Addamiano) 1504
Westly, H. with Meyrowitz, R. Stability of $AsBr_3$ immersion liquids during storage 761
White, J. F. and Corwin, J. F. Synthesis and origin of chalcedony 112
Whelan, J. A. and Goldich, S. S.

New data for hisingerite and neotocite 1412
——— and Lepp, H. Occurrence of saponite near Silver Bay, Minnesota 430
Wilkinson, J. F. G. Calciferous amphiboles, oxyhornblende, kaersutite and barkevikite .. 340
Williams, S. J. 1201
Wilson, A. and Leary, J. K. Occurrence of cuspidine in phosphorous furnace slag 759
Winsloe, E. H. with Liebhafsky, H. S., Pfeiffer, H. G. and Zemany, P. D. *X*-ray absorption and emission in analytical chemistry (Book review) 460
Wöhlerite (Vdovykin) 244
Wooster, W. A. with Henry, N. M. F. and Lipson, H. Interpretation of *x*-ray diffraction photographs (Book review) 1512
Worthing, H. W. with Waring, C. L. Microspectrochemical analysis of minerals 1177
Wurtzites, synthetic, relationship between unit-cell edges and composition (Skinner, Bethke) 1382
X-ray absorption and emission in analytical chemistry. (Liebhafsky, Pfeiffer, Winsloe and Zemany) (Book review) 460
Yang, J. S. Growth of synthetic chrysotile fiber 748
Yanshainshynite (Kuo) 1200
Yoshimuraite (Watanabe, Takeuchi, Ito) 1515
Zdorik, T. B. 1515
Zemann, A. and Zemann, J. 466, 1517
Zemany, P. D. with Liebhafsky, H. S., Pfeiffer, H. G. and Winsloe, E. H. *X*-ray absorption and emission in analytical chemistry (Book review) . 460
Zen, E-an. Mineralogy and petrology of the system Al_2O_3-SiO_2-H_2O in pyrophyllite deposits of N. Carolina 52
Zincsilite (Smol'yaninova, Moleva and Organova) 241
Zone theory in problems of sulfide mineralogy, use of. Part III. Polymorphism of Ag_2Te and Ag_2S (Frueh) 654

LOW COST . . .

"HYDROTHERMAL"

. . . REACTOR UNITS

for crystal synthesis

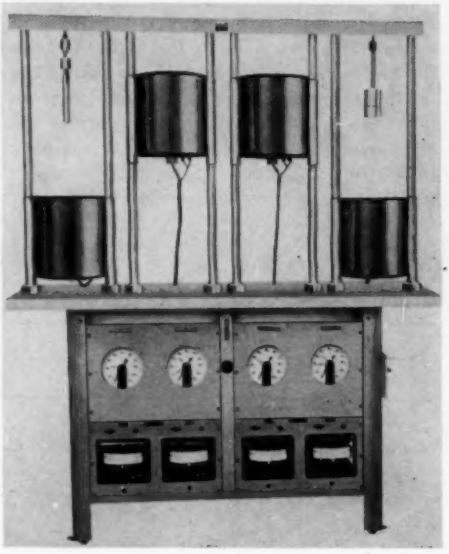

* Pressures to 60,000 psi
* Temperatures to 1200° C.
* Gases or liquids can be used to transmit pressure
* Temperature and pressure independently variable on each reactor
* Pressure indicated continuously
* Corrosion resistant
* 1-, 2-, or 4-Reactor units
* Delivered in "ready to plug in" condition

OTHER PRECISE HIGH TEMPERATURE AND HIGH PRESSURE INSTRUMENTS:

- X-ray diffraction furnaces
- Differential thermal analysis units
- Quench, gradient, and heat-treating furnaces
- Opposed anvil, ultra-high pressure devices
- Strip furnaces for rapid heating to 2400° C.

ALSO:
- Automatically-operated balanced filter x-ray units
- Automatic sample changers for x-ray fluorescence
- Noble metal arc-sealing units

RESEARCH • INSTRUMENTATION • ANALYTICAL SERVICES

TEM-PRES RESEARCH, inc.

DEPT. M, 146 N. ATHERTON ST., STATE COLLEGE, PENNA.

New American

PEAT AND MARL SAMPLER

The instrument embodies the essential features of a design by Professor Davis of the Geographical Survey. It consists of a jacketed plunger with a sharpened end. As the instrument is pressed into the ground, it remains closed. When the proper depth has been reached for taking the sample, the instrument is drawn up about 6 or 8 inches; at this point an internal locking device holds the plunger fast in the upper part of the jacket. This instrument is again forced downward, cutting and retaining the desired sample. Complete with illustrated head, 9 four foot lengths of extension rod and case; catalog number 4200 sells for $80.00.

Eberbach
CORPORATION

P.O. Box 1024 Ann Arbor, Michigan

MINERAL SPECIMENS
For teaching, display and study

New C16 Mineral Catalog listing crystals, crystal groups, rare and common minerals, now available upon request.

Filer's are interested in buying or exchanging good quality minerals, especially from foreign countries. Correspondence is invited.

FILER'S
P.O. Box 372, Redlands, California

Our Specialty is
SELECTED MINERAL SPECIMENS
FROM WORLD-WIDE LOCALITIES FOR COLLECTORS AND MUSEUMS
we also carry a complete line of
MINERALIGHTS, ESTWING PROSPECTOR PICKS, MINERALOGICAL BOOKS, ETC.
Send for free current bulletin
SCHORTMANN'S MINERALS
6 McKinley Avenue Easthampton, Massachusetts

New!

A low-priced UV lamp

that gives shortwave UV, longwave UV, or both at the same time.

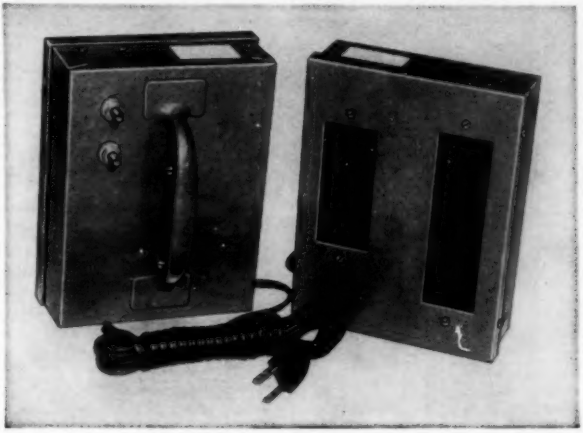

Model IS-6

Lamp measures 6½" x 5" x 1¾".
Easily held in the hand while being used.

Operates on a 115 volt AC (9-foot cord), or portable batteries can be furnished at extra cost.

It is an important aid in identification of minerals. Every Mineralogy Department, every researcher on minerals, every teacher of mineralogy and every prospector should have a source of UV.

With each lamp are furnished six fluorescent minerals for demonstration. This lamp is sold on absolute money-back guarantee of satisfaction. **$29.50**

Write for our free brochure "Uses of Ultraviolet"

R. P. Cargille Laboratories, Inc.
117 Liberty Street, New York 6, N.Y.

BIG SAVINGS NOW up to 33% off

Terrific Values on JEWELRY CRAFT and ROCKHOUNDING Supplies!

ROCKHOUNDER'S KNAPSACK

The buy of the year

Tremendous value — this is army surplus material at a low, low price. Made of a sturdy, waterproof khaki canvas, very well stitched—well made. Perfect to carry rocks, equipment, books, maps, everything you might tote on a Rockhounding trip. Sportsmen, fishermen, hunters—everybody likes them. They sling easily over your shoulder to carry any kind of load. 7½" x 5" wide x 12" deep—with shoulder strap.

M115-1 J . . . . . each only $1.50

NEW epoxy ADHESIVE

So good it's replacing rivets

MIRACLE ADHESIVE — you've seen it on T-V and in LIFE — *it bonds materials* stronger than anything else. Aircraft industry using it instead of Rivets—replaces nails and screws. Perfect for jewelry making — *Unconditionally guaranteed!* Kit of 2 jars with complete instructions.

Order as: Z1- J . . . . . only $1.50

This "15X Ruper" Magnifier with 1/2" diameter corrected lens! Full any magnifier you now use! Nickel plated metal folding frame. Equivalent to other $6 magnifiers. $1.00

Order as: T130-25 J $1.00

WE DARE YOU TO COMPARE

FLASHLIGHT MAGNIFIER

Enlarges Objects 7X

Place "Flash Magnifier" ON object under scrutiny — snap on flashlight — and get 7 times magnification exactly where you need it. Gem stones and minerals look more beautiful . . . markings, flaws, defects are easily spotted. 7" long. Metal and plastic case. Colossal value.

Z-179 J only $1.95

Complete including 2 batteries . . .

Z-180 J . only $2.15

GOLD PANNING KIT

. . . *exciting fun for the entire family*

Everything you need to pan for gold — including directions, 12" gold pan, sample of placer gold ore — ready to pan, leather pouch of ore and an alnico magnet. Shows you how to go about it . . . just like the old 49'ers did. It's a real thrill . . . and many streams in all parts of the country have gold in them. Get a kit and head for the open country. Excellent gift item too. Start panning for gold now. Order —

Z-75 J - 49'er Gold Panning Outfit . 1 for $2.95

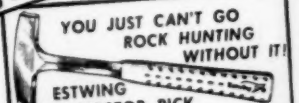

YOU JUST CAN'T GO ROCK HUNTING WITHOUT IT!

ESTWING PROSPECTOR PICK

Forged all-steel one-piece head-handle prospecting pick with the new blue everlasting nylon cushion handle grip — non slip. 13 inches long with 7" head which weighs 22 oz. Guaranteed unbreakable.

Order as Z-60- J . . . . . now only $4.75

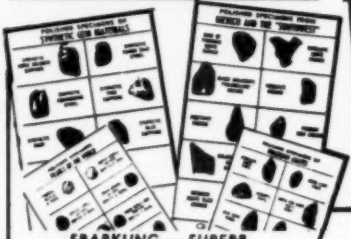

SPARKLING — SUPERB SPECIMEN CARDS!

10 different specimens on card — all tumbled and polished — many of gem quality!

Wonderful cards for everyone interested in rockhounding. Educational — instructive — good for class work — and an "absolute must" for the beginning collector.

Big value . . . terrific buy — order one or more now — you must see them to appreciate . . . we guarantee you'll be delighted!

YZ-101 J Mexico and the Southwest" only $1.00
YZ-102 J "Brazilian Agates" . . . . . only $1.00
YZ-103 J "Mother of Pearl" . . . . . only $1.00
YZ-183 J "Brazilian Gem Materials" . . only $1.00
YZ-184 J "Gem Materials of the West" . only $1.00
YZ-185 J "World Wide Gem Materials" only $1.00
YZ-186 J "International Gem Stones" . only $1.00
YZ-187 J "Colorful Gem Stones" . . . only $1.00
YZ-188 J "California Gem Materials" . only $1.00

TERRIFIC VALUES IN READER MAGNIFIERS

Imported quality — 2x magnification — optical lens. Ideal for jewelry making, rockhounding, stamp collecting, etc. Fits easily in pocket. Black Ebonite handle — polished chrome frame.

Z-181 J 2" Magnifier . each $1.00
Z-182 J; 3" Magnifier . each 1.95

YOU DO BETTER WORK WHEN YOU SEE BETTER WITH MAGNI-FOCUSER

Binocular Magnifier

Leaves both hands free to work

MAGNI-FOCUSER

Designed for All Professions and Trades

Make all precision work easier work

T131-3 J	MAGNI-FOCUSER, magnifies 1¾ times at 14" . . . $10.50	2 lbs.
T131-5 J	MAGNI-FOCUSER, magnifies 2¼ times at 10" . . . $10.50	2 lbs.
T131-7 J	MAGNI-FOCUSER, magnifies 2¾ times at 8" . . . $10.50	2 lbs.
T131-10 J	MAGNI-FOCUSER, magnifies 3½ times at 4" . . . $12.50	2 lbs.
T131-15 J	MAGNI-FOCUSER, magnifies 4¾ times at 3" . . . $15.00	2 lbs.
T131-17 J	MAGNI-FOCUSER, magnifies 5½ times at 2½" . . . $15.00	2 lbs.

Any work that requires precision can be done easier, faster and more accurately with a Magni-Focuser — the binocular magnifier.

Magni-Focuser shows an object in third dimension and greatly magnified—with the depth and clarity of normal vision. It reduces eye-strain and prevents squinting—thereby saving time, increasing accuracy, and minimizing the chance of errors and accidents.

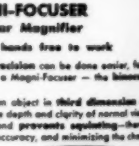

RELIEVE "EYE STRAIN" WITH A MAGNI-FOCUSER

All items sold on Money Back Guarantee!

GRIEGER'S 1633 E. WALNUT PASADENA, CALIF.

Prices include Taxes and Postage!

ALL NEW!

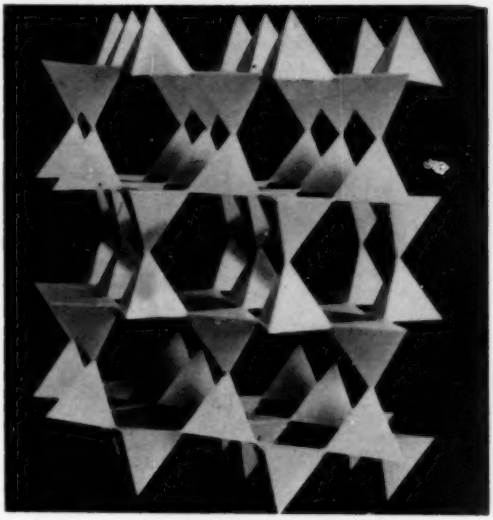

Tridymite

TETRAHEDRAL MODELS OF SILICATES

- **Durable plastic**
- **Scaled models 1″-2Å**

Available—Sets of 28 silicate-frame models
—Individual models
—Bulk tetrahedra for model construction

Models are designed to illustrate the various silicate frameworks. The 28 models include most of the known structurally distinct silicate frames. They include less known structures, such as Zunyite, Wollastonite, Xonotlite, Apophyllite, Gillespite, Prehnite, Sanbornite, Left- and Right-handed Quartz, Coesite and others.

Each model contains several unit cells.

For information and price list write to:

DYNACAST CORP.
509 Vandalia Street
St. Paul 4, Minn.

A complete system for differential thermal analysis

SYMBOL OF DEPENDABILITY AND ACCURACY

INTRODUCING
DELTATHERM

The Deltatherm is a complete measuring system which will bring economy and versatility to your laboratory or production line. It was designed and constructed by people who *know* DTA; it will provide you a degree of usefulness and accuracy well beyond that attainable with patchwork equipment.

EFFICIENCY two or more furnaces permit continuous operation.

CAPACITY each furnace holds up to four samples, their inert references, and a reference well for temperature indication.

IMMEDIATE READOUT up to four traces are permanently recorded on the twelve-inch chart and are visible immediately.

VERSATILITY sample blocks available include standard (inconel), ceramic, and controlled-atmosphere for vacuum and pressure studies.

SENSITIVITY 25 micro volts per inch, maximum (4.5″ deflection for alpha-beta quartz transition with standard chromel-alumel thermocouples).

MODULAR CIRCUIT PACKAGING rugged circuitry has been standardized to simplify maintenance; plug-in printed circuits allow rapid component exchange.

Write today for complete information contained in new bulletin and for the name of your nearby distributor.

TECHNICAL EQUIPMENT CORPORATION

917 Acoma Street • Denver 4, Colorado
MAin 3-0258

Direct Distance Dialing Code: 303
TWX: DN 955

NOW...

...a versatile, high precision

CAMBION® Monochromator *with light source*

- **Cold Intense 100 Watt Zirconium Arc Light**
- **Point Source — .08″ Diameter**
- **Convenient Circular Light Aperture**
- **Wide Range of Wavelengths — 4500A to 6400A**
- **Narrow Pass Band Width — 40A to 120A**

Here's the ideal monochromator for optical crystallography determinations. Can be used with both microscope and refractometer. Utilizes the rotary dispersion of quartz to provide a continuous selection of wavelengths. Combines highest intensity light source with large aperture. Power source, light, and lenses in compact, portable unit. Overall length 14″; height 5″; width 6″. Crackle grey finish. Send coupon for complete details.

CAMBRIDGE THERMIONIC CORPORATION
CAMBION
The guaranteed electronic components

Cambridge Thermionic Corporation
503 Concord Avenue
Cambridge 38, Massachusetts

Please send complete details on CAMBION Monochromator.

Name.....

Title.....

Address.....

City.....*Zone*....*State*.....

POTASSIUM-ARGON AGE DETERMINATIONS

can
help
solve
a variety
of geological
problems.
Perhaps we
could
help
solve
some of
yours.
Why not
write to
Department V
for our
free pamphlet,
K-Ar Age Determinations,
and find out?

GEOCHRON LABORATORIES, Inc.
24 Blackstone Street
Cambridge 39, Massachusetts,
U.S.A.

Carnotite

Of the thousands of hand specimens labeled "carnotite", in museum collections and private collections, all but a few are tyuyamunite. X-ray studies have shown these specimens to be near tyuyamunite in X-ray pattern. Carnotite from Club Mesa, Montrose County, Colorado, is actually carnotite, as shown by X-ray tests.

This material is practically pure, the only impurity being a small amount of quartz. The purity is such that it will not hold together sufficiently for use as a hand specimen.

Vials, for use as reference carnotite specimens, or for laboratory tests, or for X-ray patterns, $2.00, postpaid.

JOHN S. ALBANESE

Fine Minerals

P.O. Box 221 Union, New Jersey

SHALE'S

9226 W. Pico Blvd., Los Angeles 35, Calif.

MUSEUM SPECIMENS FOR SALE OR TRADE

Inquiries invited

MI-GEE brand

METHYLENE IODIDE

Sp.G. 3.3 M.P. 5-6°C 99.9% Minimum assay

Best quality for all laboratory, industrial and mining uses.

Lowest prices. Prompt shipment

National Biochemical Company

3127 W. Lake St., Chicago 12, Illinois

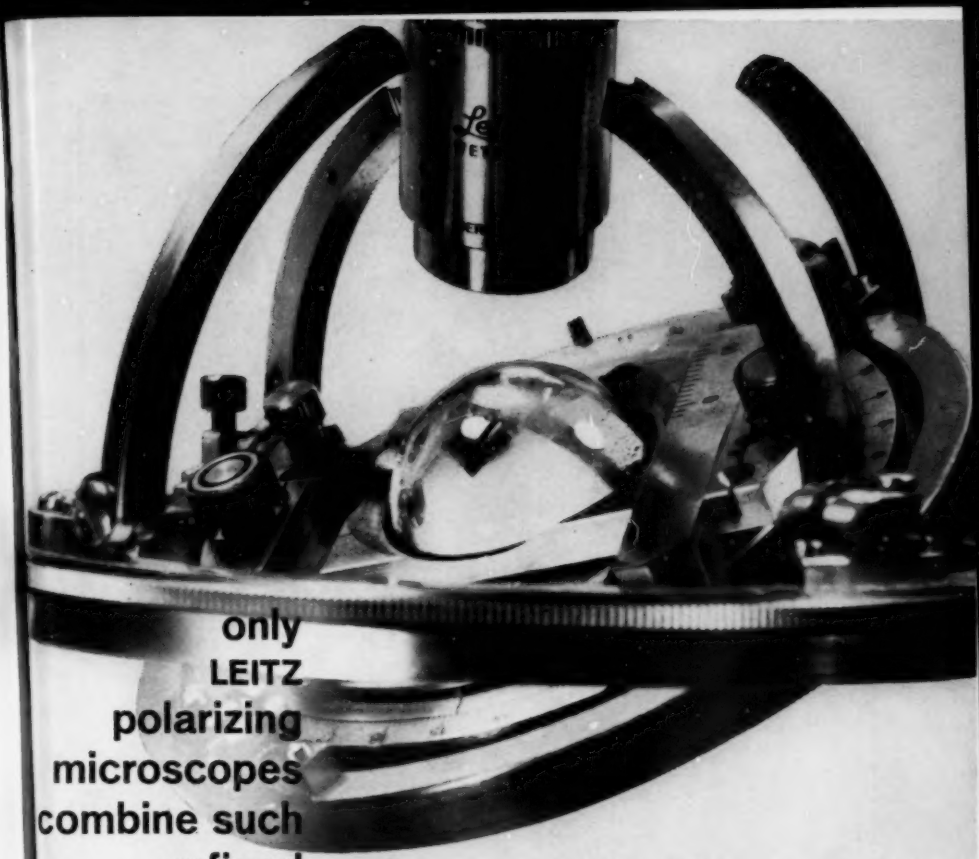

only LEITZ polarizing microscopes combine such refined precision and limitless versatility

4 specialized Polarizing Microscopes for advanced research, laboratory and student

DIALUX-POL... the world's most advanced universal polarizing research microscope. A choice of more than 100 optional interchangeable components permits almost infinitely varied combinations for precision measurement, examination and photomicrography that require polarizing techniques. Features a built-in light source and matching condenser system. Adapts for transmitted or reflected polarized light.

Exclusive Optional Features: conoscopic observation with bindcular body • single-knob coarse and fine adjustment • monocular tube with iris diaphragm for small crystal identification • combination FS tube for photography • vertical illuminator for ore microscopy • choice of polarizing filters or calcite prisms.

ORTHOLUX-POL... world's widest range universal research microscope for all types of microscopy in addition to polarizing features. Built-in system for incident and transmitted illumination, including incident phase contrast.

LABOLUX-POL... laboratory and semi-research polarizing microscope with built-in transmitted illumination and provisions for work in incident light.

SM-POL... student polarizing microscope or chemical microscope for general applications in transmitted polarized light.

ARISTOPHOT PHOTOGRAPHIC UNIT... supplements Leitz polarizing microscopes for photomicrography, macrophotography and low-power surveys with incident or transmitted light. Mirror reflex system for 3¼ x 4¼ (9 x 12cm), 4 x 5 or Polaroid; also adapts to Leica 35mm.

Yours for the asking... FREE — Complete 62-Page Manual of Leitz specialized polarizing microscopes, accessories and photomicrography units. Includes detailed bibliography on all applications.

30401

E. LEITZ, INC., 468 PARK AVENUE SOUTH, NEW YORK 16, N. Y.
Distributors of the world-famous products of Ernst Leitz G. m. b. H. Wetzlar, Germany—Ernst Leitz Canada Ltd.
LEICA AND LEICINA CAMERAS · LENSES · PROJECTORS · MICROSCOPES

The Mineralogical Society of America, in sorting out its stock of back issues of the AMERICAN MINERALOGIST, finds that it has a few copies of out-of-print issues. These are listed below and are available at the prices given. Postage is additional.

Older issues:

Volume 1, no. 6 (with index to volume), December 1916	$ 2.00	
2, no. 9, September 1917	2.00	
3, no. 6, (Renée—Just Haüy issue), June 1918	3.00	
3, no. 12 (with index to volume), December 1918	2.00	
5, nos. 1, 2, 3, 4, 5, 7, 10, 11, 12, 1920	2.00	each

Complete volumes:

Volume 20, 1935	$25.00
21, 1936	25.00
22, 1937 (includes Palache issue)	35.00
23, 1938	25.00
32, 1947	25.00

Separate issues:

Volume 22, no. 5, May 1937 (Palache issue)	$20.00
29, no. 9-10, September-October 1944	5.00
11-12, November-December 1944	5.00
30, no. 7-8, July-August 1945	5.00
31, no. 3-4, March-April 1946	5.00
32, no. 3-4, March-April 1947	5.00

Complete sets of the American Mineralogist are available with out-of-print issues supplied in microtext, with the exception of the special Palache issue (May, 1937, Vol. 22) which is available only on special order in a full size Xerox reproduction. See page xii in the March-April, 1961, issue for prices.

Send your order to the Treasurer, Marjorie Hooker
Mineralogical Society of America
U. S. Geological Survey
Washington 25, D.C.

The Name Is Appropriate . . .

MINERALS UNLIMITED

can supply most of your classroom mineral and rock needs at competitive prices. Poundage, lots of 1 × 1" specimens, larger specimens—all are available in quality material. Sorry, no school catalog available, but why not give us the opportunity of bidding on the minerals you need? We have more than 500 species in stock.

Some examples of what is available, and at what prices:

25¢ per lb.

Chromite—Phillipine "leopard ore"
Epidote—solid green massive (California)
Actinolite—coarse green crystallized masses (California)

35¢ per lb.

Anorthite—cleavages in hornblende norite (California)
Oolitic hematite—reddish pisolitic masses (New York)
Magnetite—black massive, no polarity (California)

50¢ per lb.

Psilomelane—black massive, some reniform (New Mexico)
Burkeite—buff crystalline masses (California)
Glauconite—dark green cementing sandstone (Texas)

55¢ per lb.

Knotted schist—shows incipient porphyroblasts (California)
Bishop tuff—an unwelded tuff (California)
Campito sandstone—magnetite-rich arkosic sandstone (California)
Peridotite—"Kimberlite" (Arkansas)
Olivine peridotite—"Dunite" (No. Carolina)

75¢ per lb.

Galena—good quality cleavable and cleavages (Tri-State)
Tremolite—coarse radiating silky masses, some rock (Utah)
Oligoclase—white to brown-stained, striated. Ratio AB_{80} : AN_{20} (New York)

$1.00 per lb.

Clinozoisite—yellow-green granular, with quartz, mica (Oregon)
Nephrite—grey-green crystalline masses (California)

$2.00 per lb.

Cinnabar—blood-red cleavages scattered on quartzite (Nevada)
Turquois—blue masses in rock (Arizona)

$2.25 per lb.

Smaltite—tin white metallic, very rich, with other arsenides (Canada)
Tyuyamunite—bright yellow encrustations on limestone (New Mexico)

$5.00 per lb.

Jamesonite—grey metallic in quartz, with scheelite. (Idaho)

$7.50 per lb.

Bismuthinite—rich grey metallic (Arizona-Colorado)
Melanocerite—brown to black masses in calcite, etc. (Canada)

All of the "usual" minerals in good quality—Azurite, Arsenopyrite, Hornblende, Beryl, Gypsum (many forms), Almandine, Biotite, etc.

MINERALS UNLIMITED

1724 University Avenue **Berkeley 3, California**

NEW UNIVERSAL ROCK COLLECTIONS

Ward's popular *American Rock Collection* now has two outstanding supplements. Each of the new collections contains 100 specimens selected from foreign and domestic sources to enable you to build up an impressive and valuable petrographic reference collection. Each collection will contain representative igneous, sedimentary and metamorphic rocks. Each specimen will have its own labeled tray for convenient storage and quick reference. The maximum size of the specimens will be 3 x 4", and there will be an accompanying check list of contents giving name and locality. There will be no duplication of contents in the individual collections.

MC 301. Ward's American Rock Collection. This is our standard and very popular petrographic collection. It contains 100 contrasting examples, accompanied by a manual and labeled trays.... *$150.00*

MC 301-A. Ward's Universal Rock Collection. Unit A. This contains 100 examples with labeled trays and check list. *$180.00*

MC 301-B. Ward's Universal Rock Collection. Unit B. This contains 100 examples with labeled trays and check list. *$210.00*

(WARD'S NEW POLYCRAFT TRAYS are now used for the above collections)

RECENT ACQUISITIONS

From Broken Hill, New South Wales, Australia:

Azurite. Nicely crystallized on rock 3¾ x 5¾", *$17.50;* with small embolite crystals on rock 2½ x 3", *$15.00*

Cerussite. Reticulated masses, many with crystallized anglesite 2½ x 3½", *$5.00;* 3 x 4", *$15.00, $25.00*

Embolite. Rich crystalline masses usually showing good crystallization 3 x 4", *$10.00, $15.00*

Iodyrite. Rich yellow crystalline masses frequently showing excellent crystallization 2 x 3", *$7.50;* 3 x 4", *$10.00, $15.00*

Smithsonite. Attractive partly clear to gray small crystals on coronadite 3 x 4", *$7.50, $10.00, $15.00;* 4 x 6", *$25.00*

Stolzite. Medium sized orange yellow crystals on rock 2 x 3", *$7.50;* 3 x 4", *$10.00, $15.00*

From the Camp Bird Mine, near Ouray, Colorado:

Here are but a few of the fine specimens of milky quartz with finely disseminated gold from an old collection.

1 x 2", *$17.50;* 2 x 2", *$35.00;* 3 x 3½", *$175.00.*

(Write for complete listing)

WATCH FOR ANNOUNCEMENTS OF OUR ANNIVERSARY GEOLOGY CATALOG.

WARD'S *NATURAL SCIENCE ESTABLISHMENT, INC.*
P.O. BOX 1712 ROCHESTER 3, N.Y.

GEORGE SANTA COMPANY, INC., MENASHA, WISCONSIN, U.S.A.